

Studies on Hydrodynamic and Mass Transfer Parameters in a Bubble Column

Submitted in

fulfillment of the requirements for the degree of

Doctor of Philosophy

by

Ajay Sujan

ID: 2013RCH9528

Under the Supervision of

Prof. Raj K. Vyas



**DEPARTMENT OF CHEMICAL ENGINEERING
MALAVIYA NATIONAL INSTITUTE OF TECHNOLOGY JAIPUR**

October 2018

DECLARATION

I, **Ajay Sujan**, declare that this thesis titled “**Studies on Hydrodynamic and Mass Transfer Parameters in a Bubble Column**” and the work presented in it, are my own. I confirm that:

- This work was done wholly or mainly while in candidature for a research degree at this university.
- Where any part of this thesis has previously been submitted for a degree or any other qualification at this university or any other institution, this has been clearly stated.
- Where I have consulted the published work of others, this is always clearly attributed.
- Where I have quoted from the work of others, the source is always given. With the exception of such quotations, this thesis is entirely my own work.
- I have acknowledged all main sources of help.
- Where the thesis is based on work done by myself, jointly with others, I have made clear exactly what was done by others and what I have contributed myself.

Date:

Ajay Sujan
(2013RCH9528)

CERTIFICATE

This is to certify that the thesis entitled “**Studies on Hydrodynamic and Mass Transfer Parameters in a Bubble Column**” being submitted by **Ajay Sujan (2013RCH9528)** is a bonafide research work carried out under my supervision and guidance in fulfillment of the requirement for award of the degree of **Doctor of Philosophy** in the Department of Chemical Engineering, Malaviya National Institute of Technology, Jaipur, India. The matter embodied in this thesis is original and has not been submitted to any other University or Institute for the award of any other degree.

Place: Jaipur
Date:

Raj K. Vyas
Professor
Department of Chemical Engineering
MNIT Jaipur

Acknowledgement

I am grateful to the Almighty, the most benevolent and merciful, for giving me the strength and zeal to complete this endeavor. Tremendous praise for God, who is forever a torch of guidance for knowledge seekers and whole humanity, paves the way to achieve the goal of life.

Foremost, I would like to express my sincere gratitude to my supervisor Dr. R. K. Vyas, Department of Chemical Engineering, Malaviya National Institute of Technology, Jaipur for the continuous support during my Ph.D. study and research, and also for his motivation, enthusiasm, patience and immense knowledge. His valuable guidance helped me all the time of research and writing of this thesis. I could not imagine for having a better advisor and mentor for my Ph.D. study.

I am highly thankful to Dr. Kailash Singh, Head, Department of Chemical Engineering for providing infra-structural support and facilities. I am also grateful to all the DREC members, viz. Prof. A. B. Gupta, Dr. Kailash Singh, Dr. P. Pandit and Dr. Virendra Saharan for their meticulous evaluation and suggestions throughout the tenure of my Ph.D. studies.

I would like to express my gratitude and indebtedness to my great grandfather Late Shri Ganeshi Lal, great grandmother Smt. Late Keshar Devi and grandfather Late Shri Kishan Lal, grandmother Late Smt. Ram Beti for their strong inspiration, encouragement, blessings and wishes. They offered me their silent contribution and moral support whenever it was needed.

Undoubtedly, I shall remain indebted to my father Shri Shiromani Sujan and mother Smt. Nirmala Sujan for their staunch moral support throughout my research work. They prayed for me, shared the burdens and made sure that I sailed through smoothly. Their boundless love and affection have been my great strength during the moments of stress.

I express my sincere and hearty thanks to my elder sister Mrs. Veenita Chandra, and brothers Mr. Upendra Sujan and Vivek Sujan for their persistent co-operation, patience and moral support. My brother in law Mr. Yogesh Chandra also extended his full co-operation in this mission for which I am thankful to him.

The constant co-operation, inspiration and moral support extended by my life partner Deepika Sujan is beyond any acknowledgement. Her patience and love enabled me to complete the thesis work. My lovable daughter Miss Deeksha Sujan and son Atharva Sujan also showed their patient because their childhood was affected on account of my research work.

I am extremely thankful to all the non-teaching staff of the Department namely, Mr. S.N. Reddy and Mr. Rajiv Goswami for helping me in getting the experimental set-up fabricated and in procurement of reagents and other related things.

I shall not forget to express thanks to my colleagues Dr. Komal Sharma for her assistance in preparation of the manuscript of this thesis.

I sincerely express thanks to all those persons whose names have not been mentioned here, but they contributed directly or indirectly in successful completion of this thesis.

Ajay Sujan

Abstract

Bubble columns (BC) are used widely for effecting gas–liquid mass transfer in different process industries. Applications of bubble columns include fermentation, Oxidation, chlorination, alkylation, absorption etc. Present work was targetted at single bubble modeling, bubble coalescence inhibition, volumetric mass transfer coefficient and relative power demand. A macroscopic mass transfer model based on the unsteady–state liquid film mass transfer mechanism for a single spherical bubble was formulated. Analytical solution of the model equation was obtained in Laplace transform using surface renewal rates based on Danckwerts' surface age distribution function. The mass transfer coefficient, k_L , in a slurry bubble column under different operating conditions of temperature, pressure, gas flow rate and solid concentration has been simulated using a program code 'BUBBLESIM' in MATLAB[®]. The proposed model has been validated using secondary data for a slurry system under a wide range of operating conditions. The predicted values of k_L showed very good agreement with the experimental data within an average deviation of $\pm 2\%$. The study shows that the mass transfer coefficient, k_L increased with increasing superficial gas velocity and temperature and decreased with increase in slurry concentration, while it changed slightly with pressure. Based on above, empirical correlations have been proposed for the prediction of δ in terms of dimensionless groups for H₂–, CO– and CO₂–paraffin–quartz sand systems at elevated temperatures (298 – 423 K) and elevated pressures (1 – 3MPa) in a slurry bubble column.

The bubble column was further investigated with a swarm of air bubbles dispersed in aqueous electrolyte (NaCl, MgSO₄·7H₂O, CaCl₂·2H₂O, and Na₂SO₄) solutions. In the present work, coalescence inhibition was studied by applying gas holdup enhancement and surface tension gradient approaches for aqueous solutions in single and binary mixtures (CaCl₂·2H₂O + NaCl and Na₂SO₄ + NaCl) of electrolytes. Transition concentrations of a series of coalescence inhibiting inorganic electrolytes were determined. A qualitative comparison of these electrolytes revealed that strong electrolytes (Na₂SO₄, and CaCl₂· 2H₂O) yield gas holdup enhancement $\geq 60\%$ whereas moderate electrolytes (NaCl and MgSO₄· 7H₂O) produced gas holdup up enhancement values $\leq 46\%$. It has been also found that the values of transition concentration for different electrolytes are of the same order in most of the cases and are in line with those reported in literature. Inhibition of bubble coalescence was also analyzed in terms of the

parameter $C(d\sigma/dC)^2$. The large value of the parameter $(d\sigma/dC)^2$ indicates that the electrolyte will inhibit bubble coalescence, and a smaller value indicates moderate effect on bubble coalescence. Surface elasticity values at transition concentration of various electrolytes were also determined. It was also found that the surface elasticity values at transition concentration were in the order $\text{CaCl}_2 \cdot 2\text{H}_2\text{O} > \text{MgSO}_4 \cdot 7\text{H}_2\text{O} > \text{Na}_2\text{SO}_4 > \text{NaCl}$. Surface elasticity for binary electrolytes was also estimated at their transition concentrations. The values were found in the order $\text{CaCl}_2 \cdot 2\text{H}_2\text{O} + \text{NaCl} > \text{Na}_2\text{SO}_4 + \text{NaCl}$. Furthermore, Analysis of variance (ANOVA) was employed to estimate significance of the parameters.

In this work, different types of impellers such as concave blade impellers with different curvatures, a Rushton impeller and pitch blade impellers were studied in an agitated vessel with different sparger geometries. The experiments were carried out in a flat bottom cylindrical vessel made of a transparent acrylic sheet with an internal diameter of 0.30 m and a height of 0.44 m. Response surface methodology (RSM) was applied to optimize four independent parameters, viz. curvature of blades, nozzle length, gas flow rate, and impeller speed for volumetric mass transfer coefficient (k_La) under a wide range of operational conditions in air–water system and compared its performance with a Rushton turbine. To study the mutual interaction between these four parameters and to optimize these parameters during the aeration process, a 2^4 full-factorial central composite design (CCD) and response surface methodology were employed. The optimized parameters for mass transfer coefficient k_La determined in this study are as follows: air flow rate, 22.5 L/min; agitator speed, 400 rpm; straight nozzle length, 0.10 m; and Curvature, 0.441. Under these conditions, the value of k_La was found to be 0.03716 s^{-1} . An empirical correlation for volumetric mass transfer coefficient was developed using dimensionless groups, such Froude number, impeller Weber number, impeller Reynolds number, Curvature of blade, and the ratio of $\frac{L_N}{d}$. Predicted k_La values were found to be within a variation of $\pm 10\%$ with experiments. This empirical correlation can be useful in scale –up of industrial vessel design in biological and other industries for a wide range of operational conditions. Furthermore, response surface methodology (RSM) was employed for design of experiment and different operational parameters were optimized. Curvature and nozzle length were found as the significant parameters with the help of analysis of variance (ANOVA).

The effect of gas flow rate and inter-impeller clearance on relative power demand (P_g/P_{ug}) was also studied in dual Rushton impeller configuration in a partially-baffled agitated system. The inter-impeller clearance (ΔS) was varied in the range of 3.5 – 21.5 cm. The dual Rushton impeller with minimum value of ΔS generally consumed significantly less power. In a dual Rushton impeller system, three different flow patterns were identified to explain the hydrodynamics of the vessel depending upon the impeller clearance. In the range, $0.96 \leq \Delta S/d \leq 1.54$, both impellers act independently and the power consumption of the dual Rushton impeller system was found approximately equal to one and a half times that of a single impeller at a lower impeller speed of 250 rpm. For, $\Delta S/d \leq 0.82$, when the two impellers were close to each other, the lower recirculation flow (vortices) was found absent or weakly present. In that situation, both the impellers were considered operating together like a single Rushton impeller. When the distance between the impellers became greater than $\Delta S/d \geq 1.54$, the zone between the impellers became more turbulent and large recirculation flows were visually observed above and below the impellers. In the range, $0.82 \leq \Delta S/d \leq 0.96$, a sudden transition in power consumption from a lower value to a higher value was observed for all the flow rates of air (12.5–22.5 L/min) studied during the present work. An empirical correlation for relative power demand (P_g / P_{ug}) using dimensionless groups, such as gas flow number, Froude number, and the ratio of $\Delta S/d$ was developed. Interestingly, this correlation also fits well in case of electrolyte solutions because surface tension has insignificant effect on P_g / P_{ug} . Predicted values of P_g / P_{ug} were found to be within a range of $\pm 10\%$ with experiments.

Two empirical correlations were developed for different impellers used in this study. An empirical correlation, developed for a single impeller applicable to Rushton impeller, pitch blade, and concave blade ($e = 0.441$) predicts Relative power demand (RPD) with a deviation of $\pm 15\%$. Furthermore, an empirical correlation was developed for single and multiple impeller configurations (RT+RT, CD6 + CD6, RT + RT + RT and CD6 + CD6+ CD6). Relative power demand (P_g / P_{ug}) for multiple impeller system was found to be within a variation of 10% with experimental data.

TABLE OF CONTENTS
CONTENTS

Declaration	i	
Certificate	ii	
Acknowledgements	iii	
Abstract	iv	
Table of contents	viii	
List of Tables	xiii	
List of Figures	xv	
Nomenclature	xx	
1	INTRODUCTION	1
1.1	Bubble column	1
1.2	Industrial applications of bubble columns	4
1.3	Motivations for the present work	5
1.4	Problem identification	6
1.5	Scope of present research work	7
1.6	Research objectives and Scope	8
1.7	Research outline	9
1.8	Organization of thesis	13
2	LITERATURE REVIEW	14
2.1	Introduction	14
2.2	Phenomena of coalescence	16
2.3	Flow regimes and Characteristics	17
2.4	Hydrodynamics in Newtonian liquids	17
2.5	Bubble coalescence inhibition in electrolyte solutions	18

2.6	Experimental technique for estimation of bubble coalescence estimation	22
2.7	Power consumption in stirred bubble column	29
2.8	Volumetric gas–liquid mass transfer coefficient	31
2.9	Modeling of liquid-side mass transfer coefficient	37
2.10	Hydrodynamics in non-Newtonian liquids	39
3	MATERIALS AND METHODS	41
3.1	Theory and working principle of digital dissolved oxygen electrode	41
3.2	Surface tension and density measurement	42
3.3	Experimental setup	45
3.3.1	Stirred bubble column	45
3.3.2	Bubble column	47
3.3.3	Types of impellers	48
3.3.4	Inter-impeller spacing	57
3.3.5	Spargers types and design for bubble column	57
3.3.5.1	Sparger for a stirred bubble column	59
3.3.5.2	Sparger for a bubble column	60
3.3.6	Baffles	60
3.3.7	Operating conditions	61
3.4	Power consumption measurements	67
3.5	Estimation of volumetric mass transfer coefficient (k_La)	69
3.6	Estimation of overall gas holdup	70
3.7	electrolytes and their properties	72

4	MODEL DEVELOPMENT FOR LIQUID – SIDE MASS TRANSFER COEFFICIENT	75
4.1	Introduction	75
4.2	Macroscopic model for gas–liquid mass transfer considering single spherical bubble	76
4.3	Hypotheses for model development	78
4.4	Analytical solution of model equations	80
4.5	Validation of developed model using secondary data	99
4.6	Estimation of overall mass transfer coefficient k_L using number distribution density function	100
5	RESULTS AND DISCUSSION	101
5.1	Macroscopic model development for prediction of liquid–side mass transfer coefficient k_L in a slurry bubble column	101
5.1.1	Effect of temperature	104
5.1.2	Effect of pressure	106
5.1.3	Effect of superficial gas velocity	108
5.1.4	Effect of solid concentration	110
5.1.5	Effect of liquid film thickness on k_L	112
5.1.6	Empirical correlations for liquid film thickness δ	119
5.2	Estimation of transition concentration of aqueous mixtures of single and binary electrolytes for bubble coalescence inhibition	122
5.2.1	Gas holdup enhancement in aqueous solution of single electrolyte (s)	122
5.2.2	Surface tension and surface tension gradient of a single electrolyte solution	131
5.2.3	Gas holdup enhancement in an aqueous solution of mixed electrolytes	141
5.2.4	Excess surface tension and surface tension gradient in an aqueous solution of mixed electrolytes	144
5.2.5	Surface elasticity values for single and mixed electrolytes	146

5.2.6	Analysis of variance (ANOVA)	152
5.3	Estimation of volumetric mass transfer coefficient in a partially baffled gas-liquid contactor equipped with curved and non-curved impellers	155
5.3.1	Effect of blade numbers of a pitch blade impeller	155
5.3.2	Effect of curvature of a concave blade	156
5.3.3	Effect of jet nozzle length on k_La	164
5.3.4	Empirical correlations for k_La	172
5.3.5	Development of quadratic polynomial regression model for an agitated system equipped with concave blade impeller with different curvatures	176
5.3.6	Effect of model components and their interactions on k_La	182
5.3.6.1	Effect of gas flow rate and impeller speed on k_La	182
5.3.6.2	Effect of gas flow rate and curvature of blade on k_La	183
5.3.6.3	Effect of jet nozzle length and curvature of blade on k_La	183
5.3.6.4	Effect of impeller speed and curvature of blade on k_La	183
5.3.6.5	Effect of jet nozzle length and gas flow rate on k_La	184
5.3.6.6	Effect of jet nozzle length and impeller speed on k_La	184
5.3.7	Response optimization	191
5.3.8	Development of quadratic polynomial regression model for an agitated system equipped with a Rushton impeller	194
5.3.9	Response optimization	198
5.3.10	Effect of model components their interaction on k_La	199
5.3.10.1	Effect of gas flow rate and impeller speed on k_La	200
5.3.10.2	Effect of jet nozzle length and gas flow rate on k_La	200
5.3.10.3	Effect of jet nozzle length and impeller speed on k_La	200
5.4	Estimation of relative power demand in a partially baffled gas-liquid contactor equipped with single or multiple impeller combinations	206

5.4.1	Effect of single and multiple impeller on power consumption	206
5.4.2	Effect of impeller spacings on relative power demand	209
6	CONCLUSIONS	216
6.1	Conclusions	216
6.2	Recommendations for future work	220
	References	222
	Appendix	239

List of Tables

Table 1.1 Some examples of industrial scale processes in bubble column and modifications	4
Table 2.1 Effect of air –aqueous solution of electrolyte system on gas holdup	25
Table 2.2 Empirical correlations for power consumption in the presence of gas in agitated systems	33
Table 2.3 Power consumption studies on multiple impeller configurations in stirred vessels.	35
Table 3.1 Specifications of digital dissolved oxygen probe	44
Table 3.2 Specifications of density meter	45
Table 3.3 Specifications of stirred aeration column	47
Table 3.4 Specifications of bubble column experimental setup	48
Table 3.5 Dimensions of Rushton turbine (RT), Concave-blade impeller and Pitch blade turbine (PBT)	53
Table 3.6 Specifications of jet nozzles of different lengths connected to the ring sparger	59
Table 3.7 Specifications of the multiple ring sparger	60
Table 3.8 Properties of electrolytes	73
Table 3.9 Properties of aqueous electrolytes solutions used in the experiments	74
Table 5.1: Transition concentration, C_{trans} comparison and other properties of electrolytes	128
Table 5.2: Incremental transition concentration values of electrolytes in comparison to $MgSO_4$	131
Table 5.3: Algebraic equations of excess surface tension for different electrolytes	140
Table 5.4: Algebraic equations of excess surface tension for mixed electrolyte system	145
Table 5.5: Comparison of transition concentration, C_{trans} mixed electrolytes with their component	145
Table 5.6: Gibbs elasticity and surface elasticity at transition concentration of electrolytes	151
Table 5.7: Analysis of Variance	152
Table 5.8: Experimental design layout and experimental results of the response	177
Table 5.9: Analysis of Variance (ANOVA) for mass transfer coefficient	179

Table 5.10: Estimated regression coefficients and corresponding t and P values from the data of central composite design experiment	181
Table 5.11: Optimum operating conditions of the process variable	192
Table 5.12: Estimated regression coefficients and corresponding t and P values from the data of central composite design experiment	195
Table 5.13: Analysis of Variance (ANOVA) for mass transfer coefficient	196
Table 5.14: Experimental design layout and experimental results of the response	197
Table 5.15: Optimum operating conditions of the process variable	198
Table 5.16: Power number at $\Delta S/d \geq 0.82$ for a Rushton impeller	211

List of Figures

Figure 1.1 Flow diagram of modeling of a single spherical bubble	10
Figure 1.2 Schematic diagram of work done on bubble coalescence inhibition studies in a bubble column	11
Figure 1.3 Flow diagram of relative power demand studies in a stirred bubble column.	12
Figure 2.1 Inter-relationships between various factors affecting gas holdup and mass transfer in a bubble column	40
Figure 3.1 Digital dissolved oxygen meter and electrode with its internal components	43
Figure 3.2 (a) Drop Shape Analyzer and (b) density meter	46
Figure 3.3 Schematic diagram of experimental setup of stirred bubble column	49
Figure 3.4 Photographic image of experimental setup of stirred bubble column	50
Figure 3.5 Schematic diagram of bubble column experimental setup	51
Figure 3.6 Photographic image of experimental setup of bubble column	52
Figure 3.7 Images of different types of impellers utilized in this work: (a) to (e) curved blade impellers; (f) and (g) pitch blade impellers; and (h) and (i) Rushton impellers	54
Figure 3.8 Geometrical parameters of the agitator used (a) 4 Pitch blade turbine (4PBT), (b) 6 Pitch blade turbine (6PBT), (c) Rushton turbine (RT), (d) concave blade impeller with different curvature.	56
Figure 3.9 Double and triple impeller configurations with inter impeller clearance in a stirred tank equipped with (a) Dual impeller system ($\Delta S = 0.25d-1.52d$), (b) triple impeller system ($\Delta S=d$).	58
Figure 3.10 Various types of jet nozzle length used in this study (a) Image of jet nozzle (b) Dimension of jet nozzle	62
Figure 3.11 Arrangement of jet nozzles connected to the circular ring	63
Figure 3.12 Geometrical parameters of the sparger used (a) jet nozzle, (b) ring sparger	64
Figure 3.13 Actual schematic view of different types of sparger utilized in this work: (a) ring sparger of 2.5 mm hole diameter (b) jet nozzle attached with ring	65
Figure 3.14 Schematic diagram of perforated nylon circular disc sparger	66
Figure 3.15 Bed expansion method (Kazakis et al. 2007) for gas holdup measurement (a) before air supply (b) after air injection and (c) after superimposing the images (a) and	71

(b). Reproduced from Kazakis et al. (2007) with permission from Elsevier	
Figure 4.1 Mechanism of transient mass transfer through liquid film and surface renewal by liquid element on a spherical bubble	77
Figure 5.1: Flow diagram of unsteady state mass transfer model development for k_L .	102
Figure 5.2: Flow diagram for estimation of liquid film thickness and surface renewal rate in a slurry bubble column	103
Figure 5.3: Influence of temperature on mass transfer coefficient for diffusion of H_2 , CO and CO_2 in a slurry system (liquid paraffin– Quartz sand: 150-200 μm) – comparison of experimental and predicted values.	105
Figure 5.4: Influence of pressure on mass transfer coefficient for diffusion of H_2 , CO and CO_2 in a slurry system (liquid paraffin– Quartz sand: 150-200 μm) – comparison of experimental and predicted values.	107
Figure 5.5: Influence of gas flow rate on mass transfer coefficient for diffusion of H_2 , CO and CO_2 in a slurry system (liquid paraffin– Quartz sand: 150-200 μm) – comparison of experimental and predicted values.	109
Figure 5.6: Influence of slurry (liquid paraffin – Quartz sand: 150-200 μm) concentration on mass transfer coefficient k_L .	111
Figure 5.7: Experimental vs predicted values of k_L for (a) CO – slurry system (liquid paraffin – quartz sand), (b) CO_2 – slurry system (liquid paraffin – quartz sand) and (c) H_2 – slurry system (liquid paraffin – quartz sand).	115
Figure 5.8: Effect of liquid film thickness (δ) on k_L ($S = 1-10 s^{-1}$) for (a) CO – slurry system (liquid paraffin – quartz sand), (b) CO_2 – slurry system (liquid paraffin – quartz sand) and (c) H_2 – slurry system (liquid paraffin – quartz sand).	118
Figure 5.9: Dimensionless gas holdup parameter ($\varepsilon/\varepsilon_w$) versus concentration in aqueous $CaCl_2 \cdot 2H_2O$ solutions.	124
Figure 5.10: Dimensionless gas holdup parameter ($\varepsilon/\varepsilon_w$) versus concentration in aqueous Na_2SO_4 solutions	125
Figure 5.11: Dimensionless gas holdup parameter ($\varepsilon/\varepsilon_w$) versus concentration in aqueous NaCl solutions	126

Figure 5.12: Dimensionless gas holdup parameter ($\varepsilon/\varepsilon_w$) versus concentration in aqueous $\text{MgSO}_4 \cdot 7\text{H}_2\text{O}$ solutions.	127
Figure 5.13: Qualitative comparisons between strong ($\text{CaCl}_2 \cdot 2\text{H}_2\text{O}$ and Na_2SO_4) and moderate (NaCl and $\text{MgSO}_4 \cdot 7\text{H}_2\text{O}$) electrolytes.	130
Figure 5.14: Pictorial representation of bubble coalescence inhibition by using electrolyte(s).	133
Figure 5.15: Variation of excess surface tension of solution with electrolyte concentration for strong electrolytes ($\text{CaCl}_2 \cdot 2\text{H}_2\text{O}$ and Na_2SO_4).	136
Figure 5.16: Variation of parameter $C(d\sigma/dC)^2$ with electrolyte concentration for strong electrolytes ($\text{CaCl}_2 \cdot 2\text{H}_2\text{O}$ and Na_2SO_4).	137
Figure 5.17: Variation of excess surface tension of solution with electrolyte concentration for moderate electrolytes (NaCl and $\text{MgSO}_4 \cdot 7\text{H}_2\text{O}$).	138
Figure 5.18: Variation of parameter $C(d\sigma/dC)^2$ with electrolyte concentration for moderate electrolytes (NaCl and $\text{MgSO}_4 \cdot 7\text{H}_2\text{O}$).	139
Figure 5.19: Comparison of gas hold up enhancement for mixed electrolytes ($\text{CaCl}_2 \cdot 2\text{H}_2\text{O} + \text{NaCl}$) system with individual electrolytes.	142
Figure 5.20: Comparison of gas hold up enhancement for mixed electrolytes ($\text{Na}_2\text{SO}_4 + \text{NaCl}$) system with individual electrolytes.	143
Figure 5.21: Comparison of excess surface tension of mixed electrolytes ($\text{CaCl}_2 + \text{NaCl}$) with individual electrolytes.	147
Figure 5.22: Comparison of excess surface tension of mixed electrolytes ($\text{Na}_2\text{SO}_4 + \text{NaCl}$) with individual electrolytes.	148
Figure 5.23: Comparison of parameter $C(d\sigma/dC)^2$ for mixed electrolytes ($\text{CaCl}_2 + \text{NaCl}$) system with individual electrolytes.	149
Figure 5.24: Comparison of parameter $C(d\sigma/dC)^2$ for mixed electrolytes ($\text{Na}_2\text{SO}_4 + \text{NaCl}$) system with individual electrolytes.	150
Figure 5.25: Residual plots for gas holdup.	153
Figure 5.26 At constant gas flow rate (22.5 L/min), variation of $k_L a$ values of the 4 PBT and 6 PBT at 9 cm nozzle length and Comparison with 6 PBT, dual concentric ring sparger system.	156

Figure 5.27 Effect of impeller speeds at different gas flow rates on mass transfer coefficient for Rushton agitated system equipped with dual concentric ring sparger.	158
Figure 5.28 The effect of blade curvature on k_{La} with various gas flow rate, (a) 200 rpm; (b) 250 rpm; (c) 300 rpm; (d) 350 rpm and (e) 400 rpm.	163
Figure 5.29 Effect of impeller speeds on k_{La} with various gas flow rates at different jet nozzle lengths (a) 5 cm; (b) 6 cm; (c) 7 cm; (d) 8cm; (e) 9 cm and (f) 10 cm.	171
Figure 5.30 Plot of the experimental and model predicted values of k_{La} for Rushton impeller with different jet nozzle lengths.	174
Figure 5.31 Plot of the experimental and model predicted values of k_{La} for concave impeller with different curvature.	175
Figure 5.32: (a) Response surface and (b) contour plots of k_{La} at optimized value as the function of gas flow rate (L/min) and impeller speed (rpm).	185
Figure 5.33: (a) Response surface and (b) contour plots of k_{La} at optimized value as the function of gas flow rate (L/min) and curvature (dimensionless).	186
Figure 5.34: (a) Response surface and (b) contour plots of k_{La} at optimized value as the function of gas flow rate (L/min) and nozzle length (m).	187
Figure 5.35: (a) Response surface and (b) contour plots of k_{La} at optimized value as the function of curvature (dimensionless) and nozzle length (m).	188
Figure 5.36: (a) Response surface and (b) contour plots of k_{La} at optimized value as the function of impeller speed (rpm) and nozzle length (m).	189
Figure 5.37: (a) Response surface and (b) contour plots of k_{La} at optimized value as the function of impeller speed (rpm) and curvature (dimensionless).	190
Figure 5.38: The optimum values of the process variables for k_{La} .	192
Figure 5.39: Plot of the measured and model predicted values of the response variable..	193
Figure 5.40: The optimum values of the process variables for k_{La} .	198
Figure 5.41: Plot of the measured and model predicted values of the response variable.	199
Figure 5.42: (a) response surface and (b) contour plots of k_{La} at optimized value as the function of gas flow rate (L/min) and impeller speed (rpm).	203
Figure 5.43: (a) response surface and (b) contour plots of k_{La} at optimized value as the function of impeller speed (rpm) and nozzle length (dimensionless).	204
Figure 5.44: (a) response surface and (b) contour plots of k_{La} at optimized value as the	205

function of gas flow rate (L/min) and nozzle length (dimensionless).

Figure 5.45 Comparison of predicted relative power demand from correlation and the experimental values for single impeller system. 208

Figure 5.46 Comparison of predicted relative power demand from correlation and the experimental values for different single and multiple impeller systems. 209

Figure 5.47 Effect of inter-impeller spacing on the power number N_p at (a) 12.5 L/min (b) 15 L/min (c) 17.5 L/min (d) 20 L/min (e) 22.5 L/min gas flow rate. 214

Figure 5.48 Predicted vs. experimental values of (P_g/P_{ug}) for multiple impeller system (RT-RT). 215

Nomenclature

a	Specific gas–liquid interfacial area (1/m)
a_{\pm}	Mean ion activity coefficient
a_f	Free area of the disc (m ²)
A	Hamaker constant (non-retarded) for water, ($=3.5 \times 10^{-20}$ J)
A_1, A_2	Integration constants
BCs	Boundary condition
c	Force defined by eq. (2), N
C_{trans}	Transition concentration (mol/L)
C	Electrolyte concentration (mol/L)
ΔC	Change in surface tension of solute (electrolyte) (mol/L)
C_A	Microscopic gas concentration in liquid-phase (mol/L)
\bar{C}_A	Laplace-transformed gas concentration profile outside the bubble
C_i	Gas concentration in the liquid phase at the gas–liquid interface (mol/L)
C_L	Macroscopic gas concentration in liquid bulk (mol/L)
C_S	Mass concentration in liquid (%)
C_A^*	Saturated gas concentration in liquid phase (mol/L)
$\cos \theta$	Power factor ($=0.8$ to 0.9) (dimensionless)
d_B	Mean bubble diameter (m)
d	Diameter of impeller (m)
D_T	Diameter of vessel (m)
D_a, D_L	Gas diffusivity in liquid (m ² /s)

D_C	Column diameter (m)
e	Curvature of blade (dimensionless) (I_H/I_W)
Eu	Euler number ($P/\rho_{SL}.U_g^2$)(dimensionless)
Fr	Froude number ($N^2 d/g$) and ($N^2 d_i^4 / gwV_L^{2/3}$) (dimensionless)
Fl	Gas flow number (Q/NV_L)(dimensionless)
g	Acceleration of gravity (m/s^2)
H_L	Liquid height in bubble column (m)
H_b	Aerated froth height in bubble column (m)
I	Intensity of current (A)
I_H	Impeller height (m)
I_W	Impeller width (m)
IC	Initial condition
k	Defined by Eq. (3) (1/m)
k_L	Liquid side mass transfer coefficient (m/s)
$k_L a$	Gas-liquid volumetric mass transfer coefficient in liquid (1/s)
L_N	Length of nozzle (m)
M_B, M_1, M_2	Molecular weight (kg/kmol)
N	Rotational impeller speed (rpm)
N_A	The number of moles of diffusing gas through interfacial area (mol/s)
N	Avogadro's number
P_{ug}	Ungassed power (W/m^3)

$P_{i,imp}$	$P_{i, imp} = i$ th Impeller power consumption (W)
P	Pressure (MPa)
P_c	Critical pressure (MPa)
P_g	Gassed power (W/m^3)
Q	Gas flow rate (L/min)
r	Radial position (m)
r	Bubble radius (m)
R	Radius of bubble (m)
R	Universal gas constant (J/mol. K)
Re	Reynolds number ($d \cdot \rho_{SL} \cdot U_g / \mu_{SL}$)(dimensionless)
Re	Reynolds number of impeller ($d^2 N \rho_L / \mu_L$) (dimensionless)
s	Laplace domain, 1/s
S	Fractional rate of renewal of surface of liquid, 1/s
Sc	Schmidt number ($\mu_{SL} / \rho_{SL} \cdot D_a$)(dimensionless)
Sh	Sherwood number ($k_L \cdot D_c / D_a$)(dimensionless)
ΔS	Inter-impeller spacing (m)
t	Microscopic time (s)
T	Absolute temperature (K)
T_c	Critical temperature (K)
T_r	Reduced temperature (K)
u_G	Gas flow rate (L/min)
U_g	Superficial gas velocity (m/s)
U_L	Velocity of liquid (m/s)
V	Voltage of the power supply (V)
V	Molar volume (cm^3/mol)

V_D	Molar volume of the hard sphere (cm^3/mol)
V_L	Volume of liquid (m^3)
w	Width of blade (m)
W	Impeller width (m)
$We = (d^3 N^2 \rho_L / \sigma_L)$	Weber number of impeller (dimensionless)

Greek symbols

δ	Thickness of the mass transfer liquid film (m)
η	Efficiency of the motor depending upon impeller speed (dimensionless)
μ	Mean deviation
μ_L	Viscosity of liquid i.e. liquid paraffin (Pa.s)
μ_{SL}	Viscosity of slurry (Pa.s)
ν	Number of ions formed on dissociation (i.e. $\nu = 2$ for most inorganic salt)
ν_A	Gas molar volume (m^3/kmol)
$\nu_r, \nu_\theta, \nu_\phi$	Velocity vector in r, θ and ϕ directions
ρ_L	Density of liquid i.e. liquid paraffin (kg/m^3)
ρ_a	Density of air (kg/m^3)
ρ_{SL}	Density of slurry (kg/m^3)
ρ_S	Solid density (kg/m^3)
ρ_{aqueous}	Density of aqueous solution of electrolyte (kg/m^3)
σ	Standard deviation
σ_L	Surface tension of liquid (kg/s^2)
σ_1, σ_2	Effective hard sphere diameter, \AA

σ, σ_{el} or σ_{aqueous}	Surface tension of electrolyte solutions (mN/m)
σ_w	Surface tension of water (mN/m)
$\Delta\sigma$	Mean change in surface tension (mN/m)
$d\sigma/dC$	Surface tension gradient (mN/m)/(mol/L)
ψ	Surface-age distribution function (1/s)
ψ_{aqueous}	Electrical conductivity of aqueous solution of electrolyte ($\mu\text{S/m}$)
$\varepsilon, \varepsilon_G$	Gas hold-up in aqueous solution of electrolyte (dimensionless)
ε_w	Gas hold-up in distilled water(dimensionless)

Abbreviations

<i>ANN</i>	Artificial neural network
<i>ANOVA</i>	Analysis of variance
<i>A315, A310</i>	Lightning axial flow impeller
<i>CBDT</i>	Concave bladed disc turbine
<i>CBY_N, CBY_W</i>	CBY narrow blade (N) and wide blade (W)
<i>GH</i>	Gas holdup
<i>HM</i>	Homogeneous regime
<i>HT</i>	Hetrogeneous regime
<i>HEDT</i>	Six half-elliptical blade disk turbine
<i>LTN</i>	Lightnin
<i>MOC</i>	Material of construction
<i>NS</i>	Narcissus impeller
<i>NSD</i>	Normalized standard deviation
<i>PBT</i>	Pitch blade turbine

<i>PBU</i>	Pitched blade pumping up
<i>PBD</i>	Pitched blade pumping down
<i>PBTD</i>	Pitched blade turbine pumping down
<i>PDT</i>	Parabolic-blade disk turbine
<i>WD_D</i>	Four-wide blade hydrofoil impeller pumping down
<i>WD_D</i>	Four-wide blade hydrofoil impeller pumping down
<i>RSM</i>	Response surface methodology
<i>RT</i>	Rushton turbine
<i>RTD</i>	Rushton disk turbine
<i>SS</i>	Stainless steel
<i>TXU</i>	Techmix pumping up
<i>TXD</i>	Techmix pumping down
<i>WH_D</i>	Four wide blade hydrofoil impeller pumping down

1 Introduction

1.1 Bubble columns

Bubble columns (BC) and slurry bubble columns (SBC) have gained much attention in recent years as gas-liquid based multiphase contactors have been found suitable for a wide range of industrial applications. Oxidation, chlorination, alkylation, oxychlorination, absorption, hydroformylation, oxysulphonation and carbonylation are examples of two-phase bubble column applications. Similarly, three phase slurry bubble columns are used for hydrogenation, polymerization, coal liquefaction, and Fischer-Tropsch synthesis among many other applications (Youssef et al. 2014; Possos et al 2015 Esmaeili et al 2015). In addition, bubble columns are also intensively utilized in biochemical processes such as fermentation and biological wastewater treatment, i.e. aerobic degradation of organic wastes.

Fischer-Tropsch synthesis process, in particular, is considered as one of the major promising routes for providing the world with clean fuel alternatives as well as renewable energy. Large-scale industrial applications such as Fischer-Tropsch synthesis for which bubble column reactors are preferred, require high superficial gas velocities, higher solids (catalyst) loading, higher temperature, and higher pressure in order to achieve desired volumetric productivity. Bubble columns are often preferred over multiphase reactors, since they offer excellent heat and mass transfer characteristics, low maintenance cost due to simple construction and absence of moving parts (resulting in lower power consumption), and less floor space requirements for installation, cost effective technology, and high selectivity and conversion per pass and online solid loading and withdrawal. (Maceiras et al. 2010; Youssef et al. 2014; Jhavar and Prakash 2014). Various types of bubble column reactors and modifications are available (Shah et al. 1982).

Mathematical and theoretical models have been reported in literature which provides varied details of mass transfer based on established classical concepts of film and penetration theories (Kawase et al. 1987; Cockx et al. 1995; Shimizu et al. 2000; Kittilsen et al. 2001; Garcia-Ochoa and Gomez 2004; Haut et al. 2005 Dhaouadi et al. 2008). As such the film model is not valid for the explanation of unsteady-state mass transfer mechanism and stirred systems (Wang and Langemann 1994a). Similarly, neither the penetration nor the film-

penetration model is capable of describing the mass transfer mechanism with two liquid films at the interface, particularly in the liquid-liquid systems (Wang and Langemann 1994a). Clearly, all the above mentioned models have certain limitations and cannot be used to predict gas-liquid mass transfer rates accurately in complex situations, i.e. heterogeneous regimes, under varying superficial gas velocity and higher pressures. Mass transfer models such as Danckwerts' surface renewal model and the two-film theory offer higher precision in prediction of mass transfer between two phases.

Use of organic and inorganic compounds in industrial bubble columns, particularly in bioreactors, is quite common. For instance, microorganism growth and survival in aerobic biological systems require interfacial oxygen transfer. Hence, oxygen transfer through an air-liquid interface is one of the major issues in bioreactor design due to the low solubility of oxygen in aqueous solutions of electrolytes (Jackson 1991). Only a few studies on the influence of electrolyte concentration on gas holdup in bubble columns with a diameter less than 0.12 m have been reported earlier (Syeda and Reza 2011; Nguyen et al. 2012). Effective interfacial oxygen transfer is a complex phenomenon and it is desirable that the size of bubbles remains small. Bubble size is a key parameter for hydrodynamic studies in bioreactors and it depends on parameters such as physicochemical properties of the liquid, gas flow rate, contactor geometry and type of sparger used. The presence of electrolytes in water keeps the bubbles apart and makes them stable for a longer time. The knowledge of effects of electrolytes on hydrodynamic properties in a bubble column is, therefore, important for bubble coalescence inhibition. An important effect of electrolytes is the inhibition of bubble coalescence during the approach or collision of a bubble with other bubbles. Bubble coalescence in pure water occurs when the value of surface elasticity is zero. At this point, the approaching bubbles begin to drain and form an unstable film which ruptures at a film thickness close to 110 nm (Pashley and Craig 1997). An electrolyte increases the stabilization time of liquid film by increasing the surface elasticity of the gas-liquid interface. The surface elasticity (which is quantitatively equal to half of the Gibbs elasticity) is the basis of coalescence inhibition (Christenson and Yaminsky 1995).

Mechanically agitated gas-liquid reactors with single or multiple impellers on a common shaft are often used to increase the contact between relatively small amounts of gas in a large amount of liquid in several industrial applications namely; aerobic fermentation, chlorination, hydrogenation crystallization, polymerization, and waste water treatment etc. Multiple-impeller reactors have numerous advantages over single-impeller reactors, viz. even

distribution of shear stress and power dissipation, improved liquid circulation, better gas distribution and longer gas residence time in a vessel. Thus, Multiple-impeller are more effective in gas utilization. Also multiple impellers are preferred over a single-impeller where shear sensitivity to micro-organisms is important criteria for the design (Gogate et al. 2000; Shewale and Pandit 2006; Fujasova et al. 2007; Moucha et al. 2009; Labik et al. 2014).

In the last two decades, a number of new, modified impellers have been developed to enhance and optimize gas-liquid contact in agitated gas liquid system. Modification of the flat geometry of Rushton blade affects pressure and velocity fields in the blade vicinity (Vasconcelos et al. 2000). Van't Riet (1975) studied a variety of impeller styles, and introduced the concept of using concave blades. The concave geometry of the blades did not allow large cavities to form easily at low gas flow rate; while at higher gas flow rates, the cavities behind the concave blades have smaller dimensions compared to those behind standard flat blades i.e., Rushton impeller. Moreover, the curved or hollow blade impellers, such as SCABA and concave blade turbines, also provide better gassed power characteristics and shaft stability performance than the standard Rushton impeller with much less reduction in power drawn (Khare and Niranjana 1999; Cooke et al. 2005; Chen and Chen 1999; Saito et al. 1992).

The relative power demand in mechanically agitated vessels is an important parameter in the characterization and design of agitated industrial gas-liquid contactors. Power consumption does not only depend on the impeller type, properties of fluid, agitator speed, gas flow rate combination of impellers but also on geometry of agitated system with configuration such as baffled, unbaffled or partially baffled and inter-impeller clearance.

The spacing between impellers is considered to be crucial factor in designing of stirred type gas-liquid contactors for maximizing oxygen mass transfer, and minimizing mixing time, or power consumption. A significant amount of experimental data can be found in the literature on power consumption in single-impeller systems (Smith et al. 2001; Michelan et al.2009). However, incomplete information is available for power consumption in mixing tanks provided with multiple impellers, although their industrial importance is significant. In particular, very little information is available on inter-impeller clearance in multiple impeller systems (Markopoulos et al. 2004; Markopoulos et al. 2005). The power consumed by multiple impellers and the characteristics of the flow they generate are often estimated on the basis of the power consumed by single impellers. Generally, power consumption in case of aerated conditions, is relatively smaller as compared to the nonaerated conditions. This

reduction varies depending on the type of impeller, impellers combination and inter-impeller clearance (Markopoulos et al. 2004; Markopoulos et al. 2005). In a multiple impeller system, flow pattern caused by one impeller can be significantly affected by another impeller in the system because of the flow interactions between the impellers. Mechanically agitated gas–liquid reactors with single–, double–and triple–impeller on a common shaft are often used to increase the contact between relatively small amounts of gas in a large amount of liquid. Some of the researchers reported various hydraulic and mass transfer characteristics for different types and impeller combinations in multiple-impeller vessels (Bouaifi et al., 2001; Garcia-Cortes et al., 2004; Puthli et al. 2005; Shewale and Pandit, 2006; Fujasova et al 2007).

1.2 Industrial applications of bubble columns

A comprehensive list of processes in which bubble columns are used in chemical, petro-chemical and allied industries is given in Table 1.1.

Table 1.1 Some examples of industrial scale processes in bubble column and modifications (Shah et al. 1982; Majumder 2016).

Processes	Main product
Oxidation of Ethylene in Acetic acid solutions	Vinyl acetate
Oxidation of Acetaldehyde	Acetic acid
Oxidation of sec. Butanol	Acetic acid
Oxidation of Acetaldehyde	Acetic anhydride
Oxidation of Cumene	Phenol and Acetone
Oxidation of Toluene	Benzoic acid
Oxidation of Xylene	Phthalic acid
Oxidation of Ethylbenzene	Acetophenone
Oxidation of Butanes	Acetic acid and Methyl Ethyl Ketone (MEK)
Partial Oxidation of Ethylene	Acetaldehyde
Oxidation of cuprous chloride	Copper oxychloride
Oxidation of hydroquinone	Hydrogen peroxide
Wet oxidation of waste water	Water
Absorption of CO ₂ in Ammoniated Brine	Soda Ash
Alkylation of Methanol	Acetic acid

Alkylation of Benzene	Ethylbenzene, Cumene
Carbonylation of Methanol	Acetic acid
Chlorination of Aliphatic Hydrocarbons	Chloroparaffin
Chlorination of Aromatic Hydrocarbons	Chlorinated aromatics
Oxychlorination of Ethylene	Dichloroethane
Oxysulphonation of paraffin	Paraffin sulphonate
Hydroformylation of Olefins	Aldehydes and Alcohols

1.3 Motivations for the present work

Due to the lack of information about hydrodynamic because of complicated behaviour of bubble in its various regimes (homogeneous, heterogeneous, and slug flow regimes) causes a number of operational difficulties and design uncertainties. Bubble behaviour as the key hydrodynamic factor in bubble column can drastically change due to the effect of various parameters involved in operation. According to Deckwer (1985), the hydrodynamic flow regimes in bubble columns are better explained and categorized into three definite groups namely, homogeneous (bubbly i.e. equal bubble sizes), heterogeneous (churn turbulent i.e. wide bubble sized distribution) and slug flow regimes (bubbles and slugs upto the column diameter in size) depending on superficial gas velocity, bubble column diameters and physical properties of phases. In all process, bubble size and gas holdup are important design parameter, they directly affected interfacial area available for mass transfer. It is well known that both parameters are affected by the coalescence and breakage phenomena occurring inside the column. Categorization of bubbles based on the differences in their sizes viz. macro bubbles, micro bubble, and sub-microbubbles or nano-bubbles, and ultrafine bubbles with their major properties are reported in literature (Temesgen et al. 2017).

The efficiency of most gas-liquid processes in bubble column can be affected by various parameters that play an important role in enhancing either the heat and mass transfer or interfacial areas between the contacting phases; such as operating conditions (superficial gas velocity and liquid flow rates, temperature, pressure), column geometry (diameter, height and shape), gas distributor design (single nozzle, perforated plate, porous plate, number of holes and size of hole), type and design of impeller, physical properties of liquid (surface

tension, density, viscosity), properties of gas, dispersion height of the liquid, solid loading (diameter, concentration, density), internals and surfactants as well as impurities and water contaminants. Detail effect of selected parameters for study in bubble column and stirred bubble column under heterogeneous systems will be discussed in later chapters.

1.4 Problem identification

From literature review, gaps identified in the studies reported earlier are as follows:

1. A set of research articles with different gas-liquid or gas liquid–solid systems are available in literature. However, an effective macroscopic mathematical model of k_L need to be explored which can be applied effectively in a particular application using the energy and properties of the liquid. A theoretical approach was needed for accurate estimation of overall mass transfer coefficient in a two or three phase bubble column system, if bubble size distribution is known.
2. The presence of inorganic compounds/ electrolytes in water in industrial bubble columns, particularly in bioreactors, is quite common. Knowledge of the effects of these compounds on the hydrodynamics in a bubble column is, therefore, important for knowing the extent of mass transfer taking place in such systems. Unfortunately, inadequate data are available on transition concentration of aqueous mixtures of single and binary electrolytes for bubble coalescence inhibition. The advantage of such a research is that it may provide an opportunity to utilize experimental data for judicious estimation of electrolyte requirements. Furthermore, values of surface elasticity are not available at transition concentration of electrolytes which is important for bubble coalescence inhibition.
3. Length of radial nozzles used for gas injection in a bubble column affects the value of gas–liquid mass transfer coefficient. To our knowledge, quantitative comparison studies on the effect of length of jet nozzles and ring sparger on volumetric mass transfer coefficient in partially baffled stirred vessel equipped with Rushton impeller have not been reported in literature so far. These studies may be useful in bioreactor applications where limited oxygen transfer is required.

Some of the areas which needed attention are as follows:

1. Mathematical modeling for prediction of mass transfer coefficient k_L based on unsteady state liquid film fluctuations by micro-eddies in slurry bubble column

system is scarcely reported in literature. Thus, mathematical modeling for prediction of mass transfer coefficient k_L and a method for estimation of liquid film thickness δ employing model equations of mass transfer coefficient was needed.

2. Studies on transition concentration of aqueous mixtures of single and binary electrolytes for bubble coalescence inhibition were also incomplete and asked for further exploration. Unfortunately, inadequate data were available on surface elasticity at transition concentration for single and mixed electrolyte solutions.
3. Comparative studies on the performance of various lengths of jet nozzles and ring sparger on volumetric mass transfer coefficient in partially baffled stirred vessel equipped with Rushton impeller were scarcely reported in literature. Thus, optimization study needed to be carried out for enhancing the value of mass transfer coefficient. Also, an empirical correlation for estimation of volumetric mass transfer coefficient applicable to various jet nozzle lengths based on dimensionless groups was not reported in literature
4. Studies on relative power demand (P_g / P_{ug}) in a partially baffled gas-liquid contactor equipped with single or multiple impeller combinations have been scarcely reported in literature.
5. A limited number of publications are available on parametric studies on volumetric mass transfer coefficient in stirred bubble column systems using concave blade impeller. Besides, optimization of curvature of concave blade impellers has not been reported so far. This aspect needed a study for improving gas-liquid mass transfer rate

1.5 Scope of present research work

As mentioned above, there is a need to understand the complex hydrodynamics of a bubble column and stirred bubble column, especially at higher agitator speeds and higher gas flow rates. In the present work, two systems, viz. a bubble column and a stirred bubble column were employed for hydrodynamic and mass transfer studies. The, aim of the present study is to conduct experimental studies on the effect of gas flow rate, impeller speeds, electrolyte concentration, types of impellers, and types of spargers on hydrodynamic and mass transfer parameters. For design, modeling, optimization and scale-up of gas – liquid/ slurry bubble columns, precise knowledge of gas-liquid mass transfer phenomena dictated by interfacial fluctuations are of cardinal importance. In this study, a macroscopic model for prediction of liquid –side mass transfer coefficient k_L based on unsteady state liquid film fluctuations by

micro-eddies (liquid elements) in gas – liquid/ slurry bubble columns has been presented. The experimental data generated in present study on transition concentration of electrolytes, relative power demand and volumetric mass transfer coefficient are important ingredients for design and scale up of bubble columns.

1.6 Research objectives and Scope

In the present study, experimental studies were carried out in a bubble column with 0.105 m inner diameter for investigating the coalescence behavior in presence of electrolytes and flat bottom cylindrical vessel with an internal diameter of 0.30 m and height 0.44 m used for relative power demand and volumetric mass transfer studies.

The objectives of the present research work are as follows:

1. To develop a macroscopic model for prediction of mass transfer coefficient k_L based on unsteady state liquid film fluctuations by micro-eddies in a slurry bubble column system and to develop a empirical correlations for estimation of liquid film thickness δ for H_2 , CO and CO_2 in a slurry system in terms of dimensionless groups. Also, to study the effect of process parameters such as temperature, pressure, gas flow rate, and slurry concentration on mass transfer coefficient for diffusion of H_2 , CO and CO_2 in a slurry system.
2. To study transition concentrations of aqueous mixtures of single (NaCl, $MgSO_4 \cdot 7H_2O$, $CaCl_2 \cdot 2H_2O$ and Na_2SO_4) and binary electrolytes ($CaCl_2 \cdot 2H_2O + NaCl$ and $Na_2SO_4 + NaCl$) for bubble coalescence inhibition. Also, to estimate surface elasticity at transition concentration for single and mixed electrolyte solutions.
3. To experimentally measure relative power demand (P_g / P_{ug}) in a partially baffled gas-liquid contactor equipped with single and multiple impeller combinations and to develop empirical correlations for estimation of relative power demand in terms of dimensionless groups.
4. To study the effect of length of jet nozzles on volumetric mass transfer coefficient and compare it with ring sparger in partially baffled stirred vessel equipped with Rushton impeller and to develop an empirical correlation for estimation of volumetric mass transfer coefficient in terms of dimensionless groups.
5. To study the effect of curvature of curved-blade impeller on volumetric mass transfer coefficient and identify the most effective operating parameter among gas flow rate,

impeller speed and curvature of blade using surface research methodology in a partially baffled stirred gas–liquid contactor.

1.7 Thesis outline

A brief overview of the work presented in the thesis on modeling of mass transfer in a single spherical bubble is shown in Figures 1.1. The overall work done on bubble coalescence using electrolytes is presented in Figure 1.2. Similarly, estimation of relative power demand by stirred bubble column is presented in Figure 1.3.

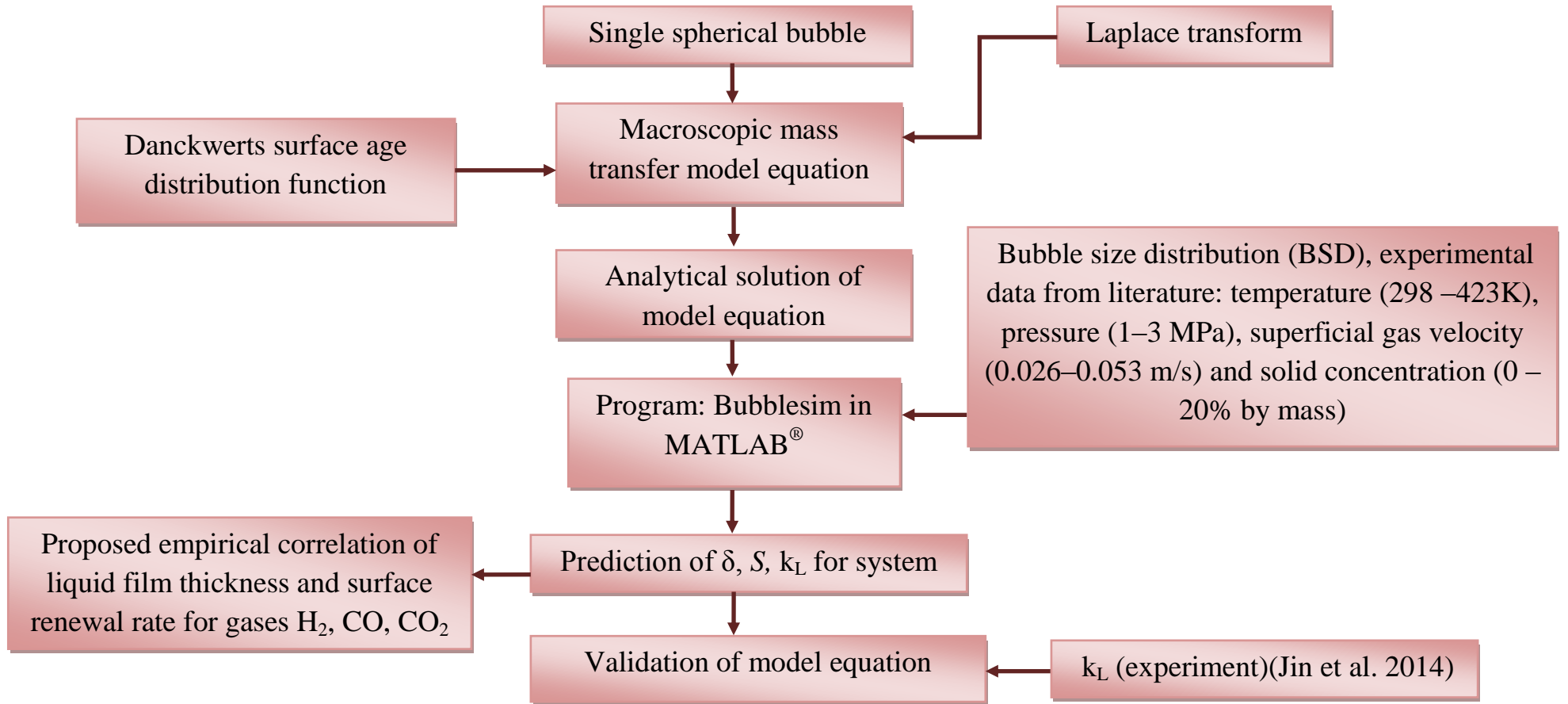


Figure 1.1 Flow diagram of modeling of a single spherical bubble.

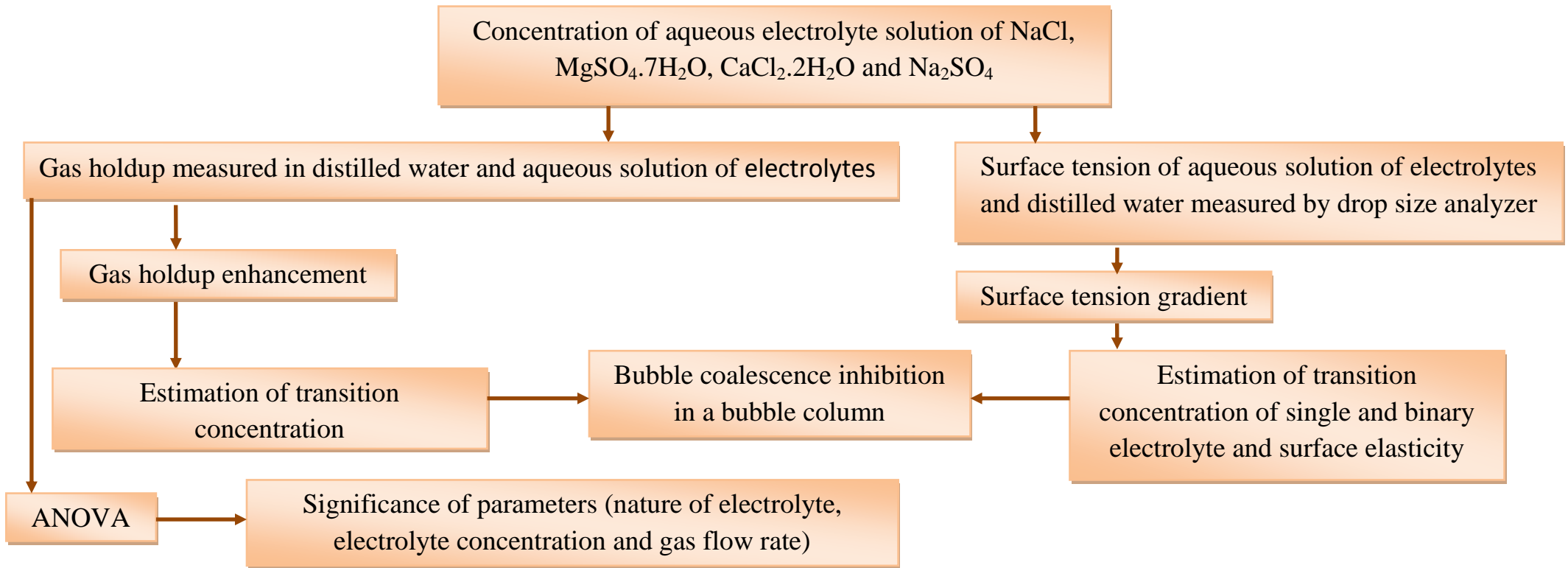


Figure 1.2 Schematic diagram of work done on bubble coalescence inhibition studies in a bubble column.

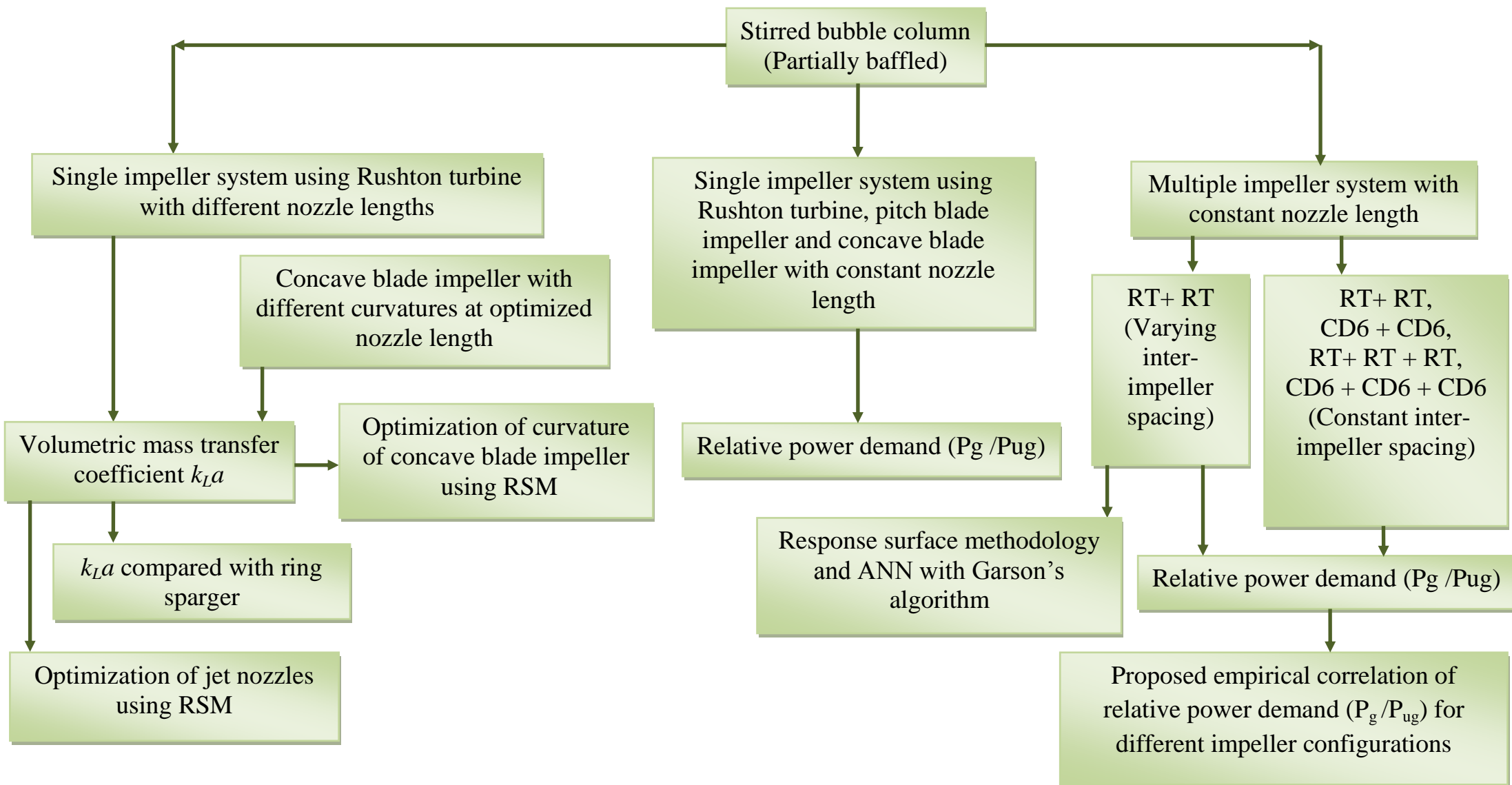


Figure 1.3 Flow diagram of relative power demand studies in a stirred bubble column.

1.8 Organization of thesis

The research work carried out has been organized into six chapters as shown below:

Chapter 1 delineates the purpose of this thesis and gives an overview of hydrodynamic studies in the process industry and discusses the details associated with bubble column study and research objectives derived from the inadequacy found in the literature and briefly describe the scope of upcoming chapters.

Chapter 2 presents a brief general review of literature on gas holdup, volumetric mass transfer coefficient and relative power consumption in a bubble column and a stirred gas-liquid contactor for Newtonian and non-Newtonian systems.

Chapter 3 describes various chemicals, impellers, and spargers used for hydrodynamic and mass transfer studies. Equipment used and analytical instruments used are also summarized. Furthermore, experimental procedures adopted for power consumption and mass transfer coefficient are given in this chapter.

Chapter 4 outlines the unsteady state macroscopic model for prediction of mass transfer coefficient k_L in a slurry bubble column system. Empirical correlation for estimation of liquid film thickness in a slurry bubble column has also been developed in this chapter.

Chapter 5 presents results and discussion of studies carried out in the present work. The chapter has been divided into four sections. *Section 1* presents macroscopic model development for prediction of liquid-side mass transfer coefficient k_L in a slurry bubble column system. *Section 2* presents estimation of transition concentration of aqueous mixtures of single and binary electrolytes for bubble coalescence inhibition in a bubble column. *Section 3* provides the effect of length of jet nozzles on volumetric mass transfer coefficient and its comparison with ring sparger in a stirred vessel equipped with Rushton impeller has also been covered. *Section 4* covers the estimation of relative power consumption in a partially baffled gas-liquid contactor equipped with single or multiple impeller combinations. In addition, effect of impeller spacing on relative power consumption in a stirred vessel with double stage Rushton impeller is also covered.

Chapter 6 provides summary of the work done, important outcomes of the thesis, and finally, potential areas for further research concerning this topic which are identified and recommended for a future study.

2 Literature review

2.1 Introduction

Bubble columns (BCs) are simple but very effective and adaptable gas – liquid contacting devices which can be used for hydrodynamic and mass transfer studies with or without chemical reaction. Bubble columns are excellent devices in terms of performance, ease of construction and low maintenance. Bubble columns (BCs) may be operated either in the homogeneous or heterogeneous flow regime. Because of their immense benefits, bubble columns are widely used in many industries including pulp and paper processing, biochemical processes such as fermentation and biological wastewater treatment, mineral processing and pharmaceutical manufacturing. The three most important key parameters which govern the performance of bubble columns are overall gas hold-up (ϵ_G), volumetric gas-liquid mass transfer coefficient (k_La), and effective interfacial area (a). The complete understanding of hydrodynamics in bubble columns has not yet been accomplished in spite of concerted research efforts. Among various parameters that are not considered is the volume occupied by tiny gas bubbles that are not accounted for while estimating effective interfacial area in the bubble column. Viscous Newtonian and non-Newtonian systems are frequently encountered in biotechnological, pharmaceutical and food processing industries. In non-Newtonian systems, gas holdup in bubbling regime strongly depends upon coalescence tendency of bubbles. The coalescing tendency of bubbles in viscous non-Newtonian systems leads to decrease in gas holdup, resulting in a decrease in effective interfacial area and thereby volumetric gas-liquid mass transfer coefficient.

Some excellent reviews are available in the literature which are focuses on the following topics: gas holdup studies (Shah et al. 1982; Joshi et al. 1982; Kantarci et al. 2005; Leonard et al. 2015), bubble characteristics (Shah et al. 1982; Kantarci et al. 2005; Kulkarni and Joshi, 2005), flow regime investigations (Shah et al. 1982; Kantarci et al. 2005; Shaikh and Al-Dahhan, 2007; Shaikh and Al-Dahhan 2013), Design and scale-up (Kantarci et al. 2005), Heat transfer

coefficient studies (Joshi et al. 1982; Shah et al. 1982; Kantarci et al. 2005), mass transfer studies (Shah et al. 1982; Joshi et al. 1982; Beenackers and Swaaij, 1993; Kantarci et al. 2005; Markopoulos et al. 2007; Ochoa and Gomez, 2009; Leonard et al. 2015), power consumption in stirred vessels (Joshi et al. 1982; Ascanio et al. 2004), surface aerators (Joshi et al. 1982), gas inducing type of agitated contactor (Joshi et al. 1982), mixing ((Joshi et al. 1982), and flow patterns of impellers ((Joshi et al. 1982).

A critical analysis of available correlations with divergent nature for gas holdup, volumetric gas liquid mass transfer coefficient, liquid side mass transfer coefficient for different gas–liquid or gas–liquid–solids systems and various types of bubble columns and their modifications are described by shah et al.(1982). Joshi et al. (1998) presented an extensive review, covering different aspects dealing with design parameters and operating parameters which influence on gas holdup structure in bubble column reactors. Furthermore, other information like holdup profiles, bubble size measurements, holdup measurement and dynamic gas disengagement has been reviewed critically. Boyer et al. (2002) presented a critical review on the various non-intrusive and intrusive measuring techniques used for investigating multiphase flow analysis either in gas/ liquid or in gas/liquid/solid reactor. Furthermore, few examples in the petrochemical and refinery are reported where these measuring techniques can be employed. Kulkarni and Joshi, (2005) critically reviewed on bubble formation at a single orifice and on multipoint sieve trays in Newtonian as well as non-Newtonian stagnant/or flowing liquids and bubble rise velocity in pure Newtonian, contaminated Newtonian liquids and non-Newtonian liquid. Furthermore, it has been discussed on various formulas of bubble size, rise velocity for Newtonian as well as non-newtonian. Kantarci et al. (2005) presented a critical review focused on description of design and scale up, application areas, fluid dynamics and flow regimes characteristics and design parameters characterizing their operation. Considerable work on flow regime transition in bubble columns has been reviewed by Shaikh and Al-Dahhan (2007). An excellent review on bubble column operating at high pressure and temperature has been given by Leonard et al. (2015). Its covered different mechanisms govern by bubble column; various influence parameters on gas holdup, interfacial area, mass transfer coefficient and volumetric gas-liquid transfer coefficient and on liquid axial dispersion coefficient. There are a large number of empirical correlations of gas holdup reported in literature which are covered wide range of physico-chemical properties of gas / liquid, column geometry, type and design of gas distributor

and the operating conditions (Shah et al. 1982; Joshi et al. 1982; Kantarci et al. 2005; Leonard et al. 2015). Gas holdup plays a significant role in design and scale-up of bubble column. It can be defined as the percentage by volume of the gas in the gas-liquid (two phase) and gas-liquid-solid (three phase) mixture in the column. Gas holdup is directly related to specific interfacial area of the bubbles which lead to higher mass transfer coefficient in results higher mass transfer in a gas-liquid system. The behaviour of the gas holdup depends on many different factors, including the physical properties of gas / liquid, column geometry, gas distributor design and the operating variables, i.e., pressure, gas velocity, temperature. Currently, there are several techniques available to measure the gas holdup, such as pressure drop measurements, electro-conductivity, X-ray transmission, γ radiation, mean residence time distribution, optical fiber probes, particle image velocimetry and computer tomography.

2.2 Phenomena of Coalescence

Knowledge of the flow regime and gas holdup is important in estimating the hydrodynamic of a gas-liquid mixture in a bubble column. In all gas-liquid system, the bubbles can increase and decrease in size due to coalescence and breakup. The phenomena of coalescence occurs when two gas bubbles first collide and trap a certain amount of liquid between them, which once drained may reduce the film thickness of the bubble to a critical value causing it to rupture and the gas bubbles to coalesce. Breakup of bubbles is caused by collisions with turbulent eddies, approximately equal in size to the bubbles (Prince and Blanch, 1990).

It has been reported earlier by several investigators (Eissa and Schügerl 1975; Bach and Pilhofer 1978; Godbole et al 1982; Khare and Joshi 1990; Ruzicka et al 2003; Olivieri et al. 2011) that viscosity of liquid has a dual effect on gas holdup. At lower viscosity, drag force exerted by the liquid is small, and therefore, the bubbles rise in the column with higher velocity leading to more coalescence among the bubbles and thus lower gas holdup. Conversely, with increase in viscosity, the coalescence of bubbles gets limited reaching its maxima as a result of increased drag and reduced bubble rise velocity. With further increase in viscosity, the tendency to coalesce prevails allowing the bubbles to rise at higher velocity (Besagni et al. 2017). Thus resulting in lowering of gas holdup upto a certain extent and then a constant gas holdup further. The value of viscosity varies with the nature and type of solid/liquid used (Eissa and Schügerl

1975; Bach and Pilhofer 1978; Godbole et al 1982; Khare and Joshi 1990; Ruzicka et al 2003; Olivieri et al. 2011).

2.3 Flow Regimes and Characteristics

It is commonly accepted that, depending on the gas flow rate, two main flow regimes can be observed in bubble columns, i.e. (i) *homogeneous* bubbly flow regime encountered at low gas velocities and characterized by a narrow bubble size distribution and uniform gas holdup. Expectant of bubble coalescence and breakup in the bubble bed is negligible and (ii) *heterogeneous* (churn turbulent flow) regime observed at higher gas velocities characterized by the appearance of large bubbles, formed by coalescence of the small bubbles and bearing a higher rise velocity, hence, leading to relatively lower gas holdup values (Besagni and Inzoli 2018; Besagni and Inzoli 2017; Zhradnik et al., 1997). The homogeneous flow regime can be further classified into (a) “mono-dispersed homogeneous” flow regime and (b) “pseudo-homogeneous” flow regime, depending on the existing bubble size distribution in the system. It is well-known that the bubble size distribution in the bubble column systems is mainly controlled by the gas sparger openings. Stability of homogeneous regime and the gas holdup values are strongly influenced by the type and geometry of the gas sparger i.e. fine pore sparger or coarse gas sparger (Besagni and Inzoli 2018; Zhradnik et al. 1997) and the properties of the liquid phase (Shah et al., 1982; Krishna et al., 1991; Krishna et al., 1999; Ruzicka et al., 2003; Kantarci et al., 2005; Shaikh and Al-Dahhan, 2007; Ruzicka et al., 2008). Either of the regimes can be obtained in a system by varying the gas flow rate.

2.4 Hydrodynamics in Newtonian liquids

To date, many investigators have carried out hydrodynamic studies in bubble columns and based on their experimental findings, the empirical correlations for overall gas hold-up have been proposed. Depending on the properties of the liquid phase and type of gas distributor, both homogeneous and heterogeneous flow regimes appeared in the same column by varying the inlet gas flow rate. The effects of liquid properties and sparger characteristics were investigated on gas holdup in bubble columns equipped with a porous sparger and correlations were formulated based on dimensionless groups for the prediction of gas holdup applicable for homogeneous (Mouza et al., 2005; Kazakis et al., 2007) and heterogeneous regimes (Kazakis et al., 2007),

respectively. It has been concluded that gas holdup depends on pore diameter of the porous sparger, and the physical properties of the liquid phase. Hughmark (1967) reported a correlation for the gas hold-up which takes into account the effect of the liquid properties only. The effect of column geometry like, diameter and operating properties like, superficial gas velocity has been ignored in the reported correlation. Akita and Yoshida, 1973 investigated the effect of various gas-liquid systems (air-water, oxygen-water, air-glycol, air-methanol, air-CCl₄, CO₂-water, helium-water, air-NaCl aqueous solution and air-Na₂SO₃ aqueous solution) on gas holdup in bubble column and developed a new correlation for gas holdup to correlate their experimental data. But the authors did not consider the effect of nature of the gas on gas holdup. Correlation earlier proposed for fractional gas holdup by Hikita et al.1980 which is valid only for pure liquid or the non-electrolyte solutions. The other effective parameters like nozzle diameter, column diameter and the clear liquid height were not considered in the reported correlation. Hikita and Kikukawa (1994) investigated the effect of physical properties of the liquids on the gas holdup in a bubble column equipped with a single nozzle sparger. It has been concluded that surface tension of the liquid has a significant effect on gas holdup. Further, they developed a new correlation to correlate quantitatively their experimental data. But the authors did not consider the other effective parameters like single nozzle diameter, column diameter, superficial gas velocity and the clear liquid height. Gestrich and Rahse (1975) proposed a gas holdup correlation and concluded that gas holdup is unaffected by mean bubble diameters ranging from 0.2 to 0.4 cm.

2.5 Bubble coalescence inhibition in electrolyte solution

Bubble coalescence inhibition is important for different liquids and solutions for improving the mass transfer performance in bubble columns, bioreactors like fermenters and aerobic wastewater treatment system. Use of organic and inorganic compounds in industrial bubble columns, particularly in bioreactors, is quite common. For instance, microorganism growth and survival in aerobic biological systems require interfacial oxygen transfer. Hence, oxygen transfer through an air-liquid interface is one of the major issues in bioreactor design due to the low solubility of oxygen in aqueous solutions of electrolytes (Jackson 1991). Effective interfacial oxygen transfer is a complex phenomenon and it is desirable that the size of bubbles remains small. Bubble size is a key parameter for hydrodynamic studies in bioreactors and it depends on

parameters such as physicochemical properties of the liquid, gas flow rate and contactor geometry. The presence of electrolytes in water keeps the bubbles apart and makes them stable for a longer time. The knowledge of effects of electrolytes on hydrodynamic properties in bubble columns is, therefore, important for bubble coalescence inhibition. An important effect of electrolytes is the inhibition of bubble coalescence during the approach or collision of a bubble with other bubbles. Bubble coalescence in pure water occurs when the value of surface elasticity is zero. At this point, the approaching bubbles begin to drain and form an unstable film which ruptures at a film thickness close to 110 nm (Pashley and Craig 1997). Thin film geometry when two air bubbles approach in a liquid are reported in literature (Horn et al. 2011). An electrolyte increases the stabilization time of liquid film by increasing the surface elasticity of the gas-liquid interface.

A number of studies have reported bubble coalescence behavior in electrolyte solutions (Marrucci and Nicodemo 1967; Lessard and Zieminski, 1971; Prince and Blanch, 1990; Craig et al., 1993; Zahradnik et al., 1995; Weissenborn and Pugh 1995; Nguyen et al. 2012). It has been observed that coalescence commonly occurs in pure water and with increasing concentration of electrolytes, there is a transition to coalescence inhibition regime. This transition occurs over a narrow concentration range (< 0.1 mol/L) which is characteristic of a particular electrolyte such as NaCl, Na₂SO₄, CaCl₂ and MgSO₄ etc (Castillo et al 2011; Craig 1993). Some of the researchers investigated the effect of electrolytes on gas holdup and coalescence behavior of bubbles in a laboratory scale bubble column (Ribeiro et al. 2007; Orvalho et al. 2009; Syeda and Reza 2011; Nguyen et al. 2012; Besagni and Inzoli 2017b). As the suppression of bubble coalescence leads to gas holdup enhancement, the concentration at which minimum bubble coalescence is achieved is likely to result in a maximum gas holdup in a bubble column. Therefore, gas hold-up enhancement in bubbling region is strongly related to the coalescence inhibition tendency of bubbles in different gas-liquid systems. Various researchers reported that electrolytes reduces the solubility of the gas molecules in aqueous solutions electrolytes and proposed as an alternative mechanism by which electrolytes inhibit bubble coalescence (Weissenborn and Pugh 1996; Geffcken 1994; Millero et al. 2002). Investigations using surface tension of electrolytes have been scarcely reported in the literature. For a very low concentration of electrolyte solutions (weak solutions), which have interfacial tensions practically same as pure water, the bubbles were reported to be much smaller and the gas hold-up much higher than that

of pure water (Lee and Meyrick 1970; Machon et al. 1977). Recently, Syeda and Reza (2011) found a strong relationship between gas holdup and surface tension gradient with the addition of electrolytes. The effect of air –aqueous solution of electrolyte system on gas holdup, ε_G is shown in Table 2.1.

The first systematic significant elementary studies of bubble coalescence were reported by Marrucci (1969). Authors developed a coalescence model to account the change in surface concentration of solute, (ΔC), caused by increase in the surface area during film stretching, leading to a change in interfacial tension, ($\Delta\sigma$) for two adjoining bubbles in aqueous electrolytes solutions and found that the drainage rate is strongly dependent on the mobility of the surface. If the bubble interface is immobile, the liquid drains from the surface between the two flattened bubbles in a slow process, whereas if the surface is mobile, drainage is much faster. In such a case, coalescence rate of bubbles is faster. In addition, the corresponding concentration of electrolytes is responsible for shifting the mobile interface into an immobile one. Thus, the bubble size would depend on the concentration of solute which controlled the type of interface and the interfacial tension gradient (Marrucci 1969; Lessard and Zieminski 1971).

In a stagnant pure water system, the rate of coalescence is at its maximum and it decreases as the concentration of electrolytes is increased. At transition coalescence concentration, the coalescence rate is drastically reduced by 50%. The transition coalescence concentration of electrolytes has been suggested as a critical key factor for characterizing the hydrodynamics behavior (Ribeiro and Mewes, 2007; Syeda and Reza, 2011) and mass transfer (Al Taweel et al., 2013) in a bubble column. The ionic strength of aqueous solution of electrolytes at the interface was a critical parameter in influencing coalescence rate and bubble diameter. The critical concentration depends on the valency of both the ions forming the electrolyte. Coalescence rate decreases from high valency ion combinations (e.g. 3–1, 2–2 type) to lower valency of combinations (type 2–1, 1–2) and type 1–1 combinations (Marrucci and Nicodemo 1967; Lessard and Zieminski 1971). In similar lines, Deschenes et al. (1998) investigated the effect of dilute 1: 1 and 2: 1 electrolyte solutions on bubble coalescence inhibition. It has been observed that anion dominating the inhibition at concentration below 0.01 M and cations dominating the inhibition at higher concentrations. Only a few studies concerning the influence of electrolyte concentration on gas holdup in bubble columns with a diameter less than 0.12 m have been reported earlier (Syeda and Reza 2011; Nguyen et al. 2012). All electrolytes reduce electrostatic

forces. Some of them reduce bubble coalescence by reducing the hydrophobic attraction above their transition concentration (Craig 1993a). Electrolytes also reduce the range of attraction force above their transition concentration. In essence, electrolytes induce bubble interactions by reducing the range of attraction force from approximately 100 nm to 50 nm (Craig 1993b). Therefore, gas holdup enhancement in bubbling region is strongly related to the coalescence inhibition tendency of bubbles in different gas-liquid systems. Various researchers reported that the use of electrolytes reduces the solubility of the gas molecules in aqueous solutions and proposed an alternative mechanism by which electrolytes inhibit bubble coalescence (Weissenborn and Pugh 1996; Geffcken 1994; Millero et al. 2002). Investigations using surface tension of electrolytes have been scarcely reported in the literature. For a very low concentration of electrolyte solutions which have interfacial tensions practically same as that of pure water, the bubbles were reported to be much smaller and the gas holdup much higher than that of pure water (Lee and Meyrick 1970; Machon et al. 1977). Recently, Syeda and Reza (2011) found a strong relationship between gas holdup and surface tension gradient with the addition of electrolytes. Slope of surface tension gradient ($d(\Delta\sigma)/dC$) was reported higher at lower concentration of strong electrolytes (Na_2SO_4 and $\text{CaCl}_2 \cdot 2\text{H}_2\text{O}$) which changes sharply as the concentration increases further. For moderate electrolytes (NaCl and $\text{MgSO}_4 \cdot 7\text{H}_2\text{O}$), the increase in surface tension was gradual. Increase in surface tension due to presence of inorganic electrolytes causes a reduction in the bubble size (Chen and Tsang 2005). Average bubble size in a bubble column remains smaller in case of some specific electrolyte solutions than in pure water (Prince and Blanch 1990; Kluytmans et al. 2001) as these electrolytes can inhibit bubble coalescence and it is called "ion-specific effect" (Craig and Pashley's 1993).

Systematic studies of ion – specific coalescence of bubbles in selected mixed electrolytes solutions were reported by Henry (2007). Mixed electrolytes follow the properties of the individual ions originally assigned earlier produced by Craig (1993). The combining rules indicated that the fundamental property of the ions controls the bubble coalescence inhibitory behavior of electrolytes. For a single electrolyte system, if the value of parameter $(d\sigma/dC)^2$ is large, then the electrolyte will inhibit bubble coalescence, and bubble coalescence behavior will remain unaffected if the value of $(d\sigma/dC)^2 < 1 \text{ (mN} \cdot \text{m}^{-1}/\text{mol} \cdot \text{L}^{-1})^2$. However, in the case of mixed electrolytes, no correlation between coalescence inhibitions and $(d\sigma/dC)^2$ is available.

The interpretation of bubble coalescence and gas holdup behavior in aqueous solutions of single and mixed electrolytes in terms of surface tension gradient is also incomplete and asks for further exploration.

2.6 Experimental techniques for estimation of bubble coalescence inhibition

Ion specificity is often found to control behaviour at interface, such as biological membrane and proteins. Various salts also change solution properties such as surface tension, viscosity, density, activity coefficient. The interpretation of bubble coalescence and gas holdup behavior in aqueous solutions of single and mixed electrolytes in terms of surface tension gradient is also incomplete and asks for further exploration. To our best knowledge, the effect of presence of mixed electrolytes on gas holdup and surface elasticity values of different electrolytes at transition concentration have not been reported in literature. Surface elasticity is increased by the use of electrolytes. Surface elasticity is proportional to the surface tension gradient and for a single electrolyte, this gives a good correlation with bubble coalescence inhibition. However, the presence of a mixture of two electrolytes has shown no correlation between surface elasticity and bubble coalescence inhibition (Henry et al. 2007). Square of surface tension gradient $(d\sigma/dc)^2$ has been found to be proportional to the value of Gibbs elasticity. The value of Gibbs elasticity was also found to be comparable to the bubble coalescence inhibition for a range of electrolyte solutions (Craig 2011).

Surface tension gradient is the key factor that provides information of coalescence-hindering tendency of bubbles in an electrolyte solution. For a single electrolyte system, if the value of parameter $(d\sigma/dC)^2$ is large, then the electrolyte will inhibit bubble coalescence, and bubble coalescence behavior will remain unaffected if the value of $(d\sigma/dC)^2 < 1 \text{ (mN. m}^{-1}/\text{mol.L}^{-1})^2$. However, in the case of mixed electrolytes, no correlation between coalescence inhibitions and $(d\sigma/dC)^2$ is available. Systematic studies of ion – specific coalescence of bubbles in selected mixed electrolytes solutions were reported by Henry (2007). Mixed electrolytes follow the properties of the individual ions originally assigned earlier produced by Craig (1993). The combining rules indicated that the fundamental property of the ions controls the bubble coalescence inhibitory behavior of electrolytes.

Bubble coalescence is an extremely rapid process in case of pure liquid like water or sufficiently dilute solutions of electrolytes for which the value of dimensionless concentration parameter crk^2/σ is ≤ 2 . For electrolyte solution, the dimensionless concentration parameter (crk^2/σ) may be expressed (Marrucci 1969) as follows

$$\frac{crk^2}{\sigma} = \frac{2}{\nu RT \sigma} C \left(\frac{d\sigma}{dC} \right)^2 \frac{1}{1 \pm \frac{(d \ln a_{\pm})}{(d \ln C)}} \left(\frac{12\pi\sigma}{A.r} \right)^{2/3} \quad \dots(2.1)$$

where,

$$c = \frac{2}{\nu RT} C \left(\frac{d\sigma}{dC} \right)^2 \frac{1}{1 \pm \frac{(d \ln a_{\pm})}{(d \ln C)}} \quad \dots(2.2)$$

and

$$k = \left(\frac{12\pi\sigma}{A.r} \right)^{1/3} \quad \dots(2.3)$$

then,

$$\frac{crk^2}{\sigma} = f \left(C \left(\frac{d\sigma}{dC} \right)^2 \right) \quad \dots(2.4)$$

where, ν is the number of ions produced upon dissociation (i.e. $\nu = 2$ for most of the inorganic electrolytes); R is the universal gas constant; T is absolute temperature; a_{\pm} is mean activity coefficient of a solution; A is the non-retarded Hamaker constant; σ and $d\sigma/dC$ are surface tension and surface tension gradient, respectively.

The dimensionless concentration parameter, i.e Marrucci's parameter ((crk^2/σ)), contains the term $C(d\sigma/dC)^2$ which may be useful for characterization of the coalescence behavior. A number of studies successfully used the Marrucci's parameter ((crk^2/σ)) to predict gas hold-up and bubble coalescence time (Sagert and Quinn, 1978; Syeda and Reza 2011).

The concentration of electrolytes which immobilizes the gas-liquid interface for bubble coalescence inhibition is known as transition concentration (C_{trans}). The transition concentration of electrolyte according to Marrucci's model, depends on the magnitude of the change in surface tension with concentration at the interface, or surface activity, ($d\sigma/dC$). The relationship

between bubble coalescence inhibition and $(d\sigma/dC)$ was originally established by Marrucci and Nicodemo (1967) using a limited experimental data set. The parameter $(d\sigma/dC)^2$ is important in bubble coalescence phenomena related to the Gibbs elasticity of the liquid film and its magnitude controls the liquid drainage from the film as per Marrucci model.

If the value of parameter $(d\sigma/dC)^2$ is large, the presence of electrolyte inhibits bubble coalescence, and if it is small, bubble coalescence remains unaffected (Christenson and Yaminsky 1995). Generally, the transition from coalescence regime to coalescence inhibition occurs when the value of $(d\sigma/dC)^2$ drops below 1 ($\text{mN} \cdot \text{m}^{-1}/\text{mol} \cdot \text{L}^{-1}$)².

The surface elasticity (which is quantitatively half of the Gibbs elasticity) is the basis of coalescence inhibition (Christenson and Yaminsky 1995). Surface elasticity is increased by the use of electrolytes. Surface elasticity is proportional to the surface tension gradient and for a single electrolytes, this gives a good correlation with bubble coalescence inhibition. However, the presence of a mixture of two electrolytes has shown no correlation between surface elasticity and bubble coalescence inhibition (Henry et al. 2007). Square of surface tension gradient $(d\sigma/dc)^2$, has been found to be proportional to the Gibbs elasticity. The value of Gibbs elasticity was also found to be comparable to the Bubble Coalescence inhibition for a range of electrolyte solutions (Craig 2011).

Table 2.1 Effect of air –aqueous solution of electrolyte system on gas holdup, ϵ_G .

System	Electrolytes ----- Parameters studied	Sparger ----- Measurement techniques	Column diameter (m) ----- Column height(m)	Regimes covered ----- Homogeneous (HM) ----- Heterogeneous (HT)	Range of Concentration ----- Gas holdup range (-)	Remarks	Author
Air- distilled water system	NaCl, Na ₂ SO ₃ ----- Gas holdup, ϵ_G	Single point sparger with 0.005 m (5 mm) dia. ----- Bed expansion Method for gas holdup.	0.152 – 0.6 m ----- 4.0 m	HM ----- HT	0.03-1.0 M ----- 0 – 0.335	Addition of electrolytes increases gas- holdup, Correlation developed for gas holdup	Akita and Yoshida (1973)
Air- distilled water system	Na ₂ SO ₄ , NaCl, CaCl ₂ ----- Gas holdup, ϵ_G	Perforated plate of 1 and 0.0016 m(1.6 mm) hole dia. ----- Manometer readings converted to absolute pressures by a simple hydrostatic head technique; to get the values of the gas holdup.	0.154 m ----- 3.25 m	HM ----- HT	0.05-1.0 M ----- 0 – 0.35	Critical electrolyte concentration determined above which no increase in gas holdup. At higher superficial gas velocity, no effect of sparger diameter on gas holdup	Kelkar et al. (1983)
Air- distilled water system	BaCl ₂ , Na ₂ SO ₄ ----- Gas holdup, ϵ_G	Perforated plates with 0.0005–0.0025 m (0.5 – 2.5 mm) hole dia. -----	0.018 m ----- N.R	HM ----- HT	0.1- 0.27 M ----- 0 – 0.32	No effect of column internal diameter and sparger hole	Koide et al. (1984)

		Bed expansion Method for gas holdup.				diameter on gas hold up(HT), Correlation for the transition regime	
Air- distilled water system	NaCl, NaSO ₄ , KCl, NaOH, CaCl ₂ , MgSO ₄	Perforated plates with 0.0005 and 0.0016 m (0.5 and 1.6 mm) hole dia.	0.15 m ----- 0.29 m	HM ----- HT	0.5 M ----- -	Above critical concentration of electrolyte, no effect on gas holdup. Correlation for gas holdup developed.	Zahradnik et al. (1987)
	----- Gas holdup, ϵ_G	----- Bed expansion Method for gas holdup.					
Air- water system	NaCl, KCl ----- Gas holdup, ϵ_G	Perforated plates ----- Bed expansion Method for gas holdup.	0.14 m ----- N.R	HM ----- HT	0.01-1.0 M ----- -	Critical concentration are given for the electrolyte	Zahradnik et al. (1995)
Air- distilled water system	NaCl, NaSO ₄ and NaI ----- Gas holdup, ϵ_G and Regime transition point	Perforated plate with 0.0007m (0.7 mm) dia. arranged on a triangular pitch of 0.006 m (6 mm). Number of holes: 216 ----- Bed expansion Method for gas holdup. The bubble swarm velocity method, the drift -flux method for regime transition point	0.12 m ----- 1.25 m	HM ----- HT	0 - 0.089 M ----- 0 - 0.8	Gas holdup continuously increase with increasing electrolyte concentration. Transition concentration for bubble coalescence exhibited the same gas holdup profile, regardless of the electrolyte added to the liquid phase.	Ribeiro Jr and Mewes (2007)

Air- distilled water system	NaSO ₄ , NaCl, NaCl (kitchen quality)	perforated plate with circular orifices of 0.0005 m (0.5 mm) dia. and relative free area 0.2% ----- Bed expansion Method for gas holdup.	0.14 m	HM	0.001 – 6.0 M	Dual effect of the salt on the gas holdup and homogeneous regime.	Orvalho et al. (2009)
	Gas holdup, ϵ_G		2.0 m	HT	0 – 0.7		
Air- distilled / deionized water system	NaCl, MgSO ₄ .7H ₂ O, NaSO ₄ ,CaCl ₂ .2H ₂ O	Circular plate with 10 orifices of 0.002m (2 mm) diameter ----- Bed expansion Method.	0.05 m	HM	0 - 0.3 M	Enhancement in gas holdup at low concentrations. Slope, (d σ /dC) is high at lower concentration and changes sharply as the concentration increases further.	Syeda and Reza (2011)
	Gas hold-up, ϵ_G		0.5 m	HT	Up to 65(%)		
Air- distilled water system	NaCl, NaF, NaBr, NaI, and CsCl	Glass frit (porosity 11- 16 μ m) ----- Light intensity method for bubble coalescence, Bed expansion Method for gas holdup	0.045 m	N.R	0.001 – 3.0 M	Transition salt concentration for bubble coalescence inhibition of all investigated salts decreases with increasing superficial gas velocity. <i>Ctrans</i> : NaI > NaBr > CsCl > NaCl > NaF	Nguyen et al. (2012)
	Gas holdup, ϵ_G		0.2 m	N.R	Up to 60(%)		

Air- deionized water system	NaCl ----- Gas holdup, Flow regime transition and bubble size distribution	Spider sparger with six arms (diameter of each hole : 0.002–0.004 m (2-4 mm) ----- Photographic methods and bed expansion method	0.24 m ----- 5.3 m	HM ----- N.R	0 – 0.170 M ----- 0 – 0.30	Bubble size distribution shifts towards lower equivalent diameter of bubbles due to the addition of NaCl resulting in increased gas holdup. NaCl concentration stabilized the homogeneous flow regime.	Besagni and Inzoli (2017b)
--------------------------------	---	--	--------------------------	--------------------	----------------------------------	--	----------------------------------

2.7 Power consumption in stirred bubble column

Mechanically agitated gas liquid contactors equipped with a single or multiple impellers on a common shaft are frequently used in various industrial applications, such as aerobic fermentation, oxidation, hydrogenation, or chlorination. Radial impellers, i.e. Rushton impellers are widely used in mechanically agitated gas-liquid systems because of the high dispersion efficiency and its flexibility of operation. However, Rushton impeller has the disadvantage that it suffers from significant drop in power input with gassing (Saito et al., 1992, Nienow, 1996). The fall in the gassed power is due to the gas-filled cavity structure formed behind the blades of the Rushton impeller (van't Riet, 1973, Bruijn et al., 1974). Van't Riet et al. (1976) first showed that the power reduction on gassing can be significantly reduced by replacing the six flat plates of the Rushton turbine with curved pipe segments concave in the direction of rotation. This reduction of the power drop can be attributed to the concave geometry of the blades which does not allow large cavities to form easily at low gas flow rates; while at higher gas flow rates, the cavities behind the concave blades have smaller dimensions compared to those behind the standard flat blades (van't Riet et al. 1976).

The power consumed in mechanically agitated vessels is an important parameter in the characterization and design of agitated industrial gas-liquid contactors. Power consumption does not only depend on the impeller type, properties of fluid, agitator speed, gas flow rate but also on the geometry and location of the impellers employed in the agitated systems with the configuration of the vessel (column) used such as baffled, unbaffled or partially baffled and inter-impeller clearance. Various empirical correlations for power consumption in the presence of gas in single impeller agitated systems are presented in Table 2.2.

Literature review revealed that empirical correlations on air–water systems have been scarcely reported (Calderbank 1958). Therefore, in the present study an empirical correlation for estimation of relative power demand of gassed and ungassed mechanically agitated air–water system using single impeller partially baffled system applicable to different impeller types that are commonly used in industrial applications namely, Rushton impeller, concave blade (with curvature = 0.441), pitch blade impeller.

Multiple impellers agitated systems

The key problem in the scale-up of bioreactors is the irregular distribution of shear and energy dissipation, which are known to be harmful to the microorganisms in the bioreactors. This problem can be effectively tackled by the appropriate selection of multiple impeller

designs (Puthli et al. 2005). Multiple impellers configuration on a common shaft are preferred over a single impeller as multiple impellers provide more effective gas utilization in gas-liquid systems due to longer gas residence time, effective gas dispersion for generating the larger interfacial area, shear sensitivity to micro-organisms, improved liquid circulation in the vessel and higher surface area per unit liquid volume for heat transfer (Gogate et al. 2000; Shewale and Pandit 2006; Fujasova et al. 2007; Moucha et al. 2009; Linek et al. 2012; Labik et al. 2014).

The spacing between impellers is considered to be crucial factor in designing of stirred type gas-liquid contactors for maximizing oxygen mass transfer, and minimizing the mixing time, or power consumption. A significant amount of experimental data can be found in the literature on power consumption in single-impeller systems (Murugesan and Degaleesan 1992; Armenante and Chang, 1998; Chen and Chen 1999; Zhu et al., 2001; Smith 2001; Bouaifi and Roustan, 2001; Fujasova et al., 2004; Shewale and Pandit, 2006; Saghatoleslami and Bakhtiari, 2006; Thakre et al., 2008; Michelan et al., 2009; Moucha et al., 2009). However, only limited information is available for power consumption in stirred bubble columns provided with multiple impellers configuration (Arjunwadkar et al., 1998; Armenante et al. 1998; Bouaifi and Roustan 2001; Shewale and Pandit, 2006; Moucha et al. 2009; Linek et al. 2012). Previous studies on Power consumption in multiple impeller configurations in stirred vessels are shown in Table 2.3 Significance of mixing tanks provided with multiple impellers lies in the fact that they require smaller mixing time and power while they increase the extent of mass transfer by enhancing gas holdup for same process conditions as compared to single impellers. In particular, very little information is available on inter-impeller clearance in multiple impeller systems (Markopoulos et al. 2004; Markopoulos et al. 2005). The power consumed by multiple impellers and the characteristics of the flow they generate are often estimated on the basis of the power consumed by single impellers. Generally, power consumption in case of aerated conditions, is relatively smaller as compared to the nonaerated conditions. The reduction in power consumption varies depending on the type of impeller, impellers combination and inter-impeller clearance (Markopoulos et al. 2004; Markopoulos et al. 2005). The inter impeller clearance is defined as the distance between the centre-line of the two impellers. Generally, this distance is kept equal to the diameter of the impeller. Beyond this value each impeller sets up its own liquid circulation loops which do not mix with that produced by the other impeller. The influence of inter-impeller clearance on power consumption may be limited with the existence of baffles (Markopoulos et al. 2004). Unbaffled and weakly (partially) baffled systems consume less

power than those with full baffles. The interaction between dual Rushton impellers increases with reduction in baffle length for a large value of $\Delta S/d$ as reported by Markopoulos et al. (2004). Markopoulos et al. 2005 reported that the power number was unaffected by Reynolds number for fully baffled agitated systems with dual pitched blade impellers as well as for weakly and the unbaffled systems. In addition, it was also reported that the power number was not affected by inter-impeller clearance for the unbaffled agitated systems. Babalona et al. (2005) worked with gas liquid contactors agitated by dual Rushton and by dual pitched blade impellers and investigated the effect of impeller spacing on power consumption. It was reported that dual Rushton impellers system acted independently for spacing greater than $1.65d$ in tap water, while $1.20d$ for glycerol solutions. In case of dual pitched blade impeller systems, inter-impeller spacing was $1.50d$ for tap water, 1.07 for relatively high viscosities and $0.53d$ for very high viscosity values. Similar results were reported earlier by Markopoulos et al. (2001) for a double stage Rushton impeller agitated system.

2.8 Volumetric gas–liquid mass transfer coefficient

Agitation is one of the essential factors in the chemical and biochemical reaction processes. For effective gas dispersion processes in precise for fermentation and a variety of oxygenation and hydrogenation processes, need a large gas handling capacity and an effective gas dispersion for generating as large an interfacial area as possible. The volumetric mass transfer coefficient is a key parameter in the characterization and design of industrial agitated gas-liquid reactors which are often equipped with single and two or more impellers. These reactors, currently used in many chemical and biological processes, are traditionally equipped with radial turbines. The disk turbines are radial-flow impellers like standard Rushton turbine that are particularly suitable for gas-liquid dispersion due to the high shear zone near the blades where bubble formation occurs and eliminate the flow instabilities (Mishra and Joshi 2000). During gas dispersion, low-pressure trailing vortices attract gas bubbles, which coalesce to form ventilated cavities behind the blades (Van't Riet et al.1973). The size and rotation of the trailing vortices were found to be influenced by both blade number (Lu and Yang 1998) and blade curvature (Van't Riet et al.1976).

Van't Riet (1976) studied a variety of impeller styles, and introduced the concept of using concave blades. The concave geometry of the blades did not allow large cavities to form easily at low gas flow rate; while at higher gas flow rates, the cavities behind the concave blades have smaller dimensions compared to those behind standard flat blades i.e., Rushton

impeller. Moreover, the curved or hollow blade impellers, such as SCABA and concave blade turbines, also provide better mass transfer and gassed power characteristics and shaft stability performance than Rushton impeller (Khare and Niranjana 1999; Cooke et al. 2005; Chen and Chen 1999; Saito et al. 1992). Warmoeskerken and Smith (1989) extended that work and explained the improved performance of the concave blades compared to flat blades in terms of reduced cavity formation behind the blades. It was also reported that the gas-liquid mass transfer in an agitated tank due to a semi-circular blade impeller is at least 20% higher than that of a Rushton impeller at the high power dissipation levels. Saito et al. (1990) studied the performance of two SRGT impellers with four and six blades, and found that parabolic shape of SRGT blades ensure that large cavities do not form. Other finding, at all gas flow rates, the gas is being dispersed from the inside of the parabolic blade, instead of from large cavities behind the blade. Chen and Chen (2000) reported that a maximum mass transfer coefficient occurred for a given impeller speed at a certain blade curvature which varied with the blade curvature. Vasconcelos et al. (2000) worked with different modifications of the Rushton turbine in dual-impeller agitated tank. It has been reported that at the same power input and superficial gas velocity, k_{La} independent on the impeller type. Zhu et al (2001) worked with six impellers consist of radial as well as axial for estimating of k_{La} . It has been reported that radial impeller produce higher mass transfer rate than axial flow impellers for a given specific power and gas sparging rate. Literature review revealed that the majority of the studies concerning the effect of curvature on k_{La} have been carried out with ring type sparger system and at single orifices connected either to gas chamber or capillary tubes. Because of the discrepancy in mass transfer results obtained by previous researchers and the fact that there is no systematic study reported for impellers with different blade curvatures with varying jet nozzle length system. Thus, in this study, mass transfer characteristics are investigated for a series of concave blade impellers with different blade curvatures and jet nozzles with different lengths. Finally, a comparison was made with the results of radial impeller (Rushton turbine) and axial impeller (4-blade pitch and 6-blade pitch).

Table 2.2 Empirical correlations for power consumption in the presence of gas in agitated systems

Gas-liquid system	Correlation proposed	Range of operating parameter / Physical properties of liquid	Sparger/ Agitator detail/baffles	Reference
Air/water	$\frac{P_g}{P_o} = 1 - 1.26 \left(\frac{Q}{Nd^3} \right) \quad \text{for} \left(\frac{Q}{Nd^3} \right) \leq 0.035$ $\frac{P_g}{P_o} = 1 - 1.26 \left(\frac{Q}{Nd^3} \right) \quad \text{for} \left(\frac{Q}{Nd^3} \right) \geq 0.035$	$\rho_L (kg/m^3) : 790 - 1600$ $\mu_L (Pa.s) \times 10^3 : 0.5 - 28.0$ $\sigma_L (N/m) \times 10^3 : 73.5 - 21.7$	N.R /six flat blade turbine./N.R	Calderbank (1958)
Air/water, Glycerol (weak & strong), CCl ₄ , Alundum	$P_g = C \left(\frac{P_o^2 Nd^3}{Q^{0.56}} \right)^{0.45}$ <p>C: dependent on the geometry of the impeller</p>	$\rho_L (g/ml) : 0.87 - 1.60$ $\mu_L (centipoise) : 0.8 - 28$	N.R /six flat blade turbine with 3-4 inch dia./N.R	Michel and Miller (1962)
Air/water, aqueous solution of Glycerol, ethylene glycol, sodium sulphate, methyl acetate, Propionic acid	$\frac{P_g}{P} = C \left(\frac{Q}{Nd^3} \right)^n \left(\frac{N^2 d^3 \rho_L}{\sigma} \right)^m \left(\frac{\rho_L}{\rho_G} \right)$ <p>$n : 0.38$ for 4 blade paddle, $m : 0.22$ for 6 blade turbine, $m : 0.25$</p>	$\rho_L (kg/m^3) : 1000 - 1057$ $\mu_L (N.s/m^2) \times 10^3 : 0.80 - 3.0$ $\sigma_L (N/m) \times 10^3 : 44.0 - 73.6$	Single -hole orifice sparger /six flat blade turbine with 3-4 inch dia., 6 blade turbine and 4 blade paddle/4	Hassan and Robinson (1977)
Air/ water, glycol Non-foaming solutions	For non-foaming systems	$\rho_L (kg/m^3) \times 10^3 : 0.803 - 1.278$ $\mu_L (Pa.s) \times 10^3 : 0.803 - 48.50$ $\sigma_L (N/m) \times 10^3 : 23 - 72$	Porous plate, open-end tube /six flat blade turbine /4	Loiseau et al.(1977)
Air/ water+ lauric, alcohol, ethanol, water+ sugar, water +HCl + CuCl, aqueous sodium, sulphite sodium, acetic acid + propionaldehyde	For foaming systems			
Non-foaming	$P_g = C \left(\frac{P_o^2 Nd^3}{Q^{0.56}} \right)^{0.45} \quad \text{if} \left(\frac{P_o^2 Nd^3}{Q^{0.56}} \right) \leq 2000$			

<p>solutions Water+ sugar, aqueous sodium sulphite solution Air/water, methanol, CMC, Glycerol, ethylene glycol</p>	$P_g = C \left(\frac{P_0^2 N d^3}{Q^{0.56}} \right)^{0.45} \quad \text{if} \quad \left(\frac{P_0^2 N d^3}{Q^{0.56}} \right) \geq 2000$	<p>$\rho_L (kg/m^3) : 983-1104$ $\mu_L (N.s/m^2) \times 10^3 : 0.85-3.00$ $\sigma_L (N/m) \times 10^3 : 55-72$</p>	<p>Single-hole orifice sparger/six flat blade turbine/4</p>	<p>Luong and Volesky (1979)</p>
<p>Air/water, aqueous solution of ethylene glycol, sodium chloride, sodium sulphate, acetone</p>	<p><i>for newtonian fluids</i></p> $\frac{P_g}{P} = 0.497 \left(\frac{Q}{N d^3} \right)^{-0.38} \left(\frac{N^2 d^3 \rho_L}{\sigma} \right)^{-0.18}$ <p><i>for non-newtonian fluids</i></p> $\frac{P_g}{P} = 0.514 \left(\frac{Q}{N d^3} \right)^{-0.38} \left(\frac{N^2 d^3 \rho_L}{\sigma} \right)^{-0.194}$ <p><i>For non-electrolyte and electrolyte solution</i></p> $P_g = C \left(\frac{P_0^2 N d^3}{Q^{0.56}} \right)^{0.45}$	<p>$\rho_L (kg/m^3) : 960-1047$ $\mu_L (mN.s/m^2) : 0.8-2.10$ $\sigma_L (mN/m) : 38.29-72.74$</p>	<p>Copper tube sparger with orifice size 0.006 m /6 blade turbine and 4 blade paddle with 0.09, 0.13 m, 0.18 m dia./4</p>	<p>Yung et al., (1979)</p>
<p>Different air/liquids systems</p>	<p><i>based on 391 data points</i></p> $\frac{P_g}{P} = 0.10 \left(\frac{Q}{N V} \right)^{-1/4} \left(\frac{N^2 D^4}{g D_L V^{2/3}} \right)^{-1/5}$	<p>Correlation Covers the large range of variables (Michel and Miller, 1962; Pharamond et al., 1975; Luong and Volesky, 1979)</p>	<p></p>	<p>Hughmark et al. (1980)</p>
<p>Air/water, toluene, carbon tetrachloride, Glycerol and sodium sulphite</p>	$\frac{P_g}{P} = C_1 \left(\frac{Q}{N d_R^3} \right)^{-0.26} \left(\frac{N^2 d_R}{g} \right)^{-0.19} \left(\frac{d_R}{d_T} \right)^{-0.28} \left(\frac{d_w}{d_R} \right)^{-0.21}$	<p>$\rho_L (g/cm^3) : 0.858-1.586$ $\mu_L (cp) : 0.8-1.980$ $\sigma_L (dyne/sec) : 27.12-72.00$</p>	<p>Gas distributor plate containing 6 orifices of 2 mm dia. / 6-flat blade turbine with 5 cm and 7 cm dia. /4</p>	<p>Murugesan and Degaleesan, (1992)</p>

Table 2.3 Power consumption studies on multiple impeller configurations in stirred vessels.

System	Configuration	Clearance	Type of vessel	Inner diameter	Reference
Air – tap water	6PBT+4PBT 6PBT+6PBT 6PBT+6PBT+6PBT	–	Flat-bottomed cylindrical Plexiglas vessels	0.289 m	Armenante et al. 1999
Air – tap water	A315+A315 A315+A310 A315+PBSD RDT+A315 RDT+A310 RDT+PBSD		Hemispherical bottomed cylindrical vessel	0.43m	Bouaifi and Roustan 2001
Air – tap water	PBSD+PBSD+DT PBSD+PBSD+PBSD	0.3 m	cylindrical acrylic vessel	0.3 m	Shewale and Pandit, 2006
Low viscous coalescing, Low viscous non- coalescing and viscous newtonian liquids	PBU+PBU+PBU TXD+TXD+TXD TXU+TXU+TXU LTN+LTN+LTN NS+NS+NS	0.29 m	Flat-bottomed cylindrical vessels	0.29 m	Fujasova et al. 2007
Air –water	RT+TXU RT+TXU+TXU RT+TXD RT+TXD+TXD	0.6 m	cylindrical dished bottom vessel	0.6 m	Moucha et al. 2009
Air –water	RT+RT RT+RT+RT	0.6 m	cylindrical dished bottom vessel	0.6 m	Linek et al. 2012
Air –water	PDT+2CBY _N	0.144 m	Dished-base cylindrical	0.30 m	Zhang et al. 2016

	PDT+2CBY _w PDT+2WH _D HEDT+2WD _D HEDT+ 2WH _U		vessel		
Air –water	RT+PBU RT+PBU+PBU RT+PBD RT+PBD+PBD RT+TXU RT+TXU+TXU RT+TXD RT+TXD+TXD RT+LTN RT+LTN+LTN	0.29 and 0.59	cylindrical vessel	0.29 m and 0.59 m	Labik et al.2016

2.9 Modeling of liquid –side mass transfer coefficient

Experimental studies on bubble column with or without modification operated under appropriate industrially conditions have been reported widely for various gas-liquid and gas-liquid-solid systems (Shah et al. 1982). However, modeling of such systems has been scarcely reported in literature. Models can be employed to study the behavior of bubble columns under varying conditions of operation, which may be required for scale up. Higher gas–liquid interfacial areas, higher values of mass-transfer coefficient and gas holdup, longer residence time of bubble for adequate gas-liquid contact and low gas-phase pressure drops are some of the significant parameters desirable for excellent performance of a gas-liquid contactors for mass transfer. Slurry bubble columns (SBC) are preferred mainly for highly exothermic processes when efficient interphase contacting is desirable. These reactors are usually difficult to scale up because of their complex hydrodynamic behavior. Performance of reactors depends on operating conditions, physical properties of gas and liquid and dimensions of the system. The performance of such reactors is also strongly dependent on the flow regime, i.e. homogeneous or heterogeneous and bubble characteristics, such as bubble size, bubble rise velocity and bubble wake phenomena. These reactors provide larger gas–liquid interfacial area, large catalyst area, lower pressure drop and a higher $k_L a$ value at low power inputs (Lemoine et al. 2008). In three–phase systems, presence of a solid particle may have a positive or negative effect on the interfacial mass transfer as it directly affects thickness and stability of the mass transfer film. The solid particles can increase or decrease the value of k_L , depending on the extent of solids loading, size of particles, particle density, nature of particles and their surface properties. The solid particles can increase k_L by enhancing turbulence at the gas–liquid interface and increase surface renewal rate (Ferreira et al. 2010). However, the presence of solid particles can also limit the diffusion path by blocking the available area for mass transfer and decrease k_L (Yang et al. 2001; Ozkan et al. 2000). The value of k_L also depends on other variables such as diffusivity of gas in the liquid, viscosity and surface tension of the liquid (Sada et al. 1985). Presence of solid particles increases the specific interfacial area by covering the bubble surface, preventing coalescence of the bubbles and thus resulting in smaller bubbles. The effect of presence of solid particles depends on the hydrophobicity of the particle surface and on the ratio of size of particles to the bubble size. Mena et al. (2011) reported that hydrophobic particles have a strong negative influence on mass transfer, and hydrophilic particles, in a certain concentration range (\leq

3 vol. %), can increase $k_L a$. In practice, several kinds of solids are used in slurries in petroleum and petro-chemical and other industries for processes such as Fischer–Tropsch synthesis, methanol synthesis, heavy oil upgrading and other processes where particles with inert surface characteristics are also employed.

Yang et al. (2001) studied gas–liquid mass transfer behavior of syngas components (H_2 and CO) in the presence of solid particles (silica gel powder, 5 – 20 vol.%) at industrial conditions ($T = 293 - 523$ K and $P = 1 - 5$ MPa) and proposed empirical correlations to predict k_L for H_2 and CO in slurry (liquid paraffin/solid particles) bubble column. On similar lines, Yang et al. (2003) worked with slurry bubble system (H_2 –, CO – liquid paraffin – silica gel powder) and proposed an empirical correlation for predicting liquid film thickness, δ and surface renewal rate, S . However, both the correlations did not use Sherwood number, which is essential (Yang et al. 2001). Besides, molecular weight and molar volume of gas was also not used. Use of these two parameters in the correlation improves the accuracy of the correlation. In industrial applications of bubble columns, it is desirable to have a large value of liquid–side mass transfer coefficient; hence, better understanding of the mass transfer mechanism is imperative. Most of the previous bubble column studies reported in the literature are at room or ordinary temperatures, mostly for less than 30°C , but the commercial bubble columns are frequently operated at elevated temperatures and pressure, often near the boiling points. At higher temperatures, liquids exhibit lower viscosities. For operation at elevated pressures, understanding of the effect of temperature and elevated pressures on mass transfer in bubble columns is essential for the optimal design and operation of bubble column, e. g. Fischer-Tropsch synthesis of heavy paraffin from synthesis gas (Krishna and Sie 2000).

Researchers have used various models for mass transfer modeling in the absence and presence of chemical reaction in gas–liquid or gas – liquid – solid systems (Wang and Langemann 1994b; Lupin and Merchuk 1971; Kastanek 1977). However, Zhao et al. (2003) presented a model for k_L estimation based on liquid film thickness and surface renewal rate. In this study, bubble size was limited to 3 mm diameter and the gas–slurry system was treated like a gas-liquid system. Macroscopic mathematical modeling of transient mass transfer for estimation of k_L and liquid film thickness for two– or three–phase systems are scarcely available in the literature. Therefore,

concise accurately analytical models are required which can predict k_L and δ without the need to use complex computational tools.

2.10 Hydrodynamic in non-newtonian liquids

Bubble columns containing non-Newtonian liquids are used in a large number of industries for gas liquid mass transfer. The applications include non Newtonian shear thinning liquids like, slurries, suspensions, emulsions, micellar solutions, polymer solutions, pulp suspensions and mixed liquor of aerobic wastewater and organic liquids, e.g. glycerol, melts, liquid crystals, gels, foams, etc. are processed in biotechnological, pharmaceutical, polymer, pulp and paper, food processing industries and wastewater treatment to accomplish gas liquid mass transfer operations. Understanding of hydrodynamics of non-Newtonian systems in industrial bubble columns is important for effective design, operation and scale up as the fundamentals of non-Newtonian systems are yet to be understood well (Haque et al., 1986; Fransolet et al., 2005; Ghosh and Upadhyay, 2007; Anastasiou et al., 2013).

Recently, Sujan and Vyas (2017) presented an extensive review, covering different aspects dealing with design parameters and operating parameters which influence on gas holdup structure of non-Newtonian liquids in bubble columns. Inter-relationships of factors affecting gas holdup and mass transfer in a bubble column (Sujan and Vyas 2017) are presented in Figure 2.1

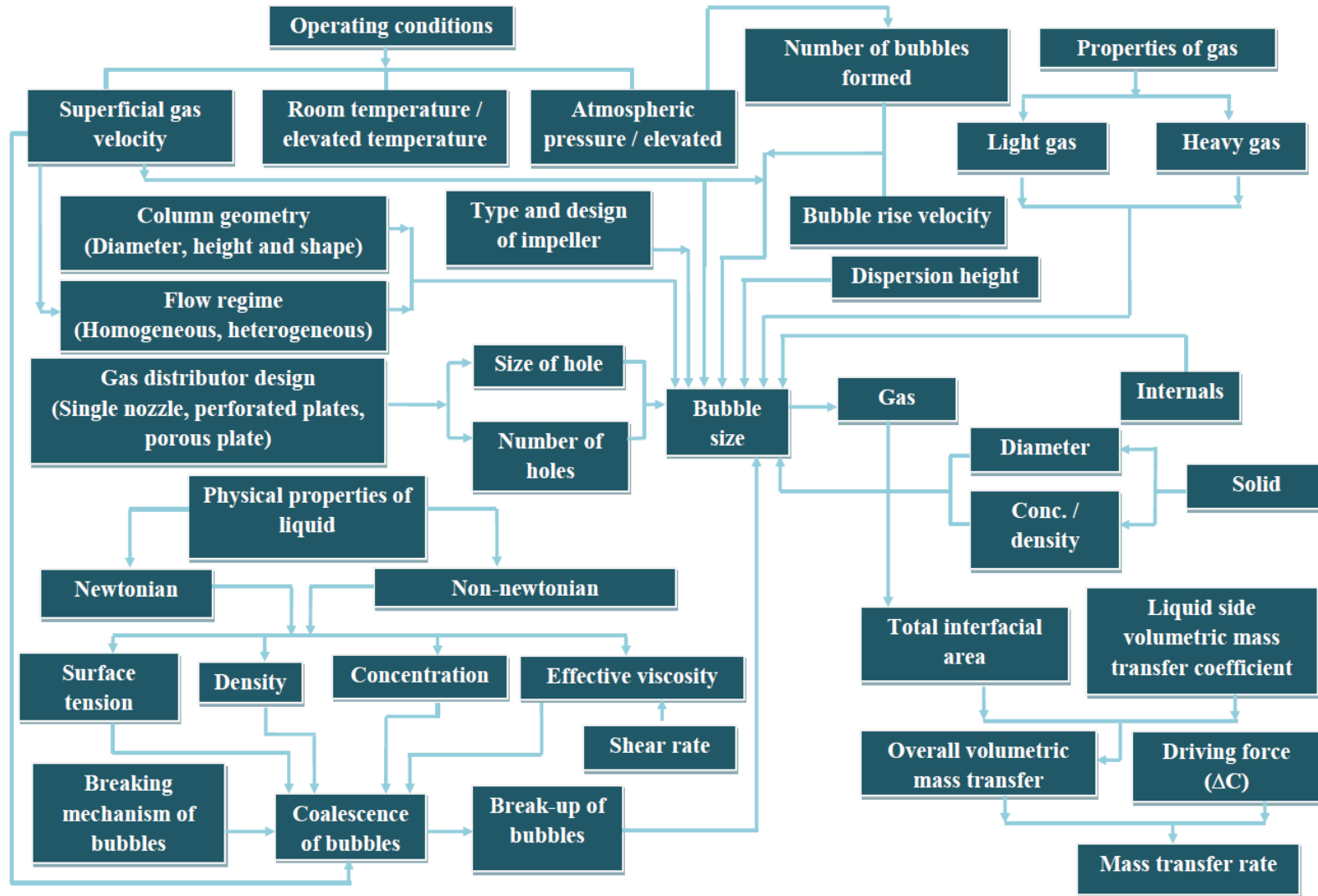


Figure 2.1 Inter-relationships between various factors affecting gas holdup and mass transfer in a bubble column (Sujan and Vyas 2017).

3 Materials and Methods

Description of materials and methods used in the research work are given in this chapter. Details of equipment/ instruments used during the experimental work are as follows:

3.1 Theory and working principle of digital dissolved oxygen electrode

Digital dissolved oxygen meter (Model: HI 2004-02 Edge®, make: Hanna instruments) was used to measure the dissolved oxygen content in the aqueous solutions during experiments. Digital dissolved oxygen meter and electrode with its internal components are presented in Figure 3.1. The Dissolved oxygen electrode (Model: HI 764080, make: Hanna instruments) has an ultra-thin, Clark-type polarographic electrode composed of a platinum cathode with a silver/silver chloride anode, an integrated temperature sensor, and a replaceable PTFE (Polytetrafluoroethylene) membrane cap. Small size 12 mm diameter membrane (ultra-thin) is suitable for measurement in narrow vessels. In the polarographic method, an external voltage is applied to the platinum cathode, silver anode, electrolyte solution and gas permeable membrane to establish a current proportional to the concentration of oxygen in a solution. A concentrated Potassium Chloride electrolyte solution from the manufacture of the instrument (HI7041S, make: Hanna instruments) is held in place over the electrode by a PTFE membrane. The specifications of digital dissolved oxygen probe are presented in Table 3.1. A zero oxygen solution (HI7040-2, make: Hanna instruments) was used for calibrating polarographic oxygen sensor by simply immersing the dissolved oxygen probe in the aqueous solution to quickly calibrate to 0% oxygen concentration. The dissolved oxygen probe is polarized with a fixed voltage of nearly 800 mV between the cathode and anode. With the probe properly polarized, oxygen is continually consumed as it passes through gas permeable PTFE membrane.

Before using dissolved oxygen probe, dissolved oxygen probe is prepared for measurement and calibrating with the zero oxygen solution. When the dissolved oxygen probe is immersed in an aqueous solution, the oxygen molecules (O_2) present in the solution diffuse through the PTFE membrane to Potassium Chloride electrolyte solution. A PTFE membrane is semi- permeable

allowing dissolved oxygen molecules to pass through it, but preventing passage of other molecules that might interface with the chemical reaction at the electrode. A voltage of approximately 800 mV goes through the electrodes to promote the chemical reaction in the probe. Chemical reaction releases electrons to generate an electrical current through the electrical circuit of the probe. Accordingly, the number of electrons produced by the redox chemical reaction of dissolved oxygen is almost directly proportional to the concentration of dissolved oxygen in the sample solution.

3.2 Surface tension and density measurement

3.2.1 Surface tension

Surface tension values of distilled water and aqueous solutions of electrolytes were accurately measured using Goniometer which utilized pendant drop method (Drop Shape Analyzer, Model No. DSA 25, Kruss, Germany). The drop Shape Analyzer is shown in Figure 3.2 (a). Drop shape analyzer consists of four main parts, namely, high resolution camera, uniform LED lighting source, syringe control mechanism, and level stage of sample. Reliable and accurate measurements are obtained using high-quality optical components in the digital camera. The surface tension can be ascertained from the image of the drop using drop shape analysis. The needle of 1.835 mm dia. is employed for drop formation. The Goniometer used for the present study has a precision up to a surface tension value of 0.05 mN/m. To eliminate any error in the surface tension results, surface tension of each sample was measured four times and an average of the four values was taken. Measured surface tension values were found within ± 0.4 mN/m of the average value. Mean surface tension of distilled water was found 72.14 mN/m with a standard deviation of 0.03 at 28 °C.

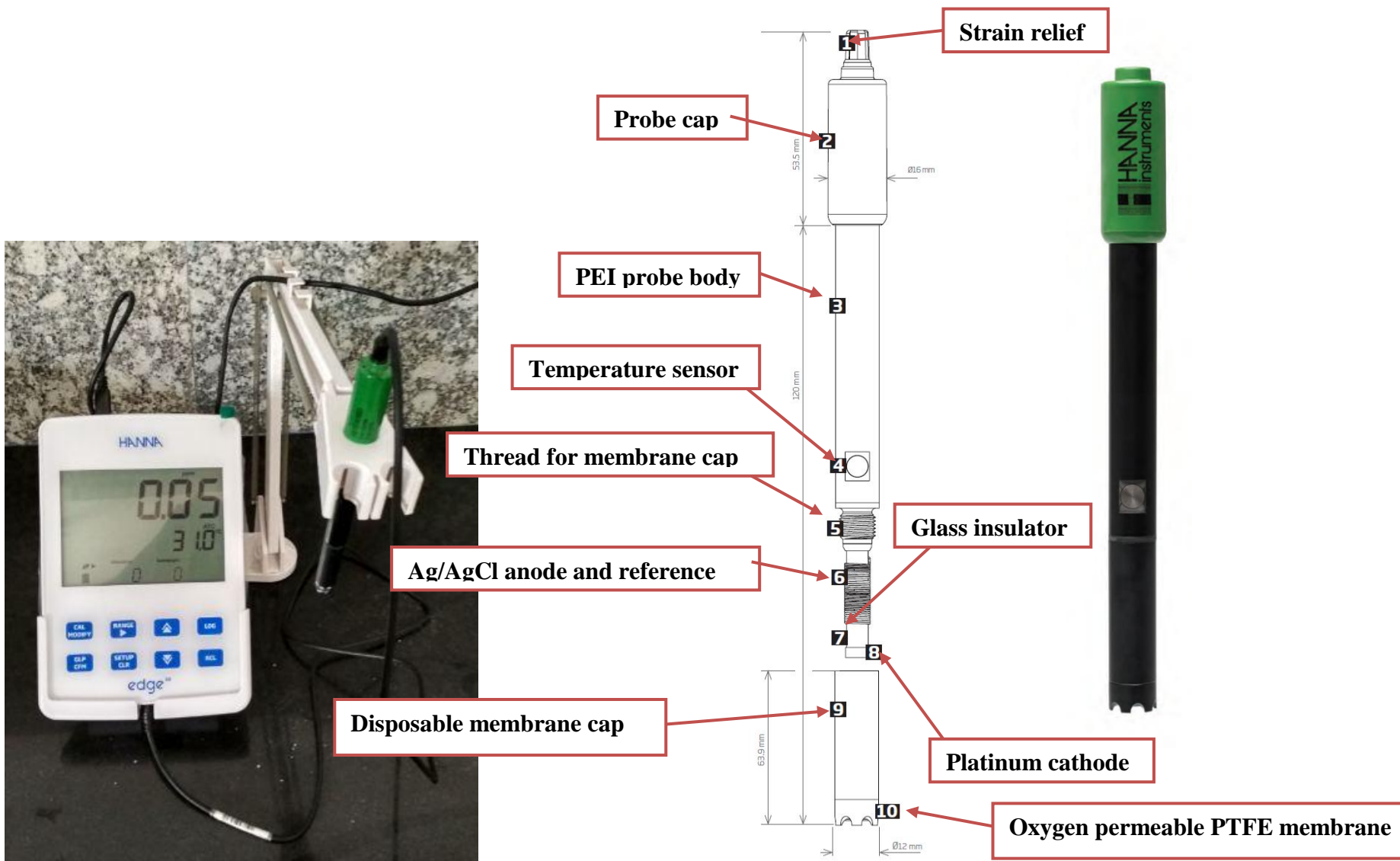


Figure 3.1 Digital dissolved oxygen meter and electrode with its internal components.

Table 3.1 Specifications of digital dissolved oxygen probe.

Particulates	Specifications
MOC of probe	Polyethylenimine (PEI)
MOC of membrane	PTFE (Polytetrafluoroethylene)
Type of probe	Polarographic
Anode	silver/silver chloride (Ag/AgCl)
Cathode	Glass encapsulated Platinum
DO Range	0.00 to 45.00 mg/L; 0.0 to 300% saturation; 0 to 50 °C
Resolution	0.01 mg/L; 0.1% saturation; 0.1 °C
Accuracy	±1.5% of reading (± 1 digit)
Calibration	one or two point at 0% (HI-7040 solution) and 100% (water saturated air)
Temperature Range	-20 to 120 °C
Power Supply	230 V AC through a 5 V DC adapter

3.2.2 Density meter

In addition, the density of each sample was also measured by density meter (Make: Kruss, Germany, Model No. DS7800). Density meters based on the oscillating U-tube method allow for a highly accurate measurement at a controlled temperature and with easily reproducible results within minutes, require a sample volume of less than 1 mL. In this method, the oscillation frequency of a body is a function of its mass. A U-shaped capillary is filled with the liquid sample and piezoelectric or magnetic oscillations are induced. The mass and thus the density of the sample can be calculated from the resulting eigen frequency of the U-tube oscillator. The density meter is shown in Figure 3.2 (b).

The samples (0.9 mL) are supplied manually via syringe in filling section, and the sample is continuously monitored for entry of air bubbles by looking through the inspection glass. A suitable medium is injected for the cleaning until all sample residues have been dissolved and removed. The drying unit (DS7060) will then remove all liquid residues. The accuracy of density meter used was $\pm 0.0001 \text{g/cm}^3$. The drying unit was connected to the peristaltic pump

and the flow of the sample or cleaning medium as well as the drying air was controlled via its 3/2-way valve. The specifications of density meter are presented in Table 3.2.

Table 3.2 Specifications of density meter (Make: Kruss, Germany, Model No. DS7800)

Particulates	Specifications
Measurement range	0–3 g/cm ³
Accuracy	±0.0001 g/cm ³
Measurement period	Typically 1–3 min including temperature control
Sample volume in case of manual injection	0.9 mL
Temperature range	10 – 40 °C
Accuracy of Temperature control	± 0.02 °C
Methods	Oscillating U-tube method

3.3 Experimental setup

3.3.1 Stirred bubble column

In this study, mechanically agitated bubble column was used for the estimation of volumetric mass transfer coefficient in air–water system. The experiments were carried out in a flat bottom cylindrical vessel made of the transparent acrylic sheet with the internal diameter of 0.30 m and height of 0.44 m. The specifications of experimental setup are presented in Table 3.3. The ratio of the diameter of the impeller used in the present studies to the diameter of the vessel was 0.467 in all the experimental runs. Schematic diagram of experimental setup of stirred bubble column is shown in Figure 3.3 and Figure 3.4 respectively.

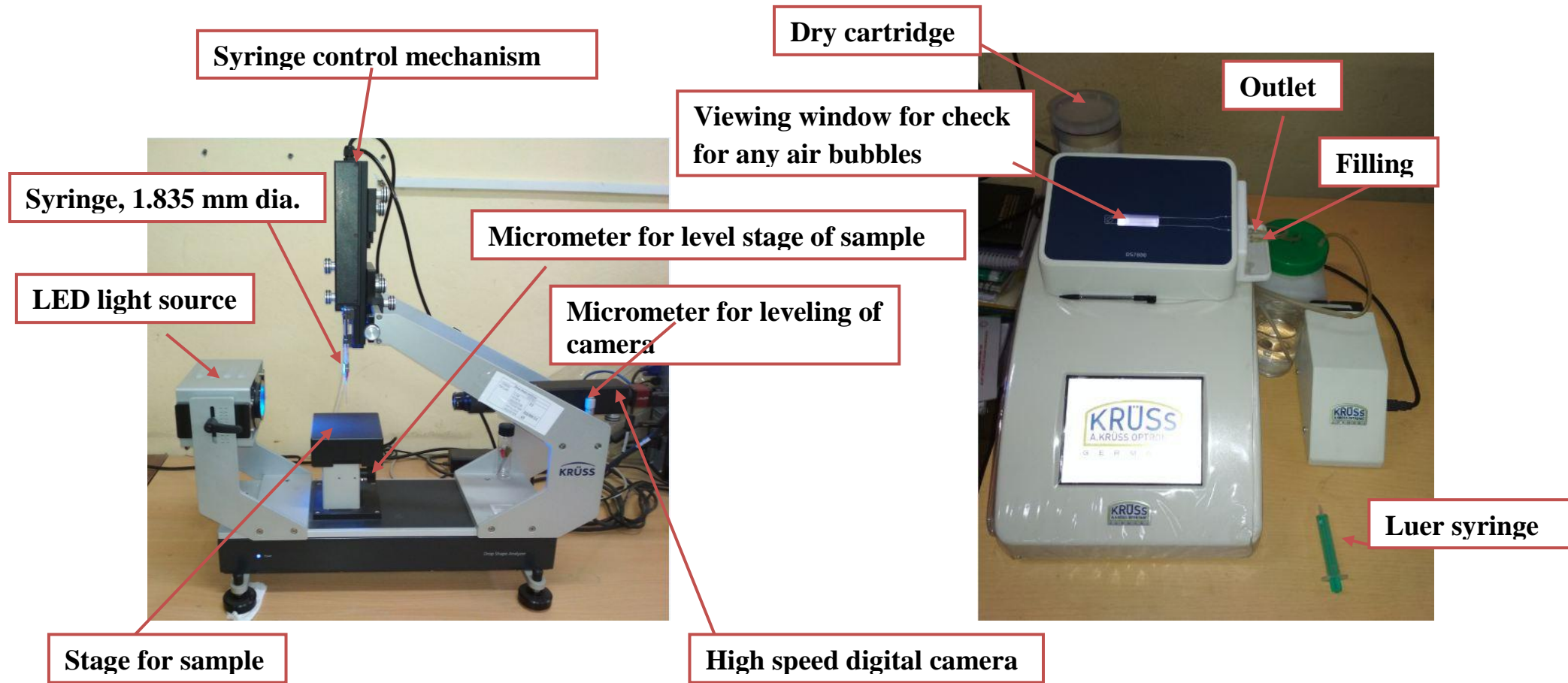


Figure 3.2 (a) Drop Shape Analyzer (Make: Krüss, Germany, Model No.: DSA 25 and (b) density meter (Make: Krüss, Germany, Model No. DS7800).

Table 3.3 Specifications of stirred aeration column.

Particulars	Specifications
MOC	Acrylic sheet
Type of vessel	Cylindrical
Working volume, L	37.5
Column height, cm	44
Column diameter, cm	30
No. of baffles / internals	2 straight cylindrical rod

3.3.2 Bubble column

In this study, bubble column was used for the experimental measurement of gas holdup in distilled water electrolyte solutions. The experiments were carried out in a borosilicate glass bubble column with an internal diameter of 0.105 m and 1.25 m height. A schematic diagram of experimental setup is shown in Figure 3.5 and Figure 3.6 respectively. A perforated nylon circular disc containing 69 orifices with a hole diameter of 2 mm each arranged in a quadrangular pattern with a pitch of 10 mm was placed at the bottom of the column and used as sparger. The free area of the disc (a_f) was 96.93% . Specifications of experimental setup are given in Table 3.4. The controlled air supply from air compressor via air control panel through air rotameter (Make: Eureka, Model No. CIVF-PG-2, Eureka industrial equipment Pvt. Ltd, Pimpri, Pune India) was sparged to bubble column. Then, the electrolyte solutions were aerated for a sufficiently long time to ensure minimum fluctuation of liquid height during bubbling. In each electrolyte solution run in the bubble column, the gas velocity was progressively increased from 17.5 to 27.5 L/m by manually adjusting the rotameter flow control valve.

Table 3.4 Specifications of bubble column experimental setup.

Parameter	Specifications
Diameter of bubble column, m	0.105
Height of bubble column, m	1.2
MOC of bubble column	Borosilicate glass
Diameter of single orifice, mm	2
Total number of orifices	69
Hole arrangement	Quadrangular pattern with a pitch of 10 mm
MOC of perforated plate	Nylon
Free perforated plate area (a_f)	96.93%

3.3.3 Types of impellers

In single impeller and all multi-impeller configurations the liquid level ($V_L = 0.0265 \text{ m}^3$) was set to 1.25D or 37.5 cm from the bottom of the vessel. Single-, Double- and triple impellers (diameter $D/3$) on a common shaft were used. Four types of impellers providing different direction of flow in the vessel were used in this study: (i) radial flow –Rushton turbine (RT) (ii) Concave blade turbine (smith turbine) (CD6) (iii) axial –Six Pitched blade impeller (blade angle 45°) and (iv) Four Pitched blade impeller (blade angle 45°). For a dual/ triple impeller system, Rushton turbine (RT) or Concave blade turbine (CD6) was mounted on a common shaft in the bottom section combined with other impeller types in the upper sections for experimental run (e.g. RT+RT, CD6 + CD6, RT + RT + RT, and CD6 + CD6 + CD6). The specifications of impellers used in the experiments are illustrated in Table 3.5. The effects of various impeller configurations on the Relative power demand (RPD) were investigated over the impeller speed range of 150–400 rpm at different gas flow rates ranging from 7.5–25 L/min in distilled water ($\rho_L = 998 \text{ kg/m}^3$, $\sigma = 0.073 \text{ N/m}$, $\mu_L = 1.037 \times 10^{-3} \text{ Pa.s}$) at a temperature of 26°C with Single-, Double- and triple impeller configurations. The schematic diagrams of all the used impeller are shown in Figure 3.7 and Figure 3.8 respectively.

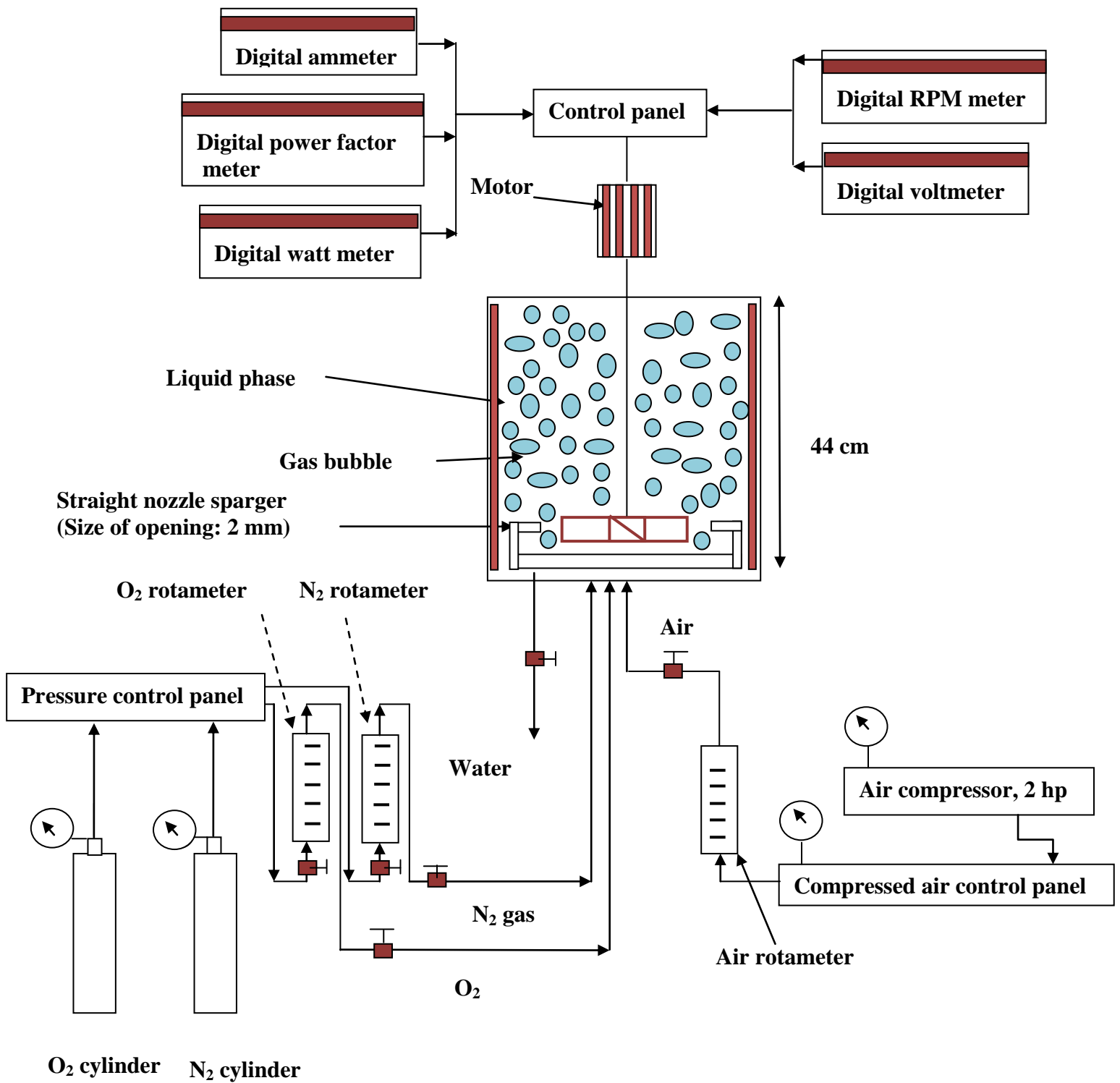


Figure 3.3 Schematic diagram of experimental setup of stirred bubble column.

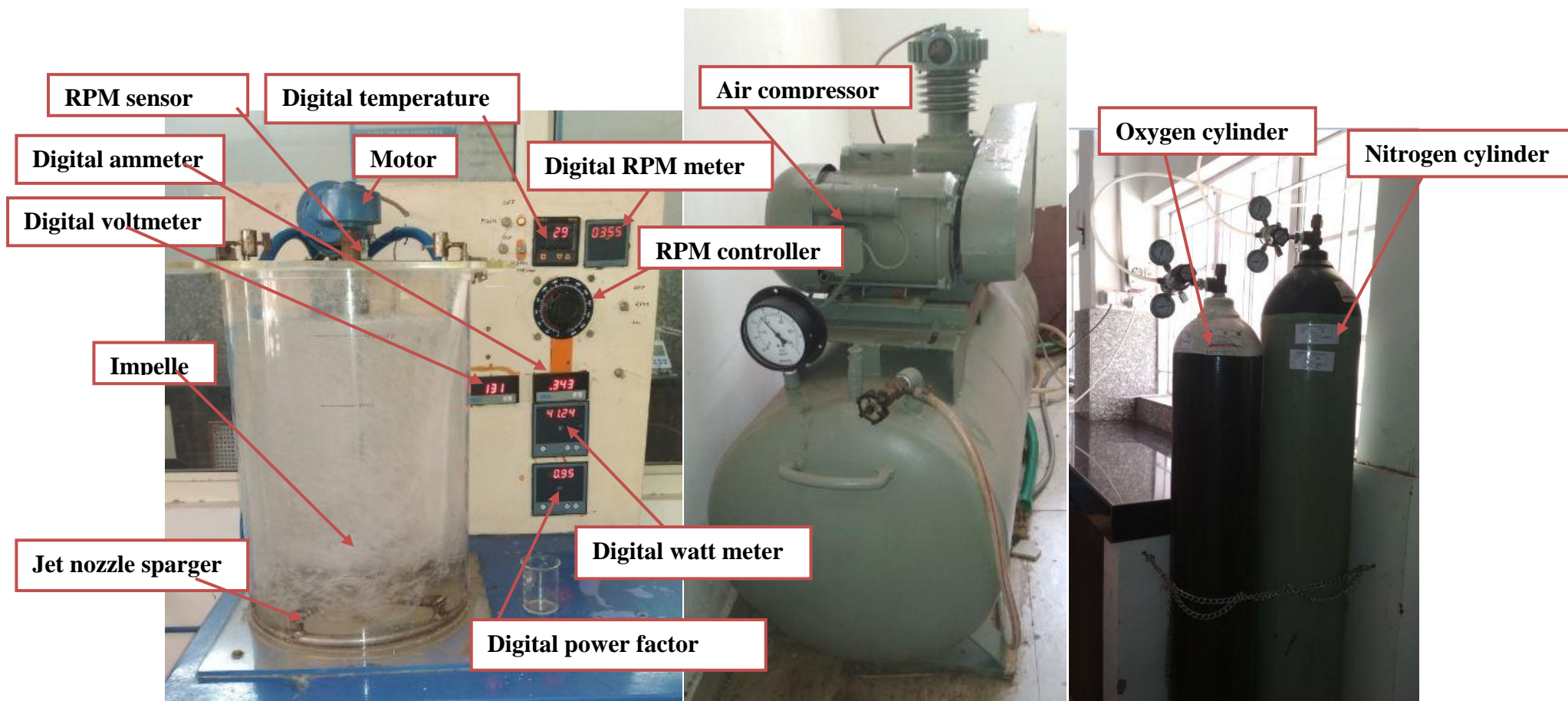


Figure 3.4 Photographic image of experimental setup of stirred bubble column.

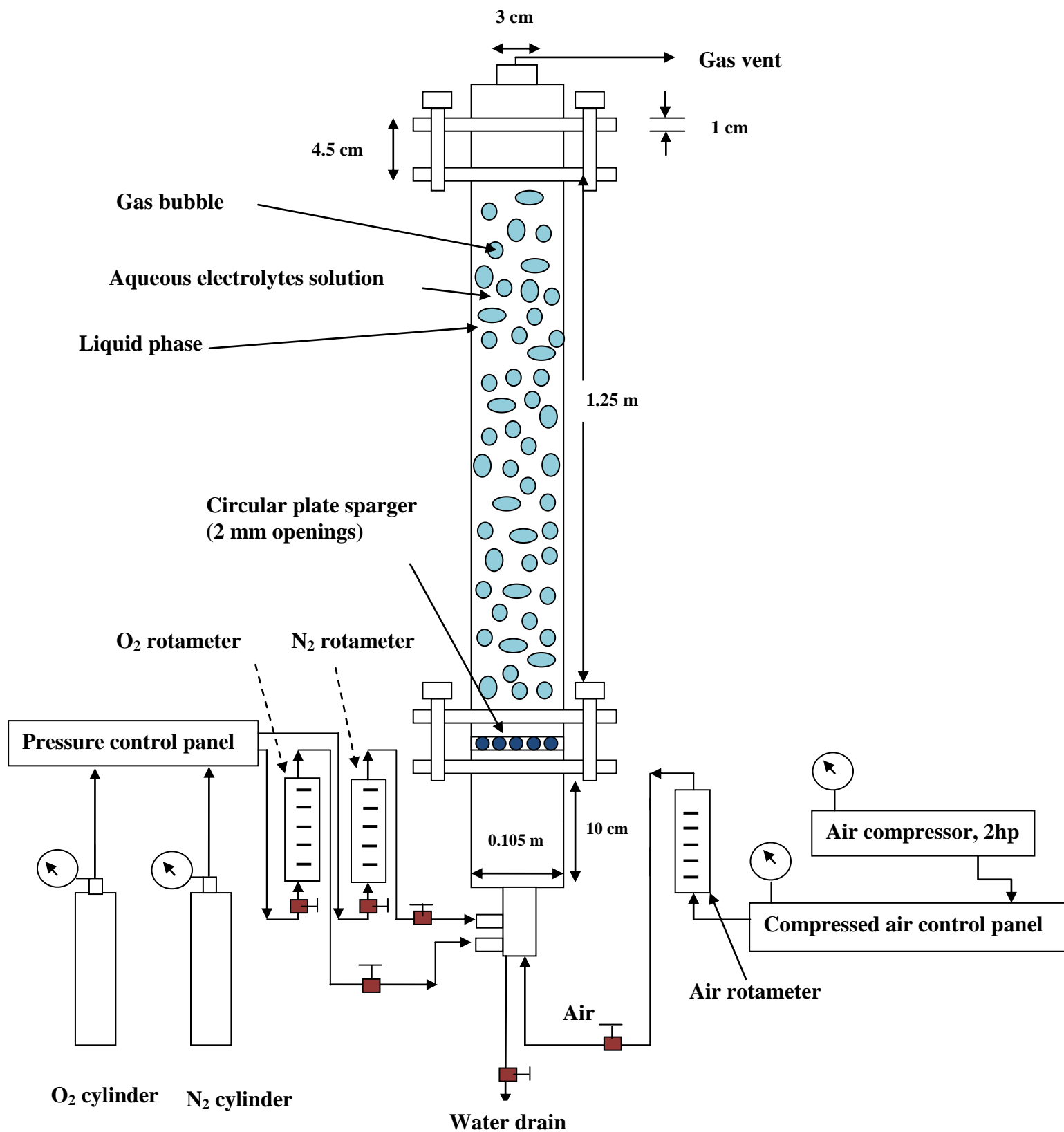


Figure 3.5 Schematic diagram of bubble column experimental setup.

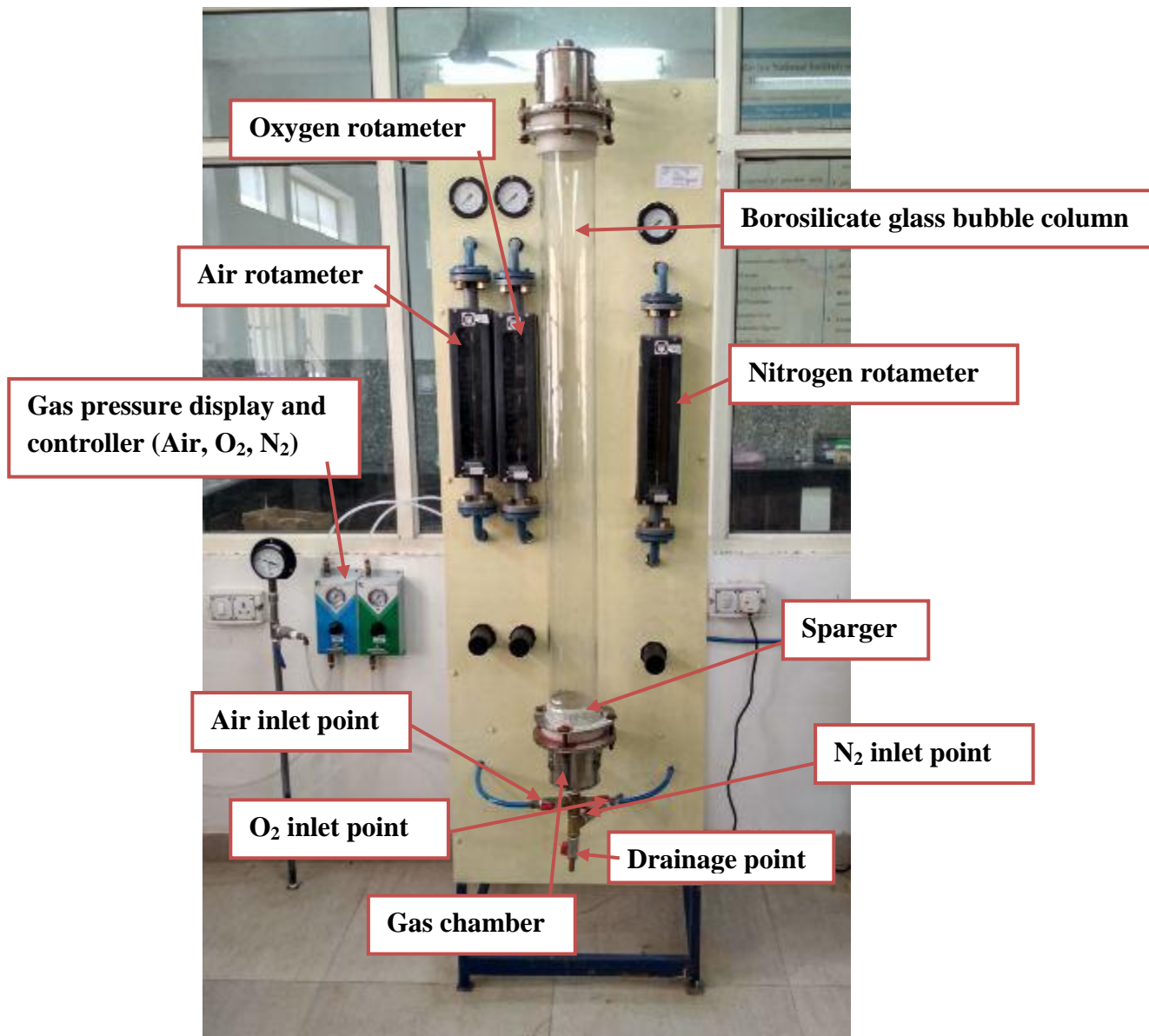


Figure 3.6 Photographic image of experimental setup of bubble column

Table 3.5 Dimensions of Rushton turbine (RT), Concave-blade impeller and Pitch blade turbine (PBT).

Impeller	Rushton turbine (RT)	Concave-blade impeller	Pitch blade turbine (PBT)
MOC	SS316	SS316	SS316
Impeller diameter (cm)	14	14	11.5
Disc diameter (cm)	10	10	–
Disc thickness (mm)	3	3	–
Hub diameter (cm)	2.5	2.5	2.5
Blade width or diameter (cm)	2.0	3.0	2.0
Blade length (cm)	2.5	2.5	4.5
Blade thickness (mm)	3	3	3
Blade curvature (–)	0	0.177, 0.243, 0.309, 0.375, 0.441	0
Number of blades (–)	6	6	4, 6
Shaft length (cm)	43	43	43
Shaft diameter (cm)	1	1	1
Blade angle	45°, 90°	0	45°

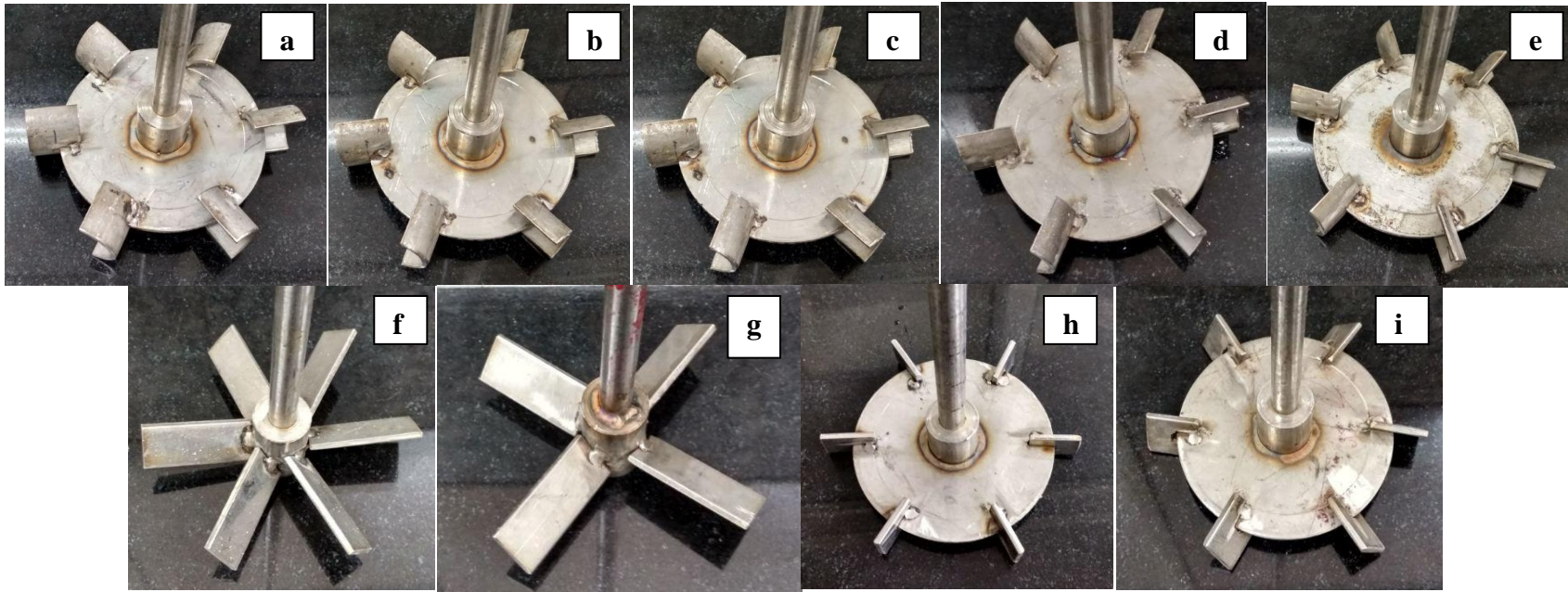
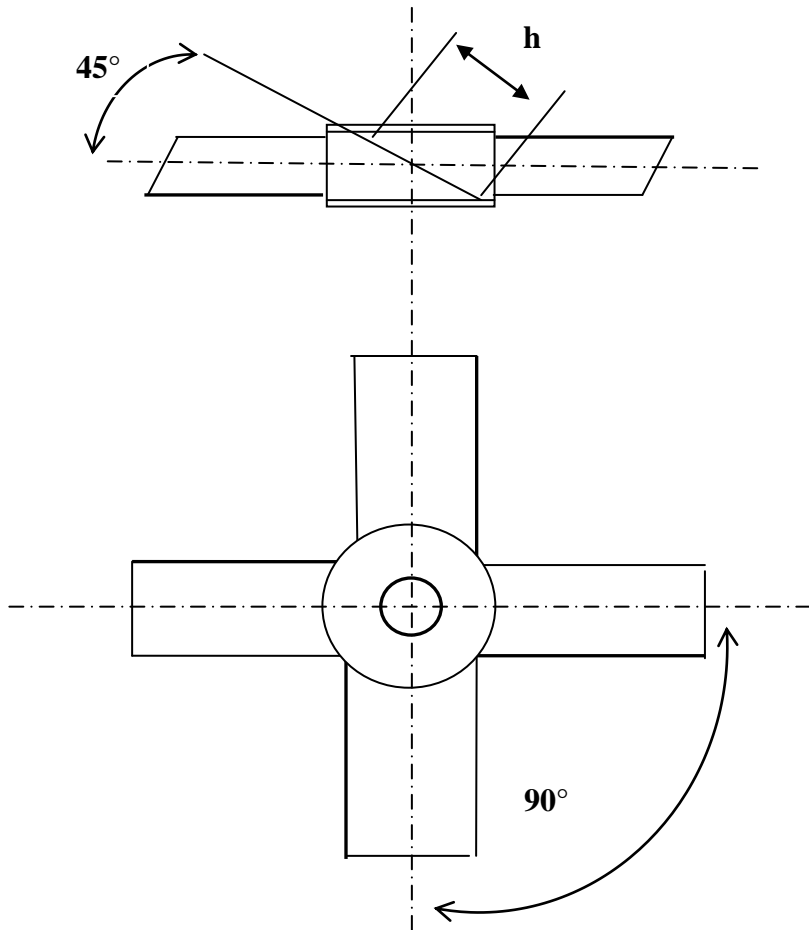
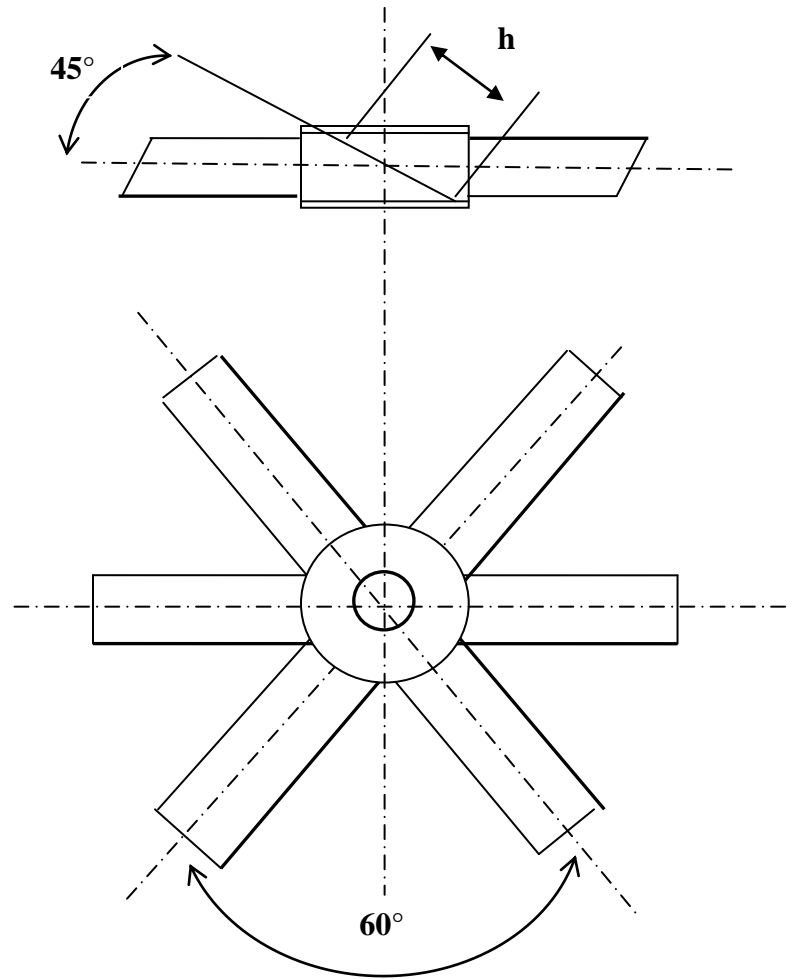


Figure 3.7 Images of different types of impellers utilized in this work: (a) to (e) curved blade impellers; (f) and (g) pitch blade impellers; and (h) and (i) Rushton impellers.



(a)



(b)

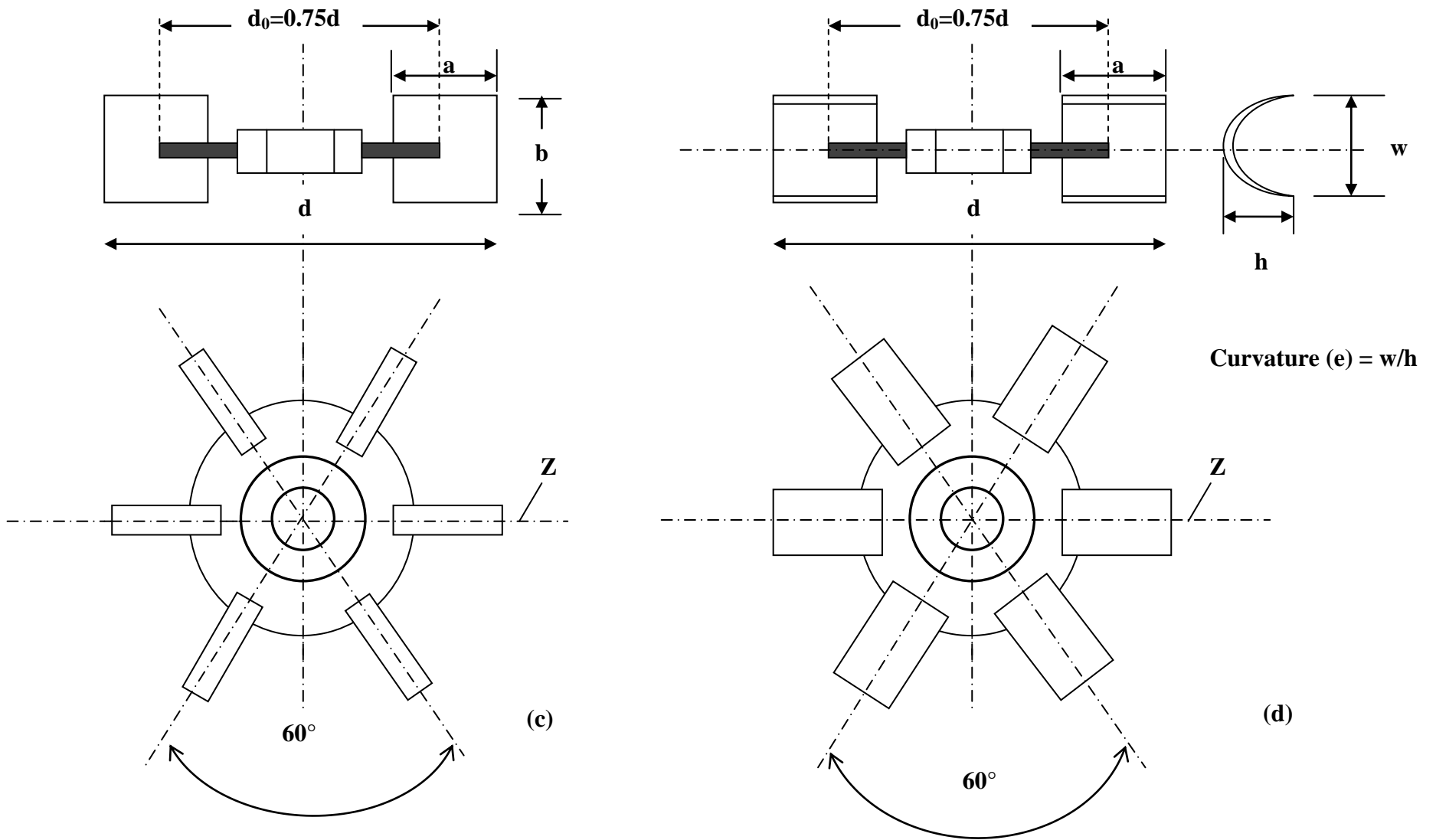


Figure 3.8 Geometrical parameters of the agitator used (a) 4 Pitch blade turbine (4PBT), (b) 6 Pitch blade turbine (6PBT), (c) Rushton turbine (RT), (d) concave blade impeller with different curvature.

3.3.4 Inter-impeller clearance

The spacing between impellers is as an essential factor for designing a dispersion and mixing system resulting in variation of oxygen mass transfer, power consumption and mixing time. For estimation of the mutual interaction between two radial impellers i.e. Rushton impeller on relative power demand which depends on the spacing between them: the clearance between impeller was varied from $0.25d$ to $1.52d$. To study the effect of dual /triple impellers (mounted on common shaft) on relative power demand, the bottom-impeller clearance was kept $D/3$, while the inter-impeller clearance was equal to the diameter of impeller (d). The bottom impeller clearance was equal to $D/3$, as it is very often used in industry and its variation in the bottom impeller clearance has weak or negligible effect on power input as shown by Cui et al. (1996). For dual Rushton impeller system, In order to detect the shifting of cavity formation during varying inter-impeller clearance for double stage impeller agitated gas-liquid contactor were identified by visual observations. The schematic diagram of clearance between impellers in stirred agitated system is shown in Figure 3.9.

3.3.5 Sparger types and design for bubble column

Sparger is the most important part of a bubble column as it determines the bubble size/rise velocity distribution. Inappropriate selection of sparger design dominates the performance of the bubble column. However, systematic route for the selection of sparger design and type are not available in the published literature. Design and operational problems such weeping, may arise due to inappropriate selection of the type/or the design of sparger. It is always desirable to ensure the uniformity of bubble sparging and no weeping conditions occurs (Kulkarni and Joshi 2011a, b).

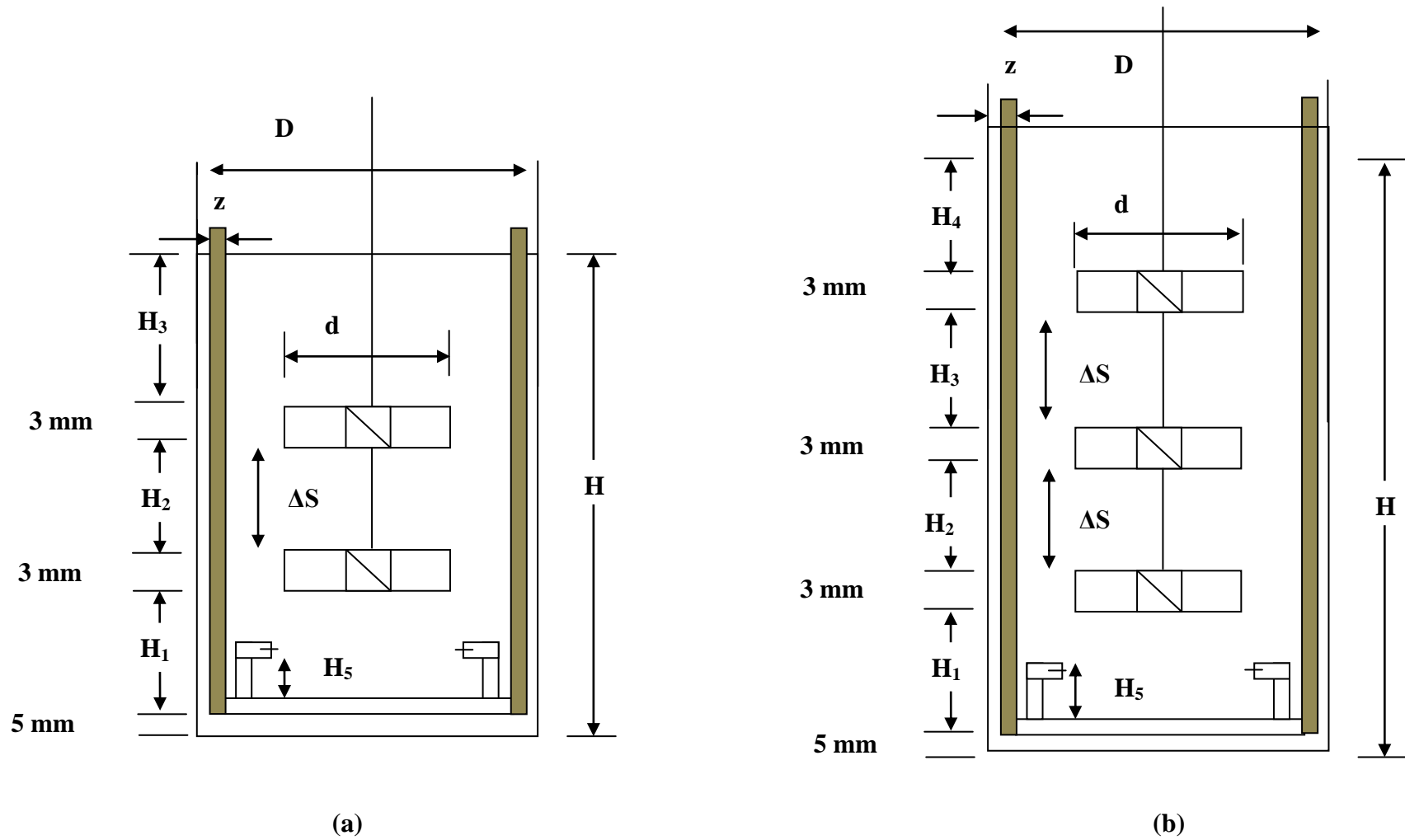


Figure 3.9 Double and triple impeller configurations with inter impeller clearance in a stirred tank equipped with (a) Dual impeller system ($\Delta S = 0.25d - 1.52d$), (b) triple impeller system ($\Delta S = d$).

3.3.5.1 Spargers for a stirred bubble column

Four jet nozzles of various lengths with orifices of 2 mm dia. made of brass ware connected to the circular ring (SS316) which has a ring diameter of 0.28 m and located at a distance of $0.24 D_T$ from the bottom of the vessel to generate smaller air bubbles. For uniformity of gas distribution in the ring, air/gas entry is provided at diametrical opposite two points. The specifications of jet nozzles attached to the circular ring are presented in Table 3.6. The jet nozzle was so designed that all the holes of the sparger should be effective over the range of gas velocities covered in this work. The schematic diagram of jet nozzles attached with circular ring and its arrangement of jet nozzles is shown in Figures 3.10 and Figures 3.11 respectively.

Multiple ring spargers (SS316) with gas entry from two ends were used to enhance volumetric mass transfer coefficient in a stirred bubble column system. Multiple ring spargers consist of two concentric circular ring with 28 cm diameter outer ring and 14 cm diameter inner ring having 142 holes of 2.5 mm hole dia. which provide large number of bubble of uniform size. The detailed specifications of multiple ring sparger are presented in Table 3.7. The schematic diagrams of multiple ring spargers are shown in Figures 3.12, and Figure 3.13 respectively.

Table 3.6 Specifications of jet nozzles of different lengths connected to the ring sparger

Parameter	Specifications
MOC (sparger)	SS316
MOC (nozzle)	Brass
Outer ring sparger diameter (cm)	28
Ring sparger tube diameter, (cm)	1.8
Jet nozzle diameter (mm)	2
Jet nozzle length (cm)	4, 5, 6, 7, 8, and 9
Jet nozzle connection points at the ring	4
Unchanging length of jet nozzle provided at ring (cm)	1
diameter of gas inlet points on ring (cm)	1.2

Table 3.7 Specifications of the multiple ring sparger.

Parameter	Specifications
MOC	SS316
Outer ring sparger diameter (cm)	28
Inner ring sparger diameter (cm)	14
Ring Sparger tube diameter (cm)	1.8
Number of holes in sparger	142
Gas inlet point diameter (cm)	1.2
Connected bridge distance (cm)	5.5
Diameter of a sparger hole (mm)	2.5
Effective area of sparger	95 (approximate)

3.3.5.2 Sparger for a bubble column

The design and performance of perforated (sieve) plate sparger depends upon number and orientation of holes, dimension of gas chamber below the perforated plate and location of gas inlet point in gas chamber. The size of the gas chamber and the location of gas inlet are selected in such a way that the gas is uniformly distributed over all the holes. In the present work, a perforated nylon circular disc containing 69 orifices with a hole diameter of 2 mm (“coarse” sparger) each arranged in a quadrangular pattern with a pitch of 10 mm was placed at the bottom of the column and it was used as sparger. The free area of the disc (a_f) was 96.93%. To ensure uniform distribution of gas in the bubble column, the gas distributor was fixed 12 cm above the air inlet. Gas holdup of a bubble column is strongly influenced by the sparger design. “Coarse gas spargers” produce the “pseudo-homogeneous” flow regimes, resulting in monotonic gas holdup curves that are concave in shape. (Sarrafı et al. 1999; Ruzicka et al. 2003; Ribeiro and Mewes 2007). The schematic diagram of perforated (sieve) disc sparger is shown in Figure 3.14.

3.3.6 Baffles

In general, there is a need to reduce energy input cost in the process industries and better performance of bioreactor system. Unbaffled agitated vessels or partially baffled system consume less power than those with full baffles. Two straight cylindrical rods of 1.5 cm

diameter, attached with ring which are act as partial baffles to prevent the tangential circulation of gas flow in the agitation system. The height of straight rod has the same height as that of the vessel.

3.3.7 Operating conditions

Agitation was provided by a 1.4 HP (220-230V) variable speed motor (Remi motor, Mumbai India) with a maximum speed of 500 rpm. The rotational speed was measured using a digital tachometer (Multispan, Model No: RPM2201, Multispan Control Instruments Pvt. Ltd. Delhi, India), with an accuracy within ± 2 rpm. An air compressor (2 HP, Crompton Greaves) was used for injecting air through a control panel to distilled water in a stirred aeration system. The gas flow rates were measured and controlled with the help of a precalibrated rotameter (Model No: CIVF-PG-2, Make: Eureka industrial equipment Pvt. Ltd, Pune, India). To prevent the holes from being blocked by particles, gas was passed through the holes continuously. These experiments were performed at different impeller speeds varying from 250 to 400 rpm with incremental changes in the gas flow rate from 12.5–22.5 L/min. The liquid level in the vessel was measured by the attached measuring scale. Temperature of water was $28 \pm 1^\circ\text{C}$ during the course of experiments and all experiments studies were carried out batch-wise at ambient conditions in lab

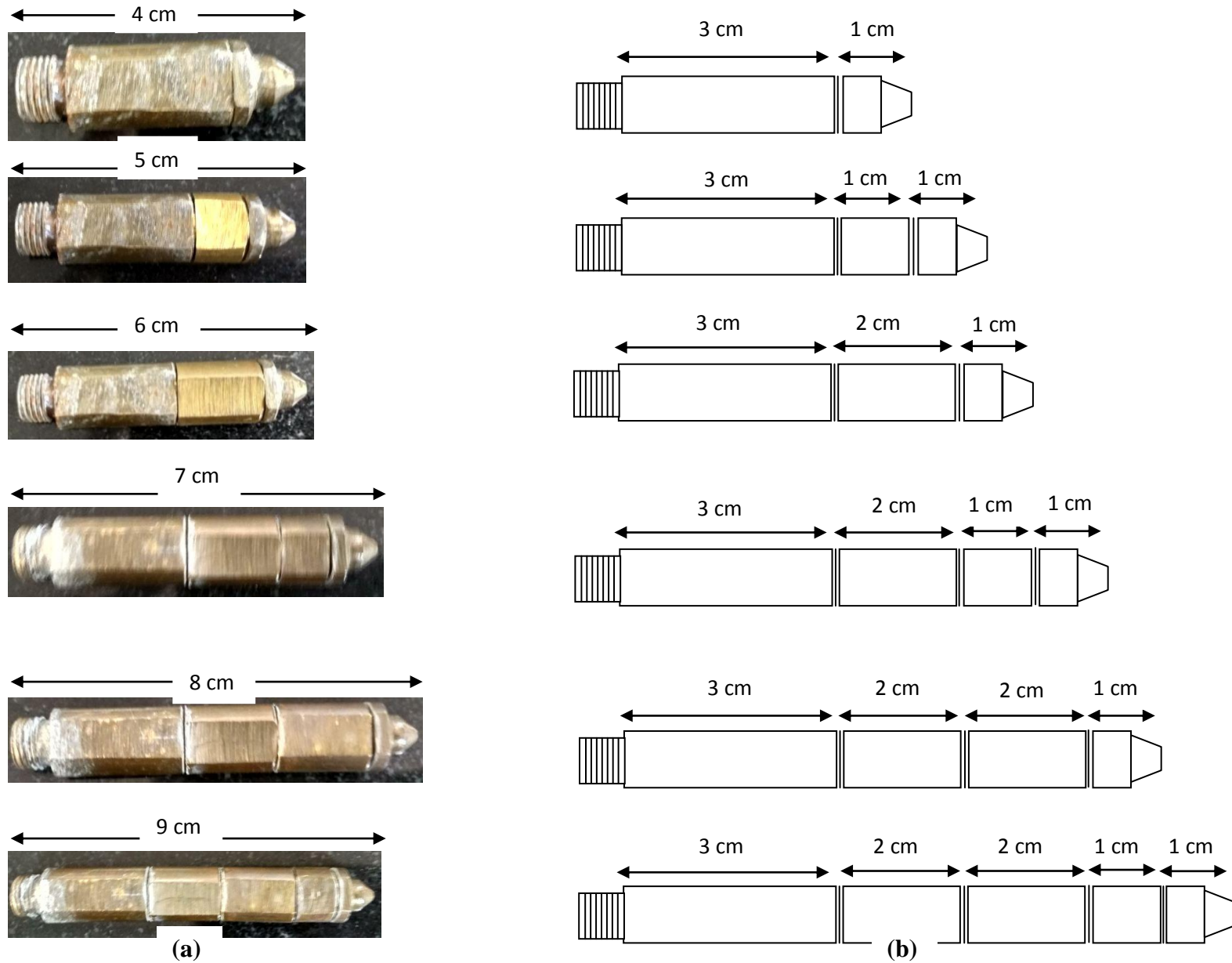


Figure 3.10 Various types of jet nozzle length used in this study (a) Image of jet nozzle (b) Dimension of jet nozzle

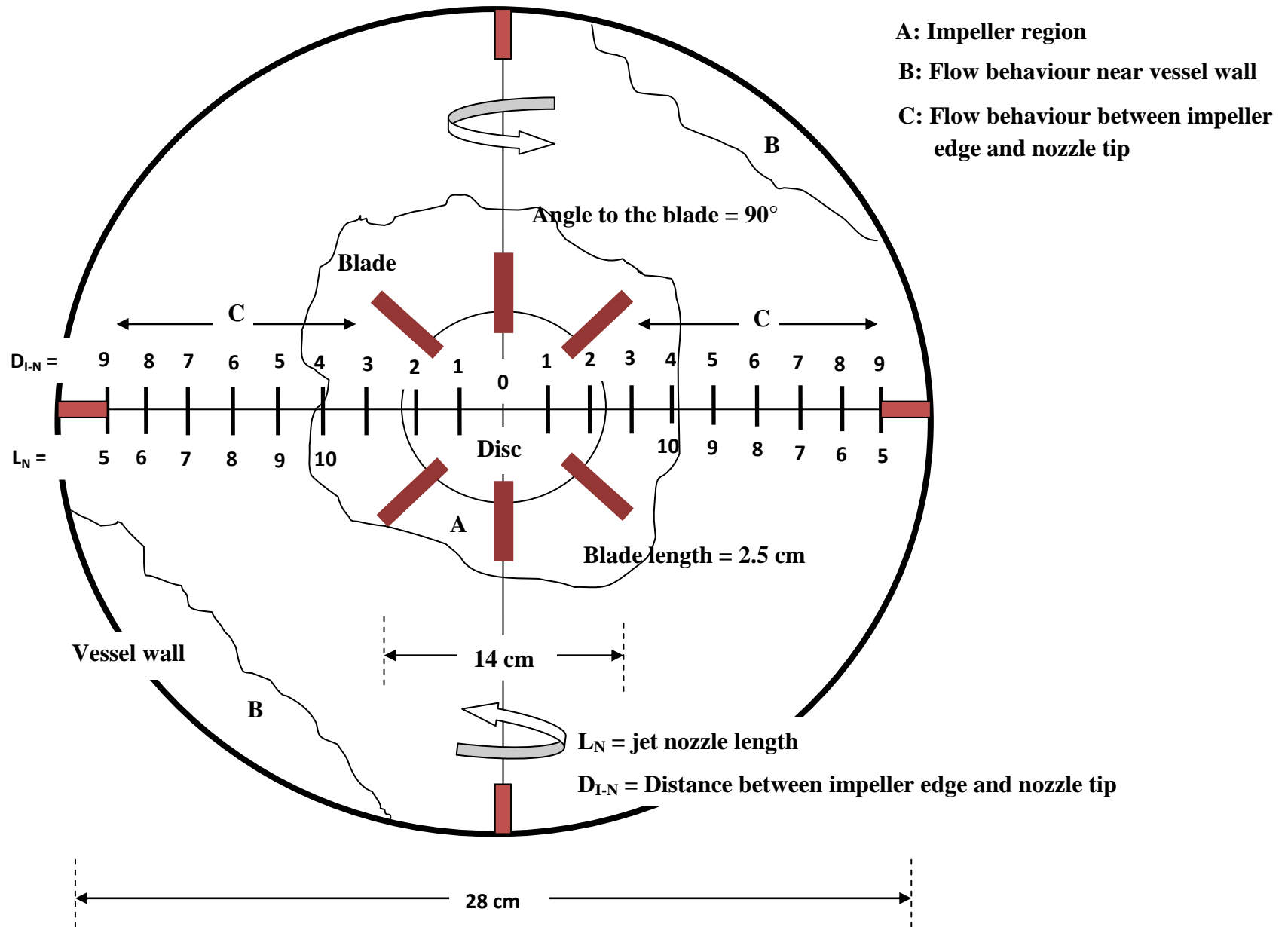


Figure 3.11 Arrangement of jet nozzles connected to the circular ring.

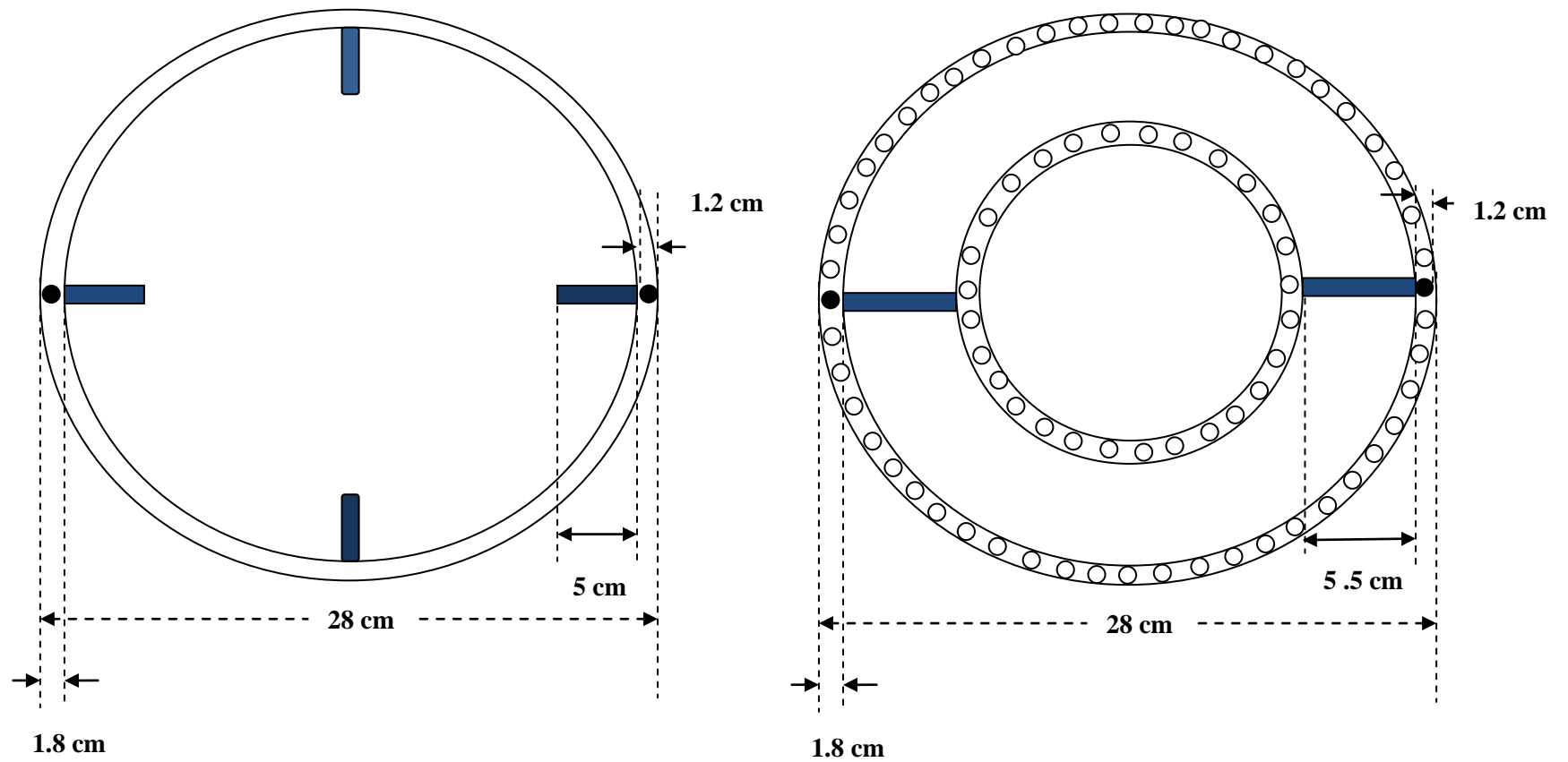


Figure 3.12 Geometrical parameters of the sparger used (a) jet nozzle, (b) ring sparger.

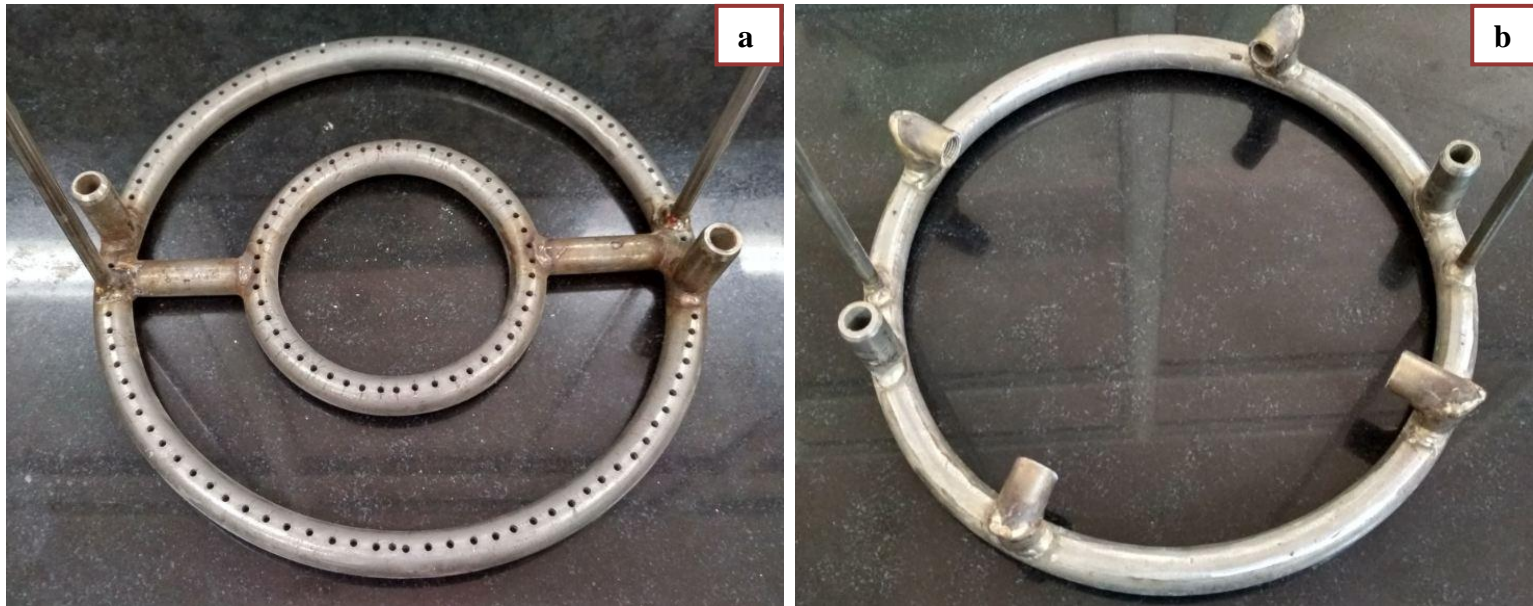


Figure 3.13 Actual schematic view of different types of sparger utilized in this work: (a) ring sparger of 2.5 mm hole diameter (b) jet nozzle attached with ring.

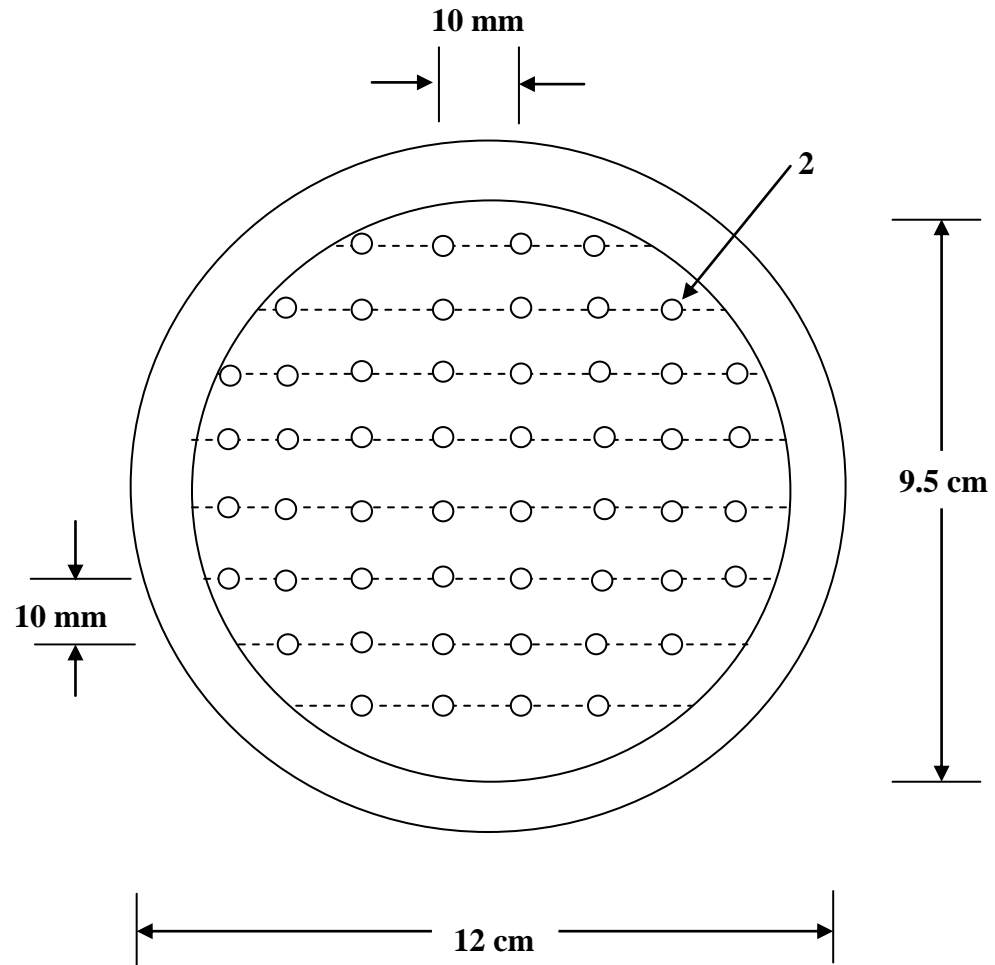


Figure 3.14 Schematic diagram of perforated nylon circular disc sparger.

3.4 Power consumption measurement

The cost of process industry products depends on the power consumption utilized in the system. It is essential to understand the hydrodynamic and mass transfer mechanisms to ensure optimum productivity of the product at optimized power consumption conditions. The stirred bubble column system equipped with the previously described impellers driven by a 1.4 HP (220-230V) motor in aerated and non-aerated condition was used to assess power consumption. Before investigating the power consumption of multiple impellers, the power consumption of single impeller was examined in terms of power number. Power consumption in an agitation system was measured in terms of electrical power input given directly to the motor through wattmeters and ammeters (Brown, 1997). The methodology reported by various authors (Shewale and Pandit 2006; Rao and Kumar 2007; Devi and Kumar 2014; Devi and Kumar 2017) was used for estimation of power consumption using the electrical power input methods in AC/DC motor employed in an agitation system. The intensity of current (I) and voltage (V) of the power supply given to the AC motor of the aerator were individually measured by a digital ammeter (Model No. SMP35S, Make: Meco Instruments Pvt. Ltd., Navi Mumbai, India) and digital voltmeter (MECO, Model No. SMP35S, Meco Instruments Pvt. Ltd., Navi Mumbai, India). Input voltage to motor oscillates between positive and negative values; therefore, the current cannot be kept constant by circuit impediment. If the current is measured as in direct current motors, an 'apparent current' is obtained. Therefore, the true power draw can be measured only by a wattmeter. Power in watts was calculated by multiplying $V \times I$ by a power factor. The ratio of true power to apparent power is known as the power factor. Most electrical motors work under low power factors for low loads and under values of 0.8–0.9 for full load (Brown, 1997; Nienow et al., 1994). Usually the power factor at full load is a technical specification of the motor. However, one of the main difficulties is the calculation of the power factor for different loads. The value of power factor was measured directly by a digital power factor meter (Multispan, Model No. PF11, Make: Multispan Control Instruments Pvt. Ltd. Delhi, India). In laboratory-scale stirred bubble column, losses occurring in the agitation system can be very important and accountable. Later, a correction was made by considering the 85–98% efficiency of the motor depending upon impeller speed. Another parameter to consider is the efficiency of the motor, which relates the output power to the input power. The manufacturer usually specifies how the efficiency factor varies according with the load (Nienow et al., 1994).

Agitation in stirred gas– liquid system was provided by a 1.0 kW (220-230V) single -phase direct current motors (Make: Remi Motor, Mumbai, India) with a maximum speed of 500 rpm. Following expression was utilized for estimating the impeller power consumption:

$$P_{\text{out}} = VI \cos \theta . \eta$$

where,

P_{out} = Impeller power consumption, W

$\cos \theta$ = Power factor (0.8 to 0.9)

V = Voltage of the power supply, V

I = Intensity of current, A

η = Efficiency of the motor depending upon impeller speed (85 – 95%)

The power factor varied only within a narrow range of ± 0.05 . The effective power consumed in the bulk agitation of a liquid is the difference between impeller power consumption measured at the experimental conditions and that measured at the same impeller speed, but in the absence of water.

Multiple impeller system

The mean specific power, $\overline{P_j^n}$ of n impellers in a liquid volume ($V_L = 0.0265 \text{ m}^3$) under both gassed ($j = g$) and ungassed ($j = 0$) conditions were calculated from the total power input of n impellers ($n = 1, 2, 3$) on a common shaft (Fujasova et al. 2007; Linek et al. 2012; Labik et al. 2014) :

$$\overline{P_j^n} = \frac{E_{j,imp}^n}{V_L} \quad (n = 1, 2, 3; j = g, 0)$$

Under gassed and ungassed conditions, the power number ($P_{ug,i}$ and $P_{g,i}$) for an impeller situated in stage i was calculated as follows:

$$N_{g,i}^P = \frac{P_{g,i}}{\rho_L N^3 D^5} \quad \text{and} \quad N_{ug,i}^P = \frac{P_{ug,i}}{\rho_L N^3 D^5}$$

3.5 Estimation of volumetric mass transfer coefficient (k_La)

To determine the volumetric mass transfer coefficient (k_La), two techniques are available, i.e. dynamic gassing out method and Sulfide method. In this work, the static gassing out method was used for the determination of volumetric mass transfer coefficient (k_La). The popularity of the gassing out method is due to its simplicity and relative accuracy. At the beginning of the experiment, oxygen present in the liquid (distilled water) was stripped out from water almost completely by injection of pure nitrogen through the gas distributor until O_2 concentration ≈ 0.5 mg/L. Purging with nitrogen is quick and effective procedure to scrub deionized water of dissolved oxygen (Ferreira et al. 2013; Mena et al. 2011). Pure nitrogen was sparged for about 15-25 min at a fixed nitrogen flow rate of 20 L/m. Purging for longer periods will not further reduce the oxygen concentration. When all the oxygen has been stripped out, air was sparged into the column and the oxygen uptake into the liquid phase was monitored continuously by means of the oxygen sensor (Model: HI764080, make: Hanna instruments). All the oxygen mass transfer experiments were conducted with distilled water (i.e., without dissolved electrolytes). A total measuring time of 210 min was used for each experiment. At this moment, the oxygen transfer process from bubbles to the liquid in order to almost reach the oxygen saturation concentration, $C_{O_2}^*$. Due to the strong dependence of the oxygen concentration at the equilibrium $C_{O_2}^*$ with respect to temperature, thermometers (Model no. TC203, make: SELEC Controls Pvt. Ltd., Mumbai, India) were used to correct $C_{O_2}^*$ at the beginning of each experiment. All the experiments were carried out at $30 \text{ }^\circ\text{C} \pm 1^\circ\text{C}$.

Oxygen mass transfer coefficient calculation utilizes the two- film theory of Lewis and Whitman (1974), where all resistances to the oxygen mass transfer have been considered to be concentrated in the liquid film while gas film resistance is ignored. The mass balance of dissolved-oxygen in a bubble column leads to the following relation:

$$\frac{dC_{O_2}}{dt} = k_La (C_{O_2}^* - C_{O_2}) \quad (3.1)$$

where, a is the interfacial area per unit volume of dispersion, k_La is the volumetric mass transfer coefficient, C_{O_2} is the dissolved-oxygen concentration in the liquid bulk and t represents the time.

Using initial (For $t = 0, C = C_0$) and final conditions ($t \rightarrow \infty, C = C_{O_2}^*$) equation (3.1) written as-

$$\frac{C(t) - C_0}{C_{O_2}^* - C_0} = 1 - \exp(-k_L a t) \quad (3.2)$$

Characteristically, dissolved oxygen concentration during the aeration has two distinguished zones, one with an intense mass transfer zone where the oxygen concentration rises quickly and other close to the saturation, when the mass transfer rate starts to decline. The solubility of oxygen at different temperatures in water was taken from the literature (Metcalf & Eddy, 2005). The total run times of experimental runs were 120 min and 210 min respectively. 120 min run was with concave blade impeller with different curvature and 210 min was with Rushton impeller. Sampling duration was 5 min in beginning up to 15 min (intense mass transfer period) and 15 min thereafter upto the end of the experimental runs. For $k_L a$ determination, experimental data of variation in dissolved oxygen concentration with air flow sparged in a stirred bubble column monitored with time and subsequently concentration gradient method (eq.3.2) was used (Metcalf & Eddy 2005).

3.6 Estimation of overall gas holdup

Overall gas holdup is one of the most important parameters characterizing the hydrodynamics of the bubble column. Gas holdup depends mainly on gas flow rate, physical properties of the liquid and type of the gas sparger. It can be defined as fractional volume of the gas in two or three-phase mixture in the column. Overall gas holdup was measured using bed expansion method (Kazakis et al. 2007). Gas holdup is the immediate increase in the dispersion height of liquid due to the macrobubbles during gas sparging in the system. As the sparging continues, the concentration of microbubble as well as sub-microbubbles (tiny bubbles) in the liquid progressively increased. This caused the liquid height to increase with time, which eventually attained a stable dispersion height. At this moment, the rate of generation of tiny bubbles was equal to the rate of disappearance. Most of the macrobubbles (large bubbles) disappeared from the system within an approximate time range of 45 to 60 s. At this moment, the dispersion consisted of microbubbles as well as sub-microbubble (tiny bubble) and its stabilized height was noted.

Bubbling height related to each individual gas velocity was noted after a stabilization period of 5 min and it was used to compute the corresponding gas holdup. All gas holdup measurements

were done in bubble column. The static height of liquid column was kept 30 cm in all experimental runs and the dynamic height of gas–liquid dispersion was measured during sparging of gas in the liquid column. Therefore, the overall gas holdup was calculated by ratio of the change in the bubbling liquid height, and that of the quiescent liquid height, using the following relation (Kazakis et al. 2007):

$$\varepsilon(u_G) = \frac{H_d(u_G) - H_s}{H_d(u_G)} \quad (3.3)$$

where, H_d is the dispersion height of the bed and H_s is the static height of the ungasged liquid in the column. Overall gas holdup measurement by visual observation of bed expansion generally exhibit, an uncertainty arising from strongly fluctuating dynamic height. In order to reduce the error associated with the visual observations of fluctuating dynamic height, average gas holdup was estimated by averaging the aforementioned liquid height differences at five consecutive instances covering a time length of 25 – 30 s for each flow rate of gas. The method of measuring liquid height difference in two different conditions (prior and after gas injection) reported earlier in literature is shown in Figure 3.15 (Kazakis et al. 2007).

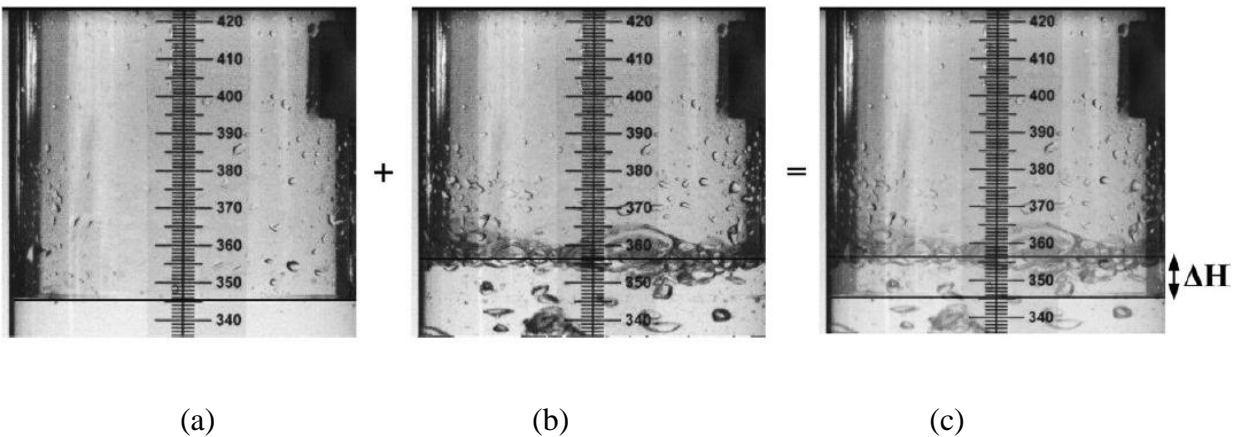


Figure 3.15 Bed expansion method (Kazakis et al. 2007) for gas holdup measurement (a) before air supply (b) after air injection and (c) after superimposing the images (a) and (b). Reproduced from Kazakis et al. (2007) with permission from Elsevier.

In the present study, gas holdup enhancement (Bed expansion method) was used for bubble coalescence inhibition. Gas holdup measurement can be conveniently measured with a reasonable accuracy. On the other hand, limitations of other techniques for studying bubble

coalescence inhibition such as thin film balance and bubble pair have already been outlined in literature (Wang et al. 2016). Use of another technique viz. microfluidics is limited due to the requirement of precise measurement of small quantity of fluids or liquid and gas needing precision measurement instruments. In view of their widespread use in process industries for bubble coalescence inhibition and other purposes due to low cost and efficiency, four electrolytes were selected to study their potential to suppress bubble coalescence moderately or strongly as the case may be.

3.7 Electrolytes used in the study

In the present work, four inorganic electrolytes (NaCl, $\text{MgSO}_4 \cdot 7\text{H}_2\text{O}$, $\text{CaCl}_2 \cdot 2\text{H}_2\text{O}$, and Na_2SO_4) were used in the experimental study. All of these electrolytes are strong electrolytes, i.e. they completely dissociate in solution and the solution will contain only ions and no molecules of the electrolyte. Depending on their effect on bubble coalescence, the electrolytes used in the present study can normally be classified into two categories, namely strongly significant effect and moderate effect. The first two electrolytes (NaCl and $\text{MgSO}_4 \cdot 7\text{H}_2\text{O}$) suppress bubble coalescence moderately, while, the remaining two (Na_2SO_4 , and $\text{CaCl}_2 \cdot 2\text{H}_2\text{O}$) to suppress bubble coalescence very strongly (Ribeiro and Mewes, 2007; Syeda and Reza 2011). Three electrolytes ($\text{CaCl}_2 \cdot 2\text{H}_2\text{O}$, Na_2SO_4 , and $\text{MgSO}_4 \cdot 7\text{H}_2\text{O}$) were supplied by Loba Chemie Pvt. Ltd., Mumbai, India, while NaCl was obtained from Rankem (RFCL Limited New Delhi, India.) Details of properties of electrolytes are summarized in Table 3.8. The electrolytes used were of analytical reagent grade and their purity was greater than 99%. Distilled water (surface tension: 72.14 ± 0.3 mN/m at 28 °C, and electrical conductivity: 200 ± 0.1 $\mu\text{S/m}$) was used to prepare the aqueous solution of electrolytes. The properties of aqueous solutions such as surface tension, density, conductivity, and pH were measured in our departmental laboratory. The solubility of oxygen is affected by the presence of electrolytes in the liquid (Narita et al. 1983). The density of each sample was also measured by density meter (Make: Kruss, Germany, Model No. DS 7800,). The accuracy of density meter used was $\pm 0.0001\text{g/cm}^3$. Electrical conductivity of aqueous solutions of electrolytes and pH were measured simultaneously by electrical conductivity and pH meter (Make: Hanna Instruments, Model No. HI5522). For proper dispersion of electrolytes in distilled water, magnetic stirrer (Make: Remi Laboratory instruments, Mumbai India, Model No. 1 MLH,) was used for 5 min for each sample. Details

properties of aqueous solutions of electrolytes used in the present study at 29 ± 1 °C are presented in Table 3.9.

Table 3.8 Properties of electrolytes.

Electrolyte	Molar mass (g mol⁻¹)	Cation	Anion	Solubility in water at 20 ° C (g L⁻¹)	Purity^{a, b}	Make
NaCl	58.44	Na ⁺	Cl ⁻	358	99.9 % ^a	Rankem ^a
MgSO ₄	246.47	Mg ²⁺	SO ₄ ²⁻	300	99.5% ^b	Loba Chemie ^b
Na ₂ SO ₄	142.04	Na ⁺	SO ₄ ²⁻	200	99.0% ^b	Loba Chemie ^b
CaCl ₂	147.01	Ca ²⁺	Cl ⁻	740	99.0% ^b	Loba Chemie ^b

^a RFCL Limited New Delhi, India

^b Loba Chemie Private Limited, Mumbai, India

Table 3.9 Properties of aqueous electrolytes solutions used in the experiments.

Conc. (mol/L)	Electrolyte															
	NaCl				MgSO ₄ ·7H ₂ O				Na ₂ SO ₄				CaCl ₂ ·2H ₂ O			
	σ_{aqueous} (mN/m)	ρ_{aqueous} g/cm ³	ψ_{aqueous} μS/cm	pH	σ_{aqueous} (mN/m)	ρ_{aqueous} g/cm ³	ψ_{aqueous} μS/cm	pH	σ_{aqueous} (mN/m)	ρ_{aqueous} g/cm ³	ψ_{aqueous} μS/cm	pH	σ_{aqueous} (mN/m)	ρ_{aqueous} g/cm ³	ψ_{aqueous} μS/cm	pH
0.0125	72.79	1.0013	1.523	7.52	72.58	1.0027	1.876	6.99	72.51	1.0022	2.792	7.21	72.339	1.0024	2.826	6.39
0.0187	72.87	1.0021	2.014	7.54	72.65	1.0031	2.261	7.13	72.64	1.0032	3.641	7.18	72.472	1.0030	3.451	6.48
0.025	72.99	1.0029	3.008	7.57	72.81	1.0036	3.254	7.14	72.88	1.0041	4.963	7.06	72.936	1.0034	5.105	6.50
0.0375	73.11	1.0032	5.114	7.51	73.14	1.0054	4.179	7.11	73.24	1.0053	5.447	7.10	73.2	1.0041	7.114	6.47
0.05	73.26	1.0038	7.142	7.55	73.57	1.0074	5.562	7.12	73.58	1.0072	8.788	6.82	73.69	1.0057	9.298	6.46
0.075	73.88	1.0044	8.105	7.56	73.6	1.0113	7.458	7.13	74.02	1.0098	9.154	6.92	74.66	1.0071	13.65	6.51
0.10	74.28	1.0052	9.862	7.51	73.66	1.0146	9.336	7.13	74.24	1.0133	15.13	6.81	75.26	1.0097	17.30	6.56
0.15	74.53	1.0072	14.14	7.53	73.68	1.0191	12.78	7.15	74.79	1.0199	22.01	6.75	76.02	1.0140	25.74	6.69
0.20	74.66	1.0099	19.09	7.50	73.7	1.0249	15.93	6.97	75.06	1.0255	27.79	7.01	75.98	1.0186	32.57	6.70
0.25	74.67	1.0113	23.15	7.51	73.7	1.0307	18.89	6.92	75.10	1.0324	33.34	6.55	75.88	1.0233	40.79	6.69
0.30	74.62	1.0127	28.12	7.53	73.75	1.0359	21.44	6.94	75.09	1.0387	38.51	6.56	76.03	1.0272	47.65	6.71

4 Model development for Liquid– side mass transfer coefficient

4.1 INTRODUCTION

Complex and diverse requirements of industrial processes warrant development of different types of gas–liquid contactors such as bubble columns and packed columns, etc. Bubble columns are commonly used for the manufacture of industrially important products in chemical, petrochemical and biochemical process industries utilizing two or three phase systems. For optimal design of gas-liquid contactors and bubble columns, understanding of gas–liquid mass transfer phenomena caused by interfacial fluctuations are of crucial importance. Reliable values of the volumetric liquid–phase mass transfer coefficient $k_L a$ cannot be obtained, if liquid–side mass transfer coefficient, k_L , and interfacial area, a , are not accurately determined. The capability of proposed model has been examined using secondary data for a slurry system with a large range of operating conditions ($T = 298 - 423$ K; $P = 1 - 3.0$ MPa; $U_g = 0.035 - 9.38$ m/s and $C_s = 0 - 20\%$ by mass) (Jin et al 2014). Despite all efforts, knowledge about the effects of solids on liquid side mass transfer coefficient k_L and the physical dimensions of liquid film (liquid film thicknesses δ) has not yet been reported in literature. Such information is important for determining the precise mass transfer rate in gas-liquid/ slurry bubble column systems.

The design, modeling, optimization and scale–up of gas – liquid/ slurry bubble columns require precise knowledge of hydrodynamic as well as mass and heat transfer parameters. The main goal of this chapter is to propose a reliable macroscopic model for prediction of mass transfer coefficient k_L which is based on unsteady–state liquid film fluctuations by micro-eddies (liquid elements) in gas – liquid/ slurry bubble columns. Bubble columns are generally operated at steady state; however, gas mass transfer in a bubble column takes place through the liquid film present at the bubble surface, which is brought about by microeddies present at the bubble surface. The microeddies continually expose fresh surface of the liquid film (surface elements) to the diffusing gas. This process is dynamic. Hence, an unsteady state model was employed. The time scale of surface renewal rate S for the estimation of k_L has been taken as $0 - 10$ s⁻¹ as reported in literature (Zhao et al. 2003).

The analytical solution of model equation was obtained by Laplace transformation using the Danckwerts' age distribution function for the surface renewal rate as a variable. Furthermore, the mathematical model is able to predict overall mass transfer coefficient in a gas-liquid/ slurry bubble column, if the distribution of bubble sizes is known. The validity of prediction of overall k_L from proposed model has been examined using experimental data reported in literature for a slurry system with a wide range of operating conditions generally encountered in industrial bubble columns (Jin et al. 2014). The effects of the model parameters such as surface renewal rate S and thickness of liquid film δ on overall mass transfer coefficient k_L were simulated. In addition, empirical correlations for estimation of liquid film thickness δ for H_2 , CO and CO_2 in slurry system (liquid paraffin–quartz sand) have been proposed in terms of dimensional groups.

4.2 Macroscopic model for gas – liquid mass transfer considering single spherical bubble

Bubble column reactors have been widely used in chemical and biochemical industries. In bubble columns, size, shape and operating / physical properties of gas and liquid are the most important parameters governing their performance. To obtain higher efficiency of the gas mass transfer, homogeneous bubbles of gas are generated at each hole of the gas sparger, which rise along the column. A schematic diagram of unsteady–state gas mass transfer through liquid film of a spherical bubble is depicted in Figure 4.1. One of the salient features of the present model is that it can be easily solved without using complex computational tools. In the analytical solution presented here, liquid phase in bubble column is considered in batch mode and gas phase in continuous mode.

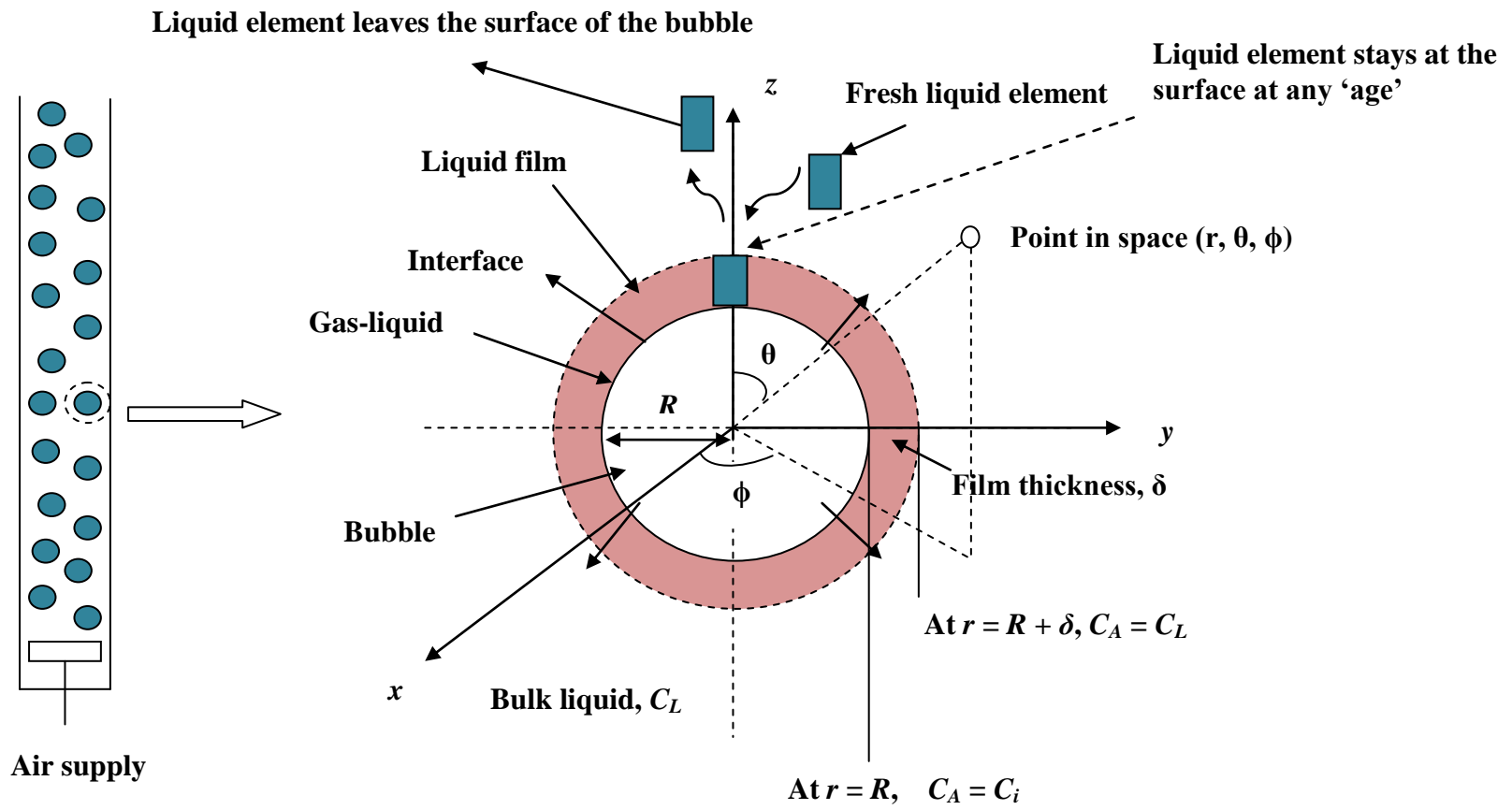


Figure 4.1 Mechanism of transient mass transfer through liquid film and surface renewal by liquid element on a spherical bubble.

4.3 Hypotheses for model development

For modeling purposes, a three-phase system can be treated same as that of a two phase (gas – liquid) system (Zhao et al. 2003). To develop an unsteady-state single liquid film model, following assumptions have been made:

- (i) In gas bubble liquid systems, liquid phase mass transfer resistance is a controlling factor (Garcia-Ochon and Gomez 2004). Therefore, it has been assumed that entire mass transfer resistance exists in the liquid film.
- (ii) Viscosity of liquid in a bubble column has been assumed to be low due to lower concentration of solids in liquid which can be treated in the same way as that of a gas-liquid system (Zhao et al. 2003).
- (iii) In quiescent liquids, gas diffusion occurs only due to molecular diffusion through the liquid film. Therefore, mass transfer has been assumed to be occurring only in r-direction perpendicular to the interface only due to molecular diffusion.
- (iv) As the rate of increase of gas concentration in the liquid bulk is small, it has been assumed that the concentration of gas in the bulk of liquid is constant.
- (v) For simplicity of model, it has been assumed that the bubble eccentricity (e) is unity and its shape is symmetric around its center.
- (vi) In order to formulate a simple model, it has been assumed that interactions between bubbles are negligible.
- (vii) Most of the industrial applications are carried out at higher intensity of turbulence (Thomas 1965). Therefore, it has been assumed that liquid film thickness (δ) is constant and bubble size is stable during the mass transfer process.
- (viii) The total surface area of a gas bubble available to micro eddies for stay at gas – liquid interface as a liquid element at any ‘age’ may belong to any ‘age’ group. The micro eddies will continually expose fresh surface of the newer liquid element to the diffusing component and sweep it away for mixing into the bulk of liquid. It has been assumed that replacement time between two liquid elements is independent of their age and has a distribution of age varying from zero to infinity at any particular instance. Therefore, it has been assumed that the rate of production of fresh surface is constant and is equal to S (surface renewal rate, 1/s) (Treybal 1981; Erkey et al 1990). It has also been assumed that ‘age’ distribution of liquid elements depends on turbulence intensity of the liquid.

- (ix) From Kolmogoroff's theory on isotropic turbulence, eddy length η , depends on kinematic viscosity, ν (m²/s) of the liquid and rate of dissipation of energy per unit mass, ε (W/kg) of liquid according to the following relationship (Lau et al. 2004; Behkish et al. 2007):

$$\eta = (\nu^3/\varepsilon)^{1/4}$$

It has been assumed that the length and width of a liquid eddy are same. If size of bubble is known then total number of liquid eddies can be easily quantified.

Frequent renewal of liquid-side film in the influence of bubble break-up and coalescence results in enhancement of mass transfer rate. Based on the above assumptions, microscopic unsteady-state mass balance of soluble gas in spherical coordinates can be written as follows:

$$\frac{\partial \rho}{\partial t} + \frac{1}{r^2} \frac{\partial}{\partial r} (\rho r^2 v_r) + \frac{1}{r \sin \theta} \frac{\partial}{\partial \theta} (\rho v_\theta \sin \theta) + \frac{1}{r \sin \theta} \frac{\partial}{\partial \phi} (\rho v_\phi) = 0 \quad (4.1)$$

The last two terms of equation 4.1 can be ignored because of negligible molecular diffusion in α and β direction.

$$\frac{\partial \rho}{\partial t} + \frac{1}{r^2} \frac{\partial}{\partial r} (\rho r^2 v_r) = 0 \quad (4.2)$$

Replacing mass density by molar density and $C_A \cdot v_r = N_A$

$$\frac{\partial C_A}{\partial t} + \frac{1}{r^2} \frac{\partial}{\partial r} (r^2 N_A) = 0 \quad (4.3)$$

Inserting Fick's law of diffusion, $N_A = -D_a \partial C_A / \partial r$, the transport of gas A in the liquid film can be expressed as follows:

$$\frac{\partial C_A}{\partial t} + \frac{1}{r^2} \frac{\partial}{\partial r} \left(-r^2 D_a \frac{\partial C_A}{\partial r} \right) = 0 \quad (4.4)$$

$$\frac{\partial C_A}{\partial t} = \frac{1}{r^2} \frac{\partial}{\partial r} \left(r^2 D_a \frac{\partial C_A}{\partial r} \right) \quad (4.5)$$

$$\frac{\partial C_A}{\partial t} = D_a \frac{1}{r^2} \frac{\partial}{\partial r} \left(r^2 \frac{\partial C_A}{\partial r} \right) ; \quad R \leq r \leq R + \delta \quad (4.6)$$

Where, t is microscopic time scale in liquid film and D_a is diffusion coefficient.

The following initial and boundary conditions are applicable:

$$IC : \{ \text{at } t = 0, C_A = C_L \} \quad (4.7)$$

$$BC : \begin{cases} \text{at } r = R, t \geq 0, C_A = C_i \\ \text{at } r = R + \delta, t \geq 0, C_A = C_L \end{cases} \quad (4.8)$$

where, R is the radius of the spherical bubble, C_i the interface concentration and C_L the concentration in the bulk phase.

4.4 Analytical solution of model equation

The linear second order partial differential equation 4.6 can be simplified to

$$\frac{\partial C_A}{\partial t} = D_a \frac{1}{r^2} \left(2r \frac{\partial C_A}{\partial r} + r^2 \frac{\partial^2 C_A}{\partial r^2} \right) \quad (4.9)$$

or

$$\frac{\partial C_A(r,t)}{\partial t} = D_a \frac{2}{r} \frac{\partial C_A(r,t)}{\partial r} + D_a \frac{\partial^2 C_A(r,t)}{\partial r^2} \quad ; [R \leq r \leq (R + \delta)] \quad (4.10)$$

The partial differential equation can be solved by Laplace transform. The Laplace transform

$\bar{C}_A(r,s)$ of the function $C_A(r,t)$ can be expressed as

$$\bar{C}_A(r,s) = \int_0^{\infty} C_A(r,t) e^{-st} dt \quad (4.11)$$

where, s (unit : s^{-1}) is variable of Laplace transformation.

The transformed equation can be written as

$$s \cdot \bar{C}_A(r,s) - C_A(r,t) = D_a \frac{2}{r} \frac{\partial \bar{C}_A(r,s)}{\partial r} + D_a \frac{\partial^2 \bar{C}_A(r,s)}{\partial r^2} \quad (4.12)$$

At initial condition, $\theta = 0, C_A = C_L$

When $C_A(r,0)$ is replaced with C_L in the transformation equation, then eq. (4.10) is rearranged in the following form:

$$s\bar{C}_A(r,s) - C_L = D_a \frac{2}{r} \frac{\partial \bar{C}_A(r,s)}{\partial r} + D_a \frac{\partial^2 \bar{C}_A(r,s)}{\partial r^2} \quad (4.13)$$

Dividing by D_a in both side

$$\frac{1}{D_a} s\bar{C}_A(r,s) - \frac{C_L}{D_a} = \frac{2}{r} \frac{\partial \bar{C}_A(r,s)}{\partial r} + \frac{\partial^2 \bar{C}_A(r,s)}{\partial r^2} \quad (4.14)$$

$$\frac{1}{D_a} s\bar{C}_A(r,s) - \frac{C_L}{D_a} = \frac{2}{r} \frac{\partial \bar{C}_A(r,s)}{\partial r} + \frac{\partial^2 \bar{C}_A(r,s)}{\partial r^2} \quad (4.15)$$

$$\frac{\partial^2 \bar{C}_A(r,s)}{\partial r^2} + \frac{2}{r} \frac{\partial \bar{C}_A(r,s)}{\partial r} - \frac{1}{D_a} s\bar{C}_A(r,s) = -\frac{C_L}{D_a} \quad (4.16)$$

Laplace transformation of boundary conditions can be written in the following form

B.C 1

$$\text{at } r = R, C_A = C_i, \text{ therefore } \bar{C}_A = \frac{C_i}{s}$$

B.C 2

$$\text{at } r = R + \delta, C_A = C_L, \text{ therefore } \bar{C}_A = \frac{C_L}{s}$$

General solution of eq. 4.16 may be written in the following form:

$$\bar{C}_A(r,s) = \frac{A_1}{r} \cos\left(\frac{r}{D_a} \sqrt{-sD_a}\right) + \frac{A_2}{r} \sin\left(\frac{r}{D_a} \sqrt{-sD_a}\right) + \frac{C_L}{s} \quad (4.17)$$

Simplification using the mathematical relationship

$$\cos\left(\frac{r}{D_a} \sqrt{-sD_a}\right) = \cos i\left(\frac{r}{D_a} \sqrt{sD_a}\right) = \cosh\left(\frac{r}{D_a} \sqrt{sD_a}\right)$$

or

$$\cos r\lambda_0 = \cosh r\lambda \quad \text{where, } \lambda_0 = \left(\frac{1}{D_a} \sqrt{-sD_a}\right) \quad \text{and} \quad \lambda = \left(\frac{1}{D_a} \sqrt{sD_a}\right)$$

$$\sin\left(\frac{r}{D_a}\sqrt{-sD_a}\right) = \sin i\left(\frac{r}{D_a}\sqrt{sD_a}\right) = -\frac{1}{i}\sinh\left(\frac{r}{D_a}\sqrt{sD_a}\right)$$

or

$$\sin r\lambda_0 = -\frac{1}{i}\sinh r\lambda$$

The following solution in terms of hyperbolic function comes out.

$$\bar{C}_A(r,s) = \frac{A_1}{r}\cosh\left(\frac{r}{D_a}\sqrt{sD_a}\right) - \frac{A_2}{r.i}\sinh\left(\frac{r}{D_a}\sqrt{sD_a}\right) + \frac{C_L}{s} \quad (4.18)$$

or

$$\bar{C}_A(r,s) = \frac{A_1}{r}\cosh(r\lambda) - \frac{A_2}{r.i}\sinh(r\lambda) + \frac{C_L}{s} \quad (4.19)$$

The integration constants A_1 and A_2 may be obtained by using the boundary condition.

For determination of integration constant A_2 :

Using B.C. 2

$$\text{at } r = R + \delta, C_A = C_L, \text{ therefore } \bar{C}_A(r,s) = \frac{C_L}{s} \quad (4.20)$$

From equation no. 4.13

$$\frac{C_L}{s} = \frac{C_L}{s} + \frac{A_1}{R+\delta}\cos\left(\frac{R+\delta}{D_a}\sqrt{-sD_a}\right) + \frac{A_2}{R+\delta}\sin\left(\frac{R+\delta}{D_a}\sqrt{-sD_a}\right) \quad (4.21)$$

$$\frac{C_L}{s} = \frac{C_L}{s} + \frac{A_1}{R+\delta}\cos((R+\delta)\lambda_0) + \frac{A_2}{R+\delta}\sin((R+\delta)\lambda_0) \quad (4.22)$$

$$0 = \frac{A_1}{R+\delta}\cos((R+\delta)\lambda_0) + \frac{A_2}{R+\delta}\sin((R+\delta)\lambda_0) \quad (4.23)$$

$$0 = A_1 \cos((R+\delta)\lambda_0) + A_2 \sin((R+\delta)\lambda_0) \quad (4.24)$$

$$0 = A_1 \cos(R\lambda_0 + \delta\lambda_0) + A_2 \sin(R\lambda_0 + \delta\lambda_0) \quad (4.25)$$

Using trigonometry formulas

$$\cos(A + B) = \cos A \cdot \cos B - \sin A \cdot \sin B$$

$$\sin(A + B) = \sin A \cdot \cos B + \cos A \cdot \sin B$$

$$0 = A_1[\cos R\lambda_0 \cdot \cos \delta\lambda_0 - \sin R\lambda_0 \cdot \sin \delta\lambda_0] + A_2[\sin R\lambda_0 \cdot \cos \delta\lambda_0 + \cos R\lambda_0 \cdot \sin \delta\lambda_0] \quad (4.26)$$

Divided by $\cos \delta\lambda$ in both side

$$0 = A_1[\cos R\lambda - \sin R\lambda \cdot \tan \delta\lambda] + A_2[\sin R\lambda + \cos R\lambda \cdot \tan \delta\lambda] \quad (4.27)$$

$$A_1[\cos R\lambda_0 - \sin R\lambda_0 \cdot \tan \delta\lambda_0] = -A_2[\sin R\lambda_0 + \cos R\lambda_0 \cdot \tan \delta\lambda_0] \quad (4.28)$$

$$A_1 \cos R\lambda_0 - A_1 \sin R\lambda_0 \cdot \tan \delta\lambda_0 = -A_2[\sin R\lambda_0 + \cos R\lambda_0 \cdot \tan \delta\lambda_0] \quad (4.29)$$

$$\left[R \frac{(C_i - C_L)}{s} - A_2 \sin R\lambda_0 \right] - \left[R \frac{(C_i - C_L)}{s \cdot \cos R\lambda_0} - A_2 \tan R\lambda_0 \right] \sin R\lambda_0 \cdot \tan \delta\lambda_0 \quad (4.30)$$

$$= -A_2[\sin R\lambda_0 + \cos R\lambda_0 \cdot \tan \delta\lambda_0]$$

$$\left[R \frac{(C_i - C_L)}{s} - A_2 \sin R\lambda_0 \right] - \left[R \frac{(C_i - C_L)}{s \cdot \cos R\lambda_0} - A_2 \tan R\lambda_0 \right] \sin R\lambda_0 \cdot \tan \delta\lambda_0 \quad (4.31)$$

$$= -A_2 \sin R\lambda_0 - A_2 \cos R\lambda_0 \cdot \tan \delta\lambda_0$$

$$R \frac{(C_i - C_L)}{s} - \left[R \frac{(C_i - C_L)}{s \cdot \cos R\lambda_0} - A_2 \tan R\lambda_0 \right] \sin R\lambda_0 \cdot \tan \delta\lambda_0 = -A_2 \cos R\lambda_0 \cdot \tan \delta\lambda_0 \quad (4.32)$$

$$R \frac{(C_i - C_L)}{s} - R \frac{(C_i - C_L)}{s \cdot \cos R\lambda_0} \sin R\lambda_0 \cdot \tan \delta\lambda_0 + A_2 \tan R\lambda_0 \cdot \sin R\lambda_0 \cdot \tan \delta\lambda_0 \quad (4.33)$$

$$= -A_2 \cos R\lambda_0 \cdot \tan \delta\lambda_0$$

$$R \frac{(C_i - C_L)}{s} \left[1 - \sin R\lambda_0 \cdot \tan \delta\lambda_0 \frac{1}{\cos R\lambda_0} \right] \quad (4.34)$$

$$= -A_2 \tan R\lambda_0 \cdot \sin R\lambda_0 \cdot \tan \delta\lambda_0 - A_2 \cos R\lambda_0 \cdot \tan \delta\lambda_0$$

Multiply by negative in both sides

$$R \frac{(C_L - C_i)}{s} \left[1 - \sin R\lambda_0 \cdot \tan \delta\lambda_0 \frac{1}{\cos R\lambda_0} \right] = A_2 \tan R\lambda_0 \cdot \sin R\lambda_0 \cdot \tan \delta\lambda_0 + A_2 \cos R\lambda_0 \cdot \tan \delta\lambda_0$$

(4.35)

$$R \frac{(C_L - C_i)}{s} [\cos R\lambda_0 - \sin R\lambda_0 \cdot \tan \delta\lambda_0] \quad (4.36)$$

$$= A_2 \tan R\lambda_0 \cdot \sin R\lambda_0 \cdot \tan \delta\lambda_0 \cdot \cos R\lambda_0 + A_2 \cos^2 R\lambda_0 \cdot \tan \delta\lambda_0$$

$$R \frac{(C_L - C_i)}{s} [\cos R\lambda_0 - \sin R\lambda_0 \cdot \tan \delta\lambda_0] \quad (4.37)$$

$$= A_2 \frac{\sin R\lambda_0}{\cos R\lambda_0} \cdot \sin R\lambda_0 \cdot \tan \delta\lambda_0 \cdot \cos R\lambda_0 + A_2 \cos^2 R\lambda_0 \cdot \tan \delta\lambda_0$$

$$R \frac{(C_L - C_i)}{s} [\cos R\lambda_0 - \sin R\lambda_0 \cdot \tan \delta\lambda_0] = A_2 \sin^2 R\lambda_0 \cdot \tan \delta\lambda_0 + A_2 \cos^2 R\lambda_0 \cdot \tan \delta\lambda_0 \quad (4.38)$$

$$R \frac{(C_L - C_i)}{s} [\cos R\lambda_0 - \sin R\lambda_0 \cdot \tan \delta\lambda_0] = A_2 \tan \delta\lambda_0 [\sin^2 R\lambda_0 + \cos^2 R\lambda_0] \quad (4.39)$$

Substituting $\sin^2 R\lambda_0 + \cos^2 R\lambda_0 = 1$

$$R \frac{(C_L - C_i)}{s} [\cos R\lambda_0 - \sin R\lambda_0 \cdot \tan \delta\lambda_0] = A_2 \tan \delta\lambda_0 \quad (4.40)$$

$$A_2 = R \frac{(C_L - C_i)}{s \cdot \tan \delta\lambda_0} [\cos R\lambda_0 - \sin R\lambda_0 \cdot \tan \delta\lambda_0] \quad (4.41)$$

using

$$\tan\left(\frac{r}{D_a} \sqrt{-sD_a}\right) = \tan i \left(\frac{r}{D_a} \sqrt{sD_a}\right) = -\frac{1}{i} \tanh\left(\frac{r}{D_a} \sqrt{sD_a}\right)$$

or

$$\tan r\lambda_0 = -\frac{1}{i} \tanh r\lambda$$

$$A_2 = -R \cdot i \frac{(C_L - C_i)}{s \cdot \tan \delta\lambda} [\cosh R\lambda + \sinh R\lambda \cdot \tanh \delta\lambda] \quad (\text{m.s.mol/L}) \quad (4.42)$$

$$\text{where, } \lambda = \left(\frac{1}{D_a} \sqrt{sD_a}\right) \quad (\text{m}^{-1})$$

For determination of constant A_1 :

Using B.C. 1

$$\text{at } r = R, C_A = C_i, \text{ therefore } \bar{C}_A(r, s) = \frac{C_i}{s}$$

From equation no. 4.13

$$\bar{C}_A(r, s) = \frac{A_1}{r} \cos\left(\frac{r}{D_a} \sqrt{-sD_a}\right) + \frac{A_2}{r} \sin\left(\frac{r}{D_a} \sqrt{-sD_a}\right) + \frac{C_L}{s} \quad (4.43)$$

$$\frac{C_i}{s} = \frac{C_L}{s} + \frac{A_1}{R} \cos\left(\frac{R}{D_a} \sqrt{-sD_a}\right) + \frac{A_2}{R} \sin\left(\frac{R}{D_a} \sqrt{-sD_a}\right) \quad (4.44)$$

$$\frac{C_i}{s} = \frac{C_L}{s} + \frac{A_1}{R} \cos(R\lambda_0) + \frac{A_2}{R} \sin(R\lambda_0) \quad (4.45)$$

$$\frac{C_i}{s} - \frac{C_L}{s} = \frac{A_1}{R} \cos(R\lambda_0) + \frac{A_2}{R} \sin(R\lambda_0) \quad (4.46)$$

$$R \frac{(C_i - C_L)}{s} = A_1 \cos(R\lambda_0) + A_2 \sin(R\lambda_0) \quad (4.47)$$

$$A_1 \cos(R\lambda_0) = R \frac{(C_i - C_L)}{s} - A_2 \sin(R\lambda_0) \quad (4.48)$$

$$A_2 \sin(R\lambda_0) = R \frac{(C_i - C_L)}{s} - A_1 \cos(R\lambda_0) \quad (4.49)$$

$$A_2 = R \frac{(C_i - C_L)}{s \cdot \sin(R\lambda_0)} - A_1 \frac{\cos(R\lambda_0)}{\sin(R\lambda_0)} \quad (4.50)$$

$$\begin{aligned} A_1 \cos R\lambda_0 - A_1 \sin R\lambda_0 \cdot \tan \delta\lambda_0 &= -R \frac{(C_i - C_L)}{s} + A_1 \cos(R\lambda_0) \\ -R \frac{(C_i - C_L) \cos R\lambda_0 \cdot \tan \delta\lambda_0}{s \cdot \sin(R\lambda_0)} + A_1 \frac{\cos(R\lambda_0)}{\sin(R\lambda_0)} \cos R\lambda_0 \cdot \tan \delta\lambda_0 & \end{aligned} \quad (4.51)$$

$$\begin{aligned}
& -A_1 \sin R\lambda_0 \cdot \tan \delta\lambda_0 = -R \frac{(C_i - C_L)}{s} - R \frac{(C_i - C_L) \cos R\lambda_0 \cdot \tan \delta\lambda_0}{s \cdot \sin(R\lambda_0)} \\
& + A_1 \frac{\cos(R\lambda_0)}{\sin(R\lambda_0)} \cos R\lambda_0 \cdot \tan \delta\lambda_0
\end{aligned} \tag{4.52}$$

$$\begin{aligned}
& R \frac{(C_i - C_L)}{s} + R \frac{(C_i - C_L) \cos R\lambda_0 \cdot \tan \delta\lambda_0}{s \cdot \sin(R\lambda_0)} \\
& = A_1 \sin R\lambda_0 \cdot \tan \delta\lambda_0 + A_1 \frac{\cos(R\lambda_0)}{\sin(R\lambda_0)} \cos R\lambda_0 \cdot \tan \delta\lambda_0
\end{aligned} \tag{4.53}$$

$$\begin{aligned}
& R \frac{(C_i - C_L)}{s} + R \frac{(C_i - C_L) \cos R\lambda_0 \cdot \tan \delta\lambda_0}{s \cdot \sin(R\lambda_0)} = \\
& A_1 \frac{\tan \delta\lambda_0}{\sin R\lambda_0} [\sin^2 R\lambda_0 + \cos^2 R\lambda_0]
\end{aligned} \tag{4.54}$$

put $\sin^2 R\lambda + C_2 \cos^2 R\lambda = 1$

$$R \frac{(C_i - C_L)}{s} + R \frac{(C_i - C_L) \cos R\lambda_0 \cdot \tan \delta\lambda_0}{s \cdot \sin(R\lambda_0)} = A_1 \frac{\tan \delta\lambda_0}{\sin R\lambda_0} \tag{4.55}$$

$$R \frac{(C_i - C_L)}{s} \left[1 + \frac{\cos R\lambda_0 \cdot \tan \delta\lambda_0}{\sin R\lambda_0} \right] = A_1 \frac{\tan \delta\lambda_0}{\sin R\lambda_0} \tag{4.56}$$

$$R \frac{(C_i - C_L)}{s} \left[\frac{\sin R\lambda_0 + \cos R\lambda_0 \cdot \tan \delta\lambda_0}{\sin R\lambda_0} \right] = A_1 \frac{\tan \delta\lambda_0}{\sin R\lambda_0} \tag{4.57}$$

$$A_1 = R \frac{(C_i - C_L)}{s \cdot \tan \delta\lambda_0} [\sin R\lambda_0 + \cos R\lambda_0 \cdot \tan \delta\lambda_0] \tag{4.58}$$

In terms of hyperbolic function

$$A_1 = R \frac{(C_i - C_L)}{s \cdot \tanh \delta\lambda} [\sinh R\lambda + \cosh R\lambda \cdot \tanh \delta\lambda] \quad (\text{m.s.mol/L}) \tag{4.59}$$

Solving eq. 4.18 with eq. 4.41 and eq. 4.58, we get

$$\begin{aligned}\bar{C}_A(r, s) &= \frac{C_L}{s} + \frac{R(C_i - C_L)}{r s \tan \delta \lambda_0} [\sin R \lambda_0 + \cos R \lambda_0 \cdot \tan \delta \lambda_0] \cos(r \lambda_0) + \\ &\frac{R(C_L - C_i)}{r s \tan \delta \lambda_0} [\cos R \lambda_0 - \sin R \lambda_0 \cdot \tan \delta \lambda_0] \sin(r \lambda_0)\end{aligned}\quad (4.60)$$

In terms of hyperbolic function

$$\begin{aligned}\bar{C}_A(r, s) &= \frac{C_L}{s} + \frac{R(C_i - C_L)}{r s \tanh \delta \lambda} [\sinh R \lambda + \cosh R \lambda \cdot \tanh \delta \lambda] \cosh\left(\frac{r}{D_a} \sqrt{s D_a}\right) + \\ &\frac{R(C_L - C_i)}{r s \tanh \delta \lambda} [\cosh R \lambda + \sinh R \lambda \cdot \tanh \delta \lambda] \sinh\left(\frac{r}{D_a} \sqrt{s D_a}\right)\end{aligned}\quad (4.61)$$

$$\begin{aligned}\bar{C}_A(r, s) &= \frac{C_L}{s} + \frac{R(C_i - C_L)}{r s \tanh \delta \lambda} [\sinh R \lambda + \cosh R \lambda \cdot \tanh \delta \lambda] \cosh r \lambda + \\ &\frac{R(C_L - C_i)}{r s \tanh \delta \lambda} [\cosh R \lambda + \sinh R \lambda \cdot \tanh \delta \lambda] \sinh r \lambda\end{aligned}\quad (4.62)$$

$$\begin{aligned}\bar{C}_A(r, s) &= \frac{C_L}{s} + \frac{R(C_i - C_L)}{r s \tanh \delta \lambda} [\sinh R \lambda \cosh r \lambda + \cosh R \lambda \cdot \tanh \delta \lambda \cosh r \lambda] + \\ &\frac{R(C_L - C_i)}{r s \tanh \delta \lambda} [\cosh R \lambda \sinh r \lambda + \sinh R \lambda \cdot \tanh \delta \lambda \sinh r \lambda]\end{aligned}\quad (4.63)$$

$$\begin{aligned}\bar{C}_A(r, s) &= \frac{C_L}{s} + \frac{R(C_i - C_L)}{r s \tanh \delta \lambda} [\sinh R \lambda \cosh r \lambda + \cosh R \lambda \cdot \tanh \delta \lambda \cosh r \lambda] - \\ &\frac{R(C_i - C_L)}{r s \tanh \delta \lambda} [\cosh R \lambda \sinh r \lambda + \sinh R \lambda \cdot \tanh \delta \lambda \sinh r \lambda]\end{aligned}\quad (4.64)$$

$$\bar{C}_A(r, s) = \frac{C_L}{s} + \frac{R(C_i - C_L)}{r s \tanh \delta \lambda} \left[\begin{array}{l} \sinh R \lambda \cosh r \lambda + \cosh R \lambda \cdot \tanh \delta \lambda \cosh r \lambda - \\ \cosh R \lambda \sinh r \lambda - \sinh R \lambda \cdot \tanh \delta \lambda \sinh r \lambda \end{array} \right] \quad (4.65)$$

$$\bar{C}_A(r, s) = \frac{C_L}{s} + \frac{R(C_i - C_L)}{r s \tanh \delta \lambda} \left[\begin{array}{l} \sinh R \lambda \cosh r \lambda - \cosh R \lambda \sinh r \lambda + \cosh R \lambda \cdot \tanh \delta \lambda \cosh r \lambda \\ - \sinh R \lambda \cdot \tanh \delta \lambda \sinh r \lambda \end{array} \right] \quad (4.66)$$

Simplification using the mathematical relationship

$$\sinh(x - y) = \sinh x \cdot \cosh y - \cosh x \cdot \sinh y$$

$$\bar{C}_A(r, s) = \frac{C_L}{s} + \frac{R(C_i - C_L)}{r \cdot s \cdot \tanh \delta \lambda} \left[\sinh(R\lambda - r\lambda) + \tanh \delta \lambda (\cosh R\lambda \cosh r\lambda - \sinh R\lambda \cdot \sinh r\lambda) \right] \quad (4.67)$$

Simplification using the mathematical relationship

$$\cosh(x - y) = \cosh x \cdot \cosh y - \sinh x \cdot \sinh y$$

$$\bar{C}_A(r, s) = \frac{C_L}{s} + \frac{R(C_i - C_L)}{r \cdot s \cdot \tanh \delta \lambda} \left[\sinh(R\lambda - r\lambda) + \tanh \delta \lambda \cosh(R\lambda - r\lambda) \right] \quad (4.68)$$

$$\bar{C}_A(r, s) = \frac{C_L}{s} + \frac{R(C_i - C_L)}{r \cdot s \cdot \tanh \delta \lambda} \left[\sinh(R - r)\lambda + \tanh \delta \lambda \cosh(R - r)\lambda \right] \quad (4.69)$$

$$\bar{C}_A(r, s) = \frac{C_L}{s} + \frac{R(C_i - C_L)}{r \cdot s \cdot \tanh \delta \lambda} \left[\sinh(R - r)\lambda + \frac{\sinh \delta \lambda}{\cosh \delta \lambda} \cosh(R - r)\lambda \right] \quad (4.70)$$

$$\bar{C}_A(r, s) = \frac{C_L}{s} + \frac{R(C_i - C_L)}{r \cdot s \cdot \tanh \delta \lambda} \left[\frac{\sinh(R - r)\lambda \cdot \cosh \delta \lambda + \sinh \delta \lambda \cdot \cosh(R - r)\lambda}{\cosh \delta \lambda} \right] \quad (4.71)$$

Simplification using the mathematical relationship

$$\sinh(x + y) = \sinh x \cdot \cosh y + \cosh x \cdot \sinh y$$

$$\bar{C}_A(r, s) = \frac{C_L}{s} + \frac{R(C_i - C_L)}{r \cdot s \cdot \tanh \delta \lambda} \left[\frac{\sinh(R - r + \delta)\lambda}{\cosh \delta \lambda} \right] \quad (4.72)$$

$$\bar{C}_A(r, s) = \frac{C_L}{s} + \frac{R(C_i - C_L) \cdot \cosh \delta \lambda}{r \cdot s \cdot \sinh \delta \lambda} \left[\frac{\sinh(R - r + \delta)\lambda}{\cosh \delta \lambda} \right] \quad (4.73)$$

$$\bar{C}_A(r, s) = \frac{C_L}{s} + \frac{R(C_i - C_L)}{r \cdot s} \left[\frac{\sinh(R - r + \delta)\lambda}{\sinh \delta \lambda} \right] \quad (4.74)$$

The inverse of the Laplace transform $f(s)$, given by

$$F(t) = \frac{1}{2\pi i} \int_{\gamma-i\infty}^{\gamma+i\infty} e^{st} f(s) ds$$

where γ is a vertical contour in the complex plane so that all singularities of $f(s)$ are to the left of it. The Laplace inverse for eq. (4.61) is difficult to find out analytically. However, Talbot algorithm (Abate et al. 2006) can be used to find numerical approximation of Laplace inverse at various values of time.

Eq. 4.61 is the Laplace transformed concentration profile. Inverse Laplace transforms of the concentration profile in the liquid film of the gas bubble presented in eq. 4.61 is cumbersome. Besides, it is the mass transfer coefficient k_L , which is important for getting interfacial mass transfer properties rather than a concentration profile in the film. Therefore, the age distribution function will be used further to get liquid phase mass transfer coefficient k_L .

Differentiating eq. (4.60) with respect to r and substituting integration constant A_1 and A_2 , we get

$$\begin{aligned} \left. \frac{d C_A(r, s)}{dr} \right|_{r=R} &= 0 + \left[\left(\frac{A_1}{r} \right) \cdot \sin \left(\frac{r}{D_a} \sqrt{-s D_a} \right) \left(\frac{1}{D_a} \sqrt{-s D_a} \right) + \left(\frac{-A_1}{r^2} \right) \cdot \cos \left(\frac{r}{D_a} \sqrt{-s D_a} \right) \right] \\ &+ \left[\left(\frac{A_2}{r} \right) \cdot \cos \left(\frac{r}{D_a} \sqrt{-s D_a} \right) \left(\frac{1}{D_a} \sqrt{-s D_a} \right) + \left(\frac{-A_2}{r^2} \right) \sin \left(\frac{r}{D_a} \sqrt{-s D_a} \right) \right] \end{aligned} \quad (4.75)$$

At $r = R$

$$\begin{aligned} \left. \frac{d C_A(r, s)}{dr} \right|_{r=R} &= 0 + \left[\left(\frac{A_1}{R} \right) \cdot \sin(R\lambda_0) \cdot \lambda_0 + \left(\frac{-A_1}{R^2} \right) \cdot \cos(R\lambda_0) \right] + \\ &\left[\left(\frac{A_2}{R} \right) \cdot \cos(R\lambda_0) \cdot \lambda_0 + \left(\frac{-A_2}{R^2} \right) \sin(R\lambda_0) \right] \end{aligned} \quad (4.76)$$

$$\left. \frac{d C_A(r, s)}{dr} \right|_{r=R} = \left(\frac{A_1}{R} \right) \left[-\sin(R\lambda_0) \cdot \lambda_0 - \left(\frac{1}{R} \right) \cdot \cos(R\lambda_0) \right] + \left(\frac{A_2}{R} \right) \left[\cos(R\lambda_0) \cdot \lambda_0 - \left(\frac{1}{R} \right) \sin(R\lambda_0) \right] \quad (4.77)$$

Substituting integration constant A_1 and A_2

$$\begin{aligned} \left. \frac{d C_A(r, s)}{dr} \right|_{r=R} &= \left(\frac{1}{R} \right) \left[R \frac{(C_i - C_L)}{s \cdot \tan \delta \lambda} [\sin R \lambda_0 + \cos R \lambda_0 \cdot \tan \delta \lambda_0] \right] \left[-\sin(R \lambda_0) \cdot \lambda_0 - \left(\frac{1}{R} \right) \cdot \cos(R \lambda_0) \right] \\ &+ \left(\frac{1}{R} \right) \left[R \frac{(C_L - C_i)}{s \cdot \tan \delta \lambda_0} [\cos R \lambda_0 - \sin R \lambda_0 \cdot \tan \delta \lambda_0] \right] \left[\cos(R \lambda_0) \cdot \lambda_0 - \left(\frac{1}{R} \right) \sin(R \lambda_0) \right] \end{aligned} \quad (4.78)$$

$$\begin{aligned} \left. \frac{d C_A(r, s)}{dr} \right|_{r=R} &= \left(\frac{(C_i - C_L)}{\tan \delta \lambda_0} \right) \left[\frac{1}{s} (\sin R \lambda_0 + \cos R \lambda_0 \cdot \tan \delta \lambda_0) \right] \left[-\sin(R \lambda_0) \cdot \lambda_0 - \left(\frac{1}{R} \right) \cdot \cos(R \lambda_0) \right] \\ &+ \left(\frac{(C_L - C_i)}{\tan \delta \lambda_0} \right) \left[\frac{1}{s} (\cos R \lambda_0 - \sin R \lambda_0 \cdot \tan \delta \lambda_0) \right] \left[\cos(R \lambda_0) \cdot \lambda_0 - \left(\frac{1}{R} \right) \sin(R \lambda_0) \right] \end{aligned} \quad (4.79)$$

$$\begin{aligned} \left. \frac{d C_A(r, s)}{dr} \right|_{r=R} &= \left(\frac{(C_i - C_L)}{\tan \delta \lambda} \right) \left[\frac{1}{s} (\sin R \lambda_0 + \cos R \lambda_0 \cdot \tan \delta \lambda_0) \right] \left[-\sin(R \lambda_0) \cdot \lambda_0 - \left(\frac{1}{R} \right) \cdot \cos(R \lambda_0) \right] \\ &- \left(\frac{(C_i - C_L)}{\tan \delta \lambda_0} \right) \left[\frac{1}{s} (\sin R \lambda_0 \cdot \tan \delta \lambda_0 - \cos R \lambda_0) \right] \left[-\cos(R \lambda_0) \cdot \lambda_0 + \left(\frac{1}{R} \right) \sin(R \lambda_0) \right] \end{aligned} \quad (4.80)$$

$$\begin{aligned} \left. \frac{d C_A(r, s)}{dr} \right|_{r=R} &= \left(\frac{(C_i - C_L)}{\tan \delta \lambda_0} \right) \left[\left\{ \frac{1}{s} (\sin R \lambda_0 + \cos R \lambda_0 \cdot \tan \delta \lambda_0) \right\} \left\{ -\sin(R \lambda_0) \cdot \lambda_0 - \left(\frac{1}{R} \right) \cdot \cos(R \lambda_0) \right\} - \right. \\ &\left. \left\{ \frac{1}{s} (\sin R \lambda_0 \cdot \tan \delta \lambda_0 - \cos R \lambda_0) \right\} \left\{ -\cos(R \lambda_0) \cdot \lambda_0 + \left(\frac{1}{R} \right) \sin(R \lambda_0) \right\} \right] \end{aligned} \quad (4.81)$$

In terms of hyperbolic function:

$$\begin{aligned} \left. \frac{d C_A(r, s)}{dr} \right|_{r=R} &= -i \frac{(C_i - C_L)}{\tanh \delta \lambda} \left[\left\{ \frac{1}{s \cdot i} (-\sinh(R \lambda) - \cosh(R \lambda) \cdot \tanh(\delta \lambda)) \right\} \left\{ \sinh(R \lambda) \cdot \lambda - \left(\frac{1}{R} \right) \cdot \cosh(R \lambda) \right\} - \right. \\ &\left. \left\{ \frac{1}{s} (-\sinh(R \lambda) \cdot \tanh(\delta \lambda) - \cosh(R \lambda)) \right\} \left\{ -\cosh(R \lambda) \cdot i \lambda - \left(\frac{1}{R \cdot i} \right) \sinh(R \lambda) \right\} \right] \end{aligned} \quad (4.82)$$

Instantaneous point mass transfer rate for a single surface element at time t , across the interface between the liquid bulk and the bubble is represented by the following equation:

$$N_A(t)\Big|_{r=R}^\bullet = -D_a \frac{\partial C_A}{\partial r} \Big|_{r=R} \quad (4.83)$$

The average mass transfer rate across the interface between the gas and liquid phase $N_A(t)\Big|_{r=R}^{Av.}$ is an integral of the instantaneous point mass transfer rates at various liquid film locations with different film age. The average mass transfer rate through the interface for the unsteady-state single film concept can be calculated using the surface age distribution function proposed by Danckwerts (1951).

$$\psi(t) = S e^{-St} \quad (4.84)$$

Where, ψ is the surface age distribution function, t is time for which a liquid surface has been exposed to gas (“age” of surface) and S is the fractional rate of renewal of surface of liquid, which is the bubble surface liquid film renewal rate. This means that the liquid film is replaced by fresh liquid element. Thus, S is the extent of surface renewal. Therefore, the average age of liquid film on the bubble surface may be given by –

$$\int_0^{\infty} \psi(t) dt = 1 \quad (4.85)$$

Average mass transfer rate across the gas–liquid bubble interface can be obtained by integrating the multiplication of instantaneous point mass transfer rate and surface age distribution function,

$$N_A(t)\Big|_{r=R}^{Av.} = \int_0^{\infty} N_A(t)\Big|_{r=R}^\bullet \psi(t) dt \quad (4.86)$$

Average mass transfer rate across the interface between the gas and liquid phase considering isolated bubble from homogeneous micro bubbling in aeration system.

$$N(t)\Big|_{r=R}^{Av.} = \frac{\left[N(t_1)\Big|_{r=R}^\bullet \psi(t_1) dt + N(t_2)\Big|_{r=R}^\bullet \psi(t_2) dt + N(t_3)\Big|_{r=R}^\bullet \psi(t_3) dt + \dots\dots\dots N(t_\infty)\Big|_{r=R}^\bullet \psi(t_\infty) dt \right]}{n}$$

(4.87)

where, n = number of micro eddies on bubble surface, and t = age of the liquid element spent on bubble surface

Average mass transfer rate across the gas- liquid bubble interface is also equal to rate of mass transfer across the interface expressed in terms of concentration difference at interface and liquid bulk.

$$N_A(t)|_{r=R}^{Av.} = k_L(C_i - C_L) \quad (4.88)$$

Now, average mass transfer rate across the film can be found out by

$$N_A(t)|_{r=R}^{Av.} = \int_0^{\infty} -D_a \frac{dC_A}{dr} \Big|_{r=R} S e^{-St} dt \quad (4.89)$$

or,

$$N_A(t)|_{r=R}^{Av.} = -D_a \frac{d \int_0^{\infty} C_A(r,t) S e^{-St} dt}{dr} \Big|_{r=R} = k_L(C_i - C_L) \quad (4.90)$$

The definition of Laplace transforms,

$$L\{f(t)\} = \int_0^{\infty} f(t) e^{-st} dt \quad (4.91)$$

By analogy, eq. (4.91) can simplify as

$$N_A(t)|_{r=R}^{Av.} = -D_a \cdot S \frac{d C_A(r, S)}{dr} \Big|_{r=R} \quad (4.92)$$

Thus,

$$N_A(t)|_{r=R}^{Av.} = -D_a \cdot S \left. \frac{d C_A(r, S)}{dr} \right|_{r=R} = k_L (C_i - C_L) \quad (4.91)$$

By rearrangement,

$$k_L = -D_a \cdot S \frac{\left. \frac{d C_A(r, S)}{dr} \right|_{r=R}}{(C_i - C_L)} \quad (4.92)$$

Substituting the value of $dC_A(r, S)/dr|_{r=R}$ from eq. (4.81) in eq. (4.92) and simplifying

$$k_L = -D_a \cdot S \frac{\left(\frac{C_i - C_L}{\tan \delta \lambda_0} \right) \left[\frac{\left\{ \frac{1}{S} (\sin R \lambda_0 + \cos R \lambda_0 \cdot \tan \delta \lambda_0) \right\} \left\{ -\sin(R \lambda_0) \cdot \lambda_0 - \left(\frac{1}{R} \right) \cdot \cos(R \lambda_0) \right\} - \left\{ \frac{1}{S} (\sin R \lambda_0 \cdot \tan \delta \lambda_0 - \cos R \lambda_0) \right\} \left\{ -\cos(R \lambda_0) \cdot \lambda_0 + \left(\frac{1}{R} \right) \sin(R \lambda_0) \right\}}{(C_i - C_L)} \right]}{(C_i - C_L)} \quad (4.93)$$

$$k_L = -D_a \frac{\left[\frac{\left\{ (\sin R \lambda_0 + \cos R \lambda_0 \cdot \tan \delta \lambda_0) \right\} \left\{ -\sin(R \lambda_0) \cdot \lambda_0 - \left(\frac{1}{R} \right) \cdot \cos(R \lambda_0) \right\} - \left\{ (\sin R \lambda_0 \cdot \tan \delta \lambda_0 - \cos R \lambda_0) \right\} \left\{ -\cos(R \lambda_0) \cdot \lambda_0 + \left(\frac{1}{R} \right) \sin(R \lambda_0) \right\}}{\tan \delta \lambda_0} \right]}{\tan \delta \lambda_0} \quad (4.94)$$

$$k_L = -D_a \frac{\left[\frac{\left(\frac{1}{R} \right) [(\sin R \lambda_0 + \cos R \lambda_0 \cdot \tan \delta \lambda_0)] [-\sin(R \lambda_0) \cdot \lambda_0 \cdot R - \cos(R \lambda_0)] - \left(\frac{1}{R} \right) [(\sin R \lambda_0 \cdot \tan \delta \lambda_0 - \cos R \lambda_0)] [-\cos(R \lambda_0) \cdot \lambda_0 \cdot R + \sin(R \lambda_0)]}{\tan \delta \lambda_0} \right]}{\tan \delta \lambda_0} \quad (4.95)$$

$$k_L = -D_a \frac{\left[\frac{[(\sin R \lambda_0 + \cos R \lambda_0 \cdot \tan \delta \lambda_0)] [-\sin(R \lambda_0) \cdot \lambda_0 R - \cos R \lambda_0] - [(\sin R \lambda_0 \cdot \tan \delta \lambda_0 - \cos R \lambda_0)] [-\cos(R \lambda_0) \cdot \lambda_0 R + \sin R \lambda_0]}{R \cdot \tan \delta \lambda_0} \right]}{R \cdot \tan \delta \lambda_0} \quad (4.96)$$

$$k_L = -D_a \frac{\left[\begin{array}{l} \left[(-\sin^2 R\lambda_0 \cdot \lambda_0 R - \cos R\lambda_0 \cdot \tan \delta\lambda_0 \cdot \sin R\lambda_0 \cdot \lambda_0 R - \cos R\lambda_0 \cdot \sin R\lambda_0 - \cos^2 R\lambda_0 \cdot \tan \delta\lambda_0) \right] \\ - \\ \left[\cos^2 R\lambda_0 \cdot \lambda_0 R - \sin R\lambda_0 \cdot \tan \delta\lambda_0 \cdot \cos R\lambda_0 \cdot \lambda_0 R - \cos R\lambda_0 \cdot \sin R\lambda_0 + \sin^2 R\lambda_0 \cdot \tan \delta\lambda_0 \right] \end{array} \right]}{R \cdot \tan \delta\lambda_0}$$

(4.97)

$$k_L = -D_a \frac{\left(\begin{array}{l} -\sin^2 R\lambda_0 \cdot \lambda_0 R - \cos R\lambda_0 \cdot \tan \delta\lambda_0 \cdot \sin R\lambda_0 \cdot \lambda_0 R - \cos R\lambda_0 \cdot \sin R\lambda_0 - \cos^2 R\lambda_0 \cdot \tan \delta\lambda_0 - \\ \cos^2 R\lambda_0 \cdot \lambda_0 R + \sin R\lambda_0 \cdot \tan \delta\lambda_0 \cdot \cos R\lambda_0 \cdot \lambda_0 R + \cos R\lambda_0 \cdot \sin R\lambda_0 - \sin^2 R\lambda_0 \cdot \tan \delta\lambda_0 \end{array} \right)}{R \cdot \tan \delta\lambda_0}$$

(4.98)

$$k_L = D_a \frac{\left(\begin{array}{l} \sin^2 R\lambda \cdot \lambda R + \cos R\lambda \cdot \tan \delta\lambda \cdot \sin R\lambda \cdot \lambda R + \cos R\lambda \cdot \sin R\lambda + \cos^2 R\lambda \cdot \tan \delta\lambda + \\ \cos^2 R\lambda \cdot \lambda R - \sin R\lambda \cdot \tan \delta\lambda \cdot \cos R\lambda \cdot \lambda R - \cos R\lambda \cdot \sin R\lambda + \sin^2 R\lambda \cdot \tan \delta\lambda \end{array} \right)}{R \cdot \tan \delta\lambda}$$

(4.99)

$$k_L = D_a \frac{(\lambda_0 R + \tan \delta\lambda_0)}{R \cdot \tan \delta\lambda_0} \quad (4.100)$$

$$k_L = D_a \frac{R \cdot \tan \delta\lambda_0 \left(\frac{\lambda_0}{\tan \delta\lambda_0} + \frac{1}{R} \right)}{R \cdot \tan \delta\lambda_0} \quad (4.101)$$

$$k_L = D_a \left(\frac{\lambda_0}{\tan \delta\lambda_0} + \frac{1}{R} \right) \quad (4.102)$$

$$\text{Put, } \lambda_0 = \left(\frac{1}{D_a} \sqrt{-SD_a} \right)$$

Final expression for gas –liquid mass transfer coefficient of a single bubble:

$$k_L = D_a \left(\frac{\frac{1}{D_a} \sqrt{-SD_a}}{\tan \delta \frac{1}{D_a} \sqrt{-SD_a}} + \frac{1}{R} \right) \quad (4.103)$$

$$k_L = D_a \left(\frac{R \frac{1}{D_a} \sqrt{-SD_a} + \tan \delta \frac{1}{D_a} \sqrt{-SD_a}}{R \cdot \tan \delta \frac{1}{D_a} \sqrt{-SD_a}} \right) \quad (4.104)$$

In terms of hyperbolic function:

$$k_L = D_a \left(\frac{R \frac{1}{D_a} \sqrt{-SD_a} + \tan \delta \frac{1}{D_a} \sqrt{-SD_a}}{R \cdot \tan \delta \frac{1}{D_a} \sqrt{-SD_a}} \right) \quad (4.105)$$

$$k_L = \left(\frac{R \sqrt{-SD_a} + D_a \tan \delta \frac{1}{D_a} \sqrt{-SD_a}}{R \cdot \tan \delta \frac{1}{D_a} \sqrt{-SD_a}} \right) \quad (4.106)$$

$$k_L = \frac{\frac{R \sqrt{-SD_a} \cos \delta \frac{1}{D_a} \sqrt{-SD_a} + D_a \sin \delta \frac{1}{D_a} \sqrt{-SD_a}}{\cos \delta \frac{1}{D_a} \sqrt{-SD_a}}}{\frac{R \cdot \sin \delta \frac{1}{D_a} \sqrt{-SD_a}}{\cos \delta \frac{1}{D_a} \sqrt{-SD_a}}} \quad (4.107)$$

$$k_L = \left(\frac{R \sqrt{-SD_a} \cos \delta \frac{1}{D_a} \sqrt{-SD_a} + D_a \sin \delta \frac{1}{D_a} \sqrt{-SD_a}}{R \cdot \sin \delta \frac{1}{D_a} \sqrt{-SD_a}} \right) \quad (4.108)$$

$$k_L = \left(\frac{R \cdot \sqrt{-1} \sqrt{SD_a} \cos \delta \frac{1}{D_a} \sqrt{-1} \sqrt{SD_a} + D_a \sin \delta \frac{1}{D_a} \sqrt{-1} \sqrt{SD_a}}{R \cdot \sin \delta \frac{1}{D_a} \sqrt{-1} \sqrt{SD_a}} \right) \quad (4.109)$$

$$k_L = \left(\frac{R \cdot i \cdot \sqrt{SD_a} \cos i\delta \frac{1}{D_a} \sqrt{SD_a} + D_a \sin i\delta \frac{1}{D_a} \sqrt{SD_a}}{R \cdot \sin i\delta \frac{1}{D_a} \sqrt{SD_a}} \right) \quad (4.110)$$

Simplification using the mathematical relationship

$$\sin i\delta \frac{1}{D_a} \sqrt{SD_a} = -\frac{\sinh \delta \frac{1}{D_a} \sqrt{SD_a}}{i} \quad \sin ix = -\frac{\sinh x}{i}$$

$$\cos i\delta \frac{1}{D_a} \sqrt{SD_a} = \cosh \delta \frac{1}{D_a} \sqrt{SD_a} \quad \cos ix = \cosh x$$

$$k_L = \left(\frac{R \cdot i \cdot \sqrt{SD_a} \cosh \delta \frac{1}{D_a} \sqrt{SD_a} - D_a \frac{\sinh \delta \frac{1}{D_a} \sqrt{SD_a}}{i}}{-R \cdot \frac{\sinh \delta \frac{1}{D_a} \sqrt{SD_a}}{i}} \right) \quad (4.111)$$

$$k_L = \frac{R \cdot i^2 \cdot \sqrt{SD_a} \cosh \delta \frac{1}{D_a} \sqrt{SD_a} - D_a \sinh \delta \frac{1}{D_a} \sqrt{SD_a}}{i} \quad (4.112)$$

$$- R \cdot \frac{\sinh \delta \frac{1}{D_a} \sqrt{SD_a}}{i}$$

$$k_L = \frac{R \cdot i^2 \cdot \sqrt{SD_a} \cosh \delta \frac{1}{D_a} \sqrt{SD_a} - D_a \sinh \delta \frac{1}{D_a} \sqrt{SD_a}}{-R \sinh \delta \frac{1}{D_a} \sqrt{SD_a}} \quad (4.113)$$

$$k_L = \frac{-R\sqrt{SD_a} \cosh \delta \frac{1}{D_a} \sqrt{SD_a} - D_a \sinh \delta \frac{1}{D_a} \sqrt{SD_a}}{-R \sinh \delta \frac{1}{D_a} \sqrt{SD_a}} \quad (4.114)$$

$$k_L = \frac{-\left[R\sqrt{SD_a} \cosh \delta \frac{1}{D_a} \sqrt{SD_a} + D_a \sinh \delta \frac{1}{D_a} \sqrt{SD_a} \right]}{-R \sinh \delta \frac{1}{D_a} \sqrt{SD_a}} \quad (4.115)$$

After simplifying,

$$k_L = \frac{R\sqrt{SD_a} \cosh \delta \frac{1}{D_a} \sqrt{SD_a} + D_a \sinh \delta \frac{1}{D_a} \sqrt{SD_a}}{R \sinh \delta \frac{1}{D_a} \sqrt{SD_a}} \quad (4.116)$$

$$k_L = \frac{R\sqrt{SD_a} \cosh \delta \frac{1}{RD_a} \sqrt{R^2SD_a} + D_a \sinh \delta \frac{1}{RD_a} \sqrt{R^2SD_a}}{R \sinh \delta \frac{1}{RD_a} \sqrt{R^2SD_a}} \quad (4.117)$$

$$k_L = \frac{R\sqrt{SD_a} \cosh \frac{\delta}{R} \sqrt{\frac{R^2S}{D_a}} + D_a \sinh \frac{\delta}{R} \sqrt{\frac{R^2S}{D_a}}}{R \sinh \frac{\delta}{R} \sqrt{\frac{R^2S}{D_a}}} \quad (4.118)$$

$$k_L = \frac{R\sqrt{SD_a} \cosh \frac{\delta}{R} \sqrt{S_M} + D_a \sinh \frac{\delta}{R} \sqrt{S_M}}{R \sinh \frac{\delta}{R} \sqrt{S_M}} \quad (4.119)$$

Where

S_M : Surface renewal modulus

$$\frac{k_L \cdot D_c}{D_a} = \frac{D_c}{D_a} \frac{R\sqrt{SD_a} \cosh \frac{\delta}{R} \sqrt{S_M} + D_a \sinh \frac{\delta}{R} \sqrt{S_M}}{R \sinh \frac{\delta}{R} \sqrt{S_M}} \quad (4.120)$$

$$\frac{k_L \cdot D_c}{D_a} = \frac{D_c}{D_a} \frac{\left[D_a R \sqrt{\frac{S}{D_a}} \cosh \frac{\delta}{R} \sqrt{S_M} + D_a \sinh \frac{\delta}{R} \sqrt{S_M} \right]}{R \sinh \frac{\delta}{R} \sqrt{S_M}} \quad (4.121)$$

$$\frac{k_L \cdot D_c}{D_a} = \frac{D_c}{R} \frac{\left[R \sqrt{\frac{S}{D_a}} \cosh \frac{\delta}{R} \sqrt{S_M} + \sinh \frac{\delta}{R} \sqrt{S_M} \right]}{\sinh \frac{\delta}{R} \sqrt{S_M}} \quad (4.122)$$

$$Sh = \frac{D_c}{R} \frac{\left[R \sqrt{\frac{S}{D_a}} \cosh \frac{\delta}{R} \sqrt{S_M} + \sinh \frac{\delta}{R} \sqrt{S_M} \right]}{\sinh \frac{\delta}{R} \sqrt{S_M}} \quad (4.123)$$

$$Sh = \frac{D_c}{R} \frac{\left[\sqrt{S_M} \cosh \frac{\delta}{R} \sqrt{S_M} + \sinh \frac{\delta}{R} \sqrt{S_M} \right]}{\sinh \frac{\delta}{R} \sqrt{S_M}} \quad (4.124)$$

$$Sh = \frac{D_c}{R} \left[\sqrt{S_M} \coth \frac{\delta}{R} \sqrt{S_M} + 1 \right] \quad (4.125)$$

Importance of eq. 4.116 lies in the fact that the mass transfer coefficient is a function of radius of bubble, surface renewal rate, thickness of liquid film and gas diffusivity in the liquid film. To the best of my knowledge the analytical solution of unsteady state diffusion equation (equation 4.9) using Laplace transformation is not available for IC (eq.4.7) and BCs (eq. 4.8) of the bubble column system studied in the present work.

4.5 validation of developed model using secondary data (Jin et al. 2014)

Details of experimental conditions used for validation of model are summarized in Table 4A.1 (Appendix 4A). Physical properties of H₂, CO, CO₂ and liquid paraffin are shown in Tables 4A.2 and 4A.3 3 respectively (Appendix 4A).

The viscosity and density of liquid paraffin were taken from the work of Huifang et al. (1999)

$$\ln \mu_L = -3.0912 + 1.7038 \times 10^3 / T \quad (4.126)$$

$$\rho_L = 171.0 \times 0.1677^{-(T-T_r)^{2/7}} \quad (4.127)$$

where, $T_r = T / T_C$ is the reduced temperature.

Apparent slurry viscosity (μ_{SL}) is estimated by the equation proposed by Thomas (1965) :

$$\mu_{SL} = \mu_L \left[1 + 2.5 C_S + 10.05 C_S^2 + 0.00273 \exp(16.6 C_S) \right] \quad (4.128)$$

where, C_S is the solid concentration in the slurry expressed as volume of solid per unit volume of slurry. In the present study, C_S is varied from 5 to 20%. The apparent density of the slurry

ρ_{SL} was predicted by using the following expression (Yang et al. 2001) :

$$\rho_{SL} = \rho_L (1 - C_S) + \rho_S C_S \quad (4.129)$$

Apparent slurry viscosities and apparent densities of slurry at 298 K and different solid concentrations are listed in Table 4A.4 (Appendix 4A).

To obtain the diffusivities of H₂, CO and CO₂ in liquid paraffin, the equation proposed by Erkey et al. (1990) was used:

$$D_a = \frac{94.5 \times 10^{-9} \sqrt{T} (V - V_D)}{M_1^{0.239} M_2^{0.781} (\sigma_1 \times \sigma_2)^{1.134}} \quad (4.130)$$

With

$$V_D = \left(1.206 + 0.0632 \frac{\sigma_1}{\sigma_2} \right) \left(\frac{N \sigma_2^3}{\sqrt{2}} \right) \quad (4.131)$$

where, N is Avogadro number, V is molar volume of liquid paraffin, V_D is molar volume of the hard sphere, M is molecular weight of gas, and σ is the effective hard-sphere diameter (Erkey et al. 1990).

4.6 Estimation of overall mass transfer coefficient, k_L using number distribution density function

Size distribution of bubbles can be described by the number distribution density function

$$f(R|\mu, \sigma)$$

$$\frac{N_{R_1, R_2}}{N_{\text{sum}}} = \int_{R_1}^{R_2=\text{max}} f(R|\mu, \sigma) dR \quad (4.132)$$

where, μ and σ are the mean and standard deviation of the variable respectively. The size distribution can be approximated by log-normal distributions

$$f(R|\mu, \sigma) = \frac{1}{R\sigma\sqrt{2\pi}} e^{-(\ln R - \mu)^2/2\sigma^2} \quad (4.133)$$

With the help of k_L for a single spherical bubble, overall mass transfer coefficient k_L of the system can be estimated by statistical integration using a log - normal distribution. Mass transfer coefficient, k_L can be approximated by the following expression:

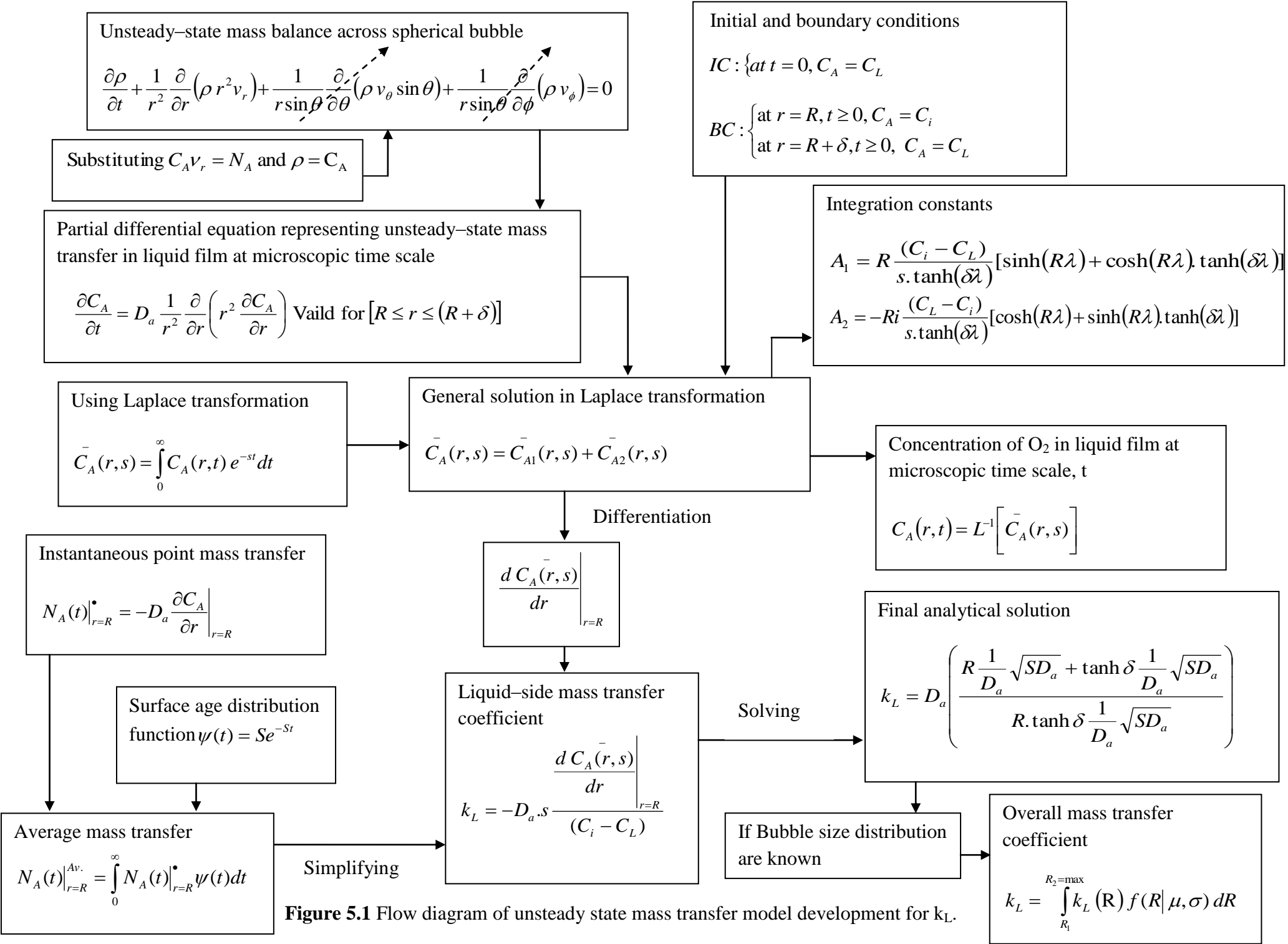
$$k_L = \int_{R_1}^{R_2=\text{max}} k_L(R) f(R|\mu, \sigma) dR \quad (4.134)$$

In this work, the values of μ and σ were obtained by trial and error for the slurry system ($\mu = 0.015$, $\sigma = 0.745$). The mean diameter of small and larger bubbles at different pressures and constant temperature ($T = 298 \text{ K}$) are listed in Table 4A.5 (Appendix 4A).

5 Results and discussion

Section 5.1: Macroscopic model development for prediction of liquid–side mass transfer coefficient k_L in a slurry bubble column system.

A macroscopic mathematical model for the mass transfer coefficient with two key parameters, viz. liquid film thickness δ and surface renewal rate S were formulated. The mathematical model is useful to predict overall k_L , if bubble size distribution is known. Effect of variations in the values of δ and S on k_L has been simulated and validated with a set of reported experimental data (Jin et al. 2014). The values of δ and S were estimated by trial and error method using a program code ‘BUBBLESIM’ in MATLAB[®]. A flow diagram of model development for k_L and estimation of δ , S and overall k_L are presented in Figure 5.1 and Figure 5.2 respectively. The model is suitable for the design and scale-up of bubble columns using liquids/ slurries of different viscosities operating at various gas velocities, temperatures and pressure.



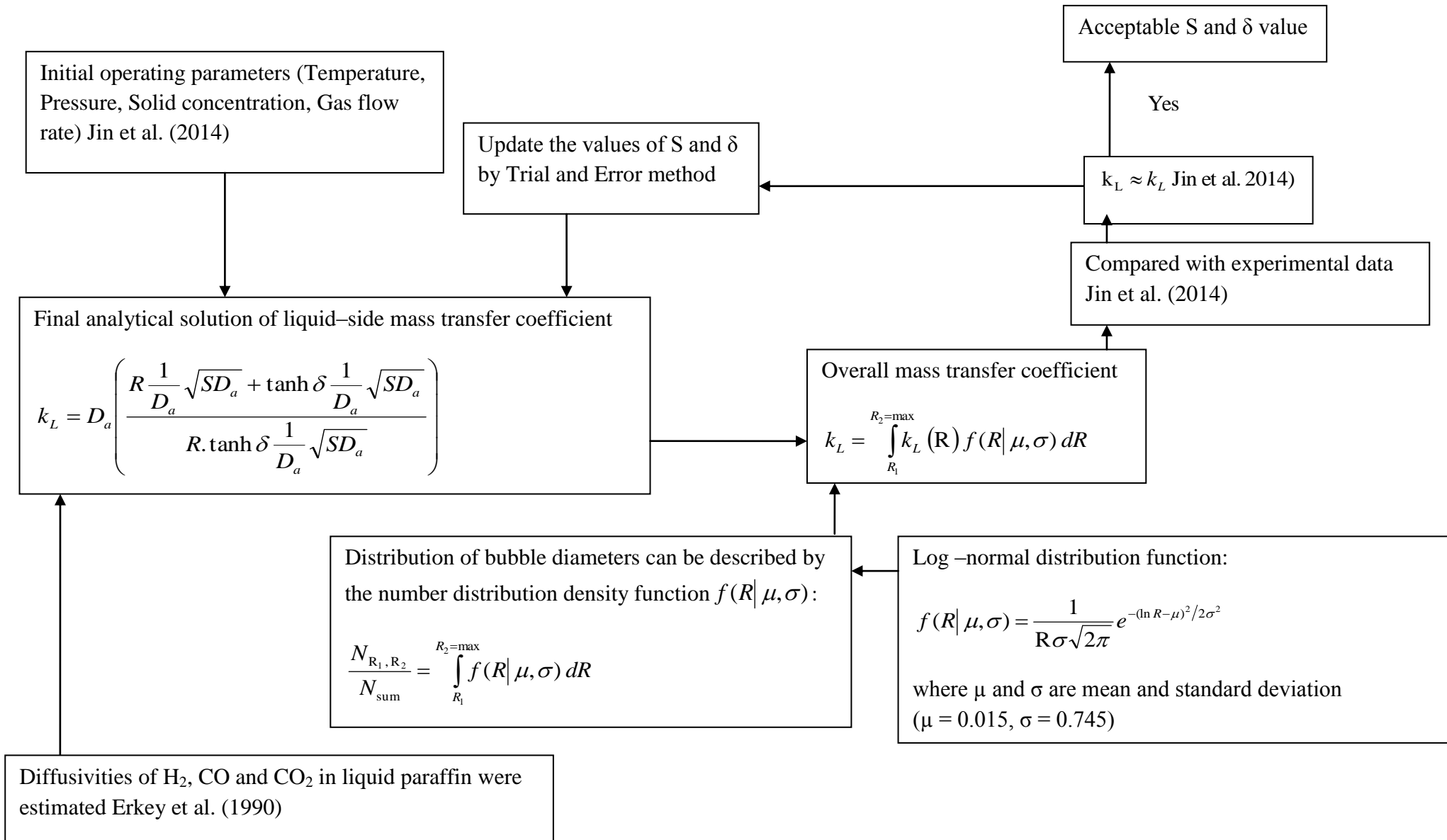


Figure 5.2 Flow diagram for estimation of liquid film thickness and surface renewal rate in a slurry bubble column

5.1.1 Effect of temperature

The mathematical model has been used to predict k_L for a range of temperatures from 298 – 423 K. Equation proposed by Erkey et al. (1990) was used to estimate diffusivity of gas (H_2 , CO, and CO_2) in liquid paraffin at different temperatures. Figure 5.3 shows the effect of temperature on k_L for diffusion of H_2 , CO and CO_2 in a slurry system comprising liquid paraffin– Quartz sand (particle size: 150-200 μm). It can be seen that the liquid–side mass transfer coefficient k_L value increases with temperature remarkably. The temperature influences both δ and S . With increase in temperature, liquid film thickness decreases while surface renewal rate increases. Both liquid viscosity and surface tension decrease with increase in temperature. Diffusion coefficient of gas in liquid and liquid properties was strongly affected by the system temperature. Mobility of liquid elements (micro eddies) on the bubble surface increases with increase in temperature due to lowering of viscosity of liquid, resulting in lower resistance of liquid film due to resultant thinning of film which promotes penetration of gas molecules from inside of the bubble to the bulk liquid phase. In other words, liquid–side mass transfer coefficient increases with decrease in liquid film thickness δ at higher temperatures due to reduction in viscosity. Diffusion coefficient of gas in liquid paraffin increased with increasing temperature and resulted in the increase in k_L . Besides, a high temperature also favors the diffusion of gas molecules in liquid film resulting in the increase in k_L value. However, a higher temperature may also promote coalescence of small bubbles into large ones (result: decreased a) with faster movement and consequently a relatively shorter contact time. This will result in a decrease in the thickness of the liquid film δ and as a result, mass transfer coefficient k_L increases (Yang et al. 2001).

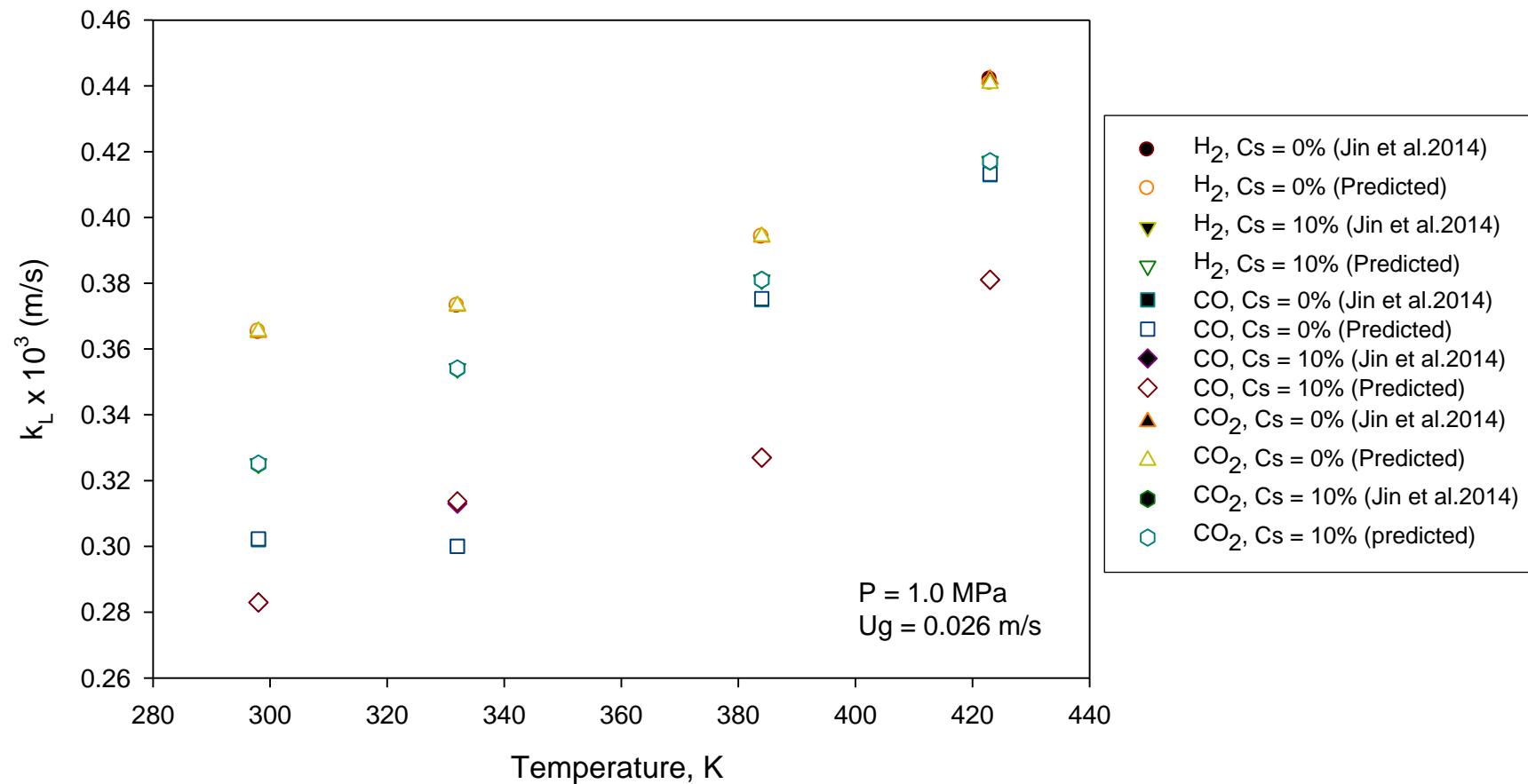


Figure 5.3 Influence of temperature on mass transfer coefficient for diffusion of H_2 , CO and CO_2 in a slurry system (liquid paraffin– Quartz sand: 150-200 μm) – comparison of experimental and predicted values.

Note: In Figure 5.3, experimental data points from literature shown in bold symbols are obscured by the symbols of model predicted data points. Therefore, are not visible.

5.1.2 Effect of pressure

Fig. 5 illustrates the influence of pressure on the mass transfer coefficient k_L in the slurry phase (liquid paraffin – quartz sand). Figure 5.4 also shows the variation of mass transfer coefficient k_L with system pressure for gases: H₂, CO and CO₂ in a slurry system (liquid paraffin – Quartz sand: 150 – 200 μm). It is obvious from Figure 5.4 that, the liquid-side mass transfer coefficient k_L increases slightly for H₂, CO and CO₂ gases with increase in pressure. The solubility of gas in the liquid phase increases with pressure, which results in decrease in liquid viscosity and surface tension (Yang et al. 2001; Lau et al. 2004). Both the liquid film thickness and surface renewal rate are influenced by the system pressure. At higher pressures, bubble breakups are enhanced and bubble coalescence is suppressed, which escalates the formation of smaller bubbles resulting in an increase in the interfacial area of the bubble. The change in k_L values at elevated pressures may be explained by the change in liquid properties, i. e. surface tension and viscosity. An increase in pressure lowers the surface tension of the liquid because of increased solubility of gas. A decrease in surface tension with pressure may allow the formation of smaller gas bubbles in the liquid phase, which will increase the interfacial area per unit volume of the bubble. The reduction in liquid viscosity also promotes mass transfer due to lower resistance of liquid film. Increase in pressure leads to the minor increase in k_L values, and an increase in the interfacial area. It may be seen from Figure 5.4 that the value of k_L for CO₂ with C_s = 10% at 2.0 MPa is lowest (0.326 m/s). It has been reported that at a pressure range of 1.7 to 3.0 MPa, increase in gas holdup for He and N₂ was reported to be within the same order of magnitude. This is because of the fact that under low pressure, large and less-dense gas bubbles are formed, whereas under high pressures, small and dense gas bubbles are formed. Under such conditions, it would not be enough to rupture the small and dense gas bubbles, and therefore, the increase in gas holdup becomes insignificant (Sujan and Vyas 2017). At higher pressures, number of bubble break-ups in the system are enhanced which escalate the formation of smaller bubbles resulting in an increase in the interfacial area of the bubble. Furthermore, several factors affect the interfacial area in a bubble column (Mena et al 2011), one of these factors may be responsible for lowering the interfacial area which results in lower k_L value.

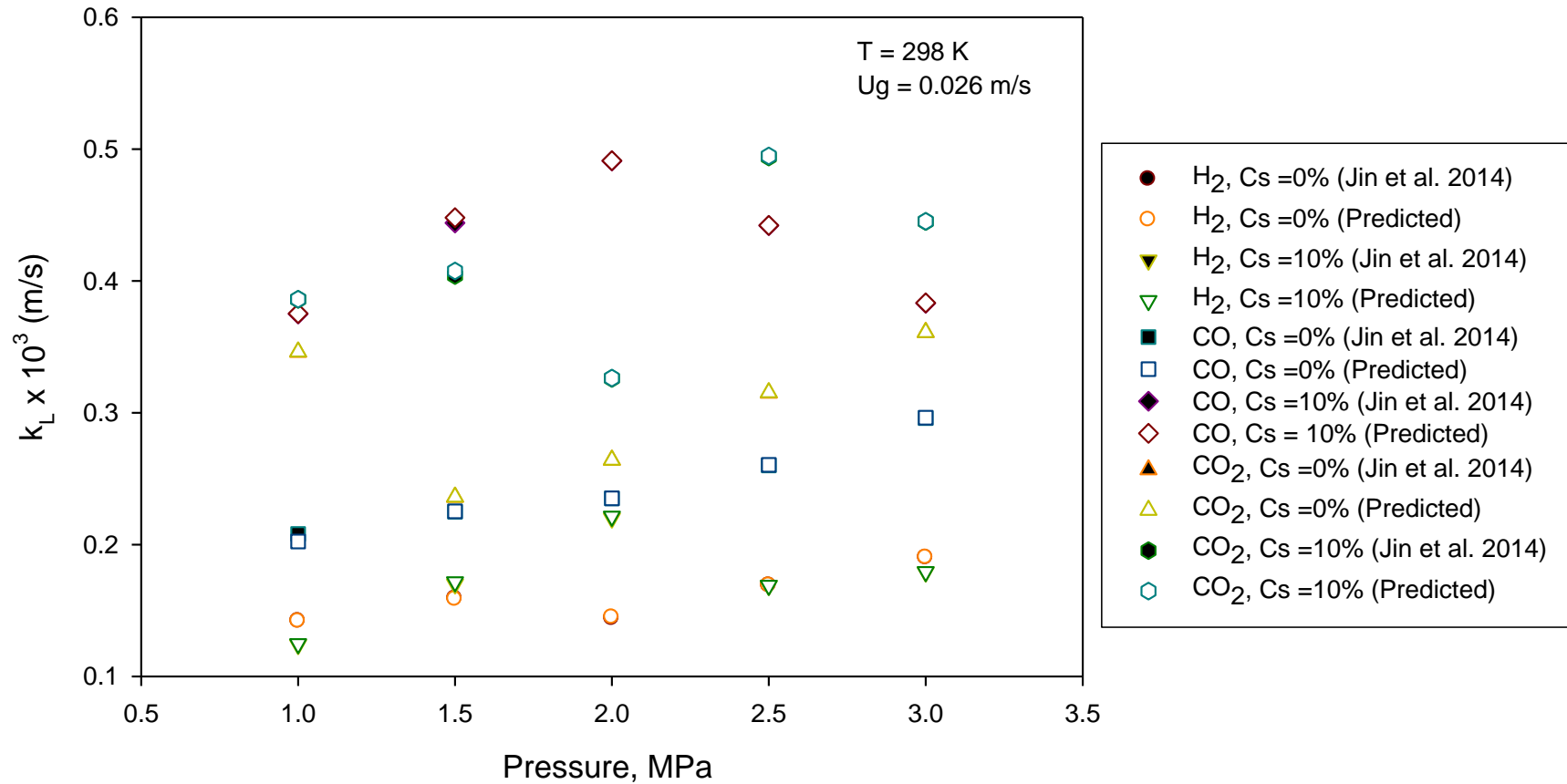


Figure 5.4 Influence of pressure on mass transfer coefficient for diffusion of H₂, CO and CO₂ in a slurry system (liquid paraffin– Quartz sand: 150-200 μm) – comparison of experimental and predicted values.

Note: In Figure 5.4, experimental data points from literature shown in bold symbols are obscured by the symbols of model predicted data points. Therefore, are not visible.

5.1.3. Effect of superficial gas velocity

Effect of the superficial gas velocity on mass transfer coefficients, k_L of H₂, CO and CO₂ in the slurry (liquid paraffin– Quartz sand: 150 – 200 μm) bubble column at 1.0 MPa is presented in Figure 5.5. As shown in Figure 5.5, when gas velocity increases, the bubble diameter would increase slightly, and the rising velocity of bubble increases, leading to the increase in turbulence and the surface renewal rate. Turbulence causes interfacial fluctuations and reduces the liquid film thickness. Higher gas velocity increases the gas holdup and decreases the mean bubble diameter leading to the increase in the specific gas-liquid interfacial area. In addition, the increase in superficial gas velocity reduces the bubble residence time leading to a decrease in the bubble surface renewal rate, S (Yang et al. 2003). Therefore, the two opposing effects result in a small influence on the superficial gas velocity and mass transfer coefficient k_L . The value of k_L for H₂ at Cs = 10% is slightly higher at a gas velocity of 4.2 m/s which is maximum among the gas velocities applied. However, this variation is small and may be attributed to experimental measurement errors. Such deviation can be found in values reported earlier also (Kluytmans et al. 2003; Sardeing et al. 2006)

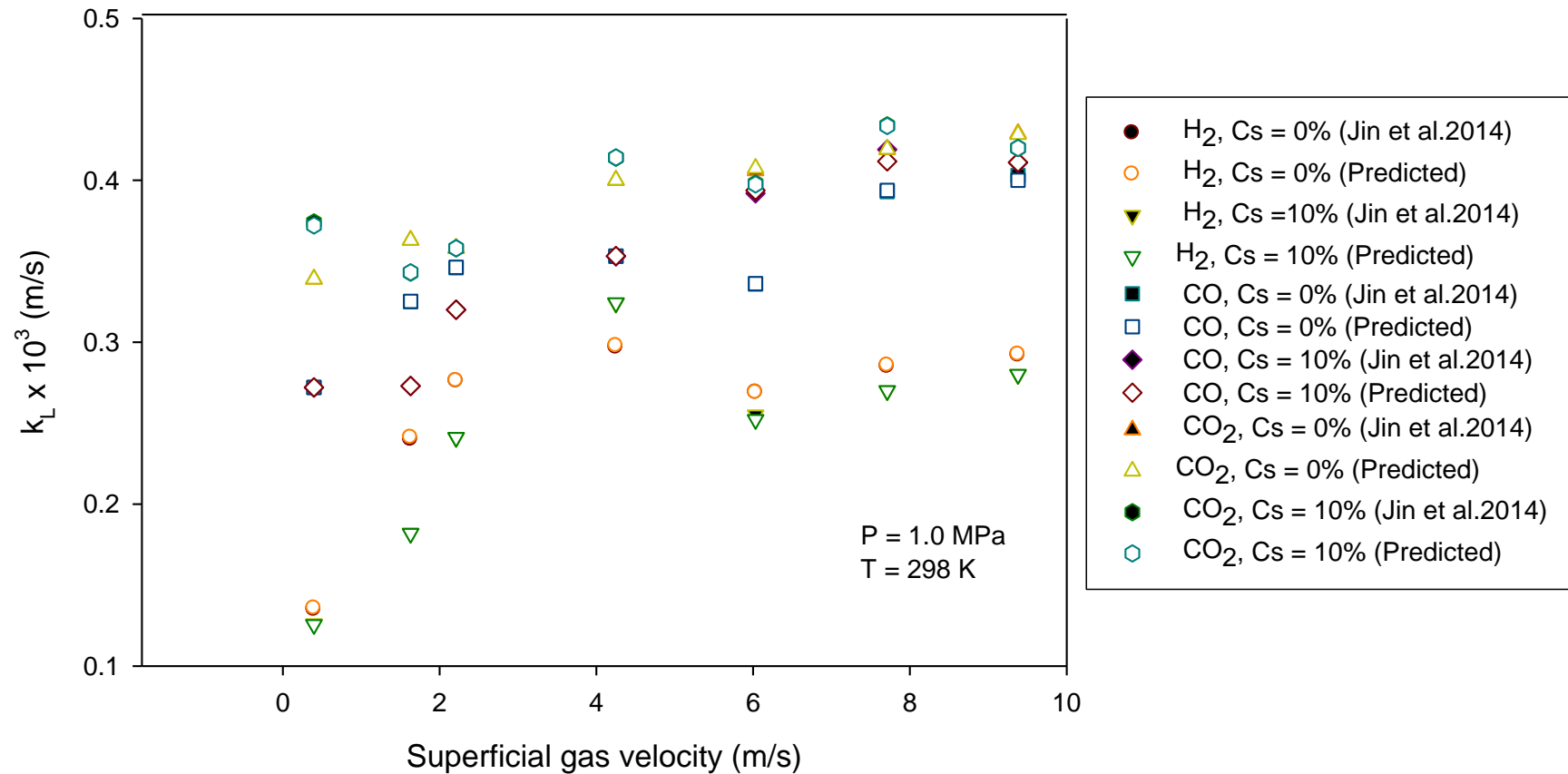


Figure 5.5 Influence of gas flow rate on mass transfer coefficient for diffusion of H₂, CO and CO₂ in a slurry system (liquid paraffin– Quartz sand: 150-200 μm) – comparison of experimental and predicted values.

Note: In Figure 5.5, experimental data points from literature shown in bold symbols are obscured by the symbols of model predicted data points. Therefore, are not visible.

5.1.4 Effect of solid concentration

Solid concentration C_s in liquid paraffin (quartz sand, particle size 150 – 200 μm) was varied from 0% to 20% by mass. Figure 5.6 shows the influence of solid concentration on the mass transfer coefficients k_L of H_2 , CO and CO_2 , respectively. It can be seen that the values of mass transfer coefficient k_L decreased slightly with an increase in the solid concentration. The enhancement of solid holdup results in increase in viscosity of the slurry, which is unfavorable to the mass transfer process. Additional solid particles may reduce the turbulence level and decrease the interface mobility. Thus, the net result will be lowering of k_L . Addition of solid concentration to a slurry system will enhance the gas bubble coalescence frequency, and as result, specific interface area will be decreased. The system viscosity also affects the surface renewal rate S (Yang et al. 2003). The surface renewal rate and mobility decrease due to addition of solid concentration and it will prevent the gas diffusion into liquid phase resulting in decrease in the value of k_L .

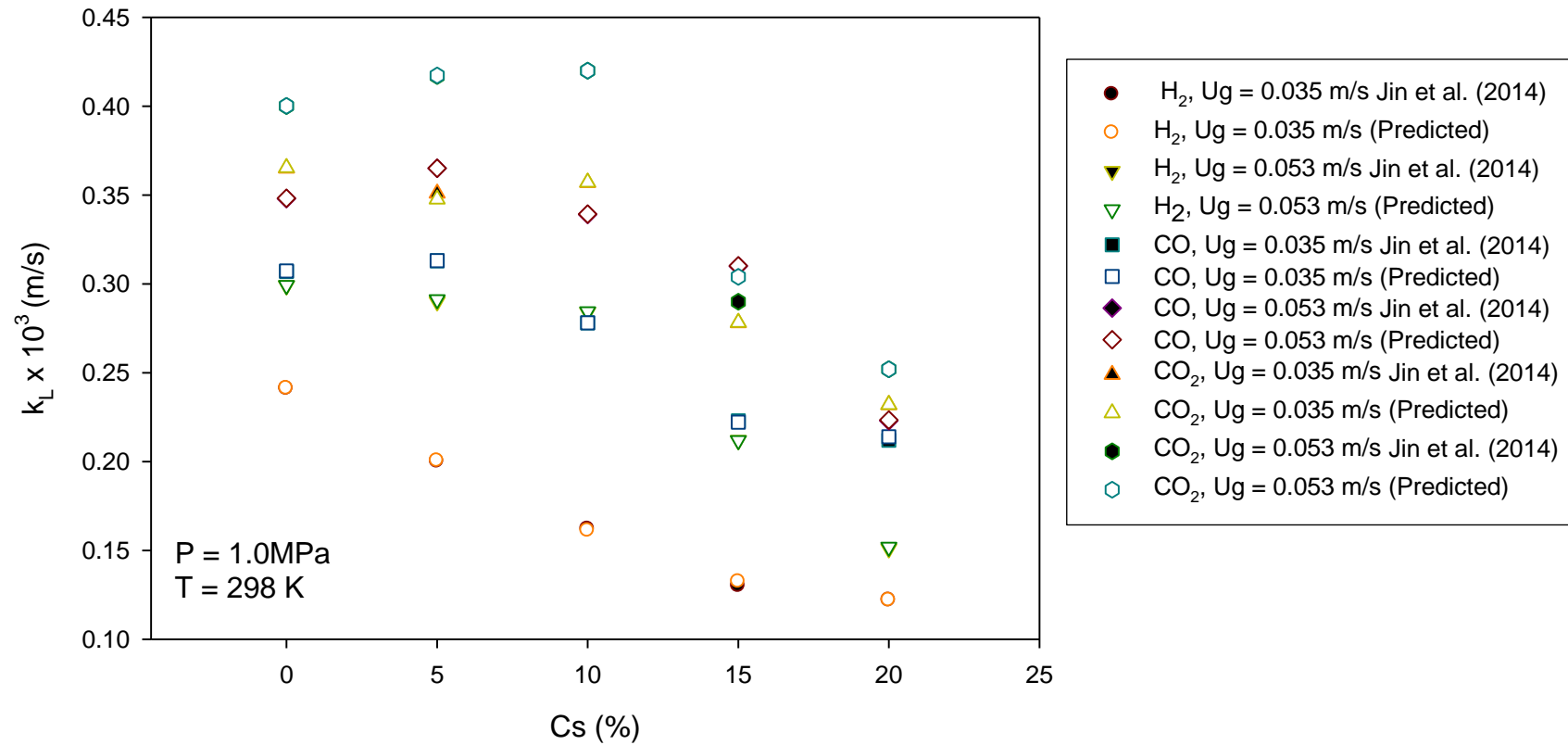
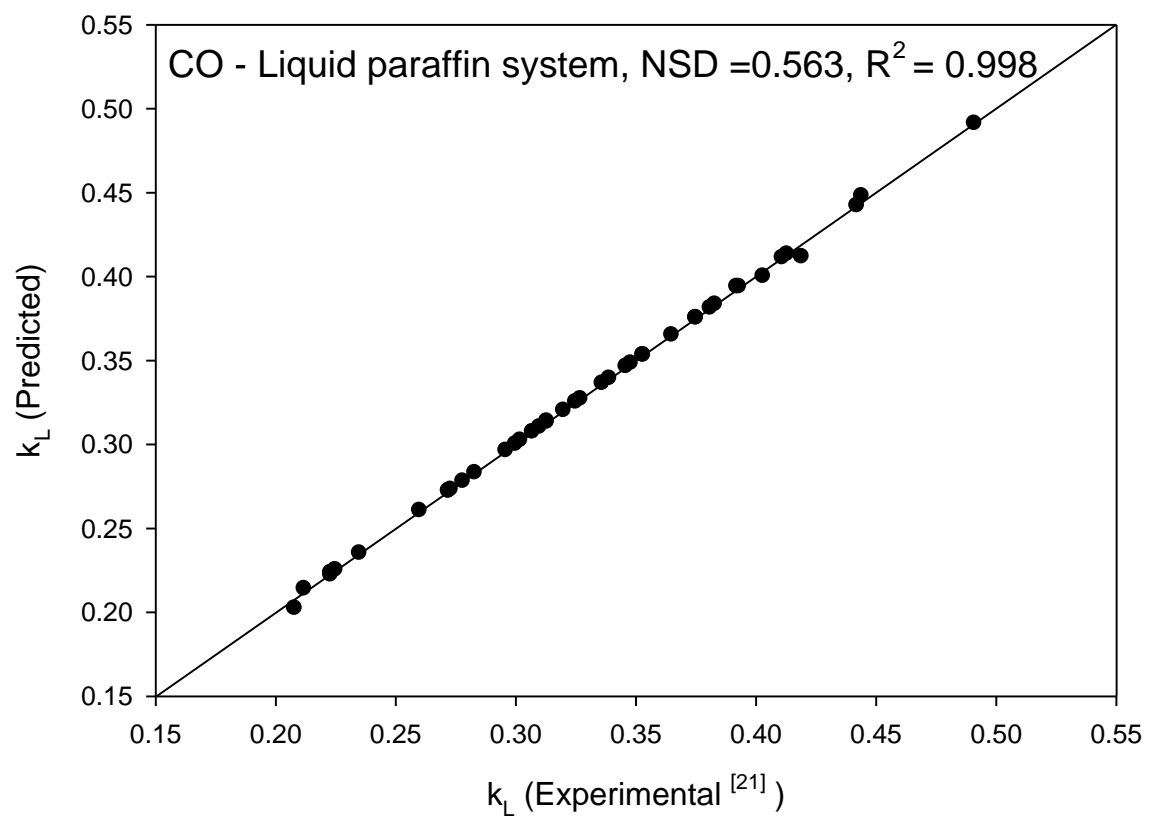


Figure 5.6 Influence of slurry (liquid paraffin – Quartz sand: 150-200 μm) concentration on mass transfer coefficient k_L .

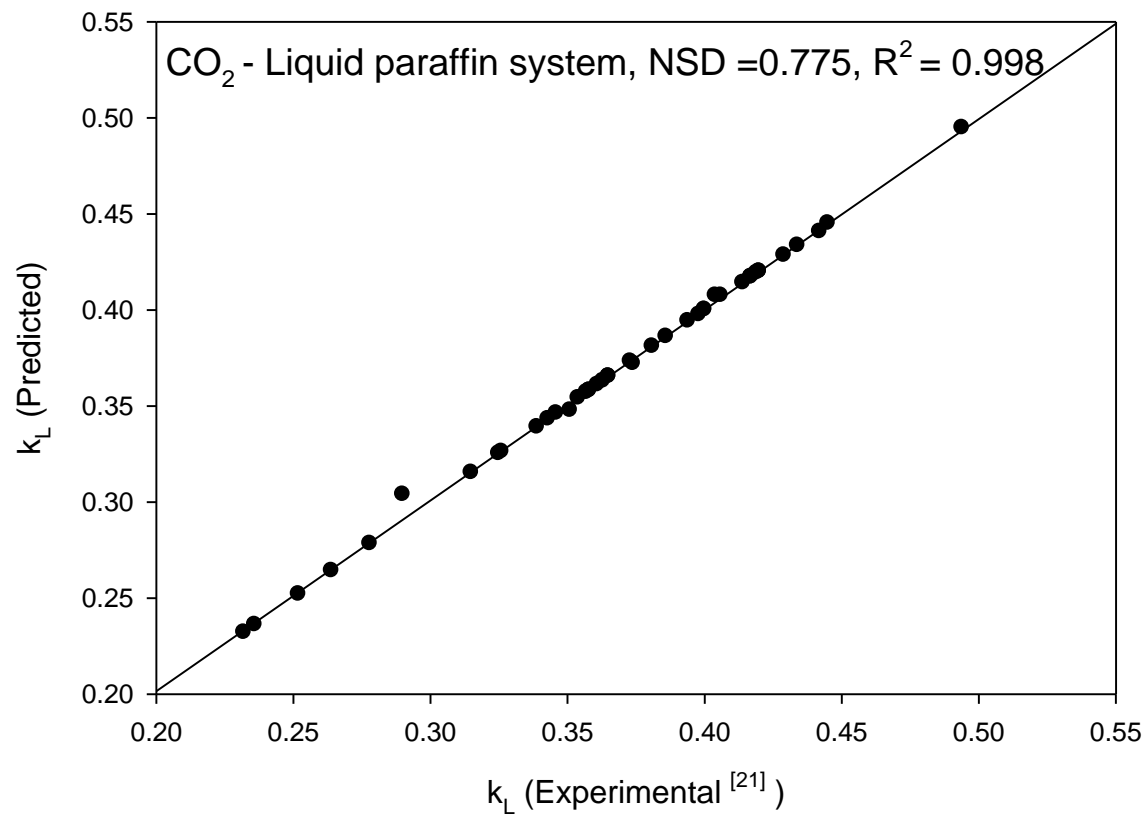
Note: In Figure 5.6, experimental data points from literature shown in bold symbols are obscured by the symbols of model predicted data points. Therefore, are not visible.

5.1. 5 Effect of liquid film thickness on k_L

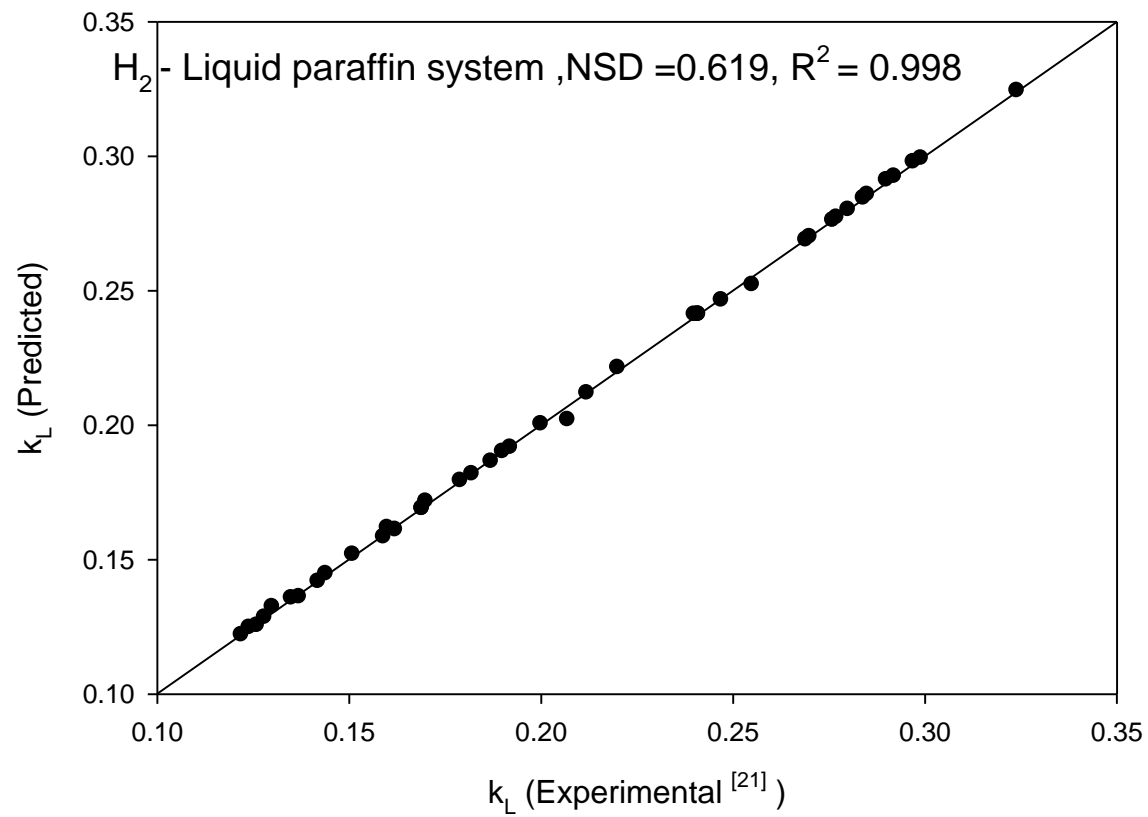
The experimental data from literature (Jin et al. 2014) and predicted values of k_L from the proposed model for CO-, CO₂- and H₂- slurry systems (liquid paraffin – Quartz sand: 150-200 μm) were plotted and are presented in Figures 5.7 (a) – (c). It may be seen from Figures 5.7 (a) – (c) that the predicted values of k_L show very good agreement with the experimental data within an average deviation of ± 2%. In addition, k_L values estimated by varying liquid film thickness (δ) for surface renewal rate ranging from 1 to 10 s⁻¹ were plotted and depicted in Figures 5.8 (a) – (c). It may be seen from Figures 5.8 (a) – (c) that variation in liquid film thickness δ values in the range from 2.5×10^{-6} to 7×10^{-6} m yields k_L values in the range of 0.2×10^{-3} to 0.5×10^{-3} m/s for CO-Liquid paraffin system. The corresponding values for CO₂-Liquid paraffin and H₂-liquid paraffin systems are for δ values range 2.14×10^{-6} to 4.70×10^{-6} m, k_L : 0.232×10^{-3} to 0.494×10^{-3} m/s and for a δ values in the range from 1.20×10^{-5} to 5.0×10^{-5} m, k_L : 0.128×10^{-3} to 0.324×10^{-3} m/s respectively. Thus, simulated results indicate that k_L is inversely proportional to δ . These trends are in order as k_L decreases with increase in δ values. It is important to mention here that values of δ are not measurable but at the same time mass transfer resistance is controlled by the magnitude of δ (Treybal 1981). The values of δ have not been reported earlier. Surface renewal rate plays an important role in maintaining the concentration gradient between the bulk gas and liquid film. Ranges of surface renewal rates have been taken in the present work from literature (Zhao et al 2003).



(a)

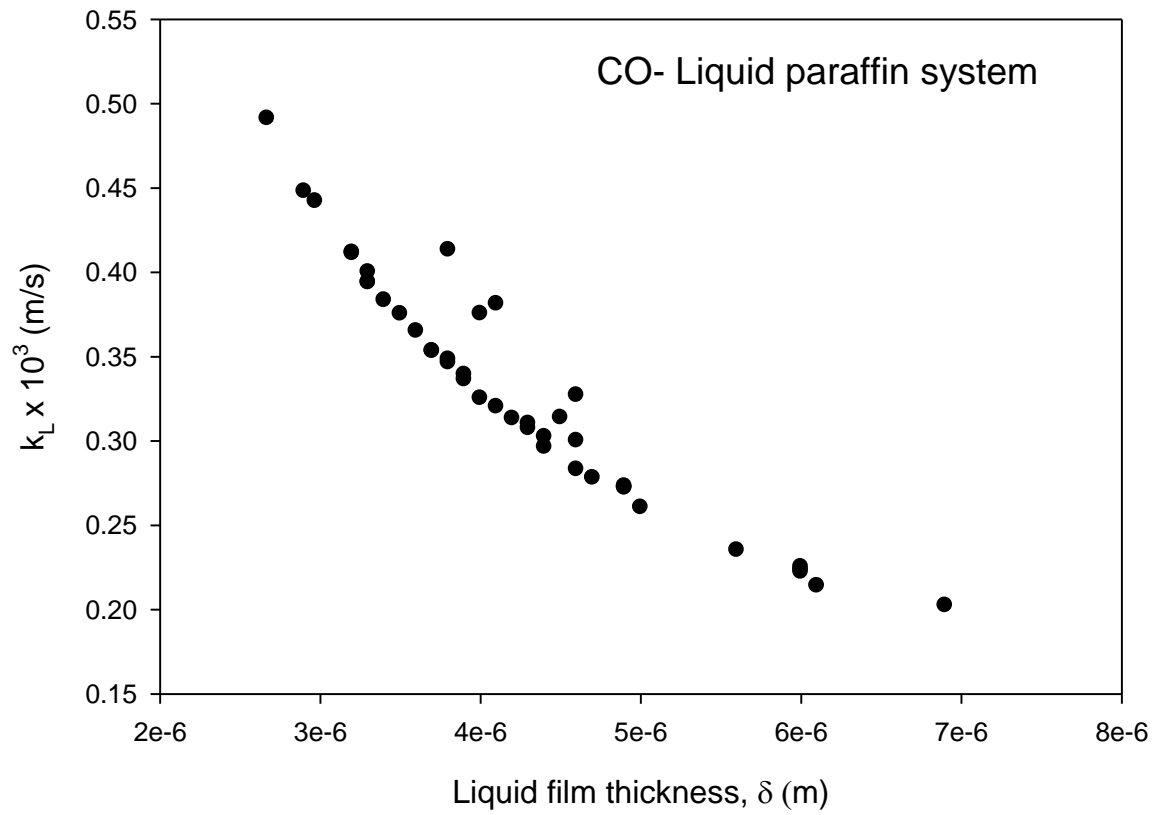


(b)

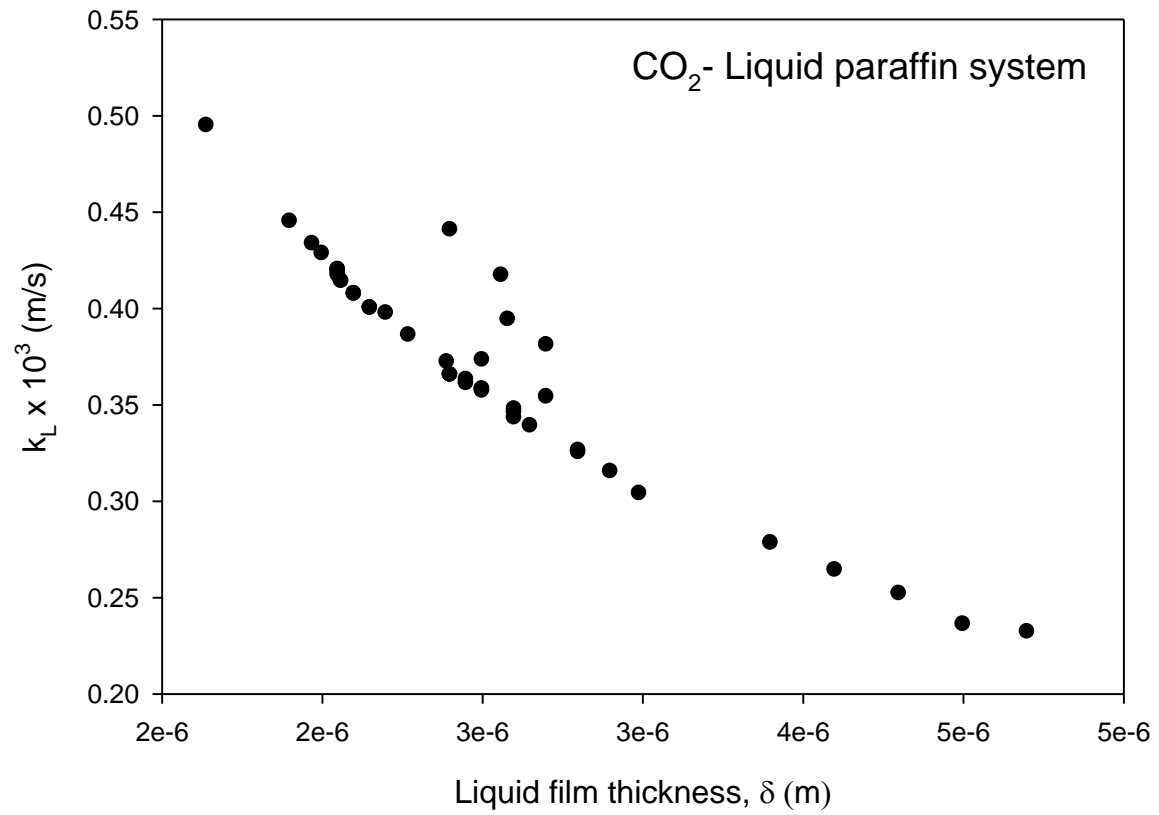


(c)

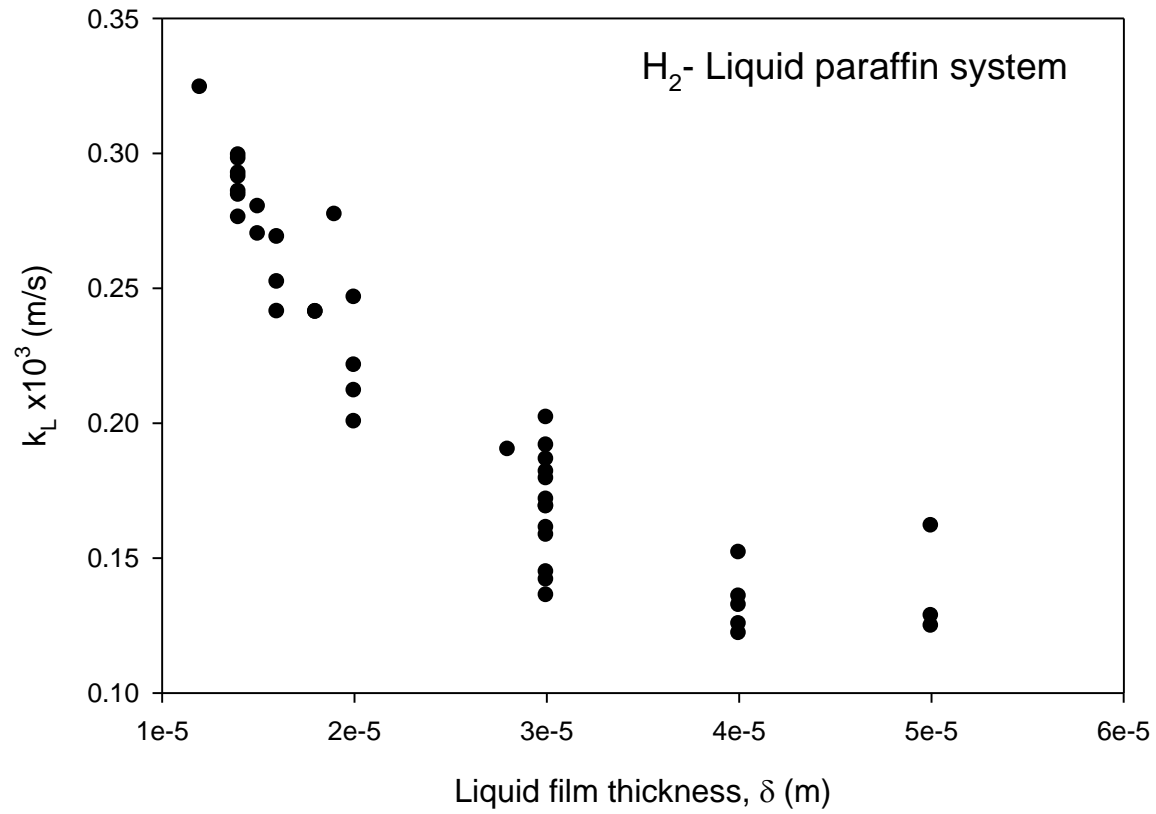
Figure 5.7 Experimental vs predicted values of k_L for (a) CO – slurry system (liquid paraffin – quartz sand), (b) CO₂ – slurry system (liquid paraffin – quartz sand) and (c) H₂ – slurry system (liquid paraffin – quartz sand).



(a)



(b)



(c)

Figure 5.8 Effect of liquid film thickness (δ) on k_L ($S = 1-10 \text{ s}^{-1}$) for (a) CO – slurry system (liquid paraffin – quartz sand), (b) CO₂ – slurry system (liquid paraffin – quartz sand) and (c) H₂ – slurry system (liquid paraffin – quartz sand).

5.1.6 Empirical correlations for liquid film thickness δ

The model developed in the present work for mass transfer coefficient (k_L) for turbulent regime is based on molecular diffusion and convective flows, which are responsible for the renewal of liquid film at the bubble surface due to microscale eddies of the turbulent field. The size of gas bubble is not a critical parameter for estimation of k_L (Sardeing et al. 2006). The development of a relationship between liquid film thickness and other variables such as pressure, temperature, superficial gas velocity, solid concentration, mass transfer coefficient, and physical properties of gas and liquid can be written in the following form:

$$\delta = f(T, P, U_g, C_s, k_L, D_a, D_c, M_A, \nu_A, \mu_{SL}, \rho_{SL})$$

Dimensional analysis was used by employing Buckingham Π (pi) theorem to obtain empirical correlations for predicting δ values for H_2 , CO and CO_2 in the form of dimensionless groups (Eu , Re , Sc , and Sh) and C_s , and ratio of slurry and gas properties. Indeed, it is not possible to fit a single correlation in good agreement with experimental data. Diffusivities of H_2 , CO and CO_2 in liquid paraffin can be calculated by Eq. (4.110) proposed by Erkey et al. (1990). Developed correlations for the three systems are as follows:

H_2 - liquid paraffin-quartz sand system

$$Sh = 1.36 \times 10^{-13} (Eu)^{0.0346} (Re)^{0.129} (Sc)^{0.118} (C_s)^{0.06} \left(\frac{\rho_{SL}}{\rho_G} \right)^{22.74} \left(\frac{\delta_{H_2}}{d_B} \right)^{-0.163} \quad (5.1)$$

Valid range : $7.26 \leq Re \leq 6.0 \times 10^4$, $2.26 \times 10^6 \leq Sh \leq 5.54 \times 10^6$, $2.41 \times 10^3 \leq Sc \leq 8.93 \times 10^4$

$12.77 \leq Eu \leq 4.9 \times 10^6$, $0 \leq C_s \leq 20(\text{mass } \%)$, $6.005 \leq \rho_{SL}/\rho_G \leq 6.312$,

$3.16 \times 10^{-4} \leq \delta/d_B \leq 9.49 \times 10^{-4}$

CO- liquid paraffin-quartz sand system

$$Sh = 1.414 \times 10^3 (Eu)^{-0.010} (Re)^{-0.021} (Sc)^{-0.2683} \left(\frac{\delta_{CO}}{d_B} \right)^{-0.966} \quad (5.2)$$

Valid range: $7.26 \leq Re \leq 6.0 \times 10^4$, $1.54 \times 10^7 \leq Sh \leq 3.74 \times 10^7$, $9.93 \times 10^3 \leq Sc \leq 3.67 \times 10^5$

$12.77 \leq Eu \leq 4.9 \times 10^6$, $0 \leq C_s \leq 20(\text{mass } \%)$, $0.997 \leq \rho_{SL}/\rho_G \leq 1.048$,

$1.69 \times 10^{-4} \leq \delta/d_B \leq 4.37 \times 10^{-4}$

CO₂- liquid paraffin-quartz sand system

$$Sh = 5.229 \times 10^3 (Eu)^{0.0012} (Re)^{0.0029} (Sc)^{0.0074} \left(\frac{\rho_{SL}}{\rho_G} \right)^{0.184} \left(\frac{\delta_{CO_2}}{d_B} \right)^{-0.974} \quad (5.3)$$

Valid range: $7.26 \leq Re \leq 6.0 \times 10^4$, $1.49 \times 10^7 \leq Sh \leq 3.39 \times 10^7$, $8.40 \times 10^3 \leq Sc \leq 3.11 \times 10^5$

$12.77 \leq Eu \leq 4.9 \times 10^6$, $0 \leq C_s \leq 20(\text{mass } \%)$, $0.653 \leq \rho_{SL}/\rho_G \leq 0.686$,

$1.35 \times 10^{-4} \leq \delta/d_B \leq 2.97 \times 10^{-4}$

Empirical correlations for the estimation of liquid film thickness presented at eq. (5.1) to eq. (5.3) indicate that the effect of solid concentration on the film thickness is negligible up to a solid concentration of 20% by vol. in case of all the three gases studied. Thus, it is obvious that mass transfer in gas-slurry systems may be treated nearly in the same way as that of a gas-liquid system. The values of the C_s term in the three eq. (5.1) to eq. (5.3) is nearly equal to 1 suggesting that the behavior of slurries of glass like solids, e.g. quartz sand will be same as that of gas-liquid systems. It may also be seen from eq. (5.1) – (5.3) that the exponent of parameter (ρ_{SL}/ρ_G) of H₂ – slurry system has a larger value than the other two systems. This fact points

out that the gas properties also play a significant role in mass transfer in bubble columns. Furthermore, the exponent of gas density (ρ_G) in eq. (5.1) – (5.3) reveals that the gas density is an important parameter in the case of H₂ gas while the same is relatively less significant in other two cases. This variation in behavior of the gases may be attributed to their molecular masses and resulting chemical behavior due to atomic orbital variations. The negative exponent in case of CO for Eu, Re and Sc may be due to mild solubility difference of these components in liquid paraffin.

Note: The correlations on film thickness δ of H₂, CO₂ and CO that has been already published in Asia pacific journals of chemical engineering entitled “Estimation of liquid–side mass transfer coefficient and liquid film thickness in a bubble column using single spherical bubble model” **13** (2), e2178 have been modified and presented in terms of dimensionless parameter Sherwood number in eq. 5.1 - 5.3.

Section 5.2: Estimation of transition concentration of aqueous mixtures of single and binary electrolytes for bubble coalescence inhibition.

Coalescence inhibition is an important requirement in industrial bubble columns for enhancement of gas holdup which in turn increases the gas –liquid interfacial area for increasing the value of overall gas – liquid mass transfer coefficient. Overall mass transfer coefficient in a bubble column is important for improving the productivity of the processes such as froth flotation or fermentation in biochemical industries.

In the present work, a study of coalescence inhibition has been targeted by applying gas holdup enhancement and surface tension gradient approaches for aqueous solutions of single and binary mixtures.

5.2.1 Gas holdup enhancement in aqueous solution of single electrolyte(s)

Gas holdup measurements were made in aqueous solutions of electrolytes in a bubble column. Dimensionless gas holdup (ϵ / ϵ_w) values for single component aqueous solutions of different electrolytes (NaCl, $MgSO_4 \cdot 7H_2O$, Na_2SO_4 , and $CaCl_2 \cdot 2H_2O$) were plotted against electrolytes concentration (C) at different gas flow rates (17.5 - 27.5 L/m). From Figure 5.9 it can be observed that dimensionless gas holdup (ϵ / ϵ_w) enhancement for a strong electrolyte ($CaCl_2$) reached a maxima of 69% at a concentration of 0.075 mol/L and a gas flow rate of 27.5 L/m. At electrolytes concentration greater than 0.075 mol/L, gas holdup enhancement decreases to 52% at an electrolyte concentration of 0.20 mol/L and then it becomes almost constant at higher concentrations. The electrolyte concentration at which the gas holdup enhancement is maximum is known as transition concentration (C_{trans}). At transition concentration, the bubble size distribution levels off and reach a constant value (Marrucci and Nicodemo 1967). From Figure 5.10, similar behavior was observed with 61% gas holdup enhancement in Na_2SO_4 solution corresponding to a concentration of 0.05 mol/L. It is remarkable to see that the gas holdup increased rapidly up to a maximum of 0.05 mol /L and thereafter the gas holdup decreased gradually (to around 11%) for a concentration increase from 0.05 mol/L to 0.10 mol/L. Thereafter, it remained almost unchanged for higher electrolytes concentration. From Figure 5.11, it is obvious that in the case of moderate electrolytes (NaCl), 47% gas holdup enhancement was observed at

the higher gas flow rate of 27.5 L/m at NaCl concentration of 0.05 mol/L. There is a slow decrease thereafter for the concentration range of from 0.05 mol/L to 0.30 mol/L. From Figure 5.12, a similar trend with 38% gas holdup enhancement was found in MgSO₄ solution. Gas holdup reached the maximum at 0.035 mol/L and decreased at to 0.075 mol/L and then almost stabilized near the same value during the increase in concentration from 0.075 mol/L to 0.3 mol/L. The inhibition of bubble coalescence results in an increase and decrease in the number and size of bubbles respectively. Comparison of measured transition concentrations and the present work with those reported in the literature doing different methods are presented in Table 5.1 along with other properties of the electrolytes studied. It may be seen from Table 5.1 that the order of the values of transition concentration for different electrolytes estimated in the present work are of the same order reported in literature. The values of C_{trans} for different electrolytes are of the same order in most of the cases. It can be seen from Table 5.1 that the value of transition concentration of the electrolyte, NaCl estimated in the present study is comparable with those reported by Syeda and Reza (2011) based on gas holdup enhancement. Similarly, the value of C_{trans} of MgSO₄ measured in the present study compares well with those reported by Zahradnik et al.(1995) and Lessard and Zieminski (1971). The comparison of values presented in Table 5.1 supports the approach and values estimated in the present work.

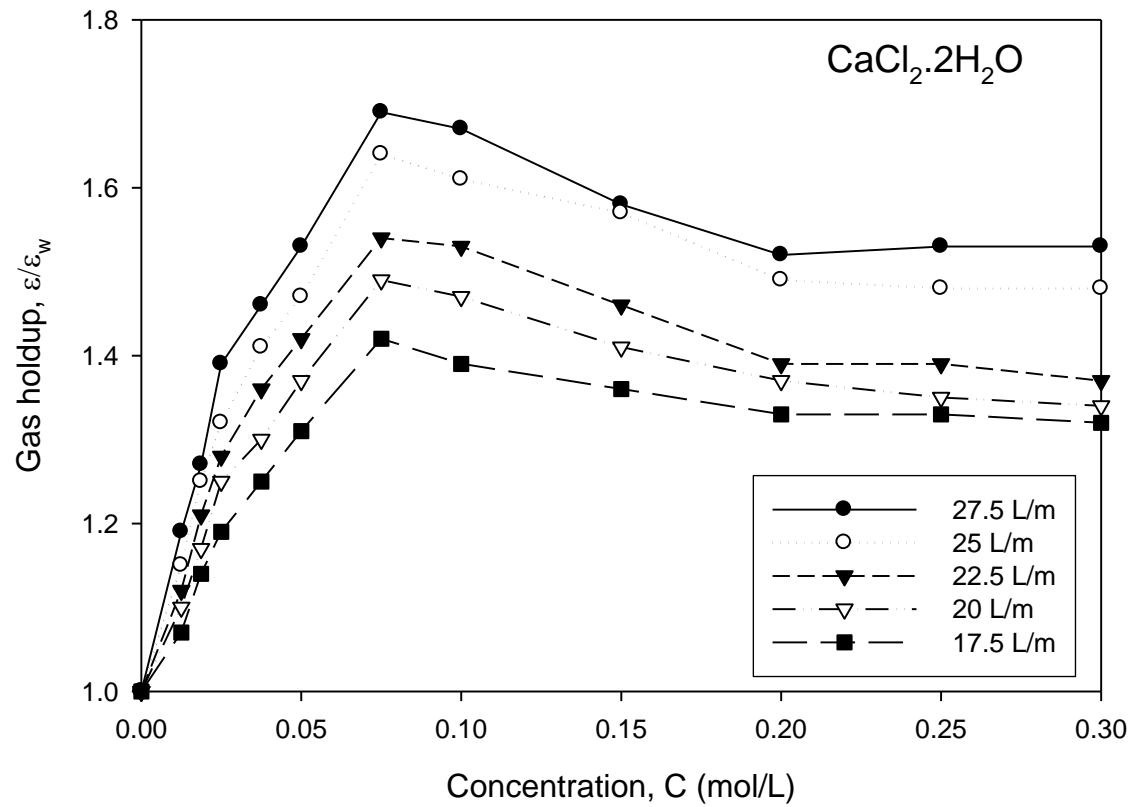


Figure 5.9 Dimensionless gas holdup parameter (ϵ/ϵ_w) versus concentration in aqueous $\text{CaCl}_2 \cdot 2\text{H}_2\text{O}$ solutions.

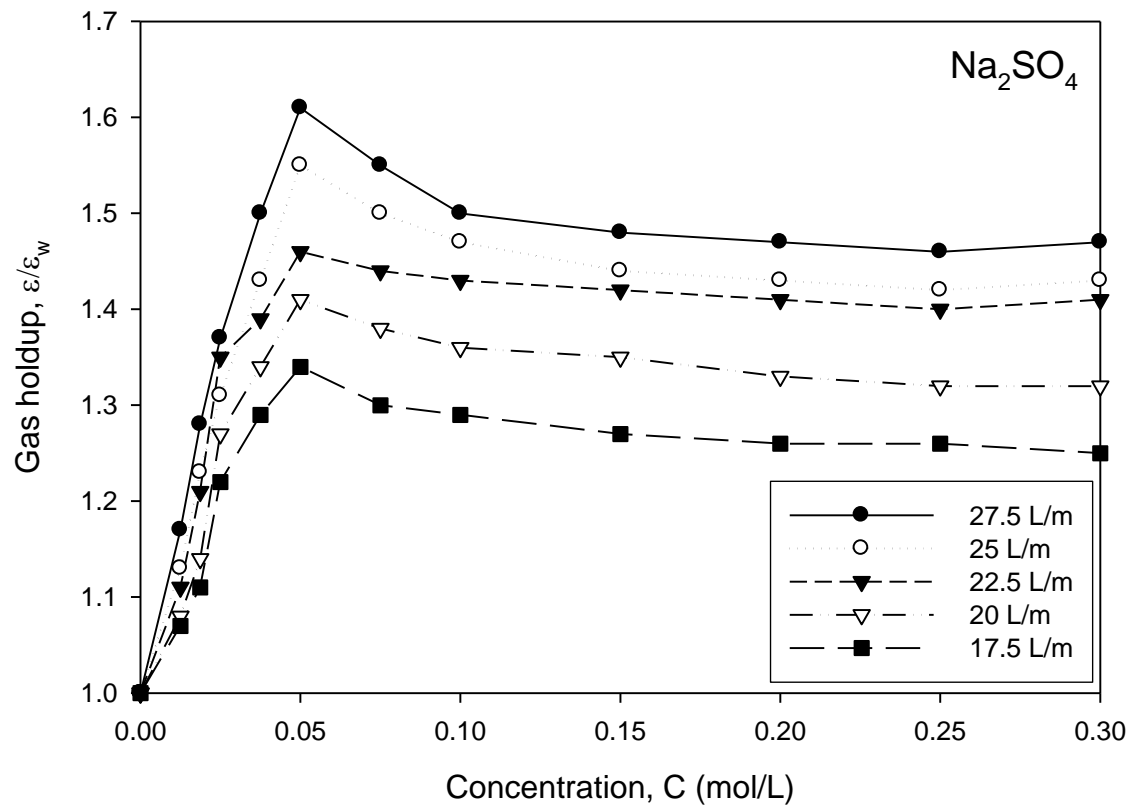


Figure 5.10 Dimensionless gas holdup parameter (ϵ/ϵ_w) versus concentration in aqueous Na_2SO_4 solutions.

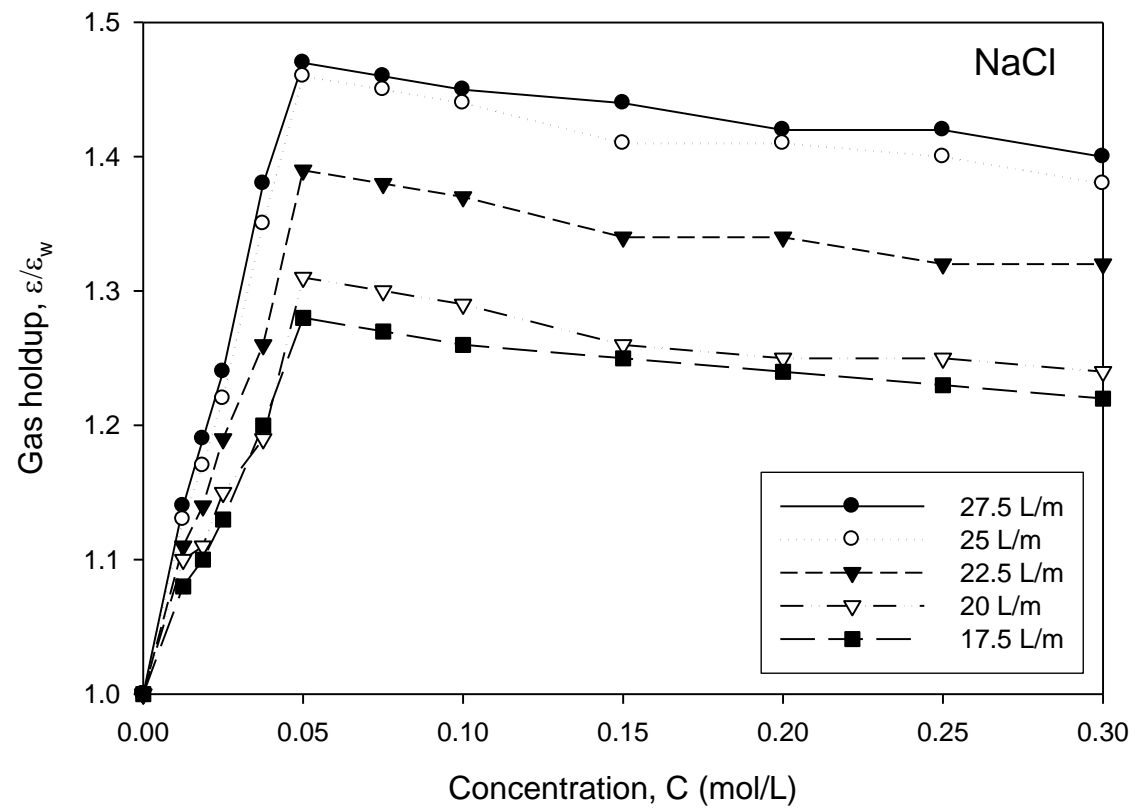


Figure 5.11 Dimensionless gas holdup parameter (ϵ/ϵ_w) versus concentration in aqueous NaCl solutions.

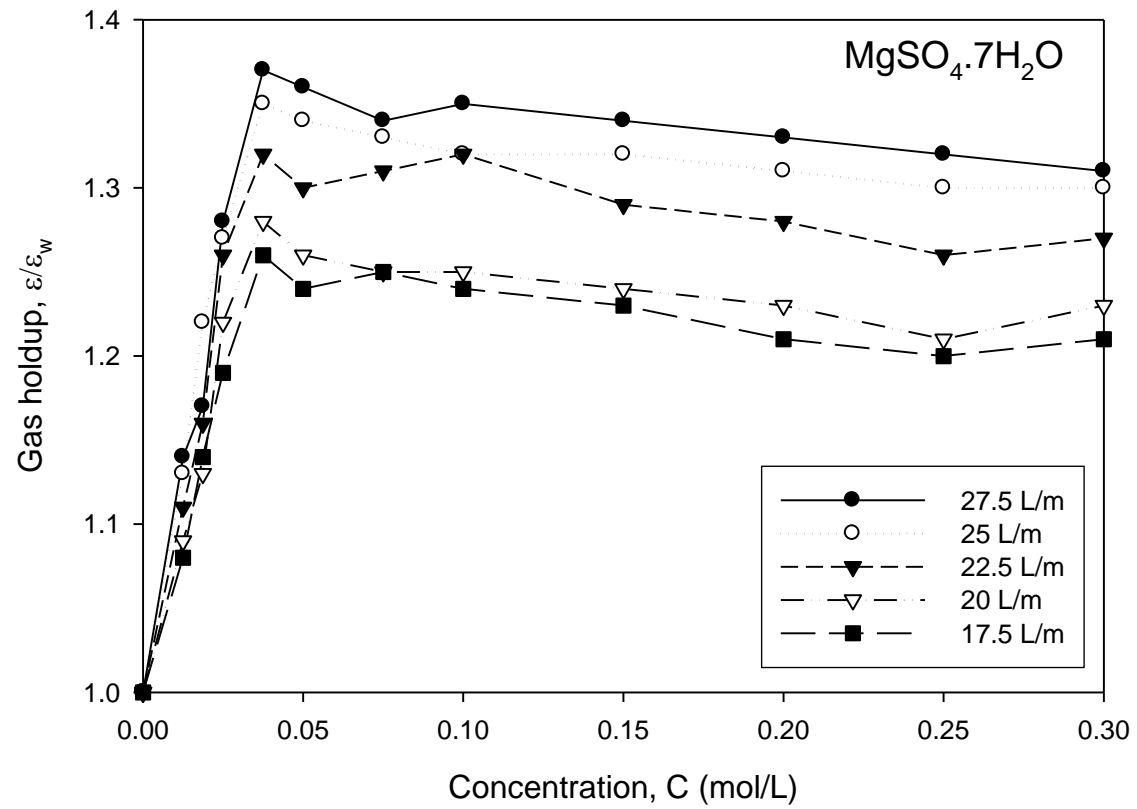


Figure 5.12 Dimensionless gas holdup parameter (ϵ/ϵ_w) versus concentration in aqueous $\text{MgSO}_4 \cdot 7\text{H}_2\text{O}$ solutions.

Table 5.1 Transition concentration, C_{trans} comparison and other properties of electrolytes.

Electrolyte	Valency type [#]	Activity coefficient for 0.1M [@]	Relative effectiveness of electrolyte [§]	Transition concentration, C_{trans} (mol/L)								
				Based on % coalescence				Based on $(\mathcal{E}/\varepsilon_w)_{\text{max}}$			Based on $C(d\sigma/dC)_{\text{max}}^2$	
				Christenson 2008	Zahradnik et al. 1995	Prince and Blanch, 1990	Lessard and Zieminski 1971	Craig et al. 1993	Syeda and Reza 2011	This work	Syeda and Reza 2011	This work
NaCl	1–1	0.7786	Moderate	0.208	0.145	0.175	0.175	0.078	0.05	0.05	0.09	0.05
MgSO ₄	2–2	0.15	Moderate	0.036	0.036	–	0.032	0.020	0.05	0.035	0.05	0.025
Na ₂ SO ₄	1–2	0.44568	Strong	–	0.051	–	0.061	–	0.25	0.05	0.03	0.05
CaCl ₂	2–1	0.51708	Strong	0.060	0.056	0.055	0.055	0.037	0.075	0.075	0.07	0.075

[#]Lee et al. 2008

[@]Zemaitis et al. 1986

[§]Ribeiro and Mewas, 2007

A qualitative comparison of gas holdup enhancement obtained for four electrolytes (2 from each strong and moderate categories) are shown in Figure 5.13. It is obvious from Figure 5.13 that the observed gas holdup enhancement behavior of these electrolytes is similar to that reported by Syeda and Reza (2011). The qualitative comparison of these electrolytes reveals that strong electrolytes yield gas holdup enhancement $\geq 60\%$ whereas moderate electrolytes give a gas holdup up enhancement values $\leq 46\%$. These values are at slight deviations with those reported by Syeda and Reza (2011). Table 5.2 presents percent incremental gas holdup enhancement of different electrolytes in comparison to the most moderate electrolyte, i.e. MgSO_4 used in the present study. In pure water, gas-liquid interface cannot sustain surface stress (Henry et al. 2008; Vakarelski et al. 2018). In such a situation, gas-liquid interface is fully mobile which leads to rapid liquid drainage from the thin film between two adjacent bubbles. This enhances coalescence phenomena due to bubble collisions. Figures 5.9 – 5.13 clearly show that in bubbling regime, gas holdup is strongly related to the coalescence tendency of bubbles in aqueous solution of electrolyte. The presence of an electrolyte establishes shear stress at the bubble interface and thus mobility of the interface is reduced or removed. During the drainage of liquid from the film in the presence of an electrolyte, surface tension gradient is established. Under such a situation, surface shear stress is created which retard surface mobility and, therefore, oppose film drainage and control drainage rate from the liquid film. This factor may contribute to the bubble stabilization process and possibly reduce the bubble size. For bubble coalescence inhibition, bubble size depends on the critical concentration of aqueous solution of an electrolyte (Prince and Blanch 1990; Chan and Tsang 2005). In fact, the critical concentration decreases with increasing bubble size. Therefore, to prevent coalescence, critical concentration increases as the equivalent diameter of bubbles decreases. In the electrolyte systems, interfacial area is 3 – 4 times higher as compared to the coalescing air-water system (Cents et al. 2005).

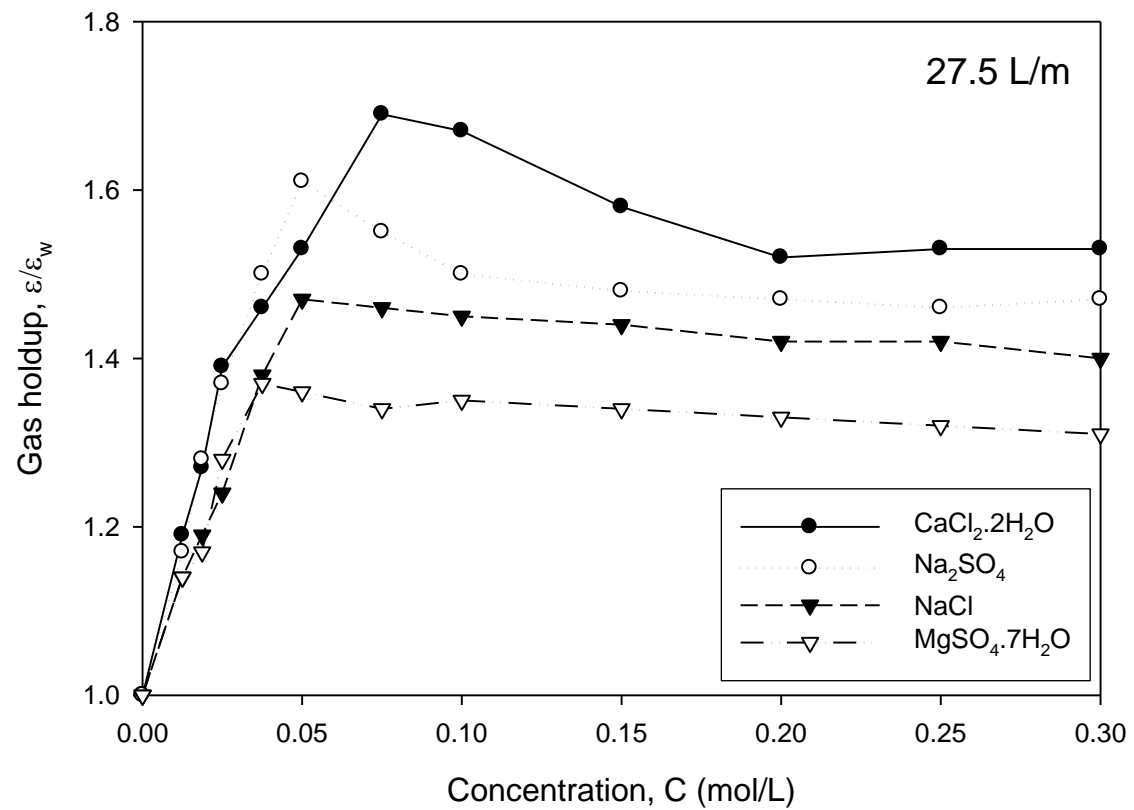


Figure 5.13 Qualitative comparisons between strong (CaCl₂·2H₂O and Na₂SO₄) and moderate (NaCl and MgSO₄·7H₂O) electrolytes.

Table 5.2 Incremental transition concentration values of electrolytes in comparison to MgSO₄ (most moderate electrolyte).

Electrolyte	Percent incremental gas holdup enhancement at transition concentration, C _{trans}
CaCl ₂	86
Na ₂ SO ₄	64
NaCl	27

These analyses indicate towards that there is only on incremental benefit of using a strong electrolyte over the most moderate electrolyte irrespective of its cost.

5.2.2 Surface tension and surface tension gradient of single electrolyte solution

Bubble coalescence is an extremely rapid process in case of pure liquid like water or sufficiently dilute solutions of electrolytes for which the value of dimensionless concentration parameter crk^2 / σ is ≤ 2 . For electrolyte solution, the dimensionless concentration parameter (crk^2 / σ) may be expressed (Marrucci 1969) as follows

$$\frac{crk^2}{\sigma} = \frac{2}{\nu RT \sigma} C \left(\frac{d\sigma}{dC} \right)^2 \frac{1}{1 \pm \frac{(d \ln a \pm)}{(d \ln C)}} \left(\frac{12\pi\sigma}{A.r} \right)^{2/3} \quad \dots(5.4)$$

where,

$$c = \frac{2}{\nu RT} C \left(\frac{d\sigma}{dC} \right)^2 \frac{1}{1 \pm \frac{(d \ln a \pm)}{(d \ln C)}} \quad \dots(5.5)$$

and

$$k = \left(\frac{12\pi\sigma}{A.r} \right)^{1/3} \quad \dots(5.6)$$

then,

$$\frac{crk^2}{\sigma} = f\left(C\left(\frac{d\sigma}{dC}\right)^2\right) \quad \dots(5.7)$$

where, ν is the number of ions produced upon dissociation (i.e. $\nu = 2$ for most of the inorganic electrolytes); R is the universal gas constant; T is absolute temperature; a_{\pm} is mean activity coefficient of a solution; A is the non-retarded Hamaker constant; σ and $d\sigma/dC$ are surface tension and surface tension gradient, respectively. The predicted values of transition concentration of electrolytes as function of surface tension and surface tension gradient given from expression could not be compared with the experimental values as bubble radius values are not available in the present work.

The concentration of electrolytes which immobilizes the gas–liquid interface for bubble coalescence inhibition is known as transition concentration (C_{trans}). Pictorial representation of bubble coalescence inhibition by using electrolyte(s) is shown in Figure 5.14. The transition concentration of electrolyte according to Marrucci’s model, depends on the magnitude of the change in surface tension with concentration at the interface, or surface activity, $(d\sigma/dC)$.

Surface tension gradient is the key factor that provides information of coalescence-hindering tendency of bubbles in an electrolyte solution. The dimensionless concentration parameter, i.e. Marrucci’s parameter $((crk^2/\sigma)$, contains the term $C(d\sigma/dC)^2$ which may be useful for characterization of the coalescence behavior. A number of studies successfully used the Marrucci’s parameter $((crk^2/\sigma)$ to predict gas hold-up and bubble coalescence time (Sagert and Quinn, 1978; Syeda and Reza 2011). The relationship between bubble coalescence inhibition and $(d\sigma/dC)$ was originally established by Marrucci and Nicodemo (1967) using a limited experimental data set. The parameter $(d\sigma/dC)^2$ is important in bubble coalescence phenomena related to the Gibbs elasticity of the liquid film and its magnitude controls the liquid drainage from the film as per Marrucci model. If the value of parameter $(d\sigma/dC)^2$ is large, the presence of electrolyte inhibits bubble coalescence, and if it is small, bubble coalescence remains unaffected (Christenson and Yaminsky 1995). Generally, the transition from coalescence regime to coalescence inhibition occurs when the value of $(d\sigma/dC)^2$ drops below $1 \text{ (mN} \cdot \text{m}^{-1}/\text{mol} \cdot \text{L}^{-1})^2$.

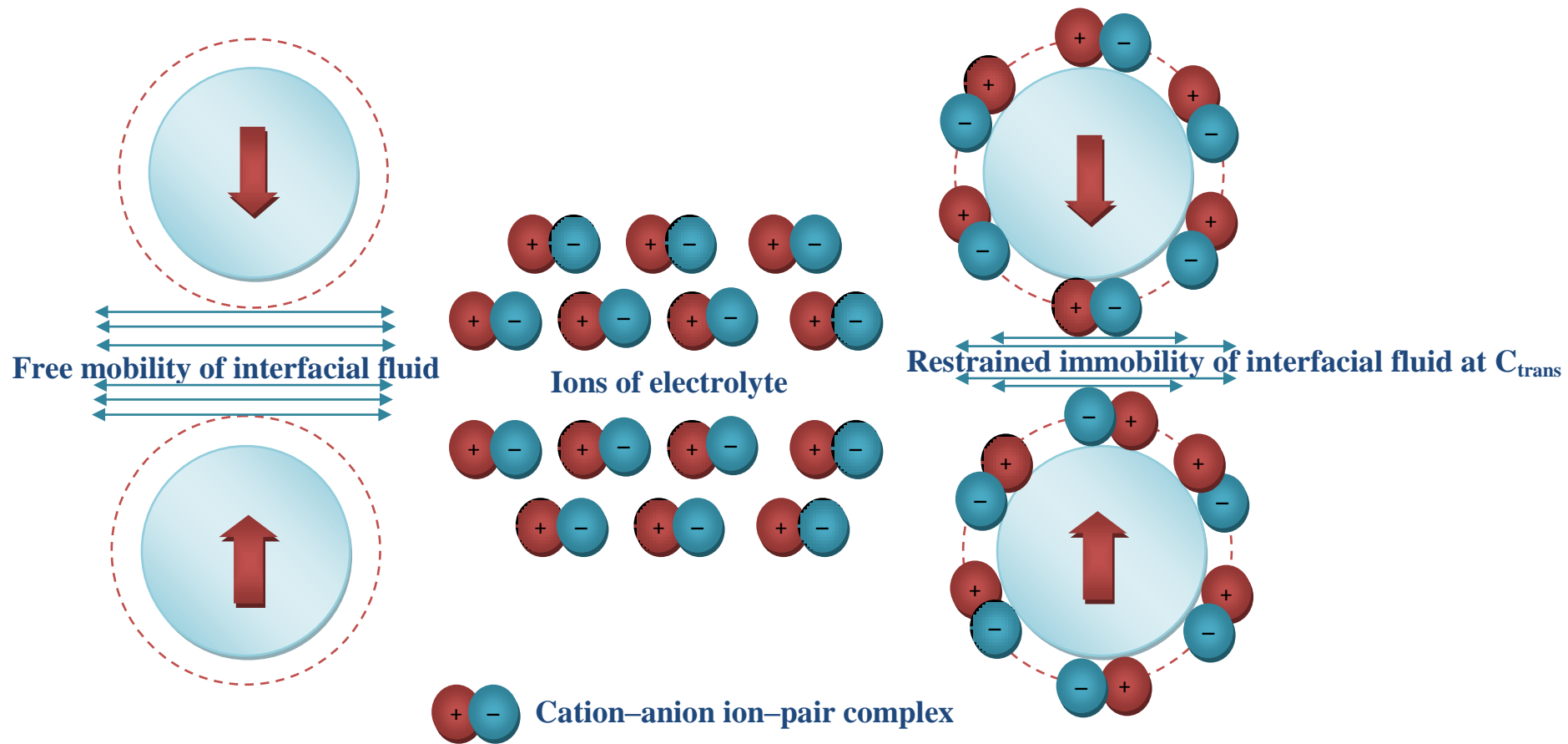


Figure 5.14 Pictorial representation of bubble coalescence inhibition by using electrolyte(s).

In this paper, the effect of electrolytes concentration on bubble coalescence behavior has been studied using the parameter $(d\sigma/dC)^2$, where $d\sigma$ is the change in surface tension and dC is the change in bulk concentration of the electrolyte. The excess surface tension $(\sigma_{el} - \sigma_w)$ due to the presence of electrolytes can be used to predict gas holdup enhancement. It can also be used to estimate transition concentration.

Plots of excess surface tension vs electrolyte concentration and parameter $C(d\sigma/dC)^2$ vs electrolyte concentration for strong electrolytes ($\text{CaCl}_2 \cdot 2\text{H}_2\text{O}$ and Na_2SO_4) are presented in Figure 5.15 and 5.16 respectively. Similarly, Plots of excess surface tension vs electrolyte concentration and parameter $C(d\sigma/dC)^2$ vs electrolyte concentration for moderate electrolytes (NaCl and $\text{MgSO}_4 \cdot 7\text{H}_2\text{O}$) are presented in Figure 5.17 and 5.18 respectively. Curves for excess surface tension vs electrolyte concentration for strong and moderate electrolyte were fitted using a non-linear polynomial fitting technique. The resulting algebraic equations were differentiated with respect to concentration to obtain $(d\sigma/dC)^2$ values. Further, the requisite parameter $C(d\sigma/dC)^2$ values for strong and moderate electrolyte were plotted against concentration. In absence of the bubble size distribution of the system, simply, algebraic equations of excess surface tension for different electrolyte concentration are presented in Table 5.3. Empirical correlation based on dimensional analysis may be proposed in future, if bubble size distribution is available.

The curve for excess surface tension vs electrolyte concentration for strong electrolytes ($\text{CaCl}_2 \cdot 2\text{H}_2\text{O}$ and Na_2SO_4) shown in Figure 5.15 increases initially up to an electrolyte concentration of 0.15 mol/L and 0.20 mol/L for $\text{CaCl}_2 \cdot 2\text{H}_2\text{O}$ and Na_2SO_4 respectively becomes almost constant thereafter at an excess surface tension value of 3.89 mN/m for $\text{CaCl}_2 \cdot 2\text{H}_2\text{O}$ and 2.95 mN/m for Na_2SO_4 respectively. A similar behavior was observed for moderate electrolytes namely NaCl and $\text{MgSO}_4 \cdot 7\text{H}_2\text{O}$ (Figure 5.17). In this curve, value of excess surface tension become constant at 2.52 mN/m for NaCl and 1.56 mN/m for $\text{MgSO}_4 \cdot 7\text{H}_2\text{O}$ corresponding to electrolyte concentration of .0.20 mol/L and 0.15 mol/L respectively. Figure 5.15 and Figure 5.17 shows that surface tension reaches to a plateau at a electrolyte concentration range of 0.2–0.3 M. The excess surface tension values of aqueous solutions of electrolytes observed in the present work are in agreement with those reported earlier (Syeda and Reza 2011).

Figure 5.16 and 5.18 show plots for parameter $C(d\sigma/dC)^2$ vs electrolyte concentration for strong and moderate electrolytes. It is obvious from these figures that parameter $C(d\sigma/dC)^2$ has higher values for strong electrolytes indicating a strong effect on bubble coalescence than moderate electrolytes.

These experimental observations are in line with those reported by Syeda and Reza (2011). It is significant to note that the concentrations at which maximum gas holdup occurs exactly matches with or close to the transition concentrations corresponding to the peak values of $C(d\sigma/dC)^2$ (Table 5.1). This implies that the peak value of $C(d\sigma/dC)^2$ can be used effectively to determine the transition concentration corresponding to the maximum gas holdup. A comparison of transition concentrations (C_{trans}) estimated by two methods in the present study with those reported literature and other properties of electrolytes are presented in Table 5.1.

For NaCl solution, the concentration corresponding to the maximum value of $C(d\sigma/dC)^2$ obtained in the present study is similar to that using gas holdup value reported by Syeda and Reza (2011). Hence, the concentration at which the maximum value of $C(d\sigma/dC)^2$ occurs may be used to approximate the transition concentration for different electrolytes. The concentration corresponding to the maximum value of $C(d\sigma/dC)^2$ in $\text{MgSO}_4 \cdot 7\text{H}_2\text{O}$ solution was found 0.025 mol/L which is close to 0.020 mol/L reported by Craig et al. (1993). The values of C_{trans} reported in literature vary from 0.037 mol/l (Craig et al., 1993) to 0.075 mol/l (Syeda and Reza 2011) for $\text{CaCl}_2 \cdot 2\text{H}_2\text{O}$ solution (Table 5.1). In the present study, the value of electrolyte ($\text{CaCl}_2 \cdot 2\text{H}_2\text{O}$) concentration corresponding to maximum value of $C(d\sigma/dC)_{\text{max}}^2$ is 0.075 mol/L which is similar to that reported by Syeda and Reza (2011). For Na_2SO_4 solution, the corresponding transition concentration is 0.05 mol/L at which $C(d\sigma/dC)_{\text{max}}^2$ occurred in the present study which is close to C_{trans} value of 0.051 mol/L reported by Zahradnik et al. (1995). In essence, the values of transition concentration of different electrolytes estimated in the present study are in line with those reported in the literature.

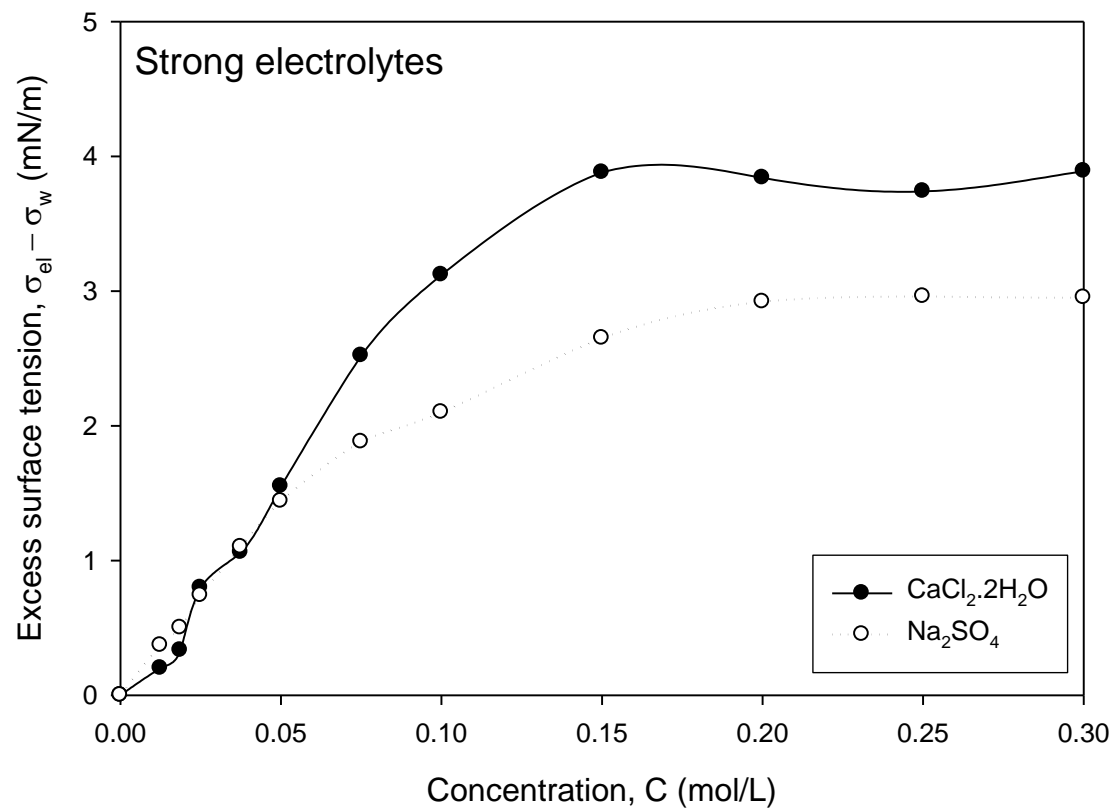


Figure 5.15 Variation of excess surface tension of solution with electrolyte concentration for strong electrolytes ($\text{CaCl}_2 \cdot 2\text{H}_2\text{O}$ and Na_2SO_4).

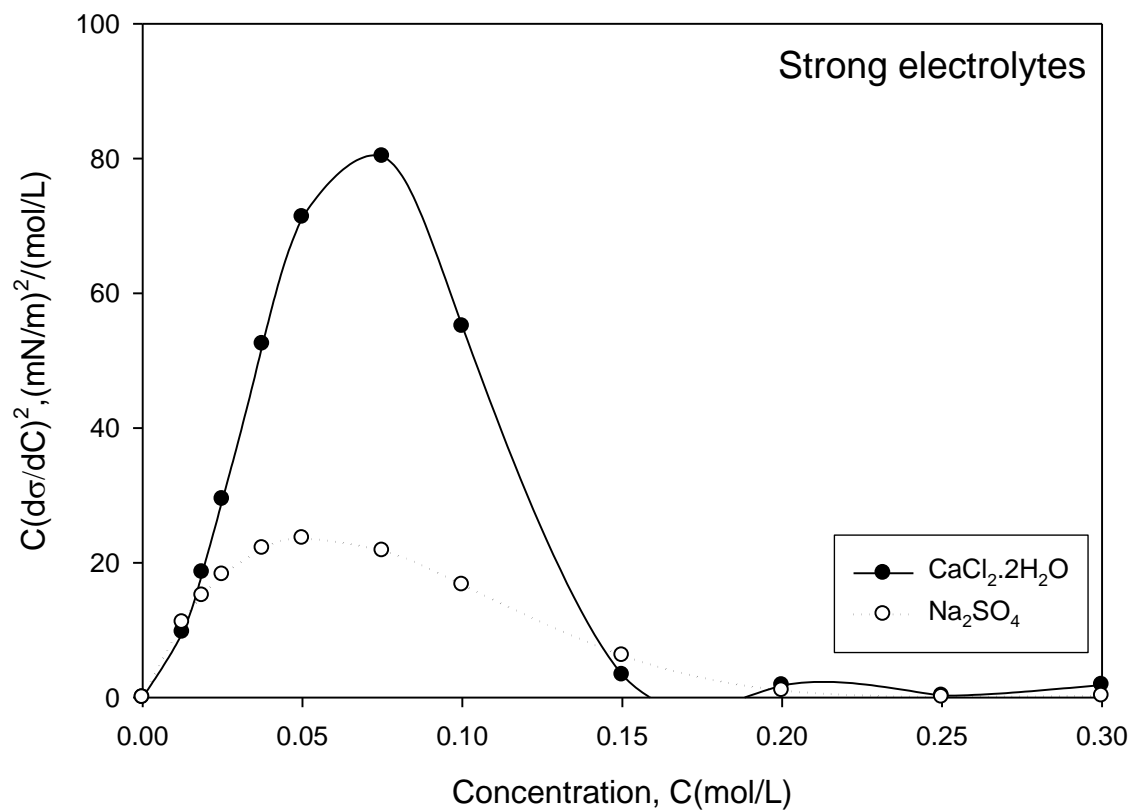


Figure 5.16 Variation of parameter $C(d\sigma/dC)^2$ with electrolyte concentration for strong electrolytes ($\text{CaCl}_2 \cdot 2\text{H}_2\text{O}$ and Na_2SO_4).

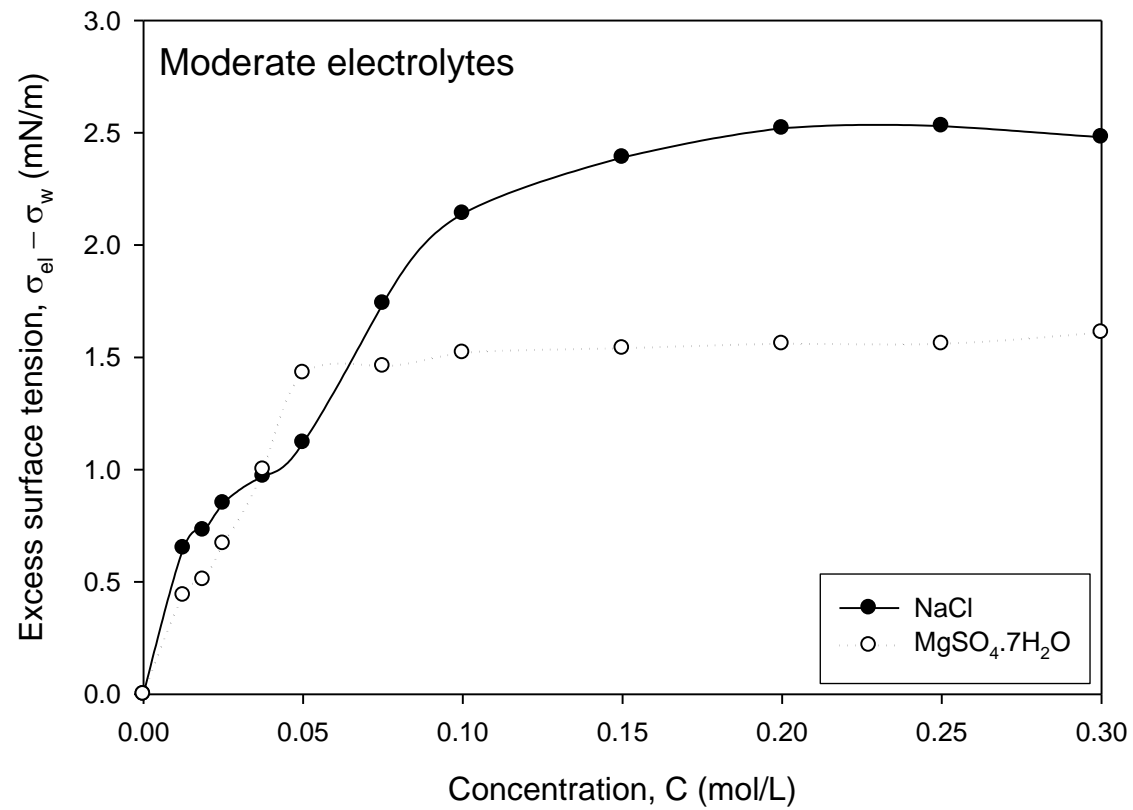


Figure 5.17 Variation of excess surface tension of solution with electrolyte concentration for moderate electrolytes (NaCl and MgSO₄·7H₂O).

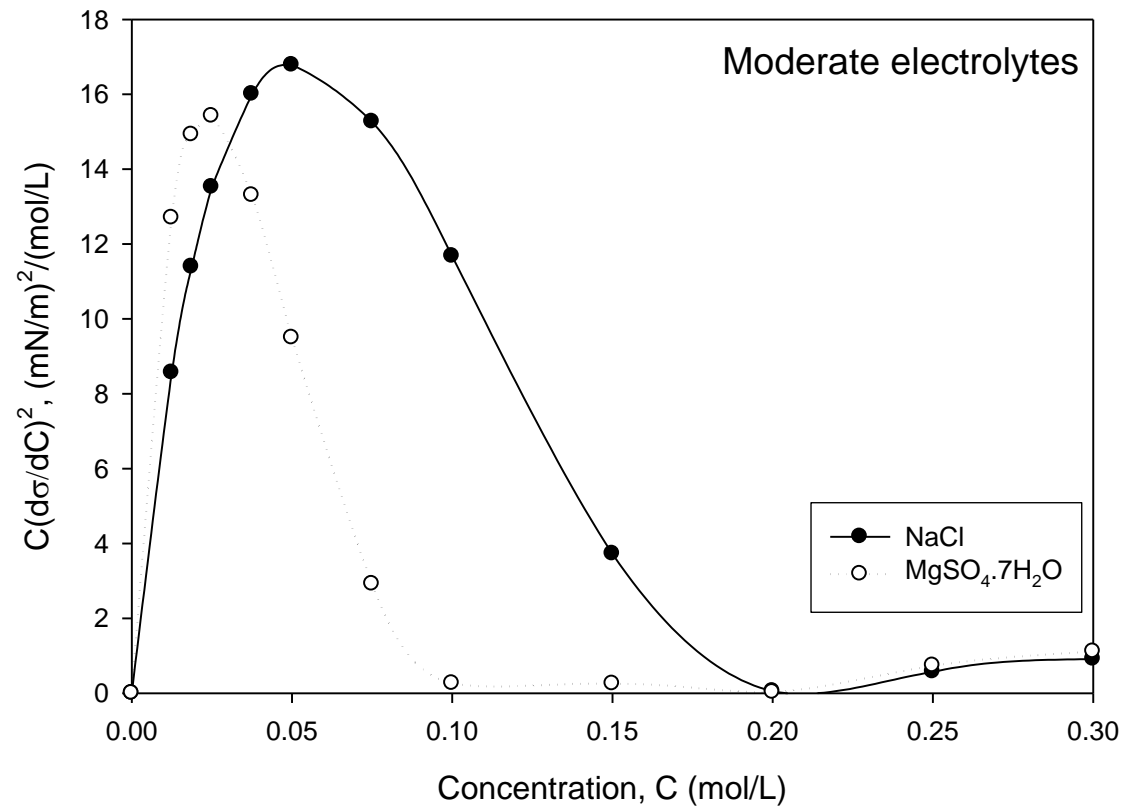


Figure 5.18 Variation of parameter $C(d\sigma/dC)^2$ with electrolyte concentration for moderate electrolytes (NaCl and MgSO₄·7H₂O).

Table 5.3 Algebraic equations of excess surface tension for different electrolytes.

Electrolyte	Algebraic equations
NaCl	$\sigma_{\text{aq.}} - \sigma_w = 2085 C^5 - 1429 C^4 + 467.5 C^3 - 140.1 C^2 + 29.47C + 0.134$
MgSO ₄ ·7H ₂ O	$\sigma_{\text{aq.}} - \sigma_w = 4.98 C^5 - 1592 C^4 + 1255 C^3 - 34804 C^2 + 40.02C - 0.041$
Na ₂ SO ₄	$\sigma_{\text{aq.}} - \sigma_w = 154.4 C^3 - 122.8 C^2 + 32.85C - 0.005$
CaCl ₂ ·2H ₂ O	$\sigma_{\text{aq.}} - \sigma_w = -19404 C^5 + 17347 C^4 - 5236 C^3 + 520.5 C^2 + 16.99C - 0.033$

5.2. 3 Gas holdup enhancement in aqueous solutions of mixed electrolytes

Experimental data of gas holdup enhancement was generated using two sets of binary mixtures of electrolytes, viz. $\text{CaCl}_2 + \text{NaCl}$ and $\text{Na}_2\text{SO}_4 + \text{NaCl}$. The combination of electrolytes is comprised one strong and one moderate electrolyte. The aqueous solution of mixed electrolytes contained equimolar concentration of both electrolytes. Gas holdup enhancement values corresponding to maximum gas flow rate of the present study (27.5 L/m) were used in the estimation of transition concentration for a mixture of electrolytes. Gas holdup enhancement data for the two combinations of electrolytes ($\text{CaCl}_2 + \text{NaCl}$ and $\text{Na}_2\text{SO}_4 + \text{NaCl}$) were plotted against total molar concentration of mixed electrolytes and are shown in Figure 5.19 and Figure 5.20. From Figure 5.19, it is obvious that gas holdup enhancement trends of a single (individual) and mixed electrolytes are similar. It has been observed from Figure 5.19 that the value of transition concentration shifted from 0.075 to 0.1 mol/L in mixed electrolyte ($\text{CaCl}_2 + \text{NaCl}$) system whereas transition concentration shifted from 0.05 to 0.075 mol/L for mixed electrolyte ($\text{Na}_2\text{SO}_4 + \text{NaCl}$) system as compared to their components viz. CaCl_2 and Na_2SO_4 respectively. The flow regime transition points in gas holdup curve based on the swarm velocity and drift-flux methods are also reported in literature (Besagni et al. 2017a; Besagni et al. 2017b; Besagni et al. 2017c; Besagni et al. 2017d; Besagni et al. 2018). The present study was aimed at determination of transition concentration of electrolytes for bubble coalescence inhibition; therefore, the selected gas velocity range was narrow. Consequently, flow regime transition points were not determined.

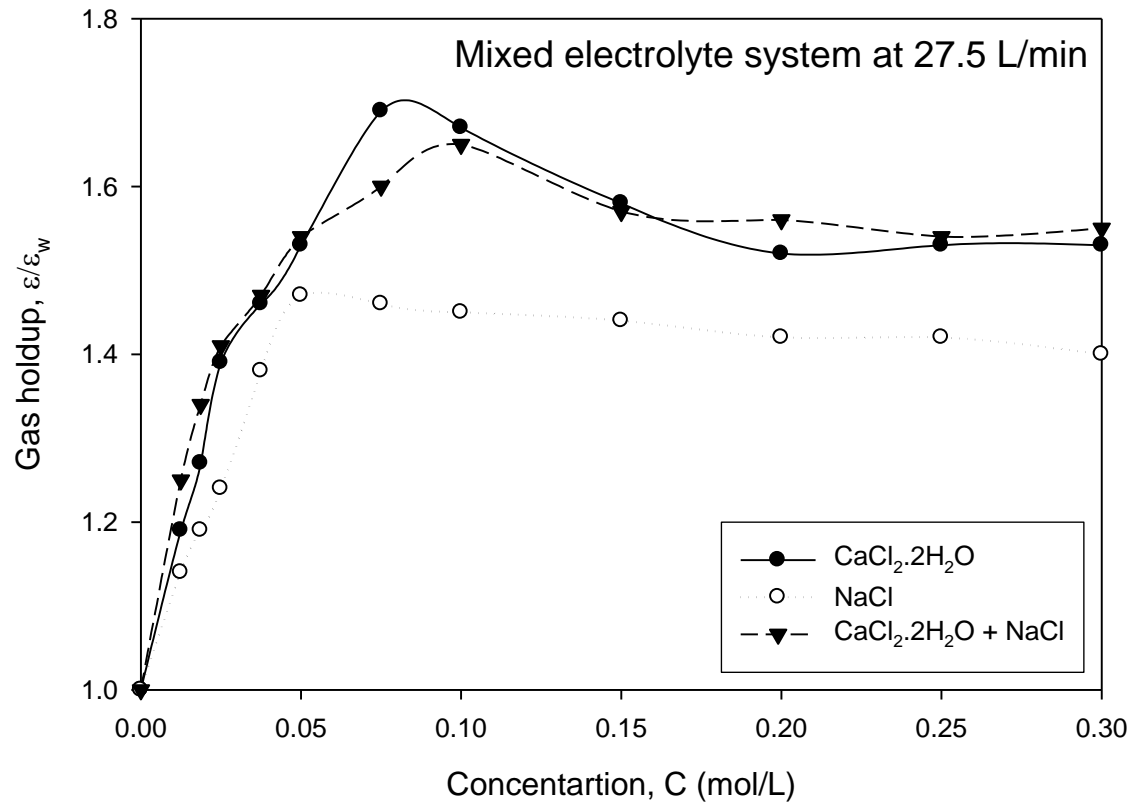


Figure 5.19 Comparison of gas hold up enhancement for mixed electrolytes ($\text{CaCl}_2 \cdot 2\text{H}_2\text{O} + \text{NaCl}$) system with individual electrolytes.

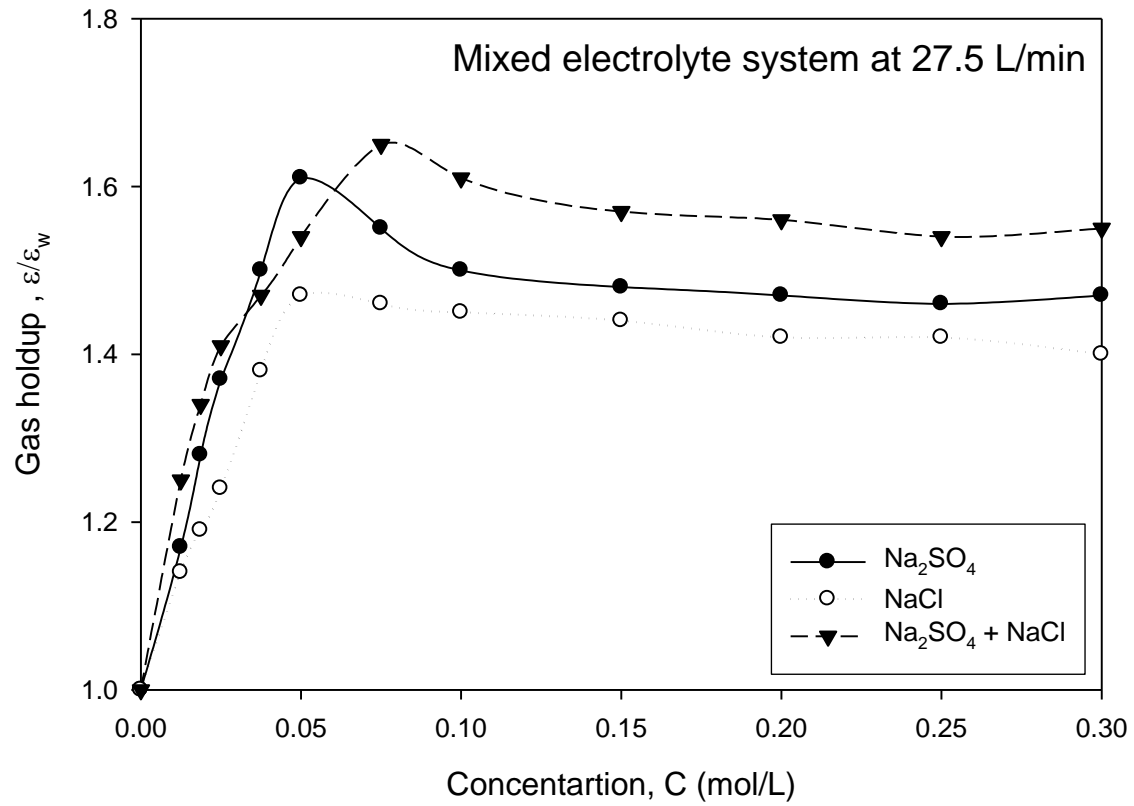


Figure 5.20 Comparison of gas hold up enhancement for mixed electrolytes (Na₂SO₄ + NaCl) system with individual electrolytes.

5.2.4 Excess surface tension and surface tension gradient in aqueous solution of mixed electrolytes

Comparison of plots of excess surface tension values and electrolyte concentration for mixed electrolyte sets and their individual electrolytes are presented in Figure 5.21 and Figure 5.22. The behavior of the curve was found similar to that of single component electrolyte solutions which increase initially up to an electrolyte concentration of 0.15 mol/L and 0.20 mol/L for $\text{CaCl}_2 \cdot 2\text{H}_2\text{O} + \text{NaCl}$ and $\text{Na}_2\text{SO}_4 + \text{NaCl}$, respectively. The curve becomes almost constant, thereafter at an excess surface tension value of 3.61 mN/m for $\text{CaCl}_2 \cdot 2\text{H}_2\text{O} + \text{NaCl}$ and 3.11 mN/m for $\text{Na}_2\text{SO}_4 + \text{NaCl}$ respectively. Parameter $C(d\sigma/dC)^2$ was also plotted against the total concentration of the two sets of mixture of electrolytes and is presented in Figure 5.23 and Figure 5.24. From the Figure 5.23, it can be observed that there is no shift in transition concentration for $\text{CaCl}_2 \cdot 2\text{H}_2\text{O} + \text{NaCl}$ mixed electrolyte system whereas transition concentration shifted from 0.05 to 0.1 mol/L for $\text{Na}_2\text{SO}_4 + \text{NaCl}$ mixed electrolytes system (Figure 5.24). Algebraic equations of excess surface tension for mixed electrolyte system and comparison of transition concentration, C_{trans} mixed electrolytes with their component are presented in Table 5.4 and Table 5.5 respectively.

Table 5.4 Algebraic equations of excess surface tension for mixed electrolyte system.

Electrolyte	Algebraic equations
CaCl ₂ .2H ₂ O + NaCl	$\sigma_{\text{aq.}} - \sigma_w = -9552 C^5 + 9733 C^4 - 3367 C^3 + 381.7 C^2 + 14.39 C - 0.005$
Na ₂ SO ₄ + NaCl	$\sigma_{\text{aq.}} - \sigma_w = 9925 C^5 - 7847 C^4 + 2216 C^3 - 318.2 C^2 + 37.86 C - 0.132$

Table 5.5 Comparison of transition concentration, C_{trans} mixed electrolytes with their component.

Mixed electrolyte/ component	Peak value		Transition concentration, C_{trans} (mol/L)	
	Based on	Based on	Based on	Based on
	$(\mathcal{E}/\varepsilon_w)_{\text{max}}$	$C(d\sigma/dC)_{\text{max}}^2$	$(\mathcal{E}/\varepsilon_w)_{\text{max}}$	$C(d\sigma/dC)_{\text{max}}^2$
CaCl ₂	1.69	80.30	0.075	0.075
Na ₂ SO ₄	1.61	23.61	0.05	0.05
NaCl	1.47	16.78	0.05	0.05
MgSO ₄ .7H ₂ O	1.37	15.42	0.0375	0.25
CaCl ₂ + NaCl	1.65	66.34	0.1	0.075
Na ₂ SO ₄ + NaCl	1.65	20.38	0.075	0.1

5.2.5 Surface elasticity values for single and mixed electrolytes

Surface elasticity of bubbles is related to bubble coalescence inhibition. Therefore, Gibbs elasticity and surface elasticity values at critical coalescence concentration for the mixed and component electrolytes solutions are presented in Table 5.6. Surface elasticity was calculated as outlined in Craig (2011). Large value of parameter $(d\sigma/dC)^2$ inhibit bubble coalescence and its value depends upon ion separation in the interfacial area (Henry et al. 2007). But the mechanism behind electrolyte inhibition of bubble coalescence is still unresolved. It is obvious from the Table 5.6 that the higher value of $\text{CaCl}_2 \cdot 2\text{H}_2\text{O}$ indicate strong bubble coalescence inhibition as compared to other electrolytes used in the study. For a combination of two electrolytes, featuring three ionic species ($\text{CaCl}_2 \cdot 2\text{H}_2\text{O} + \text{NaCl}$ and $\text{Na}_2\text{SO}_4 + \text{NaCl}$) inhibit bubble coalescence. The value of surface elasticity of combination of mixed electrolytes ($\text{CaCl}_2 + \text{NaCl}$) decreases to $442.24(\text{mN/m})^2/(\text{mol/L})^2$ from $535.33(\text{mN/m})^2/(\text{mol/L})^2$ that of CaCl_2 alone. The reduction in surface elasticity from a single component (CaCl_2) is due to the addition of a moderate electrolyte (NaCl) whose contribution to surface elasticity value is small as compared to strong one (CaCl_2). Reduction in surface elasticity will result in decrease in bubble coalescence inhibition phenomena. Similar observation was found in aqueous solution of $\text{Na}_2\text{SO}_4 + \text{NaCl}$ system. Surface elasticity values estimated in the present work could not be compared with those reported in literature (Craig 2011 and Henry et al. 2007) as values reported earlier were not estimated at critical coalescence concentration.

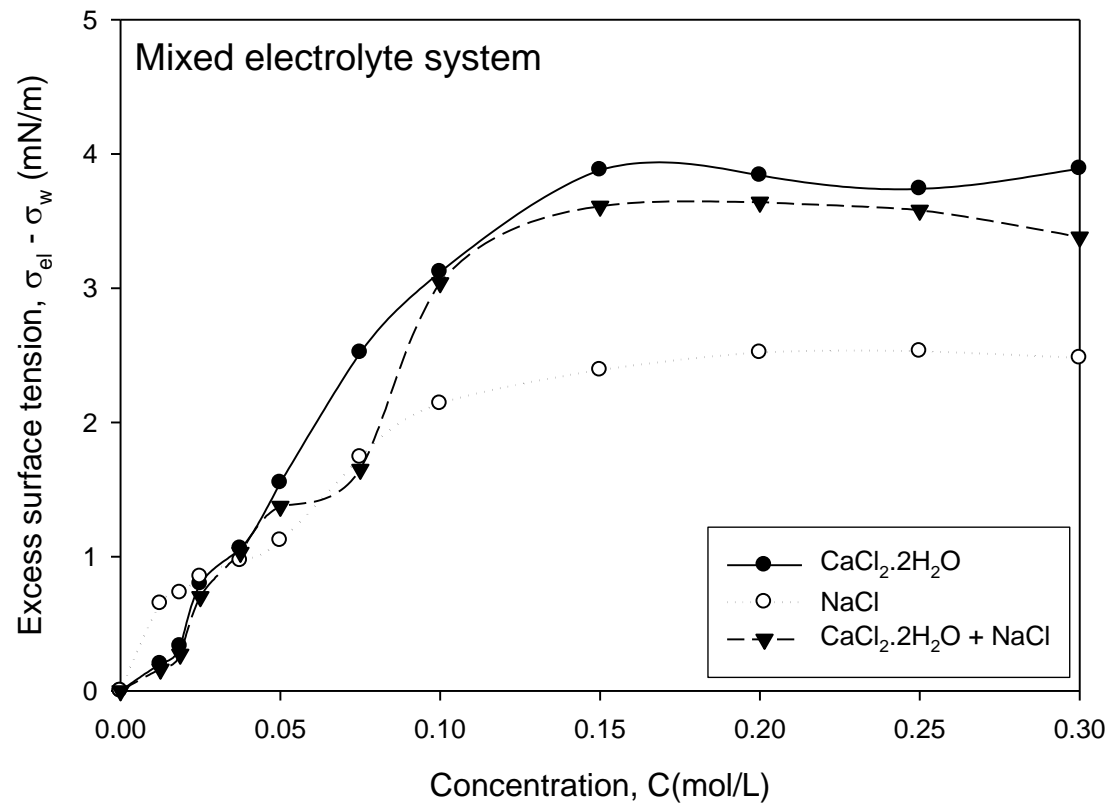


Figure 5.21 Comparison of excess surface tension of mixed electrolytes ($\text{CaCl}_2 + \text{NaCl}$) with individual electrolytes.

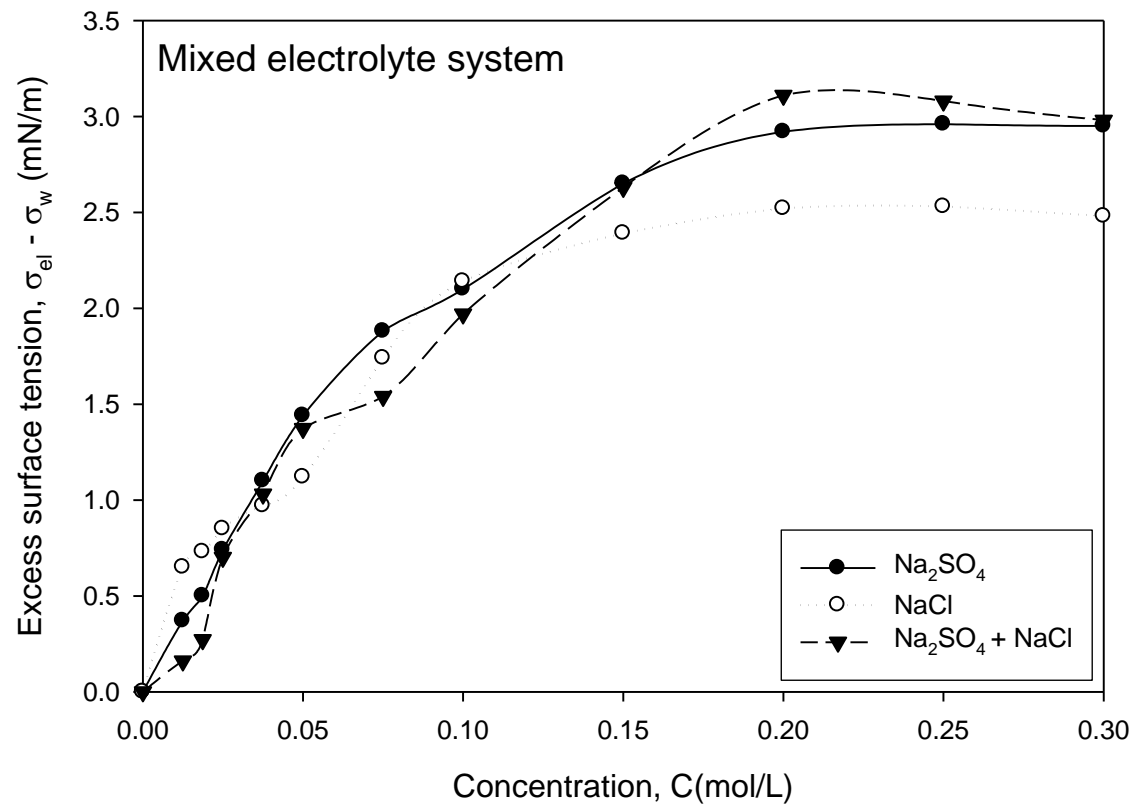


Figure 5.22 Comparison of excess surface tension of mixed electrolytes ($\text{Na}_2\text{SO}_4 + \text{NaCl}$) with individual electrolytes.

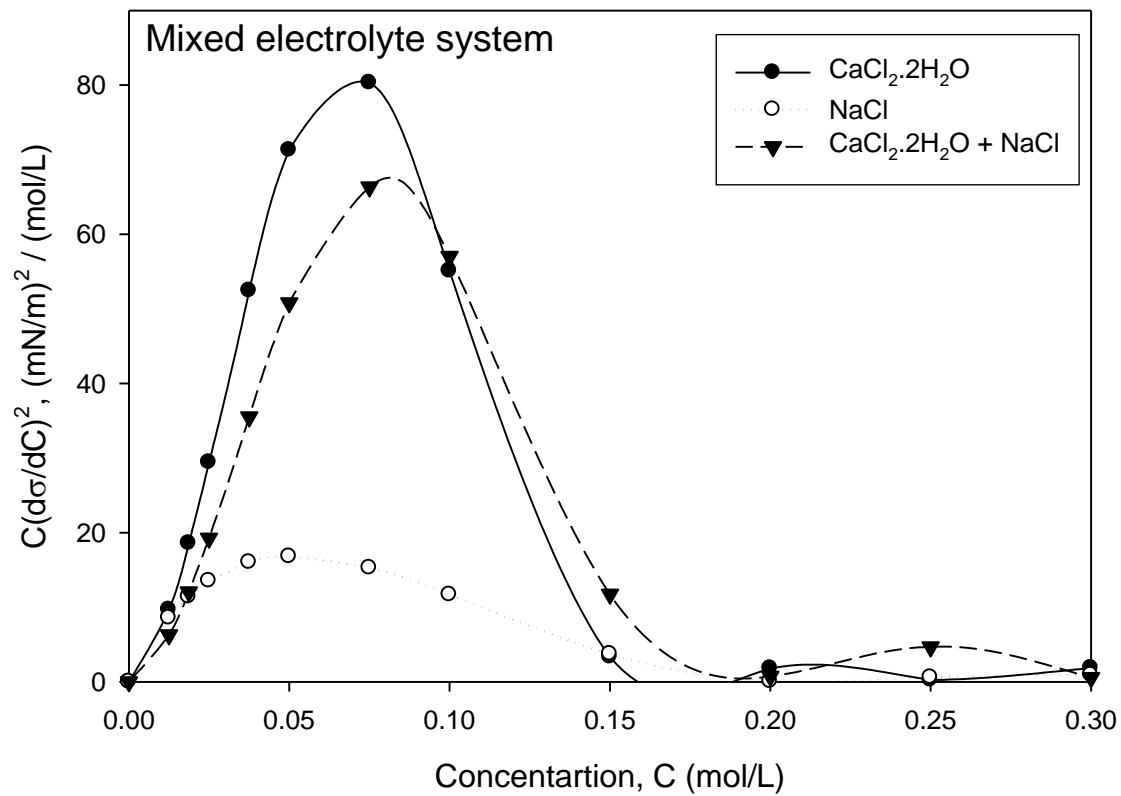


Figure 5.23 Comparison of parameter $C(d\sigma/dC)^2$ for mixed electrolytes ($\text{CaCl}_2 + \text{NaCl}$) system with individual electrolytes.

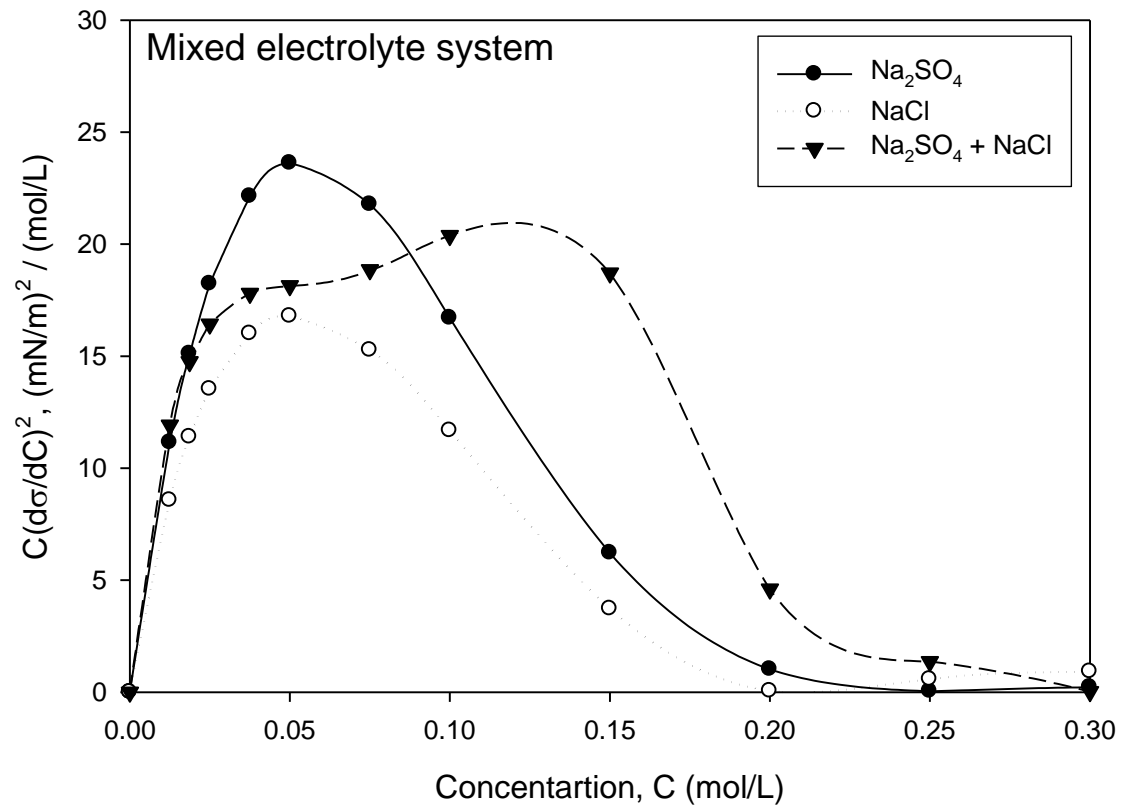


Figure 5.24 Comparison of parameter $C(d\sigma/dC)^2$ for mixed electrolytes ($\text{Na}_2\text{SO}_4 + \text{NaCl}$) system with individual electrolytes.

Table 5.6 Gibbs elasticity and surface elasticity at transition concentration of electrolytes.

Electrolyte	Bubble coalescence inhibition	$(d\sigma/dC)^2 \approx$ Gibbs elasticity (mN/m) ² /(mol/L) ²	Surface elasticity = $(1/2) \times (d\sigma/dC)^2$ (mN/m) ² /(mol/L) ²
NaCl	yes	335.51	167.76
MgSO ₄ ·7H ₂ O	yes	616.71	308.36
Na ₂ SO ₄	yes	472.11	236.06
CaCl ₂ ·2H ₂ O	yes	1070.66	535.33
CaCl ₂ ·2H ₂ O + NaCl	yes	884.48	442.24
Na ₂ SO ₄ + NaCl	yes	203.76	101.88

5.2.6 Analysis of variance (ANOVA)

In the present study, trial version of Statistical Design software (Minitab version 17) was used for regression and analysis of variance (ANOVA). Using analysis of variance, it was found that the gas flow rate, concentration of electrolytes, and the chemical nature of the electrolytes have significant effects on the average gas holdup. However, the gas flow rate and electrolyte concentration are most sensitive variable and the largest source of variation, as shown in Table 5.7.

Table 5.7 Analysis of Variance.

Source	Degrees of freedom	Sum of squares	Mean square	F-value	P-value
Gas flow rate, Ug	4	0.219258	0.054815	1646.92	0.000
electrolyte concentration, C	6	0.103789	0.017298	519.73	0.000
chemical nature of the electrolytes, N	2	0.002774	0.001387	41.68	0.000
Ug .C	24	0.012143	0.000506	15.20	0.000
Ug .N	8	0.000744	0.000093	2.79	0.009
Error	75	0.002496	0.000033		
Lack of fit	45	0.001777	0.000039	1.65	0.076
Pure error	30	0.000719	0.000024		
Total	119	0.453817			

It is obvious from the Table 5.7 that the electrolyte concentration and gas flow rate are the most sensitive variable and the largest source of variation. The fact that P-values for gas flow rate, concentration of electrolytes, and the chemical nature of the electrolytes in this table are less than the confidence level (0.05) and the P- value for the lack of fit is higher than 0.05 indicate the adequacy and significance of the model. Residual plots of gas holdup are presented in Figure 5.25.

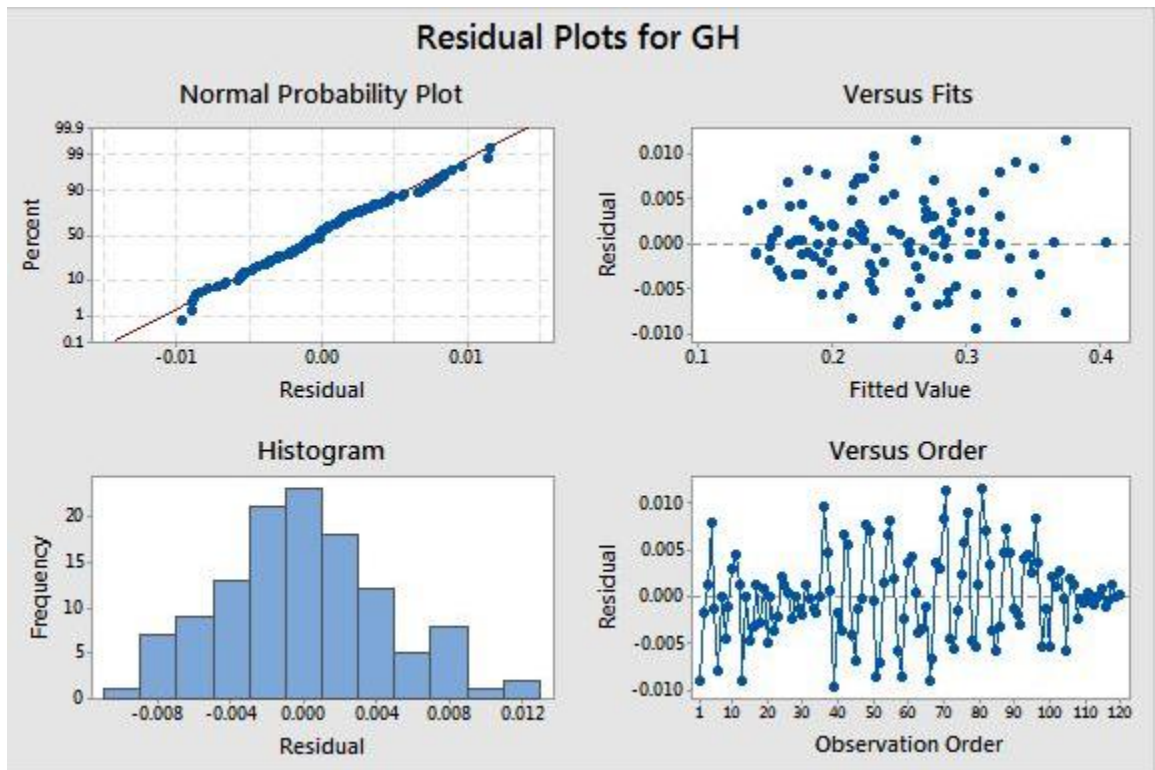


Figure 5.25 Residual plots for gas holdup.

It can be seen from Figure 5.25 that the residuals versus fits plot verify the assumption that the residuals are randomly distributed and have constant variance, because, the points fall randomly on both sides of 0, with no recognizable patterns in the points. The normal probability plot of the residuals displays the residuals versus their expected values when the distribution is normal. Normal probability plot of residuals verifies the assumption that the residuals are normally distributed as the residuals approximately follow a straight line. The residuals versus observation order plot verifies the assumption that the residuals are independent from one another as the

residuals on the plot fall randomly around the center line. The histogram of the residuals shows the distribution of the residuals for all observations. The experimental data of the average gas holdup for each of the cases studied have a log-normal distribution, as their distribution frequency is not symmetrical. Histogram of the residuals confirms that the data are not skewed and do not include outliers.

Section 5.3: Estimation of volumetric mass transfer coefficient k_{La} in a partially baffled gas-liquid contactor equipped with curved and non-curved impeller

5.3.1 Effect of blade numbers of a pitch blade impeller

In this chapter, investigation of effects of number of impeller blades on the gas dispersion and mass transfer rate within a mechanically agitated vessel has been discussed. Impeller speed is one of the important factors that affect gas liquid mass transfer in an agitated vessel. All experiments were performed in a stirred bubble column at different impeller speeds varying from 200 – 400 rpm. Volumetric mass transfer coefficient, k_{La} was estimated as described in section 3.5. Figure 5.26 shows the effect of agitation rate on volumetric mass transfer coefficient k_{La} for 4-, 6-Pitch blade turbine systems under constant air flow rate of 22.5 L/min. The increase in k_{La} values is due to the breakage of rising bubbles by the impeller blades giving rise to more interfacial area for gas transfer. From the results obtained, it was found that under the same gas flow rate (22.5 L/min) condition, the impeller with more blades always disperses gas more effectively, which results in a higher value of k_{La} . At 22.5 L/min, all three Impeller combinations show a linear increase in k_{La} values with increasing agitation. At higher impeller speeds and optimized nozzle length, a pitch blade turbine with 6 blades provides 15.3% higher mass transfer coefficient over 4 PBT. In the case of a dual concentric ring sparger with 6 PBT system, 34.3 % higher k_{La} was obtained as compared to 9 cm nozzle length. Bubble population and bubble size have a significant impact on volumetric gas-liquid mass transfer coefficient in Newtonian liquids. In the range of bubble population, many tiny bubbles (< 4 mm) appear, accumulate and circulate within the liquid during the aeration process. Tiny bubbles play a significant role in oxygen transfer because of their smaller size, which offers an extremely high interfacial area (Sujan and Vyas 2017). It has been visually observed that, concentric dual ring sparger produces more bubbles as compared to 4 jet nozzles. In contrast to the findings reported earlier (Lu and Yan1998), in the presents study, it was found that agitator rate has affects mass transfer phenomena significantly by which matches with the observation of Lu et al. (1999).

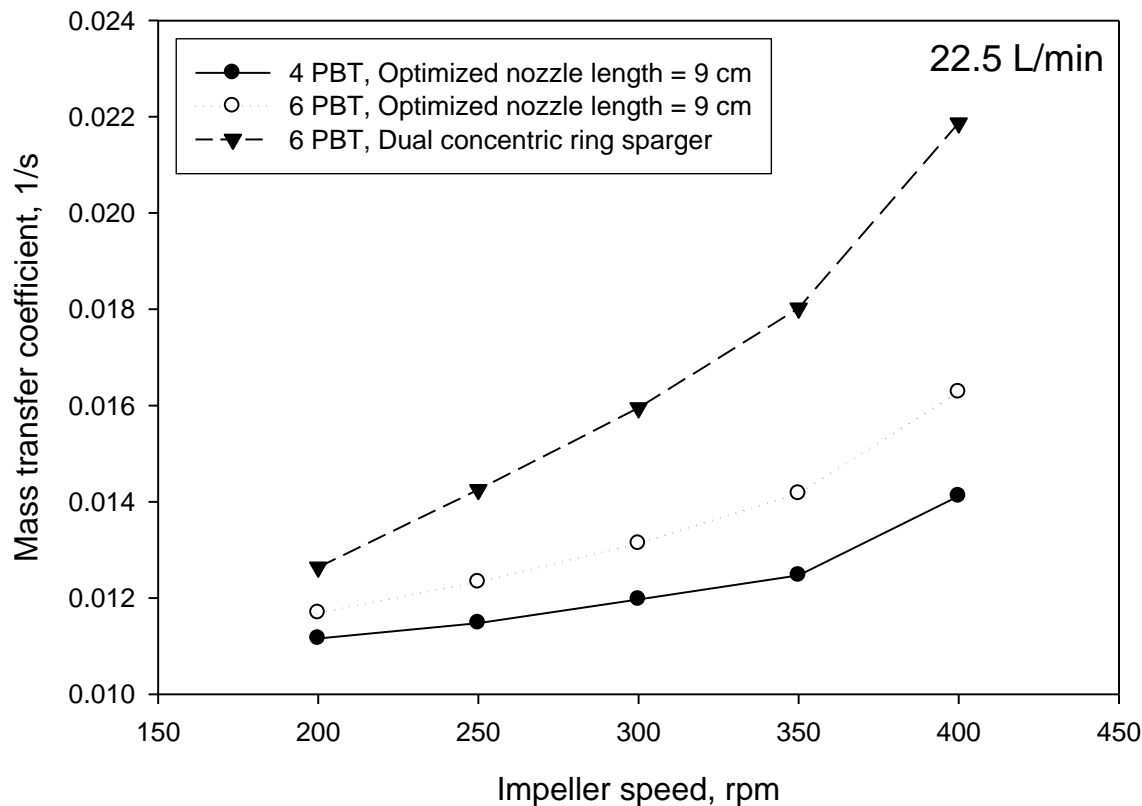


Figure 5.26 At constant gas flow rate (22.5 L/min), variation of $k_L a$ values of the 4 PBT and 6 PBT at 9 cm nozzle length and Comparison with 6 PBT, dual concentric ring sparger system.

5.3.2 Effect of curvature of concave blade

In this study, the effects of curvature of blade on volumetric gas–liquid mass transfer coefficient within the mechanically Rushton agitated system equipped with dual concentric ring sparger were investigated. Curvature of blade is one of the important factors that affects gas liquid mass transfer in an agitated vessel. All experiments were performed at gas flow rates varied from 17.5 – 22.5 L/min and different impeller speeds varied from 200 – 400 rpm. Experimental results were obtained using a Rushton impeller ($e = 0$) and a series of concave impellers ($e = 0.177 – 0.441$). For a Rushton impeller, the effect of impeller speeds on mass transfer coefficient with different gas flow rates are shown in Figure 5.27. From Figures 5.28a – 5.28e, mass transfer coefficients obtained using the concave blade impellers are slightly higher than those using the

Rushton impeller in the range of experimental conditions covered in this work. In Figure 5.28, it may also be seen that the highest mass transfer coefficient occurs for a given impeller speed at a certain blade curvature due to the cavity formed behind the blade becomes smaller with an increase in the blade curvature. From Figure 5.28e it is obvious that, at higher impeller speed (400 rpm), concave blade with 0.441 curvatures provides more than 45% improvement in mass transfer over the Rushton impeller. From Figure 5.28a–Figure5.28e, it can also be seen that the effect of curvature is insignificant at low impeller speeds. This appears to support the mass transfer results by Warmoeskerken and Smith (1989). Due to different blade curvatures and rotating speeds, the size of cavities formed behind the impeller blade significantly affects the bubble size discharged from the impeller which is responsible for higher mass transfer coefficient. It is known that the dimension of the cavity behind a flat plate blade impeller increases with an increase in the impeller speed and a smaller cavity was found to form behind a concave blade (van't Riet and Smith 1973; Saito et al 1992; Mishra and Joshi 1993). It was also visually observed that, the size of cavity to change gradually with an increase in the blade curvature at least up to $e = 0.5$. Lu et al. (1993) showed that flow pattern and size of cavities formed behind the impeller blade significantly affect the bubble size discharged from the impeller. The slightly better performance using the concave blade impellers is more clearly demonstrated in Figure 5.28a–5.28e. This figure shows that 43.18 % increment in k_La value at 17.5 L/min, 46.72 at 20 L/min and 48.35 % at 22.5 L/min respectively with that of Rushton impeller.

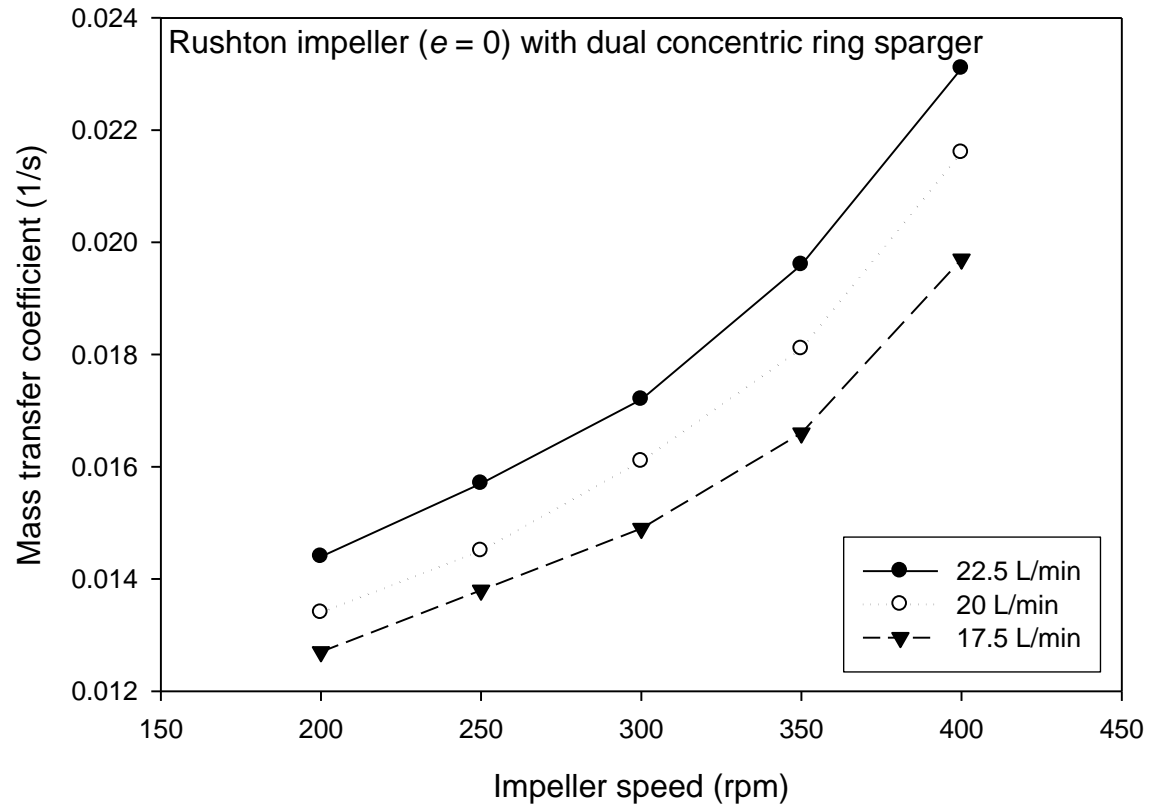
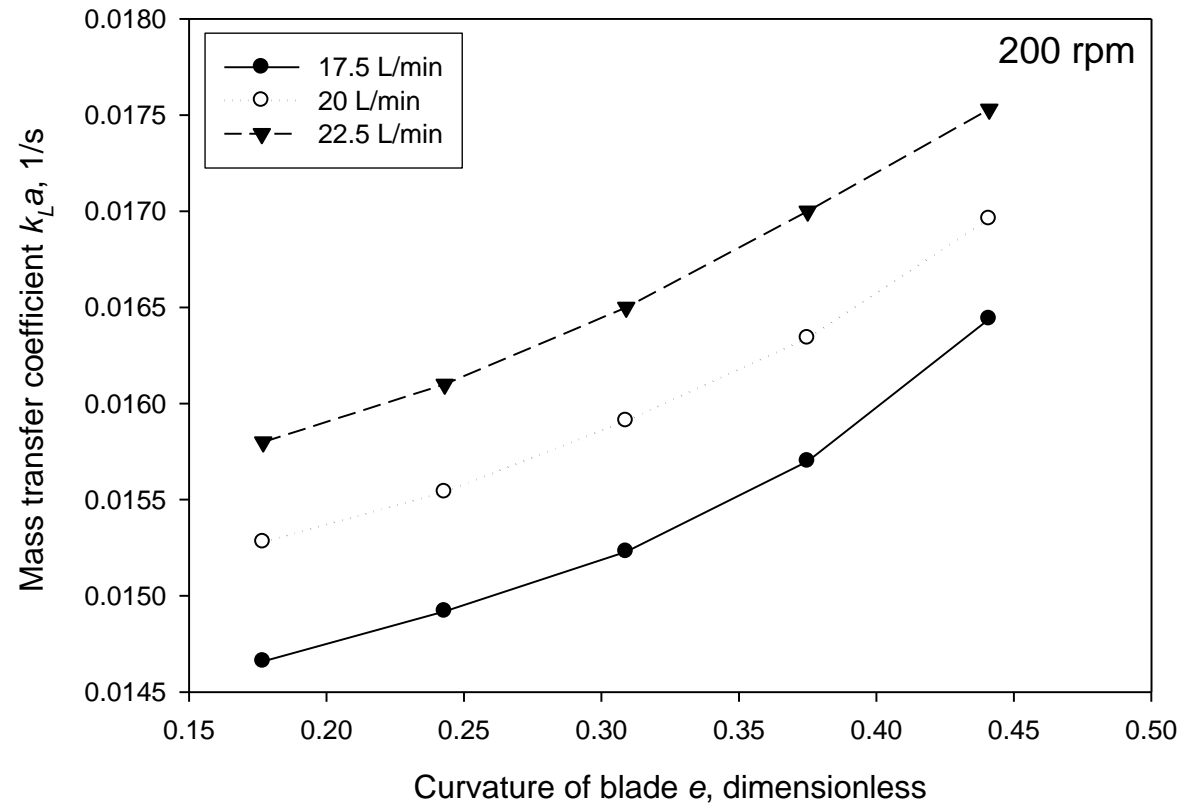
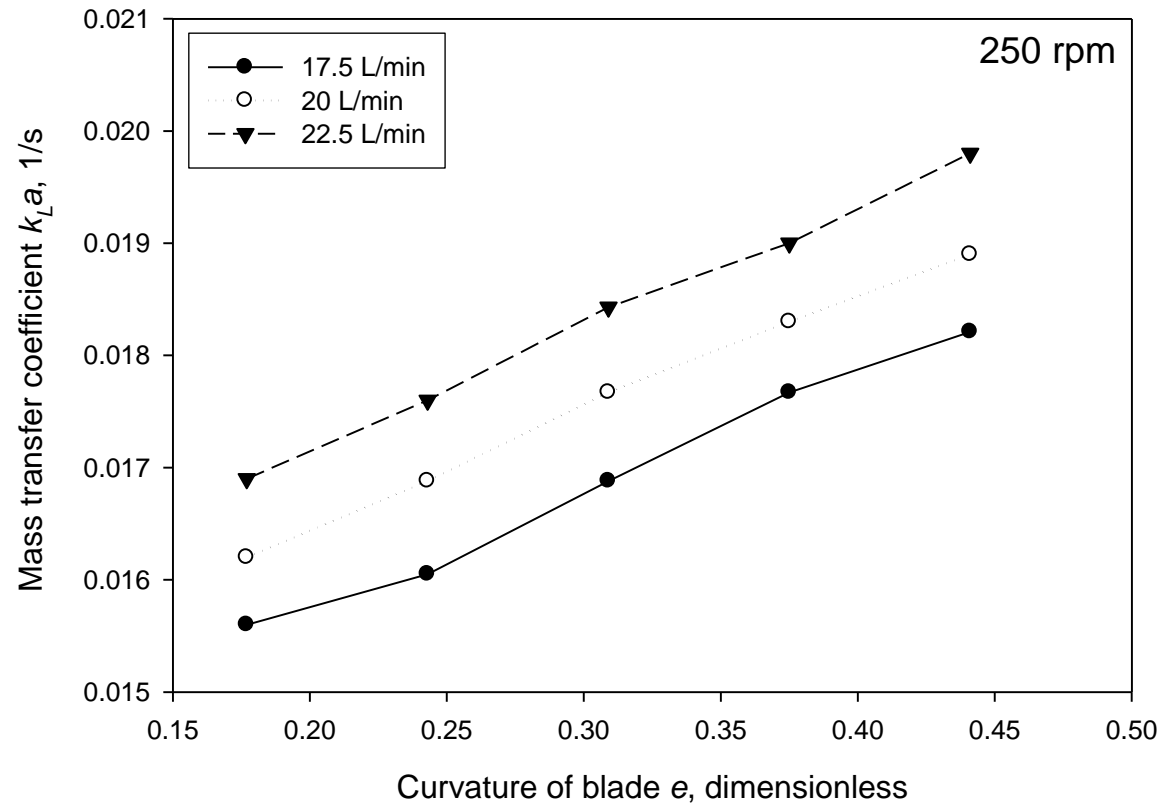


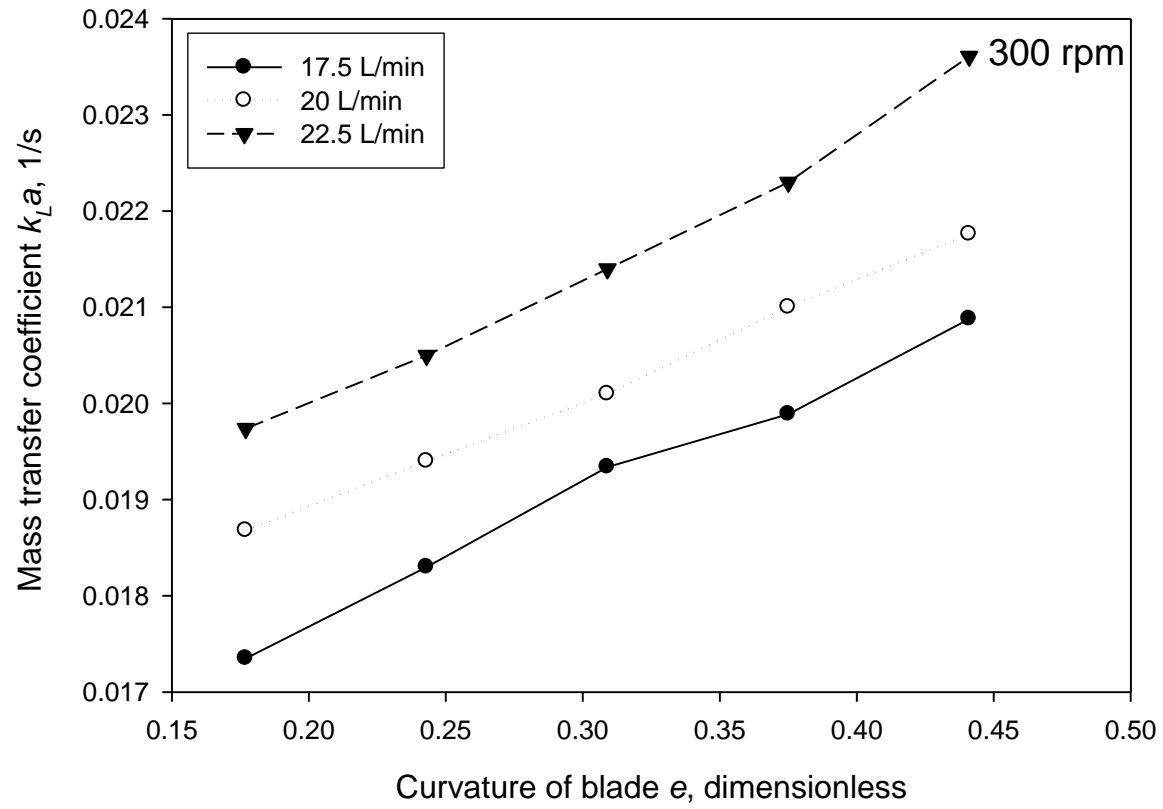
Figure 5.27 Effect of impeller speeds at different gas flow rates on mass transfer coefficient for Rushton agitated system equipped with dual concentric ring sparger



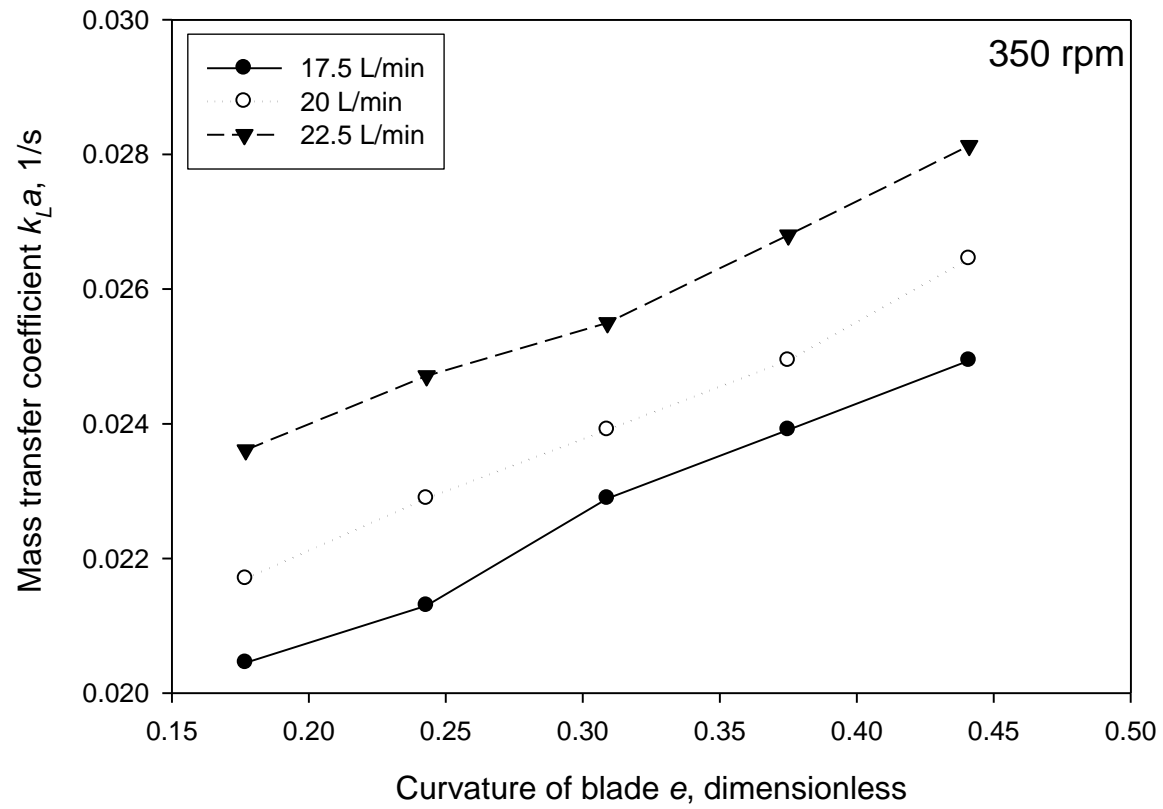
(a)



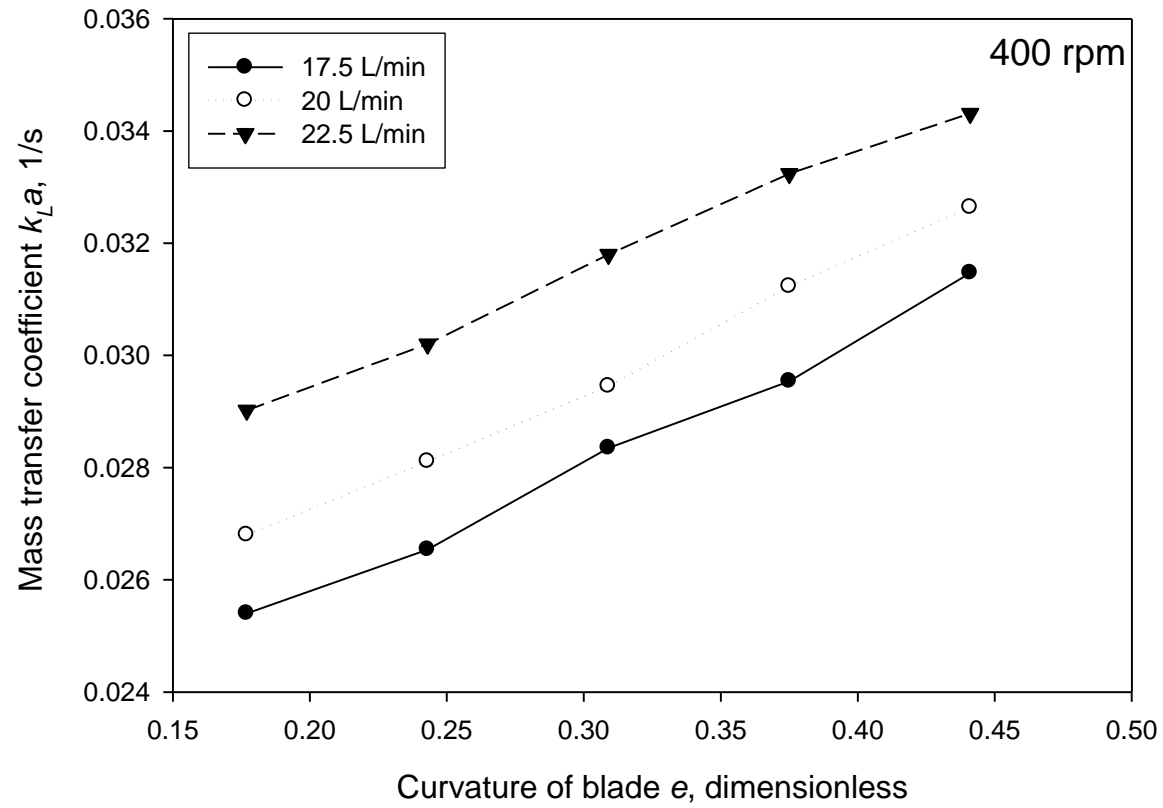
(b)



(c)



(d)



(e)

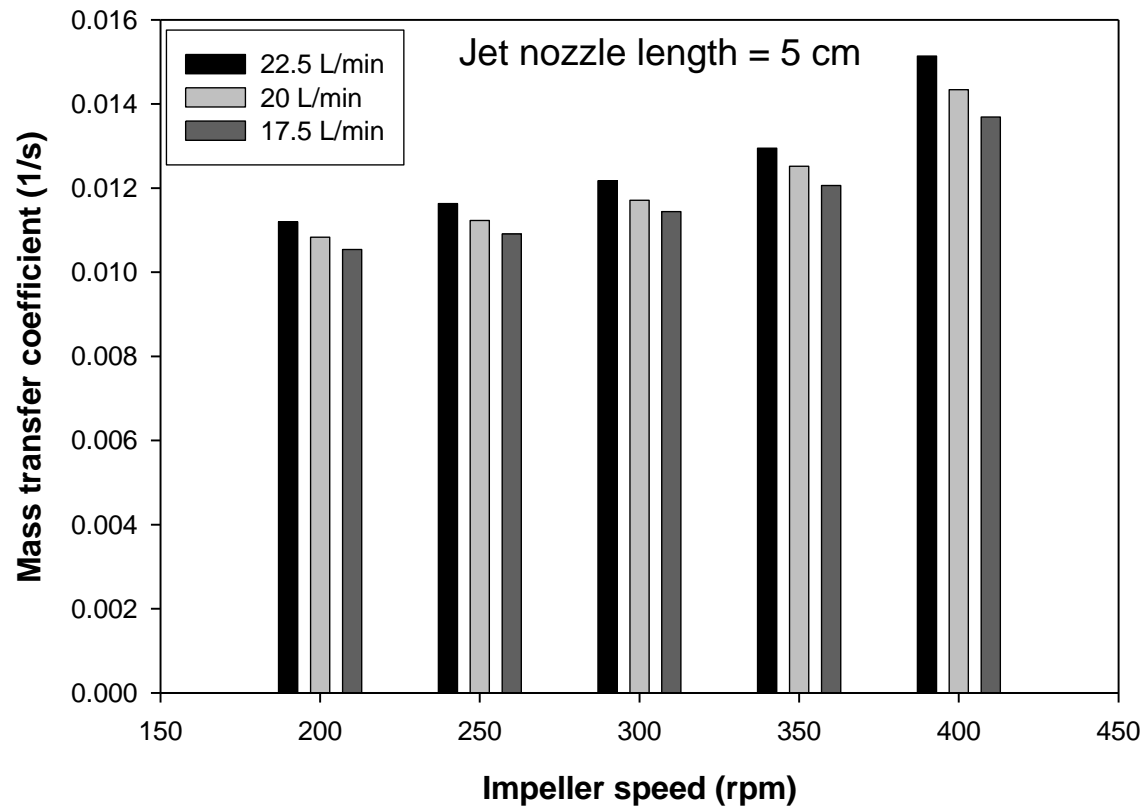
Figure 5.28 The effect of blade curvature on $k_{L}a$ with various gas flow rate, (a) 200 rpm; (b) 250 rpm; (c) 300 rpm; (d) 350 rpm and (e) 400 rpm

5.3.3 Effect of jet nozzle length on k_{La}

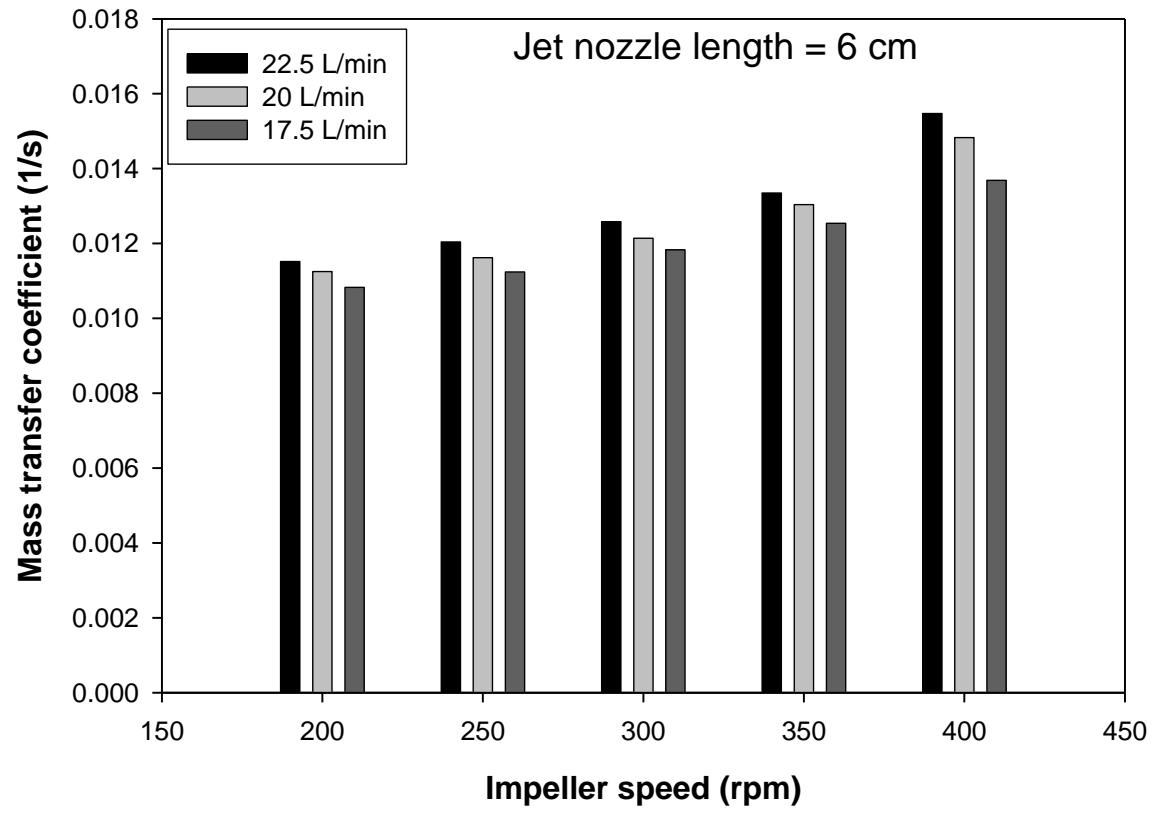
In this study, the effects of jet nozzle length on volumetric gas–liquid mass transfer coefficient within the mechanically agitated vessels equipped with Rushton impeller were investigated systematically. Nozzle length of sparger is one of the important factors in pharmaceutical and bio industries where limited oxygen is required. All experiments were performed at gas flow rates varied from 17.5 – 22.5 L/min and different impeller speeds varying from 200 – 400 rpm. Position of jet nozzle and distance between impeller edge and nozzle tip are already shown in Figure 3.11. Experimental results were obtained using a Rushton impeller ($e = 0$) and a series of jet nozzle length ($L_N = 5–10$ cm). For Rushton impeller, the effect of jet nozzle length on k_{La} with different gas flow rates was shown in Figure 5.29a–5.29f. All the figures show similar trend at different nozzles lengths under same operating conditions. From Figure 5.29e, at 9 cm nozzle length, 400 rpm and 22.5 L/min, the value of k_{La} was found to be 0.01711s^{-1} which was 13.01 % higher than that at the nozzle length of 5 cm. Similarly, 10.60 %, 7.54%, 6.07% and 4.52 % higher than those found at nozzle lengths of 6, 7, 10 and 8 cm, respectively. It was visually observed that, population and size of bubbles to change gradually with an increase in jet nozzle length up to 9 cm. but at 10 cm jet nozzle length, the value of k_{La} was found lower as compared to 9 cm jet nozzle length due to reduction in bubble population and size. It is notable to mention that a bubble which comes out of the nozzle travels the vertical distance in the stirred column on a spiral path (trajectory) and moves radially outwards as it travels up due to the centrifugal force acting on it by virtue of the circular motion of liquid water brought about by the impeller. The bubbles while crossing the impeller level which is located at a vertical distance from the jet nozzles reach at a radius greater than that of the impeller blade edge and hence experience a greater intensity of turbulence inhibiting the attraction force prevailing between the adjacent bubbles and thereby promoting coalescence inhibition.

In case of 10 cm jet nozzle, the point of delivery of nozzles was located at a significantly lower horizontal distance from the vertical axis of the agitated vessel. Thus, the spiral movement of the bubbles makes them barely reach a radial distance from the axis that is less than that of the impeller radius. The space below the impeller within its radius experiences a vortex with low pressure zone forcing the bubbles to coalesce and increase their size. The net result all these phenomena was reduction in the k_{La} value due to lower interfacial area of the coalesced bubbles.

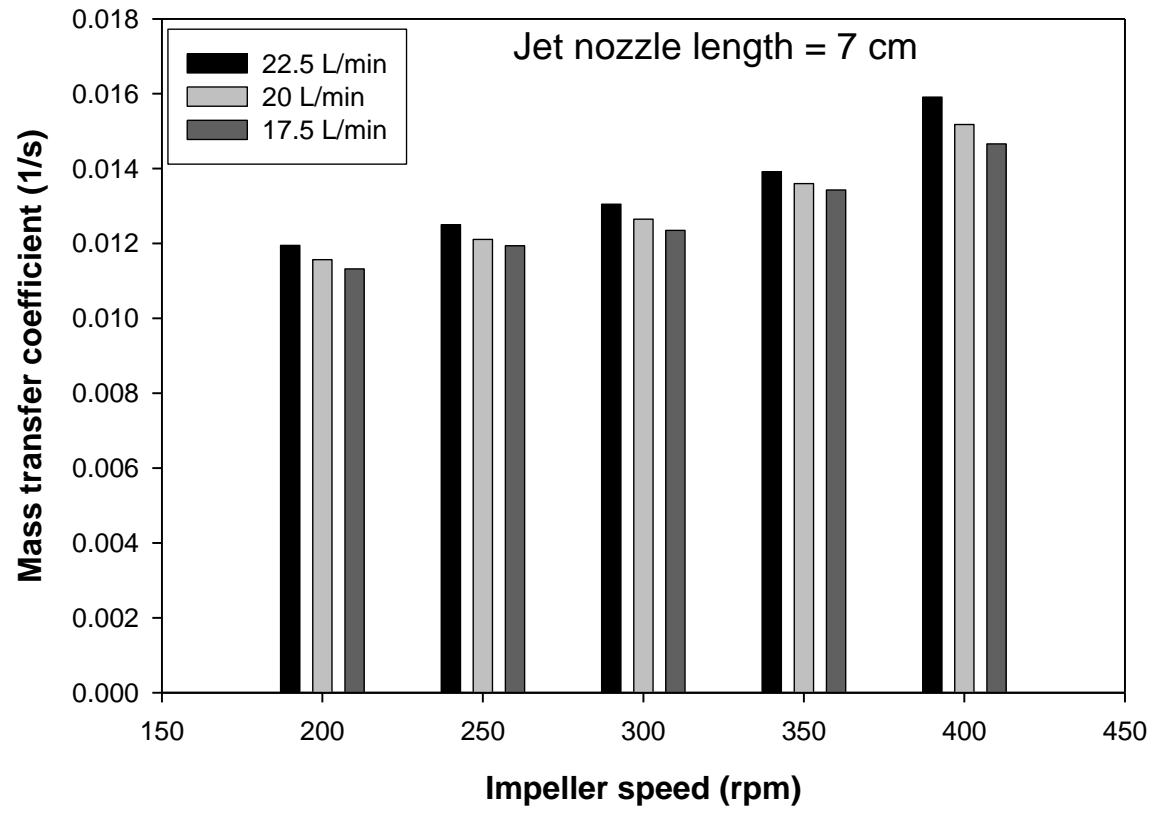
It was also visually observed during the experimental work that reduction in distance between jet nozzle and impeller blade edge significantly affects the bubble size discharged from the impeller which is responsible for higher mass transfer coefficient. It is known that the size of the cavity behind a flat plate blade impeller increases with an increase in the impeller speed (Van't Riet and Smith 1973). It is clear that large cavity traps more bubbles as compared the small cavity formed and residence time of bubbles is also higher which is responsible for higher mass transfer coefficient.



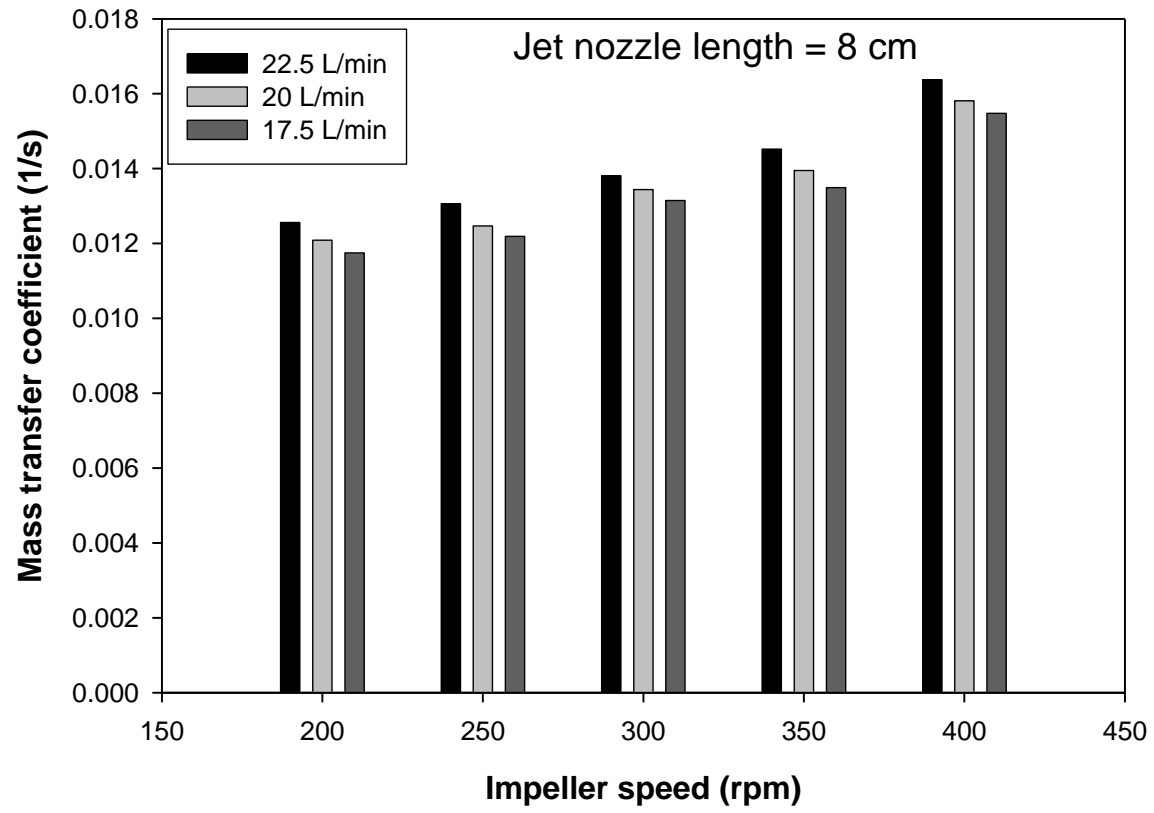
(a)



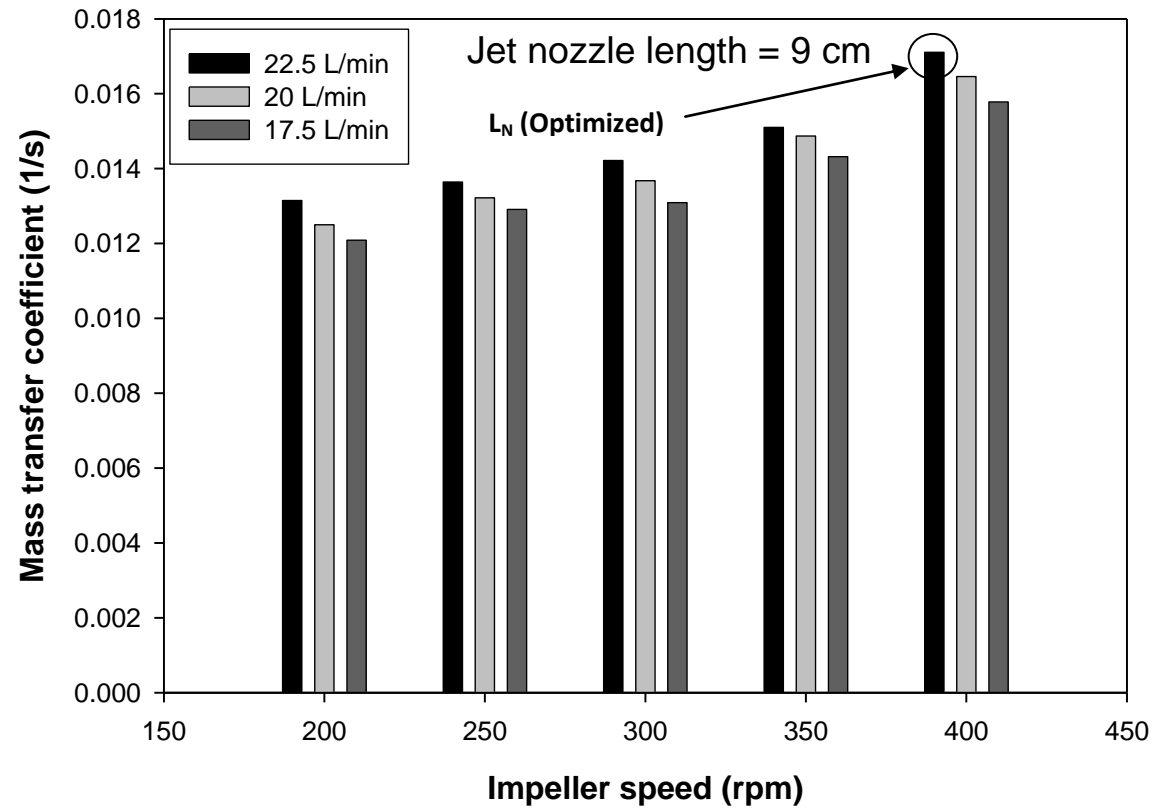
(b)



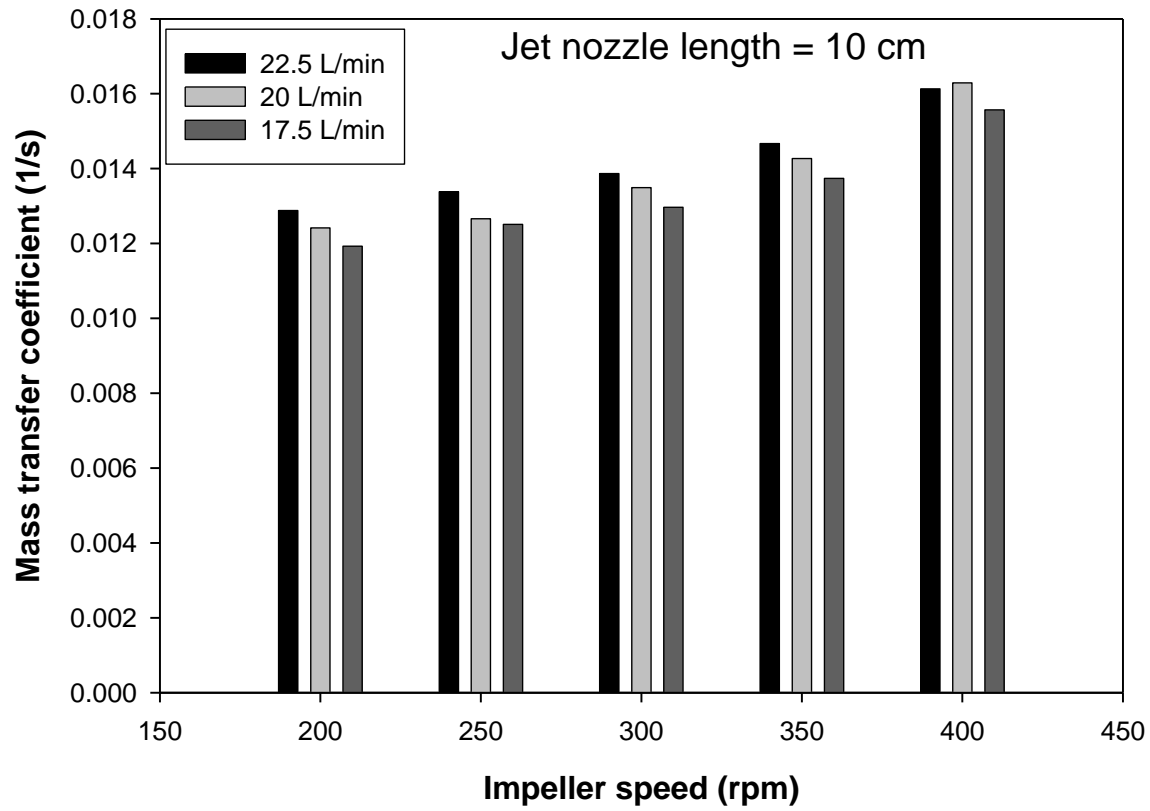
(c)



(d)



(e)



(f)

Figure 5.29 Effect of impeller speeds on $k_{L,a}$ with various gas flow rates at different jet nozzle lengths (a) 5 cm; (b) 6 cm; (c) 7 cm; (d) 8cm; (e) 9 cm and (f) 10 cm.

5.3.4 Empirical correlations for $k_L a$

Two different empirical correlations of $k_L a$ have been developed in the present work for two different systems. Empirical correlations for the estimation of $k_L a$ presented at equation 5.8 and equation 5.9 indicate that the parameter (L_N/d) is significant in both the systems. It may also be seen from equation 5.8 and equation 5.9 that the exponent of parameter (L_N/d) for the Rushton impeller has a larger value than the concave blade with different curvature systems. This fact points out that the parameter (L_N/d) also plays a significant role in the mass transfer process in bubble columns. Furthermore, the exponent of (I_H/I_W) in equation 5.8 reveals that the curvature of blade is an important parameter in the case of concave blade with different curvature blade impeller agitated system equipped with the nozzle of various lengths. Equation 5.8 shows that Froude number is relatively more significant in a curved blade agitated system as compared to Rushton blade system and reveals that the impeller speed is an important parameter. The exponent of parameter $(u_g d/D_L)$ of Rushton impeller has a larger value than concave blade system with different curvature. This point out that the gas flow rate are also plays a significant role in mass transfer in bubble columns in both systems. From equation 5.8, the exponent of Weber number is much higher as compared to Rushton impeller system. Equation 5.8 shows that Reynolds number is relatively less significant as compared to the concave blade with different curvature systems and reveals that the impeller speed is an important parameter. Experimental and model predicted values of $k_L a$ for Rushton and concave blade impeller with different jet nozzle lengths are shown in Figure 5.30 and Figure 5.31 respectively.

(a) Empirical correlation of $k_L a$ as a function of curvature of concave blade

$$\left(\frac{k_L a d_B^2}{D_L}\right) = 9.232 \times 10^3 \left(\frac{L_N}{d}\right)^{0.762} \left(\frac{I_H}{I_W}\right)^{0.463} \left(\frac{N^2 d}{g}\right)^{0.395} \left(\frac{u_g d}{D_L}\right)^{0.579} \left(\frac{d^3 N^2 \rho_L}{\sigma_L}\right)^{-0.152} \left(\frac{d^2 N \rho_L}{\mu_L}\right)^{0.607} \dots (5.8)$$

Valid range:

$$0.429 \leq L_N/d \leq 0.714 \quad 0.177 \leq I_H/I_W \leq 0.441 \quad 1.58 \leq F_r \leq 6.31$$

$$1600.632 \leq Sh \leq 4547.363 \quad 9.206 \times 10^5 \leq We \leq 6.393 \times 10^6$$

$$1.515 \times 10^6 \leq Re \leq 3.030 \times 10^6 \quad 1.429 \times 10^6 \leq u_g d/D_L \leq 2.573 \times 10^6$$

(b) Empirical correlation of $k_L a$ for Rushton impeller systems

$$\left(\frac{k_L a d_B^2}{D_L}\right) = 8.192 \times 10^3 \left(\frac{L_N}{d}\right)^{0.833} \left(\frac{N^2 d}{g}\right)^{0.330} \left(\frac{u_g d}{D_L}\right)^{0.641} \left(\frac{d^3 N^2 \rho_L}{\sigma_L}\right)^{-0.401} \left(\frac{d^2 N \rho_L}{\mu_L}\right)^{0.926} \dots(5.9)$$

Valid range:

$$1600.632 \leq Sh \leq 4547.363$$

$$0.357 \leq L_N/d \leq 0.714$$

$$1.58 \leq F_r \leq 6.31$$

$$1.429 \times 10^6 \leq u_g d / D_L \leq 2.573 \times 10^6$$

$$2.922 \times 10^6 \leq We \leq 1.169 \times 10^8$$

$$1.515 \times 10^6 \leq Re \leq 3.030 \times 10^6$$

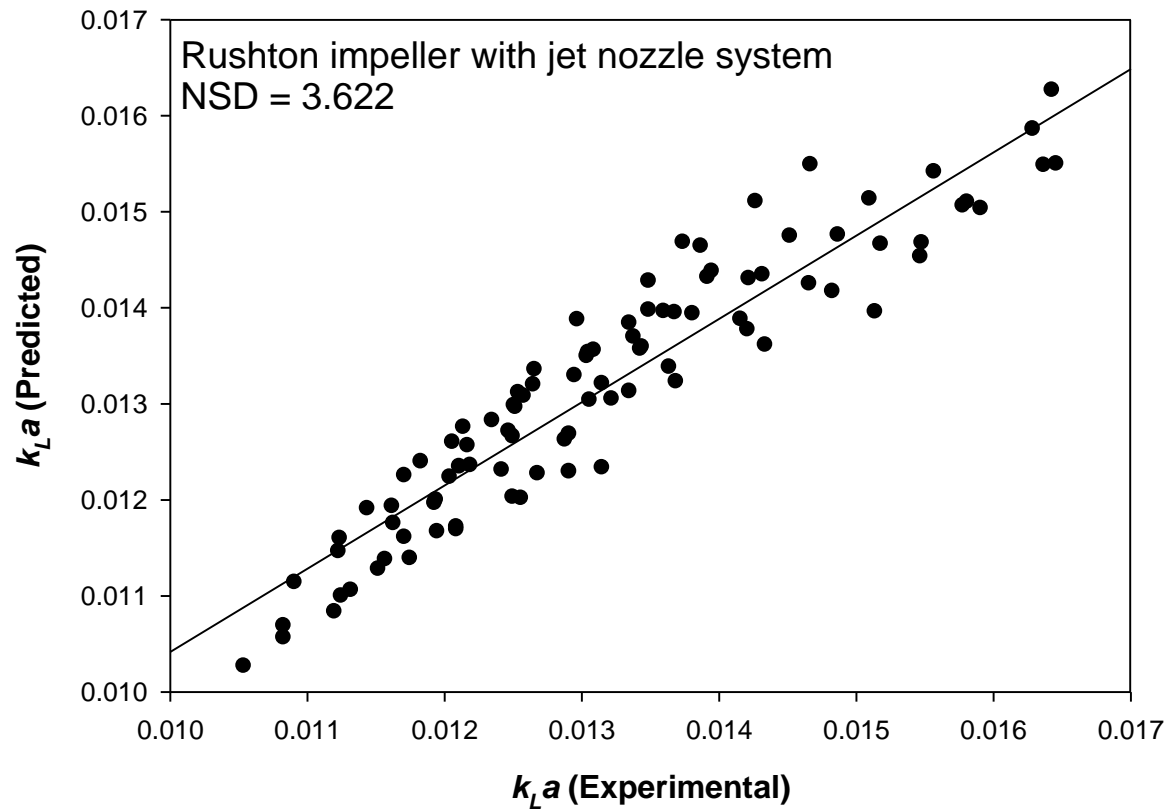


Figure 5.30 Plot of the experimental and model predicted values of $k_L a$ for Rushton impeller with different jet nozzle lengths.

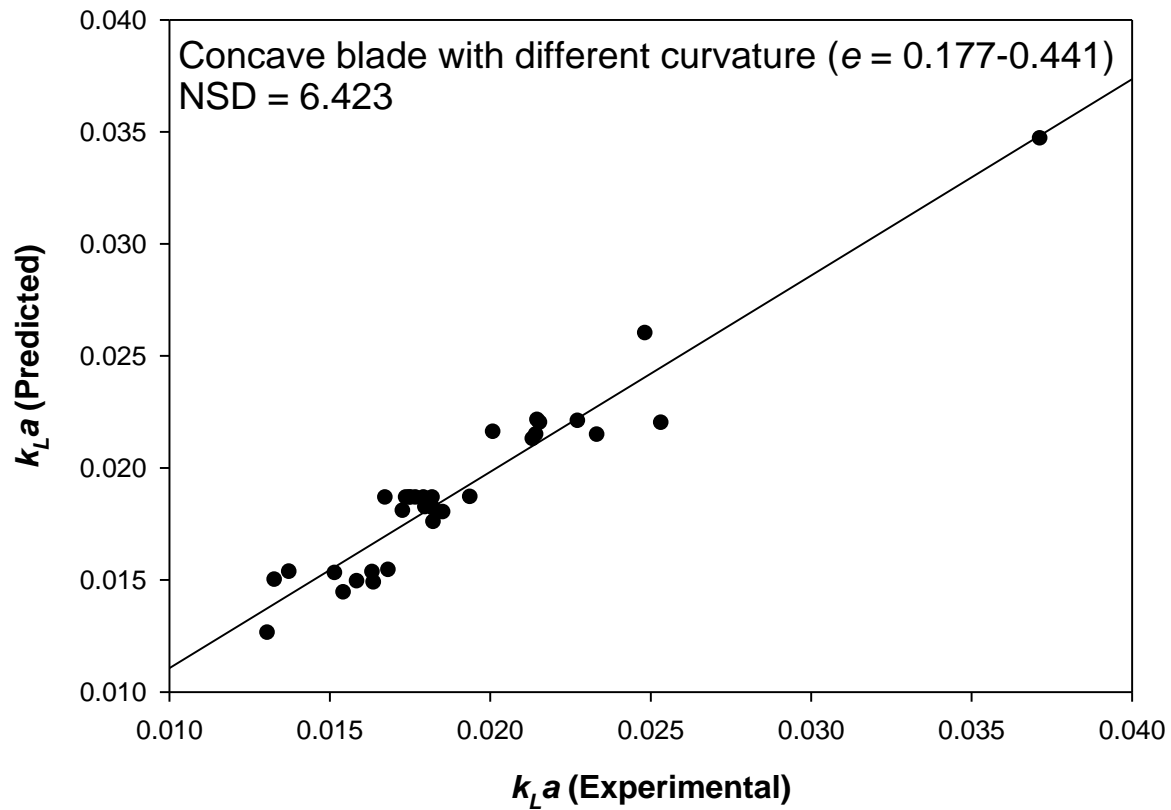


Figure 5.31 Plot of the experimental and model predicted values of $k_L a$ for concave impeller with different curvature.

5.3.5 Development of quadratic polynomial regression model for an agitation system equipped with concave blade impeller with different curvatures

The response variable, y (Volumetric mass transfer coefficient, 1/s) for agitated system equipped with concave blade impeller with different curvature can be expressed as;

$$y = f(x_{Ug}, x_N, x_{Ln}, x_C)$$

where, x_{Ug} , x_N , x_{Ln} , and x_C are the coded values of the process variables (gas flow rate, impeller speed, jet nozzle length, and curvature of blade). The experimental results and predicted values of k_{La} are presented in Table 5.8. Based on these results, an empirical relationship between the response and independent variables was attained and expressed by the following second-order polynomial equation:

$$\begin{aligned} y = & 0.0280 + 0.00048 x_{Ug} - 0.000111 x_N - 0.083 x_{Ln} - 0.0978 x_C - 0.00025 x_{Ug}^2 + 0.0000000 x_N^2 - 0.39 x_{Ln}^2 \\ & + 0.1636 x_C^2 + 0.000001 x_{Ug} \cdot x_N + 0.00637 x_{Ln} \cdot x_{Ug} + 0.00053 x_{Ug} \cdot x_C + 0.000144 x_{Ln} \cdot x_N \\ & - 0.000076 x_N \cdot x_C + 0.495 x_{Ln} \cdot x_C \end{aligned} \quad \dots(5.10)$$

Table 5.8 Experimental design layout and experimental results of the response

Run	Coded variables				Uncoded variables				Factorial design	Mass transfer coefficient, $k_L a$	
	x_1	x_2	x_3	x_4	x_{Ug}	x_N	x_{Ln}	x_C		Experimental	Predicted
1.	-1	-1	-1	-1	15.0	250	0.07	0.243	Factorial design	0.01308	0.01270
2.	+1	-1	-1	-1	20.0	250	0.07	0.243		0.01587	0.01476
3.	-1	+1	-1	-1	15.0	350	0.07	0.243		0.01639	0.01586
4.	+1	+1	-1	-1	20.0	350	0.07	0.243		0.01825	0.01835
5.	-1	-1	+1	-1	15.0	250	0.09	0.243		0.01518	0.01485
6.	+1	-1	+1	-1	20.0	250	0.09	0.243		0.01730	0.01754
7.	-1	+1	+1	-1	15.0	350	0.09	0.243		0.01855	0.01829
8.	+1	+1	+1	-1	20.0	350	0.09	0.243		0.02135	0.02142
9.	-1	-1	-1	+1	15.0	250	0.07	0.375		0.01685	0.01628
10.	+1	-1	-1	+1	20.0	250	0.07	0.375		0.01800	0.01869
11.	-1	+1	-1	+1	15.0	350	0.07	0.375		0.01825	0.01844
12.	+1	+1	-1	+1	20.0	350	0.07	0.375		0.02145	0.02128
13.	-1	-1	+1	+1	15.0	250	0.09	0.375		0.01940	0.01974
14.	+1	-1	+1	+1	20.0	250	0.09	0.375		0.02275	0.02279
15.	-1	+1	+1	+1	15.0	350	0.09	0.375		0.02157	0.02218

16.	+1	+1	+1	+1	20.0	350	0.09	0.375		0.02485	0.02567
17.	-2	0	0	0	12.5	300	0.08	0.309	Axial point	0.01376	0.01420
18.	+2	0	0	0	22.5	300	0.08	0.309		0.02011	0.01974
19.	0	-2	0	0	17.5	200	0.08	0.309		0.01635	0.01686
20.	0	+2	0	0	17.5	400	0.08	0.309		0.02335	0.02290
21.	0	0	-2	0	17.5	300	0.06	0.309		0.01330	0.01416
22.	0	0	+2	0	17.5	300	0.10	0.309		0.02149	0.02069
23.	0	0	0	-2	17.5	300	0.08	0.177		0.01545	0.01652
24.	0	0	0	+2	17.5	300	0.08	0.441		0.02535	0.02434
25.	0	0	0	0	17.5	300	0.08	0.309	Center point	0.01750	0.01758
26.	0	0	0	0	17.5	300	0.08	0.309		0.01822	0.01758
27.	0	0	0	0	17.5	300	0.08	0.309		0.01770	0.01758
28.	0	0	0	0	17.5	300	0.08	0.309		0.01675	0.01758
29.	0	0	0	0	17.5	300	0.08	0.309		0.01795	0.01758
30.	0	0	0	0	17.5	300	0.08	0.309		0.01740	0.01758
31.	0	0	0	0	17.5	300	0.08	0.309		0.01755	0.01758

Table 5.9 Analysis of Variance (ANOVA) for mass transfer coefficient

Source	Degree of freedom	Adj SS	Adj MS	F- Value	P- Value
Model	14	0.000285	0.000020	34.03	0.000
Linear	4	0.000257	0.000064	107.36	0.000
Gas flow rate, x_{Ug}	1	0.000046	0.000046	77.10	0.000
Impeller speed, x_N	1	0.000055	0.000055	91.54	0.000
Nozzle length, x_{Ln}	1	0.000064	0.000064	107.10	0.000
Curvature of blade, x_C	1	0.000092	0.000092	153.72	0.000
Square	4	0.000025	0.000006	10.27	0.000
x_{Ug}^2	1	0.000001	0.000001	1.13	0.304
x_N^2	1	0.000009	0.000009	15.83	0.001
x_{Ln}^2	1	0.000000	0.000000	0.07	0.793
x_C^2	1	0.000015	0.000015	24.31	0.000
2-Way interaction	6	0.000004	0.000001	0.98	0.472
$x_{Ug} \cdot x_N$	1	0.000000	0.000000	0.31	0.584
$x_{Ug} \cdot x_{Ln}$	1	0.000000	0.000000	0.68	0.422
$x_{Ug} \cdot x_C$	1	0.000000	0.000000	0.21	0.654
$x_N \cdot x_{Ln}$	1	0.000000	0.000000	0.14	0.715
$x_N \cdot x_C$	1	0.000001	0.000001	1.67	0.215
$x_{Ln} \cdot x_C$	1	0.000002	0.000002	2.86	0.110
Error	16	0.000010	0.000001		
Lack-of-Fit	10	0.000008	0.000000	3.85	0.056
Pure Error	6	0.000001			
Total	30	0.000294			

$R^2 = 96.7\%$, Adjusted $R^2 = 93.91\%$

Table 5.9 shows the results of the quadratic response surface model fitting in the form of analysis of variance (ANOVA). ANOVA is required to test the significance and adequacy of the model (Aleboyeh et al. 2008; Liu and Chiou 2005). The fact that p values for some terms in these tables are less than the confidence level (0.05) and the P value for lack of fit is higher than 0.05 indicate the adequacy and significance of the model. In this case, gas flow rate (x_{Ug}), impeller speed (x_N), jet nozzle length (x_{Ln}), and curvature of blade (x_C) were significant model terms with p-values less than 0.05. In addition, all interaction terms between x_{Ug} , x_N , x_{Ln} and x_C was

insignificant to the responses (term p-value >0.100 indicates the model terms are not significant) which could be manually removed from the model to improve the regression model and optimization results.

The ANOVA subdivides the total variation of the results in to two components: variation associated with the model and variation associated with the experimental error, showing whether the variation from the model is significant or not when compared with the ones associated with residual error (Liu and Chiou 2005; Singh et al. 2011). This comparison is performed by the F-value, which is the ratio between the mean square of the model and the residual error. If the model is a good predictor of the experimental results, the F-value should be greater than the tabulated value of the F-distribution for a certain number of degrees of freedom in the model at a level of significance α . The ANOVA results (Table 5.9) of the quadratic regression model (Eq. 1) suggest that the model was highly significant, as evident from the Fisher's F-test ($F_{\text{model}} = 34.03$) with a very low probability value ($p_{\text{model}} = 0.000$). Furthermore, the calculated F-value ($F_{\text{model}} = 34.03$) was compared with the critical F value ($F_{0.05,df,(n-df+1)}$) for the considered probability ($p = 0.05$) and degrees of freedom. Since, the degrees of freedom for model are 14 and $n = 31$, it gives $(n - \text{degrees of freedom} + 1) = 16$. The critical F value ($F_{0.05, 14, 16} = 2.37$) is less than the calculated F-value of 34.03. It is confirming to justify a very high degree of adequacy of the quadratic model and significance of the variables combinations (Sen et al. 2004).

The p-values were used as a tool to check the significance of each of the coefficients, which, in turn, are necessary to understand the pattern of the mutual interactions between the test variables. The larger the magnitude of the t-value and smaller the P-value, the more significant is the corresponding coefficient (Liu and Chiou 2005; Shafeeyan et al 2012). The mutual between curvature of blade and jet nozzle length, $x_{Ln} \times x_C$ ($p = 0.110$) is significant comparing to those between each other two factors. These results suggest that these interactions of each other two parameters did not improve much in increasing mass transfer value. The goodness of fit of the model was checked by the correlation coefficient (R^2) between the experimental and model predicted values of the response variable. A fairly high value of R^2 (0.967) indicated that most of the data variation was explained by the regression model. This implies that 96.7% of the variations for gassed power are explained by the independent variables and this also means that the model does not explain only about 3.3 % of variation. Moreover, a closely high value of the adjusted correlation coefficient ($R^2_{\text{adj}} = 0.939$) also showed a high significance of the model.

Table 5.10 Estimated regression coefficients and corresponding t and P values from the data of central composite design experiment.

Regression coefficient	Factor effect	Coefficient value	Standard error (SE) coefficient	t-Value	P-Value
<i>Constant</i>	–	0.017581	0.000292	60.18	0.000
Linear					
x_{Ug}	0.005542	0.002771	0.000316	8.78	0.000
x_N	0.006038	0.003019	0.000316	9.57	0.000
x_{Ln}	0.006532	0.003266	0.000316	10.35	0.000
x_C	0.007825	0.003913	0.000316	12.40	0.000
Quadratic					
x_{Ug}^2	–0.001229	–0.000614	0.000578	–1.06	0.304
x_N^2	0.004601	0.002301	0.000578	3.98	0.001
x_{Ln}^2	–0.000309	–0.000154	0.000578	–0.27	0.793
x_C^2	0.005701	0.002851	0.000578	4.93	0.000
Interaction					
$x_{Ug} \cdot x_N$	0.000865	0.000433	0.000773	0.56	0.584
$x_{Ug} \cdot x_{Ln}$	0.001275	0.000638	0.000773	0.82	0.422
$x_{Ug} \cdot x_C$	0.000705	0.000352	0.000773	0.46	0.654
$x_N \cdot x_{Ln}$	0.000575	0.000288	0.000773	0.37	0.715
$x_N \cdot x_C$	–0.001995	–0.000997	0.000773	–1.29	0.215
$x_{Ln} \cdot x_C$	0.002615	0.001307	0.000773	1.69	0.110

The factor effects of the model and associated p-values are presented in Table 5.10, it can be concluded that for predicted mass transfer coefficient responses (y), linear contribution and quadratic contribution except gas flow rate and jet nozzle length parameter of the model were more significant, whereas cross-product contribution of the model was insignificant.

For the regression coefficients, both the magnitude and sign are important, as the earlier indicates the importance or influence of the variable on the response factor, whereas, the sign determines its effect direction. A positive sign indicates a synergistic effect, while a negative sign represents an antagonistic effect of the factor on the selected response. As shown in Table 5.10, the

responses of y (k_{La}) were significantly affected by the synergistic effect of linear term of gas flow rate, impeller speed, jet nozzle length, and curvature of blade. From Table 5.10, it is evident that all the linear and quadratic (except $x_{U_g}^2$ and $x_{L_n}^2$) terms are statistically significant ($p < 0.05$). All interactions are statistically insignificant. Moreover, the first-order main effects of all the four independent variables viz. gas flow rate, impeller speed, jet nozzle length, and curvature of blade were found to be more significant than their respective quadratic effects. The t - and p -value (Tables 5.9 and 5.10) suggest that jet nozzle length and curvature of blade have a direct relationship on k_{La} . It may be noted that curvature of blade was the most significant component of the regression model for the present application, whereas, the quadratic dose term showed the lowest effect on k_{La} .

5.3. 6 Effect of model components and their interactions on k_{La}

Response surface plots provide a method to predict the value of k_{La} for different values of the tested variables and the contours of the plots help in identification of the type of interactions between these variables (Montgomery 2001). Each surface and contour plots of the quadratic model represents an infinite number of combinations of two tested variables with the other two variables kept constant (here optimized value was taken). Response surface plots provide a method to predict the k_{La} for different values of the tested variables and the contours of the plots help in identification of the type of interactions between these variables. A circular contour of response surfaces indicates that the interaction between the corresponding variables is negligible. In contrast, an elliptical or saddle nature of the contour plots indicates that the interaction between the corresponding variables is significant. The response surface contour plots for the effect of each pair of variables are shown in Figures 5.32–5.36.

5.3.6.1 Effect of gas flow rate and impeller speed on k_{La}

In Figure 5.32, the response surface and contour plots were developed as a function of agitator speed and gas flow rate while the optimized value of curvature of blade and jet nozzle length were kept constant at 0.441 and 0.1 m respectively. It can be seen from Figure 5.32, the highest mass transfer coefficient (0.0370 s^{-1}) occurred when nozzle with large length was kept at about 0.10 m under applied curvature of blade (0.441). The presumed reason is that, at constant gas flow rate, the value of k_{La} increased with increasing impeller speed due to sharp drop in bubble size which is favorable to gas–liquid mass transfer. As the air flow rate increases, the value of

k_{La} gradually increased until, at the highest gas load used, the overall effect of impeller speed becomes almost negligible. This positive effect of superficial gas velocity becomes slight due to the balance between the coalescence and breakup of the bubbles in the churn turbulent flow regime (Wilkinson et al., 1994). In other words, the increase of superficial gas velocity the gas holdup increases as well as the gas–liquid interfacial area a for aggravating bubble-bubble interactions and liquid backmixing, which is favorable to gas–liquid mass transfer, and then increases the volumetric mass transfer coefficient k_{La} .

5.3.6.2 Effect of gas flow rate and curvature of blade on k_{La}

To study the effect of curvature of blade on k_{La} , the experiments were carried out with curvature of blade varying from 0.177 to 0.441. In Figure 5.33, the response surface and contour plots were developed as a function of curvature of blade and gas flow rate while the optimum value of impeller speed and jet nozzle length were kept constant at 400 rpm and 0.1 m respectively. It can be seen from Figure 5.33, higher gas flow rate and higher curvature blade was favorable for larger value of k_{La} . As can be seen from Figure the highest mass transfer value (0.0370) occurred when curvature of blade was kept at about 0.441 under all gas flow rate conditions.

5.3.6.3 Effect of jet nozzle length and curvature of blade on k_{La}

In Figure 5.35, the response surface and contour plots were developed as a function of curvature of blade and jet nozzle length while the optimum value of impeller speed and gas flow rate were kept constant at 400 rpm and 22.5 L/m respectively. As it can be seen from Figure 5.35 the influence of these two variables on k_{La} was significant for larger value of curvature blade (0.441) and nozzle with large length (0.10 m) studied. It has been observed from Figure 5.35 that reduction in distance between jet nozzle and impeller blade edge significantly affects the bubble size discharged from the impeller which is responsible for higher mass transfer coefficient. The size of cavities formed behind the impeller blade decreased with increases blade curvature and significantly affects the bubble size discharged from the impeller which is responsible for higher mass transfer coefficient.

5.3.6.4 Effect of impeller speed and curvature of blade on k_{La}

In Figure 5.37, the response surface and contour plots were developed as a function of curvature of blade and impeller speed while the optimum value of jet nozzle length and gas flow rate were kept constant at 0.1 m and 22.5 L/m respectively. The size of cavities formed behind the blade is

believed to change gradually with increases in the blade curvature. Higher blade curvature (0.441) with higher impeller speed (400 rpm) significantly affects the bubble size and population of bubble discharged from the impeller which is accountable for higher value of k_La (0.0370 s^{-1}).

5.3.6.5 Effect of jet nozzle length and gas flow rate on k_La

In Figure 5.34, the response surface and contour plots were developed as a function of gas flow rate and jet nozzle length while the optimum value of impeller speed and curvature of blade were kept constant at 400 rpm and 0.441 respectively. As it is obvious from Figure 5.34, mass transfer coefficient increased with increase in nozzle length and reached 0.0370 s^{-1} under all gas flow rate.

5.3.6.6 Effect of jet nozzle length and impeller speed on k_La

In Figure 5.36, the response surface and contour plots were developed as a function of impeller speed and jet nozzle length while the optimum value of gas flow rate and curvature of blade were kept constant at 22.5 L/min and 0.441 respectively. As it is clear from this Figure 5.36, mass transfer coefficient reached (0.0370 s^{-1}) to the highest value when nozzle length was about 0.1 m. The reduction in gap between nozzle and impeller blade edge and impeller speed significantly affects the bubble dimension and population of bubble discharged from the impeller which is accountable to higher k_La value.

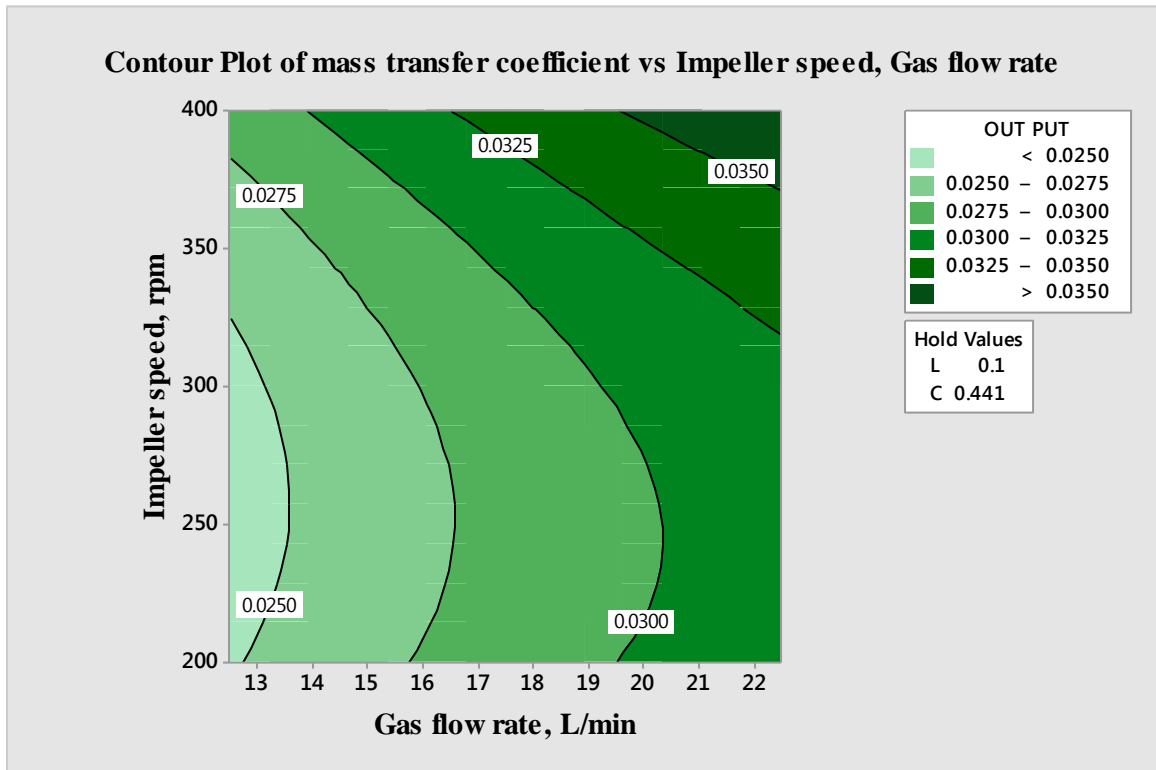
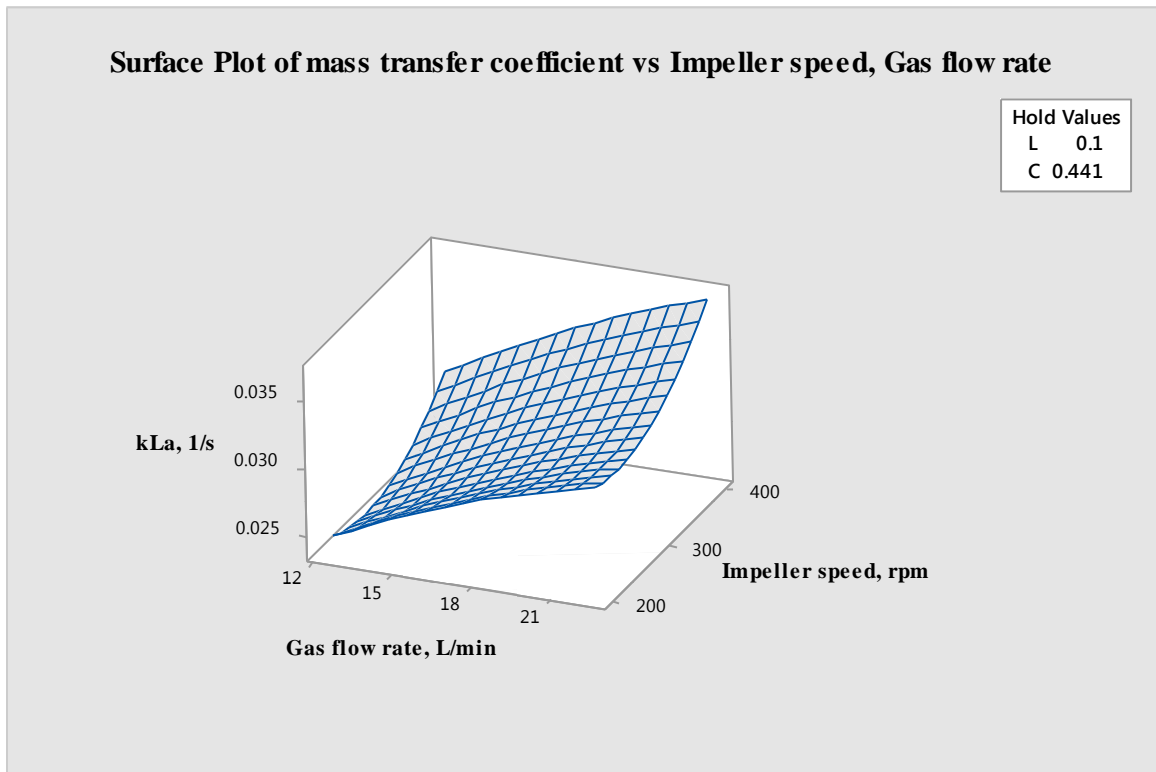


Figure 5.32 (a) Response surface and (b) contour plots of k_{La} at optimized value as the function of gas flow rate (L/min) and impeller speed (rpm)

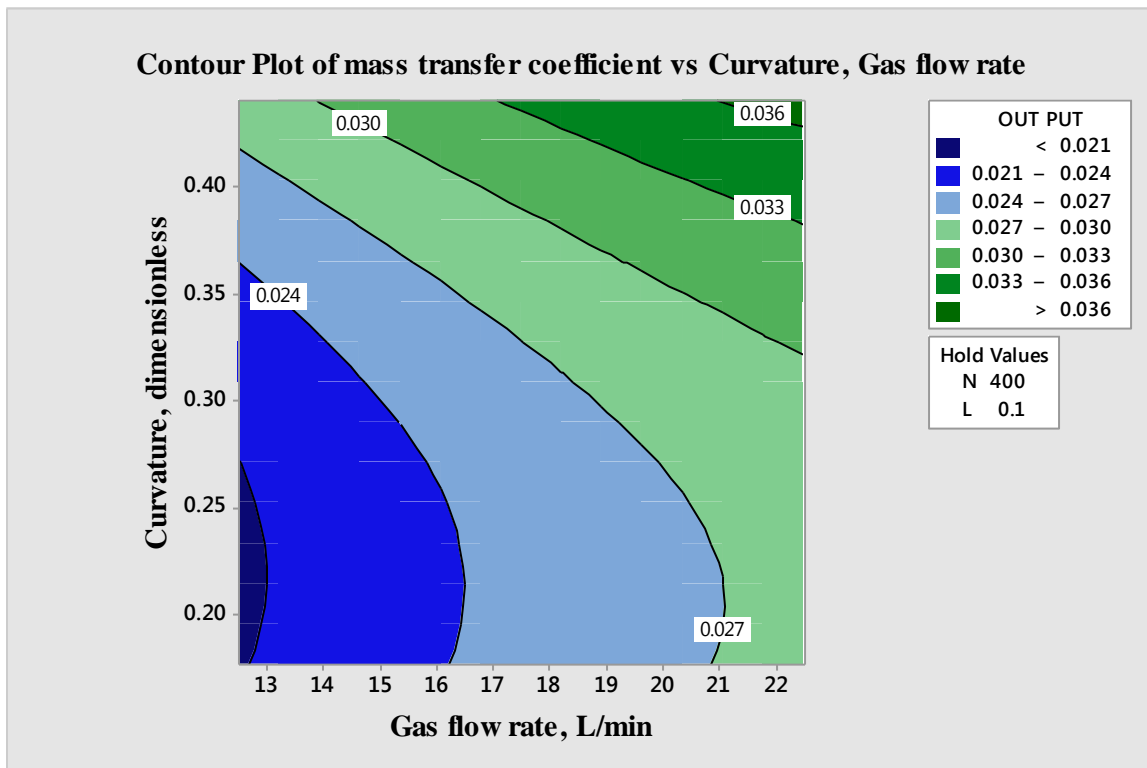
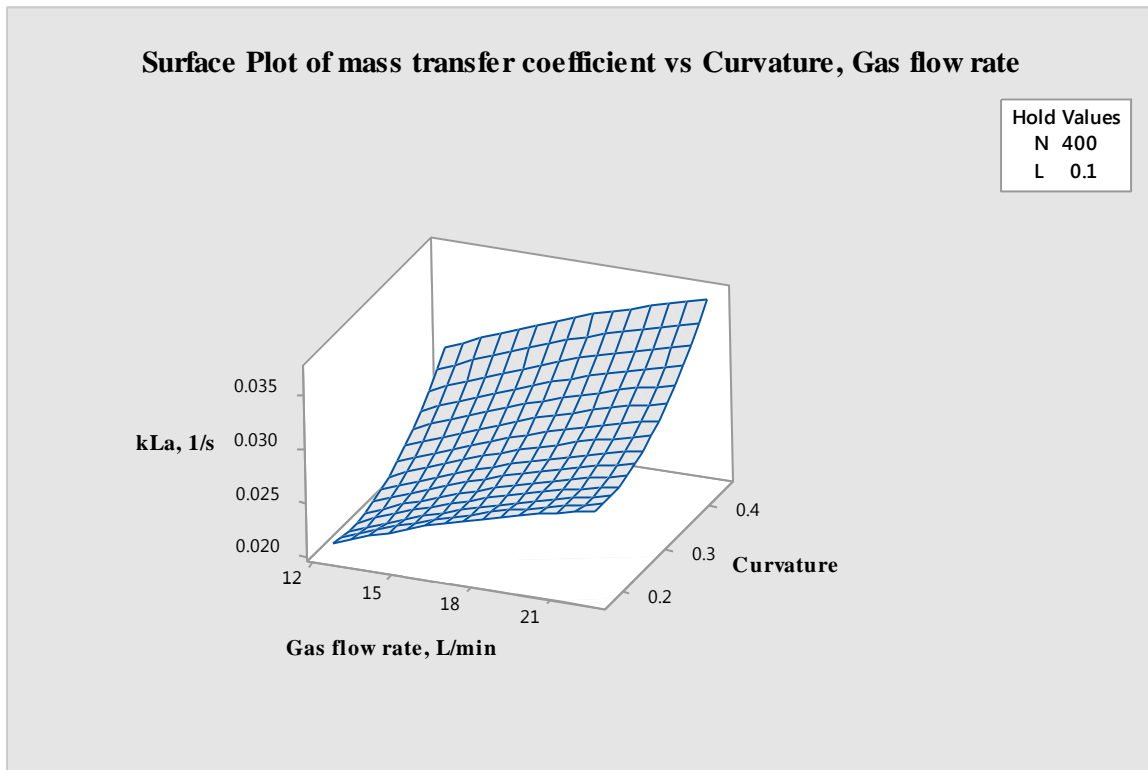


Figure 5.33 (a) Response surface and (b) contour plots of k_{La} at optimized value as the function of gas flow rate (L/min) and curvature (dimensionless).

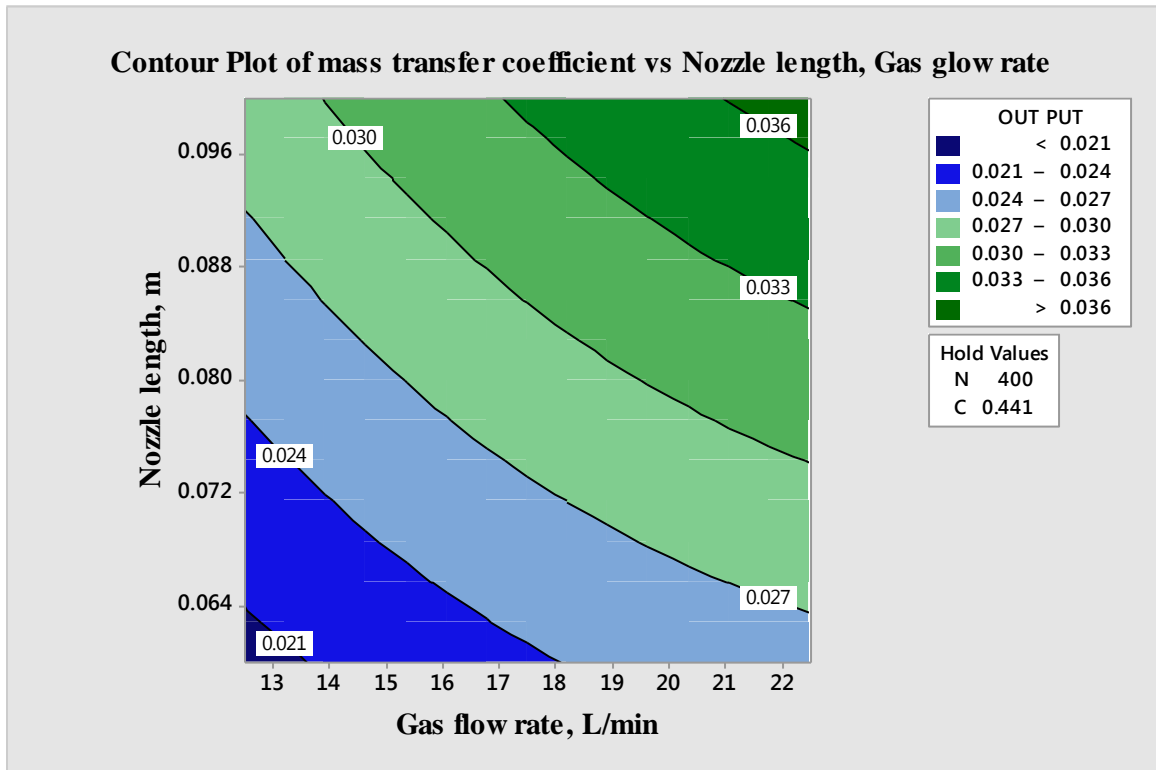
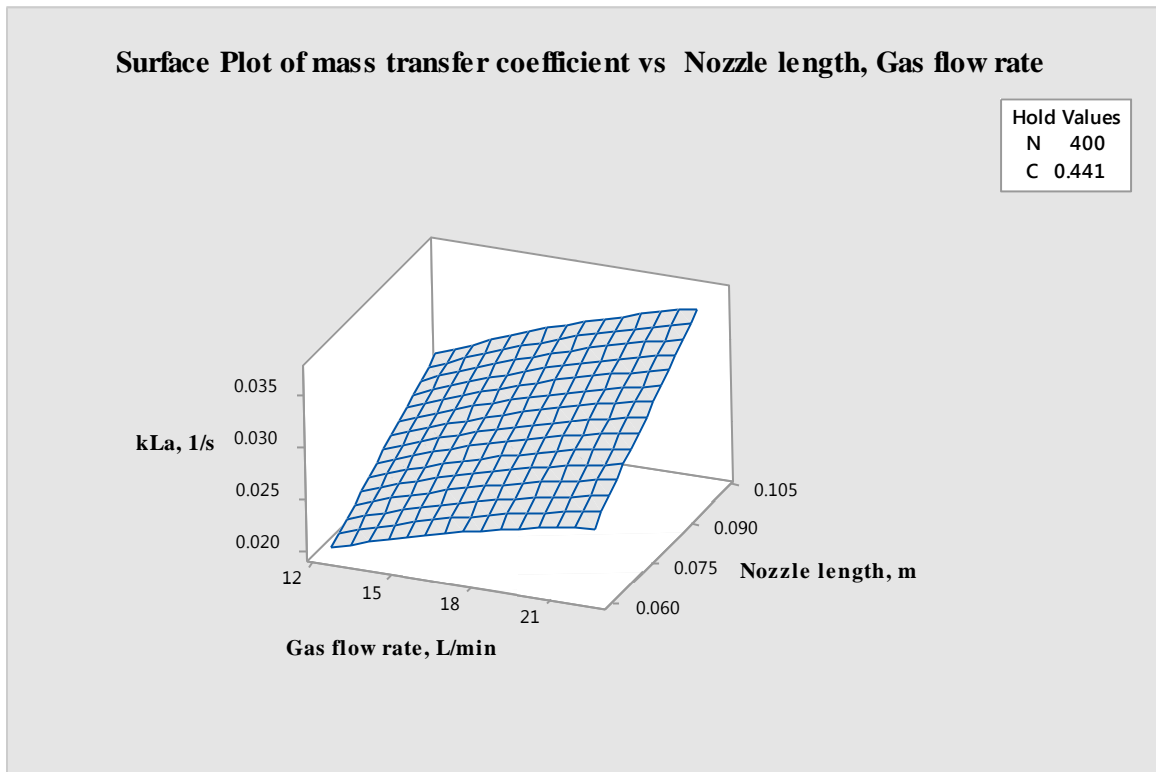


Figure 5.34 (a) Response surface and (b) contour plots of k_{La} at optimized value as the function of gas flow rate (L/min) and nozzle length (m).

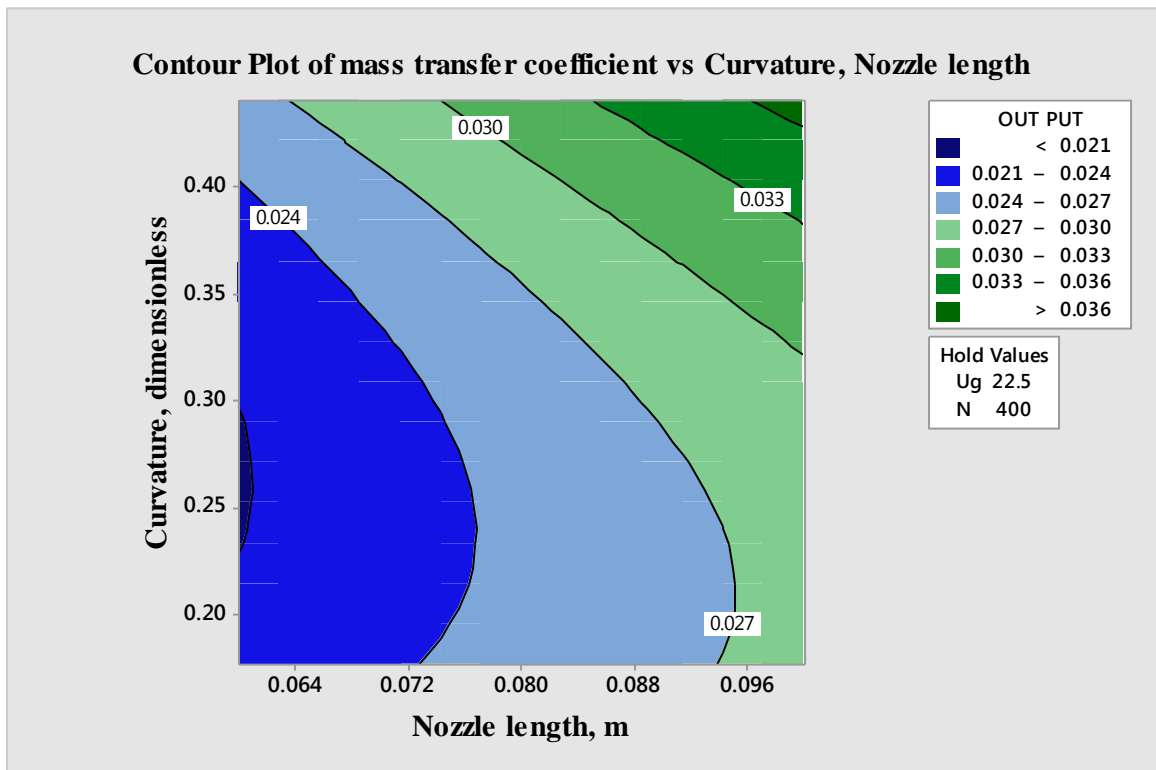
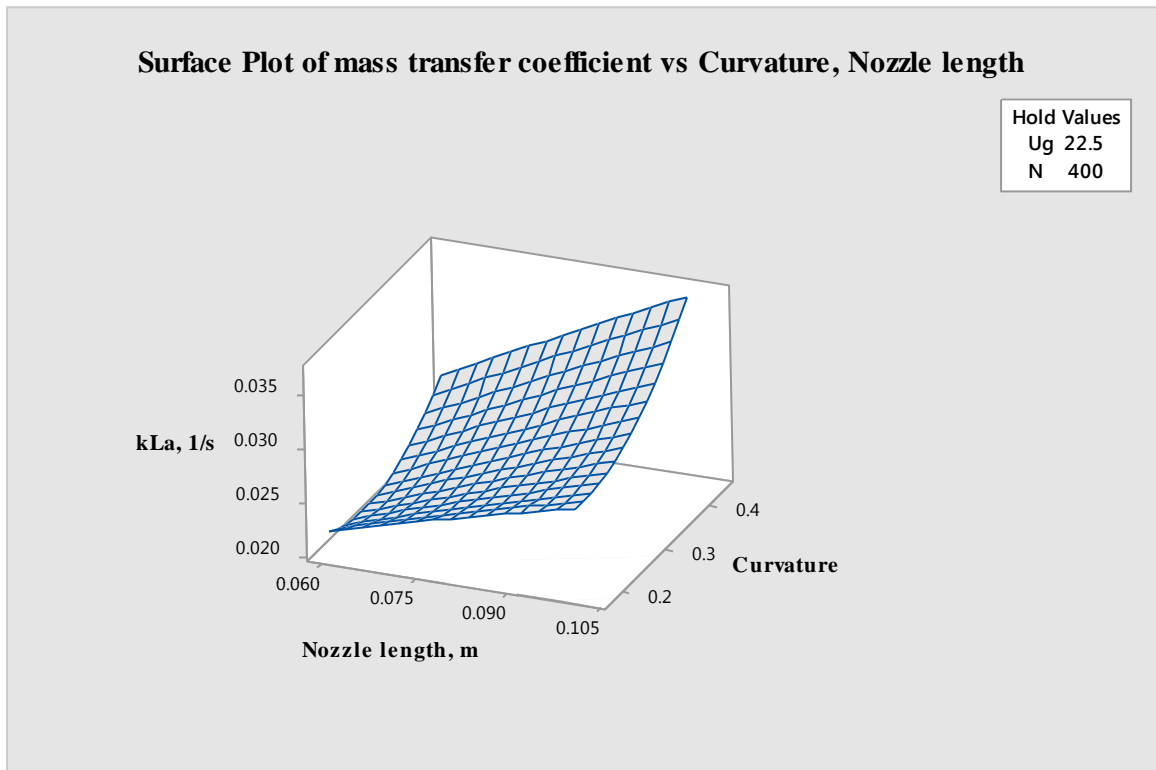


Figure 5.35 (a) Response surface and (b) contour plots of k_{La} at optimized value as the function of curvature (dimensionless) and nozzle length (m).

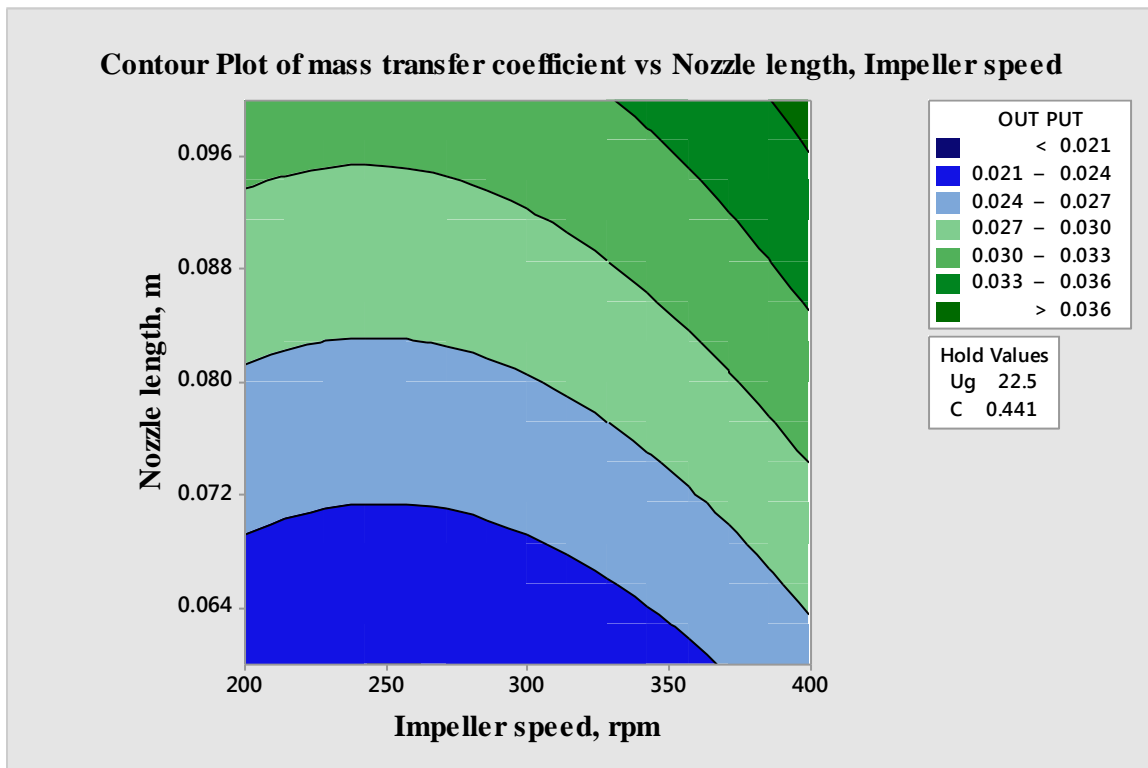
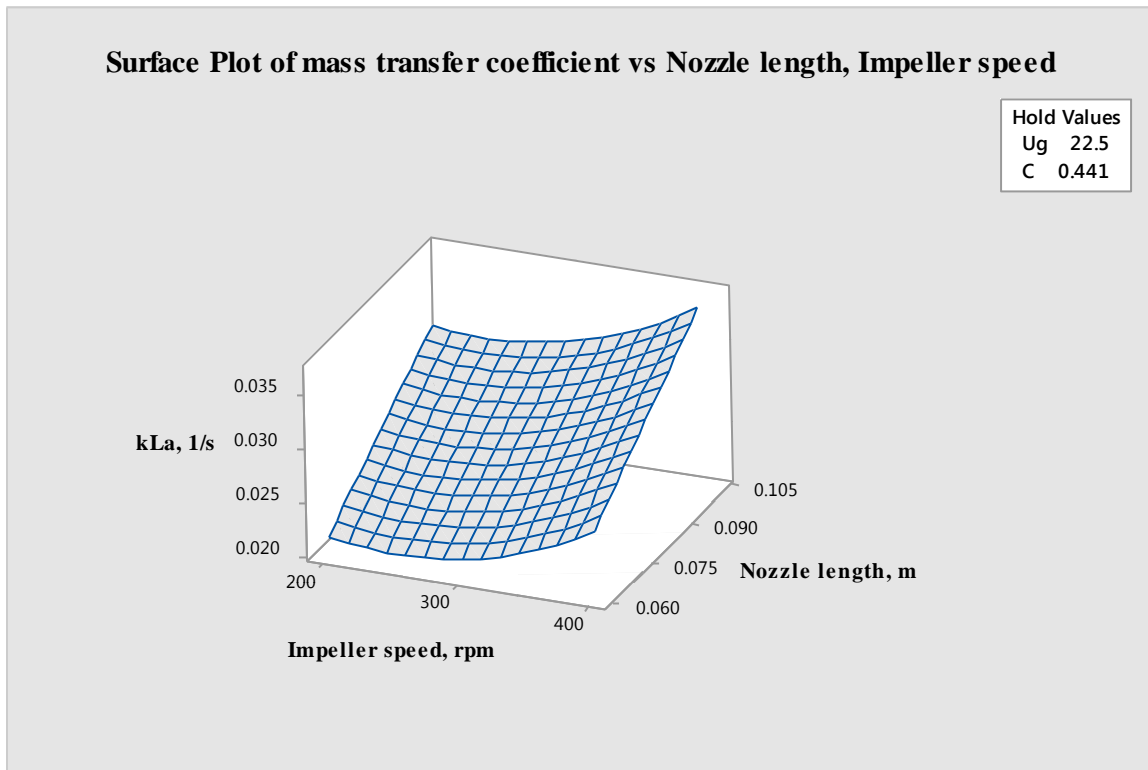


Figure 5.36 (a) Response surface and (b) contour plots of k_{La} at optimized value as the function of impeller speed (rpm) and nozzle length (m).

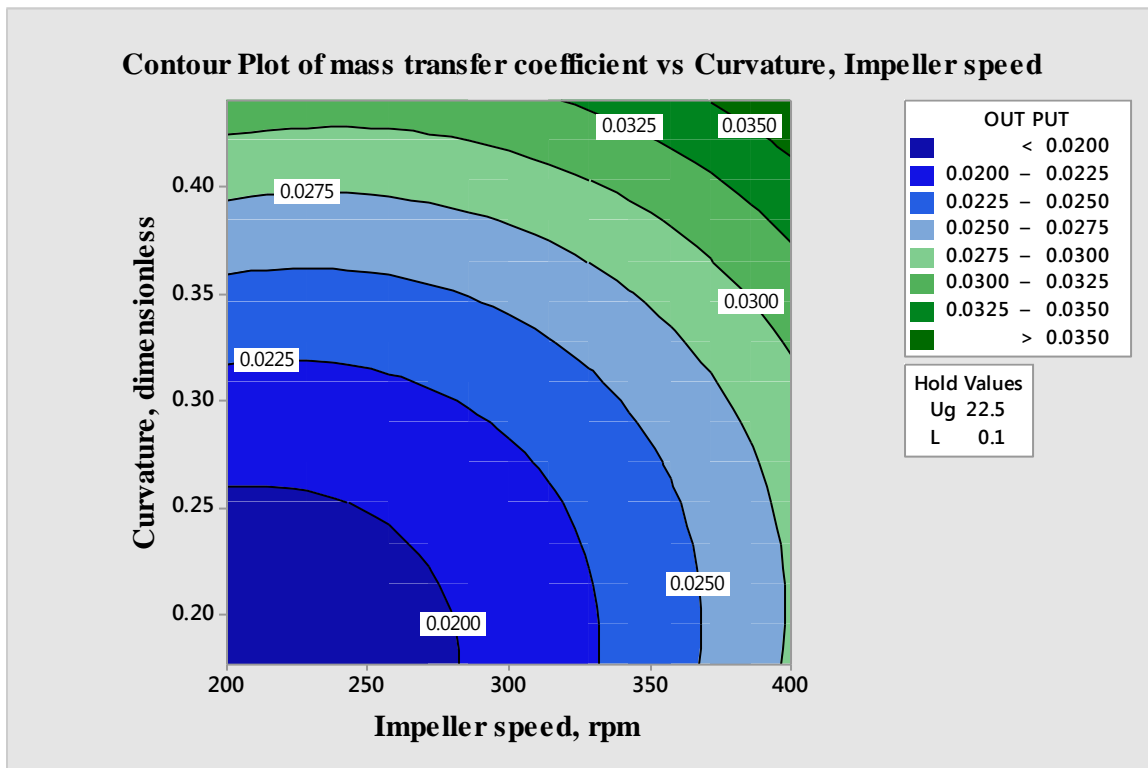
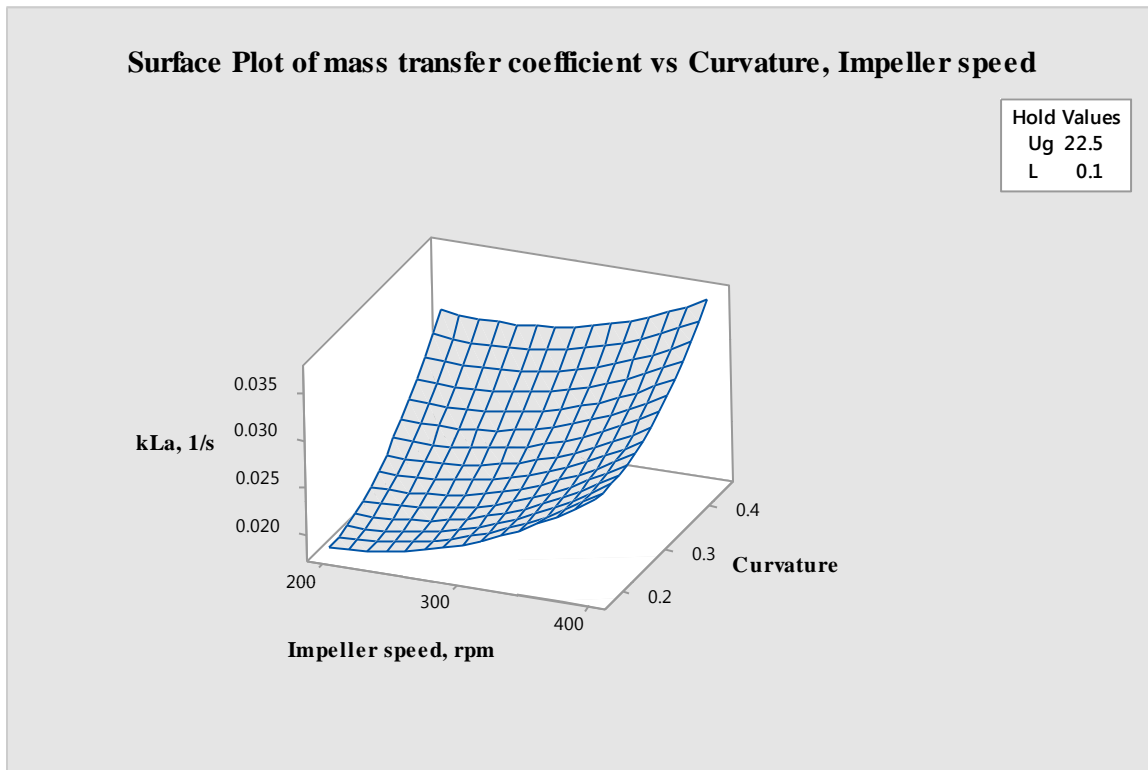


Figure 5.37 (a) Response surface and (b) contour plots of k_{La} at optimized value as the function of impeller speed (rpm) and curvature (dimensionless).

5.3.7 Response optimization

Statistical optimization method overcomes the limitations of classic empirical methods and has been proved to be a powerful tool for the optimization of mass transfer coefficient k_{La} in aeration system in this study. The high correlation of the model showed that second-order polynomials could be used to optimize aeration process condition for maximizing the value of k_{La} . The optimized parameters for mass transfer coefficient k_{La} determined in this study were set as follows: air flow rate, 22.5 L/min; agitator speed, 400 rpm; jet nozzle length, 0.10 m; Curvature, 0.441. These values were further validated by actually carrying out the experiment at the optimized values of these parameters. The optimum values of the process variables for k_{La} are shown in Table 5.11. The result shown in Figure 5.38 indicated that the optimized k_{La} was obtained when the values of each parameter were set as the optimum values, which was in good agreement with the value predicted from the model. The measured and model predicted values of the response variable are shown in Figure 5.39.

The normalized standard deviation between experimental and predicted values for each model has been calculated by following equation (Singh et al. 2008):

$$\text{Normalized standard deviation (NSD)} = 100 \sqrt{\frac{\sum \left[\frac{(k_{La}(\text{exp}) - k_{La}(\text{pred}))^2}{k_{La}(\text{exp})} \right]}{N}}$$

where $k_{La}(\text{exp})$ is the experimental k_{La} and $k_{La}(\text{pred})$ is the corresponding predicted k_{La} according to the equation under study with best fitted parameters, N is the number of measurements. It is clear that lower the values of normalized deviations, the better are the fit of experimental data.

Table 5.11 Optimum operating conditions of the process variable

Independent variables	Optimum operating conditions	$(k_{La})_{\text{experimental}}$ 1/s	$(k_{La})_{\text{predicted}}$ 1/s	Error (%)
Air flow rate, L/min	22.5	0.0370	0.03716	9.04 %
Agitator speed, rpm	400			
Jet nozzle length, m	0.10			
Curvature, dimensionless	0.441			

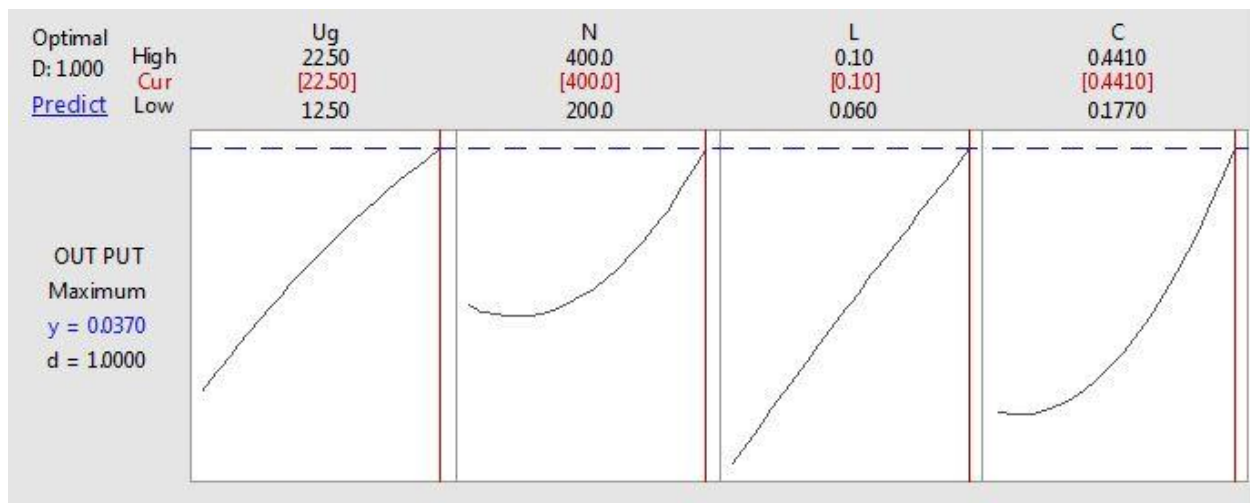


Figure 5.38 The optimum values of the process variables for k_{La} .

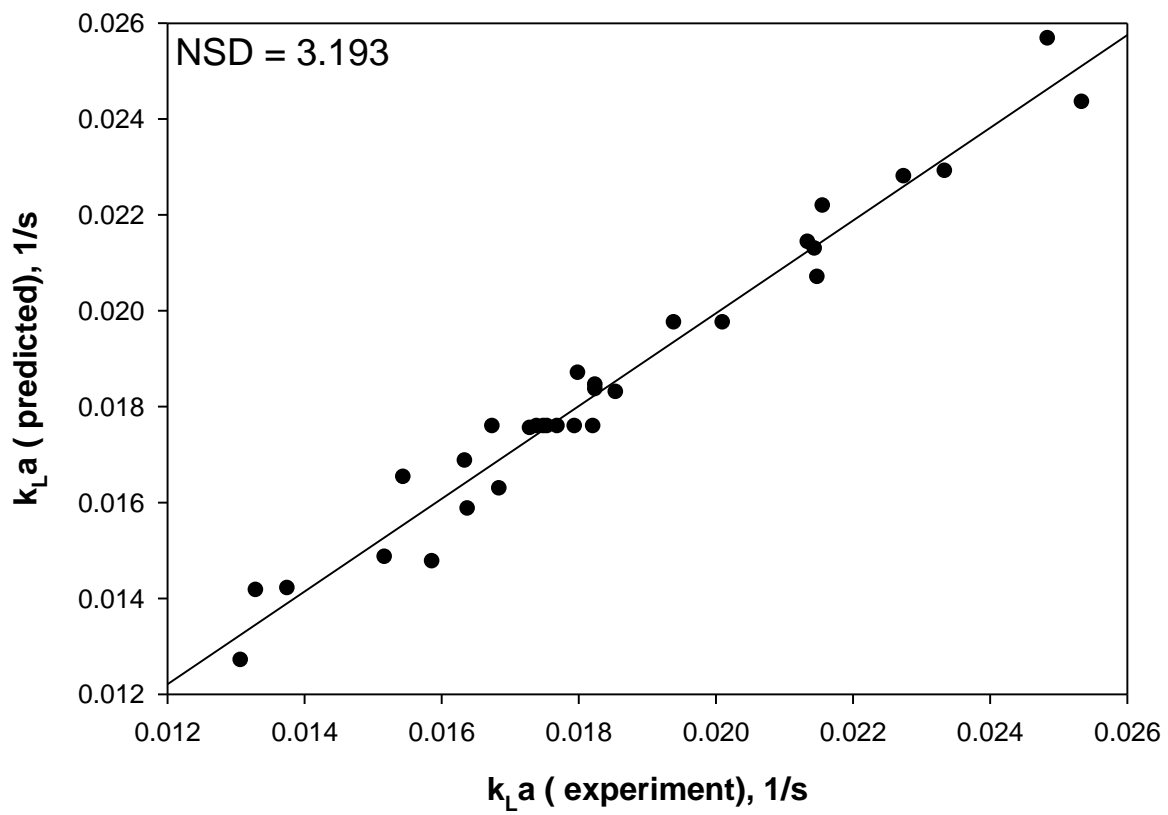


Figure 5.39 Plot of the measured and model predicted values of the response variable.

5.3.8 Development of quadratic polynomial regression model for agitation system equipped with Rushton impeller

Experimental results and the predicted values obtained using the model equation is shown in Table 5.14. The obtained R^2 value suggests good adjustments to the experimental results since this indicates that 97.49% of the variability in the response could be explained by the models. This implies that 97.49% of the variation in mass transfer coefficient in aeration system is explained by the independent variables and also suggests that only 2.51% of variation is not explained by the model. Adjusted R^2 (Adj- R^2) is also a measure of goodness of fit, but it is more suitable for comparing models with different numbers of independent variables. Here, the adjusted R^2 value (95.22%) was very close to the corresponding R^2 value. If the model is a good predictor of the experimental results, the F-value should be greater than the tabulated value of the F-distribution for a certain number of degrees of freedom in the model at a level of significance α . From Table 5.13, the F-value obtained, 43.10, is clearly greater than the tabulated F-value (2.80 at 95% significance) confirming the adequacy of the model fit.

As shown in Table 5.12, the responses of y (k_{LA}) were significantly affected by the synergistic effect of linear term of gas flow rate, impeller speed and jet nozzle length. From Table 5.12, it is evident that all the linear and quadratic (except $x_{U_g}^2$) terms are statistically significant ($p < 0.05$). All interactions are statistically insignificant. Moreover, the first-order main effects of all three independent variables viz. gas flow rate, impeller speed and jet nozzle length were found to be more significant than their respective quadratic effects. Based on these results, an empirical relationship between the response and independent variables was attained and expressed by the following second-order polynomial equation:

$$y = 0.00116 - 0.000405 x_{U_g} - 0.000009 x_N + 0.002999 x_{L_n} + 0.000007 x_{U_g}^2 + 0.000000 x_N^2 - 0.000195 x_{L_n}^2 + 0.000000 x_{U_g} \cdot x_N + 0.000030 x_{L_n} \cdot x_{U_g} - 0.000000 x_{L_n} \cdot x_N \quad \dots(5.11)$$

Table 5.12 Estimated regression coefficients and corresponding t and P values from the data of central composite design experiment.

Regression coefficient	Factor effect	Coefficient value	Standard error (SE) coefficient	t-Value	P-Value
<i>constant</i>	–	0.013217	0.000083	158.71	0.000
Linear					
Impeller speed, x_N	0.003430	0.001715	0.000104	16.43	0.000
Nozzle length, x_{Ln}	0.001610	0.000805	0.000104	7.71	0.000
Gas flow rate, x_{Ug}	0.000925	0.000462	0.000104	4.43	0.001
Quadratic					
x_N^2	0.000869	0.000435	0.000167	2.61	0.026
x_{Ln}^2	–0.001561	–0.000780	0.000167	–4.69	0.001
x_{Ug}^2	0.000359	0.000180	0.000167	1.08	0.306
Interaction					
$x_N \cdot x_{Ln}$	–0.000000	–0.000000	0.000295	–0.00	1.000
$x_{Ug} \cdot x_N$	0.000020	0.000010	0.000295	0.03	0.974
$x_{Ug} \cdot x_{Ln}$	0.000600	0.000300	0.000295	1.02	0.334

Table 5.13 Analysis of Variance (ANOVA) for mass transfer coefficient

Source	Degree of freedom	Adj SS	Adj MS	F- Value	P- Value
Model	9	0.000017	0.000002	43.10	0.000
Linear	3	0.000015	0.000005	116.32	0.000
Impeller speed, x_N	1	0.000012	0.000012	269.86	0.000
Nozzle length, x_{Ln}	1	0.000003	0.000003	59.46	0.000
Gas flow rate, x_{Ug}	1	0.000001	0.000001	16.63	0.001
Square	3	0.000002	0.000001	12.63	0.001
x_N^2	1	0.000000	0.000000	6.81	0.026
x_{Ln}^2	1	0.000001	0.000001	21.96	0.001
x_{Ug}^2	1	0.000000	0.000000	1.16	0.306
2-Way interaction	3	0.000000	0.000000	0.34	0.794
$x_N \cdot x_{Ln}$	1	0.000000	0.000000	0.00	1.000
$x_{Ug} \cdot x_N$	1	0.000000	0.000000	0.00	0.974
$x_{Ug} \cdot x_{Ln}$	1	0.000000	0.000000	1.03	0.334
Error	10	0.000000	0.000000		
Lack-of-Fit	5	0.000000	0.000000	3.75	0.087
Pure Error	5	0.000000	0.000000		
Total	19	0.000017			

$R^2 = 97.49 \%$, Adjusted $R^2 = 95.22 \%$

Table 5.14 Experimental design layout and experimental results of the response.

Coded variables			Uncoded variables				Mass transfer coefficient, $k_L a$		
Run	x_N	x_{Ln}	x_{Ug}	x_N	x_{Ln}	x_{Ug}	Experimental	Predicted	
1	-1	-1	-1	250	7	15.0	Factorial design	0.01171	0.01176
2	+1	-1	-1	350	7	15.0		0.01335	0.01347
3	-1	+1	-1	250	9	15.0		0.01268	0.01242
4	+1	+1	-1	350	9	15.0		0.01416	0.01413
5	-1	-1	+1	250	7	20.0		0.01211	0.01207
6	+1	-1	+1	350	7	20.0		0.01360	0.01379
7	-1	+1	+1	250	9	20.0		0.01322	0.01302
8	+1	+1	+1	350	9	20.0		0.01487	0.01474
9	-2	0	0	200	8	17.5	Axial point	0.01175	0.01194
10	+2	0	0	400	8	17.5		0.01548	0.01537
11	0	-2	0	300	6	17.5		0.01183	0.01163
12	0	+2	0	300	10	17.5		0.01297	0.01324
13	0	0	-2	300	8	12.5	Center point	0.01291	0.01293
14	0	0	+2	300	8	22.5		0.01381	0.01386
15	0	0	0	300	8	17.5		0.01310	0.01322
16	0	0	0	300	8	17.5		0.01315	0.01322
17	0	0	0	300	8	17.5		0.01345	0.01322
18	0	0	0	300	8	17.5		0.01325	0.01322
19	0	0	0	300	8	17.5		0.01320	0.01322
20	0	0	0	300	8	17.5		0.01308	0.01322

5.3.9 Response optimization

The optimized parameters for mass transfer coefficient k_{La} determined in this study were set as follows: air flow rate, 22.5 L/min; agitator speed, 400 rpm; jet nozzle length, 0.943 m. These values were further validated by actually carrying out the experiment at the optimized values of these parameters. The optimum values of the process variables and average values of experiments and predicted results are presented in Table 5.15 and Figure 5.40. As can be seen in this table, the deviation errors between the experimental and predicted (by regression model) a value of mass transfer coefficient k_{La} was 1.67%. The close agreement between the experimental values and those predicted from the CCD (regression) model suggests that the developed model can correlate air flow rate (L/min), impeller speed (rpm) and jet nozzle length (m) to mass transfer coefficient k_{La} with a high degree of accuracy. The measured and model predicted value of the response variable is shown in Figure 5.41. It is expected that the optimization results presented in this paper may provide background information for detailed process improvement research.

Table 5.15 Optimum operating conditions of the process variable.

Independent variables	Optimum operating conditions	$(k_{La})_{\text{experimental}}$ 1/s	$(k_{La})_{\text{predicted}}$ 1/s	Error (%)
Air flow rate, L/min	22.5	0.0164	0.01613	1.67
Agitator speed, rpm	400			
Jet nozzle length, m	0.943			

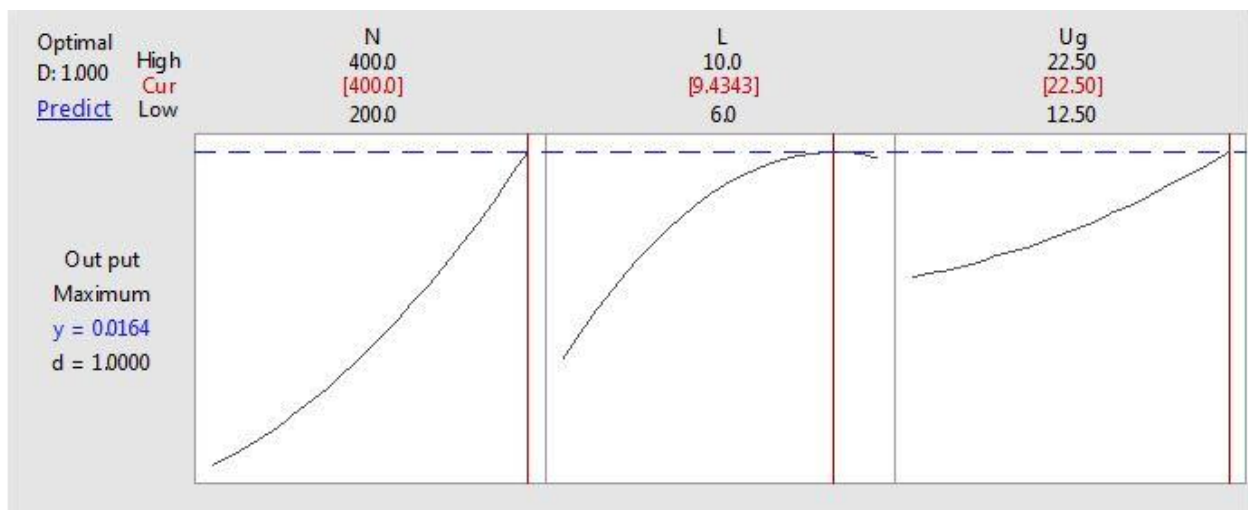


Figure 5.40 The optimum values of the process variables for k_{La} .

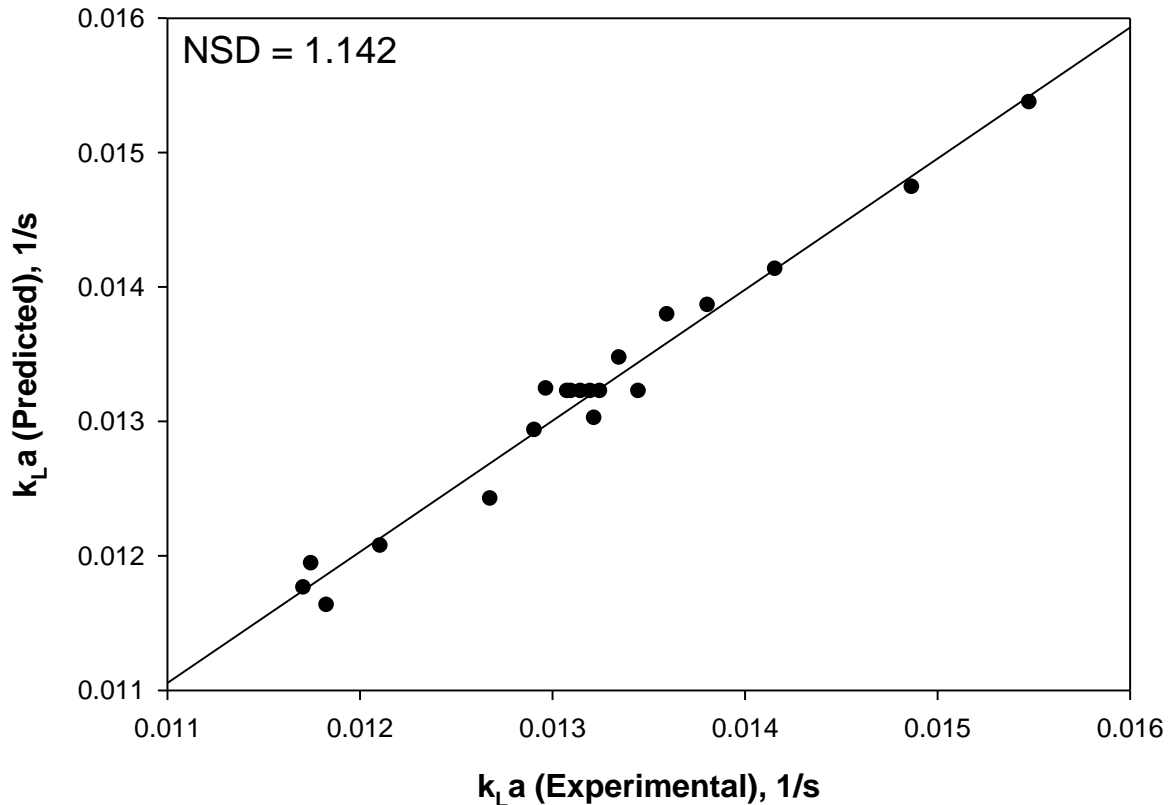


Figure 5.41 Plot of the measured and model predicted values of the response variable.

5.3.10 Effect of model components and their interactions on k_{La}

Response surface plots provide a method to predict the value of k_{La} for different values of the tested variables and the contours of the plots help in identification of the type of interactions between these variables (Montgomery 2001). Each surface and contour plots of the quadratic model represents an infinite number of combinations of two tested variables with the other two variables kept constant (here optimized value was taken). Response surface plots provide a method to predict the k_{La} for different values of the tested variables and the contours of the plots help in identification of the type of interactions between these variables. A circular contour of response surfaces indicates that the interaction between the corresponding variables is negligible. In contrast, an elliptical or saddle nature of the contour plots indicates that the interaction between the corresponding variables is significant. The response surface contour plots for the effect of each pair of variables are shown in Figures 5.42–5.44.

5.3.10.1 *Effect of gas flow rate and impeller speed on k_{LA}*

In Figure 5.42, the response surface and contour plots were developed as a function of agitator speed and gas flow rate while jet nozzle length were kept constant at 0.1 m. It can be seen from Figure 1, mass transfer coefficient increased with increase in impeller speed and reach up to 0.0164 s^{-1} . The presumed reason is that, at constant gas flow rate, the value of k_{LA} increased with increasing impeller speed due to sharp drop in bubble size which is favorable to gas–liquid mass transfer. As the air flow rate increases, the value of k_{LA} gradually increased until, at the highest gas load used, the overall effect of impeller speed becomes almost negligible. This positive effect of superficial gas velocity becomes slight due to the balance between the coalescence and breakup of the bubbles in the churn turbulent flow regime (Wilkinson et al., 1994).

5.3.10.2 *Effect of jet nozzle length and gas flow rate on k_{LA}*

In Figure 5.44, the response surface and contour plots were developed as a function of gas flow rate and jet nozzle length while the optimum impeller speed was kept constant at 400 rpm. As it clear from this figure, mass transfer coefficient reached to the highest value (0.164 s^{-1}) when nozzle length about 0.943 m. From the figure, at constant nozzle length and impeller speed, the value of k_{LA} was slightly increased with gas flow rate.

The presence of increased amounts of gas phase reduces the level of turbulence in the agitated fluid, by reducing the mechanical power dissipation through the growth of the gas cavities behind the turbine blades. Both the macro-scale and the micro-scale eddies are affected due to an increase in gas flow rate. However, it is the small eddies which are effective in breaking the bubbles whereas the large eddies are only responsible for their physical transport and distribution. It may be possible that the bubble coalescence becomes gradually more important as gas flow rate increases and this leads to higher rates of bubble collision and coalescence. At the lower gas flow rate, the cavities are of a vortex nature, whereas at the higher gas flow rate they were found to be of the clinging type.

5.3.10.3 *Effect of jet nozzle length and impeller speed on k_{LA}*

In Figure 5.43, the response surface and contour plots were developed as a function of impeller speed and jet nozzle length while optimum gas flow rate was kept constant at 22.5 L/min. It can be seen from Figure 2, the highest mass transfer coefficient (0.164 s^{-1}) occurred when nozzle with large length was kept at about 0.943 m under applied higher impeller speed (22.5 L/min).

It can be seen from Figure 5.43, at constant nozzle length, the value of k_{La} significantly increased with increasing impeller speed due to sharp fall in bubble size which is favorable to gas-liquid mass transfer. The position of jet nozzle length and distance between impeller edge and nozzle tip is shown in Figure 3.11. Each point in this figure represents the gap from impeller tip to nozzle hole over each 10 mm interval. From the Figure 3.11, in the region A and C, $5 \leq D_{I-N} \leq 8$, the distance from the blade become larger than 5 mm, the mass transfer coefficient was gradually decreases because of bubble size did not maintain its identity because of bubble coalescence taking place in radial direction. It has been also found that the value of k_{La} decreases more rapidly in the region between $4 \leq D_{I-N} \leq 5$ due to trapping some large bubbles with small and medium size bubbles in cavity present below the impeller. It is well know that the bubble size distribution is dramatic change in the hydrodynamic field around the impeller, resulting in a considerable increase in the bubble size. It was also reported that the distribution of bubble population depends on the position of the measurements and strongly depends on the associated hydrodynamic regime (Bouaifi and Roustan 1998).

In the radial direction, the bubble diameter rises towards the tank wall because of the increasing bubble population and gas hold-up which promote bubble collision and coalescence. Decreasing turbulence in the radial direction has also been lead to less bubble breakage. The effect of increasing the agitation speed is to shift the bubble distributions towards the lower end of the sparger, whereas an increase in gas flow rate has the opposite effect. Increasing the impeller speed causes a sharp drop in bubble size in the impeller tip region at low gas flow rates. At high gas flow rates, however, the effect becomes lower or insignificant, evidencing increased rates of bubble coalescence in results increase in bubble size.

The bubbles were characterized as small, medium and large size bubbles (Sujan and Vyas 2017). Visual observation confirmed that the population of small bubbles at impeller tip region (Region A) is much higher as compared to region B and C due to the high level of turbulence generated in this zone, which causes high rates of bubble breakage. The effect of agitator speed is to reduce the bubble size at this location under all conditions. Most of the investigators have reported that the bubbles size near to impeller region is less than 1 mm (Takahashi et al. 1992; Takahashi and Nienow 1993; Bouaifi and Roustan 1998). The small bubbles formed in the impeller region can be easily distributed throughout the vessel maintaining their initial sizes. At other positions (Region B and Region C), the fractions of medium size bubbles and large size bubbles are

considerably higher, indicating that high rates of bubble coalescence occur in the impeller discharge stream. The turbulence eddies with their shearing action act to reduce the bubble size on the front side of straight cylindrical rods act as a baffle. Furthermore, it has also been observed that the fraction of small size bubbles decreases near vessel wall region (Region C) compared to those in the impeller tip region (Region A). The values of k_{La} decreased with decreases in nozzle length indicate that higher coalescence rate takes place near the vessel wall region. In other words, the coalescence occurs not only near the vessel wall region but also takes place due to the difference in the rise velocities of bubbles, which significantly depend on bubble size. Large bubbles of high rise velocity catch up with small bubbles and they coalesce to form larger ones.

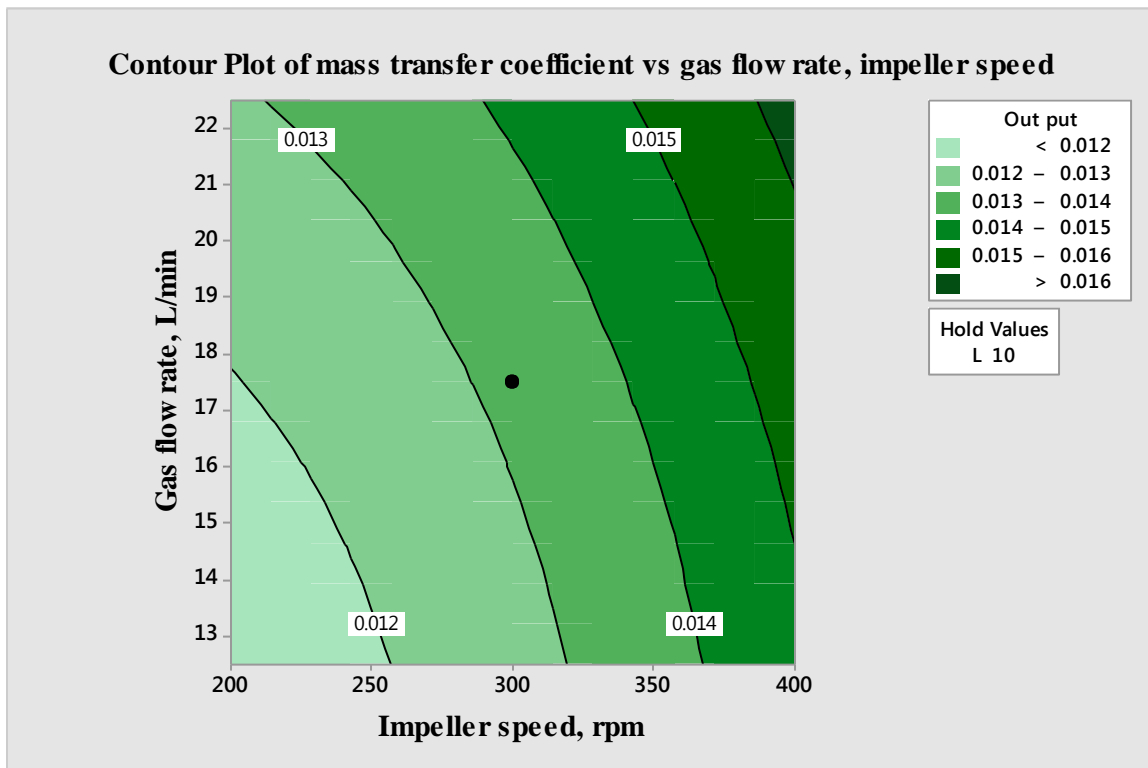
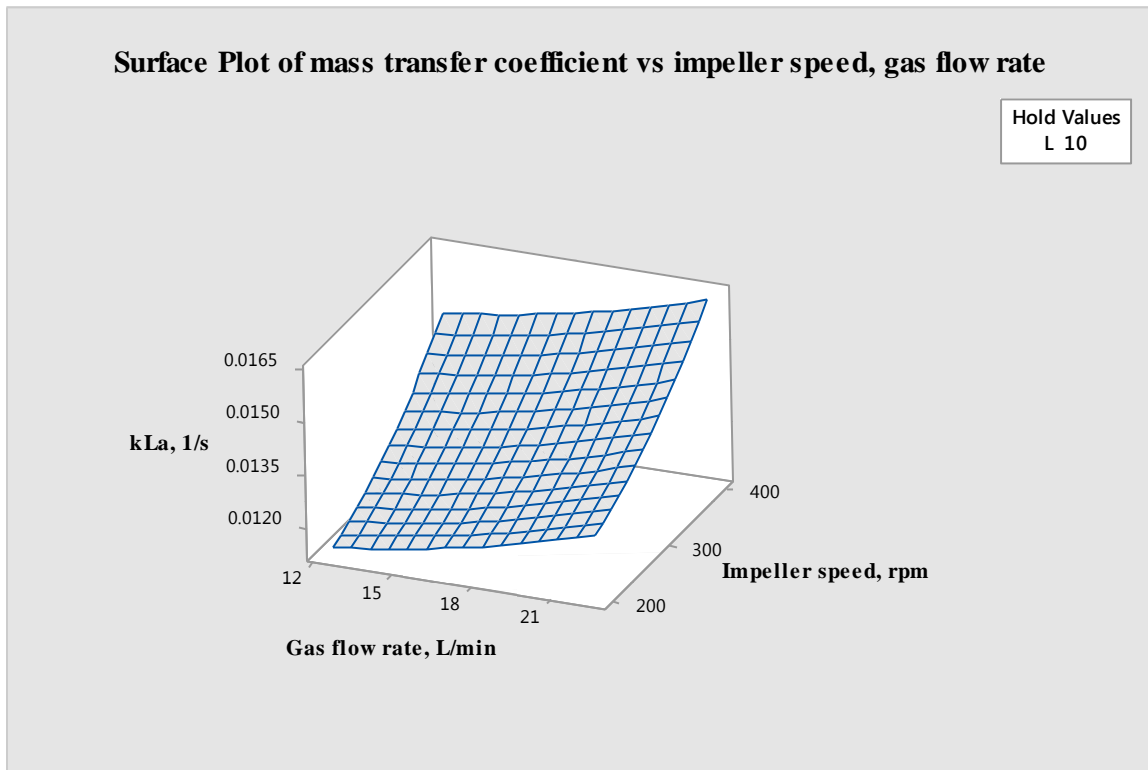


Figure 5.42 (a) response surface and (b) contour plots of k_{La} at optimized value as the function of gas flow rate (L/min) and impeller speed (rpm).

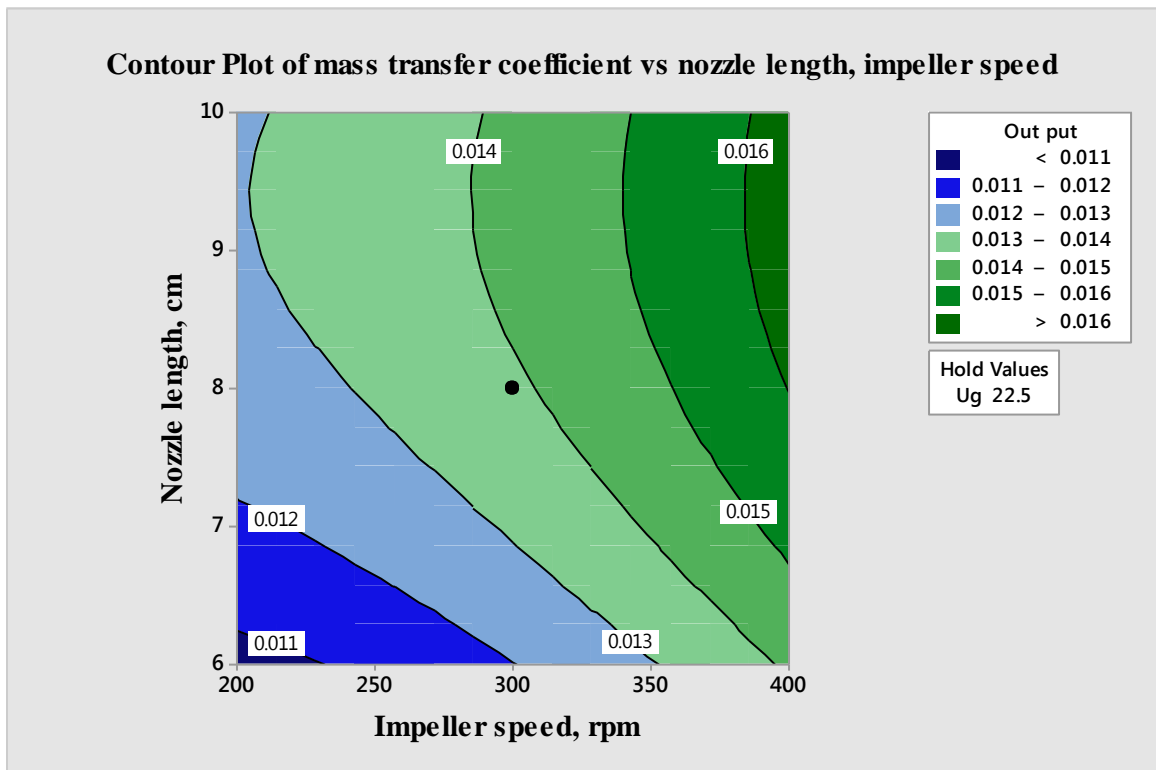
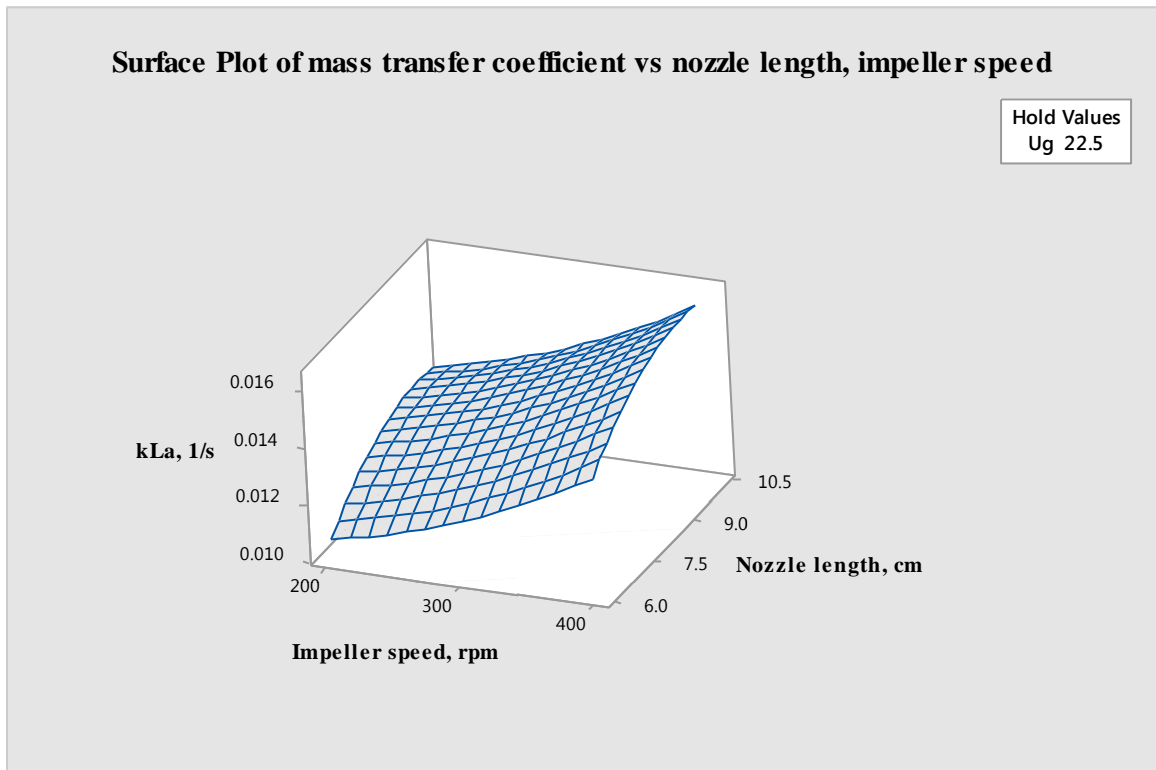


Figure 5.43 (a) response surface and (b) contour plots of k_{La} at optimized value as the function of impeller speed (rpm) and nozzle length (dimensionless)

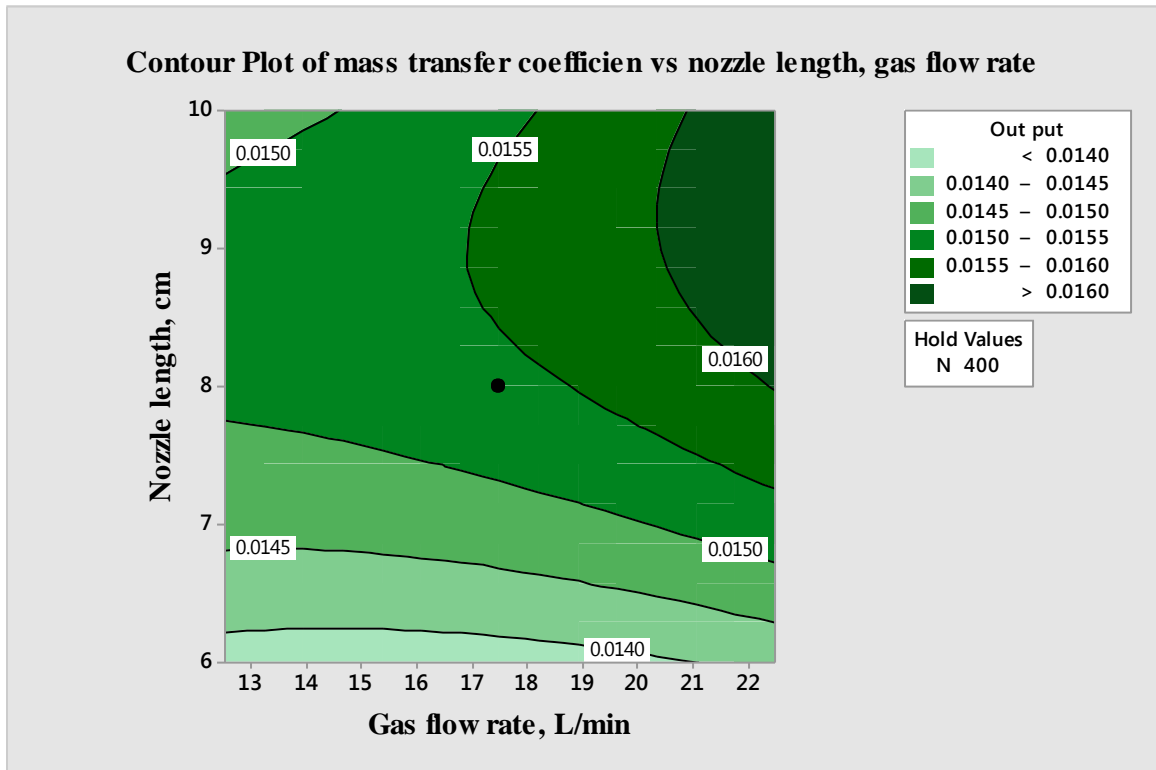
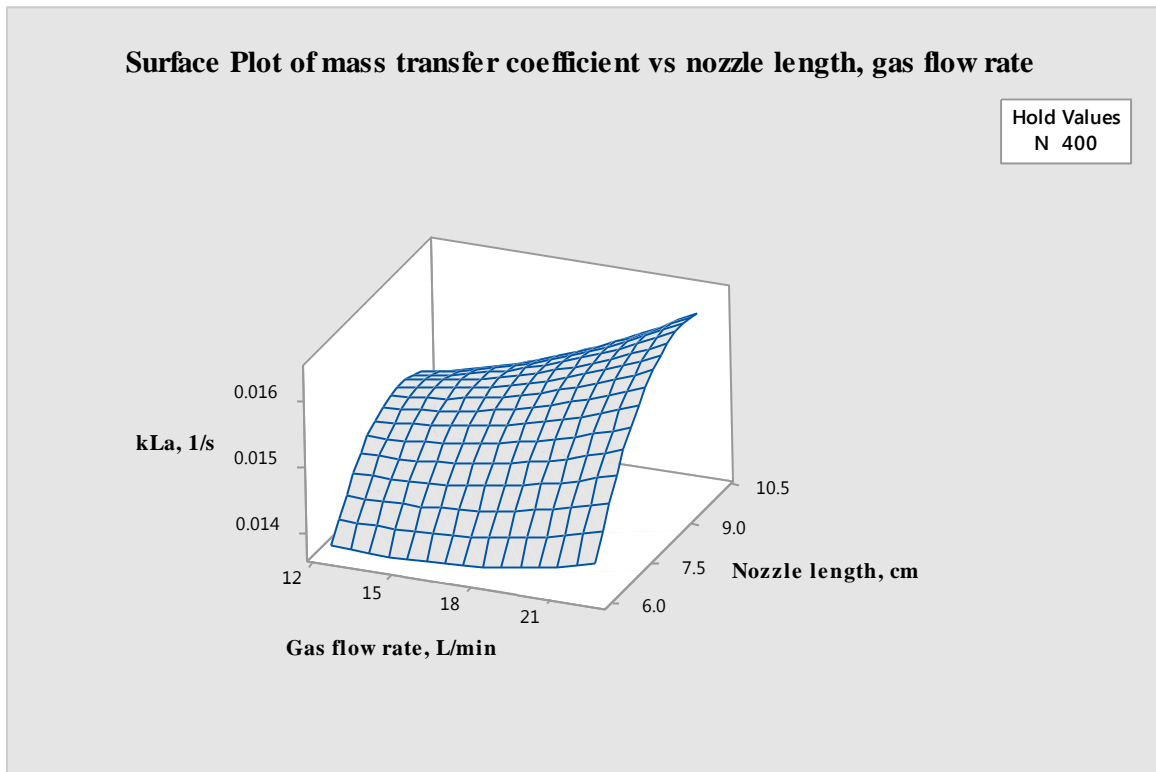


Figure 5.44 (a) response surface and (b) contour plots of k_{La} at optimized value as the function of gas flow rate (L/min) and nozzle length (dimensionless)

Section 5.4: Estimation of relative power demand in a partially baffled gas-liquid contactor equipped with single or multiple impeller combinations

5.4.1 Effect of single and multiple impeller on power consumption

Relative power demand (RPD) experiments were performed in a mechanically agitated system equipped with two cylindrical rod baffles. Single-, double- and triple- Rushton turbines (diameter $T/3$) on a common shaft were used. The bottom-impeller clearance was 0.26 m, while the inter-impeller clearance was equal to the diameter of the vessel. A sketch of arrangement of double and triple impeller configurations in the mechanically agitated system is shown in Figure 3.10. The power consumption drop was proportional to the amount of gas accumulated behind the impeller blades. In general, the power consumption P_g for the gas-liquid system depends on the type of impellers used, superficial gas velocity, agitator speed and the number of impellers installed on common shaft. Based on experimental points, the relative power consumption (RPD) was calculated for the air-water system.

Assuming the following relation

$$\frac{P_g}{P_{ug}} = f(Fl, Fr)$$

Where, Fl and Fr are the dimensionless gas flow and Froude numbers, respectively.

The correlation (equation 5.12 and equation 5.13) represents the relation suggested by Hughmark (1980) for correlating the gassed to ungassed power ratio rewritten for the data measured in a mechanically agitated system of constant geometry. Two empirical correlations were established using all impellers used in the present study. One empirical correlation valid for a single impeller (Rushton impeller, pitch blade, concave blade ($e = 0.441$) types used, predicts relative power demand (RPD) with a deviation of $\pm 10\%$. The measured and model predicted values of P_g / P_{ug} are for a single impeller agitated system is shown in Figure 5.45. Furthermore, an empirical correlation was developed for single and multiple impeller configuration systems (RT+RT, RT + RT + RT, CD6 + CD6 and CD6 + CD6 + CD6). Relative power demands (P_g / P_{ug}) for multiple impellers systems were found to be within a variation of 10% with the experiments data. The measured and model predicted values of P_g / P_{ug} for single and multiple impeller agitated systems are is shown in Figure 5.46. Three different flow patterns were observed using flow

visualization. The distance between the upper impeller and free surface of liquid becomes more turbulent due to the relative small distance are also responsible for the notable changes in power consumption. Upper impeller was not able to divert gas bubbles in radial or downward direction because of increases in central gas plume with rotating action of the upper impellers. For the middle impeller system, the two impeller streams were directed towards each other, merging together half-way between the impellers and become unstable, changing from one pattern to the other with time. In lower impeller, impeller divert gas bubbles in the radial or in the vertically downwards direction and gas bubbles get well dispersed in the region below each of the impeller.

Empirical correlation for relative power demand

(a) Single impeller system

$$\frac{P_g}{P_{ug}} = 0.163 \left(\frac{Q}{NV_L} \right)^{-0.215} \left(\frac{d_i^4 N^2}{gwV_L^{2/3}} \right)^{-0.238} \quad \dots(5.12)$$

Valid range: $2.50 \leq N(\text{rps}) \leq 6.67$, $0.000125 \leq Q(\text{m}^3/\text{s}) \leq 0.000417$

$V_L(\text{m}^3) = 0.0265$, $d_i(\text{m}) = 0.14$

(b) Single and multiple impeller system

$$\frac{P_g}{P_{ug}} = 0.209 \left(\frac{Q}{NV_L} \right)^{-0.203} \left(\frac{d_i^4 N^2}{gwV_L^{2/3}} \right)^{-0.180} (N_b)^{0.0024} \quad \dots(5.13)$$

Valid range: $2.50 \leq N(\text{rps}) \leq 6.67$, $0.000125 \leq Q(\text{m}^3/\text{s}) \leq 0.000417$

$V_L(\text{m}^3) = 0.0265$, $d_i(\text{m}) = 0.14$

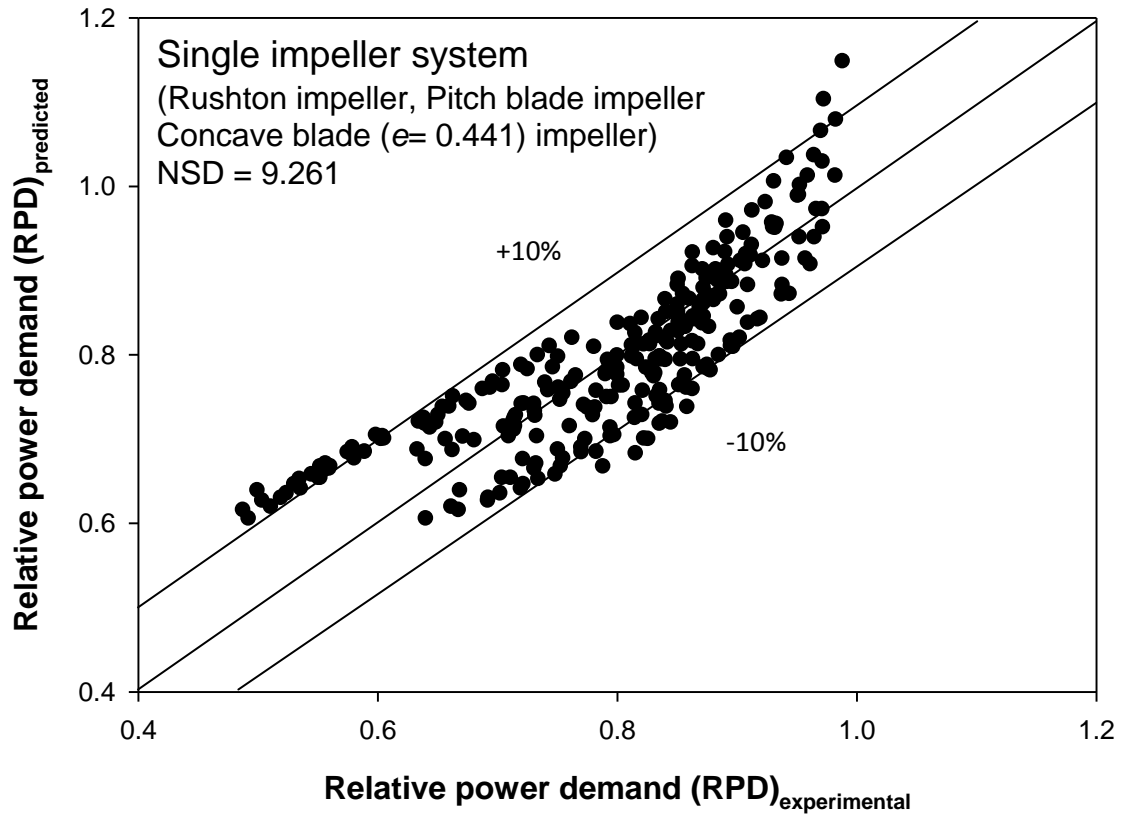


Figure 5.45 Comparison of predicted relative power demand from correlation and the experimental values for single impeller system.

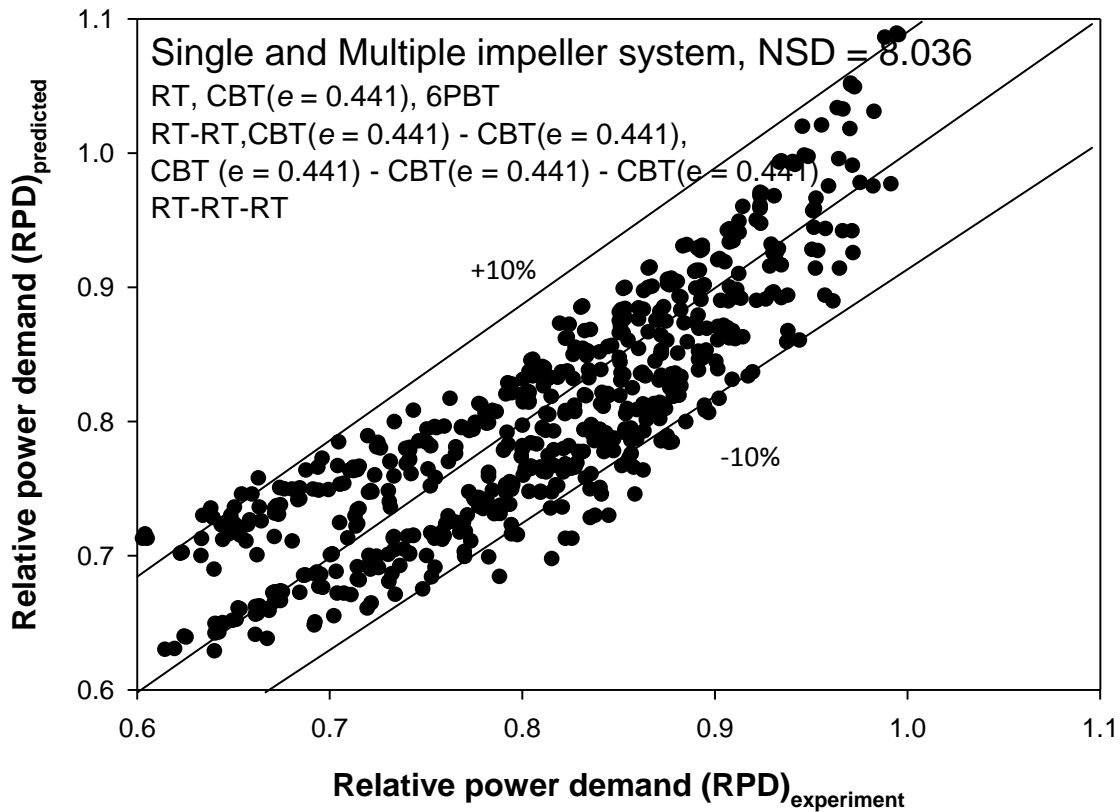


Figure 5.46 Comparison of predicted relative power demand from correlation and the experimental values for different single and multiple impeller systems.

5.4.2 Effect of impeller spacing on power consumption

The effect of impeller spacing (ΔS) on power consumption was measured in unaerated and aerated conditions for low viscosity systems agitated by double-stage Rushton impeller and compared with data reported in literature for stirrer speeds between 250 and 400 rpm. Figure 5.47a–5.47e represents the effect of inter-impeller spacing on the power number N_p at different gas flow rates and agitator speeds. For a case of $\Delta S/d \leq 0.82$, at 12.5 L/m gas flow rate, the two impellers are quite close to each other, a more or less constant value of the power number for the double impeller configuration was found and it was assumed to operate like a single Rushton impeller. But power number increases with increase in the agitator speed. At small gas flow rates, the gas is mainly dispersed by the lower impeller and thus the power consumption is

greater than that of higher aeration rates, where gas dispersion also occurs by the action of the upper impeller. In the range of $0.82 \leq \Delta S/d \leq 0.96$, at 12.5 lpm gas flow rate, the power consumption instantly increased due to the large liquid circulation by the two impellers, and it maintained more or less constant value up to an impeller spacing of 1.54 d. In this situation, both impellers act independently and the power consumption of the dual Rushton impeller system is approximately 53% higher of the impeller power at below the critical value of $\Delta S/d$. The power consumption of the system decreases from 53 to 16 % with increasing agitator speeds due to the trapping of more air bubble below the impeller. The result shows that a considerable amount of the total power dissipated is connected with the vortices below the impeller. When the gas passing through the sparger, the vortices formation below the upper impeller showed that the lower volume fraction of gas utilizes as compared to lower impeller. The different flow pattern, turbulence intensity and number of vortices present behind the Rushton impellers at different impeller spacing is shown in Table 5.16. Finally, their experimental results reveal that the power consumption in aerated systems is strongly dependent on the impeller spacing $\Delta S/d$. When the distance between the impellers becomes greater than $\Delta S/d \geq 1.54$, the zone between the impellers becomes more turbulent due to the relative small distance of the upper turbine from the liquid surface in the vessel. This is also the reason for the notable decrease in power consumption, which was always measured at larger impeller spacings.

The flow patterns in agitated systems resulting from a combination of impellers can be quite complex and may affect the power numbers obtained significantly. Three different flow patterns were observed using flow visualization. The flow patterns between two Rushton impellers were nearly horizontal and parallel when the inter-impeller spacing ($\Delta S = 21.5$ cm) was large. The mutual influence of the two impellers was weak and each impeller produced two vortices making a total of four stable vortices in this regime. The flow behavior in this regime showed that each impeller acted independently. The total power was approximately equal to the sum of the power inputs to each individual impeller. The regime between the upper impeller and the free surface of the liquid became more turbulent due to the relative small distance which is also responsible for the notable decrease in power consumption. Similar flow behavior was observed for inter-impeller spacing up to 15.5 cm. In the range of $\Delta S = 11.5$ to 13.5 cm, the two impeller streams were directed towards each other, merging together half-way between the impellers. For intermediate spacings the flow was unstable, changing from one pattern to the other with time.

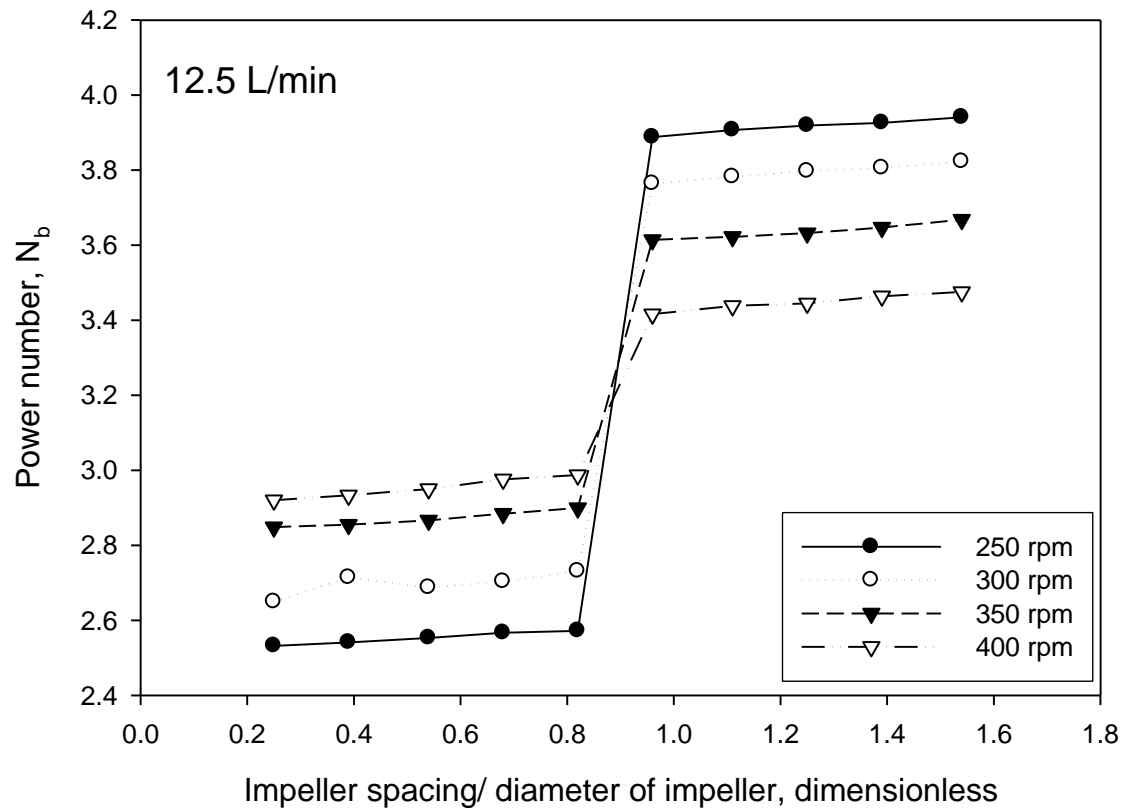
In the range $\Delta S = 5.5$ to 9.5 cm, the interaction between the two impellers became stronger. Two large vortices appeared in the whole flow field and impeller streams together completely. At $\Delta S = 3.5$ cm, the impeller stream similar to a single Rushton impeller and stronger influence with two vortices was observed. The power numbers measured for different inter-impeller spacing are given below:

Table 5.16 Power number at $\Delta S/d \geq 0.82$ for Rushton impeller system

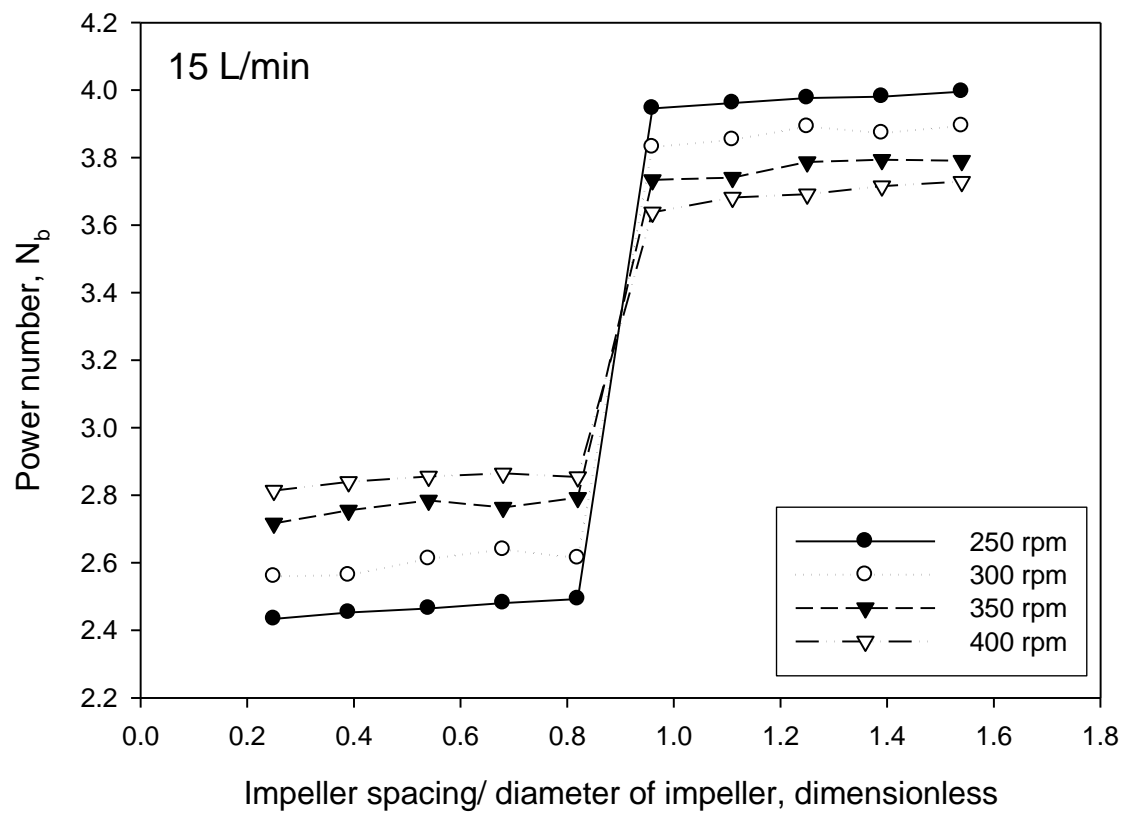
rpm	Power number at $\Delta S/d \geq 0.82$				
	12.5 L/m	15 L/m	17.5 L/m	20 L/m	22.5 L/m
250	1.53	1.61	1.63	1.77	1.83
275	1.47	1.55	1.58	1.69	1.77
300	1.41	1.48	1.54	1.62	1.73
325	1.35	1.43	1.49	1.55	1.66
350	1.26	1.36	1.46	1.50	1.54
375	1.21	1.31	1.39	1.44	1.52
400	1.16	1.29	1.34	1.38	1.44

From the Table 5.16 it is clear that at a constant gas flow rate (12.5 L/m), the power number decreases from a value of 53 to 16% with increase in impeller speeds from 250 to 400 rpm. The change in power number with $\Delta S/d$ has important guess for mixing operations as the power input to the vessel with the change from double- to single loop patterns. All five figures 5.47a –5.47e indicate that the power number decreases with increase in agitator speed from 250 to 400 rpm for all gas flow rates. The experimental results showed that the higher impeller speeds with lower gas flow rate is suitable for mixing operation because of significant reduction in power number. An empirical correlation for relative power demand with dimensionless groups, i.e. gas flow number, Froude number, the ratio of $\Delta S/d$ has been developed; however, this correlation also fits the electrolyte solutions because surface tension has insignificant effect on power demand for low viscosity system. A plot of predicted ratio of P_g / P_{ug} vs experimental P_g / P_{ug} was found to be within an error limit $\pm 10\%$. The measured and model predicted values of P_g / P_{ug} are shown in Figure 5.48

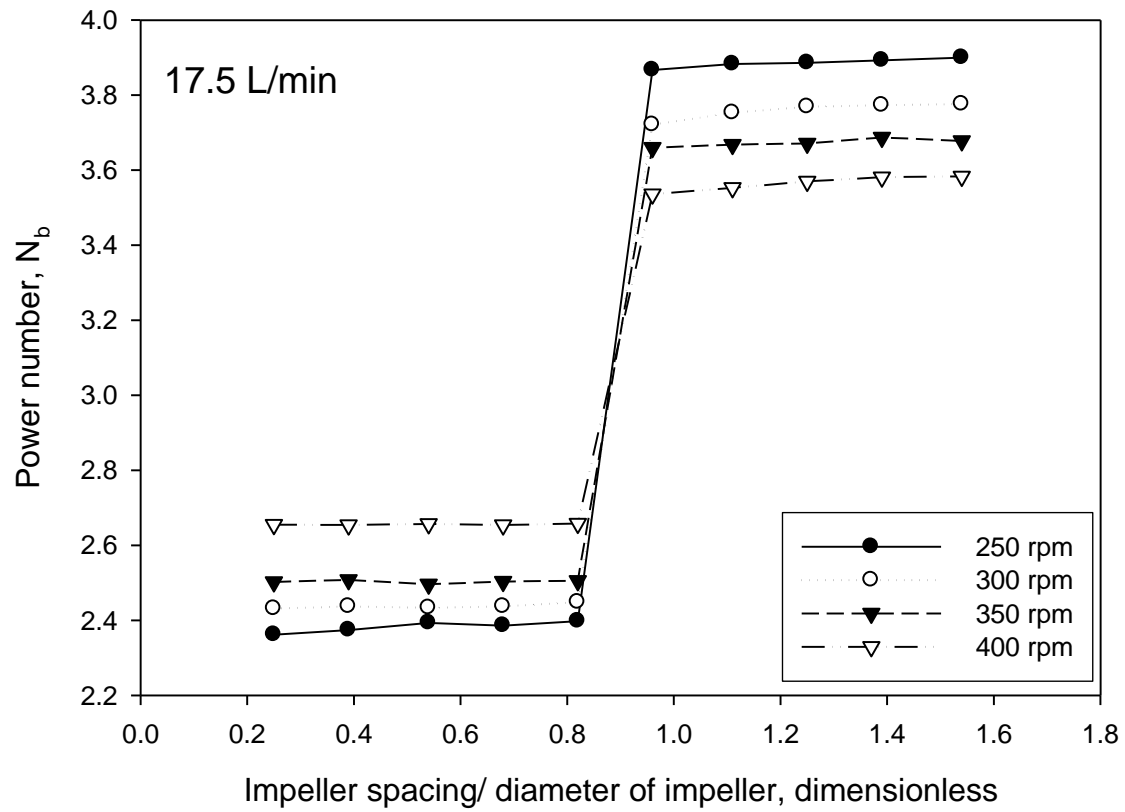
$$\frac{P_g}{P_{ug}} = 0.356 \left(\frac{Q}{NV_L} \right)^{-0.15} \left(\frac{d_i^4 N^2}{g_w V_L^{2/3}} \right)^{0.141} \left(\frac{\Delta S}{d} \right)^{-0.010} \quad \dots(5.14)$$



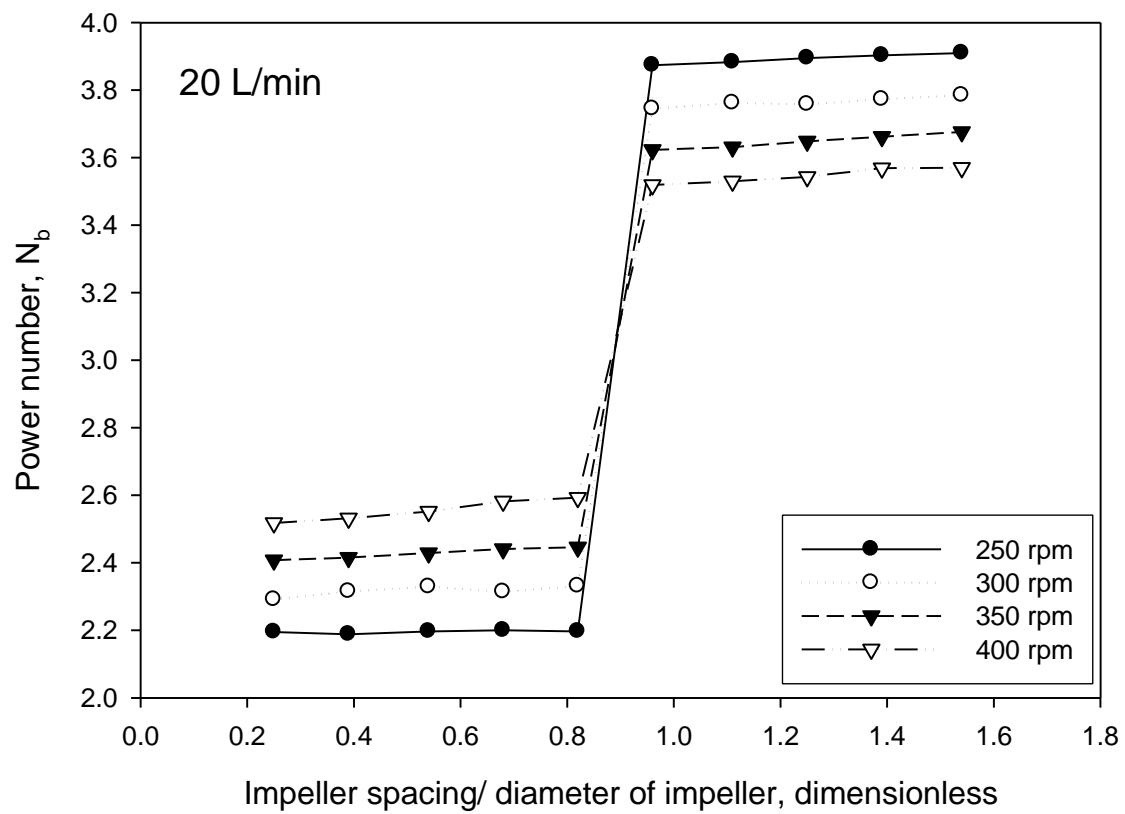
(a)



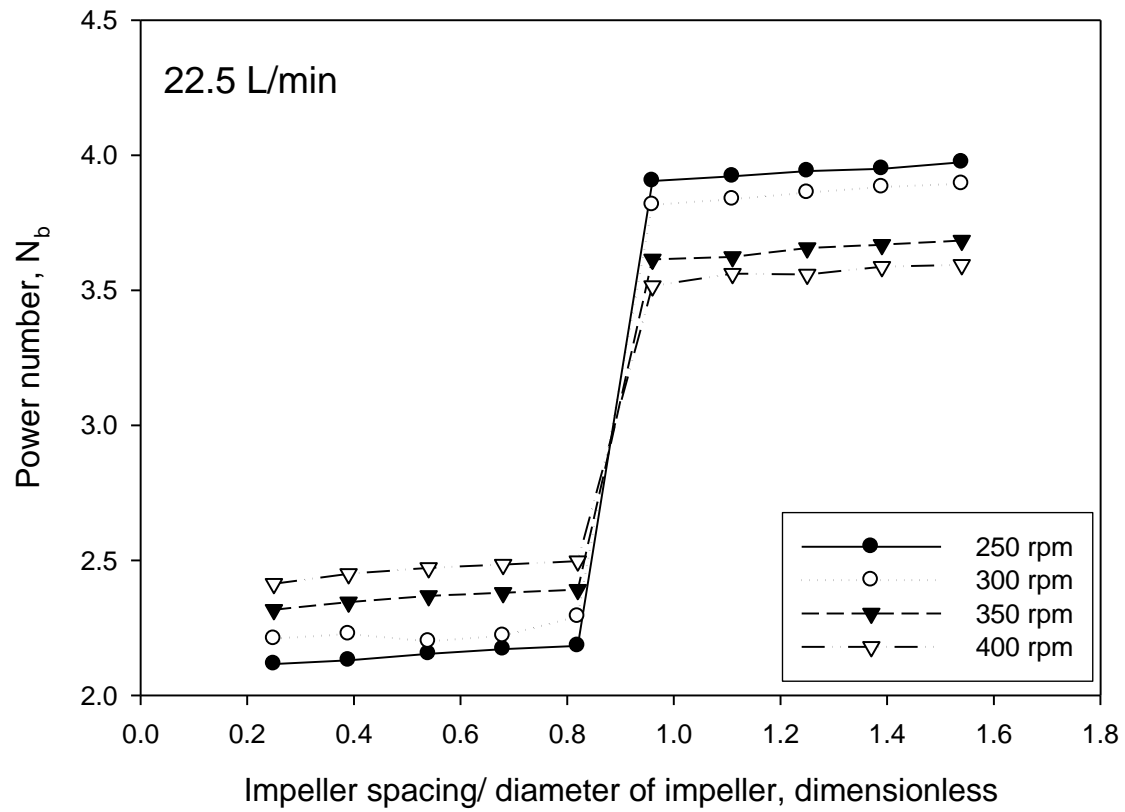
(b)



(c)



(d)



(e)

Figure 5.47 Effect of inter-impeller spacing on the power number N_p at (a) 12.5 L/min (b) 15 L/min (c) 17.5 L/min (d) 20 L/min (e) 22.5 L/min gas flow rate.

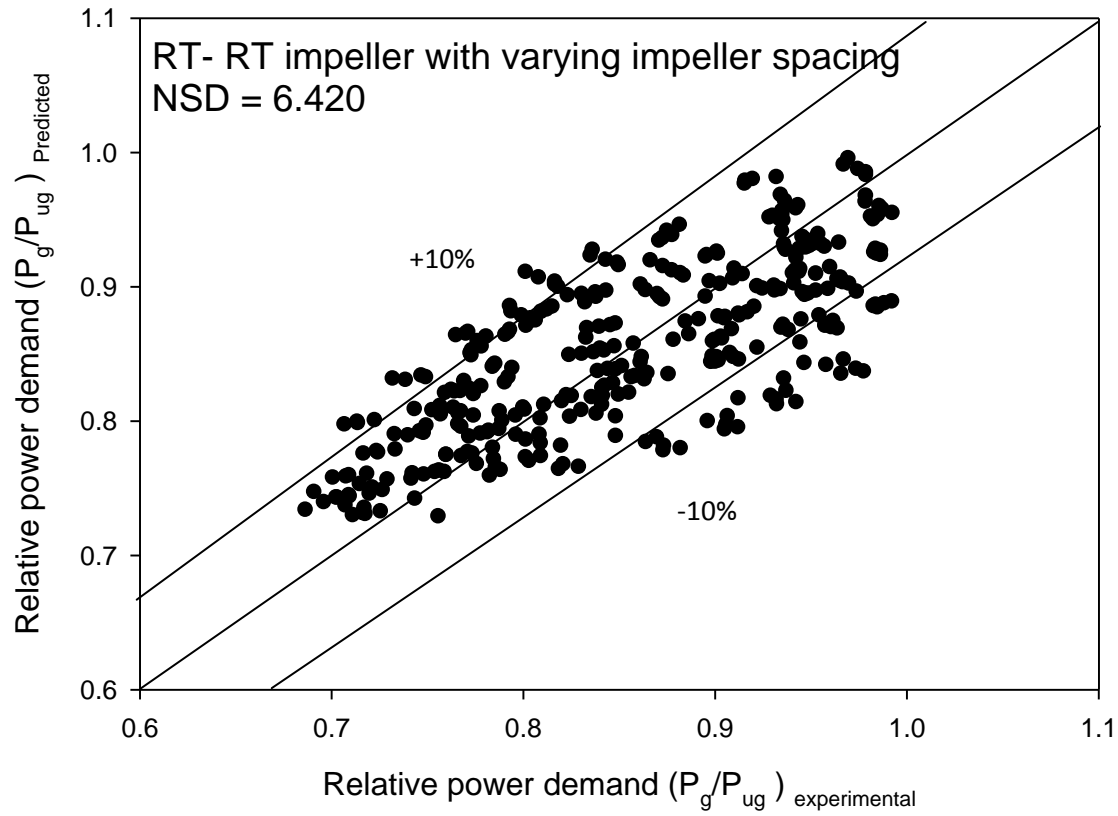


Figure 5.48 Predicted vs. experimental values of (P_g/P_{ug}) for multiple impeller system (RT–RT).

6 Conclusions

In this work, a mathematical model was established for gas-liquid/ slurry system considering surface age distribution function for a spherical bubble. The model predictions are applicable to a wide range of operating conditions for slurries with solid particles of inert surface characteristics. Using experimental data from the literature, the influence of temperature (298–423 K), pressure (1–3 MPa), superficial gas velocity (0.026–0.053 m/s) and solid concentration percent by volume (0–20%) on k_L were analyzed. The results show that the mass transfer coefficient k_L increased with increasing superficial gas velocity and temperature and decreased with increase in slurry concentration, while it changed slightly with pressure. It is clear from the simulated results that lower value of δ yields higher value of mass transfer coefficient which is supported by theory of mass transfer. Furthermore, new empirical correlations for estimation of liquid film thickness δ for H₂–, CO – and CO₂– slurry (liquid paraffin-quartz sand) systems have been developed. The predictions from the developed correlations for δ for different gas – slurry systems are fairly accurate for the applicable range which is evident from the good match of predicted and experimental values of k_L . The proposed macroscopic mathematical model is able to predict the overall k_L in a two– or three–phase bubble column system, if bubble size distribution is known. The validity of model for liquid as well as slurry systems was verified for liquid paraffin with a solid concentration range of 0 – 20%. Slurry bubble column may consist of different gases, liquid and various types of solid particles; hence, studies need to be conducted for different systems and interaction of bubbles may also be incorporated, if needed.

In the second part of the present work, study of coalescence inhibition was targetted by applying gas holdup enhancement and surface tension gradient approaches for aqueous solutions of single and binary mixtures of electrolytes. The concentration at which bubble coalescence is inhibited was determined in a 3.0 L distilled water bubble column for a series of coalescence inhibiting inorganic electrolytes (NaCl, MgSO₄.7H₂O, CaCl₂.2H₂O, and Na₂SO₄). For a single electrolyte system, maximum gas holdup (ϵ / ϵ_w) enhancement for a strong electrolyte (CaCl₂) reached a maxima of 69% at a concentration of 0.075 mol/L and at a gas flow rate of 27.5 L/m. Similar behavior was observed with 61% gas holdup enhancement in Na₂SO₄ solution corresponding to a concentration of 0.05 mol/L. In case of moderate electrolytes (NaCl), 47% gas holdup

enhancement was observed at a concentration of 0.05 mol/L. A similar trend with 38% gas holdup enhancement was found in MgSO₄ solution at a concentration of 0.035 mol/L. A qualitative comparison of these electrolytes revealed that strong electrolytes yield gas holdup enhancement $\geq 60\%$ whereas moderate electrolytes give a gas holdup up enhancement values $\leq 46\%$. It has also been found that the values of transition concentration for different electrolytes are of the same order in most of the cases and are in line with those reported in literature. In case of strong electrolytes solution, higher peak is indicative of strong effect on bubble coalescence. In case of moderate electrolytes solution, peak with shorter height is indicative of moderate effect on bubble coalescence.

In addition, the effect of electrolytes on bubble coalescence was studied using the parameter $C(d\sigma/dC)^2$ for all the electrolytes used in the study. It was verified that, as long as the value of parameter $C(d\sigma/dC)^2$ is large, the electrolyte will inhibit bubble coalescence, and if it is small, bubble coalescence will remain moderate. The importance of parameter $(d\sigma/dC)^2$ in bubble coalescence has been related to the surface elasticity of the interface of electrolyte film drainage. The drainage rate of film reduced because the duration of stability of film thickness increases due to change in elasticity of an interface surface. The variation in surface tension with the addition of electrolytes can be directly used to predict gas holdup enhancement. It can also be used for identification of electrolyte concentration for attaining highest gas holdup.

Furthermore, the effect of mixed electrolytes (CaCl₂.2H₂O + NaCl and Na₂SO₄+ NaCl) on gas holdup was also studied. From the experimental results, it was found that trends of gas holdup enhancement for single (individual) and mixed electrolytes are similar. It has been observed that the value of transition concentration shifted from 0.075 to 0.1 mol/L in mixed electrolytes (CaCl₂+ NaCl) system whereas transition concentration shifted from 0.05 to 0.075 mol/L for mixed electrolyte (Na₂SO₄ + NaCl) system as compared to their components viz. CaCl₂ and Na₂SO₄ respectively.

Besides, parameter $C(d\sigma/dC)^2$ was also plotted against the total concentration of the two sets of mixtures of electrolytes. It can be observed that there is no shift in transition concentration for CaCl₂.2H₂O + NaCl mixed electrolyte system whereas transition concentration shifted from 0.05 to 0.1 mol/L for Na₂SO₄ + NaCl mixed electrolytes system. In addition, surface elasticity of bubbles is related to bubble coalescence inhibition. Large value of parameter $(d\sigma/dC)^2$ inhibit

bubble coalescence and its value depends upon ion separation in the interfacial area. Reduction in surface elasticity will result in decrease in bubble coalescence inhibition phenomena. The value of surface elasticity of combination of mixed electrolytes ($\text{CaCl}_2 + \text{NaCl}$) decreased due to reduction in surface elasticity from a single component (CaCl_2) is due to the addition of a moderate electrolyte (NaCl) whose contribution to surface elasticity value is small as compared to the strong one (CaCl_2). Similar observation was found in aqueous solution of $\text{Na}_2\text{SO}_4 + \text{NaCl}$ system. Surface elasticity values estimated in the present work could not be compared with those reported in literature (Craig 2011 and Henry et al. 2007) as values reported earlier were not estimated at critical coalescence concentration. The density difference between the electrolytes used in the present study are not significant, therefore, the variation in the densities of their aqueous solutions will also not be considerable. Thus, difference in buoyant forces exerted by aqueous solutions of different electrolytes will be negligible regardless of the bubble size at atmospheric pressure. Furthermore, Analysis of variance (ANOVA) was employed to estimate significance of parameters (gas flow rate, electrolyte concentration and chemical nature of electrolyte) on average gas holdup. It was found that that all the parameters have significant effect on average gas holdup.

In the third part of the study on volumetric mass transfer coefficient, it was found that under the same gas flow rate (22.5 L/min) conditions, the impeller with more blades always disperses gas more effectively, which results in a higher value of $k_L a$. Bubble population and bubble size have a significant impact on volumetric gas-liquid mass transfer coefficient in Newtonian liquids. It was visually observed that concentric dual ring sparger produces more bubbles as compared to 4-jet nozzles. It was also found that highest mass transfer coefficient occurs for a given impeller speed at a certain blade curvature due to the cavity formed behind the blade becomes smaller with an increase in the blade curvature. Due to different blade curvatures and rotating speeds, the size of cavities formed behinds the impeller blade significantly affect the bubble size passing through the impeller which is responsible for higher mass transfer coefficient. A full factorial statistical approach was testified to be a powerful tool in aeration process system due to its impact on the economy and practicability of the process. The statistical analysis results suggested that the effects of all the four independent variables, viz. gas flow rate, impeller speed, jet nozzle length, and curvature of blade were found to be more significant than their respective quadratic effects. All interactions of parameters were found to be statistically insignificant. An empirical correlation for volumetric mass transfer coefficient using dimensionless groups, based on Froude

number, impeller Weber number, impeller Reynolds number, Curvature of blade, and the ratio of L_N/d was developed. Predicted values of $k_L a$ were found to be within a variation of 10% with experiments. It has been also observed that reduction in distance between jet nozzle and impeller blade edge significantly affects the bubble size discharged from the impeller which is responsible for higher mass transfer coefficient.

In the fourth part of this study, the dependence of power consumption on impeller spacing in unaerated and aerated gas-liquid systems agitated by a dual Rushton turbine system was studied. The power consumption in aerated systems was found to be strongly dependent on the inter-impeller spacing $\Delta S/d$. A gradual increase in the power number can be detected up to an impeller spacing of $1.54d$. For spacings greater than $(\Delta S/d)_{\text{critical}}$, the two impellers act independently, and the power consumption is approximately twice that of the single impeller. In aerated systems, a remarkable increase in the power consumption was observed in the range of $0.82 < \Delta S/d < 0.96$ because of large recirculation flows (vortices) above and below the impeller at a constant gas flow rate with different stirred speeds. It was also found that the gassed/ungassed power ratio P_g/P of the double impeller system was higher than that of the single Rushton turbine. In the range, $0.96 \leq \Delta S/d \leq 1.54$, two impellers act independently and the power consumption of the dual Rushton turbine system was found approximately one and half of the single impeller power at lower impeller speeds. For, $\Delta S/d \leq 0.82$, when the two impellers were close to each other, the lower recirculation flow (vortices) was found absent or weakly present. In that situation both the impellers together are considered to operate like a single Rushton impeller. When the distance between the impellers becomes greater than $\Delta S/d \geq 1.54$, the zone between the impellers becomes more turbulent. At small gas flow rates, the gas is mainly dispersed by the lower impeller and thus the power consumption is greater as compared to higher aeration rates, where gas dispersion also occurs by the action of the upper impeller. The results show that a considerable amount of the total power dissipated is connected with the vortices below the impeller. Two empirical correlations were developed using all the impellers used in this study. One empirical correlation, valid for single impeller (Rushton impeller, concave blade ($e = 0.441$) or pitch blade impeller) predicts relative power demand (RPD) with a deviation of $\pm 15\%$. Furthermore, an empirical correlation was developed for single and multiple impeller configurations (RT+RT, CD6 + CD6, RT + RT + RT, and CD6 + CD6 + CD6). Relative power demand (P_g / P_{ug}) for multiple impellers system estimate using the developed correlation was found to be within a variation of 10% with experiments.

Recommendation for future work

In a bubble column, there are many areas in which the hydrodynamics, mass transfer characteristics and bubble behavior are yet to be clearly understood because of the complex flow characteristics of bubbles in bubble columns. Studies need to be conducted to investigate other aspects. A few aspects of bubble column research that may be taken up for further study under different heads are presented below.

1. Most of the research work carried out in bubble columns are due to its advantageous properties. Yet, inadequate data are available for tapered bubble columns, square shape bubble columns, rectangular bubble columns, Co-current and counter current bubble columns. Such systems should be evaluated in more detail. Furthermore, a comparative study on the performance of various types of columns is needed to systematically explore a bubble column.
2. Gas holdups in nano-fluids have been scarcely reported in literature. A study on hydrodynamics and mass transfer in a bubble column using nano fluids may be carried out.
3. Only a limited number of studies are available on effects of various internals on bubble column hydrodynamics in Newtonian systems. It should be explored systematically.
4. Practically no data are available covering effects of various shapes of floatable materials on gas holdup. Such a study can be useful providing insight to effects of various types of solids on bubble column hydrodynamics.
5. A set of research articles with different gas-liquid or gas-liquid-solids system are available. Using wide range of reported data of physical properties, operating conditions and column and sparger geometry, new empirical correlations valid for a wide range of system parameters can be developed using artificial neural network or support vector analysis techniques.
6. The effect of a single electrolyte on gas holdup has been reported in literature. In the present work binary electrolytes were also studied. There is still a scope for further studies on binary electrolytes systems in a bubble column.

7. Gas–liquid–fiber (GLF) bubble columns have attracted recent interests, where flexible fibers consider as a solid phase. Gas–liquid–fiber systems are found in the pulp and paper industry in many unit operations. Gas flow behavior in Gas–liquid–fiber (GLF) bubble columns is very complex because the fibers are flexible with a large aspect ratio and result in complex fiber suspension rheology. Further studies are needed to explain the effect of mass fraction of fiber on gas holdup in Gas–liquid–fiber (GLF) bubble columns system.
8. Based on literature review and published work, it is evident that studies on the effect of curvature of curved blades and diameter of disk impellers on mass transfer coefficient and relative power demand (RPD) are very limited. Such a study can be taken up.
9. The effect of angled and lancet profiles blade on mass transfer coefficient and relative power demand (RPD) are scarcely reported in literature. A suitable study may be useful.

Reference

- Abate, J., & Whitt, W. (2006). A unified framework for numerically inverting Laplace transforms. *INFORMS Journal on Computing*, 18(4), 408-421.
- Akita, K., and Yoshida, F. (1973). Gas holdup and volumetric mass transfer coefficient in bubble columns. Effects of liquid properties. *Industrial and Engineering Chemistry Process Design and Development*, 12 (1), 76-80.
- Al Taweel A.M., Idhbeaa, A.O., Ghanem, A. (2013). Effect of electrolytes on interphase mass transfer in microbubble-sparged airlift reactors. *Chemical Engineering Science*, 100, 474–485.
- Aleboye, A., Daneshvar, N., & Kasiri, M. B. (2008). Optimization of CI Acid Red 14 azo dye removal by electrocoagulation batch process with response surface methodology. *Chemical Engineering and Processing: Process Intensification*, 47(5), 827-832.
- Aleboye, A., Daneshvar, N., Kasiri, M. B. (2008). Optimization of CI Acid Red 14 azo dye removal by electrocoagulation batch process with response surface methodology. *Chemical Engineering and Processing: Process Intensification*, 47(5), 827-832.
- Alim, M. A., Lee, J. H., Akoh, C. C., Choi, M. S., Jeon, M. S., Shin, J. A., & Lee, K. T. (2008). Enzymatic transesterification of fractionated rice bran oil with conjugated linoleic acid: Optimization by response surface methodology. *LWT-Food Science and Technology*, 41(5), 764-770.
- Anastasiou, A. D., Passos, A. D., Mouza, A. A. (2013). Bubble columns with fine pore sparger and non-Newtonian liquid phase: prediction of gas holdup. *Chemical Engineering Science*, 98, 331-338.
- Arjunwadkar, S. J., Saravanan, K., Pandit, A. B., Kulkarni, P. R. (1998). Optimizing the impeller combination for maximum hold-up with minimum power consumption. *Biochemical engineering journal*, 1 (1), 25-30.
- Armenante, P. M., Chang, G. M. (1998). Power consumption in agitated vessels provided with multiple-disk turbines. *Industrial and engineering chemistry research*, 37 (1), 284-291.
- Babalona, E., Babalona, D., Tagia, S., Pantouflas, E., Markopoulos, J. (2005). Power Consumption in Dual Impeller Gas–Liquid Contactors: Inter–impeller clearance, Gas Flow Rate, and Viscosity Effects. *Chemical engineering & technology*, 28(7), 802-807.
- Bach, H.F., Pilhofer, T. (1978). Variation of gas hold-up in bubble columns with physical properties of liquids and operating parameters of columns. *Ger. Chem. Eng*, 1, 270-275.

Beenackers, A. A. C. M., Van Swaaij, W. P. M. (1993). Mass transfer in gas—liquid slurry reactors. *Chemical Engineering Science*, 48(18), 3109-3139.

Behkish, A., Lemoine, R., Sehabiague, L., Oukaci, R., Morsi, B. I. (2007). Gas holdup and bubble size behavior in a large-scale slurry bubble column reactor operating with an organic liquid under elevated pressures and temperatures. *Chemical Engineering Journal*, 128(2-3), 69-84.

Besagni, G., Di Pasquali, A., Gallazzini, L., Gottardi, E., Colombo, L.P.M., Inzoli, F. (2017). The effect of aspect ratio in counter-current gas-liquid bubble columns: Experimental results and gas holdup correlations. *International Journal of Multiphase Flow*, 94, 53-78.

Besagni, G., Gallazzini, L., Inzoli, F. (2018). Effect of gas sparger design on bubble column hydrodynamics using pure and binary liquid phases. *Chemical Engineering Science*, 176, 116-126.

Besagni, G., Inzoli, F., De Guido, G., Pellegrini, L.A. (2017). The dual effect of viscosity on bubble column hydrodynamics. *Chemical Engineering Science*, 158, 509-538.

Besagni, G., Inzoli, F. (2017). The effect of electrolyte concentration on counter-current gas-liquid bubble column fluid dynamics: gas holdup, flow regime transition and bubble size distributions. *Chemical Engineering Research and Design* 118, 170–193.

Besagni, G., Inzoli, F. (2017). The effect of liquid phase properties on bubble column fluid dynamics: Gas holdup, flow regime transition, bubble size distributions and shapes, interfacial areas and foaming phenomena. *Chemical Engineering Science*. 170, 270-296.

Bouaifi, M., Hebrard, G., Bastoul, D., Roustan, M. (2001). A comparative study of gas hold-up, bubble size, interfacial area and mass transfer coefficients in stirred gas–liquid reactors and bubble columns. *Chemical Engineering and Processing: Process Intensification*, 40 (2), 97-111.

Bouaifi, M., Roustan, M. (1998). Bubble size and mass transfer coefficients in dual-impeller agitated reactors. *The Canadian Journal of Chemical Engineering*, 76(3), 390-397.

Bouaifi, M., Roustan, M. (2001). Power consumption, mixing time and homogenisation energy in dual-impeller agitated gas–liquid reactors. *Chemical Engineering and Processing: Process Intensification*, 40 (2), 87-95.

Boyer, C., Duquenne, A. M., Wild, G. (2002). Measuring techniques in gas–liquid and gas–liquid–solid reactors. *Chemical Engineering Science*, 57(16), 3185-3215.

Brown, D.E. (1997). The measurement of fermentor power input. *Chemical Industry*, 16, 684-

Bruijn, W., Vant Riet K., & Smith J. M. (1974). Power consumption with aerated Rushton turbines. *Chem. Eng. Res. Des.*, 52, 88-104.

- Cents, A. H. G., Jansen, D. J. W., Brilman, D. W. F., Versteeg, G. F. (2005). Influence of small amounts of additives on gas hold-up, bubble size, and interfacial area. *Industrial and engineering chemistry research*, **44** (14), 4863-4870.
- Chan, B.S., Tsang, Y.H. (2005). A theory on bubble-size dependence of the critical electrolyte concentration for inhibition of coalescence. *Journal of colloid and interface science* 286(1): 410 – 413.
- Chen, Z. D., Chen, J. J. J. (1999). Comparison of mass transfer performance for various single and twin impellers. *Chemical Engineering Research and Design*, 77(2), 104-109.
- Chen, Z. D., Chen, J. J. J. (2000). A study of agitated gas-liquid reactors with concave blade impellers. In *Mixing and Crystallization* (pp. 43-56). Springer, Dordrecht.
- Cho, I. H., & Zoh, K. D. (2007). Photocatalytic degradation of azo dye (Reactive Red 120) in TiO₂/UV system: Optimization and modeling using a response surface methodology (RSM) based on the central composite design. *Dyes and Pigments*, 75(3), 533-543.
- Christenson, H.K., Yaminsky, V.V. (1995) Solute effects on bubble coalescence. *The Journal of Physical Chemistry* 99(25), 10420 – 10420.
- Christenson, H.K., Bowen, R.E., Carlton, J.A., Denne, J.R.M., Lu, Y. (2008). Electrolytes that show a transition to bubble coalescence inhibition at high concentrations. *The Journal of Physical Chemistry C* 112(3), 794 – 796.
- Cockx, A., Roustan, M., Line, A., Hebrard, G. (1995). Modelling of mass transfer coefficient k_L in bubble columns. *Trans IChemE*, 73 Part A, 627-631.
- Cooke, M., Heggs, P. J. (2005). Advantages of the hollow (concave) turbine for multi-phase agitation under intense operating conditions. *Chemical Engineering Science*, 60(20), 5529-5543.
- Craig, V.S. (2011). Do hydration forces play a role in thin film drainage and rupture observed in electrolyte solutions?. *Current opinion in colloid & interface science*, 16(6), 597 – 600.
- Craig, V.S.J., Ninham, B.W., Pashley, R.M. (1993). Effect of electrolytes on bubble coalescence. *Nature*, 364(6435), 317-319.
- Craig, V.S.J., Ninham, B.W., Pashley, R.M. (1993). The effect of electrolytes on bubble coalescence in water. *J. Phys. Chem.* 97 (39), 10192 –10197.
- Cui, Y. Q., Van der Lans, R. G. J. M., Luyben, K. C. A. (1996). Local power uptake in gas-liquid systems with single and multiple Rushton turbines. *Chemical engineering science*, 51(11), 2631-2636.
- Danckwerts, P.V. (1951). Significance of liquid-film coefficients in gas absorption. *Industrial Engineering Chemistry* 43,1460–1467.

Deschenes, L.A., Barrett, J., Muller, L.J., Fourkas, J.T., Mohanty, U. (1998). Inhibition of bubble coalescence in aqueous solutions. 1. Electrolytes. *The Journal of Physical Chemistry B* 102(26), 5115-5119.

Devi, T. T., Kumar, B. (2014). Scale up criteria for dual stirred gas-liquid unbaffled tank with concave blade impeller. *Korean Journal of Chemical Engineering*, 31(8), 1339-1348.

Devi, T. T., Kumar, B. (2014). Scale up criteria for dual stirred gas-liquid unbaffled tank with concave blade impeller. *Korean Journal of Chemical Engineering*, 31(8), 1339-1348.

Devi, T. T., Kumar, B. (2017). Mass transfer and power characteristics of stirred tank with Rushton and curved blade impeller. *Engineering Science and Technology, an International Journal*, 20(2), 730-737.

Dhaouadi, H., Poncin, S., Hornut, J.M., Midoux, N. (2008). Gas-liquid mass transfer in bubble column reactor: Analytical solution and experimental confirmation. *Chemical Engineering and Processing: Process Intensification* 47, 548-556.

Eissa, S.H., Schügerl, K. (1975). Holdup and backmixing investigations in cocurrent and countercurrent bubble columns. *Chemical Engineering Science*, 30(10): 1251-1256.

Elgozali, A., Linek, V., Fialova, M., Wein, O., Zahradnik, J. (2002). Influence of viscosity and surface tension on performance of gas-liquid contactors with ejector type gas distributor. *Chemical Engineering Science*, 57(15), 2987-2994.

Erkey, C., Rodden, J.B., Akgerman, A. (1990). A correlation for predicting diffusion coefficients in alkanes. *The Canadian Journal of Chemical Engineering*, 68(4), 661-665.

Esmaeili, A., Farag, S., Guy, C., Chaouki, J. (2016). Effect of elevated pressure on the hydrodynamic aspects of a pilot-scale bubble column reactor operating with non-Newtonian liquids. *Chemical Engineering Journal*, 288, 377-389.

Esmaeili, A., Guy, C., Chaouki, J. (2015). The effects of liquid phase rheology on the hydrodynamics of a gas-liquid bubble column reactor. *Chemical Engineering Science*, 129, 193-207.

Ferreira, A., Ferreira, C., Teixeira, J.A., Rocha, F.(2010). Temperature and solid properties effects on gas-liquid mass transfer. *Chemical Engineering Journal* ,162(2),743-752.

Fransolet, E., Crine, M., Marchot, P., Toye, D. (2005). Analysis of gas holdup in bubble columns with non-Newtonian fluid using electrical resistance tomography and dynamic gas disengagement technique. *Chemical Engineering Science*, 60(22), 6118-6123.

Fujasova, M., Linek V., Moucha T., Prokopova E. (2004). Energy demands of different impeller types in gas-liquid dispersions, *Sep. Purif. Technol.* 39, 123– 131.

Fujasova, M., Linek, V., Moucha, T. (2007). Mass transfer correlations for multiple-impeller gas-liquid contactors. Analysis of the effect of axial dispersion in gas and liquid phases on “local” $k_L a$ values measured by the dynamic pressure method in individual stages of the vessel. *Chemical Engineering Science*, 62(6), 1650-1669.

Garcia-Ochoa, F., Gomez, E. (2009). Bioreactor scale-up and oxygen transfer rate in microbial processes: an overview. *Biotechnology advances*, 27(2), 153-176.

Garcia-Ochoa, F., Gomez, E.(2004). Theoretical prediction of gas-liquid mass transfer coefficient, specific area and hold-up in sparged stirred tanks. *Chemical Engineering Science*, 59, 2489–2501.

Geffcken. G. (1994) Comparative solubility of gases, etc., in water and in aqueous solutions. *Z Phys Chem* 49,257–302.

Gestrich, W., Rähse, W. (1975). Der relative Gasgehalt von Blasenschichten. *Chemie Ingenieur Technik*, 47(1), 8-13.

Ghosh, U. K., Upadhyay, S. N. (2007). Gas Holdup and Solid-Liquid Mass Transfer in Newtonian and non-Newtonian Fluids in Bubble Columns. *The Canadian Journal of Chemical Engineering*, 85(6), 825-832.

Ghotli, R. A., Aziz, A. A., Ibrahim, S., Baroutian, S., & Arami-Niya, A. (2013). Study of various curved-blade impeller geometries on power consumption in stirred vessel using response surface methodology. *Journal of the Taiwan Institute of Chemical Engineers*, 44(2), 192-201.

Godbole, S.P., Honath, M.F., Shah, Y.T. (1982). Holdup structure in highly viscous Newtonian and non-Newtonian liquids in bubble columns. *Chemical Engineering Communications*, 16(1-6), 119-134.

Gogate, P. R., Beenackers, A. A., Pandit, A. B. (2000). Multiple-impeller systems with a special emphasis on bioreactors: a critical review. *Biochemical Engineering Journal*, 6(2), 109-144.

Haque, M. W., Nigam, K. D. P., Joshi, J. B. (1986). Hydrodynamics and mixing in highly viscous pseudo-plastic non-Newtonian solutions in bubble columns. *Chemical engineering science*, 41(9), 2321-2331.

Hassan, I., Robinson, C. W. (1977). Stirred-tank mechanical power requirement and gas holdup in aerated aqueous phases. *AIChE Journal*, 23(1), 48-56.

Hassan, R., Loubiere, K., Legrand, J., & Delaplace, G. (2012). A consistent dimensional analysis of gas–liquid mass transfer in an aerated stirred tank containing purely viscous fluids with shear-thinning properties. *Chemical Engineering Journal*, 184, 42-56.

Haut, B., Cartage, T.(2005). Mathematical modeling of gas–liquid mass transfer rate in bubble columns operated in the heterogeneous regime. *Chemical Engineering Science* , 60,5937–5944.

Henry, C.L., Dalton, C.N., Scruton, L., Craig, V.S. (2007). Ion-specific coalescence of bubbles in mixed electrolyte solutions. *The Journal of Physical Chemistry C* 111(2): 1015 –1023.

Henry, C.L., Parkinson, L., Ralston, J.R., Craig, V.S. (2008). A mobile gas– water interface in electrolyte solutions. *The Journal of Physical Chemistry C*, 112(39), 15094-15097.

Hikita, H., Asai, S., Tanigawa, K., Segawa, K., Kitao, M. (1980). Gas hold-up in bubble columns. *The Chemical Engineering Journal*, 20(1), 59-67.

Hikita, H., Kikukawa, H. (1974). Liquid-phase mixing in bubble columns: effect of liquid properties. *The Chemical Engineering Journal*, 8(3), 191-197.

Horn, R. G., Del Castillo, L. A., Ohnishi, S. (2011). Coalescence map for bubbles in surfactant-free aqueous electrolyte solutions. *Advances in colloid and interface science*, 168(1-2), 85-92.

Hughmark, G. A. (1967). Holdup and mass transfer in bubble columns. *Industrial & Engineering Chemistry Process Design and Development*, 6(2), 218-220.

Hughmark, G. A. (1980). Power requirements and interfacial area in gas-liquid turbine agitated systems. *Industrial & Engineering Chemistry Process Design and Development*, 19(4), 638-641.

Huifang, Q., Shirong, W., Baiquan, D.(1999). Determination and estimation of physical property data for liquid paraffin. *Natural Gas Chemical Industry*, 24(3), 56-58.

Jackson AT (1991). *Process Engineering in Biotechnology*. Prentice Hall International, UK.

Jana, S. K., Biswas, A. B., Das, S. K. (2014). Gas holdup in tapered bubble column using pseudoplastic non-Newtonian liquids. *Korean Journal of Chemical Engineering*, 31(4), 574-581.

Jhavar, A. K., Prakash, A. (2014). Bubble column with internals: Effects on hydrodynamics and local heat transfer. *Chemical Engineering Research and Design*, 92(1), 25-33.

Jin, H., Yang, S., He, G., Liu, D., Tong, Z., Zhu, J. (2014). Gas–liquid mass transfer characteristics in a gas–liquid–solid bubble column under elevated pressure and temperature. *Chinese Journal of Chemical Engineering* , 22, 955–961.

Joshi, J. B., Pandit, A. B., Sharma, M. M. (1982). Mechanically agitated gas-liquid reactors. *Chemical Engineering Science*, 37(6), 813-844.

Joshi, J.B., Veera, V.P., Prasad, Ch. V., Phanikumar, D.V., Deshpande, N.S., Thakre, S.S., Thorat, B.N.(1998) Gas hold-up structure in bubble column reactors. *Pinna*, 64, 441-567.

Kantarci, N., Borak, F., Ulgen, K. O. (2005). Bubble column reactors. *Process Biochemistry*, **40** (7), 2263-2283.

Kastanek, F.(1977). The volume mass transfer coefficient in a bubble bed column. *Collect. Czech. Them. Commun* ,42, 2491–2497.

Kawase, Y., Halard, B., Moo-Young, M.(1987). Theoretical prediction of volumetric mass transfer coefficients in bubble columns for Newtonian and non-Newtonian fluids. *Chemical Engineering Science* ,42, 1609–1617.

Kazakis, N. A., Papadopoulos, I. D., Mouza, A. A. (2007). Bubble columns with fine pore sparger operating in the pseudo-homogeneous regime: gas hold up prediction and a criterion for the transition to the heterogeneous regime. *Chemical engineering science*, 62(12), 3092-3103.

Kazakis, N. A., Papadopoulos, I. D., Mouza, A. A. (2007). Bubble columns with fine pore sparger operating in the pseudo-homogeneous regime: gas hold up prediction and a criterion for the transition to the heterogeneous regime. *Chemical engineering science*, 62(12), 3092-3103.

Kelkar, B. G., Shah, Y. T. (1985). Gas holdup and backmixing in bubble column with polymer solutions. *AIChE journal*, 31(4), 700-702.

Kelkar, B.G., Phulgaonkar, S.R., Shah, Y.T. (1983) The effect of electrolyte solutions on hydrodynamic and backmixing characteristics in bubble columns. *The Chemical Engineering Journal*, 27(3), 125 –133.

Khare, A. S., Niranjana, K. (1999). An experimental investigation into the effect of impeller design on gas hold-up in a highly viscous Newtonian liquid. *Chemical engineering science*, 54(8), 1093-1100.

Khare, A. S., Niranjana, K. (2002). The effect of impeller design on gas hold-up in surfactant containing highly viscous non-Newtonian agitated liquids. *Chemical Engineering and Processing: Process Intensification*, 41(3), 239-249.

Khare, A.S., Joshi, J.B. (1990). Effect of fine particles on gas hold-up in three-phase sparged reactors. *The Chemical Engineering Journal*, 44(1), 11-25.

Khataee, A. R. (2010). Optimization of UV- promoted peroxydisulphate oxidation of CI Basic Blue 3 using response surface methodology. *Environmental technology*, 31(1), 73-86.

Khuri A.I, Cornell J.A., *Response Surface: Design and Analysis*, Dekker, New York, 1987.

Kittilsen, P., Togersen, R., Rytter, E., Svendsen, H. (2001). Modeling of gas-liquid mass-transfer limitations in slurry olefin polymerization. *Industrial & Engineering Chemistry Research*, 40, 1090-1096.

Kluytmans, J. H. J., Van Wachem, B. G. M., Kuster, B. F. M., and Schouten, J. C. (2003). Mass transfer in sparged and stirred reactors: influence of carbon particles and electrolyte. *Chemical Engineering Science*, 58 (20), 4719-4728.

Kluytmans, J.H.J., Van wachem, B.G.M., Kuster, B.F.M., Schouten, J.C. (2001). Gas holdup in a slurry bubble column: influence of electrolyte and carbon particles. *Industrial and Engineering Chemistry Research*, 40 (23), 5326–5333.

Koide, K., Takazawa, A., Komura, M., Matsunaga, H. (1984). Gas holdup and volumetric liquid-phase mass transfer coefficient in solid-suspended bubble columns. *Journal of chemical engineering of Japan* 17(5) :459-466.

Krishna, R., Ellenberger, J., Maretto, C. (1999). Flow regime transition in bubble columns. *International communications in heat and mass transfer*, 26 (4), 467-475.

Krishna, R., Sie. S.T. (2000). Design and scale-up of the Fischer–Tropsch bubble column slurry reactor. *Fuel Processing Technology* 2000; 64, 73–105.

Krishna, R., Van Baten, J. M., Urseanu, M. I., Ellenberger, J. (2001). A scale up strategy for bubble column slurry reactors. *Catalysis today*, 66 (2), 199-207.

Kulkarni, A. A., Joshi, J. B. (2005). Bubble formation and bubble rise velocity in gas– liquid systems: a review. *Industrial & Engineering Chemistry Research*, 44(16), 5873-5931.

Kulkarni, A. V., Joshi, J. B. (2011a). Design and selection of sparger for bubble column reactor. Part I: Performance of different spargers. *Chemical engineering research and design*, 89(10), 1972-1985.

Kulkarni, A. V., Joshi, J. B. (2011b). Design and selection of sparger for bubble column reactor. Part II: Optimum sparger type and design. *Chemical Engineering Research and Design*, 89(10), 1986-1995.

Labík, L., Vostal, R., Moucha, T., Rejl, F., Kordac, M. (2014). Volumetric mass transfer coefficient in multiple-impeller gas–liquid contactors. Scaling-up study for various impeller types. *Chemical Engineering Journal*, 240, 55-61.

Labík, L., Vostal, R., Moucha, T., Rejl, F., Kordač, M. (2014). Volumetric mass transfer coefficient in multiple-impeller gas–liquid contactors. Scaling-up study for various impeller types. *Chemical Engineering Journal*, 240, 55-61.

Lakota, A. (2007). Effect of highly viscous non-Newtonian liquids on gas holdup in a concurrent upflow bubble column. *Acta Chimica Slovenica*, 54(4), 678–688.

Lau, R., Peng, W., Velazquez-Vargas, L. G., Yang, G. Q., Fan, L. S. (2004). Gas– liquid mass transfer in high-pressure bubble columns. *Industrial & engineering chemistry research*, 43(5), 1302-1311.

Lau, R., Peng, W., Velazquez-Vargas, L.G., Yang, G.Q., Fan, L.S. (2004). Gas– liquid mass transfer in high-pressure bubble columns. *Industrial & Engineering Chemistry Research*, 43(5), 1302-1311.

Lee, J. C., Meyrick, D. L. (1970). Gas-liquid interfacial areas in salt solutions in an agitated tank. *Transactions of the Institution of Chemical Engineers and the Chemical Engineer*, 48(2), T37.

Lee, L.S., Sun, S.L., Lin, C.L. (2008). Predictions of thermodynamic properties of aqueous single-electrolyte solutions with the two-ionic-parameter activity coefficient model. *Fluid Phase Equilibria*, 233(1-2), 105-115.

Lemoine, R., Behkish, A., Sehabiague, L., Heintz, Y. J., Oukaci, R., and Morsi, B. I. (2008). An algorithm for predicting the hydrodynamic and mass transfer parameters in bubble column and slurry bubble column reactors. *Fuel Processing Technology*, **89** (4), 322-343.

Leonard, C., Ferrasse, J. H., Boutin, O., Lefevre, S., Viand, A. (2015). Bubble column reactors for high pressures and high temperatures operation. *Chemical Engineering Research and Design*, 100, 391-421.

Leonard, C., Ferrasse, J. H., Boutin, O., Lefevre, S., Viand, A. (2015). Bubble column reactors for high pressures and high temperatures operation. *Chemical Engineering Research and Design*, 100, 391-421.

Lessard, R.R., Zieminski SA (1971). Bubble coalescence and gas transfer in aqueous electrolytic solutions. *Industrial & Engineering Chemistry Fundamentals*, 10(2), 260 – 269.

Linek, V., Moucha, T., Rejl, F. J., Kordač, M., Hovorka, F., Opletal, M., Haidl, J. (2012). Power and mass transfer correlations for the design of multi-impeller gas–liquid contactors for non-coalescent electrolyte solutions. *Chemical Engineering Journal*, 209, 263-272.

Liu, H. L., Chiou, Y. R. (2005). Optimal decolorization efficiency of Reactive Red 239 by UV/TiO₂ photocatalytic process coupled with response surface methodology. *Chemical Engineering Journal*, 112(1-3), 173-179.

Loiseau, B., Midoux, N., Charpenntier, J. C. (1977). Some hydrodynamics and power input data in mechanically agitated gas–liquid contactors. *AIChE Journal*, 23(6), 931-935.

- Lu, W. M., Wu, H. Z., Chou, C. Y. (1999). Effect of impeller blade number on K_{La} in mechanically agitated vessels. *Korean Journal of Chemical Engineering*, 16(5), 703-708.
- Lu, W. M., Yang, B. S. (1998). Effect of blade pitch on the structure of the trailing vortex around Rushton turbine impellers. *The Canadian Journal of Chemical Engineering*, 76(3), 556-562.
- Luong, H. T., & Volesky, B. (1979). Mechanical power requirements of gas–liquid agitated systems. *AIChE Journal*, 25(5), 893-895.
- Lupin, H.M, Merchuk, J.C. (1971). A note on the film–penetration model for mass transfer with first order chemical reaction. *AIChE Journal* , 17, 1243–1245.
- Maceiras, R., Alvarez, E., Cancela, M. A. (2010). Experimental interfacial area measurements in a bubble column. *Chemical engineering journal*, 163 (3), 331-336.
- Machon, V., Vlcek, J., Kurdna, V. (1977). Gas hold-up in agitated aqueous solutions of strong inorganic salts, *Proc 2nd Europ Conf on Mixing, Cambridge, England; (BHRA Fluid Eng)*, F2–17–F2–34.
- Majumder, S.K. (2016). *Hydrodynamics and Transport Processes of Inverse Bubbly Flow*, 1st Edition, Elsevier, Amsterdam.
- Markopoulos, J., Babalona, E., Tsiliopoulou, E. (2004). Power consumption in agitated vessels with dual Rushton turbines: baffle length and inter–impeller clearance effects. *Chemical engineering & technology*, 27(11), 1212-1215.
- Markopoulos, J., Babalona, E., Tsiliopoulou, E., Tasopoulou, K. (2005). Power consumption in agitated vessels with dual pitched blade turbines: Baffle length and inter–impeller clearance effects. *Chemical engineering & technology*, 28(9), 978-981.
- Markopoulos, J., Christofi, C., Katsinaris, I. (2007). Mass Transfer Coefficients in Mechanically Agitated Gas-Liquid Contactors. *Chemical engineering & technology*, 30(7), 829-834.
- Markopoulos, J., Pantuflas, E. (2001). Power Consumption in Gas–Liquid Contactors Agitated by Double–Stage Rushton Turbines. *Chemical engineering & technology*, 24(11), 1147-1150.
- Marrucci, G., Nicodemo L (1967). Coalescence of gas bubbles in aqueous solutions of inorganic electrolytes. *Chem. Eng. Sci.*, 22,1257–1265.
- Marucci, G., (1969) Theory of coalescence. *Chem. Eng. Sci.*, 24, 975–985.
- Mena, P., Ferreira, A., Teixeira, J. A., Rocha, F. (2011). Effect of some solid properties on gas–liquid mass transfer in a bubble column. *Chemical Engineering and Processing: Process Intensification*, **50** (2), 181-188.
- Metcalf and Eddy, (2005), *Wastewater Engineering - Treatment, Disposal and Reuse*, 5th Edition, Tata McGraw Hill Publishing Co. Ltd., New Delhi.

- Michel, B. J., Miller, S. A. (1962). Power requirements of gas-liquid agitated systems. *AIChE Journal*, 8(2), 262-266.
- Michelan, R., Zimmer, T. R., Rodrigues, J. A., Ratusznei, S. M., de Moraes, D., Zaiat, M., Foresti, E. (2009). Effect of impeller type and mechanical agitation on the mass transfer and power consumption aspects of ASBR operation treating synthetic wastewater. *Journal of Environmental Management*, **90** (3), 1357-1364.
- Millero, F.J., Huang, F., Laferiere, A.L. (2002). Solubility of oxygen in the major sea salts as a function of concentration and temperature. *Mar Chem*, 78, 217-30..
- Mishra, V. P., Joshi, J. B. (1993). Flow generated by a disc turbine: part III. Effect of impeller diameter, impeller location and comparison with other radial flow turbines. *Transactions of the Institution of Chemical Engineers Part A: Chemical Engineering Research and Design*, 71, 563-573.
- Montgomery, D.C, *Design and Analysis of Experiments*, fifth ed., John Wiley and Sons, New York, 2001.
- Moucha, T., Linek, V., Erokhin, K., Rejl, J. F., Fujasova, M. (2009). Improved power and mass transfer correlations for design and scale-up of multi-impeller gas-liquid contactors. *Chemical Engineering Science*, **64** (3), 598-604.
- Mouza, A. A., Dalakoglou, G. K., Paras, S. V. (2005). Effect of liquid properties on the performance of bubble column reactors with fine pore spargers. *Chemical Engineering Science*, 60(5), 1465-1475.
- Murugesan, T., Degaleesan, T. E. (1992). Holdup, Interfacial Area and power requirements in turbine agitated gas-liquid contactors. *Chemical Engineering Communications*, 117(1), 263-278.
- Narita, E., Lawson, F., & Han, K. N. (1983). Solubility of oxygen in aqueous electrolyte solutions. *Hydrometallurgy*, 10(1), 21-37.
- Nedelchev, S., Jordan, U., Schumpe, A. (2006). A new correction factor for theoretical prediction of mass transfer coefficients in bubble columns. *Journal of chemical engineering of Japan*, **39** (12), 1237-1242.
- Nguyen, P. T., Hampton, M. A., Nguyen, A. V., Birkett, G. R. (2012). The influence of gas velocity, salt type and concentration on transition concentration for bubble coalescence inhibition and gas holdup. *Chemical Engineering Research and Design*, **90** (1), 33-39.
- Nienow, A. W. (1996). Gas-Liquid Mixing Studies-A Comparison of Rushton Turbines with Some Modern Impellers. *Chemical engineering research & design*, 74(4), 417-423.

- Nienow, A. W., Hunt, G., Buckland, B. C. (1994). A fluid dynamic study of the retrofitting of large agitated bioreactors: Turbulent flow. *Biotechnology and bioengineering*, 44(10), 1177-1185.
- Olivieri, G., Russo, M.E., Simeone, M., Marzocchella, A., Salatino, P. (2011) Effects of viscosity and relaxation time on the hydrodynamics of gas–liquid systems. *Chemical engineering science*, 66(14), 3392-3399.
- Orvalho, S., Ruzicka, M. C., Drahos, J. (2009). Bubble column with electrolytes: gas holdup and flow regimes. *Industrial and Engineering Chemistry Research*, **48** (17), 8237-8243.
- Oyevaar, M. H., Westerterp, K. R. (1989). The use of the chemical method for the determination of interfacial areas in gas—liquid contactors. *Chemical engineering science*, **44** (11), 2691-2701.
- Ozkan, O., Calimli, A., Berber, R., Oguz, H. (2000). Effect of inert solid particles at low concentrations on gas–liquid mass transfer in mechanically agitated reactors. *Chemical Engineering Science*, 55(14), 2737-2740.
- Pashley, R. M., Craig, V. S. J. (1997). Effects of electrolytes on bubble coalescence. *Langmuir*, 13(17), 4772-4774.
- Passos, A. D., Voulgaropoulos, V. P., Paras, S. V., Mouza, A. A. (2015). The effect of surfactant addition on the performance of a bubble column containing a non-Newtonian liquid. *Chemical Engineering Research and Design*, 95, 93-104.
- Pradhan, A. K., Parichha, R. K., De, P. (1993). Gas holdup in non-newtonian solutions in a bubble column with internals. *The Canadian Journal of Chemical Engineering*, 71(3), 468-471.
- Prince, M. J., Blanch, H. W. (1990). Bubble coalescence and break-up in air sparged bubble columns. *AIChE Journal*, 36 (10), 1485-1499.
- Prince, M.J., Blanch, H.W. (1990). Transition electrolyte concentrations for bubble coalescence. *AIChE J.* 36, 1425–1429.
- Puthli, M. S., Rathod, V. K., Pandit, A. B. (2005). Gas–liquid mass transfer studies with triple impeller system on a laboratory scale bioreactor. *Biochemical Engineering Journal*, 23 (1), 25-30.
- R.H. Myers, D.C. Montgomery, *Response Surface Methodology*, second ed., Wiley, 2001.
- Rao, A. R., Kumar, B. (2007). The use of circular surface aerators in wastewater treatment tanks. *Journal of Chemical Technology and Biotechnology*, 82(1), 101-107.
- Ribeiro CP, Mewes D (2007). The effect of electrolytes on the critical velocity for bubble coalescence. *Chemical Engineering Journal*, 126(1), 23 – 33.

- Ribeiro Jr, C. P., Mewes, D. (2007). The influence of electrolytes on gas hold-up and regime transition in bubble columns. *Chemical engineering science*, 62 (17), 4501-4509.
- Ruzicka, M. C., Drahos, J., Mena, P. C., Teixeira, J. A. (2003). Effect of viscosity on homogeneous–heterogeneous flow regime transition in bubble columns. *Chemical Engineering Journal*, 96 (1), 15-22.
- Ruzicka, M. C., Vecer, M. M., Orvalho, S., Drahos, J. (2008). Effect of surfactant on homogeneous regime stability in bubble column. *Chemical Engineering Science*, **63** (4), 951-967.
- Sada, E., Kumazawa, H., Lee, C., Fujiwara, N. (1985). Gas-liquid mass transfer characteristics in a bubble column with suspended sparingly soluble fine particles. *Industrial & Engineering Chemistry Process Design and Development* , 24(2), 255-261.
- Sagert, N.H., Quinn, M.J. (1978). The coalescence of gas bubbles in dilute aqueous solutions. *Chem. Eng. Sci.*, 33, 1087–1095.
- Saghatoleslami, N., and Bakhtiari, H. R. (2006). Experimental Investigation of Power Consumption, Mass Transfer Coefficient and Flow Regime in Gas Liquid Dispersion Systems. *Iranian Journal of Chemical Engineering*, 3 (2), 3-12.
- Saito, F., Nienow, A. W., Chatwin, S., & Moore, I. P. (1992). Power, gas dispersion and homogenisation characteristics of Scaba SRGT and Rushton turbine impellers. *Journal of chemical engineering of Japan*, 25(3), 281-287.
- Sardeing, R., Painmanakul, P., and Hébrard, G. (2006). Effect of surfactants on liquid-side mass transfer coefficients in gas–liquid systems: a first step to modeling. *Chemical Engineering Science*, 61 (19), 6249-6260.
- Sarrafi, A., Müller-Steinhagen, H., Smith, J.M., Jamialahmadi, M. (1999). Gas holdup in homogeneous and heterogeneous gas—liquid bubble column reactors. *The Canadian Journal of Chemical Engineering*, 77(1), 11-21.
- Schumpe, A., Deckwer, W. D. (1982). Gas holdups, specific interfacial areas, and mass transfer coefficients of aerated carboxymethyl cellulose solutions in a bubble column. *Industrial & Engineering Chemistry Process Design and Development*, 21(4), 706-711.
- Shafeeyan, M. S., Daud, W. M. A. W., Houshmand, A., & Arami-Niya, A. (2012). The application of response surface methodology to optimize the amination of activated carbon for the preparation of carbon dioxide adsorbents. *Fuel*, 94, 465-472.
- Shah, Y. T., Kelkar, B. G., Godbole, S. P., Deckwer, W. D. (1982). Design parameters estimations for bubble column reactors. *AIChE Journal*, **28** (3), 353-379.

Shaikh, A., Al-Dahhan, M. (2013). Scale-up of bubble column reactors: a review of current state-of-the-art. *Industrial & Engineering Chemistry Research*, 52(24), 8091-8108.

Shaikh, A., Al-Dahhan, M. H. (2007). A review on flow regime transition in bubble columns. *International Journal of Chemical Reactor Engineering*, 5(1).

Shanmugam, K., Saravanan, K., Ramamoorthy, V., Balasubramani, R. (2008). Hydrodynamic studies in stirred bubble column. *Journal of the University of Chemical Technology and Metallurgy*, 43(1), 113-118.

Shewale, S. D., and Pandit, A. B. (2006). Studies in multiple impeller agitated gas-liquid contactors. *Chemical engineering science*, 61 (2), 489-504.

Shimizu K, Takada S, Minekawa K, Kawase Y. (2000). Phenomenological model for bubble column reactors: prediction of gas hold-ups and volumetric mass transfer coefficients. *Chemical Engineering Journal*, 78, 21-28.

Singh, K. P., Gupta, S., Singh, A. K., Sinha, S. (2011). Optimizing adsorption of crystal violet dye from water by magnetic nanocomposite using response surface modeling approach. *Journal of Hazardous Materials*, 186(2-3), 1462-1473.

Singh, R. K., Kumar, S., Kumar, S., & Kumar, A. (2008). Development of parthenium based activated carbon and its utilization for adsorptive removal of p-cresol from aqueous solution. *Journal of Hazardous Materials*, 155(3), 523-535.

Smith, J. M., Gao, Z., Middleton, J. C. (2001). The unsparged power demand of modern gas dispersing impeller in boiling liquids. *Chemical Engineering Journal*, 84 (1), 15-21.

Sujan A. Studies on hydrodynamic and mass transfer parameters in a bubble column. Ph.D thesis to be submitted to Malaviya National Institute of Technology, Jaipur 2018.

Sujan, A., Vyas, R. K., & Singh, K. (2018). Estimation of liquid- side mass transfer coefficient and liquid film thickness in a bubble column using single spherical bubble model. *Asia-Pacific Journal of Chemical Engineering*.

Sujan, A., Vyas, R.K. (2017). A review on empirical correlations estimating gas holdup for shear-thinning non-Newtonian fluids in bubble column systems with future perspectives. *Reviews in Chemical Engineering* 2017. DOI: <https://doi.org/10.1515/revce-2016-0062>.

Syeda, S. R., Reza, M. J. (2011). Effect of surface tension gradient on gas hold-up enhancement in aqueous solutions of electrolytes. *Chemical Engineering Research and Design*, 89 (12), 2552-2559.

Takahashi, K., McManamey, W. J., Nienow, A. W. (1992). Bubble size distributions in impeller region in a gas-sparged vessel agitated by a Rushton turbine. *Journal of chemical engineering of Japan*, 25(4), 427-432.

Takahashi, K., Nienow, A. W. (1993). Bubble sizes and coalescence rates in an aerated vessel agitated by a Rushton turbine. *Journal of chemical engineering of Japan*, 26(5), 536-542.

Tan, I. A. W., Ahmad, A. L., & Hameed, B. H. (2008). Optimization of preparation conditions for activated carbons from coconut husk using response surface methodology. *Chemical Engineering Journal*, 137(3), 462-470.

Temesgen, T., Bui, T. T., Han, M., Kim, T. I., Park, H. (2017). Micro and nanobubble technologies as a new horizon for water-treatment techniques: A review. *Advances in colloid and interface science*, 246, 40-51.

Thakre, S. B., Bhuyar, L. B., Deshmukh, S. J. (2008). Effect of different configurations of mechanical aerators on oxygen transfer and aeration efficiency with respect to power consumption. *International Journal of Aerospace and Mechanical Engineering*, 2 (2), 100-108.

Thomas DG. (1965) Transport characteristics of suspension: VIII. A note on the viscosity of Newtonian suspensions of uniform spherical particles. *Journal of Colloid Science*, 20(3), 267-277.

Treybal, R.E. *Mass-transfer Operations*, 3rd ed., McGraw-Hill, Singapore 1981.

Vakarelski, I. U., Manica, R., Li, E. Q., Basheva, E. S., Chan, D. Y., Thoroddsen, S. T. (2018). Coalescence dynamics of mobile and immobile fluid interfaces. *Langmuir*.

Van't Riet, K., Smith, J. M. (1973). The behaviour of gas—liquid mixtures near Rushton turbine blades. *Chemical Engineering Science*, 28(4), 1031-1037.

Van't Riet, K., Smith, J. M. (1975). The trailing vortex system produced by Rushton turbine agitators. *Chemical Engineering Science*, 30(9), 1093-1105.

Vasconcelos, J. M., Orvalho, S. C., Rodrigues, A. M., Alves, S. S. (2000). Effect of blade shape on the performance of six-bladed disk turbine impellers. *Industrial & engineering chemistry research*, 39(1), 203-213.

Veera, U. P., Joshi, J. B. (2000). Measurement of gas hold-up profiles in bubble column by gamma ray tomography: effect of liquid phase properties. *Chemical engineering research and design*, 78(3), 425-434.

Wang, J., Langemann H. (1994b). Unsteady two-film model for mass transfer accompanied by chemical reaction. *Chemical Engineering Science*, 49, 3457–3463.

Wang, J., Langemann H. (1994a). Unsteady two-film model for mass transfer. *Chemical Engineering & Technology*, 17, 280–284.

Wang, J., Tan, S.H., Nguyen AV, Evans GM, Nguyen NT (2016). A Microfluidic Method for Investigating Ion-Specific Bubble Coalescence in Salt Solutions. *Langmuir*, 32(44), 11520-11524.

Warmoeskerken, M. M. C. G., Smith, J. M. (1989). Hollow blade agitator for dispersion and mass transfer. *Chemical Engineering Research and Design*, 67, 193-198.

Weissenborn, P. K., Pugh, R. J. (1995). Surface tension and bubble coalescence phenomena of aqueous solutions of electrolytes. *Langmuir*, 11, 1422 –1426.

Weissenborn, PK, Pugh RJ (1996). Surface tension of aqueous solutions of electrolytes: relationship with ion hydration, oxygen solubility, and bubble coalescence. *Journal of Colloid and Interface Science*, 184(2), 550-563.

Wilkinson, P. M., Haringa, H., Van Dierendonck, L. L. (1994). Mass transfer and bubble size in a bubble column under pressure. *Chemical Engineering Science*, 49(9), 1417-1427.

Yang, W., Wang, J., Jin, Y.(2001). Mass transfer characteristics of syngas components in slurry system at industrial conditions. *Chemical Engineering & Technology*, 24(6), 651-657.

Yang, W. G., Wang, J. F., Jin, Y. (2001). Gas-liquid mass transfer in a slurry bubble column reactor under high temperature and high pressure. *Chinese Journal of Chemical Engineering*, 9 (3), 253-257.

Yang, W., Wang, J., Zhao, B., Jin, Y. (2003). Gas–liquid mass transfer in slurry bubble systems: II. Verification and simulation of the model based on the single bubble mechanism. *Chemical Engineering Journal*, 96(1), 23-27.

Youssef, A. A., Hamed, M. E., Al-Dahhan, M. H., Duduković, M. P. (2014). A new approach for scale-up of bubble column reactors. *Chemical Engineering Research and Design*, 92(9), 1637-1646.

Zahradnik, J, Peter R, Kastanek F (1987) The effect of liquid phase properties on gas holdup in bubble column reactors. *Collection of Czechoslovak Chemical Communications*, 52(2), 335-347.

Zahradnik, J., Fialova, M., Kastanek, F., Green, K., Thomas, N. (1995). The effect of electrolytes on bubble coalescence and gas holdup in bubble column reactors. *Chem. Eng. Res. Des.*, 73, 341–346.

Zahradnik, J., Fialova, M., Ru, M., Drahos, J., Kastanek, F., Thomas, N.H. (1997). Duality of the gas-liquid flow regimes in bubble column reactors. *Chemical Engineering Science*, 52(21-22), 3811-3826.

- Zarei, M., Niaei, A., Salari, D., & Khataee, A. (2010). Application of response surface methodology for optimization of peroxi-coagulation of textile dye solution using carbon nanotube–PTFE cathode. *Journal of Hazardous Materials*, 173(1-3), 544-551.
- Zemaitis, Jr J. F., Clark, D. M., Rafal, M., Scrivner, N. C. (1986). *Handbook of Aqueous Electrolyte Thermodynamics*. DIPPR and AIChE, New York.
- Zhang, J., Gao, Z., Cai, Y., Cai, Z., Yang, J., Bao, Y. (2016). Mass transfer in gas–liquid stirred reactor with various triple-impeller combinations. *Chinese journal of chemical engineering*, 24(6), 703-710.
- Zhao, B., Wang, J., Yang, W, Jin Y.(2003). Gas–liquid mass transfer in slurry bubble systems: I. Mathematical modeling based on a single bubble mechanism. *Chemical Engineering Journal*, 96, 23–27.
- Zhu, Y., Bandopadhyay, P. C., Wu, J. (2001). Measurement of Gas-Liquid Mass Transfer in an Agitated Vessel. A Comparison between Different Impellers. *Journal of chemical engineering of Japan*, **34** (5), 579-584.

APPENDIX

APPENDIX 4A

The ranges of experimental conditions used for validation of model

4A. 1 Detail of experimental conditions (Jin et al. 2014)

Parameter(s)	Detail
Gas phase	H ₂ , CO, CO ₂
Liquid phase	Paraffin
Mass concentration of quartz sand (C _S)	0, 5%, 10%, 15%, 20%
Particle size of quartz sand	150–200 μm
Superficial gas velocity (U _g)	0.026–0.053 m · s ⁻¹
Operating pressure (P)	1.0 MPa, 1.5 MPa, 2.0 MPa, 2.5 MPa, 3.0 MPa
Temperature in the column (T)	298–423 K
Column diameter (D _T)	0.10 m

4A. 2 Physical properties of gas (Jin et al. 2014)

Gas	M _B (kg/kmol)	T _C , (K)	P _C (MPa)	ν _A × 10 ³ (m ³ /kmol)
H ₂	2.016	407.4	1.30	14.3
CO	28.010	306.5	35.0	33.0
CO ₂	44.051	304.1	7.38	34.0

4A. 3 Physical properties of paraffin

Molecular weight, kg/kmol	T _C (K)	ρ _L (kg/m ³) at 298 K	μ _L (Pa.s × 10 ³) at 298 K	σ _L × 10 ² (N/m) at 298 K
412 [@]	916.8 [@]	890 [#]	13.8 [#]	2.88 [#]

@ Weiguo et al. 2001

Jin et al. 2014

4A. 4 Physical properties of slurry at 298K

Cs (%)	ρ_{SL} (kg/m ³)	μ_{SL} (Pa.s ×10 ³)
0	890	13.8
5	879.15	47.519
10	868.3	91.215
15	857.45	188.541
20	846.6	407.960

4A. 5 Mean diameter of small and larger bubbles at different pressures and constant temperature

T = 298 K (Jin et al. 2014)

P (MPa)	Mean bubble diameter	
	$d_{B, small}$ (m)	$d_{B, larger}$ (m)
1	0.0064	0.0253
1.5	0.0067	0.0242
2	0.0073	0.0228
2.5	0.0083	0.0221
3	0.0093	0.0212

Publications

Article(s) published in journal

- Sujan A., Vyas, R. K. (2017). A review on empirical correlations for estimating gas holdup for shear–thinning non-Newtonian fluids in bubble column systems with future perspectives, *Reviews in Chemical Engineering*.
DOI: <https://doi.org/10.1515/revce-2016-0062>.
- Sujan A, Vyas RK. Singh K. (2018). Estimation of liquid–side mass transfer coefficient and liquid film thickness in a bubble column using single spherical bubble model, *Asia-Pacific Journal of Chemical Engineering*, **13** (2), e2178.
DOI: <https://doi.org/10.1002/apj.2178>,
- Sujan A, Vyas RK. (2018). Estimation of transition concentration of aqueous mixtures of single and binary electrolytes for bubble coalescence inhibition. *Chemical Papers*.**72** (10), 2539-2559. DOI: <https://doi.org/10.1007/s11696-018-0470-2>.

Article(s) in conference(s)

- Sujan, A., Vyas, R. K. (2017). Analysis of power consumption using response surface methodology in partially baffled double stage Rushton impeller gas-liquid contactor, accepted for oral presentation, CHEMCON-2017 to be held during December 27-30, 2017 at Haldia Regional Centre of Indian institute of Chemical Engineers (IChE), Haldia, West Bengal, India.
- Sujan, A., Vyas, R. K. (2017). Sensitivity analysis using Garson’s algorithm for power consumption in partially baffled gas-liquid contactor equipped with double stage Rushton impeller, accepted for oral presentation, CHEMCON-2017 to be held during December 27-30, 2017 at Haldia Regional Centre of Indian institute of Chemical Engineers (IChE), Haldia, West Bengal, India.
- Sujan, A., Vyas, R. K. Singh K. (2016). A review on relative importance of input variables for gas holdup, volumetric mass transfer coefficient and bubble diameter using weight matrix of Ann and Garson’s algorithm in gas-liquid / gas-liquid-solid bubble columns, accepted for poster presentation, CHEMCON-2016, December 27-30, 2016, held at Chennai Regional Centre of Indian institute of Chemical Engineers (IChE), Chennai, India.

- Sujan, A., Vyas, R. K. (2015). Contradictory results of Gas hold-up, Mass transfer Coefficient and Interfacial area in Bubble Column at Elevated Pressures and Temperature: A Review, accepted for poster presentation, CHEMCON-2015, December 27-30, 2015, held at Guwahati Regional Centre of Indian institute of Chemical Engineers (IChE), Guwahati, India.
- Sujan, A., Vyas, R. K. (2014). Application of Artificial Neural Network (ANN) and Support Vector Regression (SVR) for Developing Correlation for Hydrodynamic Parameters in Bubble Column, accepted for oral presentation, CHEMCON-2014, December 27-30, 2014, held at Chandigarh Regional Centre of Indian institute of Chemical Engineers (IChE), Chandigarh, India.

Ajay Sujan and Raj K. Vyas*

A review on empirical correlations estimating gas holdup for shear-thinning non-Newtonian fluids in bubble column systems with future perspectives

<https://doi.org/10.1515/revce-2016-0062>

Received December 7, 2016; accepted August 2, 2017

Abstract: Gas holdup is one of the most important parameters for characterizing the hydrodynamics of bubble columns. Modeling and design of bubble columns require empirical correlations for precise estimation of gas holdup. Empirical correlations available for prediction of gas holdup (ϵ_g) in various non-Newtonian systems for both gas-liquid and gas-liquid-solid bubble columns have been presented in this review. Critical analysis of correlations presented by different researchers has been made considering the findings and pitfalls. As the magnitude of gas holdup depends on many factors, such as physicochemical properties of gas and/or liquid, column geometry, type and design of gas distributors, operating conditions, phase properties, and rheological properties, etc., all of these have been discussed and examined. In order to emphasize the significance, relative importance of parameters such as flow behavior index, consistency index, column diameter, gas flow rate, and density of aqueous carboxymethylcellulose (CMC) solution on gas holdup has been quantified using artificial neural network and Garson's algorithm for an experimental data set of air-CMC solution from the literature. Besides, potential areas for research encompassing operating conditions, column geometry, physical properties, modeling and simulation, rheological properties, flow regime, etc., have been underlined, and the need for developing newer correlations for gas holdup has been outlined. The review may be useful for the modeling and design of bubble columns.

Keywords: artificial neural network; empirical correlations; Garson's algorithm; gas holdup; non-Newtonian systems.

1 Introduction

A large number of industries use non-Newtonian liquids in bubble columns for gas-liquid mass transfer. Several non-Newtonian shear-thinning liquids like slurries, suspensions, emulsions, micellar solutions, polymer solutions, organic liquids such as glycerol, melts, liquid crystals, gels, foams, pulp suspension, mixed liquor of aerobic wastewater, etc., are processed in biotechnological, pharmaceutical, polymer, pulp and paper, and food processing industries and wastewater treatment to accomplish gas-liquid mass transfer operation. The understanding of hydrodynamics of non-Newtonian systems in industrial bubble columns is imperative for effective design, operation, and scale up, as the fundamentals of non-Newtonian systems are yet to be understood well (Haque et al. 1986, Fransolet et al. 2005, Ghosh and Upadhyay 2007, Anastasiou et al. 2013). Empirical correlations for predicting gas holdup are developed on the basis of results of experimental studies based on inherent parameters governing mass transfer using the bubble column data. Thus, correlations provide a fundamental basis of understanding the parameters governing the hydrodynamics of bubble columns. Several authors have reported empirical correlations for gas holdup for non-Newtonian systems (Veera and Joshi 2000, Elgozali et al. 2002, Khare and Niranjana 2002, Fransolet et al. 2005, Lakota 2007, Anastasiou et al. 2013, Jana et al. 2014a, Passos et al. 2015, Esmaeili et al. 2016).

Nutrient media and liquid suspensions used in bioprocess industries generally exhibit non-Newtonian behavior. Estimation of gas holdup in bubble columns plays a significant role in the design and scale up of bubble columns. Non-Newtonian liquids containing solutes and/or suspended solids are often encountered in bioprocess, food processing, and pulp and paper industries. *A priori* accurate estimate of the gas holdup is essential for the estimation of gas-liquid mass transfer in such cases. Studies on the non-Newtonian liquid behavior in case of varying concentrations of solute(s) such as carboxymethylcellulose (CMC) and xanthan on the gas holdup have been reported earlier (Schumpe and Deckwer 1982,

*Corresponding author: Raj K. Vyas, Department of Chemical Engineering, Malaviya National Institute of Technology Jaipur, JLN Marg, Jaipur 302017, India, e-mail: rkvyas2@gmail.com

Ajay Sujan: Department of Chemical Engineering, Malaviya National Institute of Technology Jaipur, JLN Marg, Jaipur 302017, India

Kelkar and Shah 1985, Haque et al. 1986, Pradhan et al. 1993, Fransolet et al. 2005, Esmaeili et al. 2015).

Joshi et al. (1998) presented a thorough and extensive review covering different aspects dealing with design and operating parameters that influence gas holdup in bubble column reactors. Review on gas holdup by Joshi et al. (1998) is a general review and does not focus on non-Newtonian liquids. Moreover, a recent review by Leonard et al. (2015) limited their study only for high-pressure and high-temperature operation of bubble column reactors. Thus, reviews covering bubble columns with non-Newtonian systems have not received adequate attention. Bubble columns with viscous non-Newtonian systems present typical behavior in contrast to their Newtonian counterparts due to high viscosity and difference in properties such as effective viscosity and elasticity and thus require exclusive treatment due to following reasons: (i) non-Newtonian systems exhibit lower gas holdup than Newtonian systems under identical conditions of operation, in general. (ii) At relatively lower gas velocities, non-Newtonian systems attain the heterogeneous regime producing higher fraction of larger bubbles resulting in lower gas holdup. (iii) Effective viscosity is to be used in case of non-Newtonian systems as viscosity varies with shear rate. (iv) With higher effective

viscosity, both number of bubbles and coalescence of bubbles increase resulting in lower residence time and lower gas holdup. (v) Unlike Newtonian liquids, where the drag force is not strong enough to increase the coalescence rate of bubbles, smaller bubbles have a lower rise velocity resulting in higher gas holdup; in non-Newtonian liquids, higher drag force promotes bubble coalescence leading to the generation of larger bubbles at a faster rate. (vi) Coalescence of bubbles in viscous non-Newtonian systems leads to a decrease in the effective interfacial area resulting in a decrease in gas holdup. Besides, various shapes of bubbles appear in non-Newtonian systems because of higher surface tension, inertial forces, viscous drag and buoyancy together with complex rheological properties. In non-Newtonian systems, gas holdup in the bubble regime also strongly depends on coalescence tendency of bubbles.

To date, no review has specifically covered non-Newtonian systems and their properties in detail. Considering the growing use of non-Newtonian liquids in bubble columns with different applications, a comprehensive review is needed. Therefore, an attempt has been made in this review to present and critically analyze available empirical correlations for non-Newtonian systems along with their specific range of applications. The factors

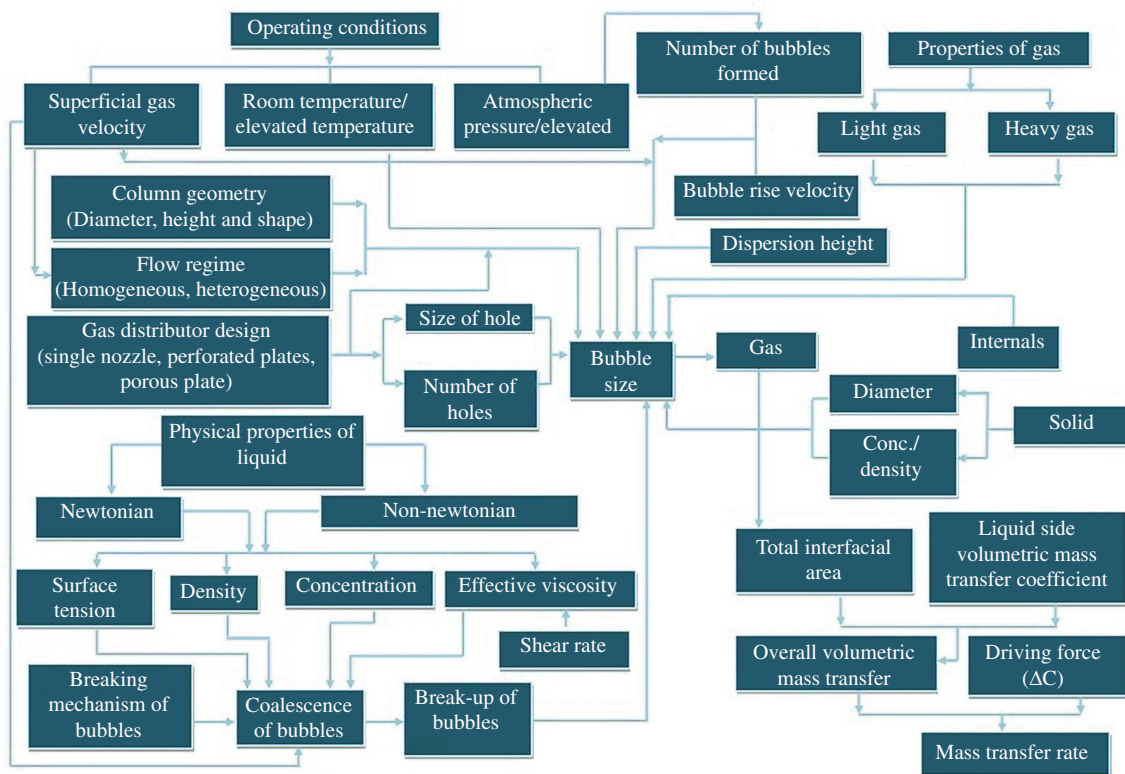


Figure 1: Inter-relationships between various factors affecting gas holdup and mass transfer in a bubble column.

affecting gas holdup such as rheological and physical properties, superficial gas velocity, column geometry, sparger geometry, internals, applications under elevated pressures, bubble characteristics, and flow regime are discussed in detail. A comparison of correlations based on regression analysis reported by the authors has also been included. Furthermore, volume occupied by tiny gas bubbles, which constitute additional effective gas-liquid interfacial area, is often not accounted for well while estimating gas holdup. Research findings on tiny bubbles along with gas holdup contribution of tiny bubbles reported in the literature have also been reviewed.

Additionally, the relative importance of parameters such as flow behavior index, consistency index, column diameter, gas flow rate and the density of aqueous CMC solution on gas holdup has been quantified using an artificial neural network (ANN) and Garson's algorithm. This underlines the relative significance of these parameters for gas holdup during the operation of the bubble column. Furthermore, detailed perspectives of future research covering various areas such as operating conditions, column geometry, physical properties, modeling and simulation, rheological properties, flow regime, bubble characteristics, sparger geometry and other miscellaneous areas are discussed in detail. Inter-relationships of factors affecting gas holdup and mass transfer in a bubble column are shown in Figure 1.

2 Empirical correlations for gas holdup and critical remarks

Numerous studies on gas holdup have been performed to investigate the hydrodynamic behavior of bubbles for proper design and scale-up of bubble column. Most of these studies have been done on laboratory-scale equipment with various gas-liquids-solid systems. Correlations for predicting gas holdup for viscous non-Newtonian systems are presented in Table 1.

In general, an empirical correlation can describe gas holdup data only within a limited range of system properties and working conditions. It is difficult to select the right empirical correlation for hydrodynamic studies applicable to large systems because all the available correlations are based on laboratory-scale columns. Predictions from correlations are based on the operating conditions (pressure, temperature and gas/liquid flow rate), physical properties of gas/liquid, and specification of the experimental setup like column geometry, sparger type and size. It is not yet certain whether these results can be extrapolated with the

same accuracy to other column geometries operated with other gases and liquids. Some researchers use the application of dimensional analysis and curve fitting techniques to develop empirical correlation for gas holdup in bubble columns. Findings of various studies on the effects of these factors are presented and critically examined. The limitation and critical remarks on gas holdup in non-Newtonian systems are presented in Table 2.

It may be observed from Table 2 that effective viscosity of the liquid has been ignored in some of the correlations (Deckwer et al. 1982, Vatai and Tekic 1989), whereas it is an established fact that the viscosity of a liquid affects gas holdup as demonstrated clearly later in Table 13. Some of the correlations are applicable only to the churn turbulent flow regime (Haque et al. 1986, Ryu et al. 1993), and such correlations have limited applications.

3 Effects of various parameters on gas holdup

Considering the fundamentals of hydrodynamics of bubbles and the empirical correlations for gas holdup, it is obvious that gas holdup is affected by rheological properties which depend on shear rate in the case of non-Newtonian systems. The important parameters required for successful design and scale up is the accurate estimation of gas holdup, which is strongly influenced by the rheological properties of non-Newtonian liquids, bubble characteristics (bubble size and shape, bubble rise velocity and pattern of bubble movement), operating parameters, column geometry, sparger geometry and the presence of internals or floating bubble breakers. In recent years, numerous researchers have focused their studies on the design and scale-up of bubble columns due to the complex nature of hydrodynamics and the underlying parameters that affect gas holdup. The flow regime (bubble flow regime, churn turbulent regime, or slug flow regime) also has a significant effect on the gas holdup and the performance of bubble columns. Details of all these properties/parameters have been discussed in the following subsection.

3.1 Rheological models

A rheological model may be considered for application, if it can provide reliable rheological data required for the system. A number of mathematical expressions of varying complexity and forms have been proposed in the literature

Table 1: Correlations for overall gas holdup for viscous non-Newtonian systems.

System (gas/liquid/solids)	Empirical correlation(s) and errors analysis	Range of parameters	Reference
Air/CMC solution	For the heterogeneous regime: $\varepsilon_G = 0.225 u_G^{0.532} \mu_L^{-0.146}$ For the slug regime: $\varepsilon_G = 0.239 u_G^{0.634} D_c^{-0.5}$ Overall error: 5%	u_G (m/s): 0.04–0.24 ρ_L (kg/m ³): 1010–1249 μ_L (Pa · s): 0.000423–0.246 μ_{eff} (Pa · s): 0.023–0.23 D_c (m) ≤ 0.3	Godbole et al. (1982)
Air/CMC/salt solution	For sintered plate in BC-I (10.2-cm diameter): $\varepsilon_G = 9.08 \times 10^{-2} u_G^{0.85}$ For 2-mm perforated plate in BC-II (14-cm diameter): $\varepsilon_G = 2.58 \times 10^{-2} u_G^{0.876}$ For both sintered and perforated plate in BC-II (14-cm diameter): $\varepsilon_G = 3.22 \times 10^{-2} u_G^{0.674}$ For the slug flow regime in BC-I (10.2 cm): $\varepsilon_G = 4.04 \times 10^{-2} u_G^{0.627}$	ρ_L (kg/m ³): 1091–1094 u_G (m/s): up to 0.18 u_G (m/s): 0.006 D_c (cm): 10.2, 14 CMC conc.: 0–1.8 wt%	Schumpe and Deckwer (1982)
Air/CMC solution	$\varepsilon_G = 0.0265 u_G^{0.82}$ Mean deviation: <2%	D_c (cm): 14 u_G (cm/s): 0.2 CMC conc.: 0.7–1.6 wt% Perforated plate (PP): 73 holes of 1-mm diameter Perforated plate (PP): 19 holes of 2-mm diameter, sintered plate (SP): 0.2-mm pore diameter, rubber plate (RP): about 1000 pricks Temperature (°C): 20 n : 0.91–0.82 k (Pa · s ^{n}): 0.04–0.23	Deckwer et al. (1982)
Air/CMC solution with addition of surfactant/ Na ₂ SO ₄ or Na ₂ SO ₃	$\varepsilon_G = K u_G^{0.6} \mu_{\text{eff}}^{-0.19}$ $K = 0.207$ for CMC solution with addition of surfactant $K = 0.255$ for CMC solution with addition of 0.8 kmol/m ³ Na ₂ SO ₄ or Na ₂ SO ₃ Mean deviation: ±4%	u_G (m/s): 0.03–0.25 ρ_L (kg/m ³): 1000–1096 μ_L (Pa · s): 0.020–0.1 σ_L (N/m): 0.0676–0.0746	Godbole et al. (1984)
Air/CMC solution	$\varepsilon_G = 0.528 u_G^{0.635}$ Average error: 4.3%	u_G (m/s): 0.01–0.410 ρ_L (kg/m ³): 987–999 μ_L (Pa · s): 0.03–0.115 σ_L (N/m): 0.068	Devine et al. (1985)
Air/CMC solution	$\varepsilon_G = u_G / C_0 (u_G + u_L) + C_1$ Values of C_0 and C_1 depend on CMC concentration	CMC conc. (ppm): 50–2300 u_G (m/s): 0.03–0.3 u_L (m/s): 0.03–0.1 D_c (m): 0.154	Kelkar and Shah (1985)
Air/CMC solution	Valid for the heterogeneous regime $\varepsilon_G = 0.171 u_G^{0.6} \mu_{\text{eff}}^{-0.22} D_c^{-0.15}$ Standard deviation: 0.01	D_c (m): 0.10–1.0 d_0 (m): 0.0003–0.002 u_G (m/s): 0.01–0.240 ρ_L (kg/m ³): 1000–1009 μ_L (Pa · s): 0.00035–0.012	Haque et al. (1986)
Air/CMC solution, glycerin + SAG	$\varepsilon_G = 0.24 n^{-0.6} \left(\frac{g D_c^3 \rho_L^2}{\mu_a^2} \right)^{0.07} \left(\frac{u_G}{\sqrt{g D_c}} \right)^{(0.84-0.14n)}$ Mean deviation: 31.4%	u_G (m/s): 0.008–0.285 D_c (m): 0.14–0.35 n : 0.28–1 μ_L (Pa · s): 0.001–1.22	Kawase and Moo-Young (1986)
Air/CMC, carboxypolymethylene, polyacrylamide	$\varepsilon_G = 1.07 n^{2/3} \left(\frac{u_G^2}{g D_c} \right)^{1/3}$	ρ_L (kg/m ³): 991–1009 n : 0.504–1.0 k (Pa · s ^{n}): 0.00090–1.65	Kawase and Moo-Young (1987)

Table 1 (continued)

System (gas/liquid/solids)	Empirical correlation(s) and errors analysis	Range of parameters	Reference
Air/ligroin, tetralin/ aluminium oxide, PVC, PE	$\varepsilon_G = F u_G^{0.77} \mu_{\text{eff}}^{-0.21}$ $F \begin{cases} 0.35 \text{ for tetralin} \\ 0.31 \text{ for ligroin} \end{cases}$	D_C (m): 0.095 Temperature (°C): 20 ± 1 ρ_s (kg/m ³): 940–3180 d_s (μm): 21.6–369 n : 0.40–1.0 k (10 ³ Pa · s ⁿ): 0.55–1010 μ_L (mPa · s): 0.54 and 2.08 ρ_L (kg/m ³): 729 (tetralin) and 968 (ligroin) Single-tube sparger: 3-mm hole diameter	Ozturk and Schumpe (1987)
Air/CMC, glycerol, PAA, and xanthan gum	$\varepsilon_G = 0.2 \left(\frac{g D_C^2 \rho_L}{\sigma_L} \right)^{-0.13} \left(\frac{g D_C^3 \rho_L^2}{\mu_{\text{eff}}^2} \right)^{0.11} \left(\frac{u_G}{\sqrt{g D_C}} \right)^{0.54}$ Average error: 8.1%	ρ_L (kg/m ³): 999–1248 n : 0.180–1.0 k (10 ⁻³ Pa · s ⁿ): 15.9–9780 σ_L (10 ⁻³ N/m): 49.5–70.7 D_L (10 ⁻⁹ m ² · s): 0.36–2.1	Schumpe and Deckwer (1987b)
Air, air + CO ₂ /CMC solution	$\varepsilon_G = 0.19 n^{-0.6} \left(\frac{g D_C^3 \rho_L^2}{\mu_a^2} \right)^{0.07} \left(\frac{u_G}{\sqrt{g D_C}} \right)^{(0.84-0.14n)}$ Mean deviation: 10.6%	u_G (m/s): 0.002–0.1 ρ_L (kg/m ³): 997–1012 $\sigma_L \times 10^3$ (N/m): 67–72 $k \times 10^3$ (Pa · s ⁿ): 1.9–66.8 n : 0.81–1.0	Vatai and Tekic (1989)
Air/CMC solution	$\varepsilon_G = 0.331 u_G^{0.663} \mu_{\text{eff}}^{-0.189} (1 + \varepsilon_F)^{1.872}$ R^2 : 0.941	D_C (m): 0.15 H_L (m): 2 Temperature (°C): 20 ± 0.5 $u_G \times 10^2$ (m/s): 2.16–9.5 $u_L \times 10^2$ (m/s): 3.5–10.5 MOC of bubble breaker: acrylic 0.019 m long, 0.015-m diameter	Kang et al. (1990)
Air/CMC solution	$\varepsilon_G = 0.107 \times 10^{-4} \left(\frac{D_C u_G \rho_G}{\mu_G} \right)^{1.09} \left(\frac{g D_C^3}{\nu_{\text{eff}}^2} \right)^{0.096} \left(\frac{d}{D_C} \right)^{-0.19}$ R^2 : 0.98 and standard deviation: 0.015	u_G (m/s): 0.01–0.07 ρ_L (kg/m ³): 997–998 C_{CMC} (wt%): 0–0.30 d_o (mm): 0.3 Number of holes = 51 σ_L (N/m): 0.07053–0.072 n (-): 0.809–1.0 k (dyne · s ⁿ /cm ³): 0.075–0.01	Mok et al. (1990)
Air/water, ethanol, acetone, CMC/glass beads	For the bubbly flow regime: $\varepsilon_G = 0.014 u_G^{0.737} u_L^{-0.182} \sigma^{-0.366} \mu_{\text{eff}}^{-0.062}$ R^2 : 0.96 For the slug or churn turbulent flow regime: $\varepsilon_G = 0.017 u_G^{0.683} u_L^{-0.103} \sigma^{-0.219} \mu_{\text{eff}}^{-0.491}$ R^2 : 0.96 For the bubbly disintegrating regime: $\varepsilon_G = 4.83 \times 10^{-3} u_G^{0.667} u_L^{-0.087} d_p^{0.196} \sigma^{-0.721} \mu_{\text{eff}}^{-0.024}$ R^2 : 0.93 For the bubble coalescing or slug flow regime: $\varepsilon_G = 6.48 \times 10^{-3} u_G^{0.74} u_L^{-0.068} d_p^{0.052} \sigma^{-0.692} \mu_{\text{eff}}^{-0.105}$ R^2 : 0.90	u_G (m/s): 0.01–0.20 u_L (m/s): 0.02–0.12 σ_L (mN/m): 42.6–72.4 n (-): 0.595–1.0 $k \times 10_3 = 1.0$ –214.2 D_C (m): 0.142 Perforated plate for liquid: 141 holes of 3-mm diameter Perforated plate for gas: 26 holes of 1-mm diameter u_G (m/s): 0.01–0.20 u_L (m/s): 0.02–0.12 d_p (mm): 1.0–8.0 ρ_s (kg/m ³): 2500 σ_L (mN/m): 42.6–72.4 n : 0.595–1.0 $k \times 10^3 = 1.0$ –214.2	Lee et al. (1993)

Table 1 (continued)

System (gas/liquid/solids)	Empirical correlation(s) and errors analysis	Range of parameters	Reference
Air/CMC	For the bubbly flow regime: $\varepsilon_G = 12.0 \left(\frac{g D_c^3 \rho_L^2}{\mu_a^2} \right)^{0.025} \left(\frac{u_G}{\sqrt{g D_c}} \right)^{1.220}$ $R^2: 0.98$ and standard deviation: 0.02 For the slug or Churn turbulent flow regime: $\varepsilon_G = 0.922 \left(\frac{g D_c^3 \rho_L^2}{\mu_a^2} \right)^{0.365} \left(\frac{u_G}{\sqrt{g D_c}} \right)^{-0.222}$ $R^2: 0.97$ and standard deviation: 0.03	u_G (m/s): 0.009–0.098 CMC conc.: 0.7 wt% D_c (m): 0.115 H_c (m): 2.0 Radial gas sparger: diameter: 0.038 m height: 0.15 m pore size: 5 μ m ρ_L (kg/m ³): 1001–1002 σ_L (N/m) $\times 10^3$: 64–65	Ryu et al. (1993)
Air/CMC	For the homogeneous regime: $\varepsilon_G = 4.1 u_G^{1.25} u_L^{0.15} S^{-0.26} p^{-0.28} d_0^{-0.17} \mu_a^{0.03}$ For the heterogeneous regime: $\varepsilon_G = 0.11 u_G^{0.86} u_L^{0.1} S^{-0.1} p^{-0.28} d_0^{-0.52} \mu_a^{-0.04}$	u_G (m/s): 0.0042–0.116 u_L (m/s): 0.007–0.012 D_c (m): 0.098 and 0.154 Height of liquid (m): 1.8 and 1.1 Perforated plate diameter d (m): 0.003–0.012 ρ_L (kg/m ³): 995–998 σ_L (N/m): 71 and 72	Vinaya and Varma (1995)
Air/CMC	$\varepsilon_G = k \times 10^{-2.1} \left(\frac{D_c u_G \rho_G}{\mu_L} \right)$ $R^2: 0.910$ k = correlation dimension	u_G (m/s): 0.02–0.2 P (bar): 1–6 D_c (m): 0.152 H_c (m): 2.0 μ_L (Pa · s): 0.001–0.038	Kang et al. (1999)
Air/CMC	For single-point sparger (25-mm diameter): $\varepsilon_G = 0.692 u_G^{0.515} \left(\frac{H}{D_c} \right)^{0.0677}$ $R^2: 0.94$ For single-point sparger (1-mm and 3-mm diameter): $\varepsilon_G = 0.6841 u_G^{0.419} \left(\frac{H}{D_c} \right)^{-0.14}$ $R^2: 0.92$	u_G (m/s): 0.06–0.3 D_c (mm): 385 Three perforated plate sparger OA: 0.42% Hole diameter: 1, 3, and 25 mm H/D_c : 0.259, 3, and 5 Power law index, n : 0.67 Consistency index, k : 0.102 Pa · s ^{n}	Veera and Joshi (2000)
O ₂ /distilled water, sucrose, SOKRAT, water + OCENOL, SOKRAT + OCENOL	$\varepsilon_G = 1.92 \times 10^6 u_G^{0.73} \left(\frac{\mu_L}{\rho_L} \right)^{0.15} \left(\frac{\sigma_L}{\rho_L} \right)^{1.3}$ Relative error: 8.0%	μ_L (mPa · s): 0.7–25.6 ρ_L (kg/m ³): 995–1270 σ_L (m): 33.5–65.4	Elgozali et al. (2002)
Air/CMC, CMC + PPG	$\varepsilon_G = x_1 (N)^{x_2} (u_G)^{x_3}$ $x_1 \begin{cases} 0.071 \text{ for DT} \\ 0.112 \text{ for CBBDT} \\ 0.153 \text{ for Scaba} \end{cases} x_2 \begin{cases} 0.0712 \text{ for DT} \\ 0.68 \text{ for CBBDT} \\ 0.73 \text{ for Scaba} \end{cases} x_3 \begin{cases} 0.36 \text{ for DT} \\ 0.44 \text{ for CBBDT} \\ 0.53 \text{ for Scaba} \end{cases}$ $R^2: 0.99$ (for DT, CBBDT, and Scaba) $\varepsilon_G = x_1 (P_g / V_L)^{x_2} (u_G)^{x_3}$ $x_1 \begin{cases} 0.35 \text{ for DT} \\ 0.53 \text{ for CBBDT} \\ 0.8 \text{ for Scaba} \end{cases} x_2 \begin{cases} 0.19 \text{ for DT} \\ 0.19 \text{ for CBBDT} \\ 0.22 \text{ for Scaba} \end{cases} x_3 \begin{cases} 0.4 \text{ for DT} \\ 0.49 \text{ for CBBDT} \\ 0.57 \text{ for Scaba} \end{cases}$ $R^2: 0.99$ (for DT, CBBDT, and Scaba)	D_c (m): 0.6 u_G (m/s): 0.01–0.006 No. of baffles: 4 Type of impellers: DT, CBBDT, Scaba6SRGT N (rps): 3–9 Ring sparger diameter: 0.16 m Average values of $n=0.57$ and $k=3.74$	Khare and Niranjana (2002)

Table 1 (continued)

System (gas/liquid/solids)	Empirical correlation(s) and errors analysis	Range of parameters	Reference
Air/xanthan solution	$\varepsilon_G = 0.26 u_G^{0.54} \mu_{\text{eff}}^{-0.147}$ Average deviation: $\pm 10\%$	μ_L (Pa · s): 0.001–0.0625 u_G (m/s) up to 0.15 D_c (m): 0.24 Conc (g/L) = 1–5	Fransol et al. (2005)
Air/aqueous CMC, aqueous propylene glycol	For both Newtonian and non-Newtonian liquids: $\varepsilon_G (\mu_L \text{ or } \mu_{\text{eff}})^{0.13} D_c^{0.15} (H_c / D_c)^{0.2} = u_G / (0.65 + 2.5 u_G^{0.666})$ Average deviation: $\pm 11.5\%$	D_c (m): 0.145 H_c (m): 2.9 Single nozzle with different diameter: 0.7, 1.0, and 1.3 mm	Ghosh and Upadhyay (2007)
Air/CMC and xanthan solution	For batch system: $\varepsilon_G = 0.0524 u_G^{0.623} \mu_{\text{eff}}^{-0.0531}$ For two-phase flow system: $\varepsilon_G = 0.0485 u_G^{0.666} \mu_{\text{eff}}^{-0.1181}$	D_c (m): 0.14 H_c (m): 2.62 d_o (mm): 1.2 Number of holes: 43 u_G (m/s) = 0.018–0.252 u_L (m/s) = 0–0.248 T (°C): ambient C_{CMC} (wt%) = 0.2–0.85 C_{xanthane} (wt%) = 0.1–0.4 n = 0.48–0.81 k = 0.30–0.505	Lakota (2007)
Air/aqueous solution of glycerin + xanthan gum	$\varepsilon_G = 2.2 \left[\left(\frac{u_G^2}{D_c g} \right)^{1.07} \left(\frac{D_c^3 \rho_L^2 g}{\mu_L^2} \right)^{0.84} \left(\frac{D_c^2 \rho_L g}{\sigma_L} \right)^{0.19} \left(\frac{d_s}{D_c} \right)^{1.16} \left(\frac{d_o}{d_s} \right)^{2.86} \right]^{0.264}$ Average deviation: $\pm 10\%$	D_c (cm): 9.0 H_c (m): 1.5 Porous disc diameter: 4.5 cm pore size: 40 μm T (°C): ambient u_G (m/s) up to 0.005 d_s / D_c : 0.3–0.6 ρ_L (kg/m ³): 1010–1180 σ_L (N/m): 0.068–0.070	Anastasiou et al. (2013)
Air/CMC	For tapered bubble column $\varepsilon_G = 3.857 \times 10^{-4} \left(\frac{u_G D_c \rho_G}{\mu_G} \right)^{0.743 \pm 0.017} \left(\frac{g \mu_{\text{eff}}^4}{\rho_L \sigma_L^3} \right)^{-0.009 \pm 0.003} \left(\frac{H_o}{D_c} \right)^{-0.565 \pm 0.038} \left(\frac{d_o}{D_c} \right)^{0.149 \pm 0.063} \theta^{0.706 \pm 0.028}$ R^2 : 0.966	H_c (m): 1.83 Top plate area (m ²): 0.0762 \times 0.0762 for TB1, 0.1016 \times 0.1016 for TB2 Bottom plate area (m ²): 0.0508 \times 0.0508 for TB1 and TB2 Taper angle (deg.): 0.86 and 0.44 Orifice diameter: 0.00277, 0.00357, and 0.00436 m Number of orifices: 50 Pitch: square Equivalent diameter, D_c (m) 0.0605–0.0614 for TB1 and 0.0692–0.0710 for TB2	Jana et al. (2014a,b)
Air/water, aqueous glycerin solution with small amount (0.35 g/L) of xanthan gum	$\varepsilon_G = 15.64 \left[\left(\frac{u_G}{\sqrt{g D_c}} \right)^{1.77} \left(\frac{D_c^3 \rho_L^2 g}{\mu_{\text{eff}}^2} \right)^{0.85} \left(\frac{d_{32}^2 \rho_L g}{\sigma_L} \right)^{0.64} \left(\frac{d_s}{D_c} \right)^{4.27} \left(\frac{d_o}{d_s} \right)^{0.02} \right]^{-0.19}$ Average deviation: $\pm 20\%$	ρ_L (kg/m ³): 998–1180 σ_L (mN/m): 31–72 D_c (cm): 9 H_c (cm): 150 Porous disc: 4.5 and 9.0-cm diameter A single nozzle: 1-cm diameter Pore size 40 μm u_G (m/s) up to 0.04	Passos et al. (2015)

Table 1 (continued)

System (gas/liquid/solids)	Empirical correlation(s) and errors analysis	Range of parameters	Reference
Air/CMC and xanthan Gum	$\varepsilon_G = 0.13 \left(\frac{gD_c^3 \rho_L^2}{\mu_a^2} \right)^{0.14} \left(\frac{u_G}{\sqrt{gD_c}} \right)^{0.73} e^{-0.1 \left(1 - \frac{G'}{G''} \right)} \left(\frac{\rho_g}{\rho_L} \right)^{0.05}$ $\varepsilon_{G,trans} = 0.13 \left(\frac{gD_c^3 \rho_L^2}{\mu_a^2} \right)^{0.14} \left(\frac{u_{G,trans}}{\sqrt{gD_c}} \right)^{0.73} e^{-0.1 \left(1 - \frac{G'}{G''} \right)} \left(\frac{\rho_g}{\rho_L} \right)^{0.05}$ $\varepsilon_{G,trans} = 0.0023 \left(\frac{gD_c^3 \rho_L^2}{\mu_a^2} \right)^{0.35} \left(\frac{d_{b,trans}}{D_c} \right)^{1.38} e^{-0.24 \left(1 - \frac{G'}{G''} \right)} \left(\frac{\rho_g}{\rho_L} \right)^{0.05}$	D_c (m): 0.15 H_c (m): 4.8 Static liquid height: 1.05 m T (°C) up to 300 P (MPa) up to 3 u_G (cm/s): 1–35 Distributor-perforated plate Plate thickness: 0.006 m Orifice arrangement: 0.027 m spaced square pitch Orifice diameter: 0.001 m Number of orifices: 24 Orifice density: 1316 (orifices/m ²)	Esmaeili et al. (2016)

(Chhabra 2006). In this article, only two models, namely, the power law model and the Carreau model, are briefly discussed with their positive and negative points.

3.1.1 Power law model

Time-independent non-Newtonian shear-thinning fluids are characterized by a decrease of the apparent viscosity with an increase of the shear rate. At very low and at very high shear rates, most shear-thinning solutions exhibit Newtonian behavior, that is, shear stress is a linear function of the shear rate. The apparent viscosities at very low and high shear rates are known as the zero shear viscosity and infinite shear viscosity, respectively. The rheological behavior of non-Newtonian (pseudoplastic) solution is described by the power law model of Ostwald-de Waele, which can be expressed as:

$$\mu_{\text{eff}} = k\gamma^{n-1} \quad (1)$$

where μ_{eff} = effective (apparent) fluid viscosity (Pa · s)

k = consistency index (Pa · s ^{n})

γ = shear rate (s⁻¹)

$$n \text{ (power law index)} = \begin{cases} n < 1, \text{ the fluid exhibits for shear-thinning (pseudoplastic) properties} \\ n = 0, \text{ the fluid shows Newtonian behavior} \\ n > 1, \text{ the fluid shows shear-thickening behavior.} \end{cases}$$

In this model, k and n are two empirical curve fitting parameters and are known as the fluid consistency index and the flow behavior index, respectively. For a shear-thinning fluid, the index may have any value between 0 and 1. The smaller the value of n , the greater is the degree

of shear thinning, the higher consistency index of solution and, the higher will be the apparent viscosity. Generally, it only applies over a limited range of shear rates, and therefore, the fitted values of k and n will depend on the range of shear rates considered. Furthermore, it does not correctly estimate the zero and infinite shear viscosities.

The effective viscosity of a non-Newtonian liquid decreases with an increase in shear rate, and higher shear rates are attained at higher gas velocities. The precise quantification of the shear rate of a non-Newtonian liquid in a bubble column is difficult because of the difficulty in exactly determining the shear rate. There are two interfaces in a bubble column; the gas-liquid interface of bubbles and the solid-liquid interface near the column wall (Joshi 1980). The flow pattern of non-Newtonian liquids is very complex. The shear rate near the column wall may be defined on the basis of average liquid circulation velocity and the column diameter. The correct measurement of circulation velocity is very difficult because it depends on superficial gas velocity, bubble rise velocity and the fractional gas holdup (Kawase and Moo-Young 1986). Hence, there is a need to accurately quantify the shear rate of a non-Newtonian fluid for its precise contribution to apparent viscosity.

Generally, flow encounters lower resistance at higher shear rates. It is well known that the molecular structure of CMC is composed of long molecular chains which are entangled and looping. These molecular chains have irregular internal order, which impart high resistance to

Table 2: Limitation and critical remarks on gas holdup correlations.

Findings/applicability	Limitation/critical remarks	Reference
Gas holdup is independent of the sparger type in the slug flow regime In the homogeneous flow regime, gas holdup increases with CMC concentration (up to 0.8 wt%) due to decreases in rise velocity of the bubble For CMC ≥ 0.8 wt%, gas holdup decreases with viscosity due to reduction in the number of small bubbles Small bubble gas holdup decreases with increases in viscosity in the slug flow regime Observed very small bubbles less than 1 mm in diameter in the slug flow regime	Extent of reduction in fraction of small bubble not mentioned when CMC concentration increased by 0.8% Correlations are applicable for both the bubbly and slug flow regimes	Schumpe and Deckwer (1982)
Flow behavior index varied from 0.495 to 1.0 and, hence, covered a wider range of non-Newtonian (pseudoplastic) solutions Lower gas holdup found in the highly viscous pseudoplastic CMC solutions viscosity > 0.02 Pa \cdot s	Correlations are valid for the churn turbulent and slug flow regimes	Godbole et al. (1982)
In the slug flow regime, gas holdup remains unaffected by viscosity of the liquid No significant effect found on gas holdup in CMC concentrations ranging from 0.7 to 1.6 in a bubble column equipped with perforated plate sparger with 1-mm holes	A proposed empirical correlation is suitable only for the slug flow regime	Deckwer et al. (1982)
Lower gas holdup found in both churn turbulent and slug flow regimes Gas holdup in large bubbles are unaffected by the presence of surfactant With increasing surfactant concentration, gas holdup increases sharply due to the presence of very small bubbles ($d_b < 1$ mm)	Correlation is suitable only for the design of fermentation tanks	Godbole et al. (1984)
Liquid velocity and apparent viscosity have no significant effect on the gas holdup Correlation for gas holdup depends only on gas velocity and is independent of apparent viscosity and column diameter	Correlation is suitable only for concurrent upflow bubble column	Devine et al. (1985)
Gas holdup increases with an increase in gas velocity but remains independent of liquid velocity Gas holdup decreases with an increase in apparent viscosity but becomes constant above 0.2 Pa \cdot s	Applicability of correlation limited only to churn turbulent flow regime only	Kelkar and Shah (1985)
Gas holdup unaffected by the sparger design in the heterogeneous and slug flow regimes Higher gas holdup values for different CMC concentrations for $H/D < 3$, and gas holdup values are independent when $H/D > 3$ Gas holdup decreases with increasing effective viscosity in the churn turbulent flow regime Gas holdup decreases with an increase in column diameter in the churn turbulent flow regime	Correlation is valid only for the churn turbulent regime	Haque et al. (1986)
Holdup number due to very small bubbles increases at lower surface tension, which is contrary to unusual trend Sparger with small openings ($d_0 \geq 0.001$) provides higher gas holdups	Correlations are valid for the heterogeneous regime only	Schumpe and Deckwer (1987a,b)
Formation of large spherical cap bubbles was found in highly viscous non-Newtonian liquid Gas holdup depends on column diameter	The theoretical model is versatile and valid for gas holdup in Newtonian as well as non-Newtonian fluids	Kawase and Moo-Young (1987)
Gas holdup decreases with an increase in the apparent viscosity in the churn turbulent flow regime Gas holdup increases with an increase in the apparent viscosity in small-diameter columns	Effect of gas properties (e.g. density) on gas holdup not considered in the proposed correlation	Vatai and Tekic (1989)
Gas holdup increases with an increase in volume fraction of bubble breakers in the column	Correlation is suitable only for floating bubble breakers in the bubble column	Kang et al. (1990)
Gas holdup increases with increasing gas velocity, while it decreases with increasing CMC concentration up to 0.3 wt% Gas holdup in the radial direction is nearly uniform at low gas velocity and low CMC concentration	Correlation is suitable only for perforated plate with 0.3-mm hole diameter	Mok et al. (1990)

Table 2 (continued)

Findings/applicability	Limitation/critical remarks	Reference
Gas holdup increases with an increase in gas velocity in the bubbly flow regime, decreases in the churn turbulent flow regime, and increases again in the slug flow regime In the churn turbulent flow regime, gas holdup decreases with an increase in apparent viscosity, whereas it is independent of apparent viscosity in the bubbly flow regime	Correlations are suitable only for radial gas sparger and applicable for the bubbly and churn turbulent flow regimes only	Ryu et al. (1993)
Gas holdup decreases with an increase in effective viscosity due to the increase in bubble size in the bed Gas holdup increases with an increase in the surfactant concentration due to the increase in bubble coalescence with increasing liquid surface tension	Correlation is suitable only for three-phase fluidized beds containing 1.7-mm glass beads and in both the bubbly and churn turbulent flow regimes	Lee et al. (1993)
Gas holdup decreases with an increase in plate perforation diameter due to increases in bubble size Increase in the spacing between adjoining plates increases the coalescence of the bubbles and reduces gas holdup Gas holdup decreases with an increase in consistency index in the churn turbulent flow regime, while it increases marginally in the bubble flow regime	Correlations are valid for the bubbly and churn turbulent flow regimes only	Vinaya and Varma (1995)
Gas holdup is higher when the bubbles are distributed symmetrically and is lowest when the bubbles are distributed asymmetrically at the distributor	Correlation is valid only for pressurized bubble column	Kang et al. (1999)
Gas holdup in the CMC solution increases with impeller speed at different gas velocities For any impeller, the gas holdup in the PPG containing the CMC solution is significantly higher than in the pure CMC solution Contribution of tiny bubbles in gas holdup is in the range of 35%–80% of total gas holdup in the PPG + CMC solution, whereas in the CMC solution, it accounts for only 15%–45%	Correlation is suitable only for stirred bubble column equipped with disc turbine and modified disc impellers	Khare and Niranjana (2002)
Gas holdup in the bubble column increases with an increase in viscosity and surface tension of the liquid	Correlation is suitable for upflow ejector-type gas distributor only	Elgozali et al. (2002)
Average gas holdup decreases with an increase in ratio of dispersion height to diameter for multipoint spargers	Free area of sparger not varied and fixed at 0.42%.	Veera and Joshi (2000)
Gas holdup values decrease with an increase in the liquid viscosity With xanthan solutions, holdup fraction of large bubbles is larger than that of small bubbles	Correlation is suitable only for perforated sparger with 1-mm hole diameter Apparent viscosity measured at a single shear rate of 100 s ⁻¹ only. Shear rates could have been varied	Fransolet et al. (2005)
Gas holdup increases with an increase in superficial gas velocity for various sizes of spargers The liquid height-to-column diameter ratio and sparger diameter have no influence on gas holdup Gas holdup decreases with an increase in effective viscosity of the liquid	Correlation is valid for large column diameters (0.145 to 0.38 m) only	Ghosh and Upadhyay (2007)
Gas holdup increases with an increase in gas superficial velocity and decreases with a decrease in effective liquid viscosity Higher gas holdup is found in the liquid batch as compared with the two-phase flow system	Correlation is only suitable for the batch and two-phase flow systems	Lakota (2007)
Gas holdup increases with an increase in superficial gas velocity Larger bubble size is produced in viscous liquids, resulting in lower gas holdup CFD simulation results were reported to be in good agreement with the proposed empirical correlations for a wide range of sparger-to-column diameter ratio (0.3–0.6)	Correlation is valid for porous sparger (pore size: 40 μm) only	Anastasiou et al. (2013)

Table 2 (continued)

Findings/applicability	Limitation/critical remarks	Reference
Higher gas holdup was found at the lower taper angle of the bubble column Gas holdup decreases with an increase in CMC concentration Gas holdup increases with a decrease in orifice size and liquid height	Correlation is suitable only for tapered bubble columns	Jana et al. (2014a)
Gas holdup increases with increasing surfactant concentration due to the lowering of surface tension At any superficial gas velocity, gas holdup increases with an increase in sparger size	Correlation is suitable only for small-diameter (9 cm) bubble columns equipped with fine pore spargers (40 μm)	Passos et al. (2015)
Gas holdup increases with both operating pressure and elasticity of the liquid phase Transition from homogeneous to heterogeneous flow regime was delayed at higher pressure	Correlation is applicable only to elevated pressure system	Esmaili et al. (2016)

flow, thereby exhibiting higher viscosity. At high shear rates, molecular chains present in CMC solutions are disentangled, stretched and reoriented parallel to the driving force in the system. This molecular realignment allows molecules to slip over each other smoothly. The net effect of all this is visible in terms of reduced viscosity of the CMC solutions. The ranges of shear rates which have been used for the estimation of apparent viscosity (effective viscosity) are listed in Table 3.

The power law viscosity model has certain limitations when used in the case of non-Newtonian fluids. Several rheological models have been classified on the basis of pseudoplastic and viscoplastic fluid behaviors (Table 4) that involve two or more adjustable parameters to describe the relationship between viscosity and shear rate of non-Newtonian fluids.

3.1.2 Carreau model

The power law model is a good approximation at high shear rates, but it fails to describe the rheological behavior at very low shear rates, where the power law model predicts viscosity value to infinity incongruently. In spite of these deficiencies, the power law model is still the most widely used in all of rheology-related studies (Nakanoh and Yoshida 1980, Godbole et al. 1982, 1984, Deckwer et al. 1982, Schumpe and Deckwer 1982, Kelkar and Shah 1985, Haque et al. 1986, Haque et al. 1987, Kawase and Moo-Young 1987, Kang et al. 1990, Pradhan et al. 1993, Ryu et al. 1993, Kantak et al. 1995, Ghosh and Upadhyay 2007, Anastasiou et al. 2013). Some typical values of flow behavior index (n) and fluid consistency index (k) are listed in Table 5 for shear-thinning non-Newtonian fluids. In view of the limitations of the power law model, another

viscosity model should be considered from the class of generalized Newtonian fluids, namely, the Carreau rheological model (1968). This model overcomes the limitations of the power law model identified above and appears to be gaining wider acceptance in chemical engineering and technological processes. Because of wider applications, the Carreau model has drawn the attention of many researchers and engineers during the last few years. For a Carreau fluid (shear thinning), the effective viscosity is equal to the zero shear rate viscosity at low shear rate, and it starts decreasing due to the shear-thinning effect only at sufficiently high shear rate. This model can describe shear-thinning behavior over a wide range of shear rates. The apparent viscosity of a Carreau fluid is given by:

$$\text{Carreau model} \quad \frac{\mu - \mu_{\infty}}{\mu_0 - \mu_{\infty}} = [1 + (\lambda\dot{\gamma})^2]^{(n-1)/2}$$

where, n (<1) and λ are two curve fitting parameters. μ_0 is the zero shear rate viscosity, μ_{∞} is the infinite shear rate viscosity and n is the power law index. The parameter λ is a constant with the unit of time, where the reciprocal of the time constant $1/\lambda$ is the critical shear rate at which viscosity begins to decrease. The Carreau model predicts Newtonian fluid behavior $\mu = \mu_0$ when either $n=1$ or λ or both. The Carreau fluids with a fluid index in the range $0 < n < 1$ are commonly referred to as shear-thinning or pseudoplastic fluids, and Carreau fluids with a fluid index in the range $n > 1$ are commonly referred to as shear-thickening or dilatant fluids. In general, the models with a large number of parameters are difficult to apply because it is seldom enough that data are available to allow good model fitting (Garakani et al. 2011). A plot of shear rate versus apparent viscosity for shear-thinning fluids identifying three separate regions is shown in Figure 2.

Table 3: Range of shear rates used and other details for the determination of gas holdup in non-Newtonian liquids.

Shear rate range, s^{-1}	Gas velocity (m/s)	Non-Newtonian liquid	Viscosity (Pa · s)	Instrument used for viscosity measurement	Reference
7–1139	u_g (m/s): up to 0.18	Aq. solution of CMC	μ_L (Pa · s): 0–0.15	Couette Viscometer (Haaka)	Schumpe and Deckwer (1982)
5.1–1022	u_g (m/s): 0.03–0.25	Aq. solution of CMC, CMC + sodium sulfate (0.8 M)	μ_L (Pa · s): 0.01–0.50	Concentric cylinder viscometer (Fann, VG-Meter)	Godbole et al. (1984)
40–600	–	Aq. solution of CMC	–	Coaxial rotating cylinder viscometer	Nakanoh and Yoshida (1980)
10–1200	u_g (m/s): 0.01–0.240	Aq. solution of CMC, CMC + electrolyte (NaCl)	μ_L (Pa · s): 0.00035–0.012	Couette Viscometer (Haaka)	Haque et al. (1986)
1.1–1021	–	Aq. solution of polyacrylamide	–	Concentric cylinder viscometer (Fann, model 35A)	Moo-Young and Kawase (1987)
0.1–1000	u_g (m/s): up to 0.08	Suspensions of kieselguhr (7 μ m), aluminium oxide (8 μ m), and activated carbon (5 μ m)	μ_L (Pa · s): 0.001–1	Rotational viscometers (Brookfield LV with UL adapter or bob 1; Contraves 115 with MS 145)	Schumpe et al. (1987)
10–1200	u_g (m/s): 0.01–0.240	Aq. solution of CMC	–	Couette Viscometer (Haaka)	Haque et al. (1987)
1.1–1021	–	Aq. solution of CMC, Carbopol, fermentation medium	–	Concentric cylinder viscometer (Fann, model 35A)	Kawase and Moo-Young (1987)
1.5–1312	u_g (m/s): 0.002–0.1	Aq. solution of CMC	–	Concentric cylinder viscometer (RHEOTEST, 2, MLW, D.D.R.)	Vatai and Tekic (1989)
100–600	u_g (m/s): 0.051 u_L (m/s): 0.077–0.121	Aq. solution of CMC, xanthan	–	Concentric cylinder viscometer (Contraves 115)	Schumpe et al. (1989)
40–750	u_g (m/s): 0–0.09	Aq. solution of CMC	–	Capillary viscometer	Pradhan et al. (1993)
28–280	u_g (m/s): 0.01–0.10	Aq. solution xanthan and hydroxypropyl guar	μ_L (Pa · s): 0.001–10	Concentric cylinder viscometer (Contraves 115)	Eickenbusch et al. (1995)
30–100	u_g (m/s): 0.01–0.06	CMC solution and CMC (1.06%) + PPG (0.11%)	–	Stress rheometer (Rheo-Tech International Ltd.)	Khare and Niranjana (2002)
100	u_g (m/s): up to 0.15	Xanthan	μ_L (Pa · s): 0.001–0.0625	Bohlin CS rheometer (Double Gap 40/50)	Fransolet et al. (2005)
10–1200	u_g (m/s): 0.018–0.252	Aq. solution of CMC, xanthan	μ_L (mPa · s): 270–10 for CMC μ_L (mPa · s): 64–5 for Xanthan	RV 100 viscometer	Lakota (2007)
0.1–1000	u_g (m^3/s): 4×10^{-6} – 20×10^{-6}	Aq. solution of CMC and PAA	μ_L (Pa · s): 0.001–1	Programmatic rheometer (Reologica Instruments AB, Sweden)	Li et al. (2012b)
1–1000	u_g (m/s): up to 0.005	Aq. solution of glycerin + xanthan gum	μ_L (Pa · s): 0.001–1	Magnetic bearing rheometer (AR-G2 TA Instruments)	Anastasiou et al. (2013)
0.1–1500	u_g (m/s): up to 0.22	Aq. solution of CMC and xanthan	μ_L (Pa · s): 0.01–10	Modular compact rheometer (MCR-501, Anton Paar) with a double gap, coquette geometry	Esmaili et al. (2015)
1–1000	u_g (m/s): up to 0.04	Aq. solution xanthan and glycerin + xanthan gum	μ_L (Pa · s): 0.001–1	Magnetic bearing rheometer (AR-G2 TA Instruments)	Passos et al. (2015)
0.1–1500	u_g (m/s) : 0.01–0.35	Aq. solution of CMC and xanthan	μ_L (Pa · s): 0.01–10	Modular compact rheometer (MCR-501, Anton Paar) with a double gap, coquette geometry	Esmaili et al. (2016)

Table 4: Classification of viscosity estimation models.

Pseudoplastic fluid	Viscoplastic fluid
Power law model	Bingham plastic model
Carreau model	Herschel-Bulkley model
Cross model	Casson fluid model
Ellis model	

3.2 Rheological and physical properties

Based on the experimental data, some researchers have formulated empirical correlations for estimating gas holdup in the churn turbulent flow regime in a bubble column with non-Newtonian liquids (Schumpe and Deckwer 1982, Haque et al. 1986, Kawase and Moo-Young 1986, 1987). Godbole et al. (1984) concluded that the gas holdup decreases with an increase in effective viscosity in the churn turbulent flow regime in a CMC solution. Furthermore, at the same viscosity, a similar trend in gas holdup in CMC/salt solution (0.8 mol/l) and pure CMC solution has been reported. Fransolet et al. (2005) studied the effect of viscosity on gas holdup in a bubble column by varying the concentration of xanthan in an aqueous solution and concluded that gas holdup decreases with an increase in the liquid viscosity. Some researchers (Godbole et al. 1982, 1984, Haque et al. 1986) have reported strong influence of effective viscosity (μ_{eff}) on gas holdup in the case of viscous non-Newtonian liquids. A similar behavior was reported by Lakota (2007). A simultaneous effect of effective viscosity (μ_{eff}) and superficial gas velocity on gas holdup was studied by Haque et al. (1986). It has been found that gas holdup ($\epsilon_G \propto \mu_{\text{eff}}^{-0.22}$) in the churn turbulent flow regime decreases with an increase in effective viscosity, and gas holdup ($\epsilon_G \propto u_G^{0.6}$) increases with an increase in superficial gas velocity. Some of the researchers (Schumpe and Deckwer 1982, Devine et al. 1985) have proposed empirical correlations which are valid for the different flow regimes. However, they have ignored the effect of effective viscosity (μ_{eff}) in the correlations. Based on experimental data, Vatai and Tekic (1989) proposed two empirical correlations which are valid for the homogeneous and slug flow regimes, respectively. The influence of effective viscosity (μ_{eff}) was not considered in the correlation proposed by these authors for the slug flow regime, whereas it has a pronounced effect on gas holdup when viscous non-Newtonian CMC solutions are used. It was further concluded that the gas holdup ($\epsilon_G \propto \mu_{\text{eff}}^{-0.19}$) decreased with an increase in effective viscosity in a churn turbulent flow regime. Fluid properties have a pronounced effect on gas holdup for a non-Newtonian liquid system, even then a set of correlations have been proposed on the basis of very limited data without

considering important fluid properties such as the surface tension of liquid and the density of gas (Godbole et al. 1982, 1984, Schumpe and Deckwer 1987a,b). The gas holdup and bubble characteristics in non-Newtonian liquids were studied by a few investigators, and correlations have been proposed for the gas holdup using dimensionless groups comprising Bond, Galilei and Froude numbers (Nakanoh and Yoshida 1980). Furthermore, Galilei number of liquid, Reynolds' number of gas and the ratio of the hole size of the perforated plate to column diameter have also been used as parameters in correlations (Mok et al. 1990). The rheological and physical properties of different non-Newtonian liquids used in various studies are listed in Table 5. For newer research, this table provides useful information for experimental as well as modeling in non-Newtonian systems within a limited range of system properties and working conditions.

Limited information on the influence of surface tension on gas holdup for non-Newtonian solutions in a bubble column was reported earlier. Schumpe and Deckwer (1987a,b) proposed an empirical correlation for aqueous solutions of CMC, sodium polyacrylamide (PAA) and xanthan. It was concluded that gas holdup increases ($\epsilon_G \propto \sigma_L^{0.13}$) with an increase in surface tension of the liquid. Flow behavior of a fluid in a bubble column is affected by the rheological properties of the non-Newtonian liquid. Fransolet et al. (2005) investigated the influence of the rheological properties of a non-Newtonian liquid, that is, xanthan on gas holdup in a bubble column.

The apparent viscosity of an aqueous solution increases with increasing concentrations of CMC due to the increase in the intermolecular interactions between the CMC molecules (Benchabane and Bekkour 2008). Ghannam and Esmail (1997), for CMC aqueous solutions (1 to 5 wt%), and Edali et al. (2001), for 5% to 8% CMC aqueous solutions, reported that flow curves of CMC solutions (τ - γ and μ - γ curves in log-log scale) followed a power law behavior over the range of shear rates between 0 and 1000 s⁻¹. Evidence of yield stress was not reported in these studies. In contrast, for the same concentration range (1%–5%), Benchabane and Bekkour (2008) found a different behavior of flow curves of CMC solutions and reported that the power law model is not suitable for fitting the flow curves (τ - γ and μ - γ curves) of CMC solutions. It must be emphasized here that this conclusion differs from the results reported earlier (Ghannam and Esmail 1997, Edali et al. 2001). The flow behavior index for 1% CMC aqueous solution is 0.95, and its flow behavior was considered to be that of a Newtonian fluid by the authors (Ghannam and Esmail 1997). For a perfect Newtonian system, the value of n is frequently constant at unity over a wide range of shear rates. The value of n is slightly less than unity and

Table 5: Rheological and physical properties of non-Newtonian liquids.

Non-Newtonian solution	Concentration (wt%)	Density (kg/m ³)	Surface tension (N/m)	Flow behavior index (n)	Consistency index, k (Pa·s ⁿ)	Reference
Aq. solution of CMC	10–17	–	–	0.82–0.75	13–25	Buchholz et al. (1978)
Aq. solution of CMC	0.7–1.6	–	–	0.91–0.82	0.04–0.23	Deckwer et al. (1982)
Aq. solution of CMC	1.0–2.0	1091–1094	–	0.860–0.749	0.048–0.721	Schumpe and Deckwer (1982)
Aq. solution of CMC	0.01–0.5	996–1008	–	1–0.495	0.0018–2.570	Godbole et al. (1982)
Aq. solution of CMC	–	1000–1006	0.0676–0.0730	0.697–0.440	0.095–7.683	Godbole et al. (1984)
CMC + sodium sulfate (0.8 M)	–	1008–1101	0.0727–0.0734	0.742–0.603	0.263–1.997	–
Aq. solution of CMC	0.50–0.75	987–999	0.068	0.56–0.440	0.921–4.614	Devine et al. (1985)
Aq. solution of CMC	50–2300 (ppm)	–	–	0.99–0.638	0.002–0.24	Keikar and Shah (1985)
Aq. solution of CMC	0.10–2.00	1000–1009	–	0.80–0.50	0.012–1.320	Haque et al. (1986)
CMC + electrolyte (NaCl)	0.10–1.50	–	–	0.82–67	0.01–0.1	–
Aq. solution of CMC, glycerine + SAG10	–	995–1018	0.0502–0.0694	1.0–0.543	0.001–1.22	Kawase and Moo-Young (1986)
Aq. solution of polyacrylamide	0.2–0.6	991–993	–	0.568–0.500	0.122–0.630	Moo-Young and Kawase (1987)
Aq. solution of CMC	0.10–2.0	1000–1009	0.069–0.073	0.80–0.50	0.012–1.320	Haque et al. (1987)
Aq. solution of CMC, Carbopol	–	991–992	0.0685–0.0711	0.820–0.476	0.0278–2.32	Kawase and Moo-Young (1987)
Aq. solution of CMC	–	991–993	–	0.770–0.504	0.034–1.65	Kawase and Moo-Young (1987)
Carbopol	–	992	–	0.816–0.656	0.0282–0.320	–
Fermentation medium	–	995	–	1.0	0.0010	–
Glycerol	–	1090–1248	–	1	3.2–588	Schumpe and Deckwer (1987a,b)
Aq. solution of CMC	–	1001–1005	0.072–0.0707	0.973–0.812	24–247	–
PAA	–	1001–1005	0.0495–0.0584	0.721–0.367	156–7851	–
Xanthan	–	999–1004	0.0583–0.0647	0.700–0.180	23–9780	–
Aq. solution of CMC	–	1002–1012	0.067–0.071	0.97–0.79	0.0019–0.0668	Vatai and Tekic (1989)
Aq. solution of CMC	0.0–0.30	997.1–998.2	70.53–72.0 (dyne/cm)	1–0.809	0.01–0.075 (dyne s ⁿ /cm ²)	Mok et al. (1990)
Aq. solution of CMC	–	1001–1003	0.0729–0.0736	0.882–0.825	0.02169–0.7164	Kang et al. (1990)
Ca(OH) ₂ suspension	5	–	–	0.87–0.54	0.0035–0.526	Kawase et al. (1992)
Ca(OH) ₂ suspension	10	–	–	–	–	–
Aq. solution of CMC	–	–	–	–	–	–
Aq. solution of CMC	0.1–0.8	995.3–1003.1	0.0658–0.068	0.92–0.80	0.0018–0.0425	Pradhan et al. (1993)
Aq. solution of CMC	0.7–1.6	1001–1002	0.064–0.065	0.870–0.825	0.027–0.232	Ryu et al. (1993)
Aq. solution of CMC	0.05–0.50	998.5–1000	0.0571–0.0693	0.8354–0.7005	0.0083–0.1551	Kantak et al. (1995)
Aq. solution of CMC	–	1000.8–1001.5	0.0735–0.0755	0.948–0.850	0.00218–0.00692	Mandal et al. (2003)
Xanthan	–	–	–	1–0.19	0.001–2.93	Fransolet et al. (2005)
Aq. solution of CMC	0.2–0.85	–	–	0.81–0.48	0.056–2.8	Lakota (2007)
Xanthan	0.1–0.4	–	–	0.505–0.30	0.168–1.50	–
Aq. solution of CMC	0.2–0.8	1001.69–1003.83	0.07834–0.08320	0.9013–0.6015	0.0138–0.6486	Jana et al. (2014a,b)
CMC and xanthan gum	0.5	995.31–995.65	0.07607–0.07392	0.68 and 0.21	0.32–3.29	Esmaili et al. (2015)
CMC and xanthan gum	0.5	995.31–995.65	0.07607–0.07392	0.68 and 0.21	–	Esmaili et al. (2016)

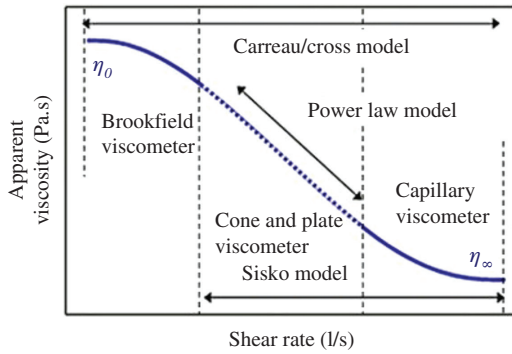


Figure 2: Demonstration of zero-shear and infinite-shear viscosities for shear-thinning fluids identifying three separate regions.

is indicative of the nonlinearity of viscosity and the shear rate curve. Furthermore, the molecular weight of CMC used in experimental studies controls the rheological properties of the diluted CMC solution, which is seldom reported by the authors (Ghannam and Esmail 1997). Thus, comparison of results of different studies becomes a real challenge. It is possible that the authors might have used low molecular weight of CMC in their study. However, Benyounes (2013) reported that the low molecular weight of CMC solution follows the Ostwald-de Waele model.

The consistency index (k) and flow index (n) are typical rheological parameters used in the power law model. The consistency index (k) is a strong function of concentration of the solution and temperature, whereas flow behavior index (n) does not have a strong dependence on concentration and temperature of the polymeric solution (Wanchoo et al. 1996, Gómez-Díaz and Navaza 2003, Cancela et al. 2005). The consistency index increases with concentration and decreases with temperature, while the opposite trend was observed with the flow behavior index (Abdelrahim and Ramaswamy 1995, Pilizota et al. 1996, Gómez-Díaz and Navaza 2003, Cancela et al. 2005).

Gas holdup decreases with reduction in the consistency index as indicated in the correlation proposed by Kawase and Moo-Young (1986). It has been reported that gas holdup in a non-Newtonian liquid depends on the flow index ($\varepsilon_g \propto n$), and some of the researchers reported that gas holdup decreases with an increase in the pseudoplasticity of the liquid or a decrease in the flow index (Kawase and Moo-Young 1986, Kawase and Moo-Young 1987, Vatai and Tekic 1989). For non-Newtonian (pseudoplastic) solutions, Haque et al. (1986) developed a correlation for the prediction of gas holdup in the churn turbulent regime for different column diameters using flow behavior index varying from 0.5 to 1.0. It was found that gas holdup decreases with an increase in the column diameter in the churn turbulent regime. In contrast to this, in some other studies, gas holdup correlations

have been proposed without considering the flow consistency index (Deckwer et al. 1982, Devine et al. 1985, Kawase and Moo-Young 1987, Elgozali et al. 2002). Such correlations would predict gas holdup less than expected in the absence of shearing. Kawase and Moo-Young (1987) developed a theoretical model with reasonable accuracy of gas holdup results, which are valid for Newtonian as well as non-Newtonian liquids. It has been reported that large spherical cap bubbles in highly viscous non-Newtonian liquid systems have limited influence on gas holdup.

Elasticity and viscosity of the non-Newtonian liquids strongly affect gas holdup. Effects of rheological properties such as elasticity and viscosity on hydrodynamics of a bubble column are yet to be fully understood. However, limited information about the effect of elasticity has been reported (Moo-Young and Kawase 1987, Suh et al. 1991, Olivieri et al. 2011, Esmaeili et al. 2015, 2016). Moo-Young and Kawase (1987) observed that elasticity of the liquid causes formation of a large number of very small bubbles, resulting in an increase of the overall gas holdup. Furthermore, it was found that the number of very small bubbles (<1-mm diameter) in the PAA solutions was much larger than in the CMC solutions. On similar lines, Esmaeili et al. (2015) investigated the effects of the rheological characteristics of xanthan gum on gas holdup in a bubble column equipped with perforated plate gas distributor. It has been found that higher gas holdup occurred at lower gas velocity because of elastic effects of the solution which prevented bubble coalescence and formation of small bubbles.

3.3 Shear rate

The bubble columns using non-Newtonian liquids are widely used in chemical, polymer, food and biochemical industries. Limited details of the effect of non-Newtonian liquids on gas holdup have been reported in the literature. Both polymer solutions and fermentation broths often behave as non-Newtonian liquids. The behavior of a liquid in a bubble column is affected by the rheological properties of the liquid, especially when using highly viscous non-Newtonian fluids. Generally, fermentation media are non-Newtonian liquids, and their rheological behavior can be acceptably simulated by aqueous solutions of CMC. The viscosity of these pseudoplastic liquids depends not only on pressure and temperature but also on shear action. Numerous non-Newtonian fluids such as CMC (Franz et al. 1980, Devine et al. 1985, Haque et al. 1986, Kawase and Moo-Young 1986, Schumpe and Deckwer 1987, Vatai and Tekic 1989, Kawase and Moo-Young 1987, Lakota 2007), PAA (Schumpe and Deckwer 1987a,b, Kawase and Moo-Young 1987), xanthan (Schumpe

Table 6: Correlations for effective shear rate in non-Newtonian liquids.

System	Approach/ basis	Correlation	Dimensions of column	Power law index range (n)	Range of superficial gas velocity, u_g (m/s)	Reference
CMC, millet jelly, glycerol	Analogical	$\gamma = 5000 u_g$	$D_c = 0.15$ m $H_c = 1.80$ m	0.72–1	≥ 0.04	Nishikawa et al. (1977)
–	Correlative	$\gamma = 1500 u_g$	$D_c = 0.14$ m $H_c = 3.9$ m	0.38–0.82	0.008–0.064	Henzler (1980)
Yeast suspension	Intuitive	$\gamma_\infty \left(\frac{\text{Bubble rise velocity in infinite medium}}{\text{Bubble equivalent diameter}} \right)^{n-1}$	$D_c = 0.15$ m $H_c = 2.0$ m	–	–	El-Temtamy et al. (1984)
CMC, glycerine+ SAG10	Intuitive	$\gamma_\infty \frac{u_g}{\text{radius of column}}$	$D_c = 0.23$ m $H_c = 1.22$ m	0.543–1	–	Kawase and Moo-Young (1986)
CMC, PAA, xanthan, glycerol	Correlative	$\gamma = 2800 u_g$ (valid for column diameter from 0.19 to 0.6 m)	$D_c = 0.06$ –0.30 m $H_c = 1.8$ –2.2 m	0.18–1	0.02–0.2	Schumpe and Deckwer (1987a,b)
CMC, xanthan	Semitheoretical	$\gamma = 2800 \left(u_g - u_L \frac{\varepsilon_g}{\varepsilon_L} + \frac{12 u_L \varepsilon_g}{d_s \varepsilon_L^2} \frac{3n+1}{4n} \right)$ (valid for upward concurrent operation)	$D_c = 1.4$ m $H_c = 2.65$ m	0.511– 0.866	–	Schumpe et al. (1989)
Glycerin-xanthan solution	Correlative	$\gamma = 70 u_g^{0.48}$	$D_c = 0.09$ m $H_c = 1.5$ m	–	0.002–0.04 m/s	Anastasiou et al. (2013)

and Deckwer 1987a,b, Fransolet et al. 2005, Lakota 2007), glycerol (Schumpe and Deckwer 1987a,b), sodium polyacrylate (Schumpe and Deckwer 1987a,b), and carboxypolyethylene (Kawase and Moo-Young 1987) were employed in previous studies for estimation of gas holdup.

All reported shear rate relationships are distinguished in four sections of analysis: (a) analogical (based on two identical but different systems operating under the same conditions), (b) theoretical (based on unrealistic assumptions in view of actual conditions), (c) correlative (based on experimental data), and (d) intuitive (difficult to evaluate). The relations proposed in the literature for the estimation of effective shear rate are given in Table 6.

Nishikawa et al. (1977) evaluated the average shear rates ($\gamma = 5000 u_c$) by fitting the heat transfer coefficient data measured from an immersed cooling coil and a jacketed wall with an aerated Newtonian and non-Newtonian liquid in a bubble column. The general applicability of this correlation is questionable as the average shear rate has stronger dependence on mass transfer coefficient than heat transfer coefficient, but it has been widely used (Nakanoh and Yoshida 1980, Godbole et al. 1982, 1984, Deckwer et al. 1982, Schumpe and Deckwer 1982, Kelkar and Shah 1985, Haque et al. 1986, 1987, Kawase and Moo-Young 1987, Kang et al. 1990, Pradhan et al. 1993, Ryu et al. 1993, Kantak et al. 1995, Lakota 2007, Ghosh and Upadhyay 2007, Anastasiou et al. 2013). This limitation has been mostly ignored. At lower gas velocities ($u_g \leq 0.04$ m/s), average shear rates are lower at the jacketed wall but higher in the center, probably due to the presence of bubble streets. However, this method has been under criticism because heat transfer in bubble column reactors is controlled by the thin boundary layer on the reactor wall or coil (Kawase and Moo-Young 1987). Henzler (1980) estimated shear rate ($\gamma = 1500 u_c$) by fitting only one data set of mass transfer coefficient data presented by Buchholz et al. (1978) in non-Newtonian liquids in a tower reactor and in sectionalized columns. This analysis may show no physical meaning. El-Temtamy et al. (1984) proposed that shear rate is proportional to the ratio of terminal velocity of the bubble to bubble diameter, but this approach is impractical as the terminal velocity of bubble and bubble diameters in highly viscous non-Newtonian liquids are non-uniform and cannot be accurately evaluated. Earlier, it was also proposed in a study that the average shear rate is proportional to the ratio of a characteristic velocity to a characteristic length. Further, for convenience of calculation, the proportionality constant was also considered as unity (Kawase and Moo-Young 1986). Schumpe and Deckwer (1987a,b) proposed shear rate ($\gamma = 2800 u_c$) based on a mass transfer coefficient experiment in

various pseudoplastic liquids in bubble column. It has been reported that liquid viscosity has a stronger effect on mass transfer as compared to heat transfer. Schumpe et al. (1989) proposed a semi-theoretical relationship of shear rate for estimating viscosity of viscous pseudoplastic liquids ($0.511 \leq n \leq 0.861$) in a three-phase fluidized column. Anastasiou et al. (2013) proposed a shear rate relationship ($\gamma = 70 u_g^{0.48}$) by correlating data of aqueous glycerin-xanthan solutions with superficial gas velocity. It is suitable for predicting shear rate for superficial gas velocity in the range of 0.002–0.04 m/s.

3.4 Superficial gas velocity and presence of CMC in aqueous solution

Gas holdup in a bubble column with non-Newtonian solution depends mainly on superficial gas velocity and concentration. A few authors have reported the effect of superficial gas velocity on gas holdup and concentration of CMC in aqueous solutions (Schumpe and Deckwer 1982, Mok et al. 1990). The value of gas holdup is strongly dependent on the concentration of non-Newtonian solutions such as CMC. Schumpe and Deckwer (1982) investigated the effect of CMC concentration (0–1.8 wt%) on gas holdup in bubble columns of different sizes with sintered plate and perforated plate spargers, respectively. It has been observed that up to 0.8 wt% CMC, the gas holdup increases with the CMC concentration due to the decrease in bubble rise velocities. Furthermore, it was observed that a smaller gas holdup is obtained with a 2-mm perforated plate in the CMC concentration range of 0.8–1.8 wt%. Based on experimental data sets, the authors have proposed separate empirical correlations valid for the homogeneous, heterogeneous and slug flow regimes, respectively. However, they have neglected the effect of effective viscosity (μ_{eff}) in the proposed correlations. Similar observations have been made by Mok et al. (1990), predicting the increase in gas holdup ($\varepsilon_g \propto u_g^{1.09}$) with increase in gas velocity. On similar lines, the authors reported that CMC concentration significantly affects gas holdup. It decreases with an increase in CMC concentration. Furthermore, Devine et al. (1985) observed that the gas holdup increases with increasing gas velocity, and it remains unaffected by apparent viscosity of the liquid. Godbole et al. (1984) investigated the effect of surfactant addition on the gas holdup at six different concentrations. It has been found that the holdup of large bubbles is unaffected by the amount of surfactant, while with increasing surfactant concentration, the gas holdup increased significantly due to the presence of very small bubbles ($d_b < 1$ mm). Another significant finding was the gas holdup due to very small bubbles. It was negligible

for pure CMC solutions. Kelkar and Shah (1985) worked with PAA and PEO (polyethylene oxide) polymer solutions in a bubble column equipped with 20 orifices 0.001 m in diameter. It has been observed that there is a consistent increase in gas holdup values with an increase in the concentration of both polymer solutions. Haque et al. (1987) investigated the effect of H/D ratio on gas holdup and bubble size in a highly viscous non-Newtonian (pseudoplastic) CMC solution in bubble columns of different sizes. It has been concluded that bubble size increases with CMC concentration, but it significantly decreased with increasing gas velocity due to increasing shear rate at a given CMC concentration. Kantak et al. (1995) observed the effect of gas and liquid properties on gas holdup in a bubble column. It has been concluded that gas holdup decreases in the presence of CMC solution. Ghosh and Upadhyay (2007) developed an empirical correlation to predict gas holdup, which is valid for both Newtonian and non-Newtonian (pseudoplastic) liquids. Lakota (2007) developed an empirical correlation to predict gas holdup as a function of gas velocity and effective viscosity of the liquid for highly non-Newtonian liquids in a co-current upflow bubble column. Jana et al. (2014a,b) worked with a non-Newtonian pseudoplastic liquid in two different tapered bubble columns and developed an empirical correlation to predict gas holdup as a function of various parameters of the system such as column diameter, effective viscosity, taper angle, gas velocity, surface tension and density of liquid, gas density and viscosity.

Enhancement of gas holdup using physical means is always desirable in order to increase the quantum of gas-liquid mass transfer. This results in increased conversion of reactant(s) to product(s). Innovative methods have been attempted for the same in the past. Kang et al. (1990) developed an empirical correlation to predict gas holdup for CMC solution in bubble columns in the presence of floating bubble breakers in the form of acrylic cylindrical blocks.

3.5 Bubble characteristics

Bubble characteristics have a significant effect on gas holdup. Some excellent reviews are available in the literature focusing on bubble characteristics (Shah et al. 1982, Craig 2004, Kantarci et al. 2005, Kulkarni and Joshi 2005, Leonard et al. 2015). Bubble population, bubble rise velocity and bubble size and shape have a significant impact on gas holdup as well as the mass transfer coefficient in non-Newtonian liquids. Factors affecting bubble characteristics such as operating conditions (pressure and temperature), rheological properties (effective viscosity and elasticity), and CMC concentration have received adequate attention

from researchers, but the effect of gas density is scarcely reported in the literature. Haque et al. (1987) reported that bubble sizes increase with increasing CMC concentration, but significantly decrease with an increase in gas velocity for a given CMC concentration. Mok et al. (1990) reported that the effect of viscosity on the mean bubble size is not significant for CMC concentration less than 0.3%. Another significant observation was the fact that the mean bubble size remained nearly the same at low gas velocity and concentration. Ryu et al. (1993) observed that mean bubble size increase with an increase in superficial gas velocity in the bubbly flow regime with a 0.7 wt% CMC solution. The bubble size distributions were found to be very narrow, approximately in the range of 2.7 to 3.7 mm.

The hydrodynamic properties of gas/non-Newtonian liquid systems have been reported by numerous authors. In highly viscous liquids, many tiny bubbles (<4 mm) appear, accumulate and circulate within the liquid during the aeration process. Tiny bubbles play a significant role in oxygen transfer because of their smaller size, which offers an extremely high interfacial area. Their main effect is to act as a high-capacity reservoir for low-solubility gases (specifically oxygen) that dampens dynamic changes of the dissolved gas concentration. The significant contribution of gas holdup due to tiny bubbles to the total gas holdup and mass transfer has been observed during bubble formation in non-Newtonian aeration systems (Buchholz et al. 1978, Franz et al. 1980, Heijnen et al. 1980, Muller and Davidson 1992, Kawalec-Pietrenko 1992, Khare and Niranjana 1994, Khare and Niranjana 1995). The contribution of tiny bubbles and their effects on gas holdup in non-Newtonian systems are listed in Table 7.

Overall gas holdup, which is the sum of the gas holdup due to tiny bubbles (residence times ≥ 10 s) and large bubble holdup ($d_b \geq 1$ cm and residence times ≤ 5 s), increases with time before attaining a stable equilibrium value. During aeration, the rate of generation of tiny bubbles is equal to the rate of their disappearance, causing their holdup to be steady. For non-Newtonian solution, such as CMC, gas holdup due to tiny bubbles depends on its rheological properties, impeller speed, gas velocity, solid concentration and presence of antifoaming agent.

Franz et al. (1980) suggested that the tiny bubbles do not actively transfer oxygen in highly viscous media; instead, tiny bubbles move to attain equilibrium with the liquid phase due to high residence time. However, the investigations of Philip et al. (1990) and Muller and Davidson (1992), referring to their steady state on airlift and bubble columns, demonstrated that the equilibrium of tiny bubbles with the liquid phase may not be achieved, but these bubbles actively contribute to oxygen transfer,

Table 7: Estimated contribution and effect of tiny bubbles on gas holdup and oxygen transfer.

System	Physical properties of liquids/operating conditions	Operating conditions	Key findings	Reference
Aqueous CMC solution	n : 0.75–0.82 k (Pa · s ⁿ): 13–50 C (wt%): 1–16 u_g (m/s): 0.008–0.0064	Column diameter: 0.14 m Height of column: 3.91 m Porous plate 2 mm in thickness and 17.5- μ m pore size Perforated plate with 150 holes of 4-mm diameter	i. Small ($d \leq 1$ mm) and large ($d \geq 5$ –10 mm) bubbles formed ii. The diameter of the column significantly influences the coalescence phenomena iii. The smaller the column diameter, the higher the coalescence frequency and the smaller the specific interfacial area	Buchholz et al. (1978)
Aqueous glycerol solution	C (v/v): 50%–95% u_g (cm/s): 1.27–7.65	Column diameter: 0.14 m Height of column: 0.35 m Perforated plate with 0.5, 1.0, and 3.0-mm hole diameter	i. Glycerol concentration in the range of 50% to 90% produced small bubble gas holdup, which was found independent of superficial gas velocity ii. With increasing hole diameter of perforated plate and increasing glycerol concentration, the small bubble gas holdup increases	Franz et al. (1980)
Aqueous PVP solution and viscous broth	N (s ⁻¹): 3.3–10	Column diameter: 0.45 and 0.36 m Six blade Rushton impeller diameter: 0.18 m	i. A fraction of very small bubbles existed ($d \leq 1$ mm) in viscous gas-liquid systems ii. Dispersion of small bubble was considered as a homogeneous phase	Heijnen et al. (1980)
Aqueous CMC solution (1 wt%)	n : 0.51–0.59 k (Pa · s ⁿ): 1.8–3.1 u_g (m/s): 0.01–0.08	Column diameter: 0.14 m	i. Contribution of tiny bubbles to the steady-state mass transfer was 20%–50% ii. Residence time of small bubbles was between 50 and 500 s, and it decreases with increasing gas flow rate iii. Equilibrium holdup of small bubbles was between 0.5% and 0.8% iv. Mass transfer coefficient of small bubbles is independent of gas flow rate v. Small bubbles have a lower driving force compared to large bubbles	Muller and Davidson (1992)
Aqueous saccharose and glycerol solution + solid phase (glass beads, magnesium oxide, synthetic resin pellets)	Shear rates (s ⁻¹): 37.69 – 226 ρ_s (kg/m ³): 1575 – 3500 d_s (mm): 0.046–0.23 u_g (m/s) \leq 0.09 $X_{\text{solid loading}} \leq 0.212$ $\mu_{\text{suspension}}$ (mPa · s) \leq 170	Column diameter: 0.105 m Perforated plate with 0.5-mm hole diameter	i. Contribution of small bubbles to the total gas holdup can be significant and was found to be about 60% ii. The small bubble holdup increases if the apparent suspension viscosity increases and decreases with an increase in the gas flow velocity iii. An increase in the apparent viscosity is due to decreases in the accumulation rate of small bubbles iv. The accumulation rate of small bubbles increases with increases in gas flow rate	Kawalec-Pietrenko (1992)

Table 7 (continued)

System	Physical properties of liquids/operating conditions	Operating conditions	Key findings	Reference
Aqueous CMC solution	n : 0.47–0.62 k (Pa · s ^{<i>n</i>}): 2.8–15 Shear rate (s ⁻¹): 2–270 u_g (m/s): 0.001–0.01 N (s ⁻¹): 4–21	Column diameter: 0.3 m Six-bladed disc turbine: 0.1 m	i. Fractional contribution of tiny bubbles to total gas holdup was as high as 70% ii. Tiny bubbles play a significant role in oxygen transfer in an agitated reactor	Khare and Niranjan (1994)
Highly viscous liquids (aqueous CMC, castor oil, rapeseed oil)	μ_L (Pa · s): 0.069–0.69 ρ_L (kg/m ³): 920–1004 σ_L (N/m): 0.0354–0.074 u_g (m/s): 0.001–0.01 N (s ⁻¹): 4–21 n : 0.47–0.67 k (Pa · s ^{<i>n</i>}): 2.8–15	Column diameter: 0.3 m Baffles: 4 Six-bladed disc turbine: 0.1 m Diameter of ring sparger: 0.24 m Number of holes: 7 Diameter of each hole: 0.5 mm	i. Tiny bubbles contributed 70%–80% of the total gas holdup ii. Contribution of tiny bubbles to oxygen transfer was greater than the contribution of large bubbles iii. Fractional contributions of tiny bubbles are reduced by the addition of antifoaming agents iv. Fractional contribution of tiny bubbles increases with an increase in viscosity and diminishes with an increase in gas velocity v. Size of tiny bubbles: 0.1–3 mm vi. Tiny bubble holdup depends on rheological properties, impeller speed, and gas velocity vii. Holdup increases up to 6 minutes for CMC solution and up to 40 minutes for castor oil	Khare and Niranjan (1995)

although with a lower driving force. The tiny bubbles are formed and destroyed continuously during the aeration.

Introductory information on the fractional contribution of tiny bubbles to the total gas holdup was reported by Khare and Niranjan (1994). The contribution of tiny bubbles to the overall gas holdup is as much as 70%–80% for Newtonian and non-Newtonian liquids (Khare and Niranjan 1995). In contrast, the experimental results of Philip et al. (1990) and Muller and Davidson (1992) for the internal loop reactor and the bubble columns reported that the contribution of tiny bubbles to the total gas holdup is only about 10%–20%. The effective contribution of the small bubbles to mass transfer is 20%–50% for the steady state (Muller and Davidson 1992). The relative contribution of tiny bubbles to the total gas holdup and oxygen transfer is more significant in the impeller-agitated reactors than in bubble columns. For impeller speed below a critical value, the contribution of tiny bubbles increases with impeller speed, whereas above it, the contribution of tiny bubble decreases due to the fact that the overall liquid circulation velocity increases, which enhances the probability of bubble coalescence (Khare and Niranjan 1995). The fraction of small bubbles in the total gas

holdup increases as the solid concentration increases. Simultaneously, particles less than 1 mm in size promote bubble coalescence, which results in higher rise velocities of the bubbles (Kawalec-Pietrenko 1992). Kawalec-Pietrenko (1992) reported that in bubble columns, the presence of suspended solids can enhance the contribution of tiny bubbles as high as 60%. The small bubble holdup increases if the apparent suspension viscosity increases and decreases with the increase in the gas flow velocity.

The contribution of tiny bubbles at low gas velocity attains an optimum value at a particular impeller speed (Figure 3). On the other hand, at higher gas velocities, the fractional contribution of tiny bubbles decreases progressively with an increase in impeller speed (Khare and Niranjan 1995). In general, the number of fine bubbles increases as the liquid viscosity increases, and consequently, the small bubble holdup increases and decreases with the increase in the gas flow rate. A similar trend has also been reported by Franz et al. (1980) and Kawalec-Pietrenko (1992).

Undesirable foaming is an essential part of aerobic biotechnology processes. To prevent undesirable foaming, antifoaming agents are generally used. The addition of anti-foam makes the liquid more coalescent and highly turbid

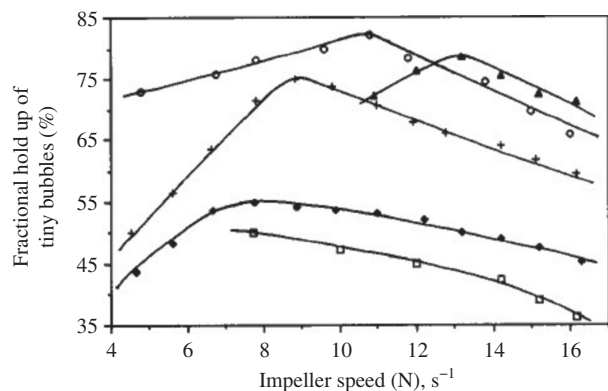


Figure 3: Variation of fractional gas holdup of tiny bubbles with impeller speed for different aqueous concentrations of CMC: for $u_g = 0.0012$ m/s, (◆) 0.75% CMC, (+) 1.0% CMC, (▲) 1.25% CMC, and (○) castor oil; for $u_g = 0.0096$ m/s, (□) 0.75% CMC. Reproduced from Khare and Niranjana (1995) with permission from Elsevier.

during aeration. The presence of antifoam reduces total gas holdup as well as the fractional contribution of tiny bubbles in 1% CMC + silicone (Khare and Niranjana 1995).

Bubble velocity and its shape in stagnant shear-thinning (pseudoplastic) non-Newtonian fluids are necessary for understanding the hydrodynamics involved in the process of gas holdup formation. Rising of bubbles is frequently encountered in non-Newtonian fluids like CMC, polyacrylamide (PAM), xanthan, etc. These are used in a wide variety of industrial applications such as chemical and biochemical processes, environmental and food processing. Because of the inherent complexity of fluids, bubbles in non-Newtonian fluids exhibit different rising velocities and shapes under the action of different forces such as drag force, buoyancy force, etc. In order to estimate the bubble terminal velocity in non-Newtonian fluids, it is necessary to be familiar with the relationship between the drag coefficient of the bubble and its Reynolds number. Empirical correlations for estimating drag coefficient for bubbles over a wide range of Reynolds numbers in different non-Newtonian fluids are listed in Table 8. The bubble rise velocity affects the gas holdup and the residence time of the gas phase. When the gas holdup increases with gas flow rate, the number of bubbles within a bubble swarm is also increased, resulting in a decrease in the drag force and an increase in the bubble rise velocity. In other words, an increased gas flow rate enhances the flow turbulence and bubble breakup and coalescence, which results in a wider distribution of the bubble rise velocity. Deng et al. (2010) reported that a higher CMC concentration led to wider distributions of the bubble size and bubble rise velocity. The average bubble rise velocity increases with an increase in gas flow rate and a decrease in CMC

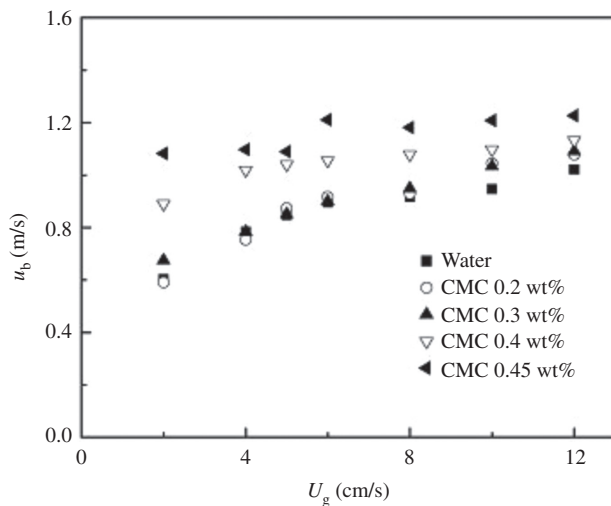
concentration. Furthermore, it was also reported that the bubble velocities were almost unchanged in the heterogeneous regime in 0.45 wt% CMC solution. The influence of the gas flow rate and CMC concentration on the average bubble rise velocity is shown in Figure 4. The frequency of bubble generation from the orifice increases with an increase in the gas flow rate, which tends to reduce apparent viscosity. Thus, the terminal velocity rises with the fall in viscous drag force of the fluid around the bubble. The influence of the injection period on the bubble rise velocity in a CMC aqueous solution was also observed by Funfschilling and Li (2006). It has been found that the bubble rise velocity in 2% CMC solution is independent of the injection period (0.3–60 s), except for the case when injection period was of 0.3-s duration as shown in Figure 5.

The bubble surface expands spherically in radial direction owing to the dominant role of surface tension in the initial stage of bubble formation. However, the influence of buoyancy on the bubble becomes significant progressive with the growth of the bubble; subsequently, the bubble is elongated vertically to an obvious teardrop shape under the common action of buoyancy and resistance of shear thinning of the fluid. Bubble shape distortion and oscillation during its rise will change the shape of a moving bubble and hence will change the drag coefficient and the terminal velocity. Distortion and oscillation tend to increase the drag resistance and reduce the terminal velocity over that of a rigid sphere of equal volume (Wanchoo et al. 2003, Gupta and Wanchoo 2009). Efforts have been made earlier in Newtonian and non-Newtonian systems to correlate the shape of bubble in shape factor term or eccentricity, which is a function of various dimensionless parameters (Wellek et al. 1966, Kojima et al. 1968, Takahashi et al. 1976, Acharya et al. 1977, Wanchoo et al. 2003, Gupta and Wanchoo 2009, Shaobai Li et al. 2012a,b,c). Details of bubbles and dependence of shape of bubbles are presented in Table 9.

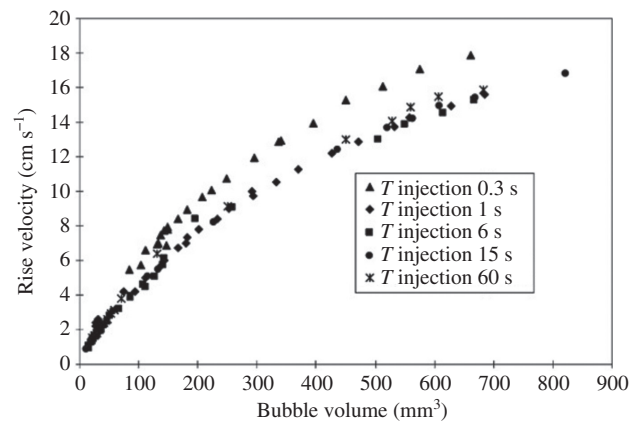
It has been reported that the rheological parameters and interfacial tension could have a strong effect on the shape of the bubble moving through a non-Newtonian liquid. A classical generalized graphical correlation in terms of the Eötvös number (Eu), Morton number (Mo) and the Reynolds number (Re) for bubbles or drops rising or falling in infinite media has been proposed earlier (Grace 1973, Clift et al. 1978). Regime-based shape graphs have been successfully used to predict the terminal velocity and the shape of a bubble/drop moving in an immiscible Newtonian liquid. The regime diagram for the shapes of gas bubbles in a quiescent fluid according to Clift et al. (1978) is shown as in Figure 6. Wenyuan et al. (2010) reported that the shape of the bubble is gradually flattened horizontally to an ellipsoid with the increase

Table 8: Correlations used for drag coefficient estimation.

System(s)	Correlation	Range	Reference
Aqueous solution of CMC	$C_D = \frac{16}{Re} (1 + 0.43 Re^{0.44}) (1 + 3.868 n^{0.7528} (1-E)^{0.6810})$	$0.95 \leq E \leq 1.05$ $0.5593 \leq n \leq 0.9377$ $1 \leq d_e \text{ (mm)} \leq 10$ $0.05 \leq Re \leq 300$	Li et al. (2012a,b,c)
Aqueous solution of CMC and PAM	$C_D = 2.173 Re^{-1.57} Ar^{0.683} Eo^{-0.0931}$	$13 \leq Re \leq 230$ $283 \leq Ar \leq 1618$ $3.2 \leq Eo \leq 9.7$	Wenyuan et al. (2010)
Aqueous solution of CMC, HEC, PAAS, and xanthan gum	$C_D = \frac{16}{Re_M} (1 + 0.12 Re_M^{0.6}) + (1 + 0.196 Ac^{0.767} Ar^{0.381})$ for $Re_M \leq 135$ and $C_D = 0.95$ for $Re_M \geq 135$ where $Re_M = \frac{\rho_l d_e U}{\mu_o} \left[1 + \left(\frac{2\lambda U}{d_e} \right)^2 \right]^{(1-s)/2}$	$0.37 \leq s \leq 0.97$ $0.062 \leq \lambda \text{ (s)} \leq 93.8$ $13.17 \leq \mu_o \text{ (mPa} \cdot \text{s)} \leq 162.73$	Zhang et al. (2008a)
Highly viscous fluids	$C_D = 2.275 Re^{-1.79} Ar^{0.801}$ $C_D = 2.275 (1 + 0.222 Sc^{0.246}) Re^{-1.79} Ar^{0.801}$	$0.013 \leq Re \leq 100$ $0.06 \leq Ar \leq 8349$ $0 \leq Ac \leq 50$	Zhang et al. (2008b)
Highly viscous fluids	$C_D = \frac{16}{Re_t} \left[\left(\frac{1}{2} + 32\theta + \frac{1}{2} \sqrt{1+128\theta} \right)^{1/3} + \left(\frac{1}{2} + 32\theta - \frac{1}{2} \sqrt{1+128\theta} \right)^{1/3} \right]^{9/4} + \left(0.036 \left(\frac{128}{3} \right)^{1/9} Re^{8/9} Mo^{1/9} \right)$	$Mo > 10^{-8}$ $\theta = (0.018)^3 \left(\frac{2}{3} \right)^{1/3} Re^{8/3} Mo^{1/3}$	Rodrigue (2001)
Aqueous solution of CMC	$C_D = \frac{16}{Re_t} (1 + 0.173 Re_t^{0.657}) + \frac{0.413}{1 + 16300 Re_t^{-1.09}}$	$6 \leq Re_t \leq 60$	Dewsbury et al. (1999)

**Figure 4:** Effects of superficial gas velocity and CMC concentration on average bubble rise velocity. Reproduced from Deng et al. (2010) with permission from Elsevier.

in Re , Eo and Mo . In addition, it was also reported that bubbles take a teardrop shape at small values of Re , Eo and Mo . In the case of polyacrylamide (PAM) aqueous

**Figure 5:** Influence of injection period on bubble rise velocity in 2% CMC solution. Reproduced from Funfschilling and Li (2006) with permission from the Institution of Chemical Engineers (IChemE).

solutions, with further increase in the values of Re , Eo and Mo , bubbles take a regular flattened shape with a tail behind the bubble, whereas the bubble shapes in CMC aqueous solutions maintain an ellipsoidal shape. Dewsbury et al. (1999) worked with low-concentration aqueous

Table 9: Classification of bubble shapes based on shape factor and Eo , Re and Mo .

System (s)	Shape factor (eccentricity)	Classified based on Eo , Re , and Mo	Shape of bubble	Reason	Reference
Aqueous solution of CMC	$0.95 < E < 1.05$	$Eo < 1$ for all $Re < 10$ and Mo range	Spherical	The surface tension tends to minimize the surface area of a bubble;	Li et al. (2012a,b,c)
	$E < 0.95$	$1 < Eo < 30$ and $\log Mo < -4$	Bubble shape: spherical to oblate (directly)	thus, the bubble shape is always spherical	
	$E > 1.05$	$Eo > 30$ for all $Re > 10$ and the entire range of Mo	Spherical cap At low Re , bubble shape: prolate	– – Small bubble rising in high concentration of CMC aqueous solutions. The normal stress acted on the side of the bubble, leading to the bubble shape becoming prolate	
Non-Newtonian liquid (CMC and PAA) and Newtonian (PVP)	$E = 1 + 0.146 Eo^{0.437}$	$Eo \rightarrow 1$ and $Re \geq 20$	Spherical \rightarrow oblate	–	Wanchoo et al. (2003)
	For oblate drops ($E > 1$)	$0.1 \leq Eo \leq 1$ and $Re \leq 20$	Spherical		
	$E = 1 - 0.086 Eo^{0.338}$	$1 \leq Eo \leq 10$ and $Re < 1$	Spherical \rightarrow prolate		
Non-Newtonian and Newtonian liquids	For prolate drops ($E < 1$)	$1 \leq Eo \leq 10$ and $Re > 1$	Oblate		Gupta and Wanchoo (2009)
	$E = 1 + 0.050 (W_i/ReWe)^{-330}$	$10 \leq Eo \leq 100$ and all Re	Prolate		
	For oblate drops ($E > 1$)	Viscoelastic fluid	Prolate	–	
	$E = 0.772 (K_1(U/R)^m/\sigma/R)^{0.125}$	$1 \leq Eo \leq 40$ and $Re \geq 1$	Shape similar to that in viscoelastic fluid	–	
	For prolate drops ($E < 1$)	$\lambda_1 \geq 1.6$ s	Spherical	–	
	$0.9 \leq E \leq 1.1$ (spherical)	$\lambda_1 \leq 1.6$ s	Spherical \rightarrow oblate	–	
		Viscoelastic fluid	Spherical \rightarrow prolate	–	
		$Eo \leq 0.1$ and all Re	Oblate	–	
		$0.1 \leq Eo \leq 1$ and all $Re \leq 20$	Prolate	–	
		$1 \leq Eo \leq 10$ and $Re \leq 1$	Oblate	–	
Aqueous solution of CMC, PAA and PEO	$E = 0.616 \left[\frac{W_i}{ReW_e} \right]^{-0.168}$	–	Prolate \rightarrow spherical	At lower Re , surface tension tends to maintain the shape perfectly spherical	Acharya et al. (1977)
	for $0.68 < E < 1$	–	Oblate	At large Re , the fluid inertia caused major distortions from sphericity	
Newtonian liquid (45 combination of liquid-liquid)	$E = 1 + 0.0083 \left[\frac{W_i}{ReW_e} \right]^{-0.87}$	–			Wellek et al. (1966)
	for $1 < E < 1.5$	–			
	$E = 1 + 0.091 W_e^{0.95}$	$0.194 \leq W_e \leq 12.6$	–	–	
	$E = 1 + 0.093 W_e^{0.98} N_{\mu r}^{0.07}$	$0.0117 \leq N_{\mu r} \leq 53.4$			
	$E = 1 + 0.129 Eo$	For the entire range of Re $6 \leq Re \leq 1354$ $0.144 \leq Eo \leq 9.59$			

Table 9 (continued)

System (s)	Shape factor (eccentricity)	Classified based on Eo , Re , and Mo	Shape of bubble	Reason	Reference
Newtonian liquid (aqueous solution of glycerine and glycerine-ethanol mixture)	$E = 1$ $E = \frac{1.14}{(Re Mo^{0.23})^{0.176}}$ $E = \frac{1.36}{(Re Mo^{0.23})^{0.28}}$ $E = 62$	For $Re Mo^{0.23} < 2$ For $2 \leq Re Mo^{0.23} \leq 6$ For $6 \leq Re Mo^{0.23} \leq 16.5$ For $Re Mo^{0.23} > 16.5$	–	–	Takahashi et al. (1976)
Newtonian liquid (glycerine, corn syrup and castor oil)	$E = 0.8 - 0.217 (\log Re) - 0.84 (\log Re)^2$	For $0.1 < Re < 20$	–	–	Kojima et al. (1968)

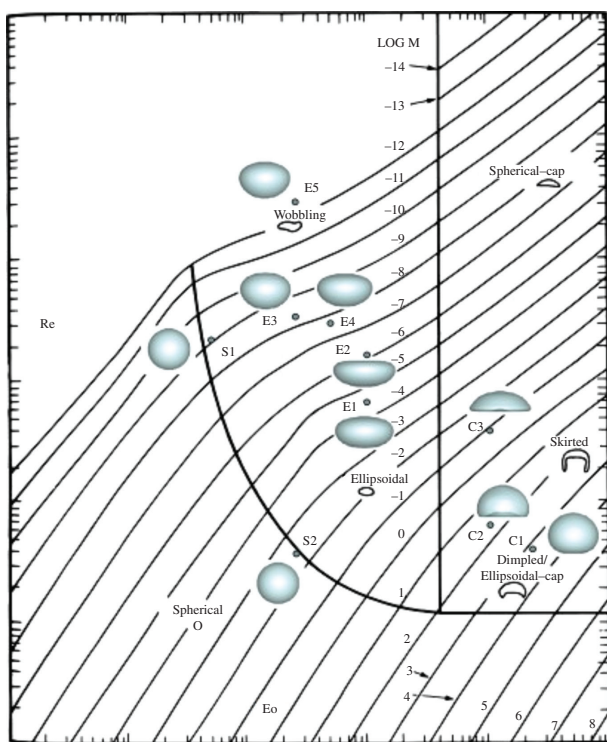


Figure 6: Regime diagram for the shape of bubbles ascending in a quiescent fluid according to Clift et al. (1978), with bubble shapes as a function of terminal Reynolds number and Eötvös number. Reproduced from Schwarz et al. (2016) with permission from Elsevier.

CMC (0.2%, w/w) solutions and found that the spherical bubbles were associated with $Re < 30$, ellipsoidal bubbles $30 < Re < 135$ and spherical cap bubbles with $Re > 135$.

The aspect ratio or eccentricity (E) of a bubble (defined as the ratio of its largest horizontal dimension to the largest vertical dimension) is used to characterize the bubble shape. Buoyancy and surface tension play an important role in determining the bubble shape. The

aspect ratio gradually decreases with an increase in Eo . Aspect ratio also depends on the types of non-Newtonian fluids used. Wenyuan et al. (2010) reported, on the basis of their study on 1.0% CMC aqueous solutions, that the bubble shape changes from spheroid to ellipsoid when Eo increases, and the bottom of the ellipsoidal bubble becomes flat in CMC aqueous solutions. Wenyuan and XiaoHong (2014) investigated the shape evolution of bubbles during bubble growth in 0.15% CMC aqueous solution and 97.3% glycerin solution at constant gas flow rate using laser image technique. It has been reported that the bubble grows into a spherical shape because of the predominant role of surface tension in the early period and thereafter is stretched gradually into a teardrop shape because of the common effect of buoyancy and shear thinning of fluid. Bubble shapes in shear-thinning fluid at different times are shown in Figure 7.

Elasticity of the non-Newtonian liquid also has a strong effect on the shape and terminal velocity of drops. Acharya et al. (1977) and Acharya and Mashelkar (1978) observed that the drag was higher in viscoelastic fluids such as polyacrylamide and polyethylene oxide than in

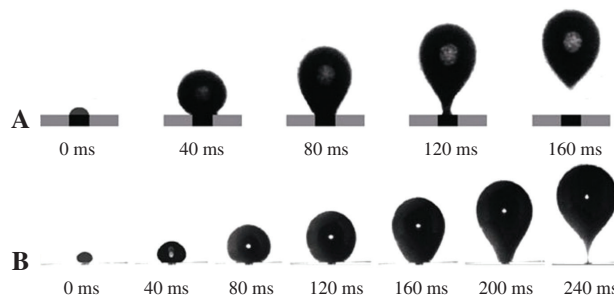


Figure 7: Regime bubble shapes in (A) CMC and (B) glycerin solutions at different times. Reproduced from Wenyuan and XiaoHong (2014) with permission from Springer.

Table 10: Different regimes of bubble shape and behavior.

Region	Galilei-Eötvös	Bubble shape
I	Low Eötvös and Galilei numbers (surface tension is high and gravity is low)	Ellipsoidal shape Bubble terminal velocity moves straight upwards
II	High Eötvös numbers and low Galilei numbers	An axisymmetric cap with a thin skirt trailing the main body of the bubble
III	Lower Eötvös and higher Galilei numbers (surface tension and inertial forces are both significant)	Bubble shape change with time Bubble rise in a zigzag or a spiral manner
IV	At low Galilei and high Eötvös numbers (that is, high Morton number)	Spherical cap and several small satellite bubbles Spherical cap bubble attains a constant shape and terminal velocity
V	High inertial force and low surface tension force	Doughnut-like or toroidal shape

viscoelastic fluids (carboxy methylcellulose) due to the large size of the wake formed in such fluids. Wanchoo et al. (2003) proposed a shape regime graph for the prediction of the shape and terminal velocity of drops moving freely under gravity in viscoelastic liquids and also correlated their drop eccentricity data in terms of Eo . On similar lines, Gupta and Wanchoo (2009) observed the shape of a single Newtonian liquid drop moving freely under gravity in a quiescent non-Newtonian liquid (both viscoelastic and viscoelastic) and proposed a correlation for the prediction of eccentricity of the Newtonian liquid drop. Furthermore, their experimental results reveal that the elasticity of fluid has a strong effect on the shape of a Newtonian liquid drop moving through a non-Newtonian viscoelastic liquid. Besides, shape regime for the Newtonian liquid drops in Newtonian and non-Newtonian (viscoelastic and viscoelastic) liquids has also been proposed by the authors. A classical review based on the motion and shape of the bubble or drop in non-Newtonian media was presented by Chhabra (2006). Recently, Tripathi et al. (2015) presented an attractive broad canvas (Galilei-Eötvös plane) of bubble behavior patterns spread into five regions (I to V) using simulated results as listed in Table 10. The authors have presented a novel bubble breakup phenomena fragmenting into a bulb-shaped bubble and a few satellite drops at low Mo values. Bubble rise velocity is generally higher in the case of strong shear-thinning fluids. Besides, bubble rise velocity becomes higher as bubble size increases. The net effect is a relatively lower gas holdup (Jana et al. 2014a,b).

3.6 Flow regimes

Different flow regimes (bubbly, churn turbulent and slug) are most frequently encountered in an industrial bubble column (Ryu et al. 1993). The knowledge of flow regime is very important for appropriate design and scale-up of bubble column reactors. Different regimes of gas-liquid flow may occur depending on the sparger geometry, superficial gas velocity, column geometry and CMC

concentration (Schumpe and Deckwer 1982, Haque et al. 1986). Gas holdup in different flow regimes has been reported in the literature and is represented by the separate empirical correlations (Schumpe and Deckwer 1982, 1987a,b, Haque et al. 1986, Lee et al. 1993, Ryu et al. 1993, Vinaya and Varma 1995). Schumpe and Deckwer (1982) observed that in the slug flow regime, the gas holdup is independent of the sparger type. For a bubble column with 0.305-m diameter, Godbole et al. (1984) reported that churn turbulent flow in CMC solution prevailed up to a viscosity of about 0.1 Pa·s. Haque et al. (1986) worked with highly viscous pseudoplastic CMC solutions in bubble columns of different diameters equipped with various sizes of spargers. It has been observed that Churn turbulent flow prevailed up to a viscosity of about 0.02 and 0.05 Pa·s for columns with 0.1- and 0.2-m diameter, respectively. Another significant finding was that slug flow regimes were not observed within the operating range of effective viscosity ($\mu_{\text{eff}} \leq 0.17$ Pa·s). Ryu et al. (1993) reported that gas holdup increases with gas velocity in the bubbly flow regime, decreases in the churn turbulent flow regime, and increases again in the slug flow regime. On similar lines, Vinaya and Varma (1995) observed that the gas flow rate, the plate perforation diameter, and the plate spacing are the significant variables influencing the three flow regimes and gas holdup. Schumpe and Deckwer (1987a,b) proposed an empirical correlation for gas holdup, which is valid for the heterogeneous flow regime. Another significant observation is that the effect of the column diameter was strong for the heterogeneous and slug flow regimes, but the trend was influenced by the small length-to-diameter ratio (L/D_c) of the columns for higher diameters.

3.7 Column geometry

Gas holdup is one of the most important parameters in the design of bubble columns. It is well established that the gas holdup depends on the superficial gas velocity and

the physical properties of the liquid. However, column diameter has been shown to have a significant effect on gas holdup when the aqueous solution of CMC was used (Godbole et al. 1982, 1984, Schumpe and Deckwer 1982, Kawase and Moo-Young 1986). On similar lines, Haque et al. (1986) investigated the effects of the column diameter using 0.10-, 0.20-, 0.38- and 1.0-m diameter on the gas holdup in bubble columns, with highly viscous pseudoplastic CMC. It was concluded that the gas holdup decreased ($\epsilon_G \propto D_c^{-0.15}$) with an increase in the column diameter in the churn turbulent regime. In the correlation proposed by Haque et al. (1986), physical properties like surface tension and liquid density were not considered.

Bubble column diameter is one of the factors that affect gas holdup (Godbole et al. 1982, Schumpe and Deckwer 1982, Haque et al. 1986, Kawase and Moo-Young 1986, Vatai and Tekic 1989, Mok et al. 1990). Based on experimental data sets, Godbole et al. (1982) proposed two correlations for pseudoplastic non-Newtonian solutions. Proposed correlation for highly viscous pseudoplastic solutions (≥ 0.02 Pa·s) in small-diameter columns indicates that the gas holdup ($\epsilon_G \propto D_c^{-0.5}$) is dependent on the reciprocal of the square root of the column diameter, while it excludes the effect of liquid viscosity on the gas holdup. The theoretical correlation proposed by Kawase and Moo-Young (1987) indicates that the gas holdup ($\epsilon_G \propto D_c^{-1/3}$) is proportional to the reciprocal of one third power of the column diameter. However, the authors did not consider the effect of effective viscosity (μ_{eff}) and surface tension of the liquid on gas holdup. Besides, gas properties like gas density and viscosity have been ignored in all the correlations mentioned above for viscous non-Newtonian systems.

In industrial applications like fluidization SO_2 scrubbing and segregation of particles in fluidized columns, flotation cells, biochemical reactions, and biological wastewater treatment, standard and tapered bubble columns play a significant role for gas-liquid mass transfer. At lower taper angles, the tapered bubble column is capable of providing higher fractional gas holdup due to the higher circulation rate of smaller bubbles in an annular region as compared to a standard bubble column under similar conditions (Jana et al. 2014a,b, 2015). The effect of the taper angle in the case of varying aqueous concentrations of non-Newtonian solutes, like CMC, on the gas holdup has been scarcely reported in the literature.

3.8 Sparger geometry

The type of gas sparger is another important parameter that characterizes the bubble size and movement in a

bubble column and in turn affects gas holdup. Various types of gas spargers that have been studied in the literature are ring type, perforated plate, porous plate, single nozzle, ejector-type gas distributor and membrane type. A few authors have reported the effect of sparger hole size on gas holdup (Franz et al. 1980, Schumpe and Deckwer 1982). Franz et al. (1980) worked with different sizes of perforated plates and estimated the gas holdup in CMC aqueous solutions. It has been concluded that a perforated plate with lower hole size produces much higher gas holdup than the corresponding higher sizes. On similar lines, Haque et al. (1986) worked on four different designs of sieve plate spargers and studied their effect on gas holdup. It has been found that gas holdup remains unaffected by the sparger design in the heterogeneous and slug flow regimes. A similar observation was made by Schumpe and Deckwer (1982). Veera and Joshi (2000) reported gas holdup profiles in CMC solutions in a bubble column equipped with perforated plate containing different sizes of holes and developed gas holdup correlation with reasonable acceptable accuracy. Anastasiou et al. (2013) worked with several non-Newtonian shear-thinning fluids in bubble columns with a porous sparger to provide very fine air bubbles and formulated an empirical correlation in terms of dimensionless numbers to predict the average gas holdup with reasonable accuracy ($\pm 10\%$). On similar lines, Passos et al. (2015) studied the addition of organic surfactant in a non-Newtonian liquid in a bubble column equipped with a porous sparger and proposed a correlation that can predict the gas holdup with a slight sacrifice in accuracy ($\pm 20\%$). Various types of spargers used in non-Newtonian systems are listed in Table 11.

As may be seen from Table 11, types of sparger and their dimensions do not have a definite trend on gas holdup. Use of radial gas sparger imparts a higher gas holdup as compared to the plate-type sparger. An empirical correlation for gas holdup in a bubble column containing aqueous CMC solution using a radial gas sparger has been reported earlier. Furthermore, a bubble column equipped with a radial gas sparger yields a higher gas holdup by 1.5–3 times than that of a bubble column or external loop airlift reactor equipped with a plate-type sparger (Ryu et al. 1993).

3.9 Internals

In commercial bubble columns using non-Newtonian solutions, internal obstacles such as perforated plates (Chen and Yang 1989), baffles (Deckwer and Schumpe 1993, Pandit and Joshi 2005), vibrating helical springs (Balamurugan et al. 2010), mixers and heat exchanger tubes

Table 11: Types of spargers used in experimental studies.

Type of sparger (s)	Specifications	Remarks	Reference
Perforated plate	Hole diameter: 0.5–3.0 mm Hole arrangement: triangle Number of holes: 141–360 Fractional free area (%): 0.040–5.64	Lower hole size produces much higher gas holdup	Franz et al. (1980)
Sintered plate, perforated plates	Sintered plate Mean pore width: 0.2 mm Perforated plate: 1 No. of holes: 421 Hole size: 0.5 mm Perforated plate: 2 No. of holes: 73 Hole size: 1.0 mm Perforated plate: 3 No. of holes: 19 Hole size: 2.0 mm	Type of gas distributor does not affect gas holdup in the slug flow regime	Schumpe and Deckwer (1982)
Sieve plate, ring sparger	Sieve plate Number of holes: 100, 109, and 168 Hole diameter: 0.3, 1.0, 1.5, and 2.0 mm Pitch: circular and square Ring sparger Number of holes: 148 Hole diameter: 2.0 mm Diameter of ring: 580 mm Inside tube diameter: 26 mm	Gas holdup unaffected by sparger design in the heterogeneous and slug flow regimes	Haque et al. (1986)
Radial gas sparger	Stainless steel 0.38 m-OD × 0.15 m-H	1.5–3 times higher gas holdup	Ryu et al. (1993)
Perforated plate	Hole diameter: 0.003–0.012 Fractional free area (%): 0.1–0.52 Plate spacing (m): 0.05–0.85	Gas holdup decreases with an increase in hole diameter Gas holdup decreases with an increase in plate spacing	Vinaya and Varma (1995)
Single-nozzle sparger	Hole diameter: 0.7, 1.0, and 1.3 mm	Gas holdup remains unaffected by the sparger diameter	Ghosh and Upadhyay (2007)
Porous disc (fine pore sparger)	SS 316 Pore size: 40 μm Sparger diameter: 4.5 and 9.0 cm	Higher gas holdup was produced using 9.0-cm sparger as compared to 4.5-cm sparger	Passos et al. (2015)

are normally used. Instrumentation probes, downcomers and risers with heat exchangers are all considered to be various forms of internal obstacles in industrial applications of bubble columns (Pradhan et al. 1993). The presence of such internals and their relative positioning in the column can significantly affect the reactor's hydrodynamics, heat and mass transfer characteristics, as well as the nature and yield of the reaction products. In addition, internal structures are also useful for controlling the flow behavior and back mixing in the column. However, most of the reported studies in the literature do not investigate the effect of internals on the hydrodynamics in bubble columns. The appropriate selection of the internal structure can lead to enhanced reactor performance, which is to be considered for proper modeling and design of bubble

columns. In order to obtain the desired performance for a given application, bubble columns often need to be equipped with internals of different types. Among the few reported studies in non-Newtonian systems, Pradhan et al. (1993) investigated the effect of volume fraction varying from 0.014 to 0.193 covered by internals on overall gas holdup. In this study, two different types of configuration of internals like helical coils and a vertical straight tube bundle were used in a 0.102-m-diameter and 2.5-m-height Plexiglas column. Gas holdup was found to increase with the increase in the volume fraction covered by the internals in the column for a particular gas velocity and type of internals. This conforms to observations made by other researchers (Yamashita 1987a,b, Saxena and Vadivel 1988, Roy et al. 1989, Pradhan et al. 1991, Youssef and Al-Dahhan

2009, Jhawar and Prakash 2014) who carried out their investigations in Newtonian systems with vertical tubes as internals in the column. Physically, the presence of an internal structure reduces the cross-sectional area available for flow, retards the bubble motions, turbulence becomes very vigorous and bubbles can move rapidly in the radial direction in spite of obstacles presented by the internals. Higher volume fraction of internals promotes breakage of large bubbles to tiny sizes, and this is more prominent in the case of coil-type internals, thereby resulting in higher gas holdup. Another significant finding was that bubbles remained dispersed in the liquid for a long period of time even after stoppage of gas flow in the column. Besides, the

pressure drop per unit height ($\Delta P/\Delta H$) decreased with the increase in superficial gas velocity for a particular value of volume fraction covered by the internals in the column. Modified gas velocity in the presence of internals in the bubble column can be written as $u_{gm} = u_g / (1 - x_v^i)$, where x_v^i is volume fraction of the internals. Recently, the effect of vibrating internals such as vibrating helical springs on gas holdup for a Newtonian liquid in bubble columns was reported by Balamurugan et al. (2010). It has been observed that gas holdup was 135% higher as compared to without an internal bubble column system. Another significant observation was that vibrating helical springs offer a simple, cost-effective and easy way to enhance gas holdup

Table 12: Configuration of internals used for Newtonian and non-Newtonian systems.

System(s)	Type of internal structure	Details of internals	Key findings	Reference
Non-Newtonian (CMC solution)	Helical coils and a vertical straight tube	Helical coils (copper) with 3.5- and 6.8-cm diameters Straight tube (stainless steel) with 1.2-, 1.5-, and 2.0-cm outer diameters	A fixed gas velocity, $\Delta P/\Delta H$, value decreases with an increase in volume fraction covered by each type of internals Gas holdup increases with an increase in superficial gas velocity for a particular volume fraction of internals	Pradhan et al. (1993)
Non-Newtonian (CMC solution)	Perforated plate	37 circular plates made of stainless steel (six mesh wire screen sheets) Fractional free area: 0.64	Six-mesh screen may have become less effective to control the growth of bubbles in highly viscous solutions	Chen and Yang (1989)
Newtonian (air-tap water)	Circular tube bundle (A)	No. of tubes: 15, tube diameter: 12.7 mm, tube length: 1.50 m, wall-to-wall spacing between tubes: 4.4 mm	Highest gas holdups found with A and AB ₂ combination internals followed by B ₂ , while lowest values are obtained with B ₁	Jhawar and Prakash (2014)
	Concentric baffle (B ₁ and B ₂)	No. of blades: 6, length of blade: 35 mm, width of blade: 19 mm, blade angle: 60° from axis, z=0.15 m for B ₁ and 0.3 m for B ₂		
Newtonian (air-tap water)	Helical springs	Range of internal diameter: 1.0–4.0 cm Wire thickness: 0.05–1.9 cm Number of internals: 1–41	Gas holdup 135% higher than without use of internals in the bubble column system	Balamurugan et al. (2010)
Newtonian (air-tap water)	Plexiglas rods	Two circles of six rods each covered 5% of the total cross section of the column 48 rods placed in a triangular pitch of 2.4 cm that covered 22% of the total cross section of the column	Gas holdup and interfacial area increase with an increase in covered area by internals	Youssef and Al-Dahhan (2009)
Newtonian (air-tap water)	Vertical pipe and rod	Pipe and rod internals Length: 250–280 cm, MOC: vinyl chloride resin and iron	Gas holdup increased with the outer diameter of pipe and rod Does not depend on the arrangement of pipes and rods	Yamashita (1987a)
Newtonian (air-tap water)	Baffle plate shapes – ring, square, equilateral triangle, cross, modified cross and rectangle	Ring diameter: 150 mm Square: 50–110 mm ² Equilateral triangle: 50–130 mm ² Cross: 120–140 mm ² Modified cross: 80 mm ² , Rectangle: 60 × 140 mm ²	Gas holdup depends on the cross-sectional area of internals but is independent of their geometrical shape	Yamashita (1987b)

Table 13: Summary of effects of variations of parameters on gas holdup.

Parameter	Variation in parameter value	Effect on gas holdup	Reason(s)	Reference
Effective viscosity	↑	↓	The more viscous fluid causes cluster formation of bubbles due to an increased coalescence phenomenon leading to a lower gas residence time and consequently to a lower gas holdup. In other words, the holdup fraction of large bubbles is always higher than the holdup of small bubbles	Godbole et al. (1984), Fransolet et al. (2005), Lakota (2007)
Column diameter	↑	↓	Higher cross-sectional area of bubble column provides large circulation rate of bubbles due to coalescence of bubbles, and it is responsible for lower gas holdup	Godbole et al. (1982), Haque et al. (1986)
Surface tension	↑	↑	Lower surface tension liquids promote small bubbles resulting in higher gas holdup	Schumpe and Deckwer (1987a,b)
Internals	↑	↑	The internals reduce the effective cross-sectional area of the bubble column, and it controls the flow behavior and back mixing in the system. As a result, the bubble motions become very vigorous and can move rapidly in radial direction in spite of interruption presented by the internals	Pradhan et al. (1993)
Gas velocity	↑	↑	Major contribution to the overall gas holdup comes from fast-rising bubbles (due to bubbles coalescence phenomena), and it significantly increases with increase in superficial gas velocity. The small bubbles gas holdup is due to slow rising and long residence time. It is unaffected with an increase in gas velocity	Devine et al. (1985), Mok et al. (1990)
Concentration (CMC and other solution)	↑	↑	Bubble size decreases with an increase in gas velocity due to increasing shear for a given CMC concentration. Bubble size increases with CMC concentration	Kantak et al. (1995)
Consistency index	↑	↑	Higher consistency index indicates higher effective viscosity of non-Newtonian liquids. The effective viscosity depends significantly on shear rate. It decreases with an increase in shear rate. Higher shear rates are attained at higher superficial gas velocities. Lower effective viscosity liquid promotes higher gas holdup	Kawase and Moo-Young (1986)
Flow behavior index	↓	↓	Reduction in gas holdup is caused by the increase of pseudoplasticity of liquid or decrease in flow index	Kawase and Moo-Young (1987)
Taper angle	↓	↑	Smaller tapered angle promotes bubble coalescence, but some smaller bubbles recirculate in the annular region, which is responsible for the higher gas holdup	Jana et al. (2014a,b)
Sparger design	Smaller/higher hole size	↔	At lower gas velocities, the smaller hole size of the perforated sparger generates shorter bubble size, which promotes higher gas holdup. It is unaffected by sparger design in the heterogeneous and slug flow regimes	Franz et al. (1980)
Elasticity of liquid	↑	↑	Higher elasticity liquid prevents bubble coalescence, and small bubbles are formed	Moo-Young and Kawase (1987)
Pressure	↑	↑	An increase in the gas density and a reduction in coalescence tendency of the gas bubbles with increase in pressure are responsible for the formation of smaller bubbles. It rises with lower velocity along the column height, and thus, the gas holdup is higher	Esmaili et al. (2016)

↑, Increasing; ↓, decreasing; ↔, unaffected.

even at higher superficial gas velocity. From the literature, the vibrating or flexible structures like helical springs have a strong potential for use as internals in industrial bubble columns; hence, studies on helical springs for non-Newtonian systems need to be conducted. For effective internals study, expectations from internals in bubble columns are the lower volume fraction of internals with higher surface area, no external energy input, reliability for higher gas flow rate, and least expenditure on maintenance cost of internals. Table 12 summarizes the various types of internals geometry used in Newtonian and non-Newtonian systems.

3.10 Elevated pressure

Physical properties of the gas and liquid phases such as gas density, liquid viscosity and surface tension of liquid are influenced by the system pressure (Kang et al. 1999, Esmaeili et al. 2016). The effects of elevated pressure and rheological properties on gas holdup in a bubble column with a non-Newtonian solution have also been reported in the literature. It has been established that application of elevated pressure leads to higher gas holdup. The effect of elevated pressure (0.1–0.6 MPa) on gas holdup has been investigated for aqueous solutions of CMC (Kang et al. 1999). At higher system pressures than atmospheric pressure, liquid viscosity and surface tension become significantly reduced with an increase in system temperature, whereas its influence on gas density is less pronounced. Thus, it tends to reduce the bubble sizes. The surface tension of liquid slightly reduces and gas density significantly increases with increases in system pressure, resulting in decreased bubble size (Lin and Fan 1999, Kang et al. 2000). Studies on the effect of elevated pressure on the gas holdup for non-Newtonian liquids (aq. CMC and xanthan gum) have been scarcely reported (Esmaeili et al. 2016). It has been found that gas holdup increases with an increase in operating pressure. Another significant finding was a delay in flow regime transition with increases in operating pressure.

It has been concluded that gas holdup remains unaffected by impeller design in a non-Newtonian liquid. The summary of effects of variations (increase/decrease) in parameters on gas holdup in non-Newtonian systems is listed in Table 13.

4 Discussion

A careful review of Tables 1 and 13 indicates that although a number of correlations have been proposed, no single

generalized correlation is applicable under different operating conditions. The approaches used are largely empirical. The empiricism has been mainly due to incomplete knowledge of the hydrodynamics of the bubble column. Although empirical correlations are useful for the design of bubble columns and modeling purposes, they give limited information about the mechanism of physical processes occurring in a bubble column. Theoretical analysis may yield some insight into the transport phenomena inside the bubble columns. Theoretical correlations based on established classical concepts are a good alternative and are applicable both to non-Newtonian fluids as well as Newtonian fluids. Unfortunately, there are few single theoretical correlations available which can provide reasonable prediction of gas holdup in bubble columns.

A significant part of the gas holdup in Newtonian and non-Newtonian liquids may be due to very small bubbles. The behavior of bubbles in highly viscous liquids (non-Newtonian liquid) is very different from that of water and other low-viscosity liquids (Newtonian liquid). The coalescence of bubbles near the sparger and the rupture of larger bubbles at the surface generate very tiny bubbles, which, due to their low rise velocity, accumulate and circulate with the liquid. These two phenomena generate a variety of bubble size distributions, which appear in both Newtonian and non-Newtonian liquids. A precise estimation of the size of tiny bubbles is useful to develop an empirical correlation which is approximately close to the realistic phenomena occurring in the bubble column. There are several possibilities to explain the hydrodynamic phenomena for Newtonian and non-Newtonian fluids in a bubble column.

Hydrodynamics of a bubble column depends on the liquid height-to-column diameter ratio (H_L/D_c). At low liquid heights, equilibrium bubble size is not attained, and hence, the bubble rise and liquid circulation velocities do not attain their equilibrium values. For larger values of H_L/D_c , the bubble breakup due to shearing leads to equilibrium bubble size, resulting in a constant gas holdup. Haque et al. (1986a,b) reported that for $H_L/D_c \leq 3$, gas holdup decreases with increasing value of H_L/D_c . Some contradictory findings have also been reported in the literature. Ghosh and Upadhyay (2007) once declared the H_L/D_c parameter to be insignificant for used range of H_L/D_c , but the same parameter was used in the correlation proposed by the authors.

The bubble column hydrodynamics are also supposed to depend on the liquid-phase viscosity. It is reported that the gas holdup is lower for fluids of higher viscosity. This effect is likely to be more pronounced for non-Newtonian fluids than for Newtonian ones, which can be attributed to the reduced surface tension of the liquid. Few investigators

involved surface tension terms in proposed correlations for non-Newtonian systems (Schumpe and Deckwer 1987a,b, Lee et al. 1993, Anastasiou et al. 2013, Jana et al. 2014a,b, Passos et al. 2015). The bubble flow is also characterized by the dispersion of the bubbles and the free space available between the bubbles. If the bubbles are small enough and there is sufficient free space, bubble population increases with an increase in gas flow rate and thus gas holdup increases. However, beyond a certain limit, there is little effect of gas flow rate on bubble population, and coalescence of bubbles increases significantly and hence gas holdup remains constant.

From the literature, gas holdups in non-Newtonian liquids such as CMC solutions are higher than those in Newtonian liquids like water. This is because of the fact that for a highly viscous CMC solution, the gas bubbles inside the column face more resistance to move. Thus, the residence time of the gas bubbles increases, which in turn increases the gas holdup. However, after a certain concentration of CMC solution, it remains more or less constant, as there are two contradictory effects of CMC concentration on gas holdup. As the concentration increases, gas holdup increases for increase in residence time of the bubbles, but simultaneously, the coalescence of bubbles increases with increase in CMC concentration, which tends to decrease the gas holdup.

5 Network development

Over the past two decades, ANNs have emerged as powerful, attractive and versatile computational tools for organizing and correlating information in ways that have proved useful for solving complex types of problems that are difficult to attempt using traditional numerical and statistical methods. They are also capable of dealing with uncertainties, noisy data and nonlinear relationships. Owing to their several attractive characteristics, ANNs have been widely used in chemical engineering applications such as steady-state and dynamic process modeling, process identification, yield maximization, nonlinear control, and fault detection and diagnosis, in addition to hydrodynamics of bubble column (Reisener et al. 1993, Bulsari and Saxen 1994, Yang et al. 1999, Alvarez et al. 2000, Garcia-Ochoa and Castro 2001, Jamialahmadi et al. 2001, Utomo et al. 2001, 2002, Lemoine et al. 2003, 2008, Lemoine and Morsi 2005, Shaikh and Al-Dahhan 2003, Yuanxin et al. 2003, Sharma et al. 2004, Behkish et al. 2005, Al-Masry and Abdennour 2006, Baawain et al. 2007, Gandhi et al. 2007, Ahmed Zeki 2009, Ibrehem and Hussain 2009, Gandhi and

Joshi 2010, Amiri et al. 2011a,b, Chen et al. 2013, Pirdashti et al. 2013, Bhunia et al. 2015). ANNs consist of a group of artificial neurons that are interconnected in a way similar to the architecture of the human brain. In this study, a multilayer feed-forward neural network has been used to design the complex nonlinear relationships between input and output layers. Each layer has a specific number of neurons that play a significant role in the modeling of the system. To identify which of the input variables have the most significant impact on gas holdup, a sensitivity analysis was carried out on the trained network. A simple and innovative technique proposed by Garson (1991) was used to define the relative importance of the input variables by examining the connection weights of the trained network. The results of the sensitivity analysis are discussed later.

The multilayer perceptron is the most popular and widely used in ANN studies. It consists of three or more layers. The first layer has the input neurons (parameters), while the last layer contains the output. In addition, one or more layers can be between the input and output layers, which are known as the hidden layers (Jana et al. 2014a,b, Mitra et al. 2014). The neural network performance is also sensitive to the number of neurons in the hidden layer. The number of hidden neurons depends on the complexity of the problem and is determined during the training process by trial and error. However, too many neurons in the hidden layer may result in the overfitting of the model and may produce large errors in the predicted output. Also, few neurons in a hidden layer may lead to unsatisfactory performance of the network. The back-propagation algorithm technique, which was developed by Rumelhart et al. (1986), is the most popular process and has been used in many fields of science and engineering. With this method, the weights of the network are adjusted during the training phase to minimize the sum of the squared errors. Rheological parameters, that is, flow behavior index (n) and consistency index (k) vary with CMC concentration (Haque et al. 1986, Kawase and Moo-Young 1987). Available literature data do not explain the parameter intensity that affect the gas holdup using the non-Newtonian system. ANN and Garson's algorithm are used for addressing this gap. For a case study, experimental data of Haque et al. (1986) were used to develop a three-layer feed-forward neural network model. In order to increase the numerical stability of the model construction, data were normalized between 0 and 1 before training. This is accomplished by using the formula (Olden and Jackson 2002):

$$x_n = \frac{(x_i - x_{\min})}{(x_{\max} - x_{\min})}$$

where x_n , x_p , x_{\min} , and x_{\max} are normalized value, actual input data, minimum and maximum input data, respectively.

5.1 Data division

The data used (49 data sets) were divided into three sets, viz., training, cross validation and testing. Seventy percent (29 data sets) of the data points were selected for training, 15% for cross validation (10 data sets) and 15% for testing the network (10 data sets). The training data points were used to train the network and compute the weights of the inputs. The test data points were used to measure the performance of the selected ANN model. The ranges of parameters used in ANN are shown in Table 14.

5.2 Activated function

There is no agreement in the literature on which type of activation function is to be used, and it depends on the type of input training data and the case under investigation. For new users, it is difficult to choose the activation function for their data as they have no guidelines to choose from (Lahiri and Ghanta 2008). Five variables such as flow behavior index, consistency index, column diameter, gas flow rate and density of aqueous CMC solution were selected for the implementation of an artificial intelligence-based approach. Multilayer networks typically use tangent sigmoid activation functions in the hidden layers. Sigmoid functions are characterized by the fact that their slope must approach zero, as the input becomes large. The tangent sigmoid activation functions for the input and hidden neurons are needed to introduce nonlinearity into the network. Without nonlinearity, hidden layers would not make networks more powerful than just plain perceptrons (Hamed et al. 2004). Based on these facts, in this study, three-layer feed-forward ANN models ($5:N_H:1$) with tangent sigmoid transfer function (tansig) at the hidden layer with N_H neurons and a

linear transfer function (purelin) at the output layer were implemented for gas holdup.

5.3 Back-propagation training algorithm

Training a network consists of an iterative process in which the network is given the desired inputs along with the correct outputs for those inputs. During training, if it fails to produce the correct output it rereads the input and again tries to produce the correct output (whining a reasonable error margin). The weights are slightly adjusted during each iteration through the training set (known as a training cycle, epoch or iteration) until the appropriate weights have been established (Lahiri and Ghanta 2008). Training is the process of optimizing the connection weights. The method most commonly used for establishing the optimum weight combination of feed-forward neural networks is the back-propagation algorithm (Rumelhart et al. 1986), which is based on first-order gradient descent. Depending on the complexity of the task to be learned, thousands of training cycles may be needed for the network to correctly identify the training set (Lahiri and Ghanta 2008). There are several different back-propagation training algorithms published in the literature (Lahiri and Ghanta 2008, Bar et al. 2010a,b, Mitra et al. 2014, Jana et al. 2014a,b). It is difficult to know which training algorithm will be the fastest for a specific data set in ANN-based problems. It may depend on many factors including the complexity of the problem and the number of data points in the training set. In this study, the Levenberg-Marquardt (LM) training algorithm was adopted for all $(5 - N_H - 1)$ network structures.

5.4 Model validation using statistics

The correlation coefficient (R^2), the root mean square error (RMSE), and the maximum average percentage error (MAPE) were the main criteria used to evaluate the prediction performance of ANN models. RMSE was used as it has the advantage that large errors receive much greater attention than small errors (Hecht-Nielson 1990). The following expressions (Pareek et al. 2002, Sharma et al. 2004, Lahiri and Ghanta 2008) were used for error analysis of network prediction:

$$\text{RMSE} = \sqrt{\frac{\sum_{i=1}^{i=N_S} (y_{\text{predicted},i} - y_{\text{experimental},i})^2}{N_S}}$$

$$\text{MAPE} = \frac{1}{N_S} \sum_{i=1}^{N_S} \frac{|y_{\text{predicted},i} - y_{\text{experimental},i}|}{y_{\text{experimental},i}} \times 100$$

Table 14: Database used in ANN (Haque et al. 1986).

Parameters	Range	
Flow behavior index	$0.50 \leq n \leq 0.80$	(-)
Consistency index	$0.012 \leq k \leq 1.320$	(Pa · s ⁿ)
Column diameter	$0.2 \leq D_c \leq 1.0$	(m)
Gas flow rate	$0.033 \leq u_g \leq 0.24$	(m/s)
Density of aqueous CMC solution	$1000 \leq \rho_{\text{aq,CMC}} \leq 1009$	(kg/m ³)
Gas holdup	$0.0447 \leq \varepsilon_g \leq 0.381$	(-)

$R =$

$$R = \frac{\sum_{i=1}^{N_s} (y_{\text{experimental},i} - y_{\text{experimental,mean}})(y_{\text{predicted},i} - y_{\text{predicted,mean}})}{\sqrt{\sum_{i=1}^{N_s} (y_{\text{experimental},i} - y_{\text{experimental,mean}})^2} \sqrt{\sum_{i=1}^{N_s} (y_{\text{predicted},i} - y_{\text{predicted,mean}})^2}}$$

where $y_{\text{experimental}}$ and $y_{\text{predicted}}$ are the experimental and predicted values from output neurons, respectively, and $y_{\text{experimental,mean}}$ and $y_{\text{predicted,mean}}$ represent the average actual and predicted values from output neurons. N_s represents the number of data sets, while the subscript i refers to the data set number.

5.5 Model optimization

Feed-forward networks trained with the back-propagation algorithm have been applied successfully by many researchers (Shaikh and Al-Dahhan 2003, Sharma et al. 2004, Behkish et al. 2005, Lahiri and Ghanta 2008). Accordingly, the back-propagation algorithm was used for optimizing the connection weights in this study. Information about the back-propagation algorithm has been reported earlier (Garcia-Ochoa and Castro 2001, Lemoine et al. 2003, Shaikh and Al-Dahhan 2003, Yuanxin et al. 2003, Sharma et al. 2004, Behkish et al. 2005, Gandhi and Joshi 2010, Bar and Das 2011, Jana et al. 2014a,b). The LM algorithm was used in this study. It is one of the most appropriate higher-order adaptive algorithms known for minimizing the mean square error of a network. The value of μ (μ) and iterations were taken as 0.001 and 1000, respectively (by default). In the present work, MATLAB R2014 (The MathWorks Inc., Natick, MA, USA) software, running on an Intel core (TM) i5-2410M Processor 2.30 GHz, 4.0 GB RAM, 64-bit based HP Laptop (HP Inc., Bangalore, Karnataka, India) was used for modeling and simulation purposes.

For optimization of the network, two neurons in the hidden layers were used as an initial guess and were run for the neural regression with tangent sigmoid transfer function (tansig) at the hidden layer and a linear transfer function (purelin) at the output layer. RMSE, MAPE and cross correlation coefficient R^2 were found for each run. The procedure was repeated by varying the hidden layer nodes from 2 to 12. Table 15 illustrates the dependence of RMSE and MAPE on the number of neurons in the hidden layer for the present output sets. For the generalization of the model, optimum iteration was found by monitoring the validation error. Training was stopped when the validation error started rising. Weights and learning rate at this iteration were considered for testing the suitability of

Table 15: Error analysis of applied ANN structures.

ANN structure	RMSE	MAPE	R^2
5-2-1	0.0039	12.8690	0.96447
5-3-1	0.0029	10.8726	0.96737
5-4-1	0.0002	9.0554	0.98993
5-5-1	0.0001	2.6043	0.99688
5-6-1	0.0004	3.2944	0.99301
5-7-1	0.0007	2.6646	0.99664
5-8-1	0.0116	6.8737	0.99312
5-9-1	0.0002	4.4138	0.99403
5-10-1	0.0048	5.2684	0.99333
5-11-1	0.0011	3.6246	0.99298
5-12-1	0.0014	10.9604	0.99309

Values in bold face represent optimized ANN structure.

the model using the test data set. As seen in Table 15, the number of neurons in the hidden layer was optimized as five ($N_h = 5$), with the minimum RMSE and MAPE of 0.0001 and 2.6043, respectively, for the estimation of gas holdup. When the number of neurons exceeded these global minima, RMSE and MAPE values increased significantly from 0.0001 to 0.0004 and from 2.6043 to 3.2944, respectively, for the training sets of gas holdup. The R^2 , RMSE and MAPE values for different ANN structures containing different neurons in the hidden layer are shown in Table 15. The output tracks the targets very well for training, testing and validation, and the correlation coefficient was found to be 0.99688 for total response. It indicates good matching between the experimental and predicted data.

5.6 Sensitivity analysis using Garson's algorithm

A method proposed by Garson (1991) is used for assessing the relative importance of various input variables on the output in a supervised neural network by using connection weight matrix. The contribution of variables in ANNs has been reported in the literature (Olden 2000, Olden and Jackson 2002, Olden et al. 2004, Sharma et al. 2004, Valente et al. 2014). The weights contain all the information about the network. The relative contribution of the independent variables to the predictive output of the neural network depends mainly on the magnitude and direction of the connection weight between the neurons (Olden 2000).

Negative connection weights represent inhibitory effects on neurons (reducing the intensity of the incoming signal) and decrease the value of the predicted response, whereas positive connection weights represent excitatory

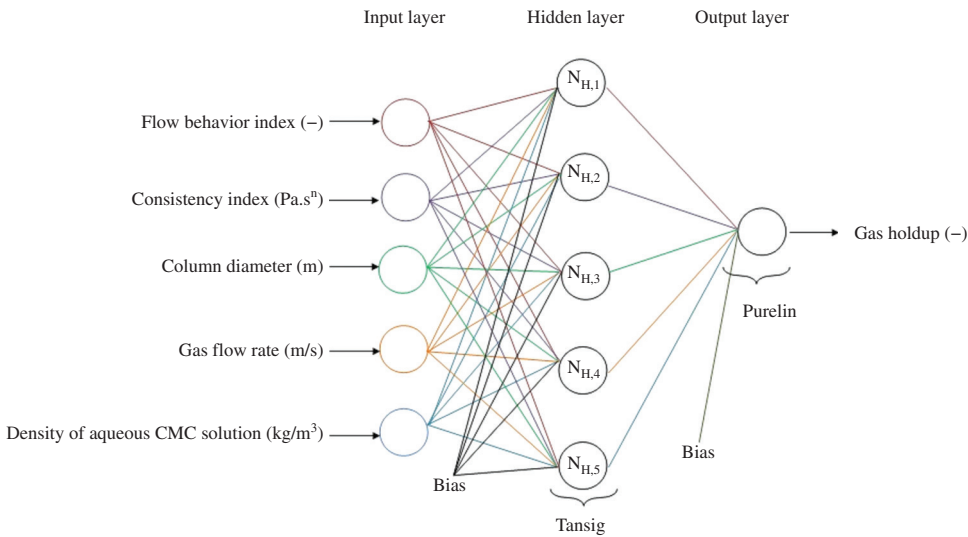


Figure 8: Graphical representation of the optimized structure of the ANN (5-5-1).

effects on neurons (increasing the intensity of the incoming signal) and increase the value of the predicted response (Olden and Jackson 2002).

Sensitivity analysis was conducted to assess the relative importance of various operating (input) parameters. The neural network weight matrix used to carry out sensitivity analysis is as follows:

$$RI_{j,n} = \frac{\sum_{m=1}^{N^h} \left\{ \left(|w_{jm}^{ih}| / \sum_{k=1}^{N^i} |w_{km}^{ih}| \right) \times |w_{mn}^{ho}| \right\}}{\sum_{k=1}^{N^i} \left\{ \sum_{m=1}^{N^h} \left(|w_{km}^{ih}| / \sum_{k=1}^{N^i} |w_{km}^{ih}| \right) \times |w_{mn}^{ho}| \right\}} \quad (2)$$

where $RI_{j,n}$ is the relative importance of the j th input variable on the n th output variable; N^i and N^h are the number of input and hidden neurons, respectively; and w s are the connection weights, with the superscripts “i”, “h” and “o” referring to input, hidden and output layers, respectively, and subscripts “k”, “m” and “n” referring to input, hidden and output neurons, respectively.

It was observed that the network performance stabilized after the inclusion of five nodes in the hidden layer (Figure 8). The optimized ANN parameters are summarized in Table 16. Therefore, based on the approximation of RMSE, MAPE and R^2 , a number of hidden neurons equal to five were adopted, and a three-layered, feed-forward, back-propagation neural network was used for modeling of the process. The relative importance of parameters that affect gas holdup is presented in Table 17.

The relative importance of various variables calculated by equation (2) is shown in Table 17. As can be seen, the variables such as flow behavior index (26.94%),

Table 16: Optimized ANN parameters for relative importance of parameters.

Particulars	Detail of optimized value of ANN
Number of training algorithm	1 (LM)
Number of neurons in input layer (flow behavior index, consistency index, column diameter, gas flow rate, and density of aqueous solution)	5
Number of hidden layer	1
Number of neurons in the hidden layer	12 (varies between 2 and 12; optimum number of neurons found by trial and error)
Number of neurons in the output layer (gas holdup)	1
Number of input data used for network training	29
Number of data used for validation	10
Number of data used for testing	10
Number of activation function tested in the hidden layer	1
Hidden layer transfer function	Tansig
Number of activation function tested in the output layer	1
Output layer transfer function	Purelin

column diameter (24.75%), and gas flow rate (20.23%) have strong effects on gas holdup; however, the consistency index (14.53%) and density of the aqueous CMC solution (13.54%) are also significant. Therefore, none of the five variables studied in this work can be neglected. The results indicate that higher flow behavior index, lower

Table 17: Relative importance of parameters affecting gas holdup.

Input variable	Connection weight					Relative importance (%)	Relative significance
	$H_{n,1}$	$H_{n,2}$	$H_{n,3}$	$H_{n,4}$	$H_{n,5}$		
Column diameter (m)	0.13539	-0.87248	-1.4549	0.29635	-2.1439	24.756	More significant
Gas flow rate (m/s)	1.9899	0.93952	-0.31921	0.073076	0.71275	20.231	More significant
Flow behavior index (-)	-0.89689	0.015978	-1.1527	1.2844	-1.1656	26.940	More significant
Consistency index (Pa · s ⁿ)	-0.29821	0.95954	-0.13155	0.61254	-0.67611	14.531	Significant
Density of aqueous CMC solution (kg/m ³)	-0.50295	-1.4677	0.16882	0.20588	-0.32647	13.540	Significant
Bias of hidden layer	2.0085	1.3475	0.278	0.58252	-2.2539		
Output weight	0.59504	-0.14884	0.4804	1.3075	0.64967		
Bias of output weight					-0.70948		

pseudoplasticity of the aqueous CMC solution and lower cross-sectional area of bubble column yield higher gas holdup. In addition, gas flow rate also plays a significant role in the estimation of higher gas holdup.

6 Perspectives of future research

Because of the complex flow characteristics of bubbles in bubble columns, there are many areas in which the hydrodynamics, mass transfer characteristics and bubble behavior are yet to be clearly understood. Studies need to be conducted to investigate other aspects. A few aspects of bubble column research that may be taken up for further study under different heads are presented below.

6.1 Operating conditions

Most of the processes operate at elevated pressure and temperature in the bubble column; however, insufficient data for non-Newtonian liquids are available in the literature to study the effect of elevated system pressure and temperature on gas holdup.

6.2 Column geometry

It is desirable to develop different types of breaking mechanisms that can be applied on large bubbles, for example, helical spring arrangements, rotational blade with floated condition, tip fin, vibration or “shaking” arrangement in bubble columns.

Summarizing the literature studies, it can be concluded that most of the research work reported were carried out in conventional stirred bubble columns due to their inherent advantages such as simple fabrication,

easier operation and getting a relatively large gas-liquid interfacial area in small volumes. Unfortunately, inadequate data are available for devices like tapered bubble columns and packed bed reactors. At lower taper angle, the tapered bubble column is capable of providing higher fractional gas holdup due to the higher circulation rate of smaller bubbles in the annular region than a standard bubble column under similar conditions. Tapered cylindrical bubble column in which the diameter of the column increases vertically upwards, the gas bubbles will have large cross-sectional area of the liquid column for vertical movement with the increased diameter of the spiral in the upward direction providing a large liquid space for movement. This will provide more contact time for bubbles, resulting in higher mass transfer. These devices need to be evaluated in more detail in terms of gas holdup because of their good accessibility for optical observations.

Comparative study on the performance of various designs like cylindrical bubble column square-shaped bubble columns, rectangular-shaped bubble columns, square-shaped tapered bubble columns, and cylindrical-shaped tapered bubble columns is not available in the published literature. Further studies should include these aspects. Use of tapered columns has also been reported in industrial practice in fluidization, SO₂ scrubbing and segregation of particles in fluidized columns. Square or rectangular cross section bubble columns will simply provide better visibility of bubbles in the liquid, which otherwise get a distorted view in the case of cylindrical columns due to curved surface.

6.3 Internals

In practice, bubble columns are usually composed of many internals such as baffles of different types, temperature, liquid level and dissolved oxygen sensors, pH

probe, types of bubble-breaking devices, etc., if any. Only a limited number of published reports is available on the effects of various internals on bubble column hydrodynamics in non-Newtonian systems. This aspect needs to be studied with varying types and designs of internals.

6.4 Physical properties

It has been concluded in earlier studies that gas holdup strongly depends on the surface tension of the liquid. Further studies are needed to explain the effect of surface tension on gas holdup for viscous non-Newtonian systems.

Accurate quantification of shear rate of a non-Newtonian liquid in a bubble column is a challenge. Generally, the flow behavior of a non-Newtonian liquid is very complex. It is also important to know the relative contribution of the two shear rates, namely, shear rate at the gas-liquid interface of bubbles and the solid-liquid interface near the column wall. Hence, there is a need to carry out studies in order to accurately quantify the shear rate of a non-Newtonian fluid for its precise contribution to apparent viscosity.

6.5 Modeling and simulation

A set of research articles with different gas-liquid or gas-liquid-solid systems are available in the literature; using a wide range of physical properties of different liquids, operating conditions, and column and sparger geometry, gas holdup data need to be generated to develop a new generalized empirical correlation which is valid for a wide range of system parameters using modeling and simulation supported by ANN or support vector regression (SVR) techniques. Use of ANN and SVR will make a more accurate prediction from empirical models.

Computational fluid dynamics (CFD) simulation has become an effective tool to get a better understanding of the complex hydrodynamics and mass transfer behavior in fluids. Such software tools help study effects of various parameters in detail. Studies are needed to find out effects of parameters such as sparger size and the effect of internals on gas holdup especially at lower superficial gas velocities in non-Newtonian systems using CFD simulation.

6.6 Rheological properties

Simultaneous effects of rheological characteristics (both elastic and viscous) of the non-Newtonian liquids on gas holdup have not been considered earlier. The effects of these properties on gas holdup need to be studied.

Non-Newtonian liquids containing varying concentrations of solutes are widely used in bubble columns in bioprocesses and other similar industries. Studies on the effect of non-Newtonian liquid behavior in the case of varying concentrations of solute(s) on the gas holdup have been scarcely reported. *A priori* estimates of gas holdup are imperative for varying concentrations of solutes in the case of fermentation of broths.

Non-Newtonian liquids such as starch, sugarcane molasses and other agricultural products/by-products are often fermented in bioreactors in the presence of other similar non-Newtonian liquids added as fermentation media containing macronutrients and other additives. Gas holdup estimates are essential for such mixtures of two or more non-Newtonian liquids in varying proportions but are currently scarcely available in the literature. At present, rheological behavior of such mixtures is approximated by using aqueous solutions of CMC possessing approximately the same behavior. Such simulated pseudoplastic liquids may often lead to poor/less-accurate estimates of gas holdup.

6.7 Flow regime

Bubble columns are operated under the homogeneous or heterogeneous regime depending on the requirement of the system/study. Gas-liquid mass transfer varies under these two conditions. Thus, a correlation developed for the same system under the two conditions will have different parameter values. The correlations reported in the literature for the prediction of gas holdup for different systems in bubble columns have not accounted for the significant changes due to the flow regime and bubble flow patterns covering the entire range of operating conditions. Correlations need to be developed for the two regimes under the range of conditions that are usually encountered but have not been reported so far.

6.8 Bubble characteristics

The contribution of tiny bubbles in gas holdup has been reported to be significant. Contradictory estimates of contribution of tiny bubble in gas holdup have been reported in earlier studies. Being a considerable source of gas-liquid mass transfer due to their larger interfacial area is a precise estimation of the contribution of tiny bubbles to gas holdup and is imperative for further research.

Bubble characteristics such as bubble size or bubble chord length, bubble velocity, bubble frequency and bubble shape play a significant role in contributing to gas

holdup in non-Newtonian systems. The effects of bubble characteristics on gas holdup are scarcely reported with contradicting results. Hence, there is a need to study different bubble characteristics aimed at estimating their precise contribution to gas holdup.

6.9 Sparger geometry

Information on gas holdup in bubble columns equipped with fine porous spargers for non-Newtonian fluids is scarcely reported in literature. Further studies are needed to confirm the validity of the earlier proposed correlations (based on larger pore spargers) on gas holdup using fine porous spargers.

6.10 Miscellaneous

In order to target reduced power requirements, newer and innovative approaches were attempted with regard to improved internals, column and sparger geometry and agitation mechanism to enhance gas holdup.

Almost all chemical process industries and municipal bodies have wastewater treatment plants. The majority of these plants are based on aerobic biological treatment. Aerobic biological treatment of wastewater is a significant area using bubble columns as aeration tanks. Gas holdup comprising air or pure oxygen is a source of oxygen transfer to wastewater containing microbes in these tanks. Probably no correlation has been proposed to predict gas holdup in aerobic biological wastewater treatment. Thus, there is a need to develop correlations for gas holdup in aeration basin equipped with a diffuser and other types of potential aerators.

Appropriate empirical correlations for hydrodynamic studies applicable to large systems are currently not available in the literature because all the available correlations are based on laboratory-scale columns. Thus, there is a need to develop correlations based on either the pilot or large scale, or the existing correlations need to be scaled up for large systems.

7 Conclusion

Gas-liquid mass transfer in bubble columns has been perceived as an area which is widely studied during the last seven decades or so and has reached a point of saturation. The applications of bubble columns are ever increasing; therefore, the present review has also delved into future

prospects of various aspects of gas holdup that need further research. This paper critically reviews the empirical correlations proposed earlier for the prediction of gas holdup in bubble columns using non-Newtonian systems. Besides, the relative importance of selected parameters such as flow behavior index, consistency index, column diameter, gas flow rate and density of aqueous CMC solution on gas holdup has been quantified using ANN and Garson's algorithm for a specific data set. It may be concluded that gas holdup in non-Newtonian systems is strongly dependent on operating conditions, rheological properties, physical properties and design parameters.

Some contradictions exist about the effect of sparger design on gas holdup. The influence of surface tension and elevated pressure on gas holdup of non-Newtonian liquids has been scarcely reported, and these parameters still remain a gray area; further investigations are needed on different systems to ascertain their effect. Apart from these, liquid flow rate temperature and gas density also have a pronounced effect on gas holdup and have by and large been ignored in the correlations proposed earlier. Furthermore, gas holdup is significantly influenced by the presence of internals in bubble columns. Gas holdup increases with an increase in surfactant concentration, and it is a strong function of a bubble size less than 1 mm. Beyond 1-mm size of bubbles, gas holdup decreases. Understanding of bubble characteristics and breaking mechanisms is imperative for improving the performance of bubble columns, and correlations need to be proposed accordingly. Recommendations have been made in the present review on future prospects for developing correlations using different parameters affecting gas holdup. The review may be useful for the design and scale up of bubble columns as it presents correlations for different applications and operating range(s).

Nomenclature

A_r	Archimedes number, dimensionless
A_c	Acceleration number, dimensionless
C_D	Drag coefficient, dimensionless
d	Impeller diameter, m
d_o	Sparger hole diameter, mm
d_p	Diameter of particle, mm
d_{32}	Sauter mean bubble diameter, m
d_e	Volume equivalent bubble diameter, m
d_s	Sparger diameter, m
D_L	Diffusivity, m ² /s
D_c	Column diameter, m
E	Elasticity or bubble aspect ratio, dimensionless
Eo	Eötvös number, dimensionless
Ga	Galilei number, dimensionless

g	Acceleration of gravity, m/s^2
G'	Storage modulus, dimensionless
G''	Loss modulus, dimensionless
H_0	Initial liquid height in column, m
H_L	Liquid height in column, m
H_c	Height of the column, m
H	Height of measurement location from the sparger, m
k	Consistency index, $Pa \cdot s^n$
Mo	Morton number, dimensionless
n	Flow behavior index, dimensionless
N	Impeller speed, rev/s or rev/min
N_H	Number of hidden layer
$N_{\mu r}$	Viscosity ratio
OA	Open area, m^2
P_g	Mechanical agitation power input in gas-liquid dispersion, W
P	Pressure, bar or atm
$\Delta P/\Delta H$	Pressure drop per unit height, kPa/m
Re_t	Terminal Reynolds number, dimensionless
Re_M	Reynolds number based on the Carreau model, dimensionless
Re	Reynolds number, dimensionless
s	Carreau model parameter, dimensionless
S	Fractional plate free area, dimensionless
T	Temperature, $^{\circ}C$ or K
u_G	Superficial gas velocity, m/s
u_L	Superficial liquid velocity, m/s
U	Bubble rise velocity, m/s
V_L	Volume of liquid, m^3
W_i	Weissenberg number, dimensionless
W_e	Weber number, dimensionless
x	Largest horizontal dimension
y	Largest vertical dimension
z	Axial location from the sparger level, m

Greek letters

λ	Carreau model parameter, s
λ_t	Fluid characteristic time, s
ϵ_G	Gas holdup, dimensionless
ϵ_F	Holdup of floating bubble breakers, dimensionless
μ_{eff}	Effective viscosity of liquid, $Pa \cdot s$
μ_a	Apparent viscosity, $Pa \cdot s$
μ_0	Zero shear rate viscosity, $Pa \cdot s$
μ_{∞}	Infinite shear rate viscosity, $Pa \cdot s$
μ_L	Liquid-phase viscosity, $Pa \cdot s$
ρ_s	Density of solid particle, kg/m^3
ρ_L	Liquid-phase density, kg/m^3
σ_L	Liquid phase surface tension, N/m
σ	Surface tension, N/m
θ	Taper angle, degree

Subscripts

G	Gas phase
L	Liquid phase
S	Solid phase

Abbreviations

CBDT	Concave bladed disc turbine
CMC	Carboxymethyl cellulose
DT	Flat bladed disc turbine
MOC	Material of construction
MAPE	Maximum average percentage error
OCENOL	A mixture of saturated and unsaturated alcohol from the fraction $C_{16}-C_{18}$
PPG	Polypropylene glycol
PAA	Polyacrylamide
PVP	Polyvinyl pyrrolidone
PAM	Polyacrylamide
RMSE	Root mean square error
SAG	Silicone antifoam emulsion
SOKRAT	A water-soluble liquid polymer based on acrylonitrile and acrylic acid in ratio 2:1
SS	Stainless steel

References

- Abdelrahim KA, Ramaswamy HS. High temperature/pressure rheology of carboxymethyl cellulose (CMC). *Food Res Int* 1995; 28: 285–290.
- Acharya A, Mashelkar RA, Ulbrecht J. Mechanics of bubble motion and deformation in non-Newtonian media. *Chem Eng Sci* 1977; 32: 863–872.
- Ahmed Zeki NS. Prediction of bubble size in bubble columns using artificial neural network. *Iraqi J Chem Pet Eng* 2009; 10: 1–8.
- Al-Masry WA, Abdennour A. Gas hold-up estimation in bubble columns using passive acoustic waveforms with neural networks. *J Chem Technol Biotechnol* 2006; 81: 951–957.
- Alvarez E, Correa JM, Riverol C, Navaza JM. Model based in neural networks for the prediction of the mass transfer coefficients in bubble columns. Study in Newtonian and non-Newtonian fluids. *Int Commun Heat Mass Transf* 2000; 27: 93–98.
- Amiri S, Mehrnia MR, Barzegari D, Yazdani A. Determination of bubble size distribution in a bubble column reactor using artificial neural network. *Asia Pac J Chem Eng* 2011a; 7: 613–623.
- Amiri S, Mehrnia MR, Barzegari D, Yazdani A. An artificial neural network for prediction of gas holdup in bubble columns with oily solutions. *Neural Comput Appl* 2011b; 20: 487–494.
- Anastasiou AD, Passos AD, Mouza AA. Bubble columns with fine pore sparger and non-Newtonian liquid phase: prediction of gas holdup. *Chem Eng Sci* 2013; 98: 331–338.
- Baawain MS, Gamal El-Din M, Smith DW. Artificial neural networks modelling of ozone bubble columns: mass transfer coefficient, gas hold-up, and bubble size. *Ozone Sci Eng* 2007; 29: 343–352.
- Balamurugan V, Subbarao D, Roy S. Enhancement in gas holdup in bubble columns through use of vibrating internals. *Can J Chem Eng* 2010; 88: 1010–1020.
- Bar N, Das SK. Comparative study of friction factor by prediction of frictional pressure drop per unit length using empirical correlation and ANN for gas-non-Newtonian liquid flow through 180 degree circular bend. *Int Rev Chem Eng* 2011; 3: 628–643.

- Bar N, Bandyopadhyay TK, Biswas MN, Das SK. Prediction of pressure drop using artificial neural network for non-Newtonian liquid flow through piping components. *J Pet Sci Eng* 2010a; 71: 187–194.
- Bar N, Biswas MN, Das SK. Prediction of pressure drop using artificial neural network for gas non-Newtonian liquid flow through piping components. *Ind Eng Chem Res* 2010b; 49: 9423–9429.
- Bekkish A, Lemoine R, Sehabiague L, Oukaci R, Morsi BI. Prediction of the gas holdup in industrial-scale bubble columns and slurry bubble column reactors using back-propagation neural networks. *Int J Chem React Eng* 2005; 3: 1–35.
- Benchabane A, Bekkour K. Rheological properties of carboxymethyl cellulose (CMC) solutions. *Colloid Polym Sci* 2008; 286: 1173–1180.
- Benyounes K. Investigation of the influence of molecular weight of polymer on the rheological behavior of carboxymethylcellulose solutions. *International Multi disciplinary Scientific GeoConference: SGEM: Surveying Geology & mining Ecology Management* 2013; 2: 951–958.
- Bhunia K, Kundu G, Mukherjee D. Prediction of gas holdup in a flotation column by artificial neural network. *Int J Coal Prep Util* 2015; 35: 165–175.
- Buchholz H, Buchholz R, Lucke J, Schugerl K. Bubble swarm behaviour and gas absorption in non-Newtonian fluids in sparged columns. *Chem Eng Sci* 1978; 33: 1061–1070.
- Bulsari AB, Saxen H. Application of artificial neural networks for filtering, smoothing and prediction for a biochemical process. *Expert Syst* 1994; 11: 159–166.
- Cancela MA, Alvarez E, Maceiras R. Effects of temperature and concentration on carboxymethylcellulose with sucrose rheology. *J Food Eng* 2005; 71: 419–424.
- Chen BH, Yang NS. Characteristics of a cocurrent multistage bubble column. *Ind Eng Chem Res* 1989; 28: 1405–1410.
- Chen Z, Liu H, Zhang H, Ying W, Fang D. Oxygen mass transfer coefficient in bubble column slurry reactor with ultrafine suspended particles and neural network prediction. *Can J Chem Eng* 2013; 91: 532–541.
- Chhabra RP. Bubbles, drops, and particles in non-Newtonian fluids. Boca Raton, FL: CRC Press, 2006: 17.
- Clift R, Grace JR, Weber ME. Bubbles, drops, and particles. Mineola, NY: Dover Publications, 1978.
- Craig VS. Bubble coalescence and specific-ion effects. *Curr Opin Colloid Inter Sci* 2004; 9: 178–184.
- Deckwer WD, Schumpe A. Improved tools for bubble column reactor design and scale-up. *Chem Eng Sci* 1993; 48: 889–911.
- Deckwer WD, Nguyen-Tien K, Schumpe A, Serpemen Y. Oxygen mass transfer into aerated CMC solutions in a bubble column. *Biotechnol Bioeng* 1982; 24: 461–481.
- Deng Z, Wang T, Zhang N, Wang Z. Gas holdup, bubble behavior and mass transfer in a 5 m high internal-loop airlift reactor with non-Newtonian fluid. *Chem Eng J* 2010; 160: 729–737.
- Devine WD, Shah YT, Morsi BI. Liquid phase axial mixing in a bubble column with viscous non-Newtonian liquids. *Can J Chem Eng* 1985; 63: 195–201.
- Dewsbury K, Karamanev D, Margaritis A. Hydrodynamic characteristics of free rise of light solid particles and gas bubbles in non-Newtonian liquids. *Chem Eng Sci* 1999; 54: 4825–4830.
- Edali M, Esmail MN, Vatisstas GH. Rheological properties of high concentrations of carboxymethyl cellulose solutions. *J Appl Polym Sci* 2001; 79: 1787–1801.
- Eickenbusch H, Brunn PO, Schumpe A. Mass transfer into viscous pseudoplastic liquid in large-diameter bubble columns. *Chem Eng Process Process Intensif* 1995; 34: 479–485.
- El-Temtamy SA, Khalil SA, Nour-el-din AA, Gaber A. Oxygen mass transfer in a bubble column bioreactor containing lysed yeast suspensions. *Appl Microbial Biotechnol* 1984; 19: 376–381.
- Elgozali A, Linek V, Fialova M, Wein O, Zahradnik J. Influence of viscosity and surface tension on performance of gas-liquid contactors with ejector type gas distributor. *Chem Eng Sci* 2002; 57: 2987–2994.
- Esmaeili A, Guy C, Chaouki J. The effects of liquid phase rheology on the hydrodynamics of a gas-liquid bubble column reactor. *Chem Eng Sci* 2015; 129: 193–207.
- Esmaeili A, Farag S, Guy C, Chaouki J. Effect of elevated pressure on the hydrodynamic aspects of a pilot-scale bubble column reactor operating with non-Newtonian liquids. *Chem Eng J* 2016; 288: 377–389.
- Fransolet E, Crine M, Marchot P, Toye D. Analysis of gas holdup in bubble columns with non-Newtonian fluid using electrical resistance tomography and dynamic gas disengagement technique. *Chem Eng Sci* 2005; 60: 6118–6123.
- Franz K, Buchholz R, Schuerl K. Comprehensive study of the gas holds up and bubble size distribution in highly viscous liquids II. CMC solutions. *Chem Eng Commun* 1980; 5: 187–202.
- Funfschilling D, Li HZ. Effects of the injection period on the rise velocity and shape of a bubble in a non-Newtonian fluid. *Chem Eng Res Des* 2006; 84: 875–883.
- Gandhi AB, Joshi JB. Unified correlation for overall gas hold-up in bubble column reactors for various gas-liquid systems using hybrid genetic algorithm-support vector regression technique. *Can J Chem Eng* 2010; 88: 758–776.
- Gandhi AB, Joshi JB, Jayaraman VK, Kulkarni BD. Development of support vector regression (SVR)-based correlation for prediction of overall gas hold-up in bubble column reactors for various gas-liquid systems. *Chem Eng Sci* 2007; 62: 7078–7089.
- Garakani AK, Mostoufi N, Sadeghi F, Fatourehchi H, Sarrafzadeh M, Mehrnia M. Comparison between different models for rheological characterization of activated sludge. *Iran J Environ Health Sci Eng* 2011; 8: 255–264.
- Garcia-Ochoa F, Castro EG. Estimation of oxygen mass transfer coefficient in stirred tank reactors using artificial neural networks. *Enzym Microb Technol* 2001; 28: 560–569.
- Garson GD. Interpreting neural-network connection weights. *AI Expert* 1991; 6: 47–51.
- Ghannam MT, Esmail MN. Rheological properties of carboxymethyl cellulose. *J Appl Polym Sci* 1997; 64: 289–301.
- Ghosh UK, Upadhyay SN. Gas holdup and solid-liquid mass transfer in Newtonian and non-Newtonian fluids in bubble columns. *Can J Chem Eng* 2007; 85: 825–832.
- Godbole SP, Honath MF, Shah YT. Holdup structure in highly viscous Newtonian and non-Newtonian liquids in bubble columns. *Chem Eng Commun* 1982; 16: 119–134.
- Godbole SP, Schumpe A, Shah YT, Carr NL. Hydrodynamics and mass transfer in non-Newtonian solutions in a bubble column. *AIChE J* 1984; 30: 213–220.
- Gómez-Díaz D, Navaza JM. Rheology of aqueous solutions of food additives: effect of concentration, temperature and blending. *J Food Eng* 2003; 56: 387–392.
- Grace JR. Shapes and velocities of bubbles rising in infinite liquids. *Trans Inst Chem Eng* 1973; 51: 116–120.

- Gupta R, Wanchoo RK. Motion of a single Newtonian liquid drop through quiescent immiscible visco-elastic liquid: shape and eccentricity. *ASME J Fluids Eng* 2009; 131: 1–11.
- Hamed MM, Khalafallah MG, Hassanien EA. Prediction of wastewater treatment plant performance using artificial neural networks. *Environ Model Softw* 2004; 19: 919–928.
- Haque MW, Nigam KDP, Joshi JB. Hydrodynamics and mixing in highly viscous pseudo-plastic non-Newtonian solutions in bubble columns. *Chem Eng Sci* 1986; 41: 2321–2331.
- Haque MW, Nigam KDP, Joshi JB, Viswanathan K. Studies on gas holdup and bubble parameters in bubble columns with (carboxymethyl) cellulose solutions. *Ind Eng Chem Res* 1987; 26: 86–91.
- Hecht-Nielson R. *Neurocomputing*. Reading, MA: Addison-Wesley, 1990.
- Heijnen JJ, Riet K, Wolthuis AJ. Influence of very small bubbles on the dynamic $K_L a$ measurement in viscous gas–liquid systems. *Biotechnol Bioeng* 1980; 22: 1945–1956.
- Henzler HJ. *Begasen hoherviskoser kltissigkeiten*. *Chem.rlng – Techn* 1980; 52: 643–652.
- Ibrehem AS, Hussain MA. Prediction of bubble size in bubble columns using artificial neural network. *J Appl Sci* 2009; 9: 3196–3198.
- Jamialahmadi M, Zehtaban MR, Müller-Steinhagen H, Sarrafi A, Smith JM. Study of bubble formation under constant flow conditions. *Chem Eng Res Des* 2001; 79: 523–532.
- Jana SK, Biswas AB, Das SK. Gas holdup in tapered bubble column using pseudoplastic non-Newtonian liquids. *Korean J Chem Eng* 2014a; 31: 574–581.
- Jana SK, Biswas AB, Das SK. Pressure drop in tapered bubble columns using non-Newtonian pseudoplastic liquid-experimental and ANN prediction. *Can J Chem Eng* 2014b; 92: 578–584.
- Jana SK, Biswas AB, Das SK. ANN applicability in gas holdup prediction in tapered bubble columns using non-Newtonian pseudoplastic liquids. *ChemXpress* 2015; 8: 102–111.
- Jhavar AK, Prakash A. Bubble column with internals: effects on hydrodynamics and local heat transfer. *Chem Eng Res Des* 2014; 92: 25–33.
- Joshi JB. Axial mixing in multiphase contactors—a unified correlation. *Trans Inst Chem Eng* 1980; 58: 155–165.
- Joshi JB, Veera VP, Prasad Ch V, Phanikumar DV, Deshpande NS, Thakre SS, Thorat BN. Gas hold-up structure in bubble column reactors. *Pinsa* 1998; 64: 441–567.
- Kang Y, Min BT, Nah JB, Kim SD. Mass transfer in continuous bubble columns with floating bubble breakers. *AIChE J* 1990; 36: 1255–1258.
- Kang Y, Cho YJ, Woo KJ, Kim SD. Diagnosis of bubble distribution and mass transfer in pressurized bubble columns with viscous liquid medium. *Chem Eng Sci* 1999; 54: 4887–4893.
- Kantak MV, Hesketh RP, Kelkar BG. Effect of gas and liquid properties on gas phase dispersion in bubble columns. *Chem Eng J Biochem Eng J* 1995; 59: 91–100.
- Kantarci N, Borak F, Ulgen KO. Bubble column reactors. *Process Biochem* 2005; 40: 2263–2283.
- Kawalec-Pietrenko BT. Time-dependent gas hold-up and bubble size distributions in a gas—highly viscous liquid—solid system. *Chem Eng J* 1992; 50: B29–B37.
- Kawase Y, Moo-Young M. Influence of non-Newtonian flow behaviour on mass transfer in bubble Columns with and without draft tubes. *Chem Eng Commun* 1986; 40: 67–83.
- Kawase Y, Moo-Young M. Theoretical prediction of gas holdup in bubble columns with Newtonian and non-Newtonian fluids. *Ind Eng Chem Res* 1987; 26: 933–937.
- Kawase Y, Umeno S, Kumagai T. The prediction of gas holdup in bubble column reactors: Newtonian and non-Newtonian fluids. *Chem Eng J* 1992; 50: 1–7.
- Kelkar BG, Shah YT. Gas holdup and backmixing in bubble column with polymer solutions. *AIChE J* 1985; 31: 700–702.
- Khare AS, Niranjana K. Mechanically agitated contactors: gas hold up in highly viscous media. *ICHEME Res Event Proc* 1994; 1: 120–122.
- Khare AS, Niranjana K. Impeller-agitated aerobic reactor: the influence of tiny bubbles on gas hold-up and mass transfer in highly viscous liquids. *Chem Eng Sci* 1995; 50: 1091–1105.
- Khare AS, Niranjana K. The effect of impeller design on gas holdup in surfactant containing highly viscous non-Newtonian agitated liquids. *Chem Eng Process Process Intensif* 2002; 41: 239–249.
- Kojima E, Akehata T, Shirai T. Rising velocity and shape of single air bubbles in highly viscous liquids. *J Chem Eng Jpn* 1968; 1: 45–50.
- Kulkarni AA, Joshi JB. Bubble formation and bubble rise velocity in gas-liquid systems: a review. *Ind Eng Chem Res* 2005; 44: 5873–5931.
- Lahiri SK, Ghanta KC. Development of an artificial neural network correlation for prediction of hold-up of slurry transport in pipelines. *Chem Eng Sci* 2008; 63: 1497–1509.
- Lakota A. Effect of highly viscous non-Newtonian liquids on gas holdup in a concurrent upflow bubble column. *Acta Chim Slovenica* 2007; 54: 678.
- Lee DH, Kim JO, Kim SD. Mass transfer and phase holdup characteristics in three-phase fluidized beds. *Chem Eng Commun* 1993; 119: 179–196.
- Lemoine R, Morsi BI. An algorithm for predicting the hydrodynamic and mass transfer parameters in agitated reactors. *Chem Eng J* 2005; 114: 9–31.
- Lemoine R, Fillion B, Behkish A, Smith AE, Morsi BI. Prediction of the gas–liquid volumetric mass transfer coefficients in surface-aeration and gas-inducing reactors using neural networks. *Chem Eng Process Process Intensif* 2003; 42: 621–643.
- Lemoine R, Behkish A, Sehabiague L, Heintz YJ, Oukaci R, Morsi BI. An algorithm for predicting the hydrodynamic and mass transfer parameters in bubble column and slurry bubble column reactors. *Fuel Process Technol* 2008; 89: 322–343.
- Leonard C, Ferrasse JH, Boutin O, Lefevre S, Viand A. Bubble column reactors for high pressures and high temperatures operation. *Chem Eng Res Des* 2015; 100: 391–421.
- Li S, Ma Y, Fu T, Zhu C, Li H. The viscosity distribution around a rising bubble in shear-thinning non-Newtonian fluids. *Braz J Chem Eng* 2012a; 29: 265–274.
- Li S, Zhu C, Fu T, Ma Y. Study on the mass transfer of bubble swarms in three different rheological fluids. *Int J Heat Mass Transf* 2012b; 55: 6010–6016.
- Li S, Ma Y, Jiang S, Fu T, Zhu C, Li HZ. The drag coefficient and the shape for a single bubble rising in non-Newtonian fluids. *J Fluids Eng* 2012c; 134: 1–4.
- Mandal A, Kundu G, Mukherjee D. Gas holdup and entrainment characteristics in a modified downflow bubble column with Newtonian and non-Newtonian liquid. *Chem Eng Process Process Intensif* 2003; 42: 777–787.
- Mitra T, Singha B, Bar N, Das SK. Removal of Pb (II) ions from aqueous solution using water hyacinth root by fixed-bed column and ANN modeling. *J Hazard Mater* 2014; 273: 94–103.

- Mok YS, Kim YH, Kim SY. Bubble and gas holdup characteristics in a bubble column of CMC solution. *Korean J Chem Eng* 1990; 7: 31–39.
- Moo-Young M, Kawase Y. Gas holdup and mass transfer in a bubble column with visco-elastic fluids. *Can J Chem Eng* 1987; 65: 113–118.
- Muller FL, Davidson JF. On the contribution of small bubbles to mass transfer in bubble columns containing highly viscous liquids. *Chem Eng Sci* 1992; 47: 3525–3532.
- Nakanoh M, Yoshida F. Gas absorption by Newtonian and non-Newtonian liquids in a bubble column. *Ind Eng Chem Process Des Dev* 1980; 19: 190–195.
- Nishikawa M, Kato H, Hashimoto K. Heat transfer in aerated tower filled with non-Newtonian liquid. *Ind Eng Chem Process Des Dev* 1977; 16: 133–137.
- Olden JD. An artificial neural network approach for studying phytoplankton succession. *Hydrobiologia* 2000; 436: 131–143.
- Olden JD, Jackson DA. Illuminating the “black box”: a randomization approach for understanding variable contributions in artificial neural networks. *Ecol Model* 2002; 154: 135–150.
- Olden JD, Joy MK, Death RG. An accurate comparison of methods for quantifying variable importance in artificial neural networks using simulated data. *Ecol Model* 2004; 178: 389–397.
- Olivieri G, Russo ME, Simeone M, Marzocchella A, Salatino P. Effects of viscosity and relaxation time on the hydrodynamics of gas–liquid systems. *Chem Eng Sci* 2011; 66: 3392–3399.
- Ozturk SS, Schumpe A. The influence of suspended solids on oxygen transfer to organic liquids in a bubble column. *Chem Eng Sci* 1987; 42: 1781–1785.
- Pandit AB, Joshi YK. Mixing time studies in bubble column reactor with and without internals. *Int J Chem React Eng* 2005; 3: 1–25.
- Pareek VK, Brungs MP, Adesina AA, Sharma R. Artificial neural network modeling of a multiphase photodegradation system. *J Photochem Photobiol A Chem* 2002; 149: 139–146.
- Passos AD, Voulgaropoulos VP, Paras SV, Mouza AA. The effect of surfactant addition on the performance of a bubble column containing a non-Newtonian liquid. *Chem Eng Res Des* 2015; 95: 93–104.
- Philip J, Proctor JM, Niranjan K, Davidson JF. Gas hold-up and liquid circulation in internal loop reactors containing highly viscous Newtonian and non-Newtonian liquids. *Chem Eng Sci* 1990; 45: 651–664.
- Pilizota V, Subaric D, Lovric T. Rheological properties of CMC dispersions at low temperatures. *Food Technol Biotechnol* 1996; 34: 87–90.
- Pirdashti M, Curteanu S, Kamangar MH, Hassim MH, Khatami MA. Artificial neural networks: applications in chemical engineering. *Rev Chem Eng* 2013; 29: 205–239.
- Pradhan AK, Parichha RK, De P. Flow behavior and gas holdup in two-phase bubble column. *Inst Eng (India)* 1991; 72: 6–9.
- Pradhan AK, Parichha RK, De P. Gas hold-up in non-Newtonian solutions in a bubble column with internals. *Can J Chem Eng* 1993; 71: 468–471.
- Reisener J, Reuter MA, Kruger J. Modelling of the mass transfer in gas-sparged electrolyzers with neural nets. *Chem Eng Sci* 1993; 48: 1089–1101.
- Rodrigue D. Drag coefficient–Reynolds number transition for gas bubbles rising steadily in viscous fluids. *Can J Chem Eng* 2001; 79: 119–123.
- Roy S, Parichha RK, De P, Ray P, Barman B. Gas holdup in bubble column with immersed tubes. *Proc Indian Chem Eng Cong* 1989; 1: 72–77.
- Rumelhart DE, Hinton GE, Williams RJ. Learning internal representation by error propagation. In: Rumelhart DE, McClelland JL, editors. *Parallel distributed processing*, Vol. 1, Chapter 8. Cambridge, MA: MIT Press, 1986.
- Ryu HW, Chang YK, Kim SD. Gas holdup and mass transfer characteristics of carboxymethyl cellulose solutions in a bubble column with a radial gas sparger. *Bioprocess Eng* 1993; 8: 271–277.
- Saxena SC, Vadivel R. Heat transfer from a tube bundle in a bubble column. *Int Commun Heat Mass Transf* 1988; 15: 657–667.
- Schumpe A, Deckwer WD. Gas holdups, specific interfacial areas, and mass transfer coefficients of aerated carboxymethyl cellulose solutions in a bubble column. *Ind Eng Chem Process Des Dev* 1982; 21: 706–711.
- Schumpe A, Deckwer WD. Organic liquids in a bubble column: holdups and mass transfer coefficients. *AIChE J* 1987a; 33: 1473–1480.
- Schumpe A, Deckwer WD. Viscous media in tower bioreactors: hydrodynamic characteristics and mass transfer properties. *Bioprocess Eng* 1987b; 2: 79–94.
- Schumpe A, Deckwer WD, Nigam KD. Gas-liquid mass transfer in three-phase fluidized beds with viscous pseudoplastic liquids. *Can J Chem Eng* 1989; 67: 873–877.
- Schwarz S, Kempe T, Fröhlich J. An immersed boundary method for the simulation of bubbles with varying shape. *J Comput Phys* 2016; 315: 124–149.
- Shah YT, Kelkar BG, Godbole SP, Deckwer WD. Design parameters estimations for bubble column reactors. *AIChE J* 1982; 28: 353–379.
- Shaikh A, Al-Dahhan M. Development of an artificial neural network correlation for prediction of overall gas holdup in bubble column reactors. *Chem Eng Process Process Intensif* 2003; 42: 599–610.
- Sharma R, Singh K, Singhal D, Ghosh R. Neural network applications for detecting process faults in packed towers. *Chem Eng Process Process Intensif* 2004; 43: 841–847.
- Suh IS, Schumpe A, Deckwer WD, Kulicke WM. Gas-liquid mass transfer in the bubble column with viscoelastic liquid. *Can J Chem Eng* 1991; 69: 506–512.
- Takahashi T, Miyahara T, Izawa H. Drag coefficient and wake volume of single bubbles rising through quiescent liquid. *Kagaku Kogaku Ronbunshu* 1976; 2: 480–487.
- Tripathi MK, Sahu KC, Govindarajan R. Dynamics of an initially spherical bubble rising in quiescent liquid. *Nat Commun* 2015; 6: 1–9.
- Utomo MB, Sakai T, Uchida S, Maezawa A. Simultaneous measurement of mean bubble diameter and local gas holdup using ultrasonic method with neural network. *Chem Eng Technol* 2001; 24: 493–500.
- Utomo MB, Sakai T, Uchida S. Use of neural network–ultrasonic technique for measuring gas and solid hold-ups in a slurry bubble column. *Chem Eng Technol* 2002; 25: 293–299.
- Valente GFS, Mendonça RCS, Pereira JAM, Felix LB. Artificial neural network prediction of chemical oxygen demand in dairy industry effluent treated by electrocoagulation. *Sep Purif Technol* 2014; 132: 627–633.

- Vatai GY, Tekic MN. Gas holdup and mass transfer in bubble columns with pseudoplastic liquids. *Chem Eng Sci* 1989; 44: 2402–2407.
- Veera UP, Joshi JB. Measurement of gas holdup profiles in bubble column by gamma ray tomography: effect of liquid phase properties. *Chem Eng Res Des* 2000; 78: 425–434.
- Vinaya M, Varma YBG. Some aspects of hydrodynamics in multistage bubble columns. *Bioprocess Eng* 1995; 13: 231–237.
- Wanchoo RK, Sharma SK, Bansal R. Rheological parameters of some water-soluble polymers. *J Polym Mater* 1996; 13: 49–55.
- Wanchoo RK, Sharma SK, Gupta R. Shape of a Newtonian liquid drop moving through an immiscible quiescent non-Newtonian liquid. *Chem Eng Process Process Intensif* 2003; 42: 387–393.
- Wellek RM, Agrawal AK, Skelland AHP. Shape of liquid drops moving in liquid media. *AIChE J* 1966; 12: 854–862.
- Wenyuan F, Youguang M, Shaokun J, Ke Y, Huaizhi L. An experimental investigation for bubble rising in non-Newtonian fluids and empirical correlation of drag coefficient. *J Fluids Eng* 2010; 132: 1–7.
- Wenyuan F, XiaoHong Y. A laser imaging-LDV coupling measurement of single bubble forming and rising in shear-thinning fluid. *J Thermal Sci* 2014; 23: 233–238.
- Yamashita F. Effects of vertical pipe and rod internals on gas holdup in bubble columns. *J Chem Eng Jpn* 1987a; 20: 204–206.
- Yamashita F. Effect of shape of baffle plates and mesh and cross-sectional area of wire gauges on gas hold-up and pressure drop in a bubble column. *J Chem Eng Jpn* 1987b; 20: 201–204.
- Yang H, Fang B, Reuss M. $k_L a$ Correlation established on the basis of a neural network model. *Can J Chem Eng* 1999; 77: 838–843.
- Youssef AA, Al-Dahhan MH. Impact of internals on the gas holdup and bubble properties of a bubble column. *Ind Eng Chem Res* 2009; 48: 8007–8013.
- Yuanxin W, Xianghua L, Qiming C, Dinghuo LI, Shirong L, Al-Dahhan MH, Dudukovic MP. Prediction of gas holdup in bubble columns using artificial neural network. *Chin J Chem Eng* 2003; 11: 162–165.
- Zhang L, Yang C, Mao ZS. An empirical correlation of drag coefficient for a single bubble rising in non-Newtonian liquids. *Ind Eng Chem Res* 2008a; 47: 9767–9772.
- Zhang L, Yang C, Mao ZS. Unsteady motion of a single bubble in highly viscous liquid and empirical correlation of drag coefficient. *Chem Eng Sci* 2008b; 63: 2099–2106.

Bionotes



Ajay Sujan

Department of Chemical Engineering,
Malaviya National Institute of Technology
Jaipur, JLN Marg, Jaipur 302017, India

Ajay Sujan is a PhD scholar under the supervision of Dr. Raj K. Vyas, Chemical Engineering Department, MNIT (Jaipur, India). He was a lecturer at the Chemical Engineering Department, Anand Engineering College (Agra, India) from 2010 to 2013. He completed his Master's degree at MNIT Jaipur. He is currently working on hydrodynamic and mass transfer parameters in a bubble column. He has published a number of articles related to international conferences.



Raj K. Vyas

Department of Chemical Engineering,
Malaviya National Institute of Technology
Jaipur, JLN Marg, Jaipur 302017, India,
rkvyas2@gmail.com

Raj K. Vyas is an Associate Professor at the Chemical Engineering Department, MNIT (Jaipur, India). He obtained his PhD from the former University of Roorkee, Roorkee (now IIT Roorkee). The major areas of his research are separation processes, environmental engineering, catalysis and biotechnology. He has published/presented over 70 research papers in various international/national journals and conferences of repute, guided five PhDs and 14 Master's theses. He has received several academic awards including a "Khosla Commendation Certificate" from the University of Roorkee, Roorkee in 1996.



Estimation of liquid-side mass transfer coefficient and liquid film thickness in a bubble column using single spherical bubble model

Ajay Sujan | Raj K. Vyas | Kailash Singh

Department of Chemical Engineering,
Malaviya National Institute of Technology
Jaipur, JLN Marg, Jaipur 302017, India

Correspondence

Raj K. Vyas, Department of Chemical
Engineering, Malaviya National Institute
of Technology Jaipur, JLN Marg, Jaipur
302017, India.

Email: rkvyas2@gmail.com

Abstract

A macroscopic mass transfer model based on the unsteady-state liquid film mass transfer mechanism for a single spherical bubble was formulated. Analytical solution of the model equation was obtained in Laplace transform using surface renewal rates based on Danckwerts' surface age distribution function. The mass transfer coefficient, k_L , in a slurry bubble column under different operating conditions of temperature, pressure, gas flow rate, and solid concentration has been simulated using a program code "BUBBLESIM" in MATLAB[®], developed by the authors. The proposed model has been validated using secondary data for a slurry system under a wide range of operating conditions. The predicted values of k_L show very good agreement with the experimental data within an average deviation of $\pm 2\%$. The results show that the mass transfer coefficient, k_L , increased with increasing superficial gas velocity and temperature and decreased with increase in slurry concentration, while it changed slightly with pressure. Based on the present work, empirical correlations have been proposed for the prediction of δ in terms of dimensionless groups for H₂-, CO-, and CO₂-paraffin-quartz sand systems under elevated temperatures (298–423 K) and elevated pressures (1–3 MPa) in a slurry bubble column.

KEYWORDS

Danckwerts' surface age distribution function, Laplace transform, liquid-side mass transfer coefficient, mathematical model, slurry bubble column, spherical bubble

Nomenclature: a , Specific gas–liquid interfacial area, 1/m; A_1, A_2 , Constants of integration; C_A , Microscopic gas concentration in liquid phase, mol/L; \bar{C}_A , Laplace-transformed gas concentration profile outside the bubble; C_b , Gas concentration in the liquid phase at the gas–liquid interface, mol/L; C_L , Macroscopic gas concentration in liquid bulk, mol/L; C_S , Mass concentration of solid in liquid (%); C_A^*, C_L^* , Saturated gas concentration in liquid phase, mol/L; d_B , Mean bubble diameter, m; D_a , Gas diffusivity in liquid, m²/s; D_C , Column diameter, m; Eu , Euler number ($P/\rho_{SL} \cdot U_g^2$); k_L , Liquid-side mass transfer coefficient, m/s; $k_L a$, Gas–liquid volumetric mass transfer coefficient in liquid, 1/s; M_B, M_1, M_2 , Molecular weight, kg/kmol; $N_A, N_2(t)$, The number of moles of diffusing gas through interfacial area, mol/s; n , Number of microeddies on bubble surface; N , Avogadro number; P , Pressure, MPa; P_C , Critical pressure, MPa; r , Radial position, m; R , Radius of bubble, m; Re , Reynolds number ($d_B \cdot \rho_{SL} \cdot U_g / \mu_{SL}$); S , Fractional rate of renewal of surface of liquid, 1/s; Sc , Schmidt number ($\mu_{SL} / \rho_{SL} \cdot D_a$); Sh , Sherwood number ($k_L \cdot D_C / D_a$); s , Laplace domain, 1/s; t , Microscopic time, s; T , Temperature, K; T_C , Critical temperature, K; T_r , Reduced temperature, K; U_g , Superficial gas velocity, m/s; V , Molar volume, cm³/mol; V_D , Molar volume of the hard sphere, cm³/mol
Greek symbols: δ , Thickness of the mass transfer liquid film, m; μ , Mean deviation; μ_L , Viscosity of liquid, that is, liquid paraffin, Pa.s; μ_{SL} , Viscosity of slurry, Pa.s; v_A , Molar volume of gas, m³/kmol; v_r, v_θ, v_ϕ , Velocity vector in r, θ , and ϕ directions; ρ_L , Density of liquid, that is, liquid paraffin, kg/m³; ρ_G , Density of gas, kg/m³; ρ_{SL} , Density of slurry, kg/m³; ρ_S , Solid density, kg/m³; σ , Standard deviation; σ_L , Surface tension of liquid, kg/s²; σ_1, σ_2 , Effective hard sphere diameter, Å; ψ , Surface age distribution function, 1/s; η , Eddy length, m; ν , Kinematic viscosity of the liquid, m²/s; ϵ , Rate of dissipation of energy per unit mass, W/kg; λ , A parameter, (=), $\left(\frac{1}{D_a} \sqrt{s D_a}\right)$, 1/m



1 | INTRODUCTION

Complex and diverse requirements of industrial processes warrant development of different types of gas–liquid contactors such as bubble columns and packed columns. Bubble columns are commonly used for the manufacture of industrially important products in chemical, petrochemical, and biochemical process industries utilizing two or three phase systems. For optimal design of gas–liquid contactors and bubble columns, understanding of gas–liquid mass transfer phenomena caused by interfacial fluctuations is of crucial importance. Reliable values of the volumetric liquid-phase mass transfer coefficient $k_L a$ cannot be obtained, if liquid-side mass transfer coefficient, k_L , and interfacial area, a , are not accurately determined.

Slurry bubble columns (SBCs) are preferred mainly for highly exothermic processes when efficient interphase contacting is desirable. These reactors are usually difficult to scale up because of their complex hydrodynamic behavior. Performance of reactors depends on operating conditions, physical properties of gas and liquid, and dimensions of the system. The performance of such reactors is also strongly dependent on the flow regime, that is, homogeneous or heterogeneous and bubble characteristics, such as bubble size, bubble rise velocity, and bubble wake phenomena. These reactors provide larger gas–liquid interfacial area, large catalyst area, lower pressure drop, and a higher $k_L a$ value at low-power inputs.¹ In three-phase systems, presence of a solid particle may have a positive or negative effect on the interfacial mass transfer as it directly affects thickness and stability of the mass transfer film. The solid particles can increase or decrease the value of k_L , depending on the extent of solids loading, size of particles, particle density, nature of particles, and their surface properties. The solid particles can increase k_L by enhancing turbulence at the gas–liquid interface and increase surface renewal rate.² However, the presence of solid particles can also limit the diffusion path by blocking the available area for mass transfer and decrease k_L .^{3,4} The value of k_L also depends on other variables such as diffusivity of gas in the liquid, viscosity, and surface tension of the liquid.⁵ Presence of solid particles increases the specific interfacial area by covering the bubble surface, preventing coalescence of the bubbles, and thus resulting in smaller bubbles. The effect of presence of solid particles depends on the hydrophobicity of the particle surface and on the ratio of size of particles to the bubble size. Mena et al.⁶ reported that hydrophobic particles have a strong negative influence on mass transfer, and hydrophilic particles, in a certain concentration range (≤ 3 vol.%), can increase $k_L a$. In practice, several kinds of solids are used in slurries in petroleum and petro-

chemical and other industries for processes such as Fischer–Tropsch synthesis, methanol synthesis, heavy oil upgrading, and other processes where particles with inert surface characteristics are also employed.

Yang et al.³ studied gas–liquid mass transfer behavior of syngas components (H_2 and CO) in the presence of solid particles (silica gel powder, 5–20 vol.%) at industrial conditions ($T = 293$ – 523 K and $P = 1$ – 5 MPa) and proposed empirical correlations to predict k_L for H_2 and CO in slurry (liquid paraffin/solid particles) bubble column. On similar lines, Yang et al.⁷ worked with slurry bubble system (H_2 –, CO–liquid paraffin–silica gel powder) and proposed an empirical correlation for predicting liquid film thickness, δ , and surface renewal rate, S . However, both correlations did not use Sherwood number, which is essential.³ Besides, molecular weight and molar volume of gas were also not used. Use of these two parameters in the correlation improves the accuracy of the correlation.

In industrial applications of bubble columns, it is desirable to have a large value of liquid-side mass transfer coefficient; hence, better understanding of the mass transfer mechanism is imperative. Most of the previous bubble column studies reported in the literature are at room or ordinary temperatures, mostly for less than 30 °C, but the commercial bubble columns are frequently operated at elevated temperatures and pressure, often near the boiling points. At higher temperatures, liquids exhibit lower viscosities. For operation at elevated pressures, understanding of the effect of temperature and elevated pressures on mass transfer in bubble columns is essential for the optimal design and operation of bubble column, for example, Fischer–Tropsch synthesis of heavy paraffin from synthesis gas.⁸

Mathematical and theoretical models have been reported in literature, which provide varied details of mass transfer based on established classical concepts of film and penetration theories.^{9–15} As such, the film model is not valid for the explanation of unsteady-state mass transfer mechanism and stirred systems.¹⁶ Similarly, neither the penetration nor the film-penetration model is capable of describing the mass transfer mechanism with two liquid films at the interface, particularly in the liquid–liquid systems.¹⁶ Clearly, all the above-mentioned models have certain limitations and cannot be used to predict gas–liquid mass transfer rates accurately in complex situations, that is, heterogeneous regimes, under varying superficial gas velocity and higher pressures. Mass transfer models such as Danckwerts' surface renewal model and the two-film theory offer higher precision in prediction of mass transfer between two phases. Researchers have used various models for mass transfer modeling in the absence and presence of chemical reaction in gas–liquid or gas–liquid–solid systems.^{17–19} However, Zhao

et al.²⁰ presented a model for k_L estimation based on liquid film thickness and surface renewal rate. In this study, bubble size was limited to 3-mm diameter and the gas-slurry system was treated like a gas-liquid system. Macroscopic mathematical modeling of transient mass transfer for estimation of k_L and liquid film thickness for two- or three-phase systems are scarcely available in the literature. Therefore, concise accurately analytical models are required that can predict k_L and δ without the need to use complex computational tools. The model proposed in the present work fulfills this requirement.

The capability of proposed model has been examined using secondary data for a slurry system with a wide range of operating conditions ($T = 298\text{--}423\text{ K}$; $P = 1\text{--}3.0\text{ MPa}$; $U_g = 0.035\text{--}9.38\text{ m/s}$ and $C_s = 0\text{--}20\%$ by mass).²¹ Despite all efforts, knowledge about the effects of solids on mass transfer coefficient k_L and the physical dimensions of liquid film (liquid film thicknesses δ) has not yet been reported in literature. Such information is important for determining the precise mass transfer rate in gas-liquid/SBC systems.

The design, modeling, optimization, and scale-up of gas-liquid/SBCs require precise knowledge of hydrodynamic as well as mass and heat transfer parameters. The main goal of this article is to propose a reliable macroscopic model for prediction of mass transfer coefficient k_L , which is based on unsteady-state liquid film fluctuations by microeddies (liquid elements) in gas-liquid/SBCs.²² The analytical solution of model equation was obtained by Laplace transformation using the Danckwerts' age distribution function for the surface renewal rate as a variable. Furthermore, the mathematical model is able to predict overall mass transfer coefficient in

a gas-liquid/SBC, if the distribution of bubble sizes is known. The validity of prediction of overall k_L from proposed model has been examined using experimental data reported in literature for a slurry system with a wide range of operating conditions generally encountered in industrial bubble columns.²¹ The effects of the model parameters such as surface renewal rate S and thickness of liquid film δ on overall mass transfer coefficient k_L were simulated. In addition, empirical correlations for estimation of liquid film thickness δ for H_2 , CO , and CO_2 in slurry system (liquid paraffin-quartz sand) have been proposed in terms of dimensional groups.

2 | MODEL DEVELOPMENT FOR GAS-LIQUID MASS TRANSFER CONSIDERING SINGLE SPHERICAL BUBBLE

Bubble column reactors have been widely used in chemical and biochemical industries. In bubble columns, size, shape, and operating/physical properties of gas and liquid are the most important parameters governing their performance. To obtain higher efficiency of the gas mass transfer, homogeneous bubbles of gas are generated at each hole of the gas sparger, which rise along the column. A schematic diagram of unsteady-state gas mass transfer through liquid film of a spherical bubble is depicted in Figure 1. One of the salient features of the present model is that it can be easily solved without using complex computational tools. In the analytical solution presented here, liquid phase in bubble column is considered in batch mode and gas phase in continuous mode.

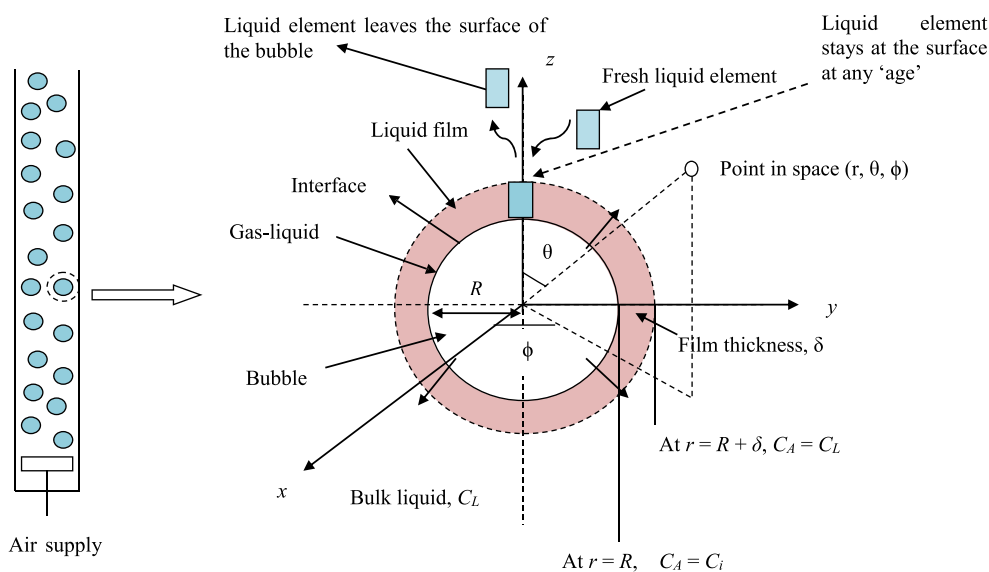


FIGURE 1 Mechanism of transient mass transfer through liquid film and surface renewal by liquid element of a spherical bubble in a bubble column



For modeling purposes, a three-phase system can be treated same as that of a two phase (gas–liquid) system.²⁰ To develop an unsteady-state single liquid film model, the following assumptions have been made:

- i. In gas bubble liquid systems, liquid-phase mass transfer resistance is a controlling factor.²³ Therefore, it has been assumed that entire mass transfer resistance exists in the liquid film.
- ii. Viscosity of liquid in a bubble column has been assumed to be low due to lower concentration of solids in liquid, which can be treated in the same way as that of a gas–liquid system.²⁰
- iii. In quiescent liquids, gas diffusion occurs only due to molecular diffusion through the liquid film. Therefore, mass transfer has been assumed to be occurring only in r-direction perpendicular to the interface only due to molecular diffusion.
- iv. As the rate of increase of gas concentration in the liquid bulk is small, it has been assumed that the concentration of gas in the bulk of liquid is constant.
- v. For simplicity of model, it has been assumed that the bubble eccentricity (e) is unity and its shape is symmetric around its center.
- vi. In order to formulate a simple model, it has been assumed that interactions between bubbles are negligible.
- vii. Most of the industrial applications are carried out at higher intensity of turbulence.²⁴ Therefore, it has been assumed that liquid film thickness (δ) is constant, and bubble size is stable during the mass transfer process.
- viii. The total surface area of a gas bubble available to microeddies for stay at gas–liquid interface as a liquid element at any “age” may belong to any “age” group. The microeddies will continually expose fresh surface of the newer liquid element to the diffusing component and sweep it away for mixing into the bulk of liquid. It has been assumed that replacement time between two liquid elements is independent of their age and has a distribution of age varying from zero to infinity at any particular instance. Therefore, it has been assumed that the rate of production of fresh surface is constant and is equal to S (surface renewal rate, 1/s).^{25,26} It has also been assumed that “age” distribution of liquid elements depends on turbulence intensity of the liquid.
- ix. From Kolmogoroff’s theory on isotropic turbulence, eddy length η , depends on kinematic viscosity, ν (m^2/s) of the liquid, and rate of dissipation of energy per unit mass, ε (W/kg) of liquid according to the following relationship^{27,28}:

$$\eta = (\nu^3/\varepsilon)^{1/4}$$

It has been assumed that the length and width of a liquid eddy are same. If size of bubble is known, then total number of liquid eddies can be easily quantified.

Frequent renewal of liquid-side film in the influence of bubble breakup and coalescence results in enhancement of mass transfer rate. Based on the above assumptions, microscopic unsteady-state mass balance of soluble gas in spherical coordinates can be written as follows:

$$\frac{\partial \rho}{\partial t} + \frac{1}{r^2} \frac{\partial}{\partial r} (\rho r^2 v_r) = 0. \quad (1)$$

Replacing mass density by molar density and $C_A \cdot v_r = N_A$

$$\frac{\partial C_A}{\partial t} + \frac{1}{r^2} \frac{\partial}{\partial r} (r^2 N_A) = 0. \quad (2)$$

Inserting Fick’s law of diffusion, $N_A = -D_a \partial C_A / \partial r$, the transport of gas A in the liquid film can be expressed as follows:

$$\frac{\partial C_A}{\partial t} = D_a \frac{1}{r^2} \frac{\partial}{\partial r} \left(r^2 \frac{\partial C_A}{\partial r} \right); \quad R \leq r \leq R + \delta, \quad (3)$$

where t is the microscopic time scale in liquid film and D_a is the diffusion coefficient.

The following initial and boundary conditions are applicable:

$$IC: \{ \text{at } t = 0, C_A = C_L, \quad (4)$$

$$BC: \begin{cases} \text{at } r = R, t \geq 0, C_A = C_i \\ \text{at } r = R + \delta, t \geq 0, C_A = C_L \end{cases}, \quad (5)$$

where R is the radius of the spherical bubble, C_i the interface concentration, and C_L the concentration in the bulk phase.

Overall mass transfer of the single bubble based on concentration gradient can be expressed by

$$\left. \frac{dC_A}{dt} \right|_{r=R} = k_L a (C_L^* - C_L), \quad (6)$$

where a is the interfacial area available for mass transfer in m^2/m^3 , C_L^* the saturation concentration of gas in mol/L, C_L the bulk concentration of gas in liquid in mol/L, and k_L the liquid-side mass transfer coefficient in m/s.

3 | ANALYTICAL SOLUTION OF MODEL EQUATION

The linear second order partial differential Equation 3 can be simplified to

$$\frac{\partial C_A}{\partial t} = D_a \frac{1}{r^2} \left(2r \frac{\partial C_A}{\partial r} + r^2 \frac{\partial^2 C_A}{\partial r^2} \right) \quad (7)$$

or

$$\frac{\partial C_A(r, t)}{\partial t} = D_a \frac{2}{r} \frac{\partial C_A(r, t)}{\partial r} + D_a \frac{\partial^2 C_A(r, t)}{\partial r^2}; \quad [R \leq r \leq (R + \delta)]. \quad (8)$$

The partial differential equation can be solved by Laplace transform. The Laplace transform $\bar{C}_A(r, s)$ of the function $C_A(r, t)$ can be expressed as

$$\bar{C}_A(r, s) = \int_0^\infty C_A(r, t) e^{-st} dt, \quad (9)$$

where s (unit: s^{-1}) is variable of Laplace transformation.

The transformed equation can be written as

$$s \bar{C}_A(r, s) - C_A(r, t) = D_a \frac{2}{r} \frac{\partial \bar{C}_A(r, s)}{\partial r} + D_a \frac{\partial^2 \bar{C}_A(r, s)}{\partial r^2}. \quad (10)$$

At initial condition, $t = 0$, $C_A = C_L$.

When $C_A(r, 0)$ is replaced with C_L in the transformation equation, then Equation 10 is rearranged in the following form:

$$\frac{d^2 \bar{C}_A(r, s)}{dr^2} + \frac{2}{r} \frac{d \bar{C}_A(r, s)}{dr} - \frac{1}{D_a} s \bar{C}_A(r, s) = -C_L \frac{1}{D_a}. \quad (11)$$

Laplace transformation of boundary conditions can be written in the following form.

B.C 1

$$\text{at } r = R, C_A = C_i, \text{ therefore } \bar{C}_A = \frac{C_i}{s}$$

B.C 2

$$\text{at } r = R + \delta, C_A = C_L, \text{ therefore } \bar{C}_A = \frac{C_L}{s}$$

General solution of Equation 11 may be written in the following form:

$$\bar{C}_A(r, s) = \frac{A_1}{r} \cosh \left(\frac{r}{D_a} \sqrt{s D_a} \right) - \frac{A_2}{r \cdot i} \sin h \left(\frac{r}{D_a} \sqrt{s D_a} \right) + \frac{C_L}{s}. \quad (12)$$

The integration constants A_1 and A_2 may be obtained by using the boundary condition of Equation 12

$$A_1 = R \frac{(C_i - C_L)}{s \cdot \tanh \delta \lambda} [\sinh R \lambda + \cosh R \lambda \cdot \tanh \delta \lambda] \quad (\text{m.s.mol/L}), \quad (13)$$

where $\lambda = \left(\frac{1}{D_a} \sqrt{s D_a} \right)$, (m^{-1});

$$A_2 = -R \cdot i \frac{(C_L - C_i)}{s \cdot \tanh \delta \lambda} [\cosh R \lambda + \sinh R \lambda \cdot \tanh \delta \lambda] \quad (\text{m.s.mol/L}). \quad (14)$$

Solving Equation 12 with Equations 13 and 14, we get

$$\begin{aligned} \bar{C}_A(r, s) = & \frac{C_L}{s} + \frac{R(C_i - C_L)}{r \cdot s \cdot \tanh \delta \lambda} [\sinh R \lambda \\ & + \cosh R \lambda \cdot \tanh \delta \lambda] \cdot \cosh \left(\frac{r}{D_a} \sqrt{s D_a} \right) \\ & + \frac{R(C_L - C_i)}{r \cdot s \cdot \tanh \delta \lambda} [\cosh R \lambda \\ & + \sinh R \lambda \cdot \tanh \delta \lambda] \cdot \sinh \left(\frac{r}{D_a} \sqrt{s D_a} \right). \end{aligned} \quad (15)$$

Equation 15 is the Laplace-transformed concentration profile. Inverse Laplace transforms of the concentration profile in the liquid film of the gas bubble presented in Equation 15 is cumbersome. Besides, it is the mass transfer coefficient k_L , which is important for getting interfacial mass transfer properties rather than a concentration profile in the film. Therefore, the age distribution function will be used further to get liquid-side mass transfer coefficient k_L .

Differentiating Equation 15 with respect to r and substituting integration constant A_1 and A_2 , we get

$$\left. \frac{d \bar{C}_A(r, s)}{dr} \right|_{r=R} = -i \frac{(C_i - C_L)}{\tanh \delta \lambda} \left[\left\{ \frac{1}{s \cdot i} (-\sinh(R \lambda) - \cosh(R \lambda) \cdot \tanh(\delta \lambda)) \right\} \left\{ \sinh(R \lambda) \cdot \lambda - \left(\frac{1}{R} \right) \cdot \cosh(R \lambda) \right\} - \left\{ \frac{1}{s} (-\sinh(R \lambda) \cdot \tanh(\delta \lambda) - \cosh(R \lambda)) \right\} \left\{ -\cosh(R \lambda) \cdot i \lambda - \left(\frac{1}{R \cdot i} \right) \sinh(R \lambda) \right\} \right]. \quad (16)$$



Instantaneous point mass transfer rate for a single surface element at time t , across the interface between the liquid bulk and the bubble, is represented by the following equation:

$$N_A(t)|_{r=R}^* = -D_a \frac{\partial C_A}{\partial r} \Big|_{r=R}. \quad (17)$$

The average mass transfer rate across the interface between the gas and liquid phase, $N_A(t)|_{r=R}^{Av.}$ is an integral of the instantaneous point mass transfer rates at various liquid film locations with different film age. The average mass transfer rate through the interface for the unsteady-state single film concept can be calculated using the surface age distribution function proposed by Danckwerts.²⁵

$$\psi(t) = S e^{-St}, \quad (18)$$

where ψ is the surface age distribution function, t is time for which a liquid surface has been exposed to gas ("age" of surface), and S is the fractional rate of renewal of surface of liquid, which is the bubble surface liquid film renewal rate. This means that the liquid film is replaced by fresh liquid element. Thus, S is the extent of surface renewal. Therefore, the average age of liquid film on the bubble surface may be given by

$$\int_0^{\infty} \psi(t) dt = 1. \quad (19)$$

Average mass transfer rate across the gas-liquid bubble interface can be obtained by integrating the multiplication of instantaneous point mass transfer rate and surface age distribution function,

$$N_A(t)|_{r=R}^{Av.} = \int_0^{\infty} N_A(t)|_{r=R}^* \psi(t) dt. \quad (20)$$

Average mass transfer rate across the interface between the gas and liquid phase considering isolated bubble from homogeneous micro bubbling in aeration system.

$$N(t)|_{r=R}^{Av.} = \frac{[N(t_1)|_{r=R}^* \psi(t_1) dt + N(t_2)|_{r=R}^* \psi(t_2) dt + N(t_3)|_{r=R}^* \psi(t_3) dt + \dots \dots N(t_\infty)|_{r=R}^* \psi(t_\infty) dt]}{n} \quad (21)$$

where, n = number of micro eddies on bubble surface, and t = age of the liquid element spent on bubble surface.

Average mass transfer rate across the gas-liquid bubble interface is also equal to rate of mass transfer across

the interface expressed in terms of concentration difference at interface and liquid bulk.

$$N_A(t)|_{r=R}^{Av.} = k_L(C_i - C_L) \quad (22)$$

Now, average mass transfer rate across the film can be found out by

$$N_A(t)|_{r=R}^{Av.} = \int_0^{\infty} -D_a \frac{dC_A}{dr} \Big|_{r=R} S e^{-St} dt \quad (23)$$

or

$$N_A(t)|_{r=R}^{Av.} = -D_a \frac{d \int_0^{\infty} C_A(r, t) S e^{-St} dt}{dr} \Big|_{r=R}. \quad (24)$$

The definition of Laplace transform,

$$L\{f(t)\} = \int_0^{\infty} f(t) e^{-st} dt. \quad (25)$$

By analogy, Equation 24 can be simplified as

$$N_A(t)|_{r=R}^{Av.} = -D_a \cdot S \frac{dC_A(\bar{r}, S)}{dr} \Big|_{r=R}. \quad (26)$$

Thus,

$$N_A(t)|_{r=R}^{Av.} = -D_a \cdot S \frac{dC_A(\bar{r}, S)}{dr} \Big|_{r=R} = k_L(C_i - C_L). \quad (27)$$

By rearrangement,

$$k_L = -D_a \cdot S \frac{dC_A(\bar{r}, S)}{(C_i - C_L)} \Big|_{r=R}. \quad (28)$$

Substituting the value of $dC_A(r, S)/dr|_{r=R}$ from Equation 16 in Equation 28 and simplifying

$$k_L = D_a \left(\frac{R \frac{1}{D_a} \sqrt{SD_a} + \tanh \delta \frac{1}{D_a} \sqrt{SD_a}}{R \cdot \tanh \delta \frac{1}{D_a} \sqrt{SD_a}} \right). \quad (29)$$



Importance of Equation 29 lies in the fact that the mass transfer coefficient k_L is a function of radius of bubble, surface renewal rate, thickness of liquid film, and gas diffusivity in the liquid film.

Details of experimental conditions used for validation of model are summarized in Table 1.

Physical properties of H₂, CO, CO₂, and liquid paraffin are shown in Tables 2 and 3, respectively.

The viscosity and density of liquid paraffin were taken from the work of Huifang et al.²⁹

$$\ln \mu_L = -3.0912 + 1.7038 \times 10^3/T, \quad (30)$$

$$\rho_L = 171.0 \times 0.1677^{-(T-T_r)^{2/7}}, \quad (31)$$

where $T_r = T/T_C$ is the reduced temperature.

Apparent slurry viscosity (μ_{SL}) is estimated by the equation proposed by Thomas³⁰:

$$\mu_{SL} = \mu_L [1 + 2.5 C_S + 10.05 C_S^2 + 0.00273 \exp(16.6 C_S)], \quad (32)$$

where C_S is the solid concentration in the slurry expressed as volume of solid per unit volume of slurry. In the present study, C_S is varied from 5% to 20% (by mass). The apparent density of the slurry ρ_{SL} was predicted by using the following expression (Yang et al.³):

$$\rho_{SL} = \rho_L(1 - C_S) + \rho_S C_S. \quad (33)$$

Apparent slurry viscosities and apparent densities of slurry at 298 K and different solid concentrations are listed in Table 4.

To obtain the diffusivities of H₂, CO, and CO₂ in liquid paraffin, the equation proposed by Erkey et al.³¹ was used:

TABLE 1 Details of experimental conditions of a bubble column²¹

Particulars	Value/detail
Gas phase	H ₂ , CO, CO ₂
Liquid phase	Paraffin
Mass concentration of quartz sand (C_S)	0%, 5%, 10%, 15%, 20%
Particle size range of quartz sand	150–200 μm
Range of superficial gas velocity (U_g)	0.026–0.053 $\text{m}\cdot\text{s}^{-1}$
Operating pressure (P)	1.0, 1.5, 2.0, 2.5, 3.0 MPa
Temperature range in the column (T)	298–423 K
Column diameter (D_C)	0.10 m

TABLE 2 Physical properties of gas²¹

Gas	M_B (kg/kmol)	T_C (K)	P_C (MPa)	$\nu_A \times 10^3$ (m ³ /kmol)
H ₂	2.016	407.4	1.30	14.3
CO	28.010	306.5	35.0	33.0
CO ₂	44.051	304.1	7.38	34.0

TABLE 3 Physical properties of liquid paraffin

Molecular weight (kg/kmol)	T_C (K)	ρ_L (kg/m ³) at 298 K	μ_L (Pa.s $\times 10^3$) at 298 K	$\sigma_L \times 10^2$ (N/m) at 298 K
412 ³	916.8 ³	890 ²¹	13.8 ²¹	2.88 ²¹

TABLE 4 Physical properties of slurry at 298 K

C_s (%)	ρ_{SL} (kg/m ³)	μ_{SL} (Pa.s $\times 10^3$)
0	890	13.8
5	879.15	47.519
10	868.3	91.215
15	857.45	188.541
20	846.6	407.960

$$D_a = \frac{94.5 \times 10^{-9} \sqrt{T}(V - V_D)}{M_1^{0.239} M_2^{0.781} (\sigma_1 \times \sigma_2)^{1.134}}, \quad (34)$$

with

$$V_D = \left(1.206 + 0.0632 \frac{\sigma_1}{\sigma_2}\right) \left(\frac{N\sigma_2^3}{\sqrt{2}}\right), \quad (35)$$

where N is Avogadro number, V is molar volume of liquid paraffin, V_D is molar volume of the hard sphere, M is molecular weight of gas, and σ is the effective hard-sphere diameter.²⁶

3.1 | Overall mass transfer coefficient, k_L

Size distribution of bubbles can be described by the number distribution density function $f(R|\mu, \sigma)$:

$$\frac{N_{R_1, R_2}}{N_{\text{sum}}} = \int_{R_1}^{R_2 = \max} f(R|\mu, \sigma) dR, \quad (36)$$

where μ and σ are the mean and standard deviation of the variable, respectively. The size distribution can be approximated by log-normal distributions



$$f(R|\mu, \sigma) = \frac{1}{R\sigma\sqrt{2\pi}} e^{-(\ln R - \mu)^2 / 2\sigma^2} \quad (37)$$

With the help of k_L for a single spherical bubble, overall mass transfer coefficient k_L of the system can be estimated by statistical integration using a log-normal distribution. Mass transfer coefficient, k_L , can be approximated by the following expression:

$$k_L = \int_{R_1}^{R_2=\max} k_L(R) f(R|\mu, \sigma) dR \quad (38)$$

TABLE 5 Mean diameter of small and larger bubbles at different pressures and constant temperature $T = 298 \text{ K}^{21}$

P (MPa)	Mean bubble diameter	
	$d_{B, \text{small}} \text{ (m)}$	$d_{B, \text{larger}} \text{ (m)}$
1	0.0064	0.0253
1.5	0.0067	0.0242
2	0.0073	0.0228
2.5	0.0083	0.0221
3	0.0093	0.0212

In this work, the values of μ and σ were obtained by trial and error for the slurry system ($\mu = 0.015$, $\sigma = 0.745$). The mean diameter of small and larger bubbles at different pressures and constant temperature ($T = 298 \text{ K}$) is listed in Table 5.

4 | RESULTS AND DISCUSSION

A macroscopic mathematical model for the mass transfer coefficient with two key parameters, viz. liquid film thickness δ and surface renewal rate S was formulated. The mathematical model is useful to predict overall k_L , if bubble size distribution is known. Effect of variations in the values of δ and S on k_L has been simulated and validated with a set of reported experimental data.²¹ The values of δ and S were estimated by trial and error method using a program code “BUBBLESIM” in MATLAB®. A flow diagram of model development for k_L and estimation of δ , S , and overall k_L are presented in Figures 2 and 3, respectively. The model is suitable for the design and scale-up of bubble columns using liquids/slurries of different viscosities operating at various gas velocities, temperatures, and pressure.

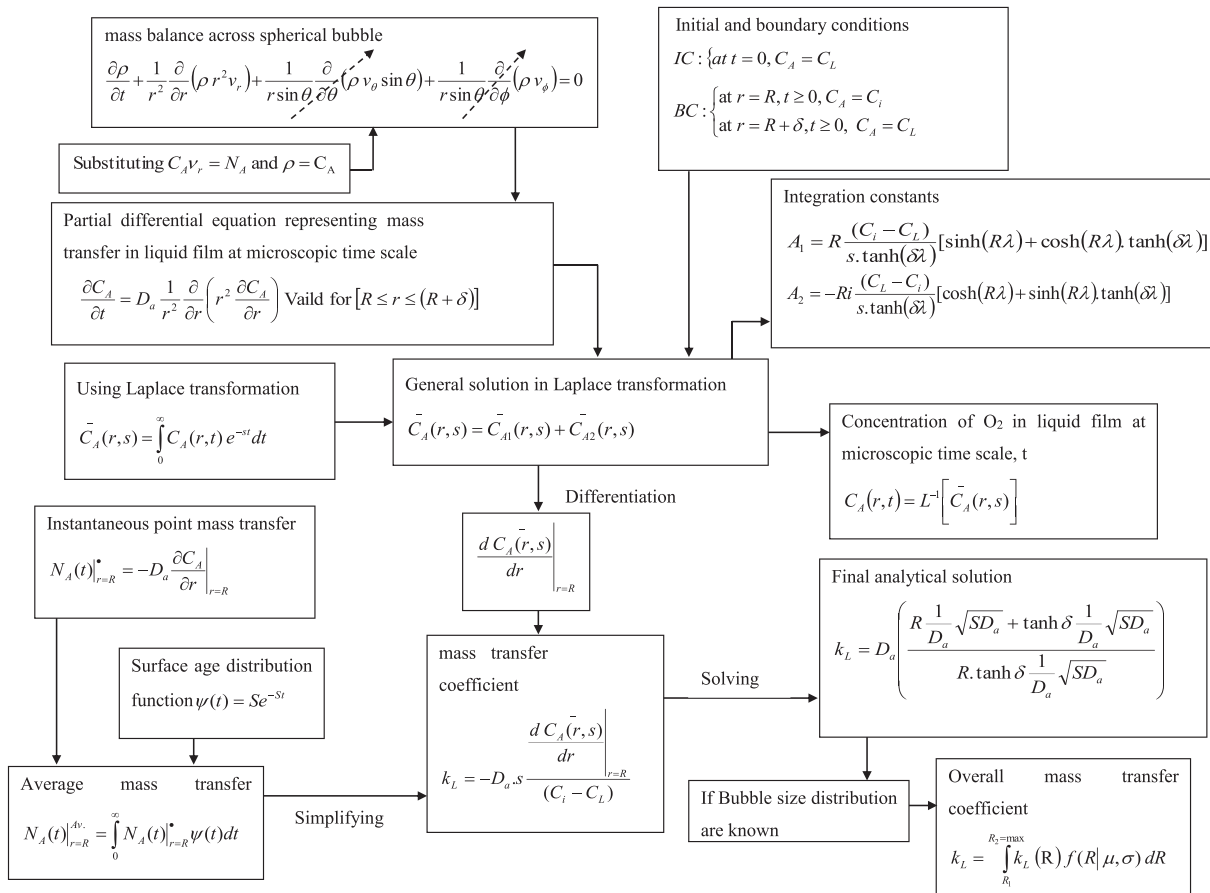


FIGURE 2 Flow diagram of unsteady-state mass transfer model development for k_L

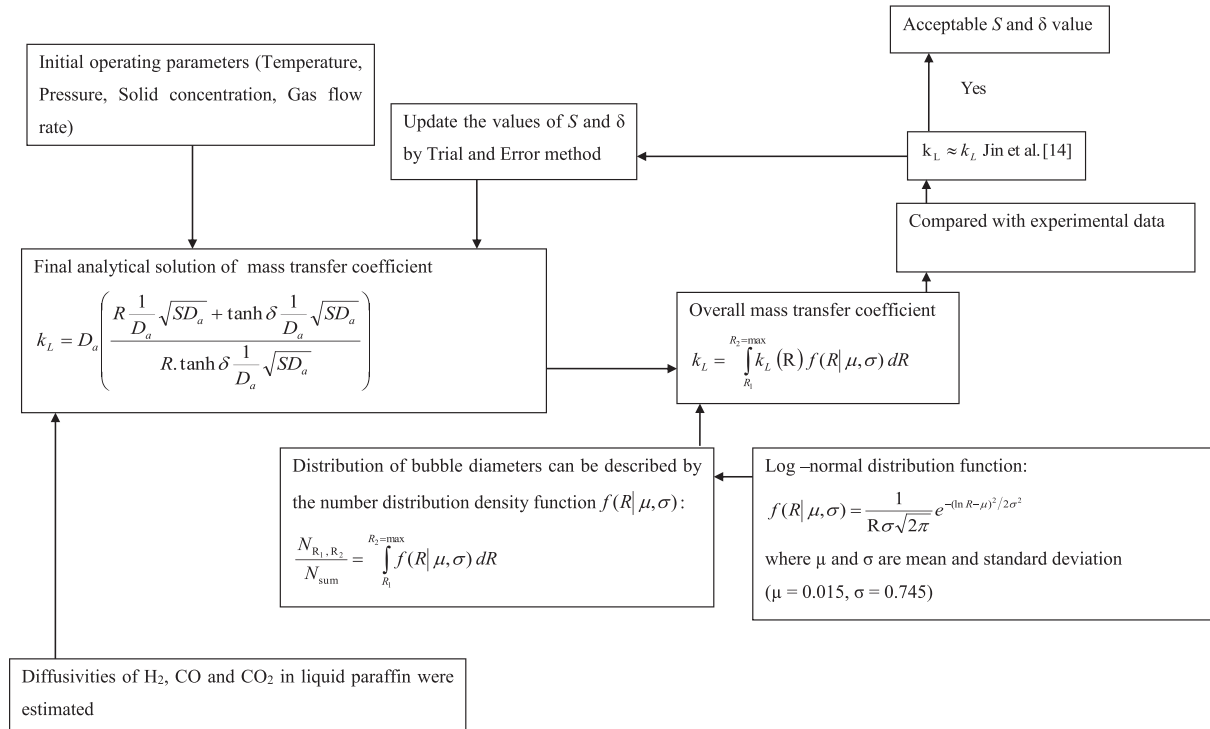


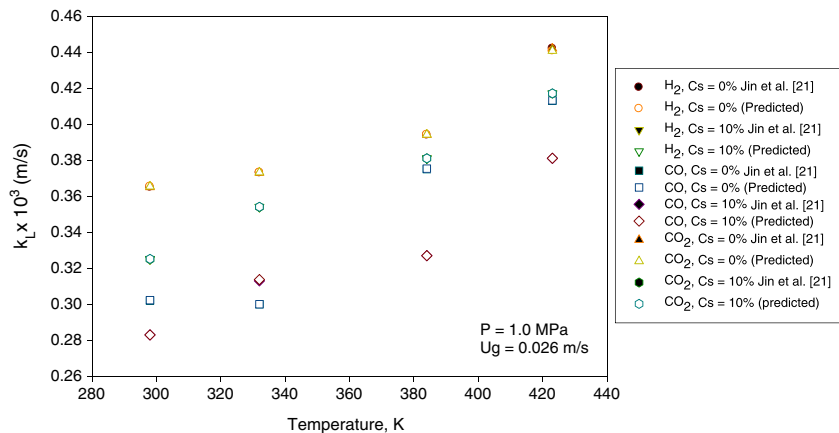
FIGURE 3 Flow diagram for estimation of liquid film thickness and surface renewal rate in a slurry bubble column

4.1 | Effect of temperature

The mathematical model has been used to predict k_L for a range of temperatures from 298 to 423 K. Equation proposed by Erkey et al.³¹ was used to estimate diffusivity of gas ($H_2, CO,$ and CO_2) in liquid paraffin at different temperatures. Figure 4 shows the effect of temperature on k_L for diffusion of $H_2, CO,$ and CO_2 in a slurry system comprising liquid paraffin–quartz sand (particle size: 150–200 μm). It can be seen that the liquid-side mass transfer coefficient k_L value increases with temperature remarkably. The temperature influences both δ and S . With increase in temperature, liquid film thickness decreases while surface renewal rate increases. Both liquid viscosity and surface tension decrease with increase in

temperature. Diffusion coefficient of gas in liquid and liquid properties was strongly affected by the system temperature. Mobility of liquid elements (microeddies) on the bubble surface increases with increase in temperature due to lowering of viscosity of liquid, resulting in lower resistance of liquid film due to resultant thinning of film, which promotes penetration of gas molecules from inside of the bubble to the bulk liquid phase. In other words, liquid-side mass transfer coefficient increases with decrease in liquid film thickness δ at higher temperatures due to reduction in viscosity. Diffusion coefficient of gas in liquid paraffin increased with increasing temperature and resulted in the increase in k_L . Besides, a high temperature also favors the diffusion of gas molecules in liquid film resulting in the increase in k_L value. However, a higher

FIGURE 4 Influence of temperature on mass transfer coefficient for diffusion of $H_2, CO,$ and CO_2 in a slurry system (liquid paraffin–quartz sand: 150–200 μm)—comparison of experimental and predicted values





temperature may also promote coalescence of small bubbles into large ones (result: decreased a) with faster movement and consequently a relatively shorter contact time. This will result in a decrease in the thickness of the liquid film δ , and as a result, mass transfer coefficient k_L increases.³

4.2 | Effect of pressure

Figure 5 illustrates the influence of pressure on the mass transfer coefficient k_L in the slurry phase (liquid paraffin–quartz sand). Figure 5 also shows the variation of mass transfer coefficient k_L with system pressure for gases: H₂, CO, and CO₂ in a slurry system (liquid paraffin–quartz sand: 150–200 μm). It is obvious from Figure 5 that the liquid-side mass transfer coefficient k_L increases slightly for H₂, CO, and CO₂ gases with increase in pressure. The solubility of gas in the liquid phase increases with pressure, which results in decrease in liquid viscosity and surface tension.^{3,32} Both the liquid film thickness and surface renewal rate are influenced by the system pressure. At higher pressures, bubble breakups are enhanced and bubble coalescence is suppressed, which escalates the formation of smaller bubbles resulting in an increase in the interfacial area of the bubble. The change in k_L values at elevated pressures may be explained by the change in liquid properties, that is, surface tension and viscosity. An increase in pressure lowers the surface tension of the liquid because of increased solubility of gas. A decrease in surface tension with pressure may allow the formation of smaller gas bubbles in the liquid phase, which will increase the interfacial area per unit volume of the bubble. The reduction in liquid viscosity also promotes mass transfer due to lower resistance of liquid film. Increase in pressure leads to the minor increase in k_L values and an increase in the interfacial area. It may be seen from Figure 5 that the value of k_L for CO₂ with $C_s = 10\%$ at 2.0 MPa is lowest (0.326 m/s). It has been

reported that at a pressure range of 1.7 to 3.0 MPa, increase in gas holdup for He and N₂ was reported to be within the same order of magnitude. This is because of the fact that under low pressure, large and less-dense gas bubbles are formed, whereas under high pressures, small and dense gas bubbles are formed. Under such conditions, it would not be enough to rupture the small and dense gas bubbles, and therefore, the increase in gas holdup becomes insignificant.³³ At higher pressures, number of bubble breakups in the system are enhanced, which escalate the formation of smaller bubbles resulting in an increase in the interfacial area of the bubble. Furthermore, several factors affect the interfacial area in a bubble column,³⁴ one of these factors may be responsible for lowering the interfacial area, which results in lower k_L value.

4.3 | Effect of superficial gas velocity

Effect of the superficial gas velocity on mass transfer coefficients, k_L , of H₂, CO, and CO₂ in the slurry (liquid paraffin–quartz sand: 150–200 μm) bubble column at 1.0 MPa is presented in Figure 6. As shown in Figure 6, when gas velocity increases, the bubble diameter would increase slightly, and the rising velocity of bubble increases, leading to the increase in turbulence and the surface renewal rate. Turbulence causes interfacial fluctuations and reduces the liquid film thickness. Higher gas velocity increases the gas holdup and decreases the mean bubble diameter leading to the increase in the specific gas–liquid interfacial area. In addition, the increase in superficial gas velocity reduces the bubble residence time leading to a decrease in the bubble surface renewal rate, S .⁷ Therefore, the two opposing effects result in a small influence on the superficial gas velocity and mass transfer coefficient k_L . The value of k_L for H₂ at $C_s = 10\%$ is slightly higher at a gas velocity of 4.2 m/s, which is maximum among the gas velocities applied. However, this variation is small and may be attributed to experimental

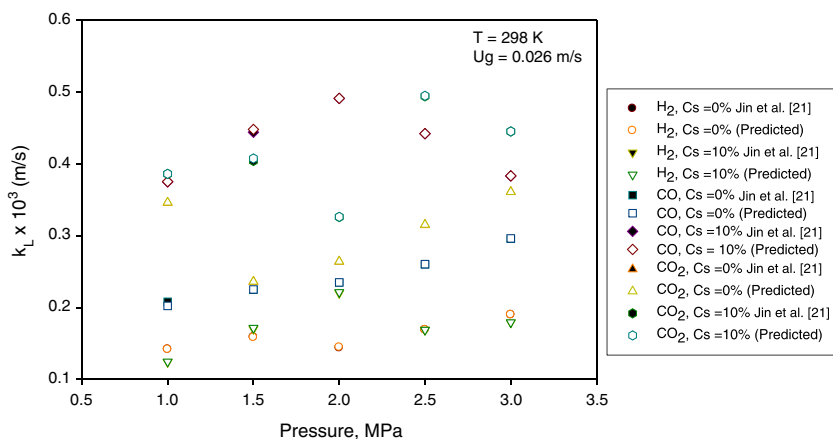


FIGURE 5 Influence of pressure on mass transfer coefficient for diffusion of H₂, CO, and CO₂ in a slurry system (liquid paraffin–quartz sand: 150–200 μm)—comparison of experimental and predicted values

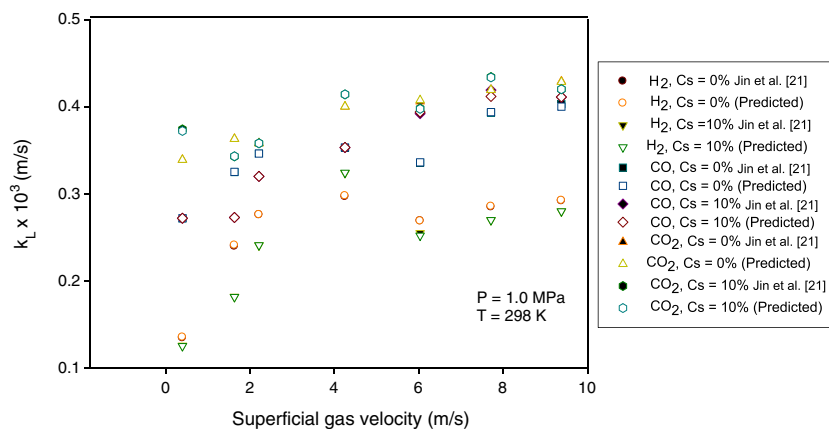


FIGURE 6 Influence of gas flow rate on mass transfer coefficient for diffusion of H_2 , CO , and CO_2 in a slurry system (liquid paraffin–quartz sand: 150–200 μm)—comparison of experimental and predicted values

measurement errors. Such deviation can be found in values reported earlier also.^{35,36}

4.4 | Effect of solid concentration

Solid concentration C_s in liquid paraffin (quartz sand, particle size 150–200 μm) was varied from 0% to 20% by mass. Figure 7 shows the influence of solid concentration on the mass transfer coefficients k_L of H_2 , CO , and CO_2 , respectively. It can be seen that the values of mass transfer coefficient k_L decreased slightly with an increase in the solid concentration. The enhancement of solid holdup results in increase in viscosity of the slurry, which is unfavorable to the mass transfer process. Additional solid particles may reduce the turbulence level and decrease the interface mobility. Thus, the net result will be lowering of k_L . Addition of solid concentration to a slurry system will enhance the gas bubble coalescence frequency, and as result, specific interface area will be decreased. The system viscosity also affects the surface renewal rate S .⁷ The surface renewal rate and mobility decrease due to addition of solid concentration, and it will prevent the gas diffusion into liquid phase resulting in decrease in the value of k_L . Finally, the effect of physical parameters on liquid film thickness, surface renewal rate, and mass transfer coefficient is presented in Table 6.

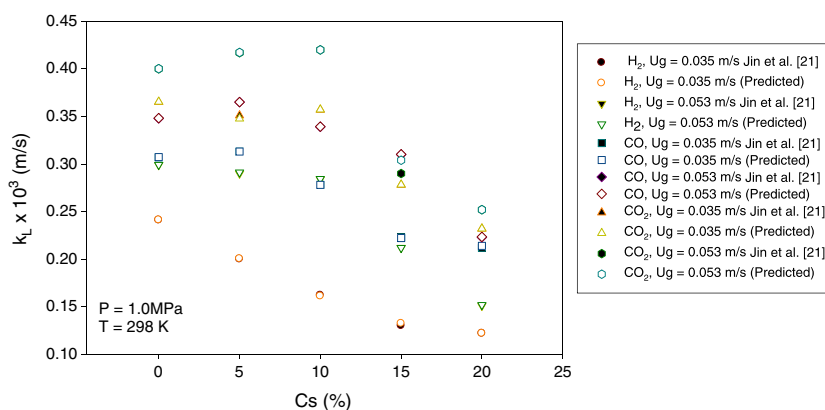


FIGURE 7 Influence of slurry (liquid paraffin–quartz sand: 150–200 μm) concentration on mass transfer coefficient k_L

4.5 | Effect of liquid film thickness on k_L

The experimental data from literature²¹ and predicted values of k_L from the proposed model for CO –, CO_2 –, and H_2 –slurry systems (liquid paraffin–Quartz sand: 150–200 μm) were plotted and are presented in Figure 8 (a–c). It may be seen from Figure 8(a–c) that the predicted values of k_L show very good agreement with the experimental data within an average deviation of $\pm 2\%$. In addition, k_L values estimated by varying liquid film thickness (δ) for surface renewal rate ranging from 1 to 10 s^{-1} were plotted and depicted in Figure 9(a–c). It may be seen from Figure 9(a–c) that variation in liquid film thickness values (δ) from 2.5×10^{-6} to 7×10^{-6} m yields k_L values in the range of 0.2×10^{-3} to 0.5×10^{-3} m/s for CO –liquid paraffin system. The corresponding values for CO_2 –liquid paraffin and H_2 –liquid paraffin systems are for δ values in the range from 2.14×10^{-6} to 4.70×10^{-6} m, k_L : 0.232×10^{-3} to 0.494×10^{-3} m/s and for a δ values in the range from 1.20×10^{-5} to 5.0×10^{-5} m, k_L : 0.128×10^{-3} to 0.324×10^{-3} m/s, respectively. Thus, simulated results indicate that k_L is inversely proportional to δ . These trends are in order as k_L decreases with increase in δ values. It is important to mention here that values of δ are not measurable, but at the same time, mass transfer resistance is controlled by the magnitude of δ .²³

**TABLE 6** Effect of operating parameters on film thickness, surface renewal rate, and overall k_L

Operating parameter	Film thickness, δ	Surface renewal rate, S	Overall k_L
Temperature	Decreases due to decrease in physical properties of liquid, that is, σ_L , ρ_L , μ_L , D_a .	Increases due to increase in mobility of liquid elements (eddies).	Increases with temperature significantly because higher temperature favors higher diffusivity of gas in the liquid film.
Pressure	At higher pressures, bubble size decreases resulting in decrease in bubble rise velocity and increase in film thickness.	Slightly affected	Slight increase with increasing in pressure because solubility of gas in the liquid phase increases with increase in pressure.
Gas flow rate	Reduction in the liquid film thickness due to interfacial fluctuations at higher value of U_g	Enhancement in the surface renewal rate	Increases with increasing superficial gas velocity.
Solid concentration	Film thickness increases because of particle covering the bubble surface.	Decreases due to increasing viscosity of the slurry, which is unfavorable to mobility of liquid elements (eddies). In other words, solid particles will reduce the turbulence level and decrease the interface mobility.	Decreases slightly with an increase in the solid concentration.

The values of δ have not been reported earlier. Surface renewal rate plays an important role in maintaining the concentration gradient between the bulk gas and liquid film. Ranges of surface renewal rates have been taken in the present work from literature.²⁰

4.6 | Empirical correlations for liquid film thickness δ

The model developed in the present work for mass transfer coefficient (k_L) for turbulent regime is based on molecular diffusion and convective flows, which are responsible for the renewal of liquid film at the bubble surface due to microscale eddies of the turbulent field. The size of gas bubble is not a critical parameter for estimation of k_L .³⁷ The development of a relationship between liquid film thickness and other variables such as pressure, temperature, superficial gas velocity, solid concentration, mass transfer coefficient, and physical properties of gas and liquid can be written in the following form:

$$\delta = f(T, P, U_g, C_S, k_L, D_a, D_C, M_A, \nu_A, \mu_{SL}, \rho_{SL}).$$

Dimensional analysis was used by employing Buckingham Π (pi) theorem to obtain empirical correlations for predicting δ values for H_2 , CO , and CO_2 in the form of dimensionless groups (Eu , Re , Sc , and Sh) and C_S , and ratio of slurry and gas properties. Indeed, it is not possible to fit a single correlation in good agreement with experimental data. Diffusivities of H_2 , CO , and CO_2 in liquid paraffin can be calculated by Equation 34

proposed by Erkey et al.³¹ Developed correlations for the three systems are as follows:

H₂-liquid paraffin-quartz sand system

$$\delta_{H_2} = 1.17 \times 10^9 (Eu)^{0.088} (Re)^{0.185} (Sc)^{0.082} (Sh)^{-1.338} (C_S)^{0.003} \left(\frac{\rho_{SL}}{\rho_G} \right)^{-7.710} \quad (39)$$

$$\text{Valid range: } 7.26 \leq Re \leq 6.0 \times 10^4, \\ 2.26 \times 10^6 \leq Sh \leq 5.54 \times 10^6, 2.41 \times 10^3 \leq Sc \leq 8.93 \times 10^4 \\ 12.77 \leq Eu \leq 4.9 \times 10^6, 0 \leq C_S \leq 20 \text{ (mass\%),} \\ 6.005 \leq \rho_{SL}/\rho_G \leq 6.312, 1.2 \times 10^{-5} \leq \delta \leq 5.0 \times 10^{-5}$$

CO-liquid paraffin-quartz sand system

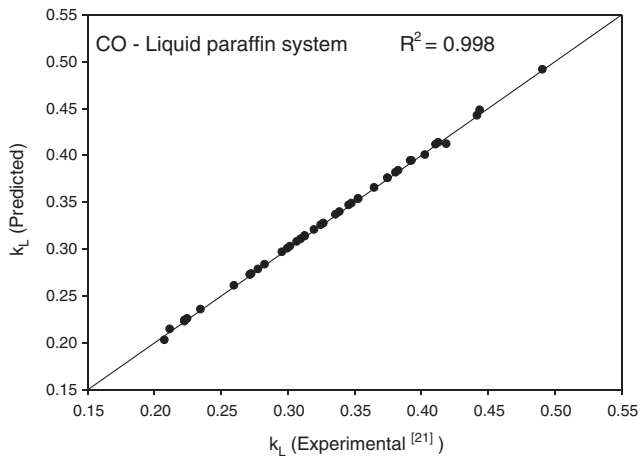
$$\delta_{CO} = 244.313 (Eu)^{-0.007} (Re)^{-0.014} (Sc)^{-0.013} (Sh)^{-1.034} (C_S)^{0.00057} \left(\frac{\rho_{SL}}{\rho_G} \right)^{0.310} \quad (40)$$

$$\text{Valid range: } 7.26 \leq Re \leq 6.0 \times 10^4, 1.54 \times 10^7 \\ \leq Sh \leq 3.74 \times 10^7, 9.93 \times 10^3 \leq Sc \leq 3.67 \times 10^5 \\ 12.77 \leq Eu \leq 4.9 \times 10^6, 0 \leq C_S \leq 20 \text{ (mass\%),} \\ 0.997 \leq \rho_{SL}/\rho_G \leq 1.048, 2.67 \times 10^{-6} \leq \delta \leq 6.0 \times 10^{-6}$$

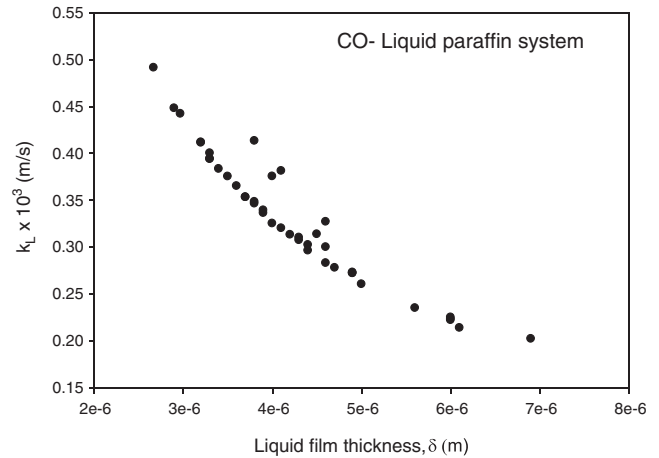
CO₂-liquid paraffin-quartz sand system

$$\delta_{CO_2} = 151.117 (Eu)^{0.003} (Re)^{0.007} (Sc)^{0.045} (Sh)^{-1.029} (C_S)^{0.00089} \left(\frac{\rho_{SL}}{\rho_G} \right)^{2.160} \quad (41)$$

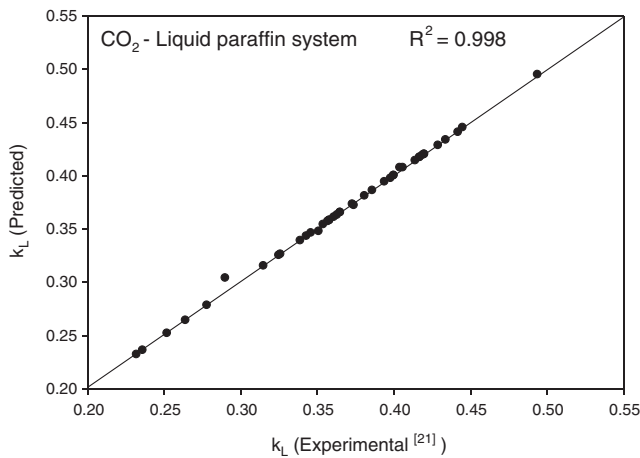
$$\text{Valid range: } 7.26 \leq Re \leq 6.0 \times 10^4, 1.49 \times 10^7 \\ \leq Sh \leq 3.39 \times 10^7, 8.40 \times 10^3 \leq Sc \leq 3.11 \times 10^5 \\ 12.77 \leq Eu \leq 4.9 \times 10^6, 0 \leq C_S \leq 20 \text{ (mass\%),} \\ 0.653 \leq \rho_{SL}/\rho_G \leq 0.686, 2.14 \times 10^{-6} \leq \delta \leq 4.7 \times 10^{-6}$$



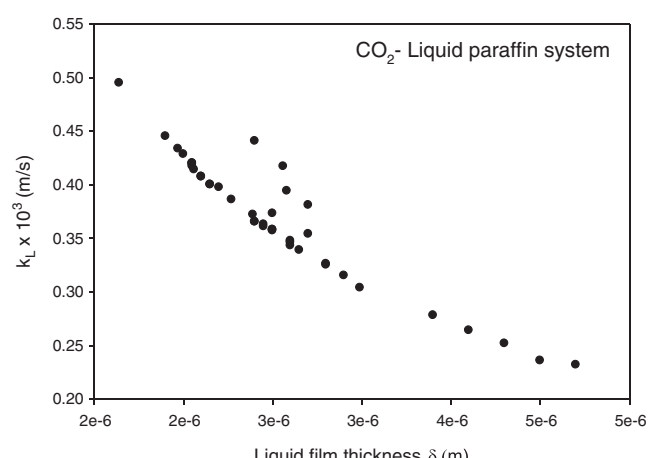
(a)



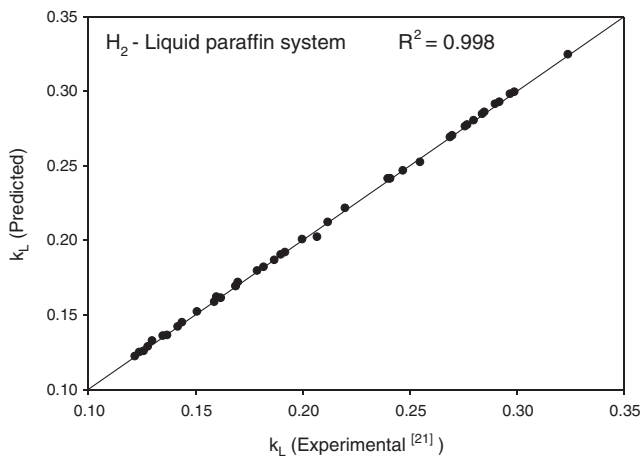
(a)



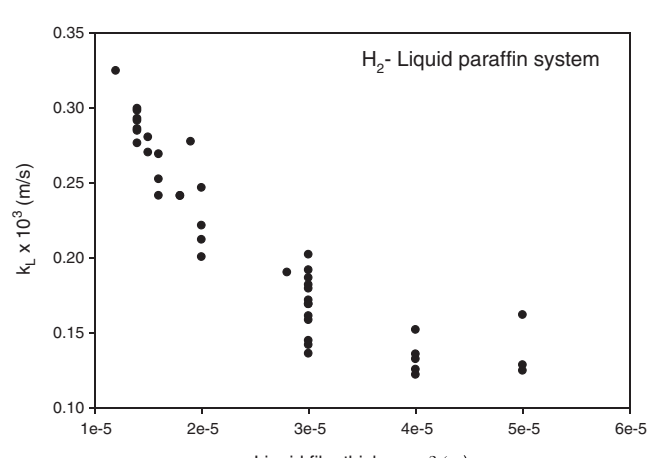
(b)



(b)



(c)



(c)

FIGURE 8 Experimental versus predicted values of k_L for (a) CO-slurry system (liquid paraffin-quartz sand), (b) CO₂-slurry system (liquid paraffin-quartz sand), and (c) H₂-slurry system (liquid paraffin-quartz sand)

Empirical correlations for the estimation of liquid film thickness presented at Equations 39 to 41 indicate that the effect of solid concentration on the film thickness is negligible up to a solid concentration of 20% by mass, in case of

FIGURE 9 Effect of liquid film thickness (δ) on k_L ($S = 1-10 \text{ s}^{-1}$) for (a) CO-slurry system (liquid paraffin-quartz sand), (b) CO₂-slurry system (liquid paraffin-quartz sand), and (c) H₂-slurry system (liquid paraffin-quartz sand)

all the three gases studied. Thus, it is obvious that mass transfer in gas-slurry systems may be treated nearly in the same way as that of a gas-liquid system. The values of the C_s term in Equations 39 to 41 are nearly equal to 1



suggesting that the behavior of slurries of glass like solids, for example, quartz sand, will be same as that of gas–liquid systems. It may also be seen from Equations 39–41 that the exponent of parameter (ρ_{SL}/ρ_G) of H₂–slurry system has a larger value than the other two systems. This fact points out that the gas properties also play a significant role in mass transfer in bubble columns. Furthermore, the exponent of gas density (ρ_G) in Equations 39–41 reveals that the gas density is an important parameter in the case of H₂ gas while the same is relatively less significant in other two cases. This variation in behavior of the gases may be attributed to their molecular masses and resulting chemical behavior due to atomic orbital variations. It was found during the testing of accuracy of prediction from the correlation that the predictions have significant deviation from the experimental values when Sherwood number is not used in the correlation.²² The deviation of predicted values of film thickness with the experimental data is due to the fact that value of mass transfer coefficient depends the film thickness.²⁰ Film thickness can be predicted without using Sherwood number also, but with the sacrifice in accuracy. The negative exponent in case of CO for *Eu*, *Re*, and *Sc* may be due to mild solubility difference of these components in liquid paraffin.

5 | CONCLUSIONS

In this work, a mathematical model was established for gas–liquid/slurry system considering surface age distribution function for a spherical bubble. The model predictions are applicable to a wide range of operating conditions for slurries with solid particles of inert surface characteristics. Using experimental data from the literature, the influence of temperature (298–423 K), pressure (1–3 MPa), superficial gas velocity (0.026–0.053 m/s), and solid concentration percent by mass (0–20%) on k_L is analyzed. The results show that the mass transfer coefficient k_L increased with increasing superficial gas velocity and temperature and decreased with increase in slurry concentration, while it changed slightly with pressure. Simulated results also indicate that k_L decreases with increase in δ values. It is clear from the simulated results that lower value of δ yields higher value of mass transfer coefficient. Furthermore, new empirical correlations for estimation of liquid film thickness δ for H₂–, CO–, and CO₂–slurry (liquid paraffin–quartz sand) systems have been developed. The predictions from the developed correlation for δ for different gas–slurry systems are fairly accurate for the applicable range, which is evident from the good match of predicted and experimental values of k_L . The proposed macroscopic mathematical model is able to predict the overall k_L in a two- or three-

phase bubble column system, if bubble size distribution is known. The validity of model for liquid as well as slurry systems was verified for liquid paraffin with a solid concentration range of 0–20%. SBC may consist of different gases, liquid, and various types of solid particles; hence, studies need to be conducted for different systems, and interaction of bubbles may also be incorporated if needed.

ACKNOWLEDGEMENTS

One of the authors (A. S.) sincerely acknowledges the helpful discussions with fellow research scholars Mr. Avdesh Singh Pundir and Mrs. Komal Sharma on MATLAB programming and model development, respectively.

ORCID

Raj K. Vyas  <http://orcid.org/0000-0001-9330-1539>

Kailash Singh  <http://orcid.org/0000-0002-2390-9239>

REFERENCE

- Lemoine R, Behkish A, Sehabiague L, Heintz YJ, Oukaci R, Morsi BI. An algorithm for predicting the hydrodynamic and mass transfer parameters in bubble column and slurry bubble column reactors. *Fuel Process Technol.* 2008;89(4):322-343.
- Ferreira A, Ferreira C, Teixeira JA, Rocha F. Temperature and solid properties effects on gas–liquid mass transfer. *Chem Eng J.* 2010;162(2):743-752.
- Yang W, Wang J, Jin Y. Mass transfer characteristics of syngas components in slurry system at industrial conditions. *Chem Eng Technol.* 2001;24(6):651-657.
- Ozkan O, Calimli A, Berber R, Oguz H. Effect of inert solid particles at low concentrations on gas–liquid mass transfer in mechanically agitated reactors. *Chem Eng Sci.* 2000;55(14):2737-2740.
- Sada E, Kumazawa H, Lee C, Fujiwara N. Gas-liquid mass transfer characteristics in a bubble column with suspended sparingly soluble fine particles. *Industr Eng Chem Process Design Develop.* 1985;24(2):255-261.
- Mena P, Ferreira A, Teixeira JA, Rocha F. Effect of some solid properties on gas–liquid mass transfer in a bubble column. *Chem Eng Process Process Intensif.* 2011;50(2):181-188.
- Yang W, Wang J, Zhao B, Jin Y. Gas–liquid mass transfer in slurry bubble systems: II. Verification and simulation of the model based on the single bubble mechanism. *Chem Eng J.* 2003;96(1):23-27.
- Krishna R, Sie ST. Design and scale-up of the Fischer–Tropsch bubble column slurry reactor. *Fuel Process Technol.* 2000;64:73-105.
- Kawase Y, Halard B, Moo-Young M. Theoretical prediction of volumetric mass transfer coefficients in bubble columns for



- Newtonian and non-Newtonian fluids. *Chem Eng Sci.* 1987;42:1609-1617.
10. Cockx A, Roustan M, Line A, Hebrard G. Modelling of mass transfer coefficient k_L in bubble columns. *Trans IChemE.* 1995;73(Part A):627-631.
11. Shimizu K, Takada S, Minekawa K, Kawase Y. Phenomenological model for bubble column reactors: prediction of gas hold-ups and volumetric mass transfer coefficients. *Chem Eng J.* 2000;78:21-28.
12. Kittilsen P, Togersen R, Rytter E, Svendsen H. Modeling of gas-liquid mass-transfer limitations in slurry olefin polymerization. *Ind Eng Chem Res.* 2001;40:1090-1096.
13. Garcia-Ochoa F, Gomez E. Theoretical prediction of gas-liquid mass transfer coefficient, specific area and hold-up in sparged stirred tanks. *Chem Eng Sci.* 2004;59:2489-2501.
14. Haut B, Cartage T. Mathematical modeling of gas-liquid mass transfer rate in bubble columns operated in the heterogeneous regime. *Chem Eng Sci.* 2005;60:5937-5944.
15. Dhaouadi H, Poncin S, Hornut JM, Midoux N. Gas-liquid mass transfer in bubble column reactor: analytical solution and experimental confirmation. *Chem Eng Process Process Intensif.* 2008;47:548-556.
16. Wang J, Langemann H. Unsteady two-film model for mass transfer. *Chem Eng Technol.* 1994a;17:280-284.
17. Wang J, Langemann H. Unsteady two-film model for mass transfer accompanied by chemical reaction. *Chem Eng Sci.* 1994b;49:3457-3463.
18. Lupin HM, Merchuk JC. A note on the film—penetration model for mass transfer with first order chemical reaction. *AICHE J.* 1971;17:1243-1245.
19. Kastanek F. The volume mass transfer coefficient in a bubble bed column. *Collect Czech Them Commun.* 1977;42:2491-2497.
20. Zhao B, Wang J, Yang W, Jin Y. Gas-liquid mass transfer in slurry bubble systems: I. Mathematical modeling based on a single bubble mechanism. *Chem Eng J.* 2003;96:23-27.
21. Jin H, Yang S, He G, Liu D, Tong Z, Zhu J. Gas-liquid mass transfer characteristics in a gas-liquid-solid bubble column under elevated pressure and temperature. *Chin J Chem Eng.* 2014;22:955-961.
22. Sujan A. Studies on hydrodynamic and mass transfer parameters in a bubble column. Ph.D thesis to be submitted to *Malaviya National Institute of Technology, Jaipur* 2018.
23. Treybal RE. *Mass-transfer Operations.* 3rd ed. Singapore: McGraw-Hill; 1981.
24. Leonard C, Ferrasse JH, Boutin O, Lefevre S, Viand A. Bubble column reactors for high pressures and high temperatures operation. *Chem Eng Res Des.* 2015;100:391-421.
25. Danckwerts PV. Significance of liquid-film coefficients in gas absorption. *Ind Eng Chem.* 1951;43:1460-1467.
26. Jajuee B, Margaritis A, Karamanev D, Bergougnou MA. Application of surface-renewal-stretch model for interface mass transfer. *Chem Eng Sci.* 2006;61:3917-3929.
27. Levins DM, Glastonbury JR. Application of Kolmogoroff's theory to particle—liquid mass transfer in agitated vessels. *Chem Eng Sci.* 1972;27:537-543.
28. Garcia-Ochoa F, Gomez E. Theoretical prediction of gas-liquid mass transfer coefficient, specific area and hold-up in sparged stirred tanks. *Chem Eng Sci.* 2004;59:2489-2501.
29. Huifang Q, Shirong W, Baiquan D. Determination and estimation of physical property data for liquid paraffin. *Natural Gas Chemical Industry.* 1999;24(3):56-58.
30. Thomas DG. Transport characteristics of suspension: VIII. A note on the viscosity of Newtonian suspensions of uniform spherical particles. *J Colloid Sci.* 1965;20(3):267-277.
31. Erkey C, Rodden JB, Akgerman A. A correlation for predicting diffusion coefficients in alkanes. *Can J Chem Eng.* 1990;68(4):661-665.
32. Lau R, Peng W, Velazquez-Vargas LG, Yang GQ, Fan LS. Gas-liquid mass transfer in high-pressure bubble columns. *Ind Eng Chem Res.* 2004;43(5):1302-1311.
33. Behkish A, Lemoine R, Sehabiague L, Oukaci R, Morsi BI. Gas holdup and bubble size behavior in a large-scale slurry bubble column reactor operating with an organic liquid under elevated pressures and temperatures. *Chem Eng J.* 2007;128:69-84.
34. Sujan A, Vyas RK. A review on empirical correlations estimating gas holdup for shear-thinning non-Newtonian fluids in bubble column systems with future perspectives. *Rev Chem Eng.* 2017.
35. Mena P, Ferreira A, Teixeira JA, Rocha F. Effect of some solid properties on gas-liquid mass transfer in a bubble column. *Chem Eng Process Process Intensif.* 2011;50:181-188.
36. Kluytmans JHI, Van Wachem BGM, Kuster BFM, Schouten JC. Mass transfer in sparged and stirred reactors: influence of carbon particles and electrolyte. *Chem Eng Sci.* 2003;58:4719-4728.
37. Sardeing R, Painmanakul P, Hebrard G. Effect of surfactants on liquid-side mass transfer coefficients in gas-liquid systems: a first step to modeling. *Chem Eng Sci.* 2006;61:6249-6260.

How to cite this article: Sujan A, Vyas RK, Singh K. Estimation of liquid-side mass transfer coefficient and liquid film thickness in a bubble column using single spherical bubble model. *Asia-Pac J Chem Eng.* 2018;e2178. <https://doi.org/10.1002/apj.2178>

*Estimation of transition concentration
of aqueous mixtures of single and binary
electrolytes for bubble coalescence
inhibition*

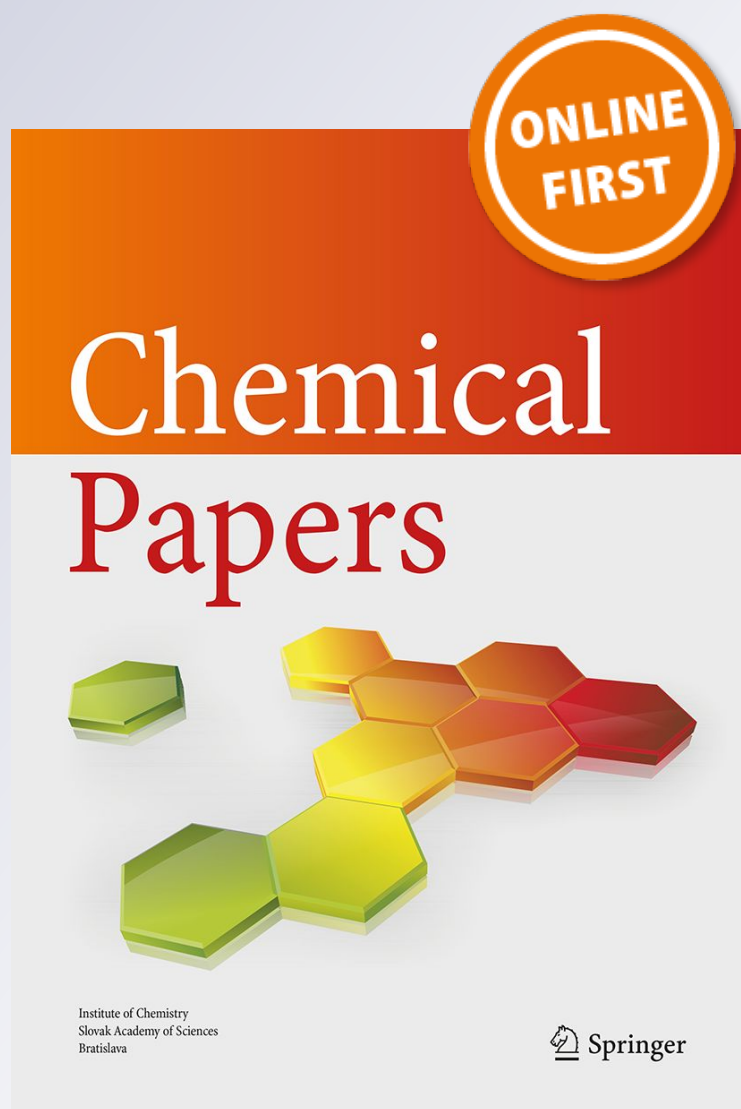
Ajay Sujan & Raj K. Vyas

Chemical Papers

ISSN 2585-7290

Chem. Pap.

DOI 10.1007/s11696-018-0470-2



Your article is protected by copyright and all rights are held exclusively by Institute of Chemistry, Slovak Academy of Sciences. This e-offprint is for personal use only and shall not be self-archived in electronic repositories. If you wish to self-archive your article, please use the accepted manuscript version for posting on your own website. You may further deposit the accepted manuscript version in any repository, provided it is only made publicly available 12 months after official publication or later and provided acknowledgement is given to the original source of publication and a link is inserted to the published article on Springer's website. The link must be accompanied by the following text: "The final publication is available at link.springer.com".



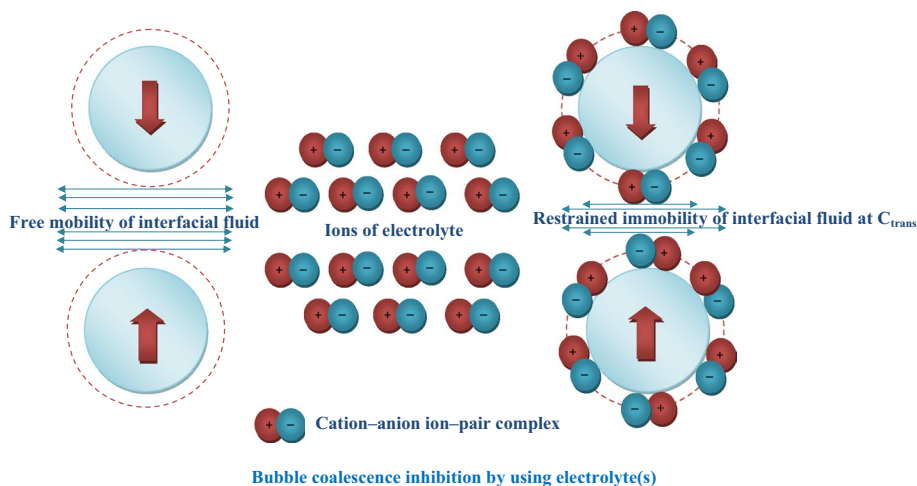
Estimation of transition concentration of aqueous mixtures of single and binary electrolytes for bubble coalescence inhibition

Ajay Sujan¹ · Raj K. Vyas¹ Received: 16 August 2017 / Accepted: 4 April 2018
© Institute of Chemistry, Slovak Academy of Sciences 2018

Abstract

A bubble column was investigated in which a swarm of air bubbles was dispersed in aqueous electrolyte (NaCl, MgSO₄·7H₂O, CaCl₂·2H₂O, and Na₂SO₄) solutions. In the present work, study of coalescence inhibition has been targeted by applying gas holdup enhancement and surface tension gradient approaches for aqueous solutions in single and binary mixtures (CaCl₂·2H₂O + NaCl and Na₂SO₄ + NaCl) of electrolytes. Transition concentrations of a series of coalescence inhibiting inorganic electrolytes were determined. A qualitative comparison of these electrolytes revealed that strong electrolytes (Na₂SO₄, and CaCl₂·2H₂O) yield gas holdup enhancement $\geq 60\%$ whereas moderate electrolytes (NaCl and MgSO₄·7H₂O) give gas holdup enhancement values $\leq 46\%$. It has been also found that the values of transition concentration for different electrolytes are of the same order in most of the cases and in line with those reported in the literature. Inhibition of bubble coalescence was also analyzed in terms of the parameter $C(d\sigma/dC)^2$. The large value of the parameter $(d\sigma/dC)^2$ indicates that the electrolyte will inhibit bubble coalescence, and a smaller value indicates moderate effect on bubble coalescence. Surface elasticity values at transition concentration of various electrolytes were also determined. It was found that the surface elasticity values at transition concentration were in the order CaCl₂·2H₂O > MgSO₄·7H₂O > Na₂SO₄ > NaCl. Surface elasticity for binary electrolytes was also estimated at their transition concentrations. The values were found in the order CaCl₂·2H₂O + NaCl > Na₂SO₄ + NaCl. Furthermore, analysis of variance was employed to estimate significance of the parameters.

Graphical abstract



Keywords Inorganic electrolyte · Surface tension gradient · Transition concentration · Bubble coalescence inhibition · Gas holdup · Bubble column

Extended author information available on the last page of the article

Abbreviations

ANOVA	Analysis of variance
GH	Gas holdup
MOC	Material of construction
HM	Homogenous regime
HT	Heterogenous regime

Symbols

A	Hamaker constant (non-retarded) for water, (3.5×10^{-20} J)
a_{\pm}	Mean ion activity coefficient
a_f	Free area of the disc
c	Force defined by Eq. (2), N
C_{trans}	Transition concentration (mol/L)
C	Electrolyte concentration (mol/L)
ΔC	Change in surface tension of solute (electrolyte)
H_L	Liquid height in bubble column (m)
H_b	Aerated froth height in bubble column (m)
k	Defined by Eq. (3) (l/m)
R	Universal gas constant, J/mol K
r	Bubble radius (m)
T	Absolute temperature (K)
U_g	Velocity of air (m/s)
U_L	Velocity of liquid (m/s)

Greek letters

$\varepsilon, \varepsilon_G$	Gas holdup in aqueous solution of electrolyte (dimensionless)
ε_w	Gas holdup in distilled water (dimensionless)
ν	Number of ions formed on dissociation (i.e., $\nu=2$ for most inorganic salt)
$\sigma, \sigma_{\text{el}}$ or σ_{aqueous}	Surface tension of electrolyte solutions (mN/m)
σ_w	Surface tension of water (mN/m)
$\Delta\sigma$	Mean change in surface tension (mN/m)
$d\sigma/dC$	Surface tension gradient
ρ_{aqueous}	Density of aqueous solution of electrolyte (kg/m^3)
ψ_{aqueous}	Conductivity of aqueous solution of electrolyte ($\mu\text{S/m}$)

Introduction

Bubble coalescence inhibition is important for different liquids and solutions for improving the mass transfer performance in bubble columns, bioreactors like fermenters and aerobic wastewater treatment systems. Use of organic and inorganic compounds in industrial bubble columns, particularly in bioreactors, is quite common. For instance, micro-organism growth and survival in aerobic biological systems

require interfacial oxygen transfer. Hence, oxygen transfer through an air–liquid interface is one of the major issues in bioreactor design due to low solubility of oxygen in aqueous solutions of electrolytes (Jackson 1991). Effective interfacial oxygen transfer is a complex phenomenon and it is desirable that the size of bubbles remains small. Bubble size is a key parameter for hydrodynamic studies in bioreactors and it depends on parameters such as physicochemical properties of the liquid, gas flow rate, contactor geometry and type of sparger used. It is commonly accepted that, depending on the gas flow rate, two main flow regimes can be observed in bubble columns, i.e., (1) homogeneous bubbly flow regime encountered at low gas velocities and characterized by a narrow bubble size distribution and uniform gas holdup. Extent of bubble coalescence and breakup in the bubble bed is negligible and (2) heterogeneous (churn turbulent flow) regime observed at higher gas velocities characterized by the appearance of large bubbles, formed by coalescence of the small bubbles and bearing a higher rise velocity, hence, leading to relatively lower gas holdup values (Besagni et al. 2018; Besagni and Inzoli 2017a, b; Majumder 2016; Besagni and Inzoli 2016; Mouza et al. 2005; Joshi et al. 2002; Zahradnik et al. 1997). The homogeneous flow regime can be further classified into (a) “mono-dispersed homogeneous” flow regime and (b) “pseudo-homogeneous” flow regime, depending on the existing bubble size distribution in the system. It is well known that the bubble size distribution in the bubble column systems is mainly controlled by the gas sparger openings. Stability of homogeneous regime and the gas holdup values are strongly influenced by the type and geometry of the gas sparger, i.e., fine pore sparger or coarse gas sparger (Besagni et al. 2018; Zahradnik et al. 1997) and the properties of the liquid phase (Mouza et al. 2005). Either of the regimes can be obtained in a system by varying the gas flow rate.

The presence of electrolytes in water keeps the bubbles apart and makes them stable for a longer time. The knowledge of effects of electrolytes on hydrodynamic properties in bubble columns is, therefore, important for bubble coalescence inhibition. An important effect of electrolytes is the inhibition of bubble coalescence during the approach or collision of a bubble with other bubbles. Bubble coalescence in pure water occurs when the value of surface elasticity is zero. At this point, the approaching bubbles begin to drain and form an unstable film which ruptures at a film thickness close to 110 nm (Pashley and Craig 1997). Empirical correlations for estimation of liquid film thickness in gas–liquid/gas–liquid–solid systems for CO, CO₂, and H₂ have been proposed recently (Sujan et al. 2018). An electrolyte increases the stabilization time of liquid film by increasing the surface elasticity of the gas–liquid interface. The surface elasticity (which is quantitatively equal to half of the Gibbs elasticity) is the basis of coalescence inhibition (Christenson

and Yaminsky 1995). Surface elasticity is increased by the use of electrolytes. Surface elasticity is proportional to the surface tension gradient and for a single electrolyte; this gives a good correlation with bubble coalescence inhibition. However, the presence of a mixture of two electrolytes has shown no correlation between surface elasticity and bubble coalescence inhibition (Henry et al. 2007). Square of surface tension gradient $(d\sigma/dc)^2$ has been found to be proportional to the value of Gibbs elasticity. The value of Gibbs elasticity was also found to be comparable to the bubble coalescence inhibition for a range of electrolyte solutions (Craig 2011).

A number of studies have reported bubble coalescence behavior in electrolyte solutions (Marrucci and Nicodemo 1967; Lessard and Zieminski 1971; Prince and Blanch 1990; Craig et al. 1993a, b; Zahradnik et al. 1995; Weissenborn and Pugh 1995; Nguyen et al. 2012). It has been observed that coalescence commonly occurs in pure water and with increasing concentration of electrolytes there is a transition to coalescence inhibition regime. This transition occurs over a narrow concentration range (<0.1 mol/L) which is characteristic of a particular electrolyte such as CH_3COOH , NH_4NO_3 , KNO_3 , KOH , KBr , NH_4Cl , NaNO_3 , KCl , NaCl , Na_2SO_4 , CaCl_2 , and MgSO_4 (Del Castillo et al. 2011; Craig et al. 1993a, b). Some of the researchers investigated the effect of electrolytes on gas holdup and coalescence behavior of bubbles in a laboratory-scale bubble column (Ribeiro and Mewes 2007a, b; Orvalho et al. 2009; Syeda and Reza 2011; Nguyen et al. 2012; Besagni and Inzoli 2017a, b). Suppression of bubble coalescence leads to gas holdup enhancement. The concentration at which minimum bubble coalescence is achieved is likely to result in the maximum gas holdup in a bubble column. It has been reported earlier by several investigators (Eissa and Schügerl 1975; Bach and Pilhofer 1978; Godbole et al. 1982; Khare and Joshi 1990; Ruzicka et al. 2003; Olivieri et al. 2011) that viscosity of liquid has a dual effect on gas holdup. At lower viscosity, drag force exerted by the liquid is small and, therefore, the bubbles rise in the column with higher velocity leading to more coalescence among the bubbles and thus lower gas holdup. Conversely, with increase in viscosity, the coalescence of bubbles gets limited reaching its maxima as a result of increased drag and reduced bubble rise velocity. With further increase in viscosity, the tendency to coalesce prevails allowing the bubbles to rise at higher velocity (Besagni and Inzoli 2017a, b), thus resulting in lowering of gas holdup up to a certain extent and then a constant gas holdup further. The value of viscosity varies with the nature and type of solid/liquid used (Eissa and Schügerl 1975; Bach and Pilhofer 1978; Godbole et al. 1982; Khare and Joshi 1990; Ruzicka et al. 2003; Olivieri et al. 2011).

Use of organic and inorganic compounds or viscous liquids affects the interfacial properties of bubbles. A change in the bubble interfacial properties reduces/promotes

coalescence phenomena, thus changing the prevailing bubble size distribution (BSD). Change in bubble size distribution has either of the following effects: (a) bubble coalescence is promoted when the prevailing bubble size distribution shifts towards larger bubbles. The lift force pushes the larger bubbles towards the center of the bubble column and, consequently, destabilizes the homogeneous flow regime and decreases gas holdup, or (b) bubble coalescence is suppressed when the prevailing bubble size distribution shifts towards smaller bubbles. The lift force pushes the small bubbles towards the wall, inducing cluster of bubbles and, consequently, stabilizes the homogeneous flow regime and increases the gas holdup (Besagni and Inzoli 2017a, b). In a recent study, it has been reported that addition of an electrolyte (NaCl) to water altered the bubble properties which shifted the bubble size distribution towards lower equivalent bubble diameters and stabilized the homogeneous flow regime and as a result the overall gas holdup increased (Besagni and Inzoli 2017a, b).

Therefore, gas holdup enhancement in bubbling region is strongly related to the coalescence inhibition tendency of bubbles in different gas–liquid systems. Various researchers reported that the use of electrolytes reduces the solubility of the gas molecules in aqueous solutions and proposed an alternative mechanism by which electrolytes inhibit bubble coalescence (Weissenborn and Pugh 1996; Geffcken 1904; Millero et al. 2002). Investigations using surface tension of electrolytes have been scarcely reported in the literature. For a very low concentration of electrolyte solutions which have interfacial tensions practically same as that of pure water, the bubbles were reported to be much smaller and the gas holdup much higher than that of pure water (Lee and Meyrick 1970; Machon et al. 1977). Recently, Syeda and Reza (2011) found a strong relationship between gas holdup and surface tension gradient with the addition of electrolytes. Slope of surface tension gradient $(d(\Delta\sigma)/dC)$ was reported to be higher at lower concentration of strong electrolytes (Na_2SO_4 and $\text{CaCl}_2 \cdot 2\text{H}_2\text{O}$) which changes sharply as the concentration increases further. For moderate electrolytes (NaCl and $\text{MgSO}_4 \cdot 7\text{H}_2\text{O}$), the increase in surface tension was gradual. Increase in surface tension due to the presence of inorganic electrolytes causes a reduction in the bubble size (Chan and Tsang 2005). Average bubble size in a bubble column remains smaller in case of some specific electrolyte solutions than in pure water (Prince and Blanch 1990; Kluytmans et al. 2001) as these electrolytes can inhibit bubble coalescence and it is called “ion-specific effect” (Craig et al. 1993a, b).

The first systematic significant elementary studies of bubble coalescence were reported by Marucci (1969). Authors developed a coalescence model to account the change in surface concentration of solute, (ΔC) , caused by increase in the surface area during film stretching, leading to a change in

interfacial tension, ($\Delta\sigma$), for two adjoining bubbles in aqueous electrolyte solutions and found that the drainage rate is strongly dependent on the mobility of the surface. If the bubble interface is immobile, the liquid drains from the surface between the two flattened bubbles in a slow process, whereas if the surface is mobile, drainage is much faster. In such a case, coalescence rate of bubbles is faster. In addition, the corresponding concentration of electrolytes is responsible for shifting the mobile interface into an immobile one. Thus, the bubble size would depend on the concentration of solute which controlled the type of interface and the interfacial tension gradient (Marucci 1969; Lessard and Zieminski 1971).

In a stagnant pure water system, the rate of coalescence is at its maximum and it decreases as the concentration of electrolytes is increased. At transition coalescence concentration, the coalescence rate is drastically reduced by 50%. The transition coalescence concentration of electrolytes has been suggested as a critical key factor for characterizing the hydrodynamic behavior (Ribeiro and Mewes 2007a, b; Syeda and Reza 2011) and mass transfer (Al Taweel et al. 2013) in a bubble column. All electrolytes reduce electrostatic forces. Some of them reduce bubble coalescence by reducing the hydrophobic attraction above their transition concentration (Craig et al. 1993a). Electrolytes also reduce the range of attraction force above their transition concentration. In essence, electrolytes induce bubble interactions by reducing the range of attraction force from approximately 100–50 nm (Craig et al. 1993b).

The critical concentration depends on the valency of both the ions forming the electrolyte. Coalescence rate decreases from high-valency ion combinations (e.g., 3–1, 2–2 type) to lower valency of combinations (type 2–1, 1–2) and type 1–1 combinations (Marrucci and Nicodemo 1967; Lessard and Zieminski 1971). On similar lines, Deschenes et al. (1998) investigated the effect of dilute 1:1 and 2:1 electrolyte solutions on bubble coalescence inhibition. It has been observed that anions dominate the inhibition at concentration below 0.01 M and cations dominate the inhibition at higher concentrations. Only a few studies concerning the influence of electrolyte concentration on gas holdup in bubble columns with a diameter less than 0.12 m have been reported earlier (Syeda and Reza 2011; Nguyen et al. 2012). Besides, only few studies are available on gas holdup characteristics of an aqueous solution of electrolytes in bubble columns as can be seen in Table 1. Empirical correlations for estimation of gas holdup in different Newtonian and non-Newtonian systems have been reported in the literature (Joshi et al. 1998; Sujana and Vyas 2017). In the present study, experiments were carried out in a bubble column with 0.105 m inner diameter, for investigating the coalescence behavior in the presence of electrolytes.

Systematic studies of ion-specific coalescence of bubbles in selected mixed electrolytes solutions were reported by

Henry et al. (2007). Mixed electrolytes follow the properties of the individual ions originally assigned earlier produced by Craig et al. (1993a, b). The combining rules indicated that the fundamental property of the ions controls the bubble coalescence inhibitory behavior of electrolytes. For a single-electrolyte system, if the value of parameter $(d\sigma/dC)^2$ is large, then the electrolyte will inhibit bubble coalescence, and bubble coalescence behavior will remain unaffected if the value of $(d\sigma/dC)^2 < 1$ ($\text{mN} \cdot \text{m}^{-1}/\text{mol L}^{-1}$)². However, in the case of mixed electrolytes, no correlation between coalescence inhibition and $(d\sigma/dC)^2$ is available.

The interpretation of bubble coalescence and gas holdup behavior in aqueous solutions of single and mixed electrolytes in terms of surface tension gradient is also incomplete and asks for further exploration. To our best knowledge, the effect of the presence of mixed electrolytes on gas holdup and surface elasticity values of different electrolytes at transition concentration have not been reported in the literature.

The aim of the present study is to fill the gap and study the effect of single and mixed electrolyte (s) on average gas holdup experimentally in a bubble column and to achieve bubble coalescence inhibition. For this purpose, transition concentrations of strong and moderate electrolytes were estimated using the parameter $C(d\sigma/dC)^2$. In addition, analysis of variance (ANOVA) was used to estimate the significance of the effect of parameters such as gas flow rate, electrolyte concentration and chemical nature of the electrolytes, on average gas holdup.

Materials and methods

The experimental study concerning gas holdup measurements was conducted in a borosilicate glass bubble column with an internal diameter of 0.105 m and 1.25 m height operated in the batch mode ($U_L \approx 0$ L/m; where U_L is the liquid flow rate). A schematic diagram of the experimental setup is shown in Fig. 1. A perforated nylon circular disc containing 69 orifices with a hole diameter of 0.002 m each arranged in a quadrangular pattern with a pitch of 0.01 m was placed at the bottom of the column and used as sparger. The free area of the disc (a_f) was 96.93%. Specifications of experimental setup are given in Table 2. To ensure uniform distribution of gas in the bubble column, the gas distributor was fixed 0.012 m above the air inlet. The electrolyte solutions were aerated for a sufficiently long time to ensure minimum fluctuation of liquid height during bubbling. The controlled air supply from air compressor via air control panel through air rotameter (Make: Eureka, Model No. CIVF-PG-2, Eureka Industrial Equipment Pvt. Ltd, Pimpri, Pune India) was sparged to the bubble column. Four inorganic electrolytes (NaCl , $\text{MgSO}_4 \cdot 7\text{H}_2\text{O}$, $\text{CaCl}_2 \cdot 2\text{H}_2\text{O}$, and Na_2SO_4) were used in the experimental study. All of

Table 1 Effect of air–aqueous solution of electrolyte system on gas holdup, ϵ_G

System	Electrolytes; parameters studied	Sparger; measurement techniques	Column diameter (m); column height (m)	Regimes covered (HM); heterogeneous (HT)	Range of concentration; gas holdup range (-)	Remarks	References
Air–distilled water system	NaCl, Na ₂ SO ₄ ; gas holdup, ϵ_G	Single point sparger with 0.005 m (5 mm) dia; bed expansion method for gas holdup	0.152–0.6 m; 4.0 m	HM; HT	0.03–1.0 M; 0–0.355	Addition of electrolytes increases gas holdup, correlation developed for gas holdup	Akita and Yoshida (1973)
Air–distilled water system	Na ₂ SO ₄ , NaCl, CaCl ₂ ; gas holdup, ϵ_G	Perforated plate of 1 and 0.0016 m (1.6 mm) hole dia; manometer readings converted to absolute pressures by a simple hydrostatic head technique; to get the values of the gas holdup	0.154 m; 3.25 m	HM; HT	0.05–1.0 M; 0–0.35	Critical electrolyte concentration determined above which no increase in gas holdup. At higher superficial gas velocity, no effect of sparger diameter on gas holdup	Kelkar et al. (1983)
Air–distilled water system	BaCl ₂ , Na ₂ SO ₄ ; gas holdup, ϵ_G	Perforated plates with 0.0005–0.0025 m (0.5–2.5 mm) hole dia; bed expansion method for gas holdup	0.018 m; N.R	HM; HT	0.1–0.27 M; 0–0.32	No effect of column internal diameter and sparger hole diameter on gas holdup (HT) Correlation for the transition regime	Koide et al. (1984)
Air–distilled water system	NaCl, NaSO ₄ , KCl, NaOH, CaCl ₂ , MgSO ₄ ; gas holdup, ϵ_G	Perforated plates with 0.0005 and 0.0016 m (0.5 and 1.6 mm) hole dia; bed expansion method for gas holdup	0.15 m; 0.29 m	HM; HT	0.5 M; –	Above critical concentration of electrolyte, no effect on gas holdup. Correlation for gas holdup developed	Zahradnik et al. (1987)
Air–water system	NaCl, KCl; gas holdup, ϵ_G	Perforated plates; bed expansion method for gas holdup	0.14 m; N.R	HM; HT	0.01–1.0 M; –	Critical concentration are given for the electrolyte	Zahradnik et al. (1995)
Air–distilled water system	NaCl, NaSO ₄ and NaI; gas holdup, ϵ_G and regime transition point	Perforated plate with 0.0007 m (0.7 mm) dia. arranged on a triangular pitch of 0.006 m (6 mm). Number of holes: 216; bed expansion method for gas holdup. The bubble swarm velocity method, the drift-flux method for regime transition point	0.12 m; 1.25 m	HM; HT	0–0.089 M; 0–0.8	Gas holdup continuously increases with increasing electrolyte concentration. Transition concentration for bubble coalescence exhibited the same gas holdup profile, regardless of the electrolyte added to the liquid phase	Ribeiro Jr and Mewes (2007a, b)
Air–distilled water system	NaSO ₄ , NaCl, NaCl (kitchen quality); gas holdup, ϵ_G	Perforated plate with circular orifices of 0.0005 m (0.5 mm) dia. and relative free area 0.2%; bed expansion method for gas holdup	0.14 m; 2.0 m	HM; HT	0.001–6.0 M; 0–0.7	Dual effect of the salt on the gas holdup and homogeneous regime	Orvalho et al. (2009)
Air–distilled/deionized water system	NaCl, MgSO ₄ ·7H ₂ O, NaSO ₄ , CaCl ₂ ·2H ₂ O; gas holdup, ϵ_G	Circular plate with 10 orifices of 0.002 m (2 mm) diameter; bed expansion method	0.05 m; 0.5 m	HM; HT	0–0.3 M; Up to 65 (%)	Enhancement in gas holdup at low concentrations. Slope (d ϵ_G /dC) is high at lower concentration and changes sharply as the concentration increases further	Syeda and Reza (2011)

Table 1 (continued)

System	Electrolytes; parameters studied	Sparger; measurement techniques	Column diameter (m); column height (m)	Regimes covered (HM); heterogeneous (HT)	Range of concentration; gas holdup range (-)	Remarks	References
Air-distilled water system	NaCl, NaF, NaBr, NaI, and CsCl; gas holdup, ϵ_G	Glass frit (porosity 11–16 μm); light intensity method for bubble coalescence, bed expansion method for gas holdup	0.045 m; 0.2 m	N.R; N.R	0.001–3.0 M; Up to 60 (%)	Transition salt concentration for bubble coalescence inhibition of all investigated salts decreases with increasing superficial gas velocity $C_{\text{trans}}:$ $\text{NaI} > \text{NaBr} > \text{CsCl} > \text{NaCl} > \text{NaF}$	Nguyen et al. (2012)
Air-deionized water system	NaCl; gas holdup, flow regime transition and bubble size distribution	Spider sparger with six arms (diameter of each hole: 0.002–0.004 m (2–4 mm)); photographic methods and bed expansion method	0.24 m; 5.3 m	HM; N.R	0–0.170 M; 0–0.30	Bubble size distribution shifts towards lower equivalent diameter of bubbles due to the addition of NaCl resulting in increased gas holdup. NaCl concentration stabilized the homogeneous flow regime	Besagni and Inzoli (2017a, b)

them are strong electrolytes, i.e., they completely dissociate in solution and the solution will contain only ions and no molecules of the electrolyte. Depending on their effect on bubble coalescence, electrolytes are normally classified into two categories, namely strongly significant effect and moderate effect. The first two (NaCl and $\text{MgSO}_4 \cdot 7\text{H}_2\text{O}$) suppress bubble coalescence moderately, whereas the remaining two (Na_2SO_4 and $\text{CaCl}_2 \cdot 2\text{H}_2\text{O}$) are known to suppress bubble coalescence very strongly (Ribeiro and Mewes 2007a; Syeda and Reza 2011).

Details of properties of electrolytes are summarized in Table 3. Stock solutions of electrolytes were prepared in distilled water. The electrolytes used were of analytical reagent grade and their purity was greater than 99%. Distilled water (surface tension: 72.14 ± 0.3 mN/m at 28 °C, and electrical conductivity: 200 ± 0.1 $\mu\text{S/m}$) was used to prepare the aqueous solution of electrolyte. In each run using electrolyte solution in the bubble column, gas flow rate was progressively increased from 7.5 to 27.5 L/m by manually adjusting the rotameter valve. Operational details of the experimental study are tabulated in Table 4. In the present study, gas holdup enhancement (bed expansion method) was used for bubble coalescence inhibition. Bubbling height related to each individual gas velocity was noted after a stabilization period of 5 min and it was used to compute the corresponding gas holdup. The reason for using the gas holdup method is that bubble column is a standard device used for contacting gases and liquids (Hecht et al. 2015). Two-phase bubble columns are widely used in chemical, petrochemical and bioprocess industries due to their inherent practical advantages in design and operation (Besagni and Inzoli 2017a, b). Besides, gas holdup measurement can be conveniently measured with a reasonable accuracy. On the other hand, limitations of other techniques for studying bubble coalescence inhibition such as thin film balance and bubble pair have already been outlined in the literature (Wang et al. 2016). Use of another technique, viz., microfluidics is limited due to the requirement of precise measurement of small quantity of fluids or liquid and gas needing precision measurement instruments. In view of their widespread use in process industries for bubble coalescence inhibition and other purposes due to low cost and efficiency, four electrolytes were selected to study their potential to suppress bubble coalescence moderately or strongly as the case may be.

It was also known that the most frequently measured fundamental parameter, i.e., gas holdup of a bubble column operation is strongly influenced by the sparger design. In this study, 2-mm sparger (“coarse” sparger) openings were used. Both “coarse gas sparger” and “fine gas sparger” would provide completely different behavior in bubble column. The shape of the gas holdup curve mainly depends on the gas sparger openings. “Coarse gas spargers” produce the “pseudo-homogeneous” flow regimes, resulting

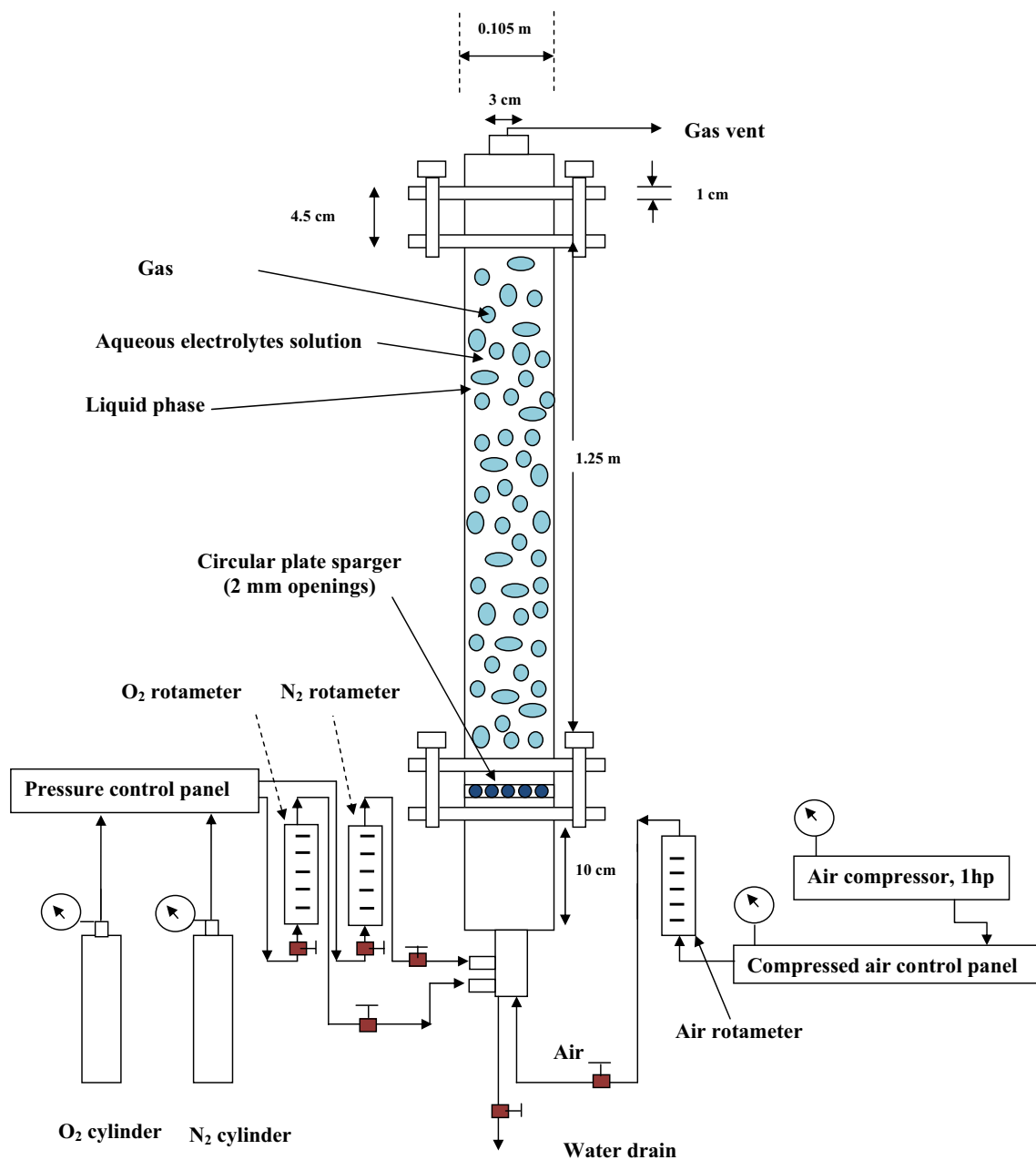


Fig. 1 Schematic diagram of experimental setup of bubble column

in monotonic gas holdup curves that are concave in shape, while “fine gas spargers” produce “mono-dispersed homogeneous” flow regimes and consequently, a peak in the gas holdup curve can appear, as observed previously by different authors (Ribeiro and Mewes 2007a; Ruzicka et al. 2003; Sharaf et al. 2016).

The objective of the present study was to determine transition concentration of some of the commonly used electrolytes at laboratory scale. Therefore, bubble column used in the present work was a laboratory size column. As per Wilkinson et al. (1992) scale-up criteria, the size, aspect

ratio (AR) and sparger opening diameter were $d_c = 0.105$ m (i.e., < 0.15 m), $AR = 3.33$ (i.e., < 5) and $d_o = 2$ mm (i.e., 1–2 mm), respectively.

Various authors have earlier reported the effect of clear liquid height on fractional gas holdup (Patil et al. 1984; Kastanek et al. 1984; Zahradnik et al. 1997; Thorat et al. 1998; Sarrafi et al. 1999; Sasaki et al. 2016; Sasaki et al. 2017). Patil et al. (1984) observed that the fractional gas holdup is independent of the sparger design (“coarse” gas sparger) and the clear liquid height, i.e., aspect ratio, AR varying from 1.8 to 3.7. Kastanek et al. (1984) found that the influence

Table 2 Specifications of experimental setup

Parameter	Specifications
Diameter of bubble column, m	0.105
Height of bubble column, m	1.2
MOC of bubble column	Borosilicate glass
Diameter of single orifice, mm	2
Total number of orifices	69
Hole arrangement	Quadrangular pattern with a pitch of 10 mm
MOC of perforated plate	Nylon
Free perforated plate area (a_f)	96.93%

of AR is negligible for H_C greater than 1–3 m and with AR larger than 5. Later, Wilkinson et al. (1992) discussed the results obtained by Kastanek et al. (1984). In a similar study, Zahradnik et al. (1997) found that the gas holdup decreases and the homogeneous flow regime is destabilized by increasing the initial liquid level up to a critical aspect ratio and concluded that their results support the assumption of a negligible influence of AR on gas holdup and flow regime transitions for AR larger than 5. These assumptions have also been confirmed by Thorat et al. (1998), who found negligible influence of AR on the gas holdup for AR larger than 5 (air–water system) or 8 for “non-coalescing” system. Sarrafi et al. (1999) did not observe any remarkable effect of the initial liquid level on the flow regime transition for $H_0 > 3$ m. Sasaki et al. (2016) found that an increase in liquid height destabilizes the homogeneous flow regime and decreases the gas holdup up when AR varied up to 5. Recently, Sasaki et al. (2017) concluded that the gas holdup is independent of the column design in large-diameter and high AR bubble columns.

Surface tension and density measurement

In the present work, static surface tension values of distilled water and aqueous solutions of electrolytes using Pendant Drop method were measured with a Goniometer (Drop Shape Analyzer, Model No. DSA 25, Kruss, Germany). The

equilibrium value was measured by effecting the change at sufficiently slow rate. Wilhelmy plate method was not used in the present study, as it suffers from possible contamination of electrolyte in the subsequent measurements. The Goniometer used for the present study has a precision up to 0.05 mN/m. To eliminate any error in the surface tension results, surface tension of each sample was measured four times and an average of the four values was taken (Sujan 2018). Measured surface tension values were found within ± 0.4 mN/m of the average value. Mean surface tension of distilled water was 72.14 mN/m with a standard deviation of 0.03 (at 28 °C). The mean change in surface tension relative to distilled water ($\Delta\sigma = \sigma - \sigma_w$, where σ_w is surface tension of distilled water) was measured for various electrolytes. A plot of the change in surface tension relative to distilled water ($\Delta\sigma$) versus electrolyte concentration (C) was used to calculate the surface tension gradient ($d(\Delta\sigma)/dC$) values. Negative values of $d(\Delta\sigma)/dC$ (decrease in σ) indicate positive surface excess concentrations of solute or positive adsorption of the solute at the gas/water interface. Positive values of $d(\Delta\sigma)/dC$ (increase in σ) indicate negative surface excess concentrations of solute or negative adsorption (depletion) of the solute from the gas/water interface. There are two cases of positive and negative values, one ion may dominate the other in terms of overall adsorption and affects measured surface tension value (Weissenborn and Pugh 1996).

Bubble coalescence is an extremely rapid process in case of pure liquid like water or sufficiently dilute solutions of electrolytes for which the value of dimensionless concentration parameter crk^2/σ is ≤ 2 . For electrolyte solution,

Table 4 Operational details of experimental study

Operational parameter	Details/values
Electrolytes used	NaCl, MgSO ₄ , Na ₂ SO ₄ and CaCl ₂
Liquid height in bubble column, m	0.35
Volume of each batch of aqueous electrolytes solution, L	3.0
Range of gas flow rate, L/min	7.5–27.5

Table 3 Properties of electrolytes

Electrolyte	Molar mass (g mol ⁻¹)	Solubility in water at 20 °C (g L ⁻¹)	Purity ^{a,b} (%)	Make of electrolyte
NaCl	58.44	358	99.9 ^a	Rankem ^a
MgSO ₄	246.47	300	99.5 ^b	Loba Chemie ^b
Na ₂ SO ₄	142.04	200	99.0 ^b	Loba Chemie ^b
CaCl ₂	147.01	740	99.0 ^b	Loba Chemie ^b

^aRFCL Limited New Delhi, India

^bLoba Chemie Private Limited, Mumbai, India

the dimensionless concentration parameter crk^2/σ may be expressed (Marucci 1969) as follows:

$$\frac{crk^2}{\sigma} = \frac{2}{vRT\sigma} C \left(\frac{d\sigma}{dC} \right)^2 \frac{1}{1 \pm \frac{(d \ln a_{\pm})}{(d \ln C)}} \left(\frac{12\pi\sigma}{A.r} \right)^{2/3} \quad (1)$$

where

$$c = \frac{2}{vRT} C \left(\frac{d\sigma}{dC} \right)^2 \frac{1}{1 \pm \frac{(d \ln a_{\pm})}{(d \ln C)}} \quad (2)$$

and

$$k = \left(\frac{12\pi\sigma}{A.r} \right)^{1/3} \quad (3)$$

then

$$\frac{E^2}{\sigma} = f \left(C \left(\frac{d\sigma}{dC} \right)^2 \right), \quad (4)$$

where v is the number of ions produced upon dissociation (i.e., $v=2$ for most of the inorganic electrolytes); R is the universal gas constant; T is absolute temperature; a_{\pm} is mean activity coefficient of a solution; A is the non-retarded Hamaker constant; σ and $d\sigma/dC$ are surface tension and surface tension gradient, respectively. The predicted values of transition concentration of electrolytes as function of surface tension and surface tension gradient given from expression could not be compared with the experimental values as bubble radius values are not available in the present work.

The concentration of electrolytes which immobilizes the gas–liquid interface for bubble coalescence inhibition is known as transition concentration (C_{trans}).

Pictorial representation of bubble coalescence inhibition using electrolyte(s) is shown in Fig. 2. The transition concentration of electrolyte according to Marrucci's model depends on the magnitude of the change in surface tension with concentration at the interface, or surface activity, $d\sigma/dC$.

Surface tension gradient is the key factor that provides information of coalescence-hindering tendency of bubbles in an electrolyte solution. The dimensionless concentration parameter, i.e., Marrucci's parameter ((crk^2/σ)), contains the term $C(d\sigma/dC)^2$ which may be useful for characterization of the coalescence behavior. A number of studies successfully used the Marrucci's parameter ((crk^2/σ)) to predict gas holdup and bubble coalescence time (Sagert and Quinn 1978; Syeda and Reza 2011).

The relationship between bubble coalescence inhibition and $(d\sigma/dC)$ was originally established by Marrucci and Nicodemo (1967) using a limited experimental data set. The parameter $(d\sigma/dC)^2$ is important in bubble coalescence phenomena related to the Gibbs elasticity of the liquid film and its magnitude controls the liquid drainage from the film as per Marrucci model.

If the value of parameter $(d\sigma/dC)^2$ is large, the presence of electrolyte inhibits bubble coalescence, and if it is small, bubble coalescence remains unaffected (Christenson and Yaminsky 1995). Generally, the transition from coalescence regime to coalescence inhibition occurs when the value of $(d\sigma/dC)^2$ drops below $1 \text{ (mN m}^{-1}/\text{mol L}^{-1})^2$.

In addition, the density of each sample was also measured by density meter (Make: Kruss, Germany, Model No. DS 7800). The accuracy of density meter used was $\pm 0.0001 \text{ g/cm}^3$. Conductivity of aqueous solution of electrolytes and pH was measured simultaneously by conductivity and pH

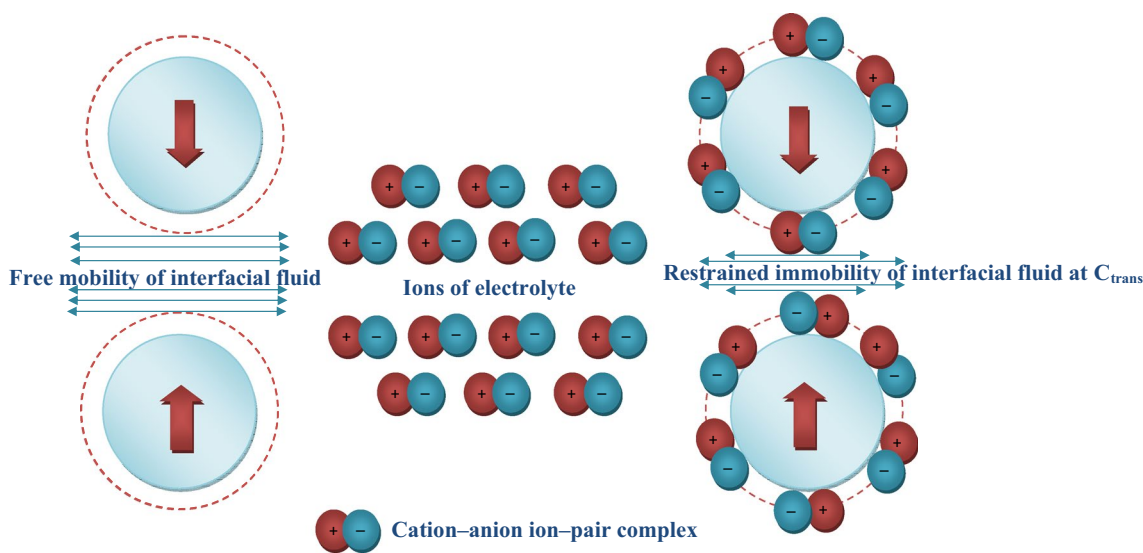


Fig. 2 Pictorial representation of bubble coalescence inhibition using electrolyte(s)

meter (Make: Hanna Instruments, Model No. HI5522). For proper dispersion of electrolytes in distilled water, magnetic stirrer (Make: Remi Laboratory instruments, Mumbai India, Model No. 1 MLH,) was used for 5 min for each sample. All experiments were carried out at ambient pressure and temperature.

Range of gas flow rate for experimental study

The froth surface of bubble bed height fluctuated mainly due to the collapse of the small, medium, and large surface bubbles. For an accurate assessment of gas holdup, the uncertainty in bed height was minimized by taking more than five sets of experimental data of H_b for a particular concentration and gas flow rate. The bubbling height related to each individual gas velocity was noted after a stabilization period of 4–5 min. The value of H_b was used to evaluate the corresponding gas holdup. The average gas holdup values at various gas flow rates for distilled water is presented in Fig. 3. Negligible gas holdup values were observed at velocities less than 5 L/m. At gas velocities beyond 30 L/m, large fluctuations in froth bubble surface were observed which introduce large errors in gas holdup estimation. For all the experiments, in the present study, the range of gas flow rates was kept around 17.5–27.5 L/m. The gas holdup values increased monotonically from 0.140 to 0.265 as the gas flow rate increased from 17.5 to 27.5 L/m.

Results and discussion

Coalescence inhibition is an important requirement in industrial bubble columns for enhancement of gas holdup which in turn increases the gas–liquid interfacial area for increasing the value of overall gas–liquid mass transfer coefficient.

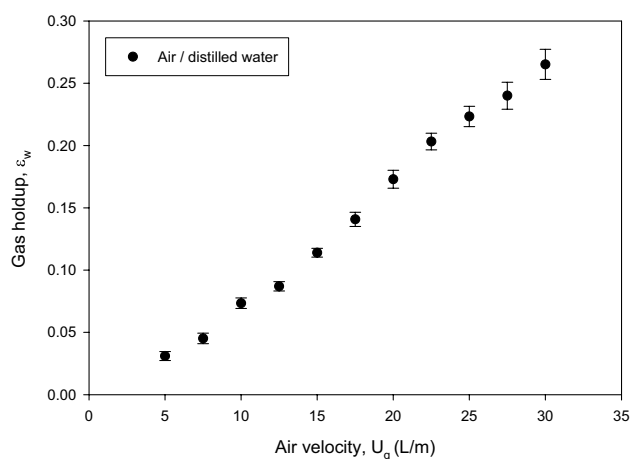


Fig. 3 Gas holdup in distilled water at various gas (air) flow rates

Overall mass transfer coefficient in a bubble column is important for improving the productivity of the processes such as froth flotation or fermentation in biochemical industries.

In the present work, a study of coalescence inhibition has been targeted by applying gas holdup enhancement and surface tension gradient approaches for aqueous solutions of single and binary mixtures.

Gas holdup enhancement in aqueous solution of single electrolyte

Dimensionless gas holdup (ϵ/ϵ_w) values for single-component aqueous solutions of different electrolytes (NaCl, $\text{MgSO}_4 \cdot 7\text{H}_2\text{O}$, Na_2SO_4 , and $\text{CaCl}_2 \cdot 2\text{H}_2\text{O}$) were plotted against electrolytes concentration (C) at different gas flow rates (17.5–27.5 L/m). From Fig. 4 it can be observed that dimensionless gas holdup (ϵ/ϵ_w) enhancement for a strong electrolyte (CaCl_2) reached a maxima of 69% at a concentration of 0.075 mol/L and a gas flow rate of 27.5 L/m. At electrolyte concentration greater than 0.075 mol/L, gas holdup enhancement decreases to 52% and at higher electrolyte concentration of 0.20 mol/L and it becomes almost constant. The electrolyte concentration at which the gas holdup enhancement is maximum is known as transition concentration (C_{trans}). At transition concentration, the bubble size distribution levels off and reaches a constant value (Marrucci and Nicodemo 1967). From Fig. 5, similar behavior was observed with 61% gas holdup enhancement in Na_2SO_4 solution corresponding to a concentration of 0.05 mol/L. It is remarkable to see that the gas holdup increased rapidly up to a maximum of 0.05 mol/L and thereafter the gas holdup decreased gradually (to around 11%) for a concentration increase from 0.05 mol/L to 0.10 mol/L. Thereafter, it remained almost unchanged for higher

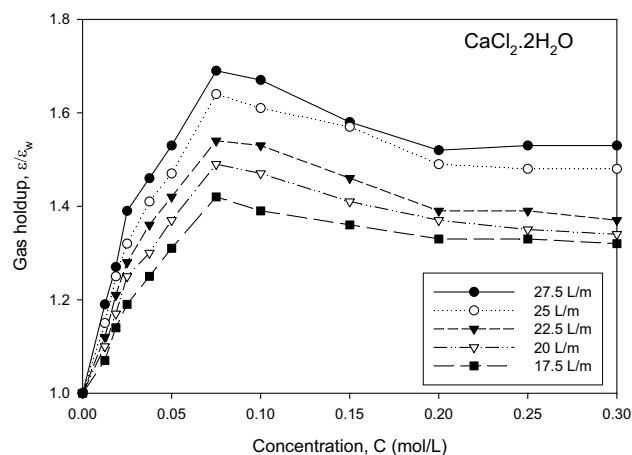


Fig. 4 Dimensionless gas holdup parameter (ϵ/ϵ_w) versus concentration in aqueous $\text{CaCl}_2 \cdot 2\text{H}_2\text{O}$ solutions

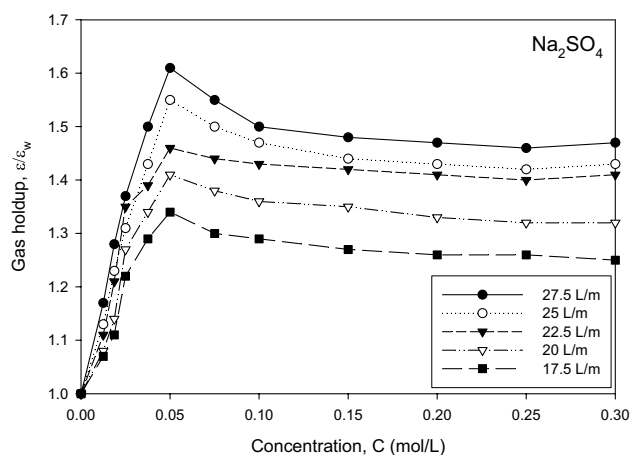


Fig. 5 Dimensionless gas holdup parameter (ϵ/ϵ_w) versus concentration in aqueous Na_2SO_4 solutions

electrolyte concentration. From Fig. 6, it is obvious that in the case of moderate electrolytes (NaCl), 47% gas holdup enhancement was observed at the higher gas flow rate of 27.5 L/m at NaCl concentration of 0.05 mol/L. There is a slow decrease thereafter for the concentration range from 0.05 to 0.30 mol/L. From Fig. 7, a similar trend with 38% gas holdup enhancement was found in MgSO_4 solution. Gas holdup reached the maximum at 0.035 mol/L and decreased at 0.075 mol/L and then almost stabilized near the same value during the increase in concentration from 0.075 to 0.3 mol/L. The inhibition of bubble coalescence results in an increase and decrease in the number and size of bubbles, respectively. Comparison of measured transition concentrations and the present work with those reported in the literature doing different methods are presented in Table 5 along with other properties of the electrolytes studied. It may be seen from Table 5 that the order of the values of

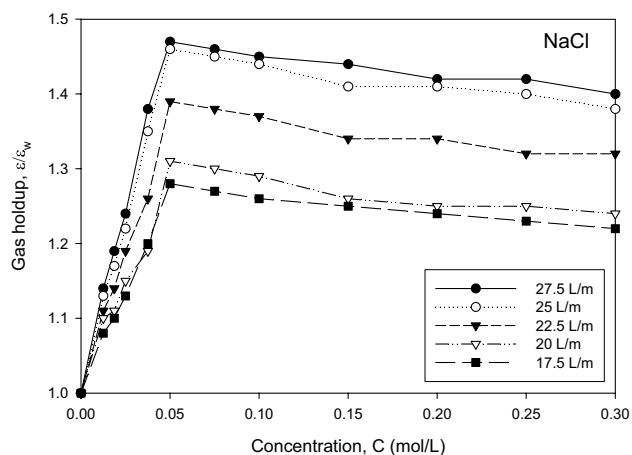


Fig. 6 Dimensionless gas holdup parameter (ϵ/ϵ_w) versus concentration in aqueous NaCl solutions

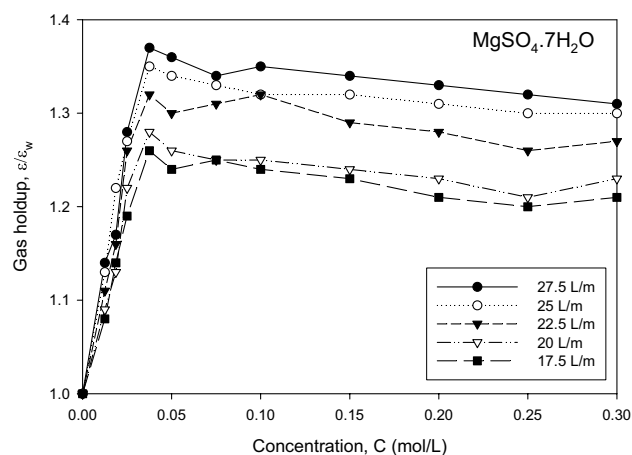


Fig. 7 Dimensionless gas holdup parameter (ϵ/ϵ_w) versus concentration in aqueous $\text{MgSO}_4 \cdot 7\text{H}_2\text{O}$ solutions

transition concentration for different electrolytes estimated in the present work are of the same order reported in the literature. The values of C_{trans} for different electrolytes are of the same order in most of the cases. It can be seen from Table 5 that the value of transition concentration of the electrolyte, NaCl estimated in the present study is comparable with those reported by Syeda and Reza (2011) based on gas holdup enhancement. Similarly, the value of C_{trans} of MgSO_4 measured in the present study compares well with those reported by Zahradnik et al. (1995) and Lessard and Zieminski (1971). The comparison of values presented in Table 5 supports the approach and values estimated in the present work.

A qualitative comparison of gas holdup enhancement obtained for four electrolytes (two from each strong and moderate categories) is shown in Fig. 8. It is obvious from Fig. 8 that the observed gas holdup enhancement behavior of these electrolytes is similar to that reported by Syeda and Reza (2011). The qualitative comparison of these electrolytes reveals that strong electrolytes yield gas holdup enhancement $\geq 60\%$ whereas moderate electrolytes give gas holdup enhancement values $\leq 46\%$. These values are at slight deviations with those reported by Syeda and Reza (2011). Table 6 presents percent incremental gas holdup enhancement of different electrolytes in comparison to the most moderate electrolyte, i.e., MgSO_4 used in the present study. In pure water, gas–liquid interface cannot sustain surface stress (Henry et al. 2008; Vakarelski et al. 2018). In such a situation, gas–liquid interface is fully mobile which leads to rapid liquid drainage from the thin film between two adjacent bubbles. This enhances coalescence phenomena due to bubble collisions. Figures 4, 5, 6, 7 and 8 clearly show that in bubbling regime, gas holdup is strongly related to the coalescence tendency of bubbles in aqueous solution of electrolyte. The presence of an electrolyte establishes shear stress at the bubble interface and

Table 5 Transition concentration, C_{trans} , comparison and other properties of electrolytes

Electrolyte	Valency type ^a	Activity coefficient for 0.1 M ^b	Relative effectiveness of electrolyte ^c	Transition concentration, C_{trans} (mol/L)				Based on $(\epsilon/\epsilon_w)_{max}$		Based on $C(d\sigma/dC)_{max}$	
				Christenson et al. (2008)	Zahradnik et al. (1995)	Prince and Blanch (1990)	Lessard and Zieminski (1971)	Craig et al. (1993a, b)	Syeda and Reza (2011)	This work	Syeda and Reza (2011)
NaCl	1-1	0.7786	Moderate	0.208	0.145	0.175	0.175	0.078	0.05	0.09	0.05
MgSO ₄	2-2	0.15	Moderate	0.036	0.036	-	0.032	0.020	0.05	0.05	0.025
Na ₂ SO ₄	1-2	0.44568	Strong	-	0.051	-	0.061	-	0.25	0.03	0.05
CaCl ₂	2-1	0.51708	Strong	0.060	0.056	0.055	0.055	0.037	0.075	0.07	0.075

^aLee et al. (2008)

^bZemaitis et al. (1986)

^cRibeiro and Mewas (2007a, b)

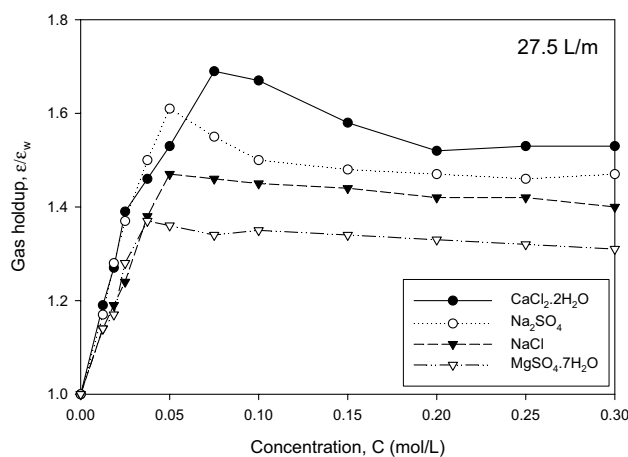


Fig. 8 Qualitative comparisons between strong (CaCl₂·2H₂O and Na₂SO₄) and moderate (NaCl and MgSO₄·7H₂O) electrolytes

Table 6 Incremental transition concentration values of electrolytes in comparison to MgSO₄ (most moderate electrolyte)

Electrolyte	Percent incremental gas holdup enhancement at transition concentration, C_{trans}
CaCl ₂	86
Na ₂ SO ₄	64
NaCl	27

This analysis indicates towards that there is only on incremental benefit of using a strong electrolyte over the most moderate electrolyte irrespective of its cost

thus mobility of the interface is reduced or removed. During the drainage of liquid from the film in the presence of an electrolyte, surface tension gradient is established. Under such a situation, surface shear stress is created which retards surface mobility and, therefore, opposes film drainage and control drainage rate from the liquid film. This factor may contribute to the bubble stabilization process and possibly reduce the bubble size. For bubble coalescence inhibition, bubble size depends on the critical concentration of aqueous solution of an electrolyte (Prince and Blanch 1990; Tsang et al. 2004; Chan and Tsang 2005). In fact, the critical concentration decreases with increasing bubble size. Therefore, to prevent coalescence, critical concentration increases as the equivalent diameter of bubbles decreases. In the electrolyte systems, interfacial area is 3–4 times higher as compared to the coalescing air–water system (Cents et al. 2005).

Surface tension and surface tension gradient of single-electrolyte solution

In this paper, the effect of electrolyte concentration on bubble coalescence behavior has been studied using the

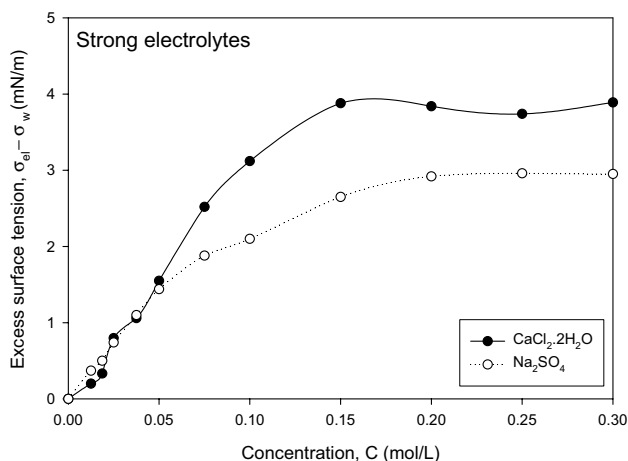


Fig. 9 Variation of excess surface tension of solution with electrolyte concentration for strong electrolytes ($\text{CaCl}_2 \cdot 2\text{H}_2\text{O}$ and Na_2SO_4)

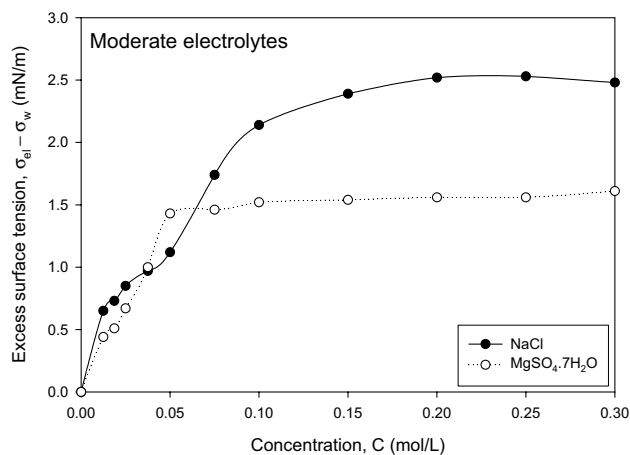


Fig. 11 Variation of excess surface tension of solution with electrolyte concentration for moderate electrolytes (NaCl and $\text{MgSO}_4 \cdot 7\text{H}_2\text{O}$)

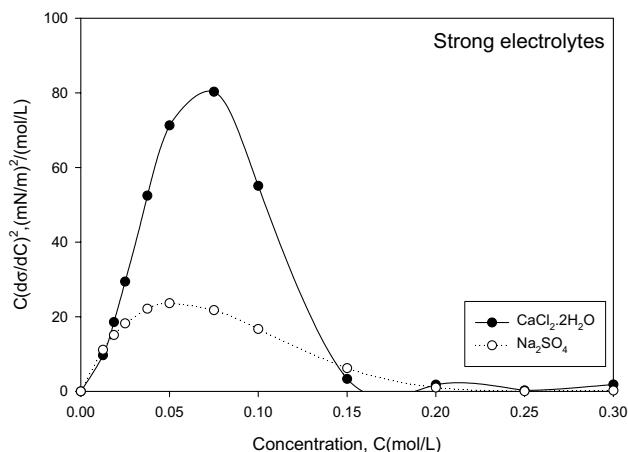


Fig. 10 Variation of parameter $C(d\sigma/dC)^2$ with electrolyte concentration for strong electrolytes ($\text{CaCl}_2 \cdot 2\text{H}_2\text{O}$ and Na_2SO_4)

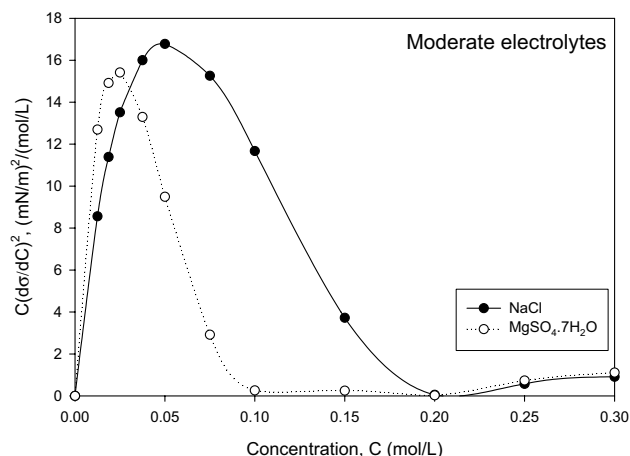


Fig. 12 Variation of parameter $C(d\sigma/dC)^2$ with electrolyte concentration for moderate electrolytes (NaCl and $\text{MgSO}_4 \cdot 7\text{H}_2\text{O}$)

parameter $(d\sigma/dC)^2$, where $d\sigma$ is the change in surface tension and dC is the change in bulk concentration of the electrolyte. The excess surface tension ($\sigma_{ei} - \sigma_w$) due to the presence of electrolytes can be used to predict gas holdup enhancement. It can also be used to estimate transition concentration.

Plots of excess surface tension vs electrolyte concentration and parameter $C(d\sigma/dC)^2$ vs electrolyte concentration for strong electrolytes ($\text{CaCl}_2 \cdot 2\text{H}_2\text{O}$ and Na_2SO_4) are presented in Figs. 9 and 10, respectively. Similarly, plots of excess surface tension vs electrolyte concentration and parameter $C(d\sigma/dC)^2$ vs electrolyte concentration for moderate electrolytes (NaCl and $\text{MgSO}_4 \cdot 7\text{H}_2\text{O}$) are presented in Figs. 11 and 12, respectively. Curves for excess surface tension vs electrolyte concentration for strong and moderate electrolyte were fitted using a non-linear

polynomial fitting technique. The resulting algebraic equations were differentiated with respect to concentration to obtain $(d\sigma/dC)^2$ values. Further, the requisite parameter $C(d\sigma/dC)^2$ values for strong and moderate electrolyte were plotted against concentration. In the absence of the bubble size distribution of the system, simple, algebraic equations of excess surface tension for different electrolyte concentration are presented in Table 7. Empirical correlation based on dimensional analysis may be proposed in future, if bubble size distribution is available.

The curve for excess surface tension vs electrolyte concentration for strong electrolytes ($\text{CaCl}_2 \cdot 2\text{H}_2\text{O}$ and Na_2SO_4) shown in Fig. 9 increases initially up to an electrolyte concentration of 0.15 and 0.20 mol/L for $\text{CaCl}_2 \cdot 2\text{H}_2\text{O}$ and Na_2SO_4 , respectively, and becomes almost constant thereafter at an excess surface tension value of 3.89 mN/m for $\text{CaCl}_2 \cdot 2\text{H}_2\text{O}$ and 2.95 mN/m for Na_2SO_4 . A similar behavior

Table 7 Algebraic equations of excess surface tension for different electrolytes

Electrolyte	Algebraic equations
NaCl	$\sigma_{\text{aq.}} - \sigma_{\text{w}} = 2085 C^5 - 1429 C^4 + 467.5 C^3 - 140.1 C^2 + 29.47C + 0.134$
MgSO ₄ ·7H ₂ O	$\sigma_{\text{aq.}} - \sigma_{\text{w}} = 4.98 C^5 - 1592 C^4 + 1255 C^3 - 34804 C^2 + 40.02C - 0.041$
Na ₂ SO ₄	$\sigma_{\text{aq.}} - \sigma_{\text{w}} = 154.4 C^3 - 122.8 C^2 + 32.85C - 0.005$
CaCl ₂ ·2H ₂ O	$\sigma_{\text{aq.}} - \sigma_{\text{w}} = -19404 C^5 + 17347 C^4 - 5236 C^3 + 520.5 C^2 + 16.99C - 0.033$

was observed for moderate electrolytes, namely NaCl and MgSO₄·7H₂O (Fig. 11). In this curve, value of excess surface tension becomes constant at 2.52 mN/m for NaCl and 1.56 mN/m for MgSO₄·7H₂O corresponding to electrolyte concentration of 0.020 mol/L and 0.15 mol/L, respectively. Figures 9 and 11 show that surface tension reaches a plateau at an electrolyte concentration range of 0.2–0.3 M. The excess surface tension values of aqueous solutions of electrolytes observed in the present work are in agreement with those reported earlier (Syeda and Reza 2011).

Figures 10 and 12 show plots for parameter $C(d\sigma/dC)^2$ vs electrolyte concentration for strong and moderate electrolytes. It is obvious from these figures that parameter $C(d\sigma/dC)^2$ has higher values for strong electrolytes indicating a strong effect on bubble coalescence than moderate electrolytes.

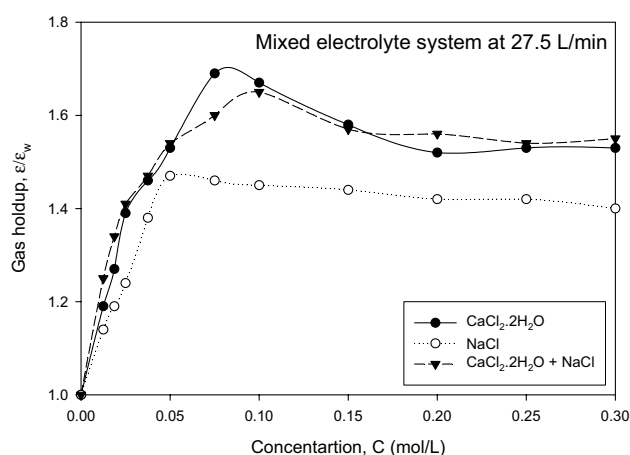
These experimental observations are in line with those reported by Syeda and Reza (2011). It is significant to note that the concentrations at which maximum gas holdup occurs exactly matches with or close to the transition concentrations corresponding to the peak values of $C(d\sigma/dC)^2$ (Table 5). This implies that the peak value of $C(d\sigma/dC)^2$ can be used effectively to determine the transition concentration corresponding to the maximum gas holdup. A comparison of transition concentrations (C_{trans}) estimated by two methods in the present study with those reported in the literature and other properties of electrolytes is presented in Table 5.

For NaCl solution, the concentration corresponding to the maximum value of $C(d\sigma/dC)^2$ obtained in the present study is similar to that using gas holdup value reported by Syeda and Reza (2011). Hence, the concentration at which the maximum value of $C(d\sigma/dC)^2$ occurs may be used to approximate the transition concentration for different electrolytes. The concentration corresponding to the maximum value of $C(d\sigma/dC)^2$ in MgSO₄·7H₂O solution was found to be 0.025 mol/L which is close to 0.020 mol/L reported by Craig et al. (1993a, b). The values of C_{trans} reported in literature vary from 0.037 mol/l (Craig et al. 1993a, b) to 0.075 mol/l (Syeda and Reza 2011) for CaCl₂·2H₂O solution (Table 5). In the present study, the value of electrolyte (CaCl₂·2H₂O) concentration corresponding to maximum value of $C(d\sigma/dC)^2_{\text{max}}$ is 0.075 mol/L which is similar to that reported by Syeda and Reza (2011). For Na₂SO₄ solution, the corresponding transition concentration is 0.05 mol/L at which $C(d\sigma/dC)^2_{\text{max}}$ occurred in the present

study which is close to C_{trans} value of 0.051 mol/L reported by Zahradnik et al. (1995). In essence, the value of transition concentration of different electrolytes estimated in the present study is in line with those reported in the literature.

Gas holdup enhancement in aqueous solutions of mixed electrolytes

Experimental data of gas holdup enhancement were generated using two sets of binary mixtures of electrolytes, viz., CaCl₂ + NaCl and Na₂SO₄ + NaCl. The combination of electrolytes is comprised of one strong and one moderate electrolyte. The aqueous solution of mixed electrolytes contained equimolar concentration of both electrolytes. Gas holdup enhancement values corresponding to maximum gas flow rate of the present study (27.5 L/m) were used in the estimation of transition concentration for a mixture of electrolytes. Gas holdup enhancement data for the two combinations of electrolytes (CaCl₂ + NaCl and Na₂SO₄ + NaCl) were plotted against total molar concentration of mixed electrolytes and are shown in Figs. 13 and 14. From Fig. 13, it is obvious that gas holdup enhancement trends of a single (individual) and mixed electrolytes are similar. It has been observed from Fig. 13 that the value of transition concentration shifted from 0.075 to 0.1 mol/L in mixed electrolyte (CaCl₂ + NaCl) system whereas transition concentration shifted from 0.05 to 0.075 mol/L for mixed electrolyte (Na₂SO₄ + NaCl) system

**Fig. 13** Comparison of gas holdup enhancement for mixed electrolyte (CaCl₂·2H₂O + NaCl) system with individual electrolytes

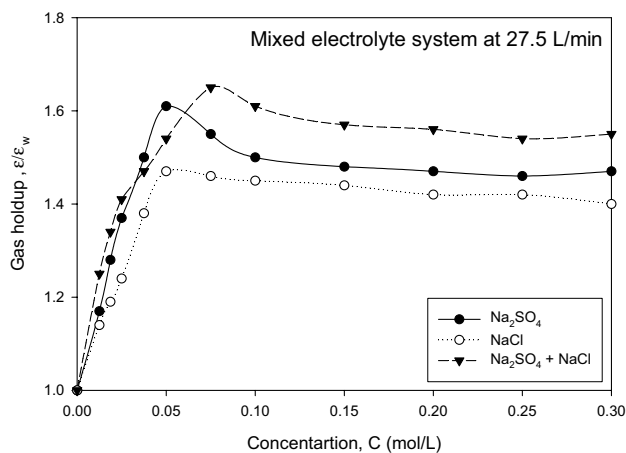


Fig. 14 Comparison of gas holdup enhancement for mixed electrolytes ($\text{Na}_2\text{SO}_4 + \text{NaCl}$) system with individual electrolytes

as compared to their components, viz., CaCl_2 and Na_2SO_4 , respectively. The flow regime transition points in gas holdup curve based on the swarm velocity and drift-flux methods are also reported in the literature (Besagni et al. 2017a, b, c, d; Besagni et al. 2018). The present study was aimed at determination of transition concentration of electrolytes for bubble coalescence inhibition; therefore, the selected gas velocity range was narrow. Consequently, flow regime transition points were not determined.

Excess surface tension and surface tension gradient in aqueous solution of mixed electrolytes

Comparison of plots of excess surface tension values and electrolyte concentration for mixed electrolyte sets and their individual electrolytes are presented in Figs. 15 and 16. The behavior of the curve was found similar to that of single-component electrolyte solutions which increases initially up to an electrolyte concentration of 0.15 mol/L and 0.20 mol/L for $\text{CaCl}_2 \cdot 2\text{H}_2\text{O} + \text{NaCl}$ and $\text{Na}_2\text{SO}_4 + \text{NaCl}$, respectively. The curve becomes almost constant, thereafter at an excess surface tension value of 3.61 mN/m for $\text{CaCl}_2 \cdot 2\text{H}_2\text{O} + \text{NaCl}$ and 3.11 mN/m for $\text{Na}_2\text{SO}_4 + \text{NaCl}$, respectively. Parameter $C(d\sigma/dC)^2$ was also plotted against the total concentration of the two sets of mixture of electrolytes and is presented in Figs. 17 and 18. From Fig. 17, it can be observed that there is no shift in transition concentration for $\text{CaCl}_2 \cdot 2\text{H}_2\text{O} + \text{NaCl}$ mixed electrolyte system whereas transition concentration shifted from 0.05 to 0.1 mol/L for $\text{Na}_2\text{SO}_4 + \text{NaCl}$ mixed electrolytes system (Fig. 18). Algebraic equations of excess surface tension for mixed electrolyte system and comparison of transition concentration, C_{trans} , of mixed electrolytes with their components are presented in Tables 8 and 9, respectively.

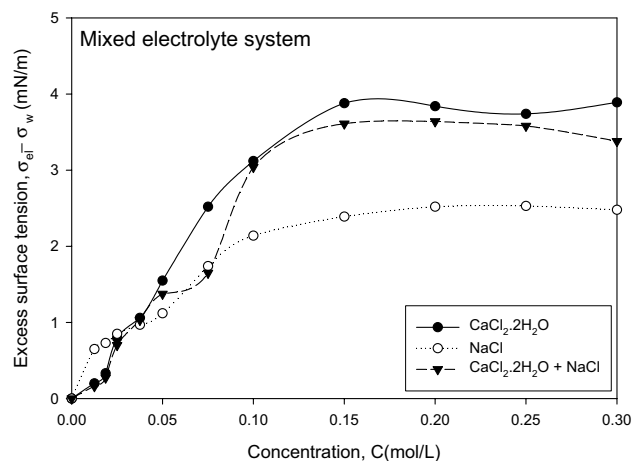


Fig. 15 Comparison of excess surface tension of mixed electrolytes ($\text{CaCl}_2 + \text{NaCl}$) with individual electrolytes

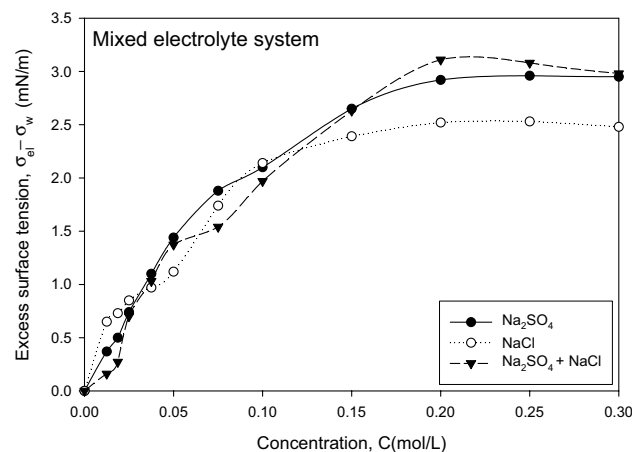


Fig. 16 Comparison of excess surface tension of mixed electrolytes ($\text{Na}_2\text{SO}_4 + \text{NaCl}$) with individual electrolytes

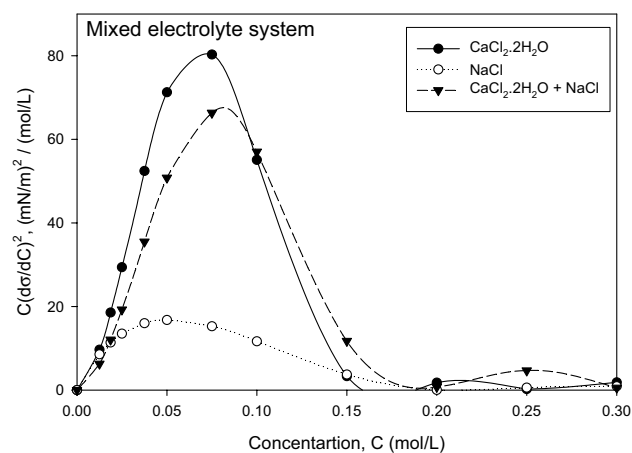


Fig. 17 Comparison of parameter $C(d\sigma/dC)^2$ for mixed electrolyte ($\text{CaCl}_2 + \text{NaCl}$) system with individual electrolytes

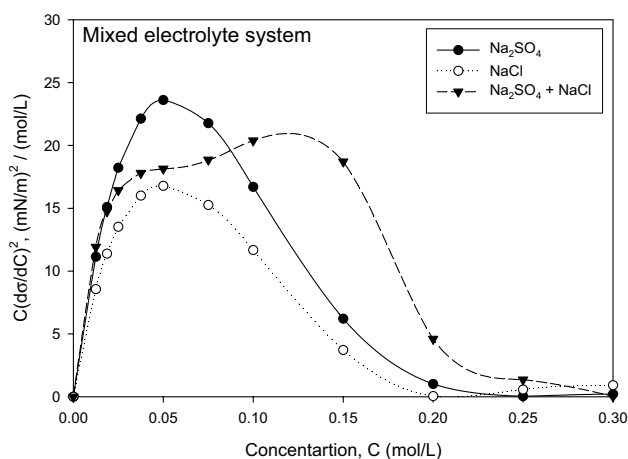


Fig. 18 Comparison of parameter $C(d\sigma/dC)^2$ for mixed electrolyte ($\text{Na}_2\text{SO}_4 + \text{NaCl}$) system with individual electrolytes

Surface elasticity values for single and mixed electrolytes

Surface elasticity of bubbles is related to bubble coalescence inhibition. Therefore, Gibbs elasticity and surface elasticity

values at critical coalescence concentration for the mixed and component electrolytes solutions are presented in Table 10. Surface elasticity was calculated as outlined in Craig (2011). Large value of parameter $(d\sigma/dC)^2$ inhibits bubble coalescence and its value depends upon ion separation in the interfacial area (Henry et al. 2007). But the mechanism behind electrolyte inhibition of bubble coalescence is still unresolved. It is obvious from Table 10 that the higher value of $\text{CaCl}_2 \cdot 2\text{H}_2\text{O}$ indicates strong bubble coalescence inhibition as compared to other electrolytes used in the study. For a combination of two electrolytes featuring three ionic species, combinations of $\text{CaCl}_2 \cdot 2\text{H}_2\text{O} + \text{NaCl}$ and $\text{Na}_2\text{SO}_4 + \text{NaCl}$ was utilized for inhibition of bubble coalescence. The value of surface elasticity of combination of mixed electrolytes ($\text{CaCl}_2 + \text{NaCl}$) decreases to $442.24(\text{mN/m})^2/(\text{mol/L})^2$ from $535.33(\text{mN/m})^2/(\text{mol/L})^2$ than that of CaCl_2 alone. The reduction in surface elasticity from a single component (CaCl_2) is due to the addition of a moderate electrolyte (NaCl) whose contribution to surface elasticity value is small as compared to strong one (CaCl_2). Reduction in surface elasticity will result in a decrease in bubble coalescence inhibition phenomena. Similar observation was found in aqueous solution of $\text{Na}_2\text{SO}_4 + \text{NaCl}$ system. Surface

Table 8 Algebraic equations of excess surface tension for mixed electrolyte system

Electrolyte	Algebraic equations
$\text{CaCl}_2 \cdot 2\text{H}_2\text{O} + \text{NaCl}$	$\sigma_{\text{aq.}} - \sigma_{\text{w}} = -9552 C^5 + 9733 C^4 - 3367 C^3 + 381.7 C^2 + 14.39 C - 0.005$
$\text{Na}_2\text{SO}_4 + \text{NaCl}$	$\sigma_{\text{aq.}} - \sigma_{\text{w}} = 9925 C^5 - 7847 C^4 + 2216 C^3 - 318.2 C^2 + 37.86 C - 0.132$

Table 9 Comparison of transition concentration, C_{trans} , of mixed electrolytes with their component

Mixed electrolyte/component	Peak value		Transition concentration, C_{trans} (mol/L)	
	Based on $(\epsilon/\epsilon_{\text{w}})_{\text{max}}$	Based on $C(d\sigma/dC)_{\text{max}}^2$	Based on $(\epsilon/\epsilon_{\text{w}})_{\text{max}}$	Based on $C(d\sigma/dC)_{\text{max}}^2$
CaCl_2	1.69	80.30	0.075	0.075
Na_2SO_4	1.61	23.61	0.05	0.05
NaCl	1.47	16.78	0.05	0.05
$\text{MgSO}_4 \cdot 7\text{H}_2\text{O}$	1.37	15.42	0.0375	0.25
$\text{CaCl}_2 + \text{NaCl}$	1.65	66.34	0.1	0.075
$\text{Na}_2\text{SO}_4 + \text{NaCl}$	1.65	20.38	0.075	0.1

Table 10 Gibbs elasticity and surface elasticity at transition concentration of electrolytes

Electrolyte	Bubble coalescence inhibition	$(d\sigma/dC)^2 \approx$ Gibbs elasticity $(\text{mN/m})^2/(\text{mol/L})^2$	Surface elasticity = $(1/2) \times (d\sigma/dC)^2 (\text{mN/m})^2/(\text{mol/L})^2$
NaCl	Yes	335.51	167.76
$\text{MgSO}_4 \cdot 7\text{H}_2\text{O}$	Yes	616.71	308.36
Na_2SO_4	Yes	472.11	236.06
$\text{CaCl}_2 \cdot 2\text{H}_2\text{O}$	Yes	1070.66	535.33
$\text{CaCl}_2 \cdot 2\text{H}_2\text{O} + \text{NaCl}$	Yes	884.48	442.24
$\text{Na}_2\text{SO}_4 + \text{NaCl}$	Yes	203.76	101.88

elasticity values estimated in the present work could not be compared with those reported in the literature (Craig 2011 and Henry et al. 2007) as values reported earlier were not estimated at critical coalescence concentration.

Analysis of variance (ANOVA)

In the present study, trial version of Statistical Design software (Minitab version 17) was used for regression and analysis of variance (ANOVA). Using analysis of variance, it was found that the gas flow rate, concentration of electrolytes, and the chemical nature of the electrolytes have significant effects on the average gas holdup. However, the gas flow rate and electrolyte concentration are the most sensitive variables and the largest source of variation, as shown in Table 11.

It is obvious from Table 11 that the electrolyte concentration and gas flow rate are the most sensitive variables and the largest source of variation. The fact that P values for gas flow rate, concentration of electrolytes, and the chemical nature of the electrolytes in this table are less than the confidence level (0.05) and the P value for the lack of fit is higher than 0.05 indicates the adequacy and significance of the model. Residual plots of gas holdup are presented in Fig. 19.

It can be seen from Fig. 19 that the residuals versus fits plot verifies the assumption that the residuals are randomly distributed and have constant variance, because the points fall randomly on both sides of 0, with no recognizable patterns in the points. The normal probability plot of the residuals displays the residuals versus their expected values when the distribution is normal. Normal probability plot of residuals verifies the assumption that the residuals are normally distributed as the residuals approximately follow a straight line. The residuals versus observation order plot verifies the assumption that the residuals are independent from one another as the residuals on the plot fall randomly around the center line. The histogram of the residuals shows the distribution of the residuals for all observations. The experimental data of the average gas holdup for each of the cases studied have a log-normal distribution, as their distribution

frequency is not symmetrical. Histogram of the residuals confirms that the data are not skewed and do not include outliers.

Conclusion

In the present work, study of coalescence inhibition was targeted by applying gas holdup enhancement and surface tension gradient approaches for aqueous solutions of single and binary mixtures of electrolytes. The concentration at which bubble coalescence is inhibited was determined in a 3.0-L distilled water bubble column for a series of coalescence inhibiting inorganic (NaCl, $\text{MgSO}_4 \cdot 7\text{H}_2\text{O}$, $\text{CaCl}_2 \cdot 2\text{H}_2\text{O}$, and Na_2SO_4) electrolytes. For a single-electrolyte system, maximum gas holdup (ϵ/ϵ_w) enhancement for a strong electrolyte (CaCl_2) reached a maxima of 69% at a concentration of 0.075 mol/L and at a gas flow rate of 27.5 L/m. Similar behavior was observed with 61% gas holdup enhancement in Na_2SO_4 solution corresponding to a concentration of 0.05 mol/L. In case of moderate electrolytes (NaCl), 47% gas holdup enhancement was observed at a concentration of 0.05 mol/L. A similar trend with 38% gas holdup enhancement was found in MgSO_4 solution at a concentration of 0.035 mol/L. A qualitative comparison of these electrolytes revealed that strong electrolytes yield gas holdup enhancement $\geq 60\%$ whereas moderate electrolytes give a gas holdup up enhancement values $\leq 46\%$. It has also been found that the value of transition concentration for different electrolytes is of the same order in most of the cases and in line with those reported in the literature. In case of strong electrolyte solution, higher peak is indicative of a strong effect on bubble coalescence. In case of moderate electrolyte solution, peak with shorter height indicated moderate effect on bubble coalescence.

In addition, the effects of electrolytes on bubble coalescence were studied using the parameter $C(d\sigma/dC)^2$ for the electrolyte. It was verified that as long as the value of parameter $C(d\sigma/dC)^2$ is large, the electrolyte will inhibit bubble coalescence, and if it is small, bubble coalescence remains

Table 11 Analysis of variance

Source	Degrees of freedom	Sum of squares	Mean square	F value	P value
Gas flow rate, U_g	4	0.219258	0.054815	1646.92	0.000
Electrolyte concentration, C	6	0.103789	0.017298	519.73	0.000
Chemical nature of the electrolytes, N	2	0.002774	0.001387	41.68	0.000
$U_g \cdot C$	24	0.012143	0.000506	15.20	0.000
$U_g \cdot N$	8	0.000744	0.000093	2.79	0.009
Error	75	0.002496	0.000033		
Lack of fit	45	0.001777	0.000039	1.65	0.076
Pure error	30	0.000719	0.000024		
Total	119	0.453817			

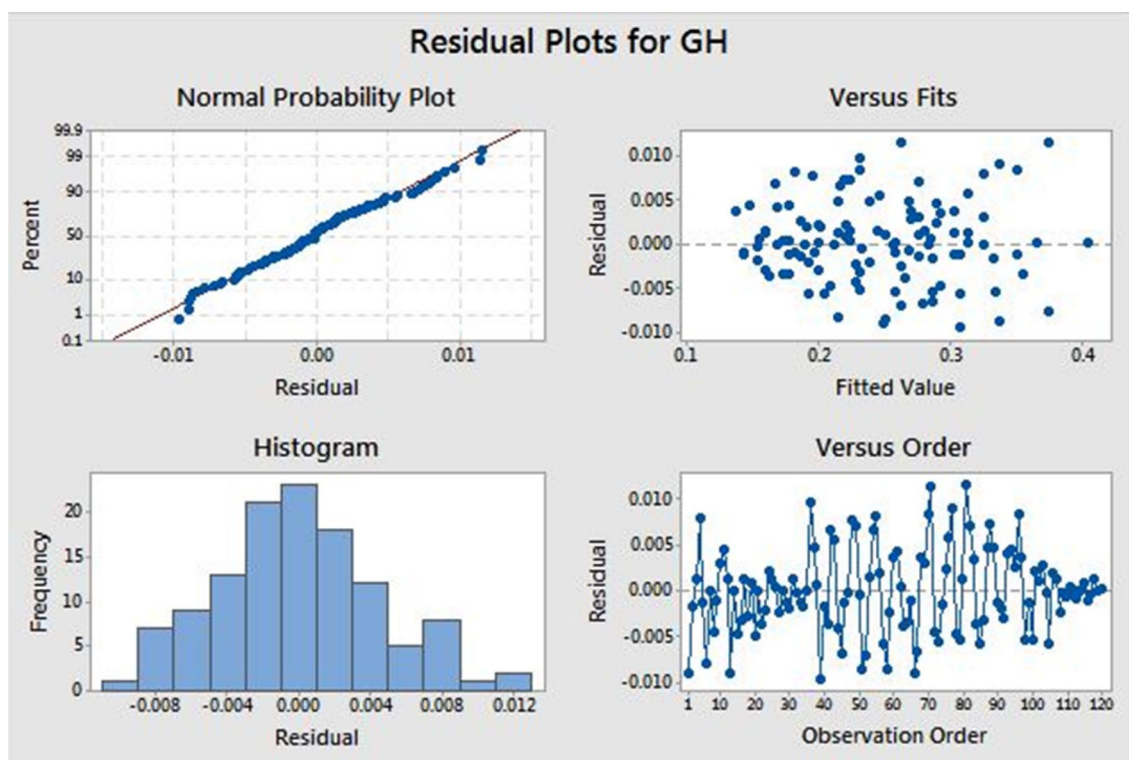


Fig. 19 Residual plots for gas holdup

moderately affected. The importance of parameter $(d\sigma/dC)^2$ in bubble coalescence has been related to the elasticity of the interface of electrolyte film drainage. The drainage rate of film reduced because the duration of stability in film thickness increases due to change in elasticity of an interface. The variation in surface tension with the addition of electrolytes can be directly used to predict gas holdup enhancement. It is also useful for the identification of electrolyte concentration for attaining highest gas holdup.

In addition, the effect of mixed electrolytes ($\text{CaCl}_2 \cdot 2\text{H}_2\text{O} + \text{NaCl}$ and $\text{Na}_2\text{SO}_4 + \text{NaCl}$) on gas holdup was also studied. From the experimental results, it was found that trends of gas holdup enhancement for single (individual) and mixed electrolytes are similar. It has been observed that the value of transition concentration shifted from 0.075 to 0.1 mol/L in mixed electrolytes ($\text{CaCl}_2 + \text{NaCl}$) system whereas transition concentration shifted from 0.05 to 0.075 mol/L for mixed electrolyte ($\text{Na}_2\text{SO}_4 + \text{NaCl}$) system as compared to their components, viz., CaCl_2 and Na_2SO_4 , respectively.

Besides, parameter $C(d\sigma/dC)^2$ was also plotted against the total concentration of the two sets of mixtures of electrolytes. It can be observed that there is no shift in transition concentration for $\text{CaCl}_2 \cdot 2\text{H}_2\text{O} + \text{NaCl}$ mixed electrolyte system whereas transition concentration shifted from 0.05 to 0.1 mol/L for $\text{Na}_2\text{SO}_4 + \text{NaCl}$ mixed electrolytes

system. In addition, surface elasticity of bubbles is related to bubble coalescence inhibition. Large value of parameter $(d\sigma/dC)^2$ inhibits bubble coalescence and its value depends upon ion separation in the interfacial area. Reduction in surface elasticity will result in a decrease in bubble coalescence inhibition phenomena. The value of surface elasticity of combination of mixed electrolytes ($\text{CaCl}_2 + \text{NaCl}$) decreased because the reduction in surface elasticity from a single component (CaCl_2) is due to the addition of a moderate electrolyte (NaCl) whose contribution to surface elasticity value is small as compared to strong one (CaCl_2). Similar observation was found in aqueous solution of $\text{Na}_2\text{SO}_4 + \text{NaCl}$ system. Surface elasticity values estimated in the present work could not be compared with those reported in the literature (Craig 2011 and Henry et al. 2007) as values reported earlier were not estimated at critical coalescence concentration. The density difference between the electrolytes used in the present study is not significant; therefore, the variation in the densities of their aqueous solutions will also not be considerable. Thus, difference in buoyant forces exerted by aqueous solutions of different electrolytes will be negligible regardless of the bubble size at atmospheric pressure. Furthermore, analysis of variance (ANOVA) was employed to estimate significance of parameters (gas flow rate, electrolyte concentration and chemical nature of

electrolyte) on average gas holdup. It was found that all the parameters have significant effects on average gas holdup.

References

- Akita K, Yoshida F (1973) Gas holdup and volumetric mass transfer coefficient in bubble columns. Effects of liquid properties, industrial and engineering chemistry process. *Des Dev* 12(1):76–80. <https://doi.org/10.1021/i260045a015>
- Al Taweel AM, Idhbeaa AO, Ghanem A (2013) Effect of electrolytes on interphase mass transfer in microbubble-sparged airlift reactors. *Chem Eng Sci* 100:474–485. <https://doi.org/10.1016/j.ces.2013.06.013>
- Bach HF, Pilhofer T (1978) Variation of gas hold-up in bubble columns with physical properties of liquids and operating parameters of columns. *Ger Chem Eng* 1:270–275
- Besagni G, Inzoli F (2016) Bubble size distributions and shapes in annular gap bubble column. *Exp Therm Fluid Sci* 74:27–48. <https://doi.org/10.1016/j.expthermfluidsci.2015.11.020>
- Besagni G, Inzoli F (2017a) The effect of electrolyte concentration on counter-current gas-liquid bubble column fluid dynamics: gas holdup, flow regime transition and bubble size distributions. *Chem Eng Res Des* 118:170–193. <https://doi.org/10.1016/j.cherd.2016.12.012>
- Besagni G, Inzoli F (2017b) The effect of liquid phase properties on bubble column fluid dynamics: gas holdup, flow regime transition, bubble size distributions and shapes, interfacial areas and foaming phenomena. *Chem Eng Sci* 170:270–296. <https://doi.org/10.1016/j.ces.2017.03.043>
- Besagni G, Di Pasquali A, Gallazzini L, Gottardi E, Colombo LPM, Inzoli F (2017c) The effect of aspect ratio in counter-current gas-liquid bubble columns: experimental results and gas holdup correlations. *Int J Multiph Flow* 94:53–78. <https://doi.org/10.1016/j.ijmultiphaseflow.2017.04.015>
- Besagni G, Inzoli F, De Guido G, Pellegrini LA (2017d) The dual effect of viscosity on bubble column hydrodynamics. *Chem Eng Sci* 158:509–538. <https://doi.org/10.1016/j.ces.2016.11.003>
- Besagni G, Gallazzini L, Inzoli F (2018) Effect of gas sparger design on bubble column hydrodynamics using pure and binary liquid phases. *Chem Eng Sci* 176:116–126. <https://doi.org/10.1016/j.ces.2017.10.036>
- Cents AHG, Jansen DJW, Brilman DWF, Versteeg GF (2005) Influence of small amounts of additives on gas hold-up, bubble size, and interfacial area. *Ind Eng Chem Res* 44(14):4863–4870. <https://doi.org/10.1021/ie049475f>
- Chan BS, Tsang YH (2005) A theory on bubble-size dependence of the critical electrolyte concentration for inhibition of coalescence. *J Colloid Interface Sci* 286(1):410–413. <https://doi.org/10.1016/j.jcis.2005.01.048>
- Christenson HK, Yaminsky VV (1995) Solute effects on bubble coalescence. *J Phys Chem* 99(25):10420. <https://doi.org/10.1021/j100025a052>
- Christenson HK, Bowen RE, Carlton JA, Denne JRM, Lu Y (2008) Electrolytes that show a transition to bubble coalescence inhibition at high concentrations. *J Phys Chem C* 112(3):794–796. <https://doi.org/10.1021/jp075440s>
- Craig VS (2011) Do hydration forces play a role in thin film drainage and rupture observed in electrolyte solutions? *Curr Opin Colloid Interface Sci* 16(6):597–600. <https://doi.org/10.1016/j.cocis.2011.04.003>
- Craig VSJ, Ninham BW, Pashley RM (1993a) Effect of electrolytes on bubble coalescence. *Nature* 364(6435):317–319. <https://doi.org/10.1038/364317a0>
- Craig VSJ, Ninham BW, Pashley RM (1993b) The effect of electrolytes on bubble coalescence in water. *J Phys Chem* 97(39):10192–10197. <https://doi.org/10.1021/j100141a047>
- Del Castillo LA, Ohnishi S, Horn RG (2011) Inhibition of bubble coalescence: effects of salt concentration and speed of approach. *J Colloid Interface Sci* 356(1):316–324. <https://doi.org/10.1016/j.jcis.2010.12.057>
- Deschenes LA, Barrett J, Muller LJ, Fourkas JT, Mohanty U (1998) Inhibition of bubble coalescence in aqueous solutions. 1. Electrolytes. *J Phys Chem B* 102(26):5115–5119. <https://doi.org/10.1021/jp980828w>
- Eissa SH, Schügerl K (1975) Holdup and backmixing investigations in cocurrent and countercurrent bubble columns. *Chem Eng Sci* 30(10):1251–1256. [https://doi.org/10.1016/0009-2509\(75\)85048-2](https://doi.org/10.1016/0009-2509(75)85048-2)
- Geffcken G (1904) Comparative solubility of gases, etc., in water and in aqueous solutions. *Z Phys Chem* 49:257–302
- Godbole SP, Honath MF, Shah YT (1982) Holdup structure in highly viscous Newtonian and non-Newtonian liquids in bubble columns. *Chem Eng Commun* 16(1–6):119–134. <https://doi.org/10.1080/00986448208911090>
- Hecht K, Bey O, Etmüller J, Graefen P, Friehmelt R, Nilles M (2015) Effect of gas density on gas holdup in bubble columns. *Chem Ing Tec* 87(6):762–772. <https://doi.org/10.1002/cite.201500010>
- Henry CL, Dalton CN, Scruton L, Craig VS (2007) Ion-specific coalescence of bubbles in mixed electrolyte solutions. *J Phys Chem C* 111(2):1015–1023. <https://doi.org/10.1021/jp066400b>
- Henry CL, Parkinson L, Ralston JR, Craig VS (2008) A mobile gas–water interface in electrolyte solutions. *J Phys Chem C* 112(39):15094–15097. <https://doi.org/10.1021/jp8067969>
- Jackson AT (1991) *Process engineering in biotechnology*. Prentice Hall International, UK
- Joshi JB, Veera VP, Prasad CV, Phanilumar DV, Deshpande NS, Thakre SS, Thorat BN (1998) Gas holdup structure in bubble column reactors. *PINSA* 64(4):441–567
- Joshi JB, Vitankar VS, Kulkarni AA, Dhotre MT, Ekambara K (2002) Coherent flow structures in bubble column reactors. *Chem Eng Sci* 57(16):3157–3183. [https://doi.org/10.1016/S0009-2509\(02\)00192-6](https://doi.org/10.1016/S0009-2509(02)00192-6)
- Kastanek F, Zahradnik J, Kratochvil J, Cermak J (1984) Modeling of large-scale bubble column reactors for non-ideal gas–liquid systems. *Front Chem React Eng* 1:330
- Kelkar BG, Phulgaonkar SR, Shah YT (1983) The effect of electrolyte solutions on hydrodynamic and backmixing characteristics in bubble columns. *Chem Eng J* 27(3):125–133. [https://doi.org/10.1016/0300-9467\(83\)80069-0](https://doi.org/10.1016/0300-9467(83)80069-0)
- Khare AS, Joshi JB (1990) Effect of fine particles on gas hold-up in three-phase sparged reactors. *Chem Eng J* 44(1):11–25. [https://doi.org/10.1016/0300-9467\(90\)80050-M](https://doi.org/10.1016/0300-9467(90)80050-M)
- Kluytmans JHJ, Van wachem BGM, Kuster BFM, Schouten JC (2001) Gas holdup in a slurry bubble column: influence of electrolyte and carbon particles. *Ind Eng Chem Res* 40(23):5326–5333. <https://doi.org/10.1021/ie001078r>
- Koide K, Takazawa A, Komura M, Matsunaga H (1984) Gas holdup and volumetric liquid-phase mass transfer coefficient in solid-suspended bubble columns. *J Chem Eng Jpn* 17(5):459–466
- Lee JC, Meyrick B (1970) Gas-liquid interfacial areas in salt solutions in an agitated tank. *Trans IChemE* 48:T37–T45
- Lee LS, Sun SL, Lin CL (2008) Predictions of thermodynamic properties of aqueous single-electrolyte solutions with the two-ionic-parameter activity coefficient model. *Fluid Phase Equilib* 264(1):45–54. <https://doi.org/10.1016/j.fluid.2007.10.015>
- Lessard RR, Zieminski SA (1971) Bubble coalescence and gas transfer in aqueous electrolytic solutions. *Ind Eng Chem Fundam* 10(2):260–269. <https://doi.org/10.1021/i160038a012>

- Machon V, Vlcek J, Kurdna V (1977) Gas hold-up in agitated aqueous solutions of strong inorganic salts. In: Proc 2nd Europ conf on mixing, Cambridge, England; (BHRA Fluid Eng), F2-17-F2-34
- Majumder SK (2016) Hydrodynamics and transport processes of inverse bubbly flow, 1st edn. Elsevier, Amsterdam
- Marrucci G, Nicodemo L (1967) Coalescence of gas bubbles in aqueous solutions of inorganic electrolytes. Chem Eng Sci 22:1257-1265. [https://doi.org/10.1016/0009-2509\(67\)80190-8](https://doi.org/10.1016/0009-2509(67)80190-8)
- Marucci G (1969) Theory of coalescence. Chem Eng Sci 24:975-985. [https://doi.org/10.1016/0009-2509\(69\)87006-5](https://doi.org/10.1016/0009-2509(69)87006-5)
- Millero FJ, Huang F, Laferiere AL (2002) Solubility of oxygen in the major sea salts as a function of concentration and temperature. Mar Chem 78:217-230. [https://doi.org/10.1016/S0304-4203\(02\)00034-8](https://doi.org/10.1016/S0304-4203(02)00034-8)
- Mouza AA, Dalakoglou GK, Paras SV (2005) Effect of liquid properties on the performance of bubble column reactors with fine pore spargers. Chem Eng Sci 60(5):1465-1475. <https://doi.org/10.1016/j.ces.2004.10.013>
- Nguyen PT, Hampton MA, Nguyen AV, Birkett GR (2012) The influence of gas velocity, salt type and concentration on transition concentration for bubble coalescence inhibition and gas holdup. Chem Eng Res Des 90(1):33-39. <https://doi.org/10.1016/j.cherd.2011.08.015>
- Olivieri G, Russo ME, Simeone M, Marzocchella A, Salatino P (2011) Effects of viscosity and relaxation time on the hydrodynamics of gas-liquid systems. Chem Eng Sci 66(14):3392-3399. <https://doi.org/10.1016/j.ces.2011.01.027>
- Orvalho S, Ruzicka MC, Drahos J (2009) Bubble column with electrolytes: gas holdup and flow regimes. Ind Eng Chem Res 48(17):8237-8243. <https://doi.org/10.1021/ie900263d>
- Pashley RM, Craig VSJ (1997) Effects of electrolytes on bubble coalescence. Langmuir 13(17):4772-4774. <https://doi.org/10.1021/la960034d>
- Patil VK, Joshi JB, Sharma MM (1984) Sectionalised bubble column: gas hold-up and wall side solid-liquid mass transfer coefficient. Can J Chem Eng 62(2):228-232. <https://doi.org/10.1002/cjce.5450620210>
- Prince MJ, Blanch HW (1990) Transition electrolyte concentrations for bubble coalescence. AIChE J 36:1425-1429. <https://doi.org/10.1002/aic.690360915>
- Ribeiro CP, Mewes D (2007a) The effect of electrolytes on the critical velocity for bubble coalescence. Chem Eng J 126(1):23-33. <https://doi.org/10.1016/j.ces.2006.08.029>
- Ribeiro CP Jr, Mewes D (2007b) The influence of electrolytes on gas hold-up and regime transition in bubble columns. Chem Eng Sci 62(17):4501-4509. <https://doi.org/10.1016/j.ces.2007.05.032>
- Ruzicka MC, Drahos J, Mena PC, Teixeira JA (2003) Effect of viscosity on homogeneous-heterogeneous flow regime transition in bubble columns. Chem Eng J 96(1):15-22. <https://doi.org/10.1016/j.ces.2003.08.009>
- Sagert NH, Quinn MJ (1978) The coalescence of gas bubbles in dilute aqueous solutions. Chem Eng Sci 33:1087-1095. [https://doi.org/10.1016/0009-2509\(78\)85014-3](https://doi.org/10.1016/0009-2509(78)85014-3)
- Sarrafi A, Müller-Steinhagen H, Smith JM, Jamialahmadi M (1999) Gas holdup in homogeneous and heterogeneous gas-liquid bubble column reactors. Can J Chem Eng 77(1):11-21. <https://doi.org/10.1002/cjce.5450770104>
- Sasaki S, Hayashi K, Tomiyama A (2016) Effects of liquid height on gas holdup in air-water bubble column. Exp. Therm Fluid Sci. 72:67-74. <https://doi.org/10.1016/j.expthermflusci.2015.10.027>
- Sasaki S, Uchida K, Hayashi K, Tomiyama A (2017) Effects of column diameter and liquid height on gas holdup in air-water bubble columns. Exp Thermal Fluid Sci 82:359-366. <https://doi.org/10.1016/j.expthermflusci.2016.11.032>
- Sharaf S, Zednikova M, Ruzicka MC, Azzopardi BJ (2016) Global and local hydrodynamics of bubble columns-effect of gas distributor. Chem. Eng. J. 288:489-504. <https://doi.org/10.1016/j.ces.2015.11.106>
- Sujan A (2018) Studies on hydrodynamic and mass transfer parameters in a bubble column. Ph.D. thesis, Malaviya National Institute of Technology, Jaipur
- Sujan A, Vyas RK (2017) A review on empirical correlations estimating gas holdup for shear-thinning non-Newtonian fluids in bubble column systems with future perspectives. Rev Chem Eng. <https://doi.org/10.1515/revce-2016-0062>
- Sujan A, Vyas RK, Singh K (2018) Estimation of liquid-side mass transfer coefficient and liquid film thickness in a bubble column using single spherical bubble model. Asia- Pac J Chem Eng 2018:e2178. <https://doi.org/10.1002/apj.2178>
- Syeda SR, Reza MJ (2011) Effect of surface tension gradient on gas hold-up enhancement in aqueous solutions of electrolytes. Chem Eng Res Des 89(12):2552-2559. <https://doi.org/10.1016/j.cherd.2011.04.013>
- Thorat BN, Shevade AV, Bhilegaonkar KN, Aglawe RH, Veera UP, Thakre SS, Joshi JB (1998) Effect of sparger design and height to diameter ratio on fractional gas hold-up in bubble columns. Chem Eng Res Des 76(7):823-834. <https://doi.org/10.1205/026387698525577>
- Tsang YH, Koh YH, Koch DL (2004) Bubble-size dependence of the critical electrolyte concentration for inhibition of coalescence. J Colloid Interface Sci 275(1):290-297. <https://doi.org/10.1016/j.jcis.2004.01.026>
- Vakarelski IU, Manica R, Li EQ, Basheva ES, Chan DY, Thoroddsen ST (2018) Coalescence dynamics of mobile and immobile fluid interfaces. Langmuir. <https://doi.org/10.1021/acs.langmuir.7b04106>
- Wang J, Tan SH, Nguyen AV, Evans GM, Nguyen NT (2016) A microfluidic method for investigating ion-specific bubble coalescence in salt solutions. Langmuir 32(44):11520-11524. <https://doi.org/10.1021/acs.langmuir.6b03266>
- Weissenborn PK, Pugh RJ (1995) Surface tension and bubble coalescence phenomena of aqueous solutions of electrolytes. Langmuir 11:1422-1426. <https://doi.org/10.1021/la00005a002>
- Weissenborn PK, Pugh RJ (1996) Surface tension of aqueous solutions of electrolytes: relationship with ion hydration, oxygen solubility, and bubble coalescence. J Colloid Interface Sci 184(2):550-563. <https://doi.org/10.1006/jcis.1996.0651>
- Wilkinson PM, Spek AP, van Dierendonck LL (1992) Design parameters estimation for scale-up of high-pressure bubble columns. AIChE J 38(4):544-554. <https://doi.org/10.1002/aic.690380408>
- Zahradnik J, Peter R, Kastanek F (1987) The effect of liquid phase properties on gas holdup in bubble column reactors. Collect Czech Chem Commun 52(2):335-347
- Zahradnik J, Fialova M, Kastanek F, Green K, Thomas N (1995) The effect of electrolytes on bubble coalescence and gas holdup in bubble column reactors. Chem Eng Res Des 73:341-346
- Zahradnik J, Fialova M, Ru M, Drahos J, Kastanek F, Thomas NH (1997) Duality of the gas-liquid flow regimes in bubble column reactors. Chem Eng Sci 52(21-22):3811-3826. [https://doi.org/10.1016/S0009-2509\(97\)00226-1](https://doi.org/10.1016/S0009-2509(97)00226-1)
- Zemaitis JF Jr, Clark DM, Rafal M, Scrivner NC (1986) Handbook of aqueous electrolyte thermodynamics. DIPPR and AIChE, New York

Affiliations

Ajay Sujan¹ · Raj K. Vyas¹ 

✉ Raj K. Vyas
rkvyas.chem@mnit.ac.in

Ajay Sujan
ajaysujan@gmail.com

¹ Department of Chemical Engineering, Malaviya National
Institute of Technology Jaipur, JLN Marg, Jaipur 302017,
India

BIO-DATA

Name	AJAY SUJAN
Father's Name	Shiromani Sujan
Mother's Name	Nirmala Sujan
Date of Birth	27.12.1977
Marital Status	Married
Educational Qualification	M.Tech. Chemical Engineering (2010) Malaviya National Institute of Technology, Jaipur, Rajasthan, India B.Tech. Chemical Engineering (2001) Institute of Engineering and Technology, Uttar Pradesh, Kanpur, India
Job Experience	4 years 6 months teaching
Scientific Memberships	Indian Institute of Chemical Engineers (IChE), Life member, Membership Number LM 52071 Indian Desalination Association (InDA), Life member, Membership Number LM 398
Publications	International Journal - 03 SCI International conference – 05 Short term course – 01